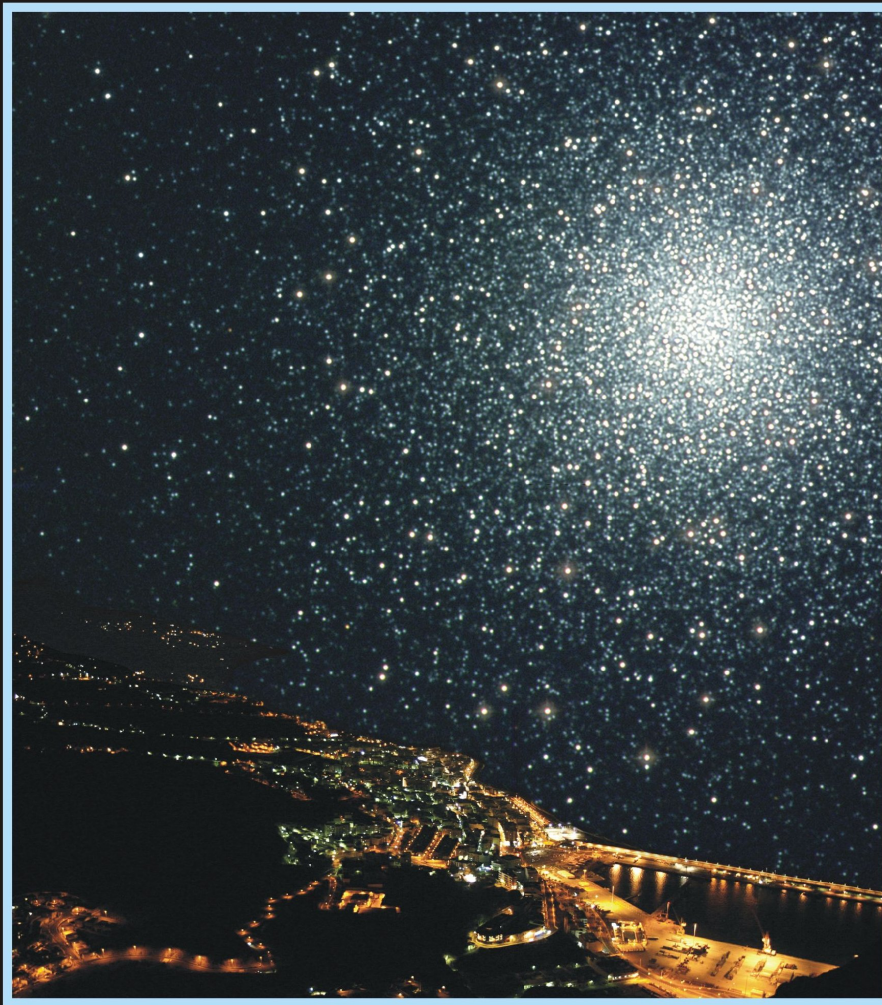


La Palma '05 **sd**^O_B Second Meeting on
Hot Subdwarf Stars
and Related Objects



Roy H. Østensen (Ed.)

6 – 10 June 2005, Santa Cruz de La Palma, Canary Islands, Spain

La Palma '05
sdo
B

THE SECOND MEETING ON
HOT SUBDWARF STARS
AND RELATED OBJECTS
PROCEEDINGS

Santa Cruz de La Palma
Canary Islands, Spain
June 6 – 10, 2005

Edited by
R. H. Østensen
Isaac Newton Group, La Palma, Spain

ISSN 1392-0049

The Proceedings of the 2nd Meeting on Hot Subdwarf Stars and Related Objects.
Baltic Astronomy, Vol. 15, Nos. 1 – 2

Editor: R. H. Østensen,

Cover design: J. Méndez and R. Østensen: Photo of Santa Cruz de La Palma by night (by Javier Méndez). M92 globular cluster image obtained with the Jacobus Kapteyn Telescope, La Palma (by Daniel Bramich and Nik Szymanek).

©Vilnius University Institute of Theoretical Physics and Astronomy,
Goštauto 12, Vilnius LT-01108, Lithuania

Printed by BMK, February 2006
Gedimino pr. 60, Vilnius LT-01110, Lithuania
Phone: 370-2396824 E-mail: bmk@lrs.lt

THE ORGANISERS

Scientific Organising Committee

Uli Heber, Simon Jeffrey, Pierre Maxted, Sabine Moehler,
Ralf Napiwotzki, Roy Østensen, Philipp Podsiadlowski,
Jan-Erik Solheim, Francois Wesemael, Sukyoung Yi

Local Organising Committee

Romano Corradi, Margie Lennon, Javier Méndez,
Roy Østensen, Saskia Prins, Peter Sørensen,
John Telting, Ángela Toledo

Organising Institutions

Isaac Newton Group (ING)
Nordic Optical Telescope (NOT)

Collaborating Institutions

Excmo. Cabildo Insular de La Palma
Patronato de Turismo de La Palma
Real Club Náutico de La Palma

CONTENTS

| | |
|---|-----|
| The organisers | iii |
| Contents | v |
| List of participants | ix |
| Conference picture | xi |
| The 2nd meeting on hot subdwarf stars and related objects. | |
| <i>R. H. Østensen</i> | 1 |
| EVOLUTIONARY MODELS AND THE UV-UPTURN PHENOMENON | |
| The look-back time evolution of the UV upturn phenomenon. | |
| <i>C. H. Ree, Y.-W. Lee, Y.-J. Sohn, S. K. Yi, S.-J. Yoon.</i> | 5 |
| Binary population synthesis, sdB stars, and the UV upturn. | |
| <i>D. Brown, S. Yi, Z. Han and S.-J. Yoon</i> | 13 |
| UV upturn of elliptical galaxies. | |
| <i>Z. Han, Ph. Podsiadlowski and A. E. Lynas-Gray</i> | 17 |
| HOT SUBDWARFS AND RELATED OBJECTS IN THE BULGE AND IN GLOBULAR CLUSTERS | |
| Hot subdwarfs in the galactic bulge. | |
| <i>G. Busso, S. Moehler, M. Zoccali et al.</i> | 25 |
| Super-Helium-rich stars in globular clusters: the origin of extreme horizontal branch. | |
| <i>S.-J. Joo, Y.-W. Lee, S.-J. Yoon et al.</i> | 33 |
| The nature of the hot stars in the bulge of globular cluster NGC 6388. | |
| <i>S. Moehler and A. V. Sweigart</i> | 41 |
| New candidate EHB stars in the open cluster NGC 6791: looking locally into the UV-upturn phenomenon. | |
| <i>L. M. Buson, E. Bertone, A. Buzzoni and G. Carraro</i> | 49 |
| Spectroscopic search for binaries among EHB stars in globular clusters. | |
| <i>C. Moni Bidin, R. A. Mendez, S. Moehler et al.</i> | 53 |
| NGC 6121-V46: a low-mass double degenerate ellipsoidal variable in a globular cluster. | |
| <i>S. J. O'Toole, R. Napiwotzki, U. Heber et al.</i> | 61 |
| Do EC 14026 stars exist in clusters? | |
| <i>M. D. Reed, D. Kilkenny and D. M. Terndrup</i> | 65 |

SURVEYS FOR HOT SUBDWARF STARS

| | |
|--|-----|
| Hot subdwarfs from low-dispersion surveys – methods of extraction and automatic analysis. <i>C. Winter, C. S. Jeffery, A. Ahmad and D. R. Morgan</i> | 69 |
| A spectroscopic search for new sdB stars from the GALEX survey. <i>J. Rhee, M. Seibert, R. H. Østensen et al.</i> | 77 |
| Searching for the “missing” PG hot subdwarfs in SDSS and GALEX data. <i>R. Wade, M. A. Stark, R. F. Green and P. R. Durrell</i> | 81 |
| The subdwarf database: released. <i>R. H. Østensen</i> | 85 |
| ATMOSPHERIC PROPERTIES OF HOT SUBDWARF STARS | |
| Subluminous O stars. <i>U. Heber, H. Hirsch, A. Ströer et al.</i> | 91 |
| Analysis of the FUSE spectra of the He-poor sdO star MCT 0019–2441. <i>M. Fontaine, P. Chayer, F. Wesemael et al.</i> | 99 |
| Metal abundances of sdB stars. <i>H. Edelmann, U. Heber and R. Napiwotzki</i> | 103 |
| NLTE analyses of sdB stars: progress and prospects. <i>N. Przybilla, M. F. Nieva and H. Edelmann</i> | 107 |
| New model atmospheres for Hydrogen-deficient stars: continuous and line opacities. <i>N. Behara and C. S. Jeffery</i> | 115 |
| Atmospheric parameters for subdwarf B stars: a consistency check between the Balmer lines and the far-ultraviolet spectrum. <i>C. Pereira, F. Wesemael and P. Bergeron</i> | 123 |
| Improved Helium line formation for extreme Helium stars. <i>N. Przybilla, K. Butler, U. Heber and C. S. Jeffery</i> | 127 |
| FUSE observations of Germanium, Zirconium and Lead in sdB Stars. <i>P. Chayer, M. Fontaine, G. Fontaine et al.</i> | 131 |
| Chemical abundances of Helium-rich subdwarf B stars. <i>A. Ahmad and C. S. Jeffery</i> | 139 |
| Multicomponent winds in sdB stars? <i>K. Unglaub</i> | 147 |
| Spectroscopic analysis of sdB binaries from the SPY project. <i>C. Karl, U. Heber, R. Napiwotzki and S. Geier</i> | 151 |
| Spectral analysis of sdB-He stars from the SDSS. <i>A. Ahmad, C. Winter and C. S. Jeffery</i> | 159 |
| Non-LTE metal abundances in V652 Her and HD 144941. <i>N. Przybilla, M. F. Nieva, U. Heber and C. S. Jeffery</i> | 163 |

HOT SUBDWARFS IN BINARY SYSTEMS

| | |
|---|-----|
| Subdwarf B star evolutionary systematics, conundrums and cautionary remarks. <i>E. Green, G. Fontaine, E. A. Hyde et al.</i> | 167 |
| The nature of the late-type companions in hot subdwarf composite-spectrum binaries. <i>M. A. Stark and R. A. Wade</i> | 175 |
| Monte Carlo simulations of post-common envelope sdB star plus white dwarf binaries. <i>B.-Q. For and E. M. Green</i> | 183 |
| Subdwarf B binaries in the Edinburgh-Cape survey. <i>L. Morales-Rueda, P. F. L. Maxted, T. R. Marsh et al.</i> | 187 |
| Discovery of 4 radial velocity variable sdB stars with eccentric orbits. <i>H. Edelmann, M. Altmann and U. Heber</i> | 191 |
| Photometric period variation of V1379 Aql. <i>E. Sipahi, S. Evren, G. Taş and C. İbanoğlu</i> | 199 |
| Helium, Carbon and Silicon abundances in the HW Virginis eclipsing binary subdwarf-B primary. <i>A. N. Mortimore and A. E. Lynas-Gray</i> | 207 |
| ASTEROSEISMOLOGY OF sdB STARS | |
| On the empirical instability domains for pulsating subdwarf B stars. <i>G. Fontaine, E. M. Green, P. Chayer et al.</i> | 211 |
| Line-profile variations in pulsating sdB stars as a pulsation mode diagnostic. <i>C. Schoenaers and A. E. Lynas-Gray</i> | 219 |
| Balloon 090100001: a link between the two classes of pulsating hot subdwarfs. <i>A. Baran, R. Oreiro, A. Pigulski et al.</i> | 227 |
| More new sdB pulsators discovered with the Nordic Optical Telescope. <i>J.-E. Solheim and R. H. Østensen</i> | 231 |
| Time-resolved spectroscopy of the bright sdBV star Balloon 090100001. <i>J. H. Telling, R. H. Østensen, U. Heber and T. Augusteijn</i> | 235 |
| Time-resolved spectroscopy of KPD 1930+2752. <i>S. Geier, U. Heber, N. Przybilla and R.-P. Kudritzki</i> | 243 |
| Time-series spectroscopy and photometry of PG 1219+534. <i>S. Harms, M. D. Reed and S. J. O'Toole</i> | 251 |
| Four rapidly pulsating sdB stars revisited. <i>D. Kilkenney, J. P. Kotze, E. Jurua et al.</i> | 255 |
| Ultracam photometry of pulsating subdwarf B stars. <i>C. S. Jeffery, C. Aerts, V. S. Dhillon and T. R. Marsh</i> | 259 |

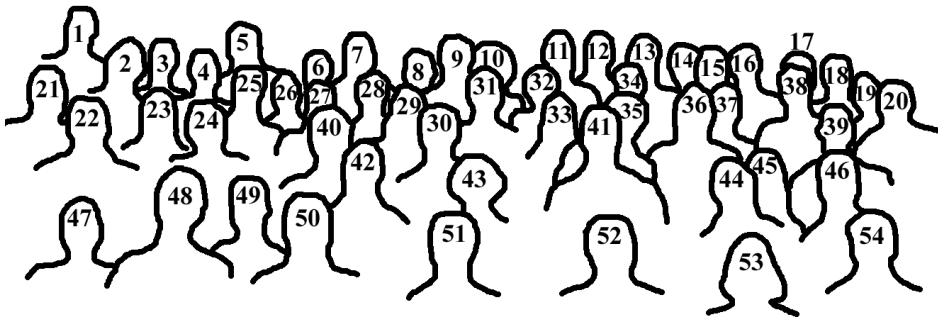
| | |
|---|------|
| Searching for observational evidence of tidally inclined pulsations. <i>M. Reed et al.</i> | 269 |
| High-speed ULTRACAM colorimetry of the subdwarf B star SDSS J171722.08+58055.8 <i>C. Aerts, C. S. Jeffery, V. S. Dhillon et al.</i> | 275 |
| Follow-up observations of known EC 14026-type pulsators. <i>G. Wolf, A.-Y. Zhou, D. M. Terndrup et al.</i> | 279 |
| PG 0014+067: WET observations and a new twist to the sdB star puzzle. <i>S. Kawaler, M. Vučković et al.</i> | 283 |
| Long-period variable subdwarf B stars: prospects for asteroseismology. <i>S. K. Randall, G. Fontaine, E. M. Green et al.</i> | 291 |
| FUSE determination of the abundances of Iron-peak elements in the PG 1716+426 stars. <i>J.-P. Blanchette, P. Chayer, F. Wesemael et al.</i> | 301 |
| The structure of subdwarf B stars as revealed by asteroseismology. <i>S. Charpinet, G. Fontaine, P. Brassard et al.</i> | 305 |
| An approach to a stability analysis of an sdO star. <i>C. Rodríguez-López, A. Moya, R. Garrido et al.</i> | 313 |
| A new large-amplitude slowly pulsating sdB star. <i>D. Kilkenny, D. O'Donoghue, M. D. Reed et al.</i> | 317 |
| The MSST campaign: 4m spectroscopy of PG 1605+072. <i>S. Jeffery, U. Heber, S. Dreizler et al.</i> | 321 |
| ABSTRACTS OF PAPERS OF THIS MEETING PUBLISHED SOMEWHERE ELSE AND NOT INCLUDED INTO THE BALTIC ASTRONOMY JOURNAL | |
| Spectroscopic detection of g -modes in a long-period pulsating sdB star – PG 1627+017. <i>B.-Q. For, E. Green, D. O'Donoghue et al.</i> | A-I |
| Magnetic fields in sdB and sdO stars <i>S. J. O'Toole, S. Jordan, U. Heber et al.</i> | A-II |
| Photometry of LS IV–14°116. <i>A. Ahmad and C. S. Jeffery</i> | A-IV |

LIST OF PARTICIPANTS

| Name | Country | E-mail | ID* |
|--------------------------|-------------|--------------------------------------|-----|
| Conny Aerts | Belgium | conny@ster.kuleuven.be | 53 |
| Amir Ahmad | N. Ireland | amir@star.arm.ac.uk | 50 |
| Javier Méndez Alvarez | Spain | jma@ing.iac.es | - |
| Thomas Augusteijn | Spain | tau@not.iac.es | - |
| Andrzej Baran | Poland | andrzej@oa.uj.edu.pl | 12 |
| Natalie Behara | N. Ireland | ntb@star.arm.ac.uk | 45 |
| Pierre Bergeron | Canada | bergeron@astro.umontreal.ca | 16 |
| Jean-Philippe Blanchette | Canada | blanchette@astro.umontreal.ca | 2 |
| David Brown | UK | dab@astro.ox.ac.uk | 18 |
| Irmela Bues | Germany | bues@sternwarte.uni-erlangen.de | 43 |
| Lucio Buson | Italy | buson@pd.astro.it | 20 |
| Giorgia Busso | Germany | busso@astrophysik.uni-kiel.de | 49 |
| Stphane Charpinet | France | scharpin@ast.obs-mip.fr | 10 |
| Pierre Chayer | USA | chayer@pha.jhu.edu | 34 |
| Heinz Edelmann | Germany | edelmann@sternwarte.uni-erlangen.de | 9 |
| Gilles Fontaine | Canada | fontaine@astro.umontreal.ca | 11 |
| Mathieu Fontaine | Canada | mfontaine@astro.umontreal.ca | 7 |
| BiQing For | USA | bfor@as.arizona.edu | 23 |
| Stephan Geier | Germany | geier@sternwarte.uni-erlangen.de | 17 |
| Elizabeth Green | USA | bgreen@as.arizona.edu | 3 |
| Zhanwen Han | P.R. China | zhanwen@public.km.yn.cn | 35 |
| Stacey Harms | USA | slh757s@smsu.edu | 6 |
| Ulrich Heber | Germany | heber@sternwarte.uni-erlangen.de | 32 |
| Simon Jeffery | UK | csj@arm.ac.uk | 38 |
| Hyunjin Jeong | S. Korea/UK | hyunjin@astro.ox.ac.uk | 33 |
| Seok-Joo Joo | S. Korea | nespat25@csa.yonsei.ac.kr | 31 |
| Christian Karl | Germany | karl@sternwarte.uni-erlangen.de | 39 |
| Steve Kawaler | USA | sdk@iastate.edu | 21 |
| David Kilkeny | S. Africa | dmk@saa.ac.za | 5 |
| Danny Lennon | Spain | djl@ing.iac.es | - |
| Anthony E. Lynas-Gray | UK | aelg@astro.ox.ac.uk | 14 |
| Pierre Maxted | UK | pflm@astro.keele.ac.uk | - |
| Sabine Moehler | Germany | smoehler@eso.org | 51 |
| Christian Moni Bidin | Chile | mbidin@das.uchile.cl | 36 |
| Luisa Morales-Rueda | Netherlands | lmr@astro.ru.nl | 26 |
| Darragh O'Donoghue | S. Africa | dod@saa.ac.za | 22 |
| Simon O'Toole | Germany | otoole@sternwarte.uni-erlangen.de | 8 |
| Raquel Oreiro | Spain | ror@iac.es | 27 |
| Caroline Pereira | Canada | pereira@astro.umontreal.ca | 19 |
| Philipp Podsiadlowski | UK | podsi@astro.ox.ac.uk | 1 |
| Norbert Przybilla | Germany | przybilla@sternwarte.uni-erlangen.de | 46 |

* Number in conference photo identification picture on next page.

| | | | |
|--------------------------|------------|------------------------------------|----|
| Suzanna Randall | Canada | randall@astro.umontreal.ca | 28 |
| Chang Hee Ree | S. Korea | chr@csa.yonsei.ac.kr | 40 |
| Mike Reed | USA | MikeReed@missouristate.edu | 42 |
| Jaehyon (Jay) Rhee | USA | rhee@srl.caltech.edu | 30 |
| Cristina Rodriguez-Lopez | Spain | cristinatrl@uvigo.es | 29 |
| Caroline Schoenaers | UK | cxs@astro.ox.ac.uk | 25 |
| Esin Sipahi | Turkey | sipahi@astronomy.sci.ege.edu.tr | 47 |
| Jan-Erik Solheim | Norway | j.e.solheim@astro.uio.no | 44 |
| Michele Stark | USA | stark@astro.psu.edu | 4 |
| John Telting | Spain | jht@not.iac.es | 41 |
| Klaus Unglaub | Germany | unglaub@sternwarte.uni-erlangen.de | 52 |
| Richard Wade | USA | wade@astro.psu.edu | 37 |
| Franois Wesemael | Canada | wesemael@astro.umontreal.ca | 13 |
| Christopher Winter | N. Ireland | cwr@arm.ac.uk | 48 |
| George Wolf | USA | georgewolf@smsu.edu | 54 |
| Suk-Jin Yoon | UK | sjyoon@astro.ox.ac.uk | 15 |
| Roy Østensen | Spain | roy@ing.iac.es | 24 |





THE 2ND MEETING ON HOT SUBDWARF STARS AND RELATED OBJECTS

R. H. Østensen

Isaac Newton Group, Apartado 321, E-38700 Santa Cruz de La Palma, Spain

1. INTRODUCTION

The first meeting dedicated to hot subdwarf stars was held in Keele, U.K. on June 16–20 2003. The idea of such a meeting was conceived by Pierre Maxted, and in his report in the proceedings of that meeting the full background is given (Maxted 2004). When I went to that meeting, I had just started a new three-year contract as a PPARC research fellow at the Isaac Newton Group of Telescopes (ING) on La Palma, Canary Islands. Since it has been a tradition for the research fellows at ING to organise a conference or workshop during their contract period, the possibility of hosting a follow-up meeting to the Keele event was on my mind. When several people suggested La Palma as a good option for the next meeting, I was not slow to accept, and on the last day of the Keele meeting, the offer to hold another meeting on La Palma in 2005 was presented.

The title of the first meeting was Extreme Horizontal Branch Stars and Related Objects. After a lengthy discussion in the SOC it was decided to change that to Hot Subdwarf Stars and Related Objects instead. The terms EHB stars and sdB/sdO stars are often used interchangeably, but the EHB term implies a specific evolutionary history. Recently, evidence has accumulated that many of the stars that appear similar to EHB stars in spectroscopic studies may have completely different evolutionary histories. From the beginning, the intention of the meeting was to keep it open to all these similar stars, which is why the extension *and related objects* was included. The term *hot subdwarf stars*, however, has no evolutionary implications, but is a classical term used in spectral classifications of blue stars. This term encompasses the sdB, sdOB and sdO stars as well as the helium rich varieties usually referred to as He-sdB or He-sdO stars. With *hot subdwarf stars* we include all objects that appear in the HR diagram below the main sequence and above the white dwarf cooling track, regardless of how they got there. The *related objects* extension was kept in order to make sure that objects such as the extreme helium (EHe) stars were not left out. (Technically they are subluminous, but due to their low gravities they are not classified as He-sdB stars.)

2. THE MEETING

The meeting took place in Santa Cruz de La Palma between the 6th and the 10th of June 2005. 58 participants arrived from all over the world, almost half again as many as at the first meeting. The organisation of the meeting was carried out in a collaboration between the Isaac Newton Group (ING) and the

Nordic Optical Telescope (NOT), both which contributed a considerable amount toward the budget of the meeting. Support for specific social events was provided by the local government (Excmo. Cabildo Insular de La Palma) and the tourist board (Patronato de Turismo de La Palma). Additionally, the Real Club Náutico de Santa Cruz de La Palma has been extremely helpful by making their excellent locales available to us at no cost. Thanks to all this financial support we were able to keep a very reasonable registration fee, and even waive it completely for about a third of the participants who were students or without financial support at the time. On behalf of all the participants who enjoyed the hospitality of La Palma, I would like to thank all the organisations involved.

The meeting room at the Real Club Náutico provided an excellent environment for the event. The Club's restaurant also managed to provide excellent coffee breaks with delicious and varied snacks, as well as a very impressive conference dinner. Being in the center of the city allowed people to use the extended lunch break to explore the old city and find their own places to eat.



Fig. 1. At the meeting.

3. THE SESSIONS

The meeting was divided into sessions that covered a broad range of topics related to the hot subdwarf stars. They were:

- Evolutionary models and the UV-upturn phenomenon
- Hot subdwarfs and hot HB stars in the field, clusters and galaxies
- Atmospheric properties of hot subdwarf stars
- Hot subdwarfs in binary systems
- Asteroseismology of sdB stars

Eight half-day sessions were completed during the meeting, with three sessions dedicated to asteroseismology, two sessions for atmospheric properties and the remaining topics filling one session each. The contributions in these proceedings are arranged roughly along the order of the listed sessions. All the talks were limited to 30 minutes, with 5 minutes extra for discussions. Interleaved with the talks were short oral presentations with discussions of the posters.

4. THE ISLAND

The island of La Palma is one of the smaller of the Canary Islands, with a surface area of 706 km² and a population of only 80 000. It is unusual in that it rises exceptionally steeply from the ocean floor (from a depth of 4000 m) to a volcanic crater rim at an altitude of between 2000 and 2500 meters. The Observatory is located around the highest point, the Roque de los Muchacos (2426 m).



Fig. 2. At the William Herschel Telescope.

The participants of the meeting were invited to tour the observatory area and visit the 4.2 m William Herschel Telescope (WHT, see Fig. 2), the 2.5 m Nordic Optical Telescope (NOT) and the 10 m Gran Telescopio Canarias (GTC) which is currently being assembled in its enormous dome.



Fig. 3. Exploring the volcanoes.

opportunity to stay another day were invited to a tour around the island, including a visit to some recent volcanoes (Fig. 3).

5. THE PROCEEDINGS

For the first meeting it was decided by the SOC to submit all contributions to a thorough refereeing process, and the participants were called to assist with the reviewing of the papers (Maxted 2004). For this second meeting we have even called upon experts not present at the meeting, in order to ensure that all papers have been refereed by qualified researchers. This process has gone exceptionally smoothly thanks to the prompt response of (almost) all the referees.

An issue that the SOC was not happy with from the proceedings of the first

On Friday evening, after the end of the meeting, a farewell party was held at the swimming-pool resort of the Real Club Náutico, in the harbor of Santa Cruz de La Palma. Most of the participants also enjoyed the entertainment provided by the local observatory band *Manifold*, and some even braved the dance floor.

On Saturday the participants who had the opportunity to stay another day were invited to a tour around the island, including a visit to some recent volcanoes (Fig. 3).

meeting was the long printing time. The SOC felt that the purpose of publishing results from work in progress was somewhat defeated if the time between the original presentation and the printed version was more than a year. For this reason we sought to find a publisher who could promise us quick printing and freely accessible on-line versions at an affordable price. Baltic Astronomy was quick to promise us the first issue of 2006 for our purposes. In addition to the regular journal issues, we could obtain special hard-back copies for the participants at a very reasonable price.

Oral presentations from the meeting have been given a page limit of eight pages (although a few participants have been allowed to exceed this), and short “poster” presentations were limited to four pages. Three contributions are published in other journals, and for this reason only an abstract version is presented at the end of the proceedings book, with reference to the journal paper.

6. OTHER REMARKS

The LOC put a lot of effort into designing useful web-pages to assist the participants with information about the meeting, registration and manuscript submission. (<http://www.ing.iac.es/conferences/subdwarf/>). All the pages are written in PHP¹ and changes dynamically according to what information is available. A registration system was made using a PHP interface to a MySQL² database. The on-line registration form allowed participants to enter their registration data, update information such as talk titles and abstracts, and the database allowed automatic update of the conference program. An automatic interface for submission of the proceedings which also did some basic checks on the manuscripts, was also provided. The pages will remain accessible for the foreseeable future, and anybody interested in reworking this system for other events can contact the author.

The SOC wishes to thank the members of the LOC for their work in managing the event. Special thanks goes to Javier Méndez of the Isaac Newton Group for his excellent work in managing the venue and all the social events, as well as the design of the poster and the photos for the meeting.

After the success of this second meeting, the group in Bamberg has offered to host the 3rd meeting in 2007. It is clear that a new tradition for a biennial series of meetings on hot subdwarf stars has been established.

REFERENCES

Maxted P. F. L. 2004, *Ap&SS*, 291, 193

¹ PHP (www.php.net) is a script language that generates HTML documents.

² MySQL (www.mysql.com) is an open source database system.

THE LOOK-BACK TIME EVOLUTION OF THE UV UPTURN PHENOMENON

C. H. Ree¹, Y.-W. Lee¹, Y.-J. Sohn¹, S. K. Yi^{1,2}, S.-J. Yoon^{1,2}
and the GALEX Science Team

¹ *Center for Space Astrophysics and Department of Astronomy, Yonsei
University, 134 Shinchon, Seoul 120-749, Korea*

² *Department of Physics, University of Oxford, Keble Road, Oxford OX1 3RH,
U.K.*

Received 2005 August 1

Abstract. In order to investigate the origin of the far-UV (FUV) flux from early-type galaxies, *Galaxy Evolution Explorer* (GALEX) is collecting the UV data for the elliptical-rich clusters at moderate redshifts ($z < 0.25$) where the dominant FUV source is predicted to be hot horizontal-branch (HB) stars and their post-HB progeny. The early results show that the FUV flux of quiescent early-type galaxies *does* evolve substantially during the last 1–2 Gyr of look-back time, and the observed UV fading is consistent with the variation predicted by the population synthesis models where the mean temperature of HB stars declines rapidly with increasing look-back time.

Key words: galaxies: elliptical – galaxies: evolution – galaxies: stellar content – ultraviolet: galaxies

1. INTRODUCTION

It is now well established that the far-UV (FUV) flux (“UV upturn”) of nearby early-type galaxies originates from a minority population of old hot helium-burning horizontal-branch (HB) stars (O’Connell 1999; Brown et al. 2000b). Stellar evolution models of HB predict that the mean temperature of HB distribution declines rapidly with decreasing age (e.g., Lee et al. 1994), and therefore the FUV flux from ellipticals should fade rapidly with look-back time (Greggio & Renzini 1990; Tantalo et al. 1996). Population synthesis models of Yi et al. (1999) also indicate that careful observations for the UV look-back time evolution could also discriminate two alternative HB solutions on the origin of UV flux, i.e., “metal-poor” and “metal-rich” HB models, which predict different ages for giant ellipticals.

The *Hubble Space Telescope* (HST) has obtained FUV images for several elliptical-rich clusters in the redshift range of $0.3 < z < 0.6$ (Brown et al. 2000a, 2003), but stellar evolution models (Lee et al. 1999; Yi et al. 1999) predict that hot HB stars must be absent at these relatively high redshifts, as no stars of low enough mass have yet evolved. Therefore, UV observations covering a lower redshift range ($z < 0.25$) are still required, in order to test the look-back

time evolution effect of HB stars in giant ellipticals. Here we present the early results from the *Galaxy Evolution Explorer* (GALEX) UV observations for the Abell clusters in this redshift range, and also for the Fornax cluster as a local calibrator.

2. GALEX UV OBSERVATIONS

GALEX UV deep imaging survey for the UV upturn early-type galaxies aims at the elliptical-rich Abell clusters at $z < 0.25$. The first deep imaging target for this study was Abell 2670 at $z = 0.076$. Figure 1 shows the GALEX FUV and optical images of the early-type galaxies successfully identified within 25 arcmin² field of view centered on the brightest giant elliptical galaxy, a19 (Lee et al. 2005a). From a subsequent observation, we also successfully detected several early-type galaxies in Abell 951 at $z = 0.143$ in the GALEX UV images (see Figure 2; Ree et al. 2005). In most cases, their FUV lights are concentrated in the central region of the red galaxies without recent massive star formation, which is analogous to the smooth UV profiles of the quiescent UV upturn galaxies in the local Universe (Ohl et al. 1998; O’Connell 1999), with a few exceptions discussed below. The multi-orbit deep imaging UV observations with GALEX dedicated for more other elliptical-rich clusters at moderate redshifts are ongoing.

In order to compare the remote targets at various redshifts with the local samples without any systematic effect that may arise from the different aperture sizes used in the photometry, we should measure the total luminosities with sufficiently large, variable apertures. The total luminosities of those cross-matched early-type galaxies in remote clusters were measured by the elliptical aperture photometry (MAG_AUTO) with SExtractor image analysis package (Bertin & Arnouts 1996) in both FUV and optical passbands. The Galactic foreground extinctions were then corrected with $R_V = 3.1$, $R_{FUV} = 8.16$ (Cardelli et al. 1989). We do *not* convert the observed values into the restframe ones, as the *empirical k*-corrections may cause uncertainties in the comparison between the data samples at different redshifts. Instead, we will compare the apparent values with the model synthetic spectra redshifted to the target distances.

Nearby clusters of galaxies, e.g., Fornax, Virgo and Coma, are the best places to find the local early-type galaxies with various UV strengths, and they provide constraints to the model parameters in the local Universe. GALEX observations for the early-type galaxies in the Fornax cluster are presented in Figure 3. Their FUV magnitudes were measured from the surface photometry using ellipse fitting. The FUV surface brightness profiles extend smoothly, out to $r > 80''$ in the case of NGC 1399 and NGC 1404. In order to minimize the aperture effect induced by UV/optical radial gradient (Ohl et al. 1998), we estimated the FUV total magnitudes by integration of the radial profiles. We have also corrected for the Galactic foreground extinctions ($A_{FUV} = 0.09 - 0.14$), and their total magnitudes in *V*-band were adopted from the Third Reference Catalog of Bright Galaxies (RC3; de Vaucouleurs et al. 1991). Our FUV photometry for the elliptical galaxies in the Fornax cluster, when measured within the *International Ultraviolet Explorer satellite* (IUE) aperture ($20'' \times 10''$), agrees well with the IUE measurements (Burstein et al. 1988) to within 0.01–0.06 mag.

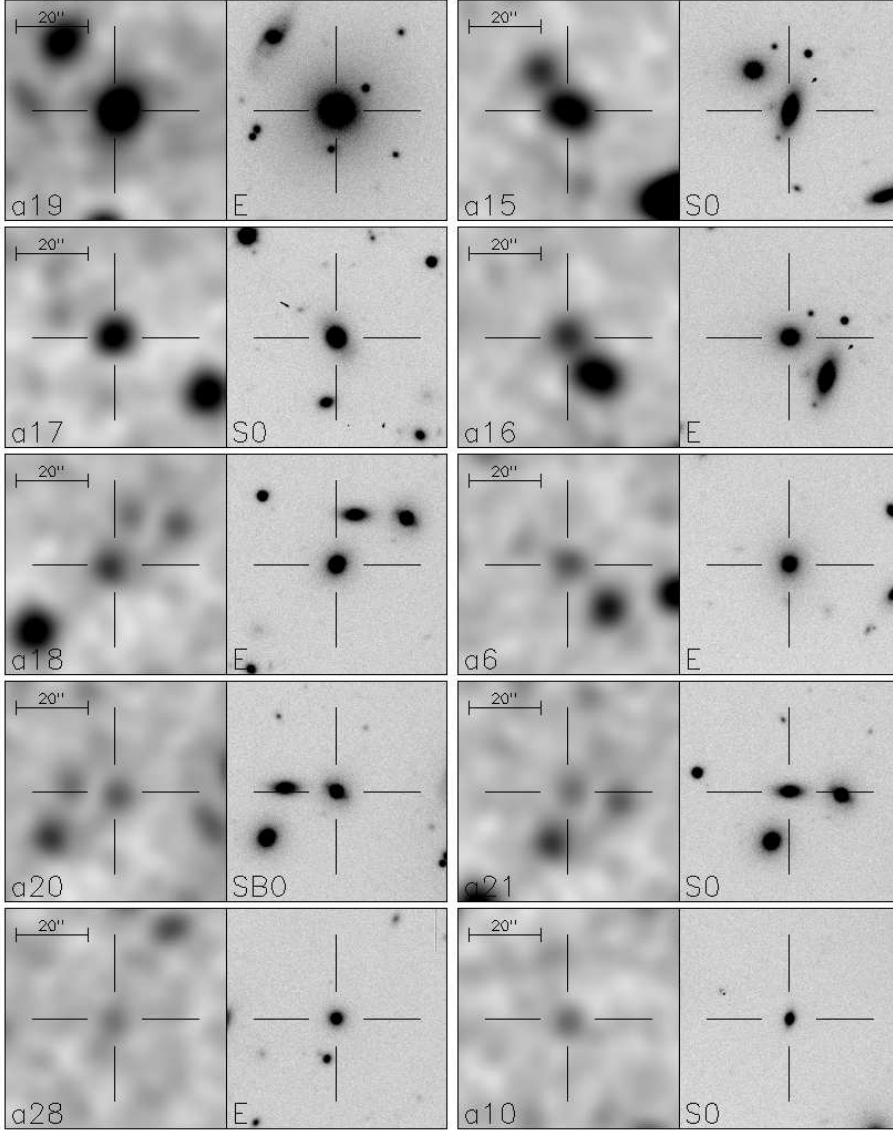


Fig. 1. GALEX FUV (*left panels*) and optical *r*-band (*right panels*) images ($1' \times 1'$) of the early-type galaxies in Abell 2670 ($z = 0.076$). The optical images are from Fasano et al. (2002). For some of UV-strong galaxies here, a15 and a16, there are strong evidences of young populations based on strong near-UV flux or $H\alpha$ emission feature due to the residual star formation (Lee et al. 2005a).

3. MORE DISTANT CLUSTERS

Even the most massive giant elliptical galaxies ($M_V \leq -22$) should be fainter than 25th magnitude (AB) in FUV at $z > 0.3$. It would be very difficult to detect such faint *red* galaxies at high redshift with a small telescope like GALEX.

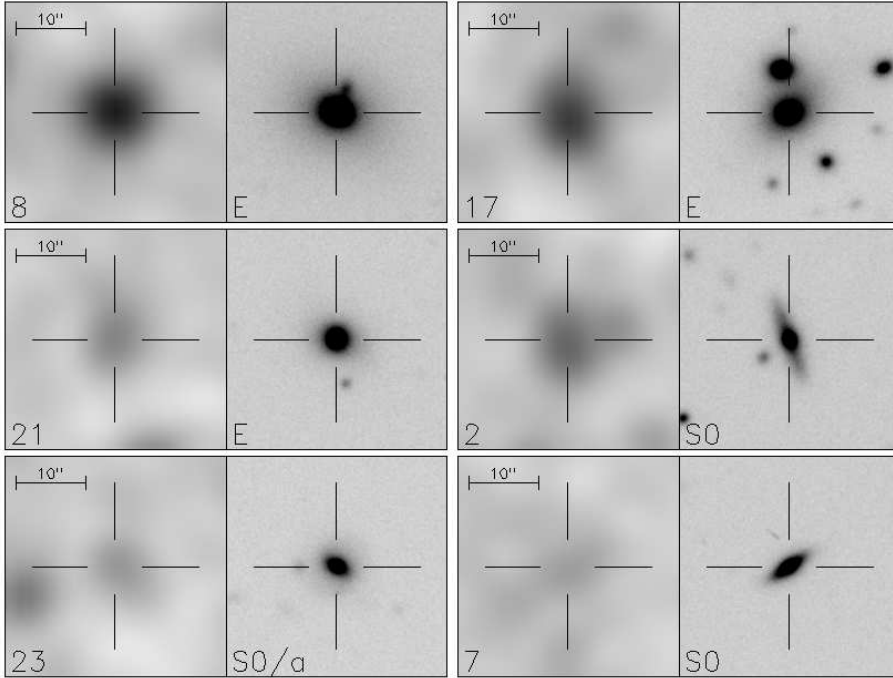


Fig. 2. GALEX FUV (*left panels*) and optical *r*-band (*right panels*) images ($30'' \times 30''$) of early-type galaxies in Abell951 ($z = 0.143$). The optical images are from Fasano et al. (2000). Optical spectroscopic follow-ups are underway searching for the recent star formation signatures, if any, in these galaxies.

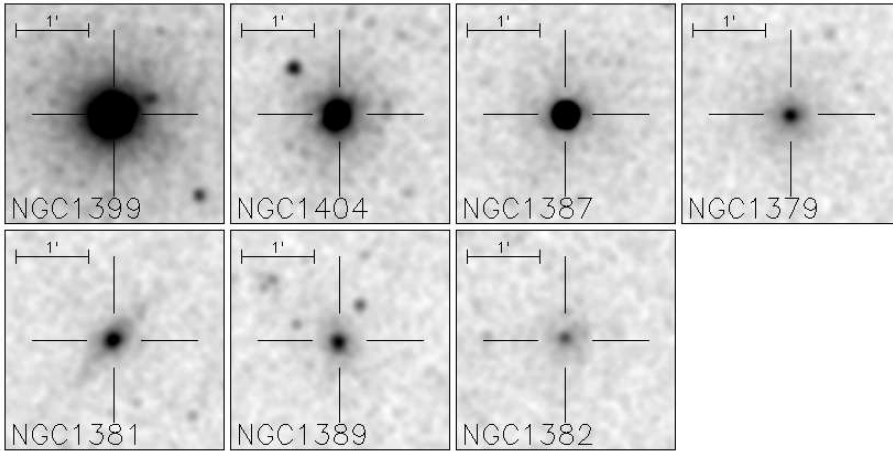


Fig. 3. GALEX FUV images ($3' \times 3'$) of the early-type galaxies in the Fornax cluster as a local calibrator. Their FUV lights are concentrated in the central region, and the radial profiles extend smoothly to $r > 1'$ for UV-strong galaxies.

However, there are several HST UV observations for the distant galaxy clusters at $0.3 < z < 0.6$ with the *Space Telescope Imaging Spectrograph* (STIS). From the literatures, we have taken the photometric measurements for the early-type galaxies in two distant clusters, CL1358+62 at $z = 0.33$ and CL0016+16 at $z = 0.55$, observed in UV by Brown et al. (2000a, 2003) and in optical passbands by van Dokkum et al. (1998) and Smail et al. (1997), respectively. The HST *Faint Object Camera* data for Abell 370 at $z = 0.375$ (Brown et al. 1998) are not included here, as they may have significant systematic errors according to Brown et al. (2003).

For the comparison with GALEX data, we converted those HST measurements to the AB magnitude system using the photometric zero-points and pivot wavelengths defined in the HST image headers ($m_{\text{AB}} = m_{\text{ST}} - 5 \log \lambda_p + 18.6921$). Model spectral energy distributions (SEDs) redshifted to $z = 0.33$ and 0.55 were then used to estimate the systematic difference between the HST and GALEX filter systems. Since the aperture radii in their analyses ($0.4''$ in *FUV* for both clusters, and $1.5''$ in *V* for CL 1358+62) are not large enough to represent total magnitudes, we applied appropriate aperture corrections, -0.32 (*FUV*) and -0.22 (*V*) for CL 1358+62. For the galaxies in CL 0016+16, we applied a correction only in *FUV* (-0.17 mag), as we adopted the total *V* magnitude from the catalog in Smail et al. (1997). The aperture correction values were obtained by utilizing the *FUV* (Lee et al. 2005a) and *V* (Marcum et al. 2001) radial profiles of NGC 1399, assuming that these clusters are at 75 (CL 1358+62) and 117 (CL 0016+16) times the distance of the Fornax cluster adopting the currently favored cosmological parameters $(\Omega_M, \Omega_\Lambda, H_0) = (0.3, 0.7, 70)$. Finally, foreground extinction corrections are applied.

4. DISCUSSION

From the extinction-corrected apparent total magnitudes in both *FUV* and *V* passbands, we have derived the *FUV* – *V* colors of the early-type galaxies in clusters, measured by GALEX (Fornax, Abell 2670 and *preliminary* analysis of Abell 951) and by HST (CL 1358+62 and CL 0016+16). The apparent redshift evolution of the observed *FUV* – *V* colors is then presented in Figure 4, along with the two alternative model predictions. The “metal-poor HB model” suggests that the dominant FUV sources are very old ($t > 12$ Gyr) hot metal-poor HB stars and their post-HB progeny, and the FUV flux is expected to increase with age due to the smaller main-sequence turnoff and HB envelop masses. In the “metal-rich HB model”, on the other hand, the dominant sources are old ($t = 10$ – 12 Gyr) hot super metal-rich HB and post-HB stars, and the FUV flux is predicted to increase with metallicity due to the enhanced helium enrichment and mass-loss. Even if these two alternative models are almost equally capable of reproducing the observed *FUV* – *V* colors in present-epoch giant ellipticals, their evolutionary predictions are quite different from one another (see Yi et al. 1999).

The models in Figure 4 are specifically constructed to match the *FUV* – *V* color of the local giant elliptical galaxy NGC 1399, the brightest galaxy in the Fornax cluster, and then passively evolved with look-back time. The model spectra and colors are then redshifted and the look-back times are converted to the equivalent redshift values, with the cosmological parameters above. Therefore, the foreground extinction-corrected observed data can be directly compared with the models. Since the NGC 1399 is a typical FUV-strong giant elliptical galaxy in the local

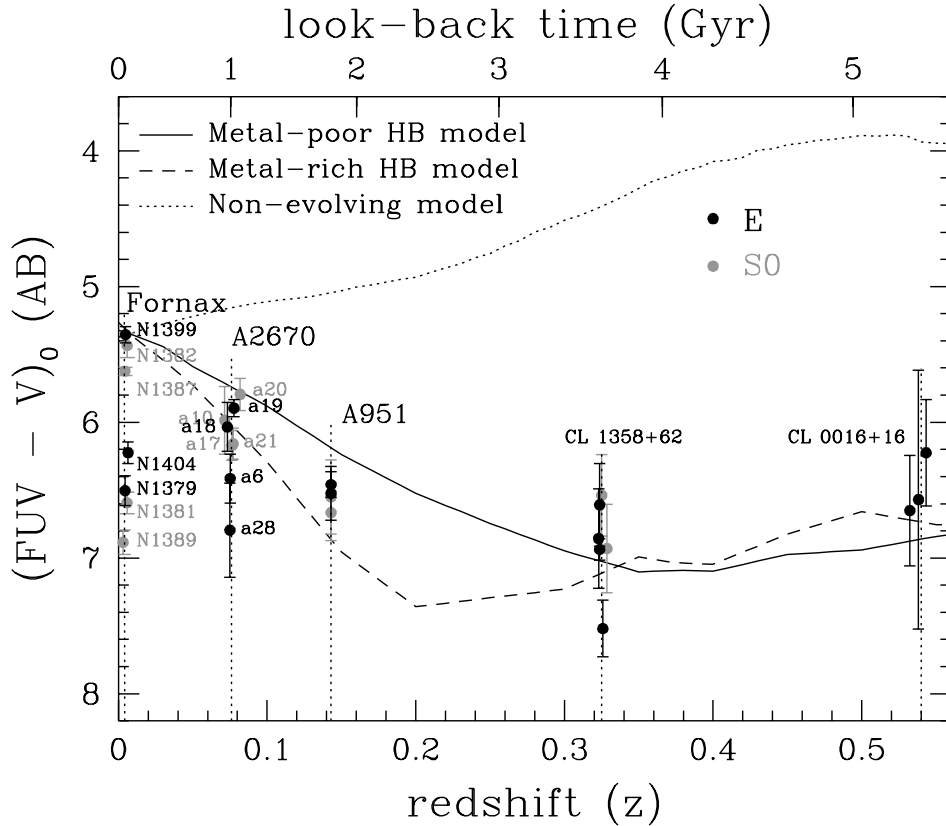


Fig. 4. Evolution of the UV upturn as a function of redshift. The observed apparent $FUV - V$ colors of the early-type galaxies in clusters at various redshifts are compared with the “metal-poor” (*solid*) and “metal-rich” (*dashed*) HB evolutionary models. The *dotted* line is for the case that the model spectrum of NGC 1399 is redshifted with no stellar evolution considered. Only the *quiescent* type of galaxy samples, without any strong star-formation signatures, are plotted (see text).

Universe, the model lines would represent the redshift (look-back time) evolution of giant ellipticals, and hence should be compared with the brightest ellipticals in each cluster. Note that there is a distinguishable amount of difference between the two alternative evolutionary models, up to ~ 1 mag. in $FUV - V$ color at $z \approx 0.2$, for the massive giant elliptical galaxies ($M_V \approx -22$).

It is clear from Figure 4 that we have detected the fading of the UV upturn expected at moderate redshifts. Compared to NGC 1399, the nearby giant elliptical galaxy in the Fornax cluster, an apparent extinction-corrected $FUV - V$ color of the giant elliptical galaxy (a19) in Abell 2670 gets redder by ~ 0.55 mag at $z = 0.076$ (look-back time ~ 1.0 Gyr). For the restframe $FUV - V$ color, this corresponds to 0.70 mag, which is consistent with the variation predicted by the models (Lee et al. 2005a). A preliminary analysis for Abell 951 ($z = 0.143$) confirms this by showing a similar amount of evolution again in the $FUV - V$ color of UV-strong giant elliptical galaxies between the look-back time of 1 and 2 Gyr. In

these models, the dominant FUV source is hot HB stars for $z < 0.25$, and therefore the FUV flux fades rapidly with look-back time (redshift) as the HB temperature distribution becomes cooler with decreasing age (increasing look-back time).

For $z > 0.3$, the HST data also appear to be in reasonable agreement with our model predictions, to within the errors. Note, however, that the models become more uncertain at these relatively higher redshifts, as the dominant FUV source changes from hot HB stars to post-asymptotic giant branch (PAGB) stars for $z > 0.25$. In particular, Lee et al. (1999, see their Fig. 1) predict that the HB contribution to the total FUV flux becomes almost negligible for $z > 0.4$. At relatively higher redshifts, the total FUV flux would therefore increase as the mass of PAGB stars decreases because their lifetimes correlate inversely with their mass. Consequently, the available HST data may provide no direct test of HB evolution effect. Nevertheless, they provide a useful test on the adopted mass ($0.565 M_{\odot}$) of PAGB stars in our models.

Although we are witnessing the growing body of evidence indicating the FUV flux of quiescent early-type galaxies evolves substantially at moderate redshifts ($z < 0.25$) as the deep imaging survey with GALEX UV telescope continues, there are some issues to be solved. On the observational side of this study, UV blending and contamination by young stars are serious issues. With the given spatial resolution of GALEX (1.5 "/pixel), it becomes difficult to de-blend properly the UV lights purely from the old stellar population in elliptical galaxies and the possible UV contaminations by neighboring dwarf galaxies, as we reach out to $z \sim 0.2$. Furthermore, some early-type galaxies show contamination from the residual star formation in their UV spectra (Burstein et al. 1988; Yi et al. 2005), and therefore it is important to check whether our sample galaxies are not affected by a minority population of young stars. As described in Lee et al. (2005a), we found two of the UV-strong early-type galaxies in Abell 2670, a15 (S0) and a16 (E), show the evidence of young populations inferred by unusually strong near-UV flux or by strong H α emission. Some of HST data samples also show unexpectedly strong UV flux. All of these abnormal galaxies with recent star-forming signatures are excluded in Figure 4. The optical follow-up spectroscopy continues for the other GALEX target clusters in order to discriminate such star-forming red galaxies.

On the theoretical side, the nature of extreme HB (EHB) stars and their contribution to the UV flux should be understood. The effect of EHB stars are *not* fully included in the current population synthesis models presented here. Particularly, the excessively large age (up to 30% older than the Galactic globular clusters) required for the local giant ellipticals in the "metal-poor" HB model would be reduced significantly, if the EHB stars are explained as the minority population of super helium-rich stars (Lee et al. 2005b). In any case, the observed rapid evolution of FUV flux with look-back time at moderate redshifts, if confirmed by further observations, would infer the strong age dependency in the evolution of UV sources in old stellar systems (Lee et al. 1994; Yi et al. 1999).

ACKNOWLEDGMENTS. GALEX is a NASA Small Explorer, launched in April of 2003. We gratefully acknowledge NASA's support for construction, operation and science analysis for the GALEX mission, developed in cooperation with the Centre National d'Etudes Spatiales of France and the Korean Ministry of Science and Technology. Yonsei University participation is funded by the Korean Ministry of Science & Technology, for which we are grateful.

REFERENCES

- Bertin E., Arnouts S. 1996, *A&A*, 117, 393
- Brown T. M., Ferguson H. C., Deharveng J.-M., Jedrzejewski R. I. 1998, *ApJ*, 508, L139
- Brown T. M., Bowers C. W., Kimble R. A., Ferguson H. C. 2000a, *ApJ*, 529, L89
- Brown T. M., Bowers C. W., Kimble R. A., Sweigart A. V., Ferguson H. C. 2000b, *ApJ*, 532, 308
- Brown T. M., Ferguson H. C., Smith E., Bowers C. W., Kimble R. A., Renzini A., Rich R. M. 2003, *ApJ*, 584, L69
- Burstein D., Bertola F., Buson L. M., Faber S. M., Lauer T. R. 1988, *ApJ*, 328, 440
- Cardelli J. A., Calyton G. C., Mathis J. S. 1989, *ApJ*, 345, 245
- de Vaucouleurs G., de Vaucouleurs A., Corwin H. G., Buta R. J., Paturel G., Fouque P. 1991, *Third Reference Catalog of Bright Galaxies*, Springer (RC3)
- Fasano G., Bettoni D., D'Onofrio M., Kjærgaard P., Moles M. 2002, *A&A*, 387, 26
- Fasano G., Poggianti B. M., Couch W. J., Bettoni D., Kjærgaard P., Moles M. 2000, *ApJ*, 542, 673
- Greggio L., Renzini A. 1990, *ApJ*, 364, 35
- Lee Y.-W., Demarque P., Zinn R. 1994, *ApJ*, 423, 248
- Lee Y.-W. et al. 2005a, *ApJ*, 619, L103
- Lee Y.-W. et al. 2005b, *ApJ*, 621, L57
- Lee Y.-W., Woo J.-H., Yi S., Park J.-H. 1999, in *Spectrophotometric Dating of Stars and Galaxies*, eds. I. Hubeny, S. Heap & R. Cornett, ASP Conf. Ser., 192, 307
- O'Connell R. W. 1999, *ARA&A*, 37, 603
- Ohl R. G. et al. 1998, *ApJ*, 505, L11
- Ree C. H. et al. 2005, in preparation
- Smail I., Dressler A., Couch W. J., Ellis R. S., Oemler A. 1997, *ApJS*, 110, 213
- Tantalo R., Chiosi C., Bressan A., Fagotto F. 1996, *A&A*, 311, 361
- van Dokkum P. G., Franx M., Kelson D. D., Illingworth G. D., Fisher D., Fabricant D. 1998, *ApJ*, 500, 714
- Yi S., Lee Y.-W., Woo J.-H., Park J.-H., Demarque P., Oemler A. 1999, *ApJ*, 513, 128
- Yi S. et al. 2005, *ApJ*, 619, L111

BINARY POPULATION SYNTHESIS, SDB STARS AND THE UV UPTURN

D. Brown¹, S. Yi², Z. Han³ and S.-J. Yoon²

¹ *Department of Physics and Astrophysics, University of Oxford, Oxford, OX1 3RH, U.K.*

² *Department of Astronomy, Yonsei University, Sinchon 134, Seoul 120-749, Korea*

³ *Yunnan Observatory, National Astronomical Observatories, Chinese Academy of Sciences, P.O. Box 110, Kunming, 650011, China*

Received 2005 September 19

Abstract. We aim to use the methods of binary population synthesis (BPS) to study the ultraviolet upturn (UVX) in the spectra of giant elliptical galaxies with emphasis being placed on those binary channels which could lead to the formation of stars that can account for it. This project will combine Sukeyoung Yi's single star population synthesis methodology with that of Zhanwen Han's binary population synthesis methods in order to provide a more coherent study of the origin of the UV upturn, the focus being on sdB stars as the possible source of the UV upturn. The primary approach of the project will be to explore the UV upturn, with sdBs included, for several different metallicities in order to examine the UVX in composite populations.

Key words: stars: hot subdwarfs – stars: binaries: general – galaxies: elliptical – galaxies: stellar content

1. THE UV UPTURN (UVX)

At present, a moderate consensus suggests that low-mass core helium burning stars, which are in the HB phase of their evolution, serve as the strongest candidates for sources of the UVX in stellar populations. The UVX is characterized by a high increase in rest-frame UV flux (in the range of $\lambda \sim 1000\text{--}2500 \text{ \AA}$) in the spectra of elliptical (E) galaxies, S0 galaxies and in the bulges of spiral galaxies.

2. UVX HYPOTHESES

Most population synthesis studies of the UVX, including those of Yi (1997, 1998), assume that it arises from the evolution of single HB stars. However, others, such as Han and Podsiadlowski (HP), having conducted an extensive binary population synthesis study of the origin of sdB stars (Han et al. 2002, 2003) formed via binary channels, note that sdB stars could help account for a significant portion of UV radiation in galaxies; in fact, HP have also conducted an extensive study of the UVX at solar metallicity. In the single star scenario, two hypotheses make

contradictory claims as to how the UVX originates from low-mass HB stars. The metal-rich hypothesis (Yi et al. 1997, 1998) claims that the UVX originates in metal-rich stars characterized by a high He abundance, and, hence, high mass-loss. In contrast, the metal-poor hypothesis (Park & Lee 1997) claims that the UVX is the natural consequence of the oldest, metal-poor stars in a giant elliptical galaxy (GE) having evolved into the HB phase of their lives. In the binary scenario, the UVX originates from EHB stars in the form of sdBs which result from several different types of binary evolution channels: (1) common envelope (CE) ejection; (2) Roche lobe overflow (RLOF) in one binary component and (3) merger of two WDs.

3. INPUT MODELS

EPS models for single star evolution are here combined with the products of binary population synthesis models to produce a combined population synthesis. The EPS models and methods employed are those of Sukyoung Yi and Seok-Jin Yoon. In these, data from the Y^2 isochrones and realistic synthetic HB constructions have been reduced and processed into synthetic CMD and spectral energy distributions (SED) models by Seok-Jin Yoon. The sdB models are products of Han (1995) binary population synthesis code, which uses an input grid generated by an updated version of Eggleton’s original stellar evolution code (Eggleton 1971, 1972, 1973). The spectral library employed is that assembled by Lejeune et al. (1997). Tables 1 and 2 list the model input parameters.

Table 1. General input parameters.

| | |
|---------------------------------------|--|
| Stellar population: | 10^7 single stars; 10^7 binaries |
| IMF: | Miller-Scalo |
| Age range: | 1 – 20 Gyr |
| Metallicity: | $Z = 0.02$ (single abundance population) |
| Stellar mass range: | $0.1 M_{\odot} < m < 100 M_{\odot}$ |
| Binary input parameters: | |
| Binary fraction: | 67% |
| Flat distribution in q : | $n(q) = 1$ |
| Critical mass ratio: | $q_{\text{crit}} = 1.5$ |
| Reimers mass-loss coefficient: | $\eta = 0.25$ |
| Common ejection frequency: | $\alpha_{\text{CE}} = 0.75$ |
| Thermal energy conversion efficiency: | $\alpha_{\text{TH}} = 0.75$ |

Table 2. Model input parameters.

| Parameter | Yi | Han |
|--|-----------|-----------|
| Convective core overshoot: | $0.20H_p$ | $0.25H_p$ |
| Mixing length parameter (l/H_p): | 1.7431 | 2.0 |
| Helium abundance (Y): | 0.27 | 0.28 |
| He enrichment parameter ($\Delta Y/\Delta Z$): | 2.0 | 2.0 |

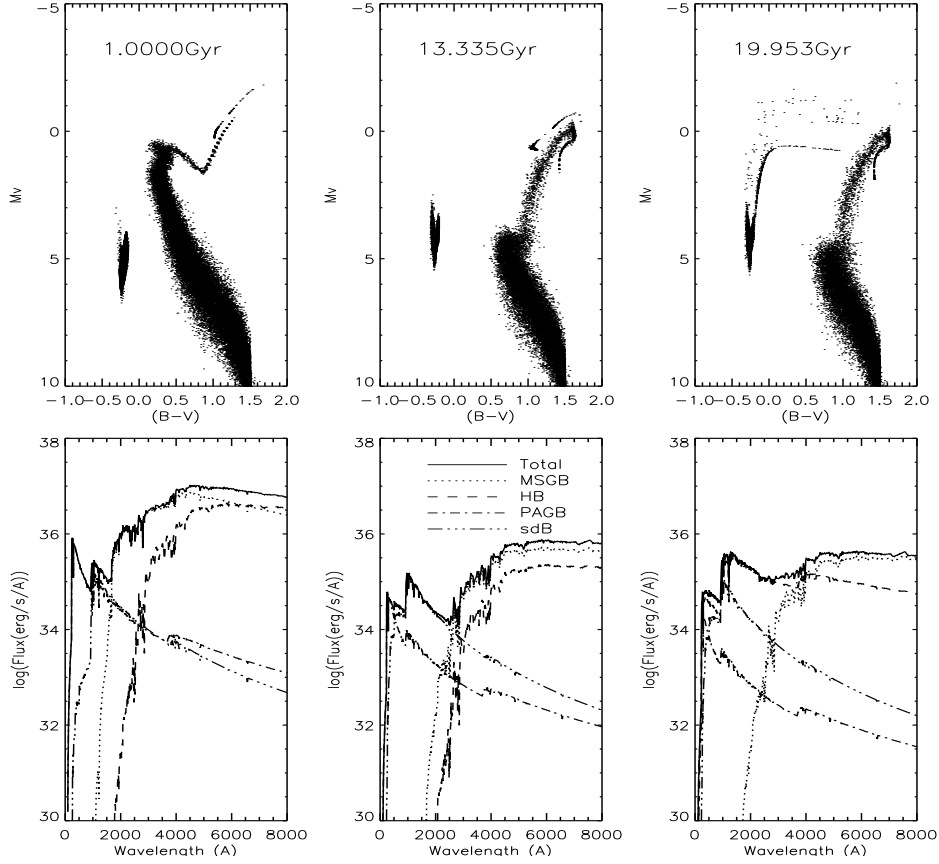


Fig. 1. Time evolution of the SSP as shown in the given CMDs and SEDs.

4. PRELIMINARY RESULTS

As a prelude to studying the UVX in composite systems (GEs), the first step of this inquiry has been to examine the UVX in a simple stellar population (SSP) for a single abundance of $Z = 0.02$. Both single and binary stars have been included in the population synthesis study. Figure 1 shows the CMD and SED time evolution of the population, respectively, for the given ages. With sdBs included, the total FUV flux decreases with increasing age until the trend is reversed by a contribution from single HB stars for late ages. The corresponding color evolution of $1500-V$ with redshift z is given in Figure 2 (the solid line) along with two other models for composite systems obtained by Yi et Yoon (Lee et al. 2005). As seen, there is an increase of $1500-V$ for the redshift range $0.0 < z < 0.2$ in contrast to that suggested by the other two models and empirical data points of NGC 1399 and Abell 2670. Incidentally, the cosmological parameters are $\Omega = 0.15$, $\Lambda = 0.85$, $z_F = 4.9$ and $H_o = 64.0$.

5. SUMMARY AND FUTURE PROSPECTS

Since the parameter space over which this study has been conducted is very limited ($Z = 0.02$ and $\eta = 0.25$), the results presented here are inconclusive in regard to the UVX hypotheses discussed earlier. Interestingly though, the given SSP does exhibit a UVX due to the presence of sdBs at early ages and later. However, the downward trend in $1500-V$ for lower redshifts is not reversed, which differs from an increase in $1500-V$ near low redshifts in GEs. The difference in results can stem from the fact that the SSP is a single abundance population whereas giant elliptical galaxies are composite metal-rich systems. Much is still to be learned from a study of Population II and super-solar stellar populations. Both abundance domains are the primary aims of this project in the future through an adaptation of Han's BPS code for different metallicities, mass-loss prescriptions and binary input parameters to see how the UV contribution from sdBs is affected.

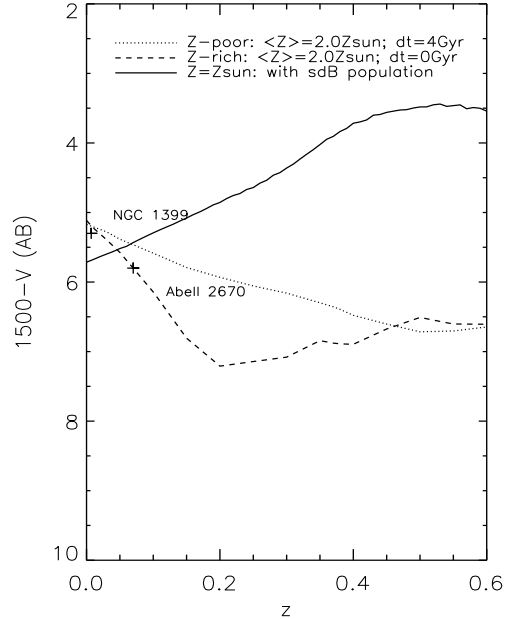


Fig. 2. Evolution of $1500-V$ with z . Data points for NGC 1399 and Abell 2670 are from the GALEX survey (Lee et al. 2005).

REFERENCES

- Eggleton P. P. 1971, MNRAS, 151, 351
 Eggleton P. P. 1972, MNRAS, 156, 361
 Eggleton P. P. 1973, MNRAS, 163, 179
 Han Z. 1995, PhD thesis, Cambridge University
 Han Z., Podsiadlowski P., Maxted P. F. L., Marsh T. R., Ivanova N. 2002, MNRAS, 336, 449
 Han Z., Podsiadlowski P., Maxted P. F. L., Marsh T. R., Ivanova N. 2003, MNRAS, 341, 669
 Lee Y. W., Ree C. H. et al. 2005, ApJ, 619, L103
 Lejeune T., Cuisinier F., Buser R. 1997, A&AS, 125, 229
 Park J. H., Lee Y. W. L. 1997, ApJ, 476, 28
 Yi S., Demarque P., Oemler A. 1997, ApJ, 486, 201
 Yi S., Demarque P., Oemler A. 1998, ApJ, 492, 480
 Yi S., Lee Y. W., Woo J. H., Park J. H., Demarque P., Oemler A. 1999, ApJ, 513, 128

UV UPTURN OF ELLIPTICAL GALAXIES

Z. Han¹, Ph. Podsiadlowski² and A. Lynas-Gray²

¹ *National Astronomical Observatories, Yunnan Observatory, Chinese Academy of Sciences, PO Box 110, Kunming 650011, China*

² *University of Oxford, Department of Astrophysics, Keble Road, Oxford OX1 3RH, U.K.*

Received 2005 August 1

Abstract. We investigate the UV upturn phenomenon of elliptical galaxies by applying the binary model of hot subdwarfs of Han et al. (2002, 2003). Preliminary results show that the model provides a natural explanation for the UV upturn phenomenon and that the model could be used to detect low level recent star formation.

Key words: galaxies: elliptical – ultraviolet: galaxies – stars: binaries: close – stars: subdwarfs

1. INTRODUCTION

For old stellar populations, such as giant elliptical galaxies, far-UV radiation was expected to be almost completely dark. However, this is not the case. As surprisingly discovered by *Orbiting Astronomical Observatory 2* (OAO-2) mission in 1969, there exists a flux increase in spectral energy distributions of early-type galaxies from 2000 to 1200 Å, known as UV upturn (also referred as UV excess, UV rising-branch, UV rising flux, UVX) (see the review by O’Connell 1999). The origin of the UV upturn remained a mystery for many years ever since (see, e.g., Kjær-gaard 1987). Ferguson et al. (1991), Dorman et al. (1995) and Brown et al. (1995, 1997) identified that UV upturn is mainly from extreme horizontal branch (EHB) stars. Brown et al. (2000) resolved hot HB stars for the first time in an elliptical galaxy (the core of M32).

EHB stars are core-helium burning stars with very thin hydrogen envelopes ($M_{\text{env}} \leq 0.02M_{\odot}$). They are the major source of far UV radiation in the evolutionary population synthesis study of giant elliptical galaxies. There are two schools of thought about the UV upturn, metal-poor school (Lee 1994; Park & Lee 1997) and metal-rich school (Bressan et al. 1994, 1996; Tantalo et al. 1996; Yi et al. 1995, 1997a, 1997b, 1998). Both schools adopt the formation channel of EHB stars from single stellar evolution, in which stellar wind mass-loss near the tip of the first giant branch (FGB) may strip off a giant’s envelope and leave an almost bare helium core (e.g., D’Cruz et al. 1996).

The metal-poor school ascribes the UV-upturn to an old metal-poor population (the metal-poor tail of the wide metallicity distribution). An uncomfortably large age (~ 20 Gyr) is required to explain observations. In the metal-rich school, the UV-upturn results from the metal-rich population of giant elliptical galaxies. In

order to fit observations, some assumptions need to be made, i.e., helium enrichment parameter $\Delta Y/\Delta Z > 2.5$, a fine-tuning of Reimer's mass-loss coefficient and its dependence on metallicity, a metallicity of 1–3 Z_{\odot} and an age usually larger than 10 Gyr. Some of the assumptions are not justified.

In both schools, the formation of EHB stars is due to stellar wind mass-loss near the tip of the FGB, and therefore there is a sudden onset of the formation of EHB stars when a stellar population evolves. In other words, the UV upturn of elliptical galaxies declines rapidly with redshift. However, this is not the case, as shown by HST observations of Brown et al. (1998, 2000, 2003).

However, more than half of hot subdwarfs are found in binaries observationally (e.g., Maxted et al. 2001). Han et al. (2002, 2003) therefore proposed a binary model for the formation of EHB stars (or hot subdwarfs). In the model, there are three channels for the formation of hot subdwarfs, i.e., common envelope ejection for hot subdwarf binaries with short orbital periods, stable Roche lobe overflow for hot subdwarfs with long orbital periods, and merger of helium white dwarfs to form single hot subdwarfs. The model can explain the main observational characteristics of hot subdwarfs, in particular their distributions in the orbital period vs. minimum companion mass diagram and in the effective temperature vs. surface gravity diagram, their distributions of orbital period and mass function, their binary fraction and the fraction of hot subdwarf binaries with white dwarf (WD) companions, their birth rates and their space density.

In this paper we apply the binary model of Han et al. (2002, 2003) to the study of UV upturn and give the preliminary results. A more systematic and comprehensive study will be published elsewhere.

2. THE APPROACH

Han et al. (1994, 1995a, 1995b, 1998, 2003) developed a binary population synthesis (BPS) code, with which millions of stars (including binaries) can be evolved simultaneously from the zero-age main sequence (ZAMS) to white dwarfs or supernova explosion. The code can simulate in a Monte Carlo way the formation of many interesting stellar objects, such as type Ia supernovae, cataclysmic variables, double degenerates, barium stars, etc.

We incorporate the binary hot subdwarf model of Han et al. (2002, 2003) into the BPS code so that we can carry out Monte Carlo simulations and obtain the hot subdwarf population and its evolution. In the simulations, we adopt a metallicity of $Z = 0.02$, the critical mass ratio $q_{\text{crit}} = 1.5$ for stable Roche lobe overflow on first giant branch (FGB) or asymptotic giant branch (AGB), common envelope ejection efficiency $\alpha_{\text{CE}} = 0.75$ and thermal contribution to the ejection $\alpha_{\text{th}} = 0.75$ (see section 7.4 of Han et al. 2003 for details). In addition, the simulations also require as input the star formation rate (SFR), the initial mass function (IMF) of the primary, the initial mass-ratio distribution and the distribution of initial orbital separations as follows.

- (1) The SFR is taken to be a single burst.
- (2) A simple approximation to the IMF of Miller & Scalo (1979) is used; the primary mass is generated with the formula of Eggleton, Fitchett & Tout (1989)

$$M_1 = \frac{0.19X}{(1-X)^{0.75} + 0.032(1-X)^{0.25}}, \quad (1)$$

where X is a random number uniformly distributed between 0 and 1. The adopted ranges of primary masses are 0.8 to $100.0 M_{\odot}$. The studies by Kroupa, Tout & Gilmore (1993) and Zoccali et al. (2000) support this IMF.

(3) We take a constant mass-ratio distribution in the current study,

$$n(1/q) = 1, \quad 0 \leq 1/q \leq 1, \quad (2)$$

where $q = M_1/M_2$.

(4) We assume that all stars are members of binary systems and that the distribution of separations is constant in $\log a$ (a is the separation) for wide binaries and falls off smoothly at close separations:

$$an(a) = \begin{cases} \alpha_{\text{sep}} \left(\frac{a}{a_0}\right)^m, & a \leq a_0; \\ \alpha_{\text{sep}}, & a_0 < a < a_1, \end{cases} \quad (3)$$

where $\alpha_{\text{sep}} \approx 0.070$, $a_0 = 10 R_{\odot}$, $a_1 = 5.75 \times 10^6 R_{\odot} = 0.13 \text{ pc}$ and $m \approx 1.2$. This distribution implies that there is an equal number of wide binary systems per logarithmic interval and that approximately 50 per cent of stellar systems are binary systems with orbital periods less than 100 yr.

In order to convolve the simulation result into colors or spectral energy distribution (SED), we adopt the latest version of BaSeL library (see Lejeune et al 1997, 1998 for a description), which gives the colors and SEDs of stars with a wide range of metallicity Z , surface gravity $\log g$ and effective temperature T_{eff} . The library does not cover the surface gravity range for hot subdwarfs, and we therefore calculated emergent fluxes for solar metallicity hot subdwarfs using plane-parallel static model stellar atmospheres computed with ATLAS9 (Kurucz 1992) and adopting the assumption of local thermodynamic equilibrium, and the range for $\log g$ is 5.0 to 7.0 with a spacing of $\Delta \log g = 0.2$, the range for T_{eff} is 10 000 K to 40 000 K with $\Delta T = 1000 \text{ K}$.

3. RESULTS AND DISCUSSION

In our investigation, we evolve a simple stellar population (SSP), in which all the stars have the same metallicity and the same age, or a mixed stellar population (MSP) which consists of two SSPs, a major one and a minor one. The major population has solar metallicity and an age of 10 Gyr, while the minor one has a solar metallicity and an age t . The minor population fraction f is the ratio of minor population mass to the total mass of the MSP, and $f = 100 \%$ means the MSP is actually a SSP with an age t .

Figure 1 is a comparison between the UV spectrum from our model and that of M 49 from the Hopkins Ultraviolet Telescope (HUT) (from Brown et al. 1997). The model is a solar metallicity MSP with a total stellar mass of $4.7 \times 10^{10} M_{\odot}$ and a major population age of 10 Gyr. The minor population fraction is $f = 0.28 \%$, and the minor population has an age of 0.5 Gyr. Actually we fixed the age of the major population according to local galaxy ages derived by Terlevich & Forbes (2002) and the minor population fraction, and obtained the best fit when the minor population age is 0.5 Gyr (the details of the fitting process will be described in another publication). The fraction of $f = 0.28 \%$ is below the detecting limit for recent star formation. We see that the fit is satisfactory.

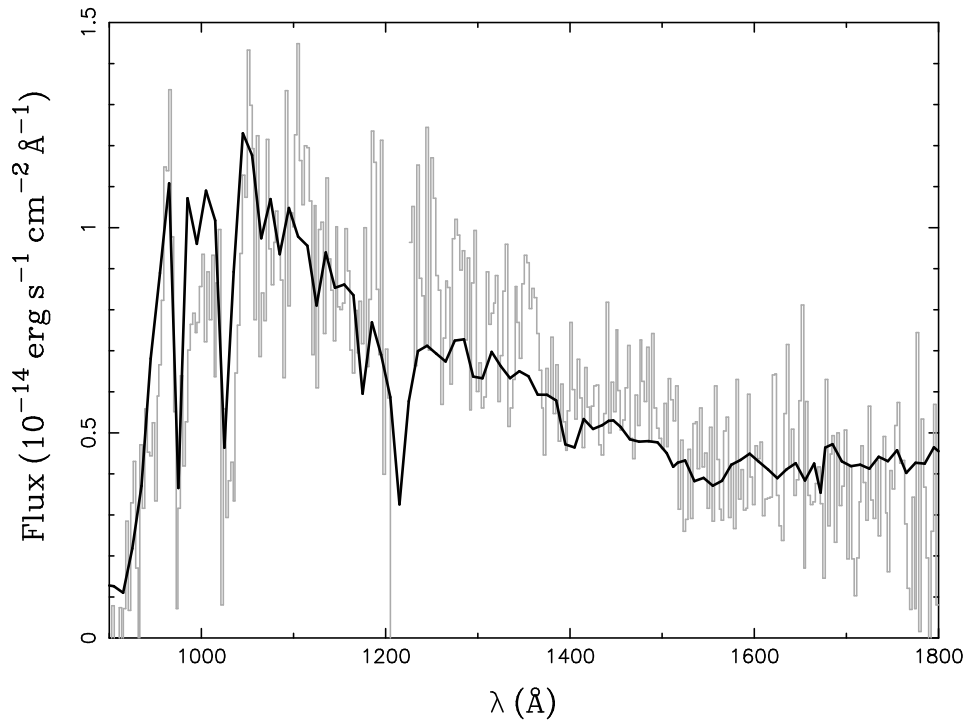


Fig. 1. A fit to the UV spectrum of elliptical galaxy M49 obtained using the Hopkins Ultraviolet Telescope (HUT) (taken from Brown et al. 1997). The HUT data are shown by the grey histogram, while the thick solid line is from our model.

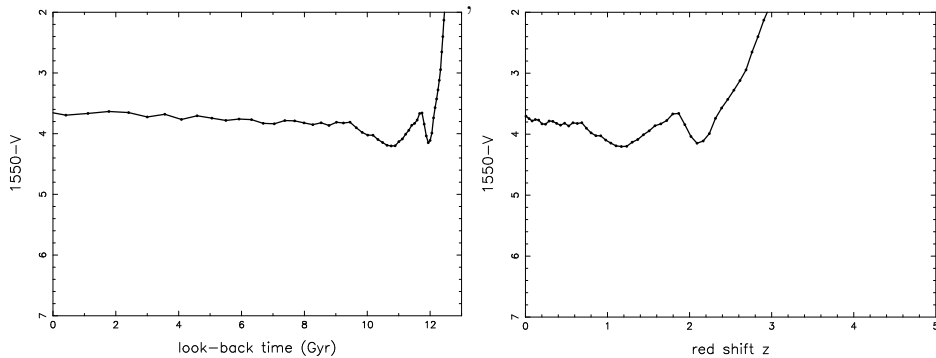


Fig. 2. The UV-upturn vs. look-back time (the left panel) and the UV-upturn vs. redshift (the right panel) from our model.

The magnitude of UV-upturn is defined by Burstein et al. (1988) as $1550-V = -2.5 \log(f_{1550}/f_V)$, where f_{1550} is the energy flux at 1550 \AA and f_V – the flux in the V passband. Figure 2 is the UV-upturn versus the look-back time or the redshift for a SSP. The look-back time is defined as $t_L = 13 \text{ Gyr} - t_{\text{SSP}}$, where t_{SSP}

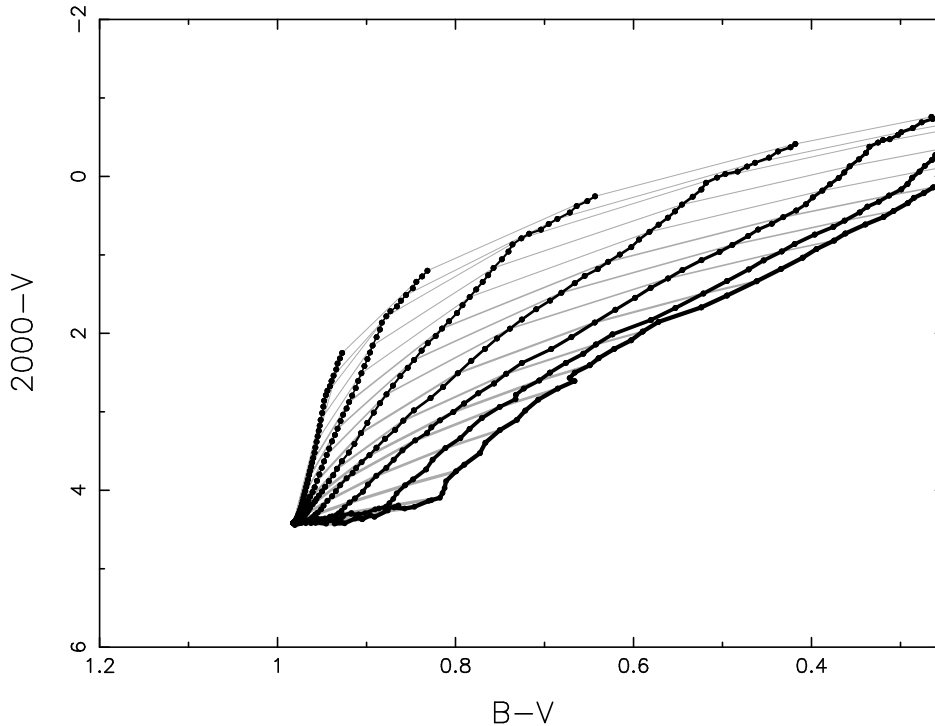


Fig. 3. $2000-V$ vs. $B-V$ for a mixed stellar population composed of a major and a minor population. The major population is with solar metallicity and with an age of 10 Gyr. The grey lines from top to bottom are for minor population age of $\log(t/\text{Gyr}) = -1.0, -0.9, -0.8, -0.7 \dots$, the dark solid lines from left to right are for minor population fractions of 0.1 %, 0.32 %, 1 %, 3.2 %, 10 %, 32 % and 100 %, while 100 % means that the mixed population is actually a single population (i.e., minor population only).

is the age of the SSP. We also convert the look-back time to redshift by adopting a flat universe and a Hubble time of 13.7 Gyr. As we see from Brown et al. (2003), UV-upturn does not depend much on redshift, and Figure 2 is consistent with the observations. Lee et al. (2005) tried to explain UV upturn-redshift relation by assuming that the post AGB (PAGB) mass decreases with redshift. However, the mass should increase with redshift from standard stellar evolution theory.

Figure 3 is the diagram of $2000-V$ vs. $B-V$ for a solar metallicity MSP with a major population of 10 Gyr and a minor population of varying age and fraction. The figure can be used to explain the observation of far-ultraviolet emission of early-type galaxies (see Fig. 2 of Deharveng et al. 2002).

Figure 4 is the diagram of $FUV-NUV$ vs. $FUV-r$, where FUV and NUV are magnitudes in the FUV and NUV passbands of the *Galaxy Evolution Explorer* (GALEX) and r is the magnitude in the r passband of the Sloan Digital Sky Survey (SDSS). If we compare our result to the systematics of the UV-upturn in a GALEX/SDSS sample of early-type galaxies (Fig. 3 of Rich et al. 2005), we find that the red-quietest early-type galaxies in their sample have low level recent star formation.

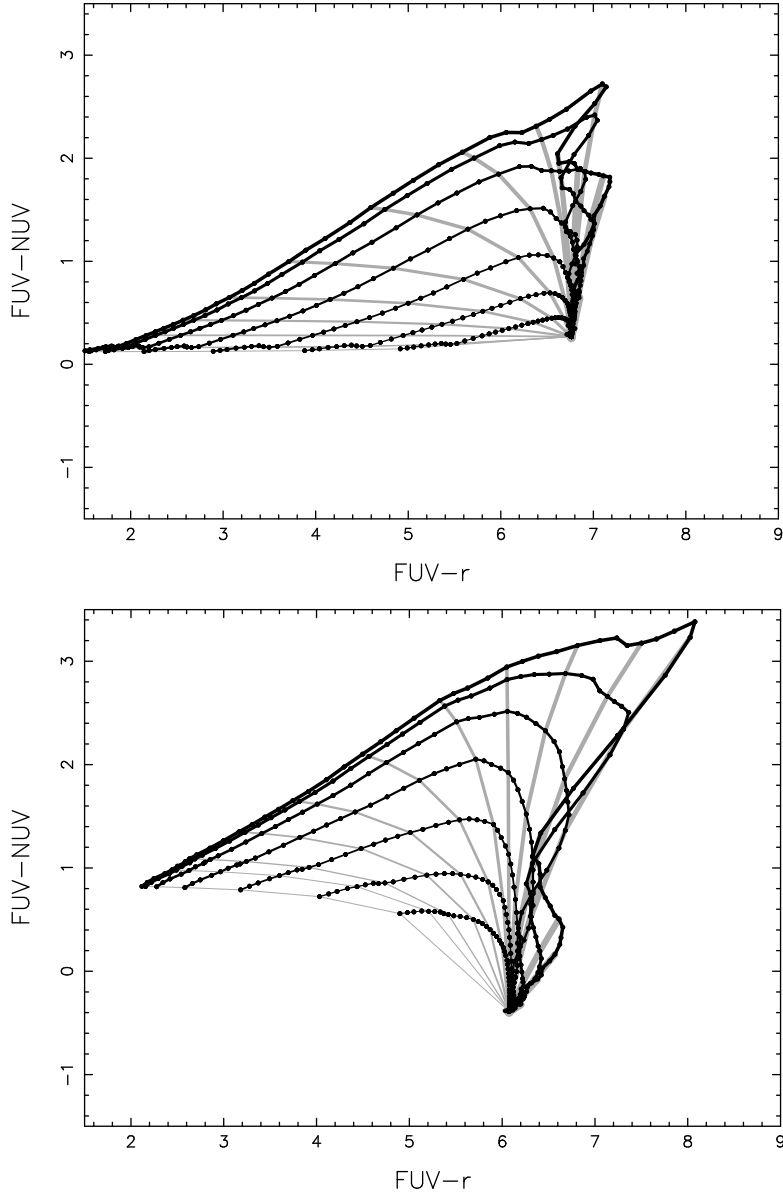


Fig. 4. $FUV-NUV$ vs. $FUV-r$ for a mixed stellar population composed of a major and a minor population. The major population is with solar metallicity and with an age of 10 Gyr. The grey lines from bottom-left to top-right are for minor population age of $\log(t/\text{Gyr}) = -1.0, -0.9, -0.8, -0.7 \dots$, the dark solid lines from bottom to top are for minor population fractions of 0.1%, 0.32%, 1%, 3.2%, 10%, 32% and 100%, while 100% means that the mixed population is actually a single population (i.e., minor population only). The top panel is for population at redshift $z = 0$, while the bottom panel is for $z = 0.2$.

4. CONCLUSIONS

We conclude that the binary model of hot subdwarfs of Han et al. (2002, 2003) is needed to understand the UV-upturn phenomenon of elliptical galaxies. Our model could be a useful tool in finding low level recent star formation.

REFERENCES

- Bressan A., Chiosi C., Fagotto F. 1994, *ApJS*, 94, 63
- Brown T. M., Bowers C. W., Kimble R. A., Ferguson H. C. 2000, *ApJ*, 529, L89
- Brown T. M., Bowers C. W., Kimble R. A., Sweigart A. V. 2000, *ApJ*, 532, 308
- Brown T. M., Ferguson H. C., Davidsen A. F. 1995, *ApJ*, 454, L15
- Brown T. M., Ferguson H. C., Davidsen A. F., Dorman B. 1997, *ApJ*, 482, 685
- Brown T. M., Ferguson H. C., Deharveng J. M., Jedrzejewski R. I. 1998, *ApJ*, 508, L139
- Brown T. M. et al. 2003, *ApJ*, 584, L69
- Burstein D., Bertola F., Buson L. M., Faber S. M., Lauer T. R. 1988, *ApJ*, 328, 440
- D’Cruz N. L., Dorman B., Rood R. T., O’Connell R. W. 1996, *ApJ*, 466, 359
- Deharveng J.-M., Boselli A., Donas J. 2002, *A&A*, 393, 843
- Dorman B., O’Connell R. W., Rood R. T. 1995, *ApJ*, 442, 105
- Eggleton P. P., Tout C. A., 1989, in *Algols*, ed. A. H. Batten, Kluwer Academic Publishers, Dordrecht, p. 164
- Ferguson H. C. et al. 1991, *ApJ*, 382, L69
- Han Z. 1998, *MNRAS*, 296, 1019
- Han Z., Podsiadlowski Ph., Eggleton P. P. 1994, *MNRAS*, 270, 121
- Han Z., Podsiadlowski Ph., Eggleton P. P. 1995a, *MNRAS*, 272, 800
- Han Z., Eggleton P. P., Podsiadlowski Ph., Tout C. A. 1995b, *MNRAS*, 277, 1443
- Han Z., Podsiadlowski Ph., Maxted P. F. L., Marsh T. R., Ivanova N. 2002, *MNRAS*, 336, 449
- Han Z., Podsiadlowski Ph., Maxted P. F. L., Marsh T. R. 2003, *MNRAS*, 341, 669
- Kjærgaard P. 1987, *A&A*, 176, 210
- Kurucz R. L. 1992, in *The Stellar Populations in Galaxies*, IAU Symp. 149, eds. B. Barbuy & A. Renzini, Kluwer Academic Publishers, Dordrecht, p. 225
- Lee Y. W. 1994, *ApJ*, 430, L113
- Lee Y. W. et al. 2005, *ApJ*, 619, L103
- Lejune T., Cuisinier F., Buser R. 1997, *A&AS*, 125, 229
- Lejune T., Cuisinier F., Buser R. 1998, *A&AS*, 130, 65
- Maxted P. F. L., Heber U., Marsh T. R., North R. C. 2001, *MNRAS*, 326, 1391
- Miller G. E., Scalo J. M. 1979, *ApJS*, 41, 513

- O'Connell R. W. 1999, *ARA&A*, 37, 603
Park J. H., Lee, Y. W. 1997, *ApJ*, 476, 28
Rich R. M. et al. 2005, *ApJ*, 619, L107
Tantalo R., Chiosi C., Bressan A., Fagotto F. 1996, *A&A*, 311, 361
Terlevich A. I., Forbes D. A. 2002, *MNRAS*, 330, 547
Yi S. K., Demarque P., Kim Y. C. 1997a, *ApJ*, 482, 677
Yi S. K., Afshari E., Demarque P., Oemler Jr. A. 1995, *ApJ*, 453, L69
Yi S. K., Demarque P., Oemler Jr. A. 1997b, *ApJ*, 486, 201
Yi S. K., Demarque P., Oemler Jr. A. 1998, *ApJ*, 492, 480

HOT SUBDWARFS IN THE GALACTIC BULGE

G. Busso¹, S. Moehler¹, M. Zoccali², U. Heber³ and S. K. Yi⁴

¹ *Institut für Theoretische Physik und Astrophysik der Universität Kiel, Leibnizstrasse 12, D-24098 Kiel, Germany*

² *Departamento de Astronomía y Astrofísica, Pontificia Universidad Católica de Chile, Avenida Vucuna Mackenna 4860, 782-0436 Macul, Santiago, Chile*

³ *Remeis-Sternwarte, Astronomisches Institut der Universität Erlangen-Nürnberg, Sternwartstrasse 7, 96049 Bamberg, Germany*

⁴ *Department of Physics, University of Oxford, Keble Road, Oxford OX1 3RH, U.K.*

Received 2005 August 1

Abstract. Recent observations and theories suggest that extreme horizontal branch (EHB) stars and their progeny should be the cause of the UV excess that many elliptical galaxies show in their spectra. Since the Galactic bulge is the closest representation of an old, metal-rich spheroid in which we are able to study the EHB scenario in detail, we obtained spectra of bulge EHB star candidates and we confirm their status as hot evolved stars. It is the first time that such stars are unambiguously observed in the Galactic bulge.

Key words: galaxies: elliptical – Galaxy: bulge – stars: hot subdwarfs

1. INTRODUCTION

The spectra of elliptical galaxies and bulge regions of spiral galaxies in many cases show a strong and unexpected increase in flux at wavelength shorter than 2500 Å. This feature, called “UV excess”, was one of the most important discoveries of satellite-based UV astronomy (Code & Welch 1969) but also a puzzle, since it required the existence of hot stars in these old metal-rich systems (see Burstein et al. 1988 and references therein). After a long debate, most people agree that the observed UV radiation is mainly produced by very hot extreme horizontal branch stars (burning helium in their core) and their progeny, as Post-EarlyAGB and AGB-manqué stars (O’Connell 1999; Greggio & Renzini 1990, 1999; Dorman et al. 1995; Yi et al. 1998). This view is supported by spectroscopic (Ferguson et al. 1991; Brown et al. 1997, 2002) and photometric (Brown et al. 2002) UV observations of extragalactic systems. Near-UV HST observations of Brown et al. (2000) in M32 detected for the first time individual EHB star candidates in an elliptical galaxy. The best fit to the observations is achieved with evolutionary tracks for helium- and metal-rich populations, since in this case EHB stars have the longest lifetimes in the temperature range required to reproduce the UV excess (cf. Bressan et al. 1994).

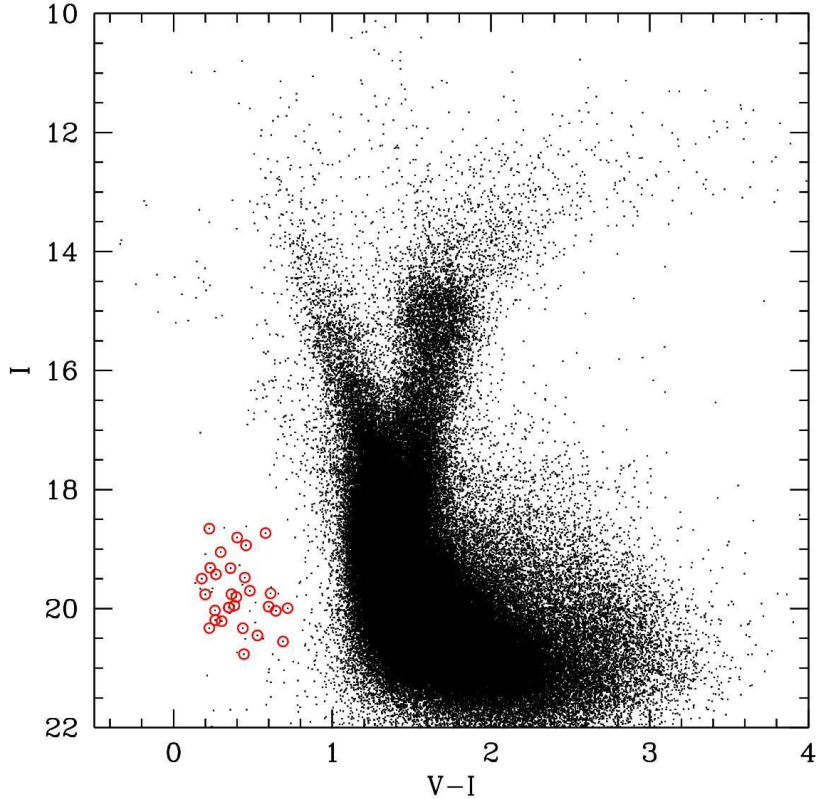


Fig. 1. Color-magnitude diagram of the Galactic bulge. Our targets are marked by circles.

The closest system similar to an elliptical galaxy with respect to age and metallicity for which it is possible to resolve stars is the Galactic bulge. The vast majority of EHB stars known in the Milky Way belongs however, to the metal-poor spheroid or to the disk population (where they show up as so-called subdwarf B (sdB) stars).

The only sdB candidates known in the bulge were found in the two massive globular cluster NGC 6388 and NGC 6441 (Rich et al. 1997; Busso et al. 2004), which are anyway not typical for the bulge population. The situation changed recently: Terndrup et al. (2004) found candidates in their survey for EHB stars in the Galactic bulge, and Wide Field Imager observations of a field toward the Galactic bulge (Zoccali et al. 2003) show a sequence of hot stars that are good candidates for EHB stars (see Figure 1). Using the values of Villeneuve et al. (1995) for scale height and space density of local field sdB stars, along a distance of 4.5 to 11 kpc within the field of view of WFI only less than 10 sdB stars are expected, while in our case about 140 candidates are found. Since they could be cool foreground stars (instead of reddened hot stars), we obtained spectroscopy of 29 candidates in order to derive effective temperatures and surface gravities and then, by means of comparison with HB models, to check their evolutionary status.

2. OBSERVATIONS

2.1. Target selection

Our spectroscopic targets were selected from the photometric catalogue of bulge stars obtained from Zoccali et al. 2003 (see Figure 1). We have chosen the stars with magnitude $18 < I < 21$ and color $0 < V - I < 0.8$ and among them we selected the most isolated ones.

2.2. VLT observations

We obtained medium-resolution spectra ($R \sim 1200$) of 29 candidates EHB stars at the VLT-UT1 (Antu) with FORS2. We used the multi-object spectroscopy (MXU) mode of FORS2 with the standard collimator, a slit width of $0.7''$ and grism B600, which allows to obtain spectra in the range between 3650 and 5200 Å (not all candidates though have spectra so extended because of the different positions on the CCD).

2.3. Data reduction

The data reduction was performed as described in Moehler et al. (2004) except for the following points. Due to the long exposure times (from 2700 s to 5400 s) the scientific observations contained a large number of cosmic rays and were therefore corrected with the algorithm described in Pych (2004). Regarding the subtraction of the sky background, we used two different methods depending on whether the target star in the slitlet was isolated or not. If the star was isolated, meaning any other stars in the slitlets were well enough separated from our target to identify regions uncontaminated by any stellar source, we approximated the spatial distribution of the sky background by a constant. If the slitlet showed severe crowding, meaning that the spectra of different stars were overlapping, we fitted each stellar profile with a Lorentzian function so that the whole spatial profile was reproduced by the sum of all the profiles; all the profiles but that one of the target were then subtracted (for details see Moehler & Sweigart 2006). With the extraction of the spectra, we saw that some (5 of 29) of our targets were actually cool stars. Therefore we did not proceed further with the reduction for these stars. The spectra were flux calibrated using standard stars spectra and corrected for any Doppler shifts determined from Balmer lines, as in Moehler et al. (2004).

3. ANALYSIS

Some examples of the spectra are shown in Figure 2. To fit the spectra (except for one He-rich one) we used ATLAS9 model atmospheres for solar metallicity (Kurucz 1993) to account for effects of radiative levitation (see Moehler et al. 2000 for details), from which we calculated spectra with Lemke's version of the LINFOR program (developed originally by Holweger, Steffen and Steenbock at Kiel University). The use of NLTE models or of LTE models with higher metallicity does not significantly change the results.

To establish the best fit, we used the routines developed by Bergeron et al. (1992) and Saffer et al. (1994), as modified by Napiwotzki et al. (1999), which employ a χ^2 test. The 1σ error necessary for the calculation of χ^2 is estimated from the noise in the continuum regions of the spectra. The fit program normalizes model spectra and observed spectra using the same points for the continuum definition.

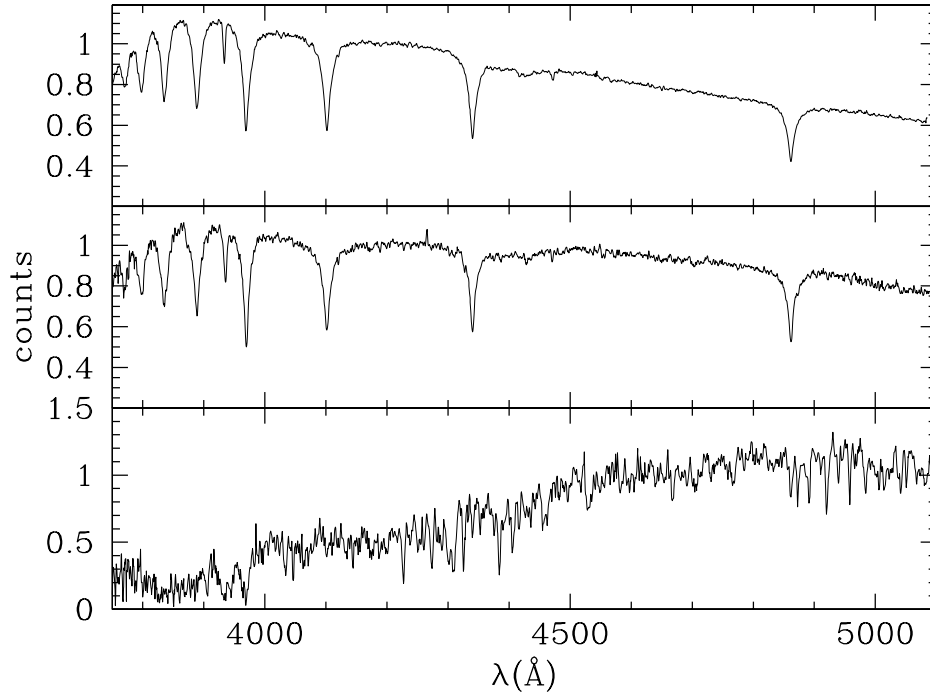


Fig. 2. Spectra of a few sdB star candidates. Top and central panel: typical spectra of newly detected hot stars with strong Balmer lines. Bottom panel: for comparison the totally different spectrum of a cool star.

We used the Balmer lines $H\beta$ to $H10$ (excluding $H\epsilon$ to avoid the Ca II H line), the He I lines at 4026, 4388, 4471, 4921 Å and the He II lines at 4542 and 4686 Å.

We obtained the atmospheric parameters T_{eff} , $\log g$ and helium abundances, and we calculated the absolute V and I magnitudes expected for these values, assuming $M_{\star} = 0.5 M_{\odot}$. We left out one star because the fit was really bad. Considering a distance from the Galactic center of ~ 8.5 kpc and a bulge radius of ~ 1.5 kpc, we found that most of these objects are indeed bulge stars: of 23 hot stars, 13 stars are in the bulge within 1σ and 3 are in the bulge within 3σ .

This is also confirmed by the radial velocities found from the Doppler shift. The field we explored is centered at Galactic coordinates $\ell = 0^{\circ}$, $b = -6^{\circ}$, toward the Galactic center, so that the expected radial velocities for disk stars are around 0 km s^{-1} . Our velocities are distributed in a range between -200 and $+300 \text{ km s}^{-1}$, in agreement with Terndrup et al. (1995).

Finally we compared our results with horizontal branch theoretical tracks: in Figure 3 we plotted in the T_{eff} vs. $\log g$ diagram the values found for those stars which belong to the bulge. The error bars are the formal errors from the fit procedure, but we are aware that the formal errors are underestimates (Napiwotzki, priv. comm.). The evolutionary tracks are from Yi et al. (1997) with metallicity $Z = 0.004$ and helium abundance $Y = 0.2416$. The Zero Age Horizontal Branch

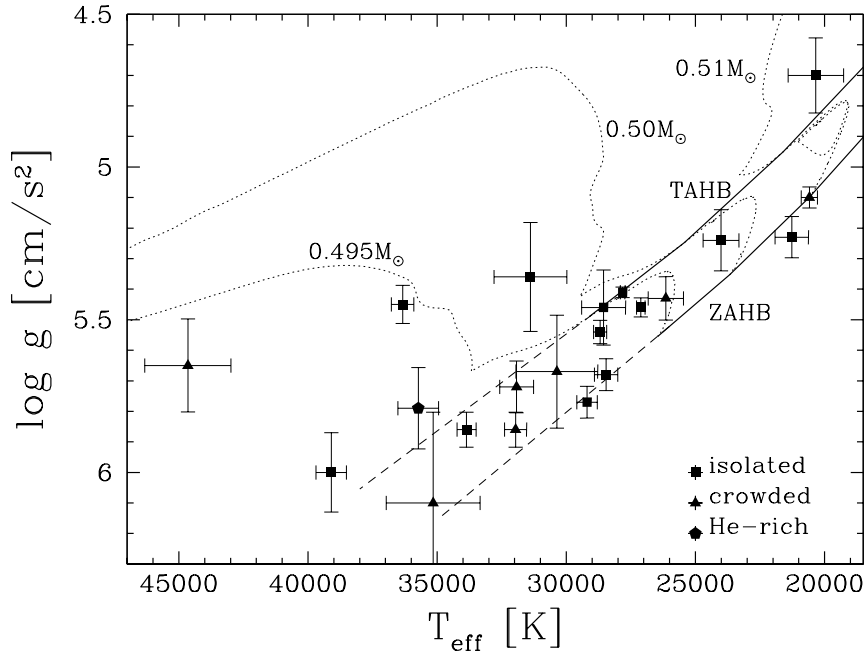


Fig. 3. T_{eff} vs. $\log g$ diagram. The squared symbols indicate the isolated stars; the triangles indicate the crowded stars and the pentagon is the He-rich star. The ZAHB and TAHB (Yi et al. 1997) and evolutionary tracks with metallicity $Z = 0.004$ and helium abundance $Y = 0.2416$ for 0.495 , 0.50 and $0.51 M_{\odot}$ are plotted. The dashed lines are extrapolated from the ZAHB and TAHB tracks.

(ZAHB), where the star starts to burn helium in its core quietly, and the Terminal Age Horizontal Branch, where the star burned the 99% of the helium, are shown together with evolutionary tracks for stars with total masses of 0.495 , 0.50 and $0.51 M_{\odot}$. Since the theoretical lower limit for the mass of an EHB star is the core mass of the progenitor on the red giant branch ($\sim 0.45 M_{\odot}$) while our tracks end at $0.495 M_{\odot}$, we extrapolated the ZAHB and TAHB to lower masses (dashed curves in Figure 3). Proper models for lower masses will be calculated and used in a later paper. The observed points agree quite well with the theoretical tracks, therefore these objects are indeed EHB stars; some objects are above the TAHB meaning that they are in the post-HB phase and then evolving as AGB-manqué stars.

Finally we want to mention that all stars except one (which is helium-rich) are helium deficient as expected from diffusion.

5. CONCLUSIONS

We observed spectra of EHB star candidates in the Galactic bulge, from which we estimated the atmospheric parameters T_{eff} and $\log g$, confirming their evolutionary status. From the calculated radial velocities and distances we verified their membership to the bulge. This is the first time that such kind of stars are observed in the bulge, and with their spectra we are going to construct the integrated spectrum of the Galactic bulge from the UV to the optical, following the

method described in Santos et al. (1995). The method consists in the construction of the integrated spectrum using a spectral library (in our case it will have to be a library extended to the UV) and the information contained in the spectroscopic and photometric observations. Regarding the spectral library, we will group the similar spectra, obtaining various groups of different spectral type, luminosity class and metallicity. For each group the average spectrum will be calculated, in order to obtain a better S/N . We will divide the color-magnitude diagram of the bulge in boxes, and each box will be associated to one of the library average spectra by means of the color index. The integrated spectrum will be the sum of the average spectra, scaling the contribute of each component keeping in account how many stars there are in each box.

This study will verify the role, so far only predicted, of EHB stars regarding the UV excess in elliptical galaxies.

ACKNOWLEDGMENTS. We are grateful to the ESO staff, especially those at the Paranal Observatory, for all their help during the observations. G.B. acknowledges support from the Deutsche Forschungsgemeinschaft via grant Mo 602/8.

REFERENCES

- Bergeron P., Saffer R. A., Liebert J. 1992, *ApJ*, 394, 228
 Bressan A., Chiosi C., Fagotto F. 1994, *ApJS*, 94, 63
 Brown T. M., Ferguson H. C., Davidsen A. F., Dorman B. 1997, *ApJ*, 482, 685
 Brown T. M., Bowers C. W., Kimble R. A., Sweigart A. V., Ferguson H. C. 2000, *ApJ*, 532, 308
 Brown T. M., Ferguson H. C., O'Connell R. W., Ohl R. G. 2002, *ApJ*, 568, 19
 Burstein D., Bertola F., Buson L. M., Faber S. M., Lauer T. R. 1988, *ApJ*, 328, 440
 Busso G., Piotto G., Cassisi S. 2004, in *Stars in Galaxies*, eds. M Bellazzini, A. Buzzoni & S. Cassisi, *Mem. Soc. Astron. Italiana*, 75, 46
 Code A. D., Welch G. A. 1969, *ApJ*, 228, 95
 Dorman B., O'Connell R. W., Rood R. T. 1995, *ApJ*, 442, 105
 Ferguson H. C., Davidsen A. F., Kriss G. A. et al. 1991, *ApJ*, 382, L69
 Greggio L., Renzini A. 1990, *ApJ*, 364, 35
 Greggio L., Renzini A. 1999, in *UV Astronomy in Italy*, eds. L. M. Buson & D. de Martino, *Mem. Soc. Astron. Italiana*, 70, 691
 Kurucz R. L. 1993 in *ATLAS9 Stellar Atmospheric Program*, <http://kurucz.harvard.edu>
 Moehler S., Sweigart A. V., Landsman W. B., Heber U. 2000, *A&A*, 360, 120
 Moehler S., Sweigart A. V., Landsman W. B., Hammer N. J., Dreizler S. 2004, *A&A*, 415, 313
 Moehler S., Sweigart A. V. 2006, *Baltic Astronomy*, 15, 41 (these proceedings)
 Napiwotzki R., Green P. J., Saffer R. A. 1999, *ApJ*, 517, 399
 O'Connell R. W. 1999, *ARA&A*, 37, 603

Pych W. 2004, PASP, 116, 148
Rich R. M., Sosin C., Djorgovski S. G. et al. 1997, ApJ, 484, L25
Saffer R. A., Bergeron P., Koester D., Liebert J. 1994, ApJ, 432, 351
Santos J. F. C., Bica E., Dottori H., Ortolani S., Barbuy B. 1995, A&A, 303, 753
Terndrup D. M., Sadler E. M., Rich R. M. 1995, ApJ, 110, 1774
Terndrup D. M., An D., Hansen A. et al. 2004, Ap&SS, 291, 247
Villeneuve B., Wesemael F., Fontaine G., Carignan C., Green R. F. 1995, ApJ, 446, 646
Yi S. K., Demarque P., Oemler A. J. 1997, ApJ, 486, 201
Yi S. K., Demarque P., Oemler A. J. 1998, ApJ, 492, 480
Zoccali M., Renzini A., Ortolani S. et al. 2003, A&A, 399, 931

**SUPER-HELIUM-RICH STARS IN GLOBULAR CLUSTERS:
THE ORIGIN OF EXTREME HORIZONTAL-BRANCH**

S.-J. Joo¹, Y.-W. Lee¹, S.-J. Yoon^{1,2}, S.-I. Han¹, C. Chung¹, C. H. Ree¹,
Y.-C. Kim¹, Y.-J. Sohn¹ and S. K. Yi^{1,2}

¹ *Center for Space Astrophysics and Department of Astronomy, Yonsei University, Seoul 120-749, Korea*

² *Department of Physics, University of Oxford, Keble Road, Oxford OX1 3RH, U.K.*

Received 2005 August 1

Abstract. Recent observations of the globular cluster ω Centauri have shown that it has a double main sequence (MS), with a minority population of bluer and fainter MS well separated from a majority population of MS stars. Here we confirm that this special feature can only be reproduced by assuming a large range of helium abundance among several distinct populations in this cluster. We further show that the same helium enhancement required to reproduce this special feature on the MS can by itself reproduce the extreme horizontal-branch (EHB) stars observed in ω Cen, which are hotter than and separated from the majority population of normal HB stars. We also discuss the possibility that similar phenomena observed in the HB of other globular clusters are also due to the helium enhancement. If confirmed by further observations, this would establish that the third parameter that influences globular cluster color-magnitude diagram (CMD) morphology, in addition to metallicity and age, is indeed helium abundance.

Key words: globular clusters: individual (ω Centauri) – stars: abundances – stars: evolution – stars: horizontal-branch

1. INTRODUCTION

The Hubble Space Telescope snapshot survey of Galactic globular clusters has shown that the presence of extreme horizontal-branch (EHB) stars is not an unusual phenomenon among relatively massive globular clusters, which suggests that a third parameter, in addition to metallicity and age, is needed in order to explain the peculiar features observed on the HBs of these clusters (Piotto et al. 2002). It has been suggested for some time that more than one epoch of star formation and the accompanying helium and other elements enhancements in some globular clusters might be responsible for the presence of bimodal HBs and the EHB stars (D’Antona et al. 2002; D’Antona & Caloi 2004). While it has already been known that the HB morphology is very sensitive to helium abundance (see, e.g., Lee et

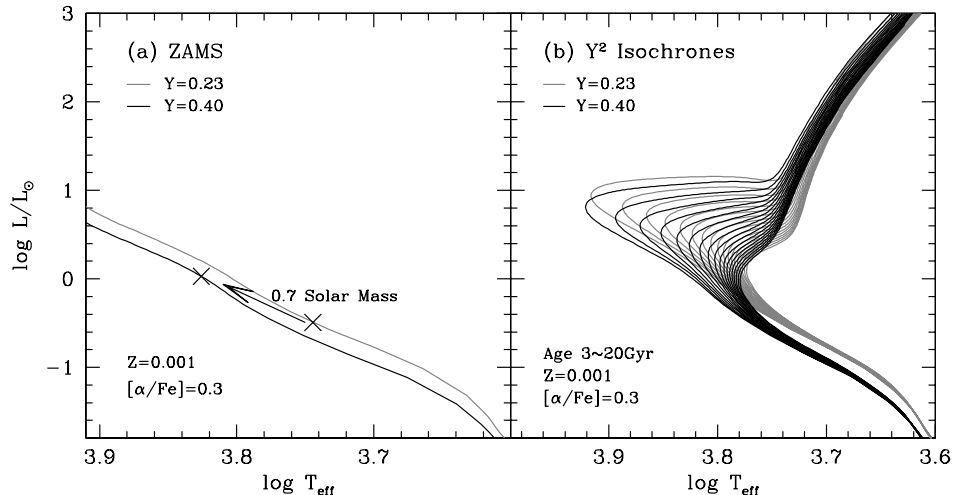


Fig. 1. New sets of Y^2 isochrones with helium enhancement. Panel (a) demonstrates the effect of helium enhancement on the zero-age main sequence for a given mass, while panel (b) illustrates the effect on the isochrones.

al. 1994), what is needed is a firm evidence that such a special helium enrichment indeed occurs in some globular clusters. This is because a star cluster is widely believed to be a coeval and chemically homogeneous system, and also the required helium enrichment is far more than that expected from standard chemical evolution models in galactic scales (i.e., $\Delta Y/\Delta Z = 1\sim 2$).

The first good evidence that some stars in a globular cluster are actually enhanced in helium came from the recent observations of ω Cen. In particular, recent analyses with isochrones (Norris 2004) and spectroscopy (Piotto et al. 2005) of the MS stars in ω Cen have shown that a large helium abundance variation is needed to reproduce the double MS (Bedin et al. 2004) observed in this cluster. Although more work is needed for a specific chemical evolution model devoted for ω Cen to understand the origin of this unusually strong helium enrichment, these observations and analyses have nevertheless provided a compelling evidence that a minority population of stars at least in one globular cluster are indeed enhanced in helium. In this paper, we report our progress in constructing population models with the super-helium-rich scenario.

2. EFFECT OF HELIUM ENHANCEMENT

In order to investigate the effect of helium abundance on the observed features in the CMD, we have first calculated new sets of Yonsei-Yale (Y^2) stellar evolutionary tracks and isochrones with helium enhancements (Kim et al. 2002; Kim et al. 2005). These tracks adopted most up-to-date input physics including a new equation of state for the low mass stars. Figure 1 demonstrates the effect of helium enrichment on the HR diagram. Helium-rich stars, in general, are brighter and bluer for a given mass because of their higher core temperature (Fig. 1a), however, since they evolve faster than helium-poor stars, they would have smaller masses for a given age, and therefore the helium-rich MS appears both bluer and

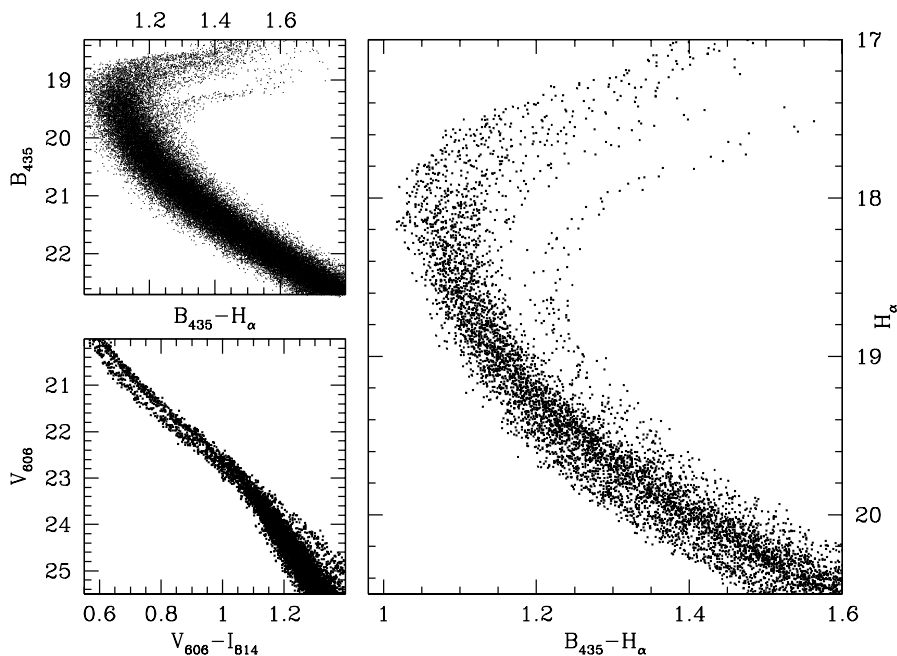


Fig. 2. Model CMDs for the main-sequence and subgiant-branch parts of ω Cen. These figures are to be directly compared with the observations by Bedin et al. (2004; see their Fig. 1).

fainter than the helium-poor MS on the isochrone (Fig. 1b). For the same reason, the mass at the tip of the red-giant-branch (RGB) of a helium-rich population is smaller than that of a helium-poor one, so that helium-rich HB stars have smaller total masses than helium-poor stars, which shifts their positions to the blue in the CMD (Lee et al. 1994).

3. POPULATION MODELS

Based on our new isochrones and the HB evolutionary tracks of Sweigart (1987) extrapolated to $Y \sim 0.4$,¹ population synthesis models are constructed following the techniques developed by Lee et al. (1990) and Park & Lee (1997). In Figure 2 we present the model CMDs for the MS and subgiant-branch (SGB) parts, based on the assumption that the helium abundances for the three most metal-rich populations are significantly enhanced among five populations with different metallicities in ω Cen (Sollima et al. 2005). These CMDs were specifically constructed with the passbands, photometric errors and total numbers of stars comparable to the observed ones of Bedin et al. (2004; see their Fig. 1), so that they can be directly compared with each other. The values of helium abundance and age are

¹ We are now in the process of constructing new sets of helium enhanced HB tracks fully consistent with our isochrones. Based on our preliminary models for ZAHB, we have confirmed that there is no serious systematic difference between our HB models and those of Sweigart (1987). We also verified that the extrapolation in Y does not produce a critical problem, by using the Sweigart & Gross (1976) HB tracks where the helium abundance is extended to $Y = 0.4$.

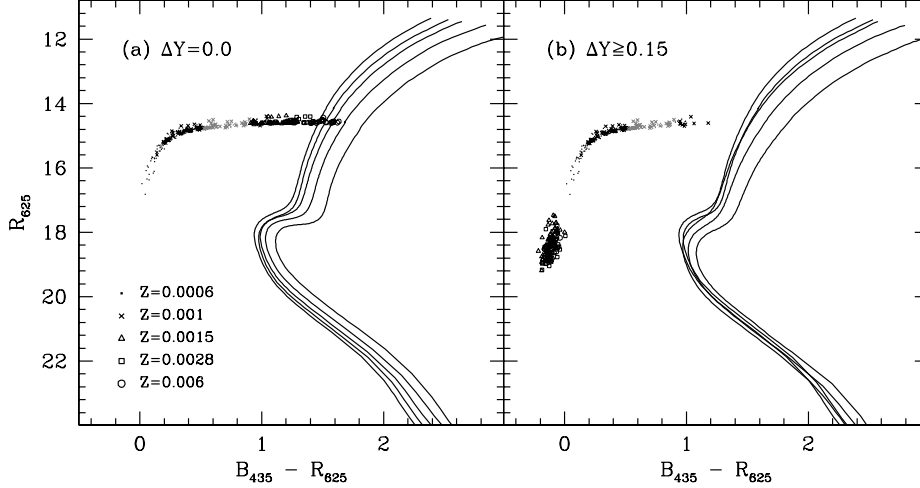


Fig. 3. Model CMDs for ω Cen. Panel (a) is for the case in which all five populations in ω Cen have the same helium abundance, while panel (b) is for the case in which the helium abundances for the metal-rich populations are significantly enhanced as in Table 1. Only the case of $\Delta Y \geq 0.15$ can reproduce the observed features on the MS and HB simultaneously. We adopted $(m - M)_R = 14.3$ and $E_{B-R} = 0.19$ in our models.

adjusted until the best matches between the models and the observed CMDs are obtained, while those for the metallicity are mostly fixed by the RGBs. Table 1 lists the input parameters used in our best model simulations. Similarly, in Figure 3, we compare two models constructed under different assumptions regarding the helium enhancement. As is clear from Figures 2 and 3, we confirm the conclusion from previous works that a large variation in helium abundance is indeed needed to reproduce the observed features on the MS to RGB, including the double MS, where the minority population of the bluer and fainter MS is both more metal-rich and super-helium-rich ($\Delta Y = 0.15$) compared to the majority population of the metal poor redder one.

In Figure 3 we have also presented corresponding synthetic HB models, which should be compared with the observed CMD by Ferraro et al. (2004; see their

Table 1. Input parameters in our best simulation of ω Cen. We adopted $[\alpha/\text{Fe}]=0.3$ and $\eta=0.46$ for the mean mass-loss on the RGB. Population ratios were from Sollima et al. (2005).

| Population | Z | Y | Age (Gyr) | Mass Loss (M_{\odot}) | Fraction |
|------------|--------|-------|--------------|------------------------------|----------|
| 1 | 0.0006 | 0.231 | 13 | 0.168 | 0.42 |
| 2 | 0.001 | 0.232 | 13 | 0.178 | 0.27 |
| 3 | 0.0015 | 0.38 | 12 | 0.172 | 0.17 |
| 4 | 0.0028 | 0.40 | 11.5 | 0.177 | 0.08 |
| 5 | 0.006 | 0.42 | 11.5 | 0.201 | 0.05 |

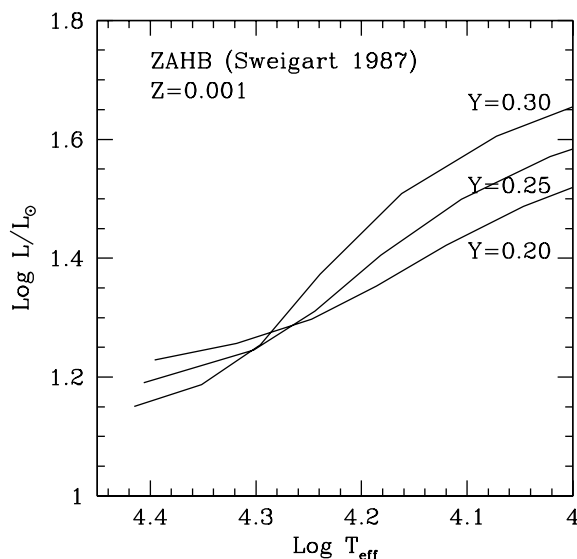


Fig. 4. The zero-age HB sequences with different helium abundances (Sweigart 1987).

Fig. 2, also see Fig. 1 of Lee et al. 2005). From models in Fig. 3a, we can see that the HB morphology generally gets redder with increasing metallicity, and the models fail to reproduce the EHB population. However, the models in Fig. 3b naturally reproduce the EHB stars observed in ω Cen with the same helium enhancements needed to reproduce the unique features on the MS. The fact that the three most metal-rich populations, including progeny of the bluer and fainter MS, all piled up on the extremely blue HB in Fig. 3b is a consequence of the large difference in helium abundance that easily overcomes the metallicity effect. In our model calculations, nothing other than the standard Reimers (1977) empirical relation was employed to estimate the amount of mass-loss on the RGB as a function of the input parameters adopted, and therefore the presence of extreme HB stars is solely the effect of helium enhancement. Under the same scenario, the complex features on the HBs of other globular clusters, such as NGC 2808, can be also explained by large internal variations of helium abundance (Lee et al. 2005; see also D’Antona et al. 2005).

An independent test for the helium-rich scenario might be provided from the FUV photometry of extreme HB stars, because the zero-age HB (ZAHB) locus is very sensitive to helium abundance. As Figure 4 illustrates, in general, helium-rich HB stars are brighter than helium-poor ones, but this trend is reversed when the effective temperature reaches ~ 19000 K. This is because extremely hot HB stars have very thin envelopes, with an almost negligible energy output from the hydrogen-burning shell. The total energy output is then mostly sustained by the helium-burning core, and since helium rich stars have a smaller core mass, they have a lower surface luminosity (Sweigart 1987). According to Sweigart (1987), EHB stars, therefore, would be fainter than HB stars as a result of the helium enhancement. The observed trends in UV CMD of EHB and blue HB stars in NGC 2808 (Brown et al. 2001) and ω Cen (Whitney et al. 1994) support our

prediction (see Fig. 4 of Lee et al. 2005). It is important to note that spectroscopic analyses of the EHB stars in ω Cen and NGC 2808 (Moehler et al. 2002; Moehler et al. 2004) have shown anomalously high helium abundances up to about 0.3–1.0. While Moehler et al. interpreted this with the late hot flasher scenario (Brown et al. 2001), we believe that at least some of this helium enrichment might be also understood from our scenario.

4. DISCUSSION

The good agreements between the models and the observations for the appearance and population ratio of EHB stars in ω Cen suggest that the third parameter that controls HB morphology, in addition to metallicity and age, might be helium abundance. This in turn suggests that whenever the relative age is estimated from the HB morphology (Lee et al. 1994; Rey et al. 2001), a better result would be obtained by ignoring extreme HB stars or similar peculiar features on the HB. Fortunately, the effect of helium abundance on the MS and RGB is relatively small, and in most globular clusters with EHB stars, the expected helium-rich populations are a minority in terms of the population ratio. Therefore, the age dating from MS and RGB is likely to be less affected by the minority populations of helium-rich stars in these clusters. However, when one infers the relative age or other physical parameters from the integrated-light colors and spectra of globular clusters and early-type galaxies, the possible contamination from helium-rich populations should still be carefully considered, as they would make the observed colors bluer, especially in the UV. Further observations and modeling of globular clusters with peculiar features on their HBs will undoubtedly help us to establish the super-helium-rich scenario as the origin of EHB stars found in globular clusters.

ACKNOWLEDGMENTS. Support for this work was provided by the creative research initiative program of the Korean ministry of science and technology, for which we are grateful.

REFERENCES

- Bedin L. R., Piotto G., Anderson J., Cassisi S. et al. 2004, *ApJ*, 605, L125
 Brown T. M., Sweigart A. V., Lanz T., Landsman W. B., Hubeny I. 2001, *ApJ*, 562, 368
 D’Antona F., Bellazzini M., Caloi V., Fusi Fecci F., Galletti S., Rood R. T. 2005, *ApJ*, in press
 D’Antona F., Caloi V. 2004, *ApJ*, 611, 871
 D’Antona F., Caloi V., Montalbán J., Ventura P., Gratton R. 2002, *A&A*, 395, 69
 Ferraro F. R., Sollima A., Pancino E., Bellazzini M. et al. 2004, *ApJ*, 603, L81
 Kim Y.-C., Demarque P., Yi S. K., Alexander D. R. 2002, *ApJS*, 143, 499
 Kim Y.-C. et al. 2005, in preparation
 Lee Y.-W., Demarque P., Zinn R. 1990, *ApJ*, 350, 155
 Lee Y.-W., Demarque P., Zinn R. 1994, *ApJ*, 423, 248
 Lee Y.-W., Joo S.-J., Han S.-I., Chung C. et al. 2005, *ApJ*, 621, L57

- Moehler S., Sweigart A. V., Landsman W. B., Dreizler S. 2002, *A&A*, 395, 37
- Moehler S., Sweigart A. V., Landsman W. B., Hammer N. J., Dreizler S. 2004, *A&A*, 415, 313
- Norris J. E. 2004, *ApJ*, 612, L25
- Park J.-H., Lee Y.-W. 1997, *ApJ*, 476, 28
- Piotto G., King I. R., Djorgovski S. G., Sosin C. et al. 2002, *A&A*, 391, 945
- Piotto G., Villanova S., Bedin L. R., Momany Y. et al. 2005, *ApJ*, 621, 777
- Reimers D. 1977, *A&A*, 57, 395
- Rey S.-C., Yoon S.-J., Lee Y.-W., Chaboyer B., Sarajedini A. 2001, *AJ*, 122, 3219
- Sollima A., Ferraro F. R., Pancino E., Bellazzini M. 2005, *MNRAS*, 357, 265
- Sweigart A. V. 1987, *ApJS*, 65, 95
- Sweigart A. V., Gross P. G. 1976, *ApJS*, 32, 367
- Whitney J. H., O'Connell R. W., Rood R. T. et al. 1994, *AJ*, 108, 1350

**THE NATURE OF THE HOT STARS IN THE BULGE
OF GLOBULAR CLUSTER NGC 6388 [†]**

S. Moehler¹ and A. V. Sweigart²

¹ *Institut für Theoretische Physik und Astrophysik, Christian-Albrechts-Universität zu Kiel, D-24098 Kiel, Germany*

² *NASA Goddard Space Flight Center, Code 681, Greenbelt, MD 20771, U.S.A.*

Received 2005 August 1

Abstract. The metal-rich bulge globular clusters NGC 6388 and NGC 6441 show distinct blue horizontal-branch tails in their color-magnitude diagrams. They are thus strong cases of the well known *Second Parameter Problem*. In addition, the horizontal branches in these globular clusters show an upward tilt toward bluer colors, which cannot be explained by canonical evolutionary models. We will discuss several scenarios which have been proposed to explain these two features and present observations obtained to test these scenarios.

Key words: stars: horizontal branch, stars: evolution, globular clusters: individual: NGC 6388

1. INTRODUCTION

Ever since its discovery over 30 years ago (Sandage & Wildey 1967; van den Bergh 1967), the 2nd parameter effect has stood as one of the major unsolved challenges in the study of the Galactic globular clusters. While it was recognized quite early that the horizontal branch (HB) becomes redder on average with increasing metallicity, many pairs of globular clusters are known with identical metallicities but markedly different HB morphologies, e.g., M3 versus M13. Thus some parameter(s) besides metallicity (the 1st parameter) must affect the evolution of the HB stars in these globular clusters. Possible 2nd parameter candidates include the globular cluster age, mass-loss along the red giant branch (RGB), helium abundance Y , α -element abundance, cluster dynamics, stellar rotation, deep mixing, etc.

HST observations by Rich et al. (1997) have found that the metal-rich globular clusters NGC 6388 and NGC 6441 ($[\text{Fe}/\text{H}] \approx -0.5$) contain an unexpected population of hot HB stars and therefore show a prominent 2nd parameter effect. Ordinarily metal-rich globular clusters have only a red HB clump. However, NGC 6388 and NGC 6441 possess extended blue HB tails containing $\sim 15\%$ of the total HB population. Quite remarkably, the HBs in both clusters slope upward with decreasing $B-V$ with the stars at the top of the blue tail being nearly 0.5 mag brighter in V than the well-populated red HB clump. Moreover, the RR Lyrae variables in these clusters have unusually long periods for the cluster metallicity,

[†] Based on observations from the European Southern Observatory, Chile (prop. 69.D-0231)

leading Pritzl et al. (2000) to suggest that NGC 6388 and NGC 6441 may represent a new Oosterhoff group. For all of these reasons the HBs of NGC 6388 and NGC 6441 are truly exceptional.

In the next section we will discuss the implications of NGC 6388 and NGC 6441 for the 2nd parameter effect and will review a number of scenarios for explaining the HB morphology of these clusters. The following sections will then describe the high and medium resolution spectra that we have obtained to test these scenarios.

2. HB MORPHOLOGY: PROBLEMS AND SCENARIOS

The presence of hot HB stars in globular clusters as metal-rich as NGC 6388 and NGC 6441 may provide an important diagnostic for understanding the 2nd parameter effect for the following reason. In intermediate-metallicity globular clusters such as M 3 the HB spans a wide range in color that extends both blueward and redward of the instability strip. The location of a star along the HB is then quite sensitive to changes in the stellar parameters. In fact, this is why the HB is “horizontal”. In metal-rich globular clusters, however, the situation is quite different. Due to their high envelope opacity, metal-rich HB stars are normally confined to a red clump. To move such stars blueward requires a larger change in the stellar structure. Thus any 2nd parameter candidate capable of producing hot HB stars in a metal-rich globular cluster might also have other observational consequences. Indeed, the upward sloping HBs in NGC 6388 and NGC 6441 suggest that the 2nd parameter in these globular clusters is affecting both the temperature and luminosity of the HB stars.

Can canonical models explain the upward sloping HBs in NGC 6388 and NGC 6441? In principle, one could produce hot HB stars in these globular clusters by increasing the cluster age or by enhancing the amount of mass-loss along the RGB. Rich et al. (1997) considered both of these possibilities but found neither of them to be satisfactory because the required increase in the cluster age is quite large and because the frequency of stellar interactions within the cores of these clusters seems too low to produce the additional RGB mass-loss. This conclusion was further supported by the theoretical HB simulations of Sweigart & Catelan (1998, hereafter SC98). They found that the HB morphology predicted by canonical HB models is flat in the (M_V vs. $B-V$) plane. Increasing the cluster age or the RGB mass-loss simply moves the models blueward in $B-V$ without increasing their luminosity. Thus canonical HB models cannot account for the HB morphology of NGC 6388 and NGC 6441. In particular, two of the most prominent 2nd parameter candidates – age and RGB mass-loss – do not work.

This failure of canonical HB models to produce upward sloping HBs has prompted the study of other noncanonical solutions. Theoretical models show that the HB luminosity at a fixed metallicity depends on two parameters: the helium abundance Y and the core mass M_c . This fact led SC98 to suggest three noncanonical scenarios involving increases in either Y or M_c which might potentially produce upward sloping HBs.

The first (“high- Y ”) scenario assumes that the stars in NGC 6388 and NGC 6441 formed with a high primordial helium abundance due to a peculiar chemical enrichment history in these clusters. From theoretical models we know that HB tracks at high helium abundances have very long blue loops which deviate considerably from the zero-age HB (ZAHB). The HB simulations of SC98 show that such high- Y tracks can indeed produce upward sloping HBs as seen in NGC 6388

and NGC 6441 provided Y is very large ($\gtrsim 0.4$). However, this scenario can be ruled out because it predicts too large a value for the number ratio R of HB stars to RGB stars brighter than the HB (Layden et al. 1999) as well as too bright a luminosity for the RGB bump (Raimondo et al. 2002).

The second (“rotation”) scenario is based on the fact that internal rotation within an RGB star can delay the helium flash, thereby leading to a larger core mass and to greater mass-loss near the tip of the RGB. This increase in M_c together with the corresponding decrease in M will shift a star’s HB location towards higher effective temperatures and luminosities. HB simulations show that this scenario can also produce upward sloping HBs similar to those observed in NGC 6388 and NGC 6441. The problem, however, is to understand how the blue HB stars could have the high rotation rates required by this scenario.

The third (“helium-mixing”) scenario is motivated by the large star-to-star abundance variations which are found among the red-giant stars within individual globular clusters and which are sometimes attributed to the mixing of nuclearily processed material from the vicinity of the hydrogen shell out to the stellar surface (Kraft 1994). The observed enhancements in Al are particularly important because they indicate that the mixing is able to penetrate deeply into the hydrogen shell (Cavallo et al. 1998). Such mixing would dredge up fresh helium together with Al, thereby enhancing the envelope helium abundance and leading to a brighter RGB tip luminosity and hence greater mass-loss. Thus a helium-mixed star would arrive on the HB with both a higher envelope helium abundance and a lower mass and would therefore be both bluer and brighter than its canonical counterpart - just what is needed to produce an upward sloping HB. Indeed, the HB simulations of SC98 confirm that helium mixing can produce HB morphologies similar to those in NGC 6388 and NGC 6441. However, the existence of helium mixing can be questioned on several grounds. The O-Na and Mg-Al anticorrelations observed in turnoff stars of NGC 6752 by Gratton et al. (2001) indicate that the Al enhancements are more likely due to primordial pollution from an earlier generation of asymptotic-giant-branch (AGB) stars than to deep mixing on the RGB. It is also questionable whether the mixing currents could overcome the large gradient in the mean molecular weight within the hydrogen shell of a RGB star. Thus helium mixing seems unlikely.

A number of additional solutions have been offered to explain the HB morphologies of NGC 6388 and NGC 6441. One of the earliest solutions, suggested by Piotto et al. (1997), was a spread in metallicity. In this case the blue HB stars would be metal-poor compared to the stars in the red HB clump. Because the HB becomes brighter in V with decreasing metallicity, the blue HB stars would also be brighter. Thus a metallicity spread might also produce an upward sloping HB. This possibility was studied by Sweigart (2002), who showed that upward sloping HBs similar to those in NGC 6388 and NGC 6441 would require the stars at the top of the blue HB tail to be approximately 2 dex more metal-poor than the stars in the red HB clump. However, Raimondo et al. (2002) have noted that the progenitors of the blue HB stars should appear as a population of metal-poor giants lying well to the blue of the metal-rich RGB. Since such metal-poor giants are not seen in the color-magnitude diagrams of NGC 6388 and NGC 6441, Raimondo et al. (2002) conclude that any metallicity spread must be small.

Piotto et al. (1997) also suggested that NGC 6388 and NGC 6441 might contain two stellar populations with different ages. This possibility has been further ex-

plored by Ree et al. (2002). Their population models for NGC 6388 and NGC 6441 are able to produce blue HB stars provided these stars are older by 1.2 Gyr and metal-poor by 0.15 dex compared to the stars in the red HB clump. Such a small difference in metallicity between the blue and red HB stars avoids the problem with the missing metal-poor giants discussed above. However, while such models might produce bimodal HBs, they do not produce an upward sloping HB. As shown by SC98, differences in age merely move an HB star horizontally along the HB, and, as shown by Sweigart (2002), a metallicity difference of 0.15 dex is too small to produce a significant HB slope. Thus the Ree et al. (2002) models do not account for a key property of the HBs in NGC 6388 and NGC 6441. Ree et al. (2002) also suggest that the long RR Lyrae periods might be explained if these stars are highly evolved from the blue HB. While such stars would have long periods, they would also evolve rapidly across the instability strip on their way to the AGB. Explaining the observed number of RR Lyrae stars under such a scenario would therefore be very difficult (Pritzl et al. 2002).

A more promising possibility is based on the suggestion by D’Antona & Caloi (2004) that the stars in globular clusters with blue HB tails are born in two events: a first generation of helium-normal stars and a second generation of helium-rich stars which subsequently form from the ejecta of the intermediate-mass AGB stars of the first generation. Since a helium-rich star has a lower turnoff mass at a given age, it will be bluer on the HB than a helium-normal star. It will also be brighter due to the increased energy output of the hydrogen-burning shell. Thus the spread in the internal helium abundance predicted by this scenario will lead to a spread in color along the HB, with the red clump stars corresponding to the helium-normal, first generation stars and the blue tail stars being progressively more helium-rich as the effective temperature increases. An upward sloping HB is a natural consequence of this spread in helium. The fact that the HB slope is more prominent in NGC 6388 and NGC 6441 than in other blue tail globular clusters may be simply due to their higher metallicity which requires a larger increase in helium in order to force a star blueward of the red clump. We emphasize that this scenario differs from the high- Y scenario, mentioned above, in which all of the stars are helium-rich and the helium-mixing scenario in which the spread in helium arises from deep mixing on the RGB.

All of the above scenarios which can produce an upward sloping HB predict that the gravities of the blue HB stars should be lower than the gravities of canonical blue HB stars. In 1998 we observed some of the brighter objects in both clusters ($B < 18$; four stars in NGC 6388, three in NGC 6441) to test this prediction. Unfortunately the results only added to the confusion as most of the stars had *higher gravities* than predicted by canonical evolution (Moehler et al. 1999). It took us four years and three rejected proposals to convince the ESO TAC to give us observing time for another test of the above described scenarios: With proposal 69.D-0231 we obtained high resolution spectra of four cool blue HB stars in NGC 6388 to determine their metallicities and rotation velocities. In addition, we observed medium resolution spectra of about a dozen blue HB stars along the blue tail to determine their effective temperatures and surface gravities. By comparing the observed values to those predicted by the various scenarios, we hope to distinguish among the scenarios.

3. HIGH RESOLUTION SPECTROSCOPY

The high resolution spectra were obtained with the UVES spectrograph at the ESO VLT with the standard setting DIC1 (390+564) and a slit width of $1''$. This setting covers the wavelength ranges 3720–4520 Å in the blue arm and 4605–5585 Å and 5674–6610 Å in the red arm (2 CCDs) at a resolution of 45 000 (blue) and 37 000 (red). This is the same setting as used by the SPY project (Karl et al., these proceedings). We therefore reduced the data with the UVES context within MIDAS, with the additional correction by a flat field shifted in wavelength direction as done by the SPY consortium to avoid ripples in the resulting one-dimensional spectrum. The details will be described in a forthcoming paper.

3.1. Analysis and results

To analyze the high resolution spectra, we first estimated effective temperatures from $B-V$ colors corrected for a reddening of 0.37 mag. Keeping these temperatures fixed, we estimated the surface gravities by fitting the Balmer line profiles as described in Moehler et al. (2004). Using these values we did a first abundance determination by spectrum synthesis, using the LINFOR program*. Then we changed the effective temperature until the abundances from Fe I and Fe II agreed to within 0.15 dex. The surface gravity was again determined by fitting the Balmer line profiles.

Figure 1 shows a section of the spectra of three HB stars together with the synthesized spectrum (the fourth star is the coolest one and therefore most difficult to analyze due to severe line blending). We find no significant deviations from the overall metallicity of NGC 6388 in these spectra and therefore no supporting evidence for a possible metal deficiency in these blue HB stars. We also do not find rotation velocities in excess of 10 km s^{-1} , which is in good agreement with the values found for blue HB stars in other globular clusters. We do find a *very tentative* evidence for a possible helium enrichment. In this temperature range, however, the helium lines are very weak and extremely sensitive to temperature variations, so that we do not want to place much emphasis on this *possible* result.

4. MEDIUM RESOLUTION SPECTROSCOPY

The medium resolution spectra of stars along the blue tail were obtained with the multi-object spectroscopy mode MOS of FORS2, again at the ESO VLT.

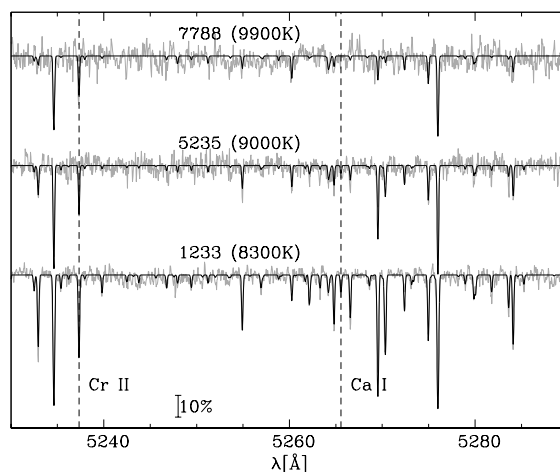


Fig. 1. Small section of the UVES spectra for the three hotter stars. The black line is the synthetic spectrum for each star and the unmarked lines are all iron lines.

* For a description see <http://a400.sternwarte.uni-erlangen.de/~ai26/linfit/linfor.html>

We used the grism 600B with a slit width of $0.6''$, corresponding to a resolution of 1200 and a wavelength range of 3700 \AA to 5200 \AA for all spectra. The wavelength range extended to blue or redder regions depending on the position of the slitlet on the CCD. The data were reduced as described in Moehler et al. (2004), except for the sky subtraction.

The MOS observations were obtained in very crowded fields, and due to the fact that several stars were observed simultaneously, we could not orient the individual slitlets in a way to avoid nearby stars. Therefore most slitlets contain spectra of several stars, in many cases overlapping so strongly that it is impossible to directly extract the spectrum of our intended target (see Figure 2). In order to account for this overlap we proceeded as follows.

- We corrected the curvature of the FORS2 spectra.
- We averaged the wavelength-calibrated two-dimensional spectra along their dispersion axis between 3500 and 5200 \AA (roughly the range which is later used for fitting the line profiles), thereby producing a one-dimensional spatial profile along the slitlet (cf. Figure 2, upper histogram).
- The one-dimensional spatial distribution of light was fitted with a combination of Moffat functions, i.e.,

$$I_{(x)} = bck + \sum_{j=1}^n I_{j(x)}$$

$$\text{with } I_{j(x)} = a_j \left(1 + \frac{4(x - b_j)^2}{c^2} \right)^{-d}.$$

For each profile the parameters a_j (amplitude) and b_j (position) were fitted individually, whereas the parameters c and d , which determine the profile width and shape (and should depend only on the seeing and instrumental broadening), had to be the same for all objects within one slitlet. We used up to 13 individual profiles to fit the full spatial light distribution along one slitlet (see Figure 2, light solid line).

- After achieving a good fit to the observed spatial profiles we kept the parameters b_j , c and d fixed and used these profiles to fit the spatial profile now at

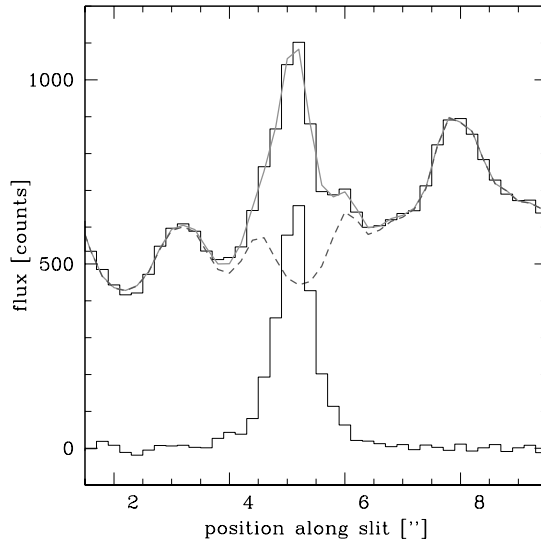


Fig. 2. The spatial light distribution along one slitlet. The upper histogram is the observed light distribution, the light continuous line gives the fit of all sources, the light dashed line marks the subtracted sky background. The lower histogram is the spatial profile of the sky subtracted image.

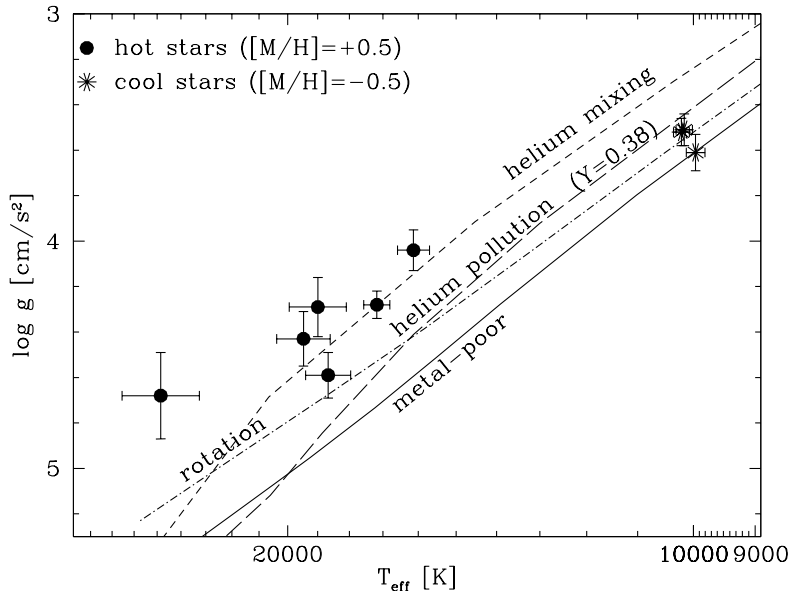


Fig. 3. Effective temperatures and surface gravities for our target stars as derived from line profile fits. Three stars have temperatures below 8000 K, where we do not trust the fit procedure, and one star showed a prominent G-band in its spectrum after the sky subtraction and was therefore not analyzed. For comparison we show the tracks discussed in Section 2.

every wavelength step. The amplitudes a_j and the spatial constant bck (for the true sky background) were allowed to vary with wavelength, in order to describe the various spectra.

- The sum of all profiles *minus the target profile* were then used as sky background (cf. Figure 2, dashed line) and subtracted from the wavelength calibrated two-dimensional image. The resulting image – containing only the target spectrum – was again averaged over the same wavelength range as above to verify the quality of the sky correction (see Figure 2, lower histogram).

4.1. Analysis and results

We then fitted the Balmer and helium line profiles to determine effective temperatures, surface gravities and helium abundances as described in Moehler et al. (2004), using a solar metallicity model grid to account for the effects of radiative levitation. The resulting values of T_{eff} and $\log g$ are shown in Figure 3, together with tracks describing the scenarios mentioned in Section 2. Obviously the hot stars show significantly lower gravities than expected. To verify if this is a luminosity effect or rather a reduction and/or analysis artifact, we used these values to estimate masses for the stars. While the three stars around 10 000 K show an average mass of $0.52 M_{\odot}$, the hot stars have an average mass of $0.28 M_{\odot}$, which is too low by almost a factor of 2. We therefore suspect that the sky subtraction did not work sufficiently well to really isolate the light from the hot stars. Tests with the spectra indicate that sky subtraction problems may also be the cause for the unexpectedly high gravities found previously by Moehler et al. (1999).

5. CONCLUSIONS

From our high resolution data (which include two of the three stars at 10 000 K in Figure 3) we find no supporting evidence for the low metallicity scenario. The atmospheric parameters of the stars at about 10 000 K also do not support the helium mixing scenario. The medium resolution data of the hotter and visually fainter stars unfortunately yield results that are apparently affected by systematic errors. As the hotter stars are fainter by at least 1.2 mag in B compared to the stars at about 10 000 K, the systematic problems are most probably due to crowding problems, which are more severe for fainter stars. Despite our best efforts, which yielded spectra without obvious evidence for contamination in all but one case, we apparently did not succeed in extracting from the observed data the information related *only* to the intended target. This should serve as a warning that observations in crowded regions are difficult, especially, if the targets are selected from HST observations (as was the case here).

ACKNOWLEDGMENTS. We want to thank the staff at the Paranal Observatory for obtaining the observations for us.

REFERENCES

- Cavallo R. M., Sweigart A. V., Bell R. A. 1998, ApJ, 492, 575
 D’Antona F., Caloi V. 2004, ApJ, 611, 871
 Gratton R. G., Bonifacio P., Bragaglia A. et al. 2001, A&A, 369, 87
 Kraft R. P. 1994, PASP, 106, 553
 Layden A. C., Ritter L. A., Welch D. L., Webb T. M. A. 1999, AJ, 117, 1313
 Moehler S., Sweigart A. V., Catelan M. 1999, A&A, 351, 519
 Moehler S., Sweigart A. V., Landsman W. B., Hammer N. J., Dreizler S. 2004, A&A, 415, 313
 Piotto G., Sosin C., King I. R. et al. 1997, in *Advances in Stellar Evolution*, eds. R. T. Rood & A. Renzini, Cambridge University Press, Cambridge, p. 84
 Pritzl B. J., Smith H. A., Catelan M., Sweigart A. V. 2000, ApJ, 530, L41
 Pritzl B. J., Smith H. A., Catelan M., Sweigart A. V. 2002, AJ, 124, 949
 Raimondo G., Castellani V., Cassisi S., Brocato E., Piotto G. 2002, ApJ, 569, 975
 Ree C. H., Yoon S.-J., Rey S.-C., Lee Y.-W. 2002, in *Omega Centauri, a Unique Window into Astrophysics*, eds. F. van Leeuwen, J. D. Hughes & G. Piotto, ASP Conf. Ser., 265, 101
 Rich R. M., Sosin C., Djorgovski S. G. et al. 1997, ApJ, 484, L25
 Sandage A., Wildey R. 1967, ApJ, 150, 469
 Sweigart A. V. 2002, in *Highlights of Astronomy*, ed. H. Rickman, ASP, San Francisco, p. 292
 Sweigart A. V., Catelan M. 1998, ApJ, 501, L63 (SC98)
 van den Bergh S. 1967, AJ, 72, 70

**NEW CANDIDATE EHB STARS IN THE OPEN CLUSTER
NGC 6791: LOOKING LOCALLY INTO THE UV-UPTURN
PHENOMENON**

L. M. Buson¹, E. Bertone², A. Buzzoni³ and G. Carraro^{4,5,6}

¹ *INAF - Osservatorio di Padova, Italy*

² *INAOE, Puebla, Mexico*

³ *INAF - Osservatorio di Bologna, Italy*

⁴ *Dept. de Astron. Univ. de Chile, Santiago, Chile*

⁵ *Astronomy Dept., Yale Univ., USA*

⁶ *Dip. di Astronomia, Univ. di Padova, Italy*

Received 2005 August 1

Abstract. Relying on *U* and *B* imagery at the Italian Telescopio Nazionale Galileo (TNG), we report here the discovery of a sample of 13 new UV-bright post-HB candidate stars in the field of the Galactic open cluster NGC 6791. Owing to its super-solar metal content ($[\text{Fe}/\text{H}] \gtrsim 0.2$ dex) and estimated age ($t \gtrsim 8$ Gyr), this cluster represents the nearest and ideal stellar aggregate to match the distinctive properties of the evolved stellar populations possibly ruling the UV-upturn phenomenon in elliptical galaxies and bulges of spirals. Our ongoing spectroscopic follow-up of this unique UV-bright sample will allow us to assess – once cluster membership of the candidates is properly checked – the real nature (e.g., sdB, sdO, AGB-manqué or EHB stars) of these hot sources and their link with the ultraviolet excess emerging from low-mass, metal-rich evolutionary environments of external galaxies.

Key words: stars: sudwarfs – stars: horizontal-branch – ultraviolet: stars

1. INTRODUCTION

Since its early discovery (Code 1969), the so-called UV-upturn phenomenon in old stellar populations of ellipticals and spiral bulges (namely the abrupt rise in the UV continuum emission shortward of $\lambda \sim 2000$ Å) has been the subject of growing theoretical analyses intended to establish its origin and evolution (see, e.g., Greggio & Renzini 1990 and O’Connell 1999, for reviews).

Both theory and observations currently seem to converge towards the “Extreme Horizontal Branch” (EHB) scenario as the main factor responsible for the phenomenon (Dorman et al. 1995; Brown 2004). If this is the case, models show that hot HB stars with helium core mass $M_{\text{core}} \lesssim 0.52 M_{\odot}$ can escape the stan-

ard post-HB evolution (that would culminate with the planetary-nebula event at the end of the asymptotic giant branch evolution), and directly reach the high-temperature region of the HR diagram ($T_{\text{eff}} \gtrsim 30\,000$ K) to fade then along the white-dwarf cooling sequence (Dorman et al. 1993).

In this framework, the role of metallicity cannot yet be confidently assessed, however, as we face two conflicting scenarios relying either on a metal-poor evolution (naturally giving rise to a blue HB morphology, see Park & Lee 1997) or a metal-rich case, where the onset of UV emission needs at least a fraction of stars to exceed some critical threshold in $[\text{Fe}/\text{H}]$ (Greggio & Renzini 1990; Bressan et al. 1994; Buzzoni 1995; Dorman et al. 1995). In this regard, one should be aware that even the high-resolution UV spectroscopy provided by FUSE for the UV-brightest elliptical NGC 1399 turned out to be inadequate to solve the problem, as it mainly probes the photospheric abundance of hot stars, likely perturbed by diffusion effects and therefore not fully indicative of the true metallicity of the whole galaxy stellar population (Brown et al. 2002).

2. NGC 6791: THE UNEXPECTED SHORTCUT

Photometric observations of evolved UV-bright stars in external galaxies are still confined to the relevant case of M31 and its satellite system (e.g., Bertola et al. 1995; Brown et al. 1998, 2000), and no suitable spectroscopy for single stars is available to date.

Surprisingly enough, the close Galactic open cluster NGC 6791, less than 5 kpc away (Friel 1995; Carraro et al. 1999), turned out to be a highly valuable candidate to address the issue of the EHB UV-bright stars, standing out as a sort of backyard “Rosetta Stone” to assess the UV emission of spheroids much farther away. This cluster is actually one of the brightest ($L_V \sim 6.3 \cdot 10^3 L_\odot$), oldest ($t \gtrsim 8$ Gyr) and metal-rich ($[\text{Fe}/\text{H}] \gtrsim +0.2$) ones (King et al. 2005; Stetson et al. 2003; Carraro et al. 1999), and hosts a significant fraction of sdB/O stars (Kaluzny & Rucinski 1995; Kaluzny & Udalski 1992, see Fig. 1) interpreted by Yong et al. (2000) as EHB stars with T_{eff} in the range 24–32 000 K, as confirmed by ground and space-borne (UIT and HST) observations (Liebert et al. 1994; Landsman et al. 1998).

3. OBSERVATIONS AND REDUCTIONS

In 2003 we started a specific observing program aiming at imaging a large field of NGC 6791 in the Johnson U and B passbands with the LRS FOSC camera at the 3.5 m Italian Telescopio Nazionale Galileo (TNG) at La Palma. Taking advantage of its 0.275 arcsec/px scale and its wide (9.4×9.4 arcmin) field of view, this imager allowed us to carry out a suitable (16×16 arcmin) and accurate (± 0.01 mag) survey of the cluster region. Resulting CMDs, based on 330 s B and 1200 s U exposures, are shown in Fig. 2. Data have been reduced with IRAF packages CCDRED, DAOPHOT, ALLSTAR and PHOTCAL, making use of the point spread function method (Stetson 1987).

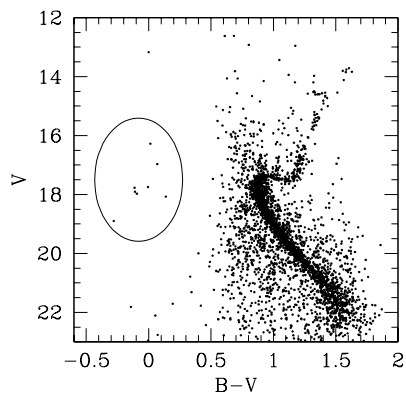


Fig. 1. The Kaluzny & Rucinski (1995) C-M diagram of NGC 6791, based on CCD photometry at the ESO 2.1 m telescope (only best photometric sample plotted here). Yong et al. (2000) provided a good fit to these data with a $([\text{Fe}/\text{H}], t) = (0.33 \text{ dex}, 8 \text{ Gyr})$ model, predicting however a red HB morphology clumped about $(B - V) \simeq 1.3$, and clearly missing the eight hot (supposedly EHB) stars singled out in the plot.

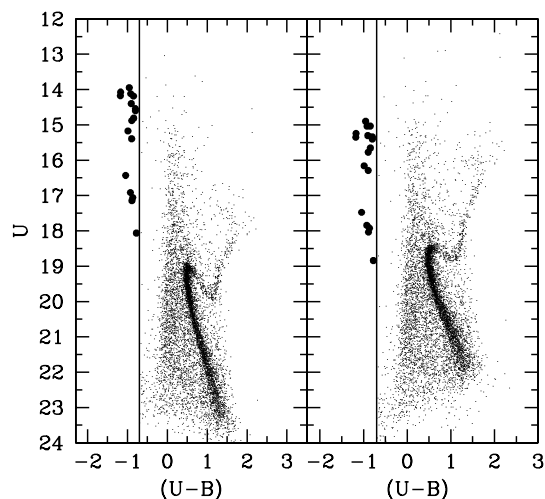


Fig. 2. Combined U vs. $U-B$ and B vs. $U-B$ diagrams of the field of NGC 6791 explored with TNG LRS. Big solid dots mark our 13 newly discovered UV-bright sources with $U-B < -0.7$ (vertical line) together with four objects (the clump about $U \sim 17$) including three member sdB and one sdO from the sample of faint blue stars by Kaluzny & Udalski (1992).

4. TOWARDS THE FUTURE

The analysis of Fig. 2 shows a cleanly detected sample of 13 new UV-bright objects, bluer than $U-B < -0.7$, and consistent with sdB/O stars, that sums up to the four EHB candidates (the clump of stars around $U \sim 17$) previously found in this color range by Kaluzny & Udalski (1992).*

Our current observational campaign, making use of several spectroscopic facilities at TNG and other telescopes, will provide us with both low- ($\sim 10 \text{ \AA}$ FWHM) and mid- ($\sim 6 \text{ \AA}$) resolution spectra along the full optical range (3500–8000 \AA) for these newly identified targets, assessing their cluster membership and, for those positive cases, allowing us to settle the effective temperature and surface gravity of each star by fitting the observed spectral energy distribution with the new

* Although about 2 mag brighter than the Kaluzny & Udalski (1992) candidates, our targets might still be consistent with an sdB/O classification, recalling the large spread in the bolometric correction to U and B magnitudes and the allowed temperature range compatible with the observed scatter in the $U-B$ color (see Johnson 1966).

UVBLUE and BLUERED synthetic spectral libraries (Rodriguez-Merino et al. 2005; Bertone et al. 2003) of appropriate metallicity. Among others, such a complete sample of *bona fide* EHB stars will also provide a first reliable estimate of the lifetime and global UV energetic budget associated to the EHB evolution relying on the so-called “Fuel Consumption Theorem” of Renzini & Buzzoni (1986).

REFERENCES

- Bertola F., Bressan A., Burstein D., Buson L. M., Chiosi C., di Serego Alighieri S. 1995, ApJ, 438, 680
- Bertone E., Buzzoni A., Rodriguez-Merino L. H., Chavez M. 2003, in *Modelling of Stellar Atmospheres*, IAU Symp. 210, eds. N. E. Piskunov, W. W. Weiss & D. F. Gray, ASP, San Francisco
- Bressan A., Chiosi C., Fagotto F. 1994, ApJS, 94, 63
- Brown T. M. 2004, Ap&SS, 291, 215
- Brown T. M., Ferguson H. C., Deharveng J.-M., Jędrzejewski R. I. 1998, ApJ, 508, L139
- Brown T. M., Bowers C. W., Kimble R. A., Sweigart A. V., Ferguson H. C. 2000, ApJ, 532, 308
- Brown T. M., Ferguson H. C., O’Connell R. W., Ohl R. G. 2002, ApJ, 568, L19
- Buzzoni A. 1995, ApJS, 98, 69
- Carraro G., Girardi L., Chiosi C. 1999, MNRAS, 309, 430
- Code A. D. 1969, PASP, 81, 475
- Dorman B., Rood R. T., O’Connell R. W. 1993, ApJ, 419, 596
- Dorman B., O’Connell R. W., Rood R. T. 1995, ApJ, 442, 105
- Friel E. D. 1995, ARA&A, 33, 381
- Greggio L., Renzini A. 1990, ApJ, 364, 35
- Johnson H. L. 1966, ARA&A, 4, 193
- Kaluzny J., Rucinski S. M. 1995, A&AS, 114, 1
- Kaluzny J., Udalski A. 1992, Acta Astron., 42, 29
- King I. R., Bedin L. R., Piotto G., Cassisi S., Anderson J. 2005, AJ, 130, 626
- Landsman W., Bohlin R. C., Neff S. G., O’Connell R. W., Roberts M. S., Smith A. M., Stecher T. P. 1998, AJ, 116, 789
- Liebert J., Saffer R. A., Green E. M. 1994, ApJ, 107, 1408
- O’Connell R. W. 1999, ARA&A, 37, 603
- Park J.-H., Lee Y.-W. 1997, ApJ, 476, 28
- Renzini A., Buzzoni A. 1986 in *Spectral Evolution of Galaxies*, eds. C. Chiosi & A. Renzini, Reidel, Dordrecht, p. 195
- Rodriguez-Merino L. H., Chavez M., Bertone E., Buzzoni A. 2005, ApJ, 626, 411
- Stetson P. B. 1987, PASP, 99, 191
- Stetson P. B., Bruntt H., Grundahl F. 2003, PASP, 115, 413
- Yong H., Demarque P., Yi S. 2000, ApJ, 539, 928

SPECTROSCOPIC SEARCH FOR BINARIES AMONG EHB STARS IN GLOBULAR CLUSTERS *

C. Moni Bidin^{1,2}, R.A. Mendez², S. Moehler³, G. Piotto¹, A. Recio-Blanco^{1,4}
and Y. Momany¹

¹ *Dipartimento di Astronomia, Università di Padova, Vicolo dell'Osservatorio
2, 35122 Padova, Italy*

² *Departamento de Astronomía, Universidad de Chile, Casilla 36-D, Santiago,
Chile*

³ *Institut für Theoretische Physik und Astrophysik, Christian-Albrechts-Universität
zu Kiel, D-24098 Kiel, Germany*

⁴ *Observatoire de la Côte d'Azur, Dpt. Cassiopée, CNRS UMR 6202, B.P. 4229,
F-06304 Nice, Cedex 04, France*

Received 2005 August 1

Abstract. We performed a spectroscopic search for binaries among hot horizontal branch stars in globular clusters. We present final results for a sample of 51 stars in NGC 6752 and preliminary results for the first 15 stars analyzed in M 80. The observed stars are distributed along all the HBs in the range $8000 \leq T_{\text{eff}} \leq 32000$ K, and have been observed during four nights. Radial velocity variations were measured with the cross-correlation technique. We analyzed the statistical and systematic errors associated with the measurements in order to evaluate the statistical significance of the observed variations. No close binary system has been detected, neither among cooler stars nor among the sample of hot EHB stars (18 stars with $T_{\text{eff}} \geq 22000$ K in NGC 6752). The data corrected for instrumental effects indicate that the radial velocity variations are always below the 3σ level of ~ 15 km s⁻¹. These results are in sharp contrast with those found for field hot subdwarfs, and open new questions about the formation of EHB stars in globular clusters and possibly of the field subdwarfs.

Key words: stars: horizontal branch – hot subdwarfs – binaries: spectroscopic – globular clusters: individual (NGC 6752, M 80)

1. INTRODUCTION

Although stellar evolution theory has successfully identified horizontal branch (HB) stars as post-core helium flash stars of low initial mass (Hoyle & Schwarzschild 1955; Faulkner 1966), we still lack a comprehensive understanding of their nature. There is a general agreement that the hottest HB stars (EHB) must have suffered a heavy mass-loss during their evolution, keeping only a thin envelope ($\sim 0.02 M_{\odot}$), but their specific formation mechanism remains unclear. The bi-

* Based on observations with the ESO Very Large Telescope at Paranal Observatory, Chile (proposal ID 69.D-0682).

narity of EHB stars, as proposed by many authors (Mengel et al. 1976; Heber et al. 2002) can provide an explanation, since in a close binary system the mass-loss can be enhanced through a number of different binary evolution channels (Han et al. 2002). Binaries have been found to be very common among field subdwarf B-type stars (sdBs), considered to be the counterparts of the cluster EHB stars. Maxted et al. (2001) estimated that $69\pm 9\%$ of sdB stars are close binaries with periods $P \leq 10$ days, and Han et al. (2003) by binary population synthesis techniques predicted a 76–89% binary fraction. From the recent investigation of Morales-Rueda et al. (2003) it appears clear that close binaries with periods $P \leq 5$ days and semiamplitudes of the radial velocity variation $K \geq 50$ km s⁻¹ are very common among sdBs. Nevertheless the binary scenarios, extensively investigated by Han et al. (2002), are not free from problems as shown by Lisker et al. (2005). Moreover a more recent survey of Napiwotzki et al. (2004) found a significantly lower binary fraction among the sdB sample (42%), showing that we are still far from a full understanding of this kind of stars. With this contribution we investigate a sample of EHB stars in globular clusters, searching for evidence of the presence of close binaries among them.

2. OBSERVATIONS AND DATA REDUCTION

In the globular cluster NGC 6752 we selected 51 target stars from the photometric data of Momany et al. (2002). We chose to perform a more complete investigation distributing the sample along the entire HB, from cooler stars ($T_{\text{eff}} \approx 8000$ K) to hot EHB stars ($T_{\text{eff}} \geq 20000$ K), although our attention was focused toward the EHB sample among which we expected to find a high fraction of close binary systems. The targets were divided into three stellar fields for multiobject spectroscopy. The positions of the targets in the color-magnitude diagram of the cluster are shown in Figure 1. In Figure 2 we indicate their radial distribution

Table 1. UT of the start of the exposures (hours and minutes).

| Field | Night | | | |
|-------|--------------|--------------|--------------|------|
| | 12 | 13 | 14 | 15 |
| A | 8:43 | 2:44 3:56 | 9:34 | 7:47 |
| B | 5:55 6:59 | 5:08 | 8:33 | 8:58 |
| C | – | 8:04 | 6:39 7:33 | 6:36 |

with respect to the cluster center. The spectra were collected during four nights of observation (2002 June 12–15) at the VLT-UT4 telescope with the FORS2 spectrograph in MXU mode. During each night, up to two pairs of 1800 s exposures were obtained in each field with a grism 1400V+18 (0.5'' wide slits, 1.2 Å resolution), except in the third night in field A, where only one single exposure was acquired, and the first night in field C, where no observations were performed. In Table 1, the UT of the start of the pair of 1800 s exposures is shown.

Due to different positions of the slits on the mask, the spectra covered slightly different spectral ranges, but in each spectrum the H β line was always present, except for star 14 in field C, that has been excluded from our analysis.

The data reduction has been performed with standard MIDAS procedures, as described in detail in Moehler et al. (2004) and Moni Bidin et al. (2005). During the same observing run similar data were acquired also for 32 HB stars in M 80.

3. MEASUREMENTS

Radial velocity (RV) variations have been measured with the cross-correlation (CC) technique (Tonry & Davis 1979) with the *fxcor* IRAF task. Before coadding the single 1800 s exposures in pairs we performed a CC between them in order to verify that no significant RV variation had occurred. For every star each spectrum has been cross-correlated with all the others, performing 10 CCs for each star in fields A and B, and 6 in field C, covering different temporal intervals from one hour to 3.1 days.

Our analysis was focused on the $H\beta$ line, cross-correlating the 4830–4890 Å spectral range. Nevertheless, all the measurements have been repeated also at other wavelengths, cross-correlating the entire spectra, with and without $H\beta$ and $H\gamma$ when present in the spectral range. In each CC the position of the center of the cross-correlation function (CCF) has been determined with a Gaussian fit (for example, see Recio-Blanco et al. 2004 for a description of the procedure). In the measurements of hot stars it has been often impossible to cross-correlate the entire spectra without the $H\beta$ line, and we selected spectral intervals with the strongest He lines instead, in order to minimize the noise included in the CC procedure and obtain a CCF with a clear peak. We also applied a Fourier filter of various shapes (Brault & White 1971) to the noisy spectra, obtaining always better CCFs but substantially unchanged results.

The [OI] 5577 Å sky line has been used as zero-point in order to correct the spectral shifts due to differences between lamp and star spectra.

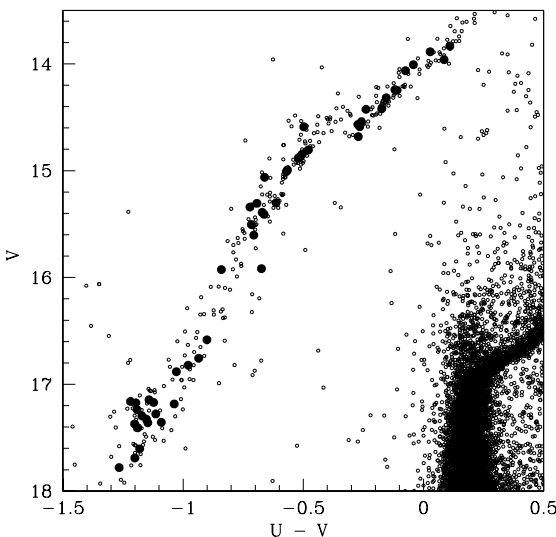


Fig. 1. Positions of the observed stars in the color-magnitude diagram of NGC 6752. Data from Momany et al. (2002).

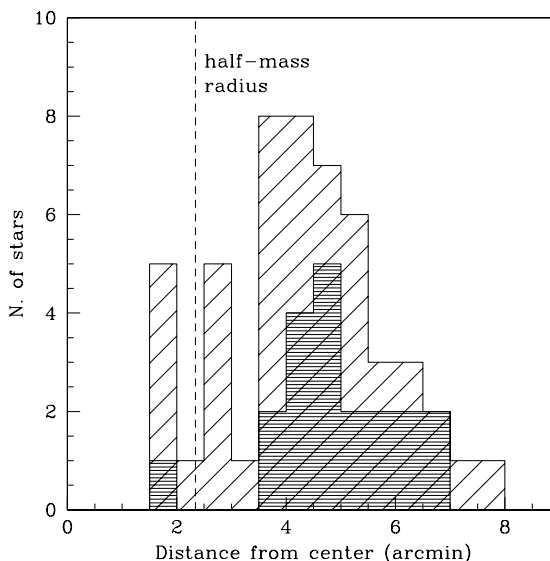


Fig. 2. Radial distribution of the observed stars. The dark shaded area indicates hot stars ($T_{\text{eff}} \geq 20\,000$ K). The half-mass radius from Harris (1996) is also indicated.

We have been forced to correct the data for a systematic effect due to different positions of stars inside the slits in different nights. The effect was up to 10–12 km s^{-1} . On the slit images (without grism), acquired just before each pair of exposures, we measured the position of the stars with respect to the center of the slit with a Gaussian fit of the stellar profile parallel to the dispersion direction. Then we translated the displacements between the frames to km s^{-1} with the instrumental relation $1 \text{ pixel} = 38.2 \text{ km s}^{-1}$ and applied them as corrections to the RV variations. A trend with Y position was evident, but with a certain scatter due to random errors, and we opted to derive the final corrections from the values obtained from the least-square solution of this relation, in order to avoid to introduce additional noise to the results.

This procedure gave corrections very similar to the RV variations measured, indicating both that the removal of the systematic effect had been successful and that the RV variations observed were due only to it.

We measured absolute RVs in order to check the cluster membership of our targets, by means of CCs with the template star HD 188112, a binary sdB star with known ephemeris (Heber et al. 2003). These RVs have undergone similar correction procedures as described before. The errors (1σ) of these measures are 6–10 km s^{-1} . All the stars show an absolute RV in agreement with that of the cluster (-27.9 km s^{-1} , Harris 1996) within 2σ and can be considered RV cluster members.

4. ERROR ANALYSIS

The detection of binary systems in our survey is strongly dependent on a proper estimate of the error budget. We performed an accurate analysis of all the sources of errors and estimated their values (σ). Finally, all the error sources have been combined in quadrature. The resulting errors are about 3–5 km s^{-1} , with the exception of some measurements for hotter stars, where the low S/N sometimes increased the total error up to 7.5 km s^{-1} . In Table 2 we summarize the contribution of each error source and the corresponding ranges (1σ). The CC error is evaluated directly from the CC theory (Tonry & Davis 1979).

The wavelength calibration (wlc) error has been measured on the lamp images calibrated with the coefficients obtained in the wlc procedure, analyzing the position of nine bright lamp lines.

The errors introduced by the corrections for the sky line position, σ_{sky} , and for the displacement of the star inside the slits, σ_{disp} , have been estimated from the dispersion of the corrections around the least-square solution when plotted against the Y positions.

We identified two additional sources of errors: the choice of the “best fit” of CCF peak and the extraction of the spectra. In fact a different extraction can

Table 2. Estimates of errors.

| Error | Range of values (km s^{-1}) |
|---------------------------|--|
| σ_{CC} | 0.5-2 ($\text{H}\beta$) 1-5 (weak lines) |
| σ_{wlc} | 1.4-1.6 |
| σ_{sky} | 1.5 |
| σ_{disp} | 0.7-1.4 |
| $\sigma_{\text{fit+ext}}$ | 0.7-1.5 (cooler stars) 2.1-3.5 (hotter stars) |

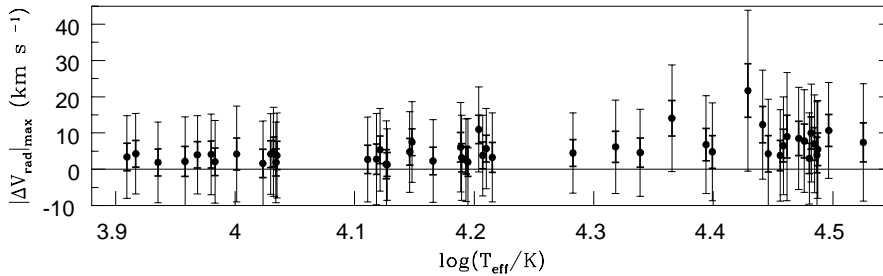


Fig. 3. Maxima of RV variations (in absolute value) measured in $H\beta$ as a function of the temperature of the stars. The thick error bar indicates the 1σ interval, the thin one -3σ .

cause a slightly different line profile; the CC procedure is sensitive enough to reveal it. In measurements on hot stars these have been identified as the main source of error. We evaluated them together extracting all the spectra a second time in a different manner and performing new measures in $H\beta$ with different fits and, finally, measuring the dispersion $\sigma_{\text{fit+ext}}$ of the differences between these new data and the previous ones. This error was strongly dependent on the S/N of the spectra. Then we divided the targets into two groups (stars cooler and hotter than $\sim 20\,000$ K).

5. RESULTS

5.1. Results from $H\beta$

In Figure 3 we summarize the results obtained from measurements in the $H\beta$ wavelength range, where we obtained the most reliable data. All the RV variations are small, lower than 15 km s^{-1} , except for one star, and are never greater than the estimated 3σ interval. They are only slightly higher for hotter stars, but with larger errors due to decreasing S/N in the spectra. We therefore conclude that *none of the observed RV variations can be considered statistically significant*.

Star 15 in field A exhibited higher RV variations in the third night, and the higher datum plotted in the figure (21.7 km s^{-1}) refers to these measurements. We consider this result interesting but particularly dubious, because it was obtained in the only not-summed spectrum (a single 1800 s exposure, as mentioned before), where all the stars tended to show higher RV variations due to the increased noise, and a comparable variation is never seen in any of the other observing nights.

5.2. Results from other lines

The results from CCs involving the entire spectral range did not provide additional information, because they always repeated the results already obtained with $H\beta$. This is due to the sensitivity of CC technique to the stronger line, and the extreme difference in strength between Balmer and others lines in our spectra.

The results obtained with $H\gamma$, when present in the spectra, always confirm the ones obtained in $H\beta$ wavelength range. The differences are always lower than 10 km s^{-1} , with just a handful of exceptions in agreement with a Gaussian distribution given the evaluated σ value.

None of the variations measured with weak lines ever exceeds the evaluated

3σ value, confirming the previous conclusions. The measurements with weak metallic lines have given very good results for cooler stars, mainly in the range $11\,500 \leq T_{\text{eff}} \leq 18\,000$ K due to the presence of many lines induced by radiative levitation of heavy elements (Glaspey et al. 1989; Behr 2003). In these cases the differences between the measured variations and the ones in H β are really small, always below 4 km s^{-1} . For hotter stars the low S/N and the lack of lines complicated the measurements, and the results are less reliable. Occasionally the difference reaches 30 km s^{-1} , but always in the sense of limiting the highest RV variations measured in H β and never emphasizing them. In fact, the stars, that show the highest variations in Figure 3, do not show great variation in these measurements.

5.3. Detection probability

In order to better understand our results, we calculated the probability of detecting a binary in our observations as a function of the period P . We assumed circular orbits and a mass of $0.5 M_{\odot}$ for each component, in order to relate the semiamplitude of the RV variation to the period. These assumptions are representative of typical binary systems observed among field sdBs. We repeated the calculations assuming a companion of $0.1 M_{\odot}$. Systems with a low-mass companion are a minority among field sdBs, but their presence is well established. Our survey is not sensitive enough for this kind of systems, except for the shortest periods, and from our results we cannot draw interesting conclusions about them. The probabilities are shown in Figure 4 (the solid line for a $0.5 M_{\odot}$ companion and the dotted line – for $0.1 M_{\odot}$).

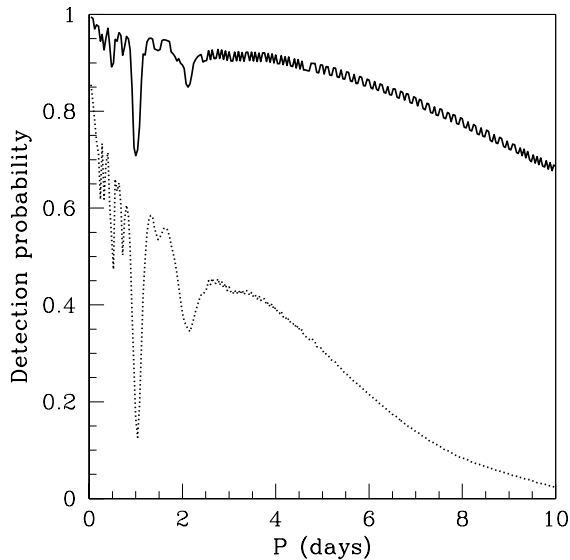


Fig. 4. Probability of detecting a binary in our observations.

our observations. The probabilities are shown in Figure 4 (the solid line for a $0.5 M_{\odot}$ companion and the dotted line – for $0.1 M_{\odot}$).

5.4. Results for M 80

Since this is a work in progress we are still unable to show a plot similar to Figure 3 for the stars observed in M 80. Nevertheless we can point out that the preliminary analysis of the first 15 stars in this cluster gives the results similar to what obtained in NGC 6752. The variations are small, the highest values being around 20 km s^{-1} . Only two RV variations exceed 15 km s^{-1} , similarly to what was observed in NGC 6752. It must be emphasized that the results on M 80 are going to be less significant than in the case of NGC 6752 both because the stars are much fainter and the errors are larger, and because strong wind from north during the observing run prevented us from observing this cluster in the first two nights, so that the detection probability is reduced. We evaluated a loss of sensitivity of

about 20–25 % for periods up to 5 days (compared to that in NGC 6752), which, for longer periods, drops rapidly to very low values.

6. CONCLUSIONS

The results shown in Figure 3 indicate that there is no close binary system in our sample, neither among cooler stars, nor among EHB targets. All the RV variations are within the estimated errors and are significantly lower than what expected. In the compilation of Morales-Rueda et al. (2003) for all field binary sdB stars with known periods, the RV semi-amplitudes are always greater than 30 km s^{-1} . These binary systems would be easily detectable in our survey. If the binary fraction of EHB stars in NGC 6752 were 69 %, as found by Maxted et al. (2001) in the field, we would expect that 13 ± 2 of our 18 stars with $T_{\text{eff}} \geq 22000 \text{ K}$ should be binaries. According to the period distribution found by Morales-Rueda et al. (2003) 80 % of them should have $P \leq 5$ days, and thus 9 ± 2 binary systems should have been detected in our sample. The absence of evidence of their presence is in sharp contrast with these previous results, and can indicate a significant difference between sdB stars in and outside globular clusters.

In conclusion, most of the EHB stars in NGC 6752, and possibly in M 80, are not close binaries. These results pose a number of problems. First of all, we are forced to conclude that the dominant mechanism for the formation of these stars in globular clusters does not involve the interactions within a close binary system. Although the high close binary fraction among field sdBs indicates that binary interactions can play an important role, our results on the EHB stars in NGC 6752 indicate that there must be other mechanisms at work.

It is possible that in GCs there are different formation channels of EHB stars with respect to the main ones in the field. For example, dynamical evolution of GCs could remove the primordial binaries able to produce sdB stars, at least in the inner part of the cluster. This is an interesting possibility, which has already been proposed also to explain why the frequency of blue stragglers (BSs) in GCs is significantly smaller than the frequency of field BSs (Piotto et al. 2004), and the anticorrelation between the frequency of BSs in GC cores and the GC total mass (Davies et al. 2004). At the same time, the GC environment can favor different formation mechanisms for the EHB stars, like close encounters and collisions among stars (at least in the cluster cores), or even more complex scenarios like the ones proposed to explain the anomalous double main sequence population in Omega Centauri (Bedin et al. 2004 and Piotto et al. 2005) and in NGC 2808 (D’Antona et al. 2005). Apparently, in these two clusters, a second generation of stars could have formed from material polluted by SNe and/or intermediate mass AGB star ejecta. These stars have an enhanced He content and could explain the presence of the EHB in both clusters.

An extended survey of the presence of close binaries among cluster EHB stars, from the inner core to the outskirts of NGC 6752, and of the presence of binaries with low companions or with longer (100 days or so) periods in NGC 6752 and other clusters with EHBs, is absolutely needed in order to test the hypothesis of the environment effects on the main production channels of these stars.

We note also that Peterson et al. (2002) reported a high fraction of binaries among the same type of stars in the same cluster, but Peterson (priv. comm.) also pointed out that their sample is mainly located in the outer regions of the cluster.

In concluding this brief discussion, we note that Napiwotzki et al. (2004) suggested that the low binary fraction among field sdBs found in their survey could be due to contamination of the sample by halo and thick disk stars, absent in Maxted et al. (2001) sample since it included only bright (thin disk) stars. On average, our cluster EHB stars are expected to be older and possibly more metal-poor than the Napiwotzki et al. sample, and apparently, the fraction of binaries among them is even smaller than among thick disk-halo sdBs, suggesting a possible dependence on ages or metallicities or on a combination of these parameters.

ACKNOWLEDGMENTS. C.M.B. and R.A.M. acknowledge support by the Chilean Centro de Astrofísica FONDAF (No. 15010003). G.P. acknowledges support by MIUR, under the program PRIN03.

REFERENCES

- Bedin L. R., Piotto G., Anderson J. et al. 2004, ApJ, 605, L125
 Behr B. B. 2003, ApJS, 149, 67
 Brault J. W., White O. R. 1971, A&A, 13, 169
 D’Antona F., Bellazzini M., Caloi V. et al. 2005, ApJ, 631, 868
 Davies M. B., Piotto G., De Angeli F. 2004, MNRAS, 349, 129
 Faulkner J. 1966, ApJ, 144, 978
 Glaspey J. W., Michaud G., Moffat A. F. J., Demers S. 1989, ApJ, 339, 926
 Han Z., Podsiadlowski P., Maxted P. F. L., Marsh T. R., Ivanova N. 2002, MNRAS, 336, 449
 Han Z., Podsiadlowski P., Maxted P. F. L., Marsh T. R. 2003, MNRAS, 341, 669
 Harris W. E. 1996, AJ, 112, 1487
 Heber U., Edelmann H., Lisker T., Napiwotzki R. 2003, A&A, 411, L477
 Heber U., Moehler S., Napiwotzki R., Thejll P., Green E. M. 2002, A&A, 383, 938
 Hoyle F., Schwarzschild M. 1955, ApJS, 2, 1
 Lisker T., Heber U., Napiwotzki R. et al. 2005, A&A, 430, 223
 Maxted P. F. L., Heber U., Marsh T. R., North R. C. 2001, MNRAS, 326, 1391
 Mengel J. G., Norris J., Gross P. G. 1976, ApJ, 204, 488
 Moehler S., Sweigart A. V., Landsman W. B., Hammer N. J., Dreizler S. 2004, A&A, 415, 313
 Momany Y., Piotto G., Recio-Blanco A. et al. 2002, ApJ, 576, L65
 Moni Bidin C., Moehler S., Piotto G. et al. 2005, A&A, submitted
 Morales-Rueda L., Maxted P. F. L., Marsh T. R., North R. C., Heber U. 2003, MNRAS, 338, 752
 Napiwotzki R., Karl C. A., Lisker T. et al. 2004, Ap&SS, 291, 321
 Peterson R. C., Green E. M., Rood R. T., Crocker D. A., Kraft R. P. 2002, in *Omega Centauri, a Unique Window into Astrophysics*, ASP Conf. Ser., 265, 255
 Piotto G., De Angeli F., King I. R. et al. 2004, ApJ, 604, L109
 Piotto G., Villanova S., Bedin L. R. et al. 2005, ApJ, 621, 777
 Recio-Blanco A., Piotto G., Aparicio A., Renzini A. 2004, A&A, 417, 597
 Tonry J., Davis M. 1979, AJ, 84, 1511

NGC 6121-V46: A LOW-MASS DOUBLE DEGENERATE ELLIPSOIDAL VARIABLE IN A GLOBULAR CLUSTER

S. J. O’Toole¹, R. Napiwotzki², U. Heber¹, H. Drechsel¹, S. Frandsen³,
F. Grundahl³ and H. Bruntt⁴

¹ *Remeis-Sternwarte Bamberg, Astronomisches Institut der Universität Erlangen-Nürnberg, Sternwartstrasse 7, D-96049 Bamberg, Germany*

² *Centre for Astrophysics Research, University of Hertfordshire, Hatfield AL10 9AB, U.K.*

³ *Department of Physics and Astronomy, University of Aarhus, Ny Munkegade, DK-8000 Aarhus C, Denmark*

⁴ *Niels Bohr Institute, Juliane Maries Vej 30, DK-2100 Copenhagen Ø, Denmark*

Received 2005 August 1

Abstract. The variable sdB known as V46 in the globular cluster M4 has remained enigmatic since its discovery almost 10 years ago. We present here radial velocity measurements obtained from medium-resolution VLT/FORS2 spectra that show variations at twice the period of the luminosity changes. This implies that the system is an ellipsoidal variable. Unlike the other sdB binaries of this nature, the fundamental parameters of this star we derive suggest that it lies below the Zero Age Extreme Horizontal Branch. From the cluster distance and the gravity we determine the mass of V46 to be $\sim 0.19 M_{\odot}$. This is too low to sustain core helium burning. From the mass function we derive a lower limit for the companion of only $0.26 M_{\odot}$. We discuss the star’s origin in the context of close binary evolution in the field and globular clusters.

Key words: stars: variable: general – stars: individual (NGC 6121-V46)

1. HISTORY AND MOTIVATION

It is now known that while the mass distribution of DA white dwarfs peaks at $\sim 0.6 M_{\odot}$, there is also a subset of objects with masses $\leq 0.46 M_{\odot}$ (Bergeron et al. 1992). Their low mass implies that they cannot ignite helium in their cores, and must have lost most of their envelope mass before reaching the tip of the red giant branch. The implication of this is that the stars must be in close binary systems, although recent results suggest that fewer than 50% show radial velocity variations (Napiwotzki et al. 2005).

There are two kinds of known binaries containing helium-core white dwarfs (HeWDs): double degenerate systems, typically containing two low-mass white dwarfs (e.g., Nelemans & Tout 2005) and millisecond pulsar (MSP) systems. In the former case the lowest mass HeWD companion known has $0.31 M_{\odot}$ (Marsh et al. 1995), while in the latter the masses are $\leq 0.2 M_{\odot}$ (e.g., Callanan et al. 1998).

Recent discoveries suggest a link between HeWDs and a small subset of sdB stars. As part of a program to measure radial velocities of sdBs, Heber et al. (2003)

discovered that the apparently normal sdB HD 188112 lies below the Zero-Age Extreme Horizontal Branch (ZAEHB). The star’s mass, determined from its trigonometric parallax, T_{eff} and $\log g$, to be only $0.24 M_{\odot}$, is inconsistent with the lowest mass for the common envelope ejection model of Han et al. (2003). HD 188112 is a radial velocity variable with a minimum companion mass of $0.73 M_{\odot}$, suggesting the primary is the progenitor of a helium core white dwarf, while the unseen companion is most likely a C/O white dwarf. Comparison with the evolutionary tracks of Driebe et al. (1998) supports this conclusion.

Since then, Liebert et al. (2004) have discovered another object lying below the ZAEHB. Comparison of the parameters of SDSS J123410.37-022802.9 (hereafter SDSS J1234) with the evolution tracks of Althaus et al. (2001) shows that this star has a mass in the range $0.18\text{--}0.19 M_{\odot}$. Note that the mass is dependent on the evolution models adopted. A higher mass is found ($\sim 0.23 M_{\odot}$) for SDSS J1234 when it is compared to the Driebe et al. tracks.

Kaluzny et al. (1997) discovered intensity variations with amplitude $\sim 1.9\%$ and period 1.045 h in the star now known as V46 in NGC 6121 (= M4). The system was a puzzle from the beginning, with colors consistent with those of a cataclysmic variable, but no emission lines present in its spectrum. Mochejska et al. (2002) found that the spectrum is consistent with an sdB star. With the discovery of pulsations in sdB stars with periods of 0.75–2 hours (Green et al. 2003), it seemed possible that V46 was a member of this class. We therefore set out to clarify the object’s nature.

2. IS IT AN EHB STAR?

A low resolution spectrum of V46 taken with the MMT was kindly provided by Janus Kaluzny. By means of Balmer line profile fitting we find $T_{\text{eff}} = 16197 \pm 546$ K and $\log g = 5.75 \pm 0.108$; the star shows no helium lines. We used Detlev Koester’s DA white dwarf grid (Finley et al. 1997) to derive these parameters. When we examine the position of V46 in the T_{eff} vs. $\log g$ plane (Figure 1), we find that it, like HD 188112 and SDSS J1234, lies below the ZAEHB. This means the star has not evolved via the EHB and strongly suggests that it too is the progenitor of a HeWD (similar to HD 188112).

If we consider the distance to the cluster M4 (2.2 kpc, Rosenberg et al. 2000) and the surface gravity of V46, we find that it should have a mass of $\sim 0.19 M_{\odot}$. In Figure 1 we show the post-RGB evolutionary tracks of Driebe et al. (1998) which suggest that V46 should have a mass of $\sim 0.195 M_{\odot}$. This is very good agreement considering the uncertainties of the model physics, and is strong evidence that the star is a member of the cluster and not a foreground object. Using the VLT we have determined the nature of this system by measuring the radial velocity of V46.

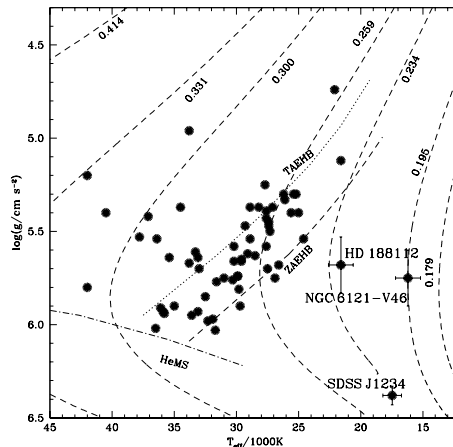


Fig. 1. Position of V46 in the T_{eff} vs. $\log g$ diagram.

3. THE NATURE OF NGC 6121-V46

We obtained 81 spectra with resolution ~ 2100 using VLT/FORS2 with the 1400V grating in service mode. The only line visible in the spectra is $H\beta$, and the resulting S/N per 4 min exposure was 10–15. We measured the radial velocity of $H\beta$ by cross correlation with a model spectrum at the temperature and gravity derived above. The velocity curve is shown at the top of Figure 2, while the power spectrum is shown at the bottom. It was calculated by fitting the curve with a range of periods using χ^2 minimization. Based on this method, we measure the period and ephemeris to be $\text{HJD}(T_0) = 2453134.496797 + 0.087159 \times E$, while the system velocity and semi-amplitude of the system are $\gamma = 31.3 \pm 1.6$ km/s and $K = 211.6 \pm 2.3$ km/s, respectively. Using this period and semi-amplitude we derive the mass function of the system to be $f(m) = 0.0855 \pm 0.0028 M_\odot$. Taking the mass of the sdB to be $0.195 M_\odot$, the minimum mass of the secondary is $0.26 M_\odot$. We note that the period of the radial velocity variation is exactly twice that of the intensity variation, indicating that V46 is an ellipsoidal variable, similar to the previously known systems KPD 0422+5421 (Koen et al. 1998) and KPD 1930+2752 (Billères et al. 2000; Maxted et al. 2000).

4. LIGHT CURVES

As well as a velocity curve, we have also obtained BVR light curves. These observations were made over April–June of 2001 to search for oscillations in red giants in M 4 (Bruntt 2003). They were obtained at the Danish 1.54 m at La Silla, Chile with DFOSC. We have attempted to determine the inclination angle of the system using a light curve analysis similar to that used for the sdB HS 2333+3927 (Heber et al. 2004). No eclipses have been detected. Due to the low amplitude of the ellipsoidal variations, the analysis is difficult. We kept the T_{eff} and mass of the sdB fixed at 16 200 K and $0.2 M_\odot$, respectively, during the analysis, but could not find a unique solution. Even fixing the mass ratio arbitrarily at, e.g. $q = 3.0$, does not help. The fits from all solutions appear identical and have very similar χ^2 values. There must be a lower limit for the inclination since at some angle the deformation of the sdB will no longer be visible. To find this limit, we first set $q = 6.0$ and then decreased it in steps of 1.0. Again no unique solution could be found, meaning that unfortunately the light curves cannot place any constraints on the system. Nevertheless we can conclude that the companion must be a white dwarf, because the variations are ellipsoidal in nature and there is no sign of a reflection effect. The latter would be expected if it were a low-mass main-sequence star.

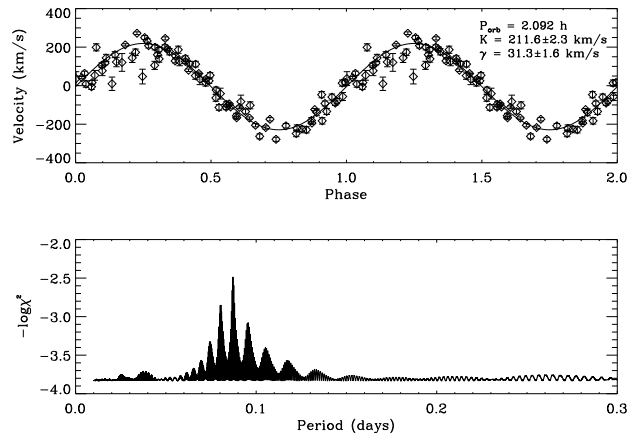


Fig. 2. Radial velocity curve and corresponding power spectrum of V46.

5. IMPLICATIONS

Despite not being able to constrain the inclination of the V46 system, we can still discuss the implications of its existence for close binary formation in globular clusters. Hansen et al. (2003) discussed low-mass HeWDs in globular clusters from a theoretical standpoint, and found that for the population of these stars in the core of NGC 6397 the companions are most likely C/O white dwarfs and not neutron stars. The likelihood of the companion of V46 being a neutron star is not high, since the inclination angle of the system would have to be $\leq 26^\circ$, and there has been no detection at radio wavelengths of any neutron star in M 4 other than PSR B1620-26 (Lyne et al. 1988). We suggest therefore that V46’s companion is either a C/O or HeWD. At the most probable inclination of 52° the mass of the companion is $\sim 0.40 M_\odot$, making it an object with a helium core. We also point out that V46 lies outside the central part of M 4; more massive objects are expected to settle towards the core of a globular cluster.

REFERENCES

- Althaus L. G., Serenelli A. M., Benvenuto O. G. 2001, MNRAS, 323, 471
 Bergeron P., Saffer R. A., Liebert J. 1992, ApJ, 394, 228
 Billères M., Fontaine G., Brassard P. et al. 2000, ApJ, 530, 441
 Bruntt H. 2003, PhD dissertation, University of Aarhus
 Callanan P. J., Garnavich P. M., Koester D. 1998, MNRAS, 298, 207
 Driebe T., Schönberner D., Blöcker T., Herwig F. 1998, A&A, 339, 123
 Finley D. S., Koester D., Basri G. 1997, ApJ, 488, 375
 Green E. M., Fontaine G., Reed M. D. et al. 2003, ApJ, 583, L31
 Han Z., Podsiadlowski P., Maxted P. F. L., Marsh T. R. 2003, MNRAS, 341, 669
 Hansen B. M. S., Kalogera V., Rasio F. A. 2003, ApJ, 586, 1364
 Heber U., Drechsel H., Østensen R. et al. 2004, A&A, 420, 251
 Heber U., Edelmann H., Lisker T., Napiwotzki R. 2003, A&A, 411, L477
 Kaluzny J., Thompson I. B., Krzeminski W. 1997, AJ, 113, 2219
 Koen C., Orosz J. A., Wade R. A. 1998, MNRAS, 300, 695
 Liebert J., Bergeron P., Eisenstein D. et al. 2004, ApJ, 606, L147
 Lyne A. G., Biggs J. D., Brinklow A., McKenna J., Ashworth M. 1988, Nature, 332, 45
 Marsh T. R., Dhillon V. S., Duck S. R. 1995, MNRAS, 275, 828
 Maxted P. F. L., Marsh T. R., North R. C. 2000, MNRAS, 317, L41
 Mochejska B. J., Kaluzny J., Thompson I., Pych W. 2002, AJ, 124, 1486
 Nelemans G., Tout C. A. 2005, MNRAS, 356, 753
 Rosenberg A., Piotto G., Saviane I., Aparicio A. 2000, A&AS, 144, 5

DO EC 14026 STARS EXIST IN CLUSTERS?

M. D. Reed¹, D. Kilkenny² and D. M. Terndrup³

¹ *Missouri State University, Springfield, MO 65804, U.S.A.*

² *South African Astronomical Observatory, Cape Town, South Africa*

³ *The Ohio State University, 140 W. 18th Avenue, Columbus, OH 43210, U.S.A.*

Received 2005 August 1

Abstract. We have began a program to search for pulsating sdB stars in open and globular clusters. Detection of pulsators in clusters would aid the understanding of their evolution, since the masses and metal content of the main-sequence progenitors would be known. Here we describe the beginning of our search during which we plan to observe about 100 sdB stars. A failure to detect any pulsators would suggest differences between sdB stars in clusters and in the field of the Milky Way (e.g., metallicity, binarity) which would need to be taken into account by any pulsation/evolution scenario.

Key words: stars: AGB and post-AGB, variable: general – clusters: individual (NGC 6791, NGC 188, NGC 6571, M 13, M 15, NGC 2808)

1. OBSERVATIONS AND ANALYSIS

To date we have observed more than 50 stars during 54 short data runs. Data were obtained for the open clusters using McDonald Observatory’s 2.1 m telescope and for the globular clusters using the MDM Observatory’s 2.4 m and the SAAO 1.9 m telescopes. All data were obtained using high-speed CCDs and processing was done using standard IRAF routines.

Differential light curves were produced using MOMF (Kjeldsen & Frandsen 1992). The accuracy of the photometry depended on several factors including the signal-to-noise (brightness) of the target and comparison stars, the number of available comparison stars, and of utmost importance for globular cluster fields, the seeing and how crowded the fields are compared to the resolution. A selection of some of the light curves and temporal spectra for sdB stars in NGC 6752 are provided in Figures 1 and 2. The dotted lines in Fig. 2 is the detection threshold discussed below.

Limits on time-series photometry can be a bit tricky as even noisy data can result in relatively flat temporal spectra (Howell 1992; Breger et al. 1994). To quantify the detection limits of our data, we used the 4σ approach of Breger et al. (1994). However, it is actually easier to detect pulsations than it might seem as during short data runs, the power can combine into unresolved peaks. (Likewise, unresolved pulsations can also cancel each other during a “beat.”) For example, the highest amplitude mode of the known pulsator Feige 48 is about 5 mma when

Table 1. Detection limits for the target stars. Column 1 gives the star designation, column 2 the 4σ limit and column 3 indicates the percentage of (24) known pulsators that would be detectable at our threshold limit.

| Target | Limit (mma) | % | Target | Limit (mma) | % | Target | Limit (mma) | % |
|--------------|----------------|----|--------|----------------|----|---------|----------------|----|
| NGC 6791 | | | | | | | | |
| B3 | 3.9 | 92 | B5 | 5.8 | 75 | B9 | 4.6 | 92 |
| B4 | 4.8 | 92 | B6 | 3.0 | 92 | B10 | 3.2 | 92 |
| NGC 188 | | | | | | | | |
| II-91 | 3.1 | 92 | D702 | 1.9 | 96 | | | |
| NGC 1904 | | | | | | | | |
| Hill11 | 3.1 | 92 | Hill34 | 3.1 | 92 | Hill70 | 1.9 | 96 |
| NGC 2808 | | | | | | | | |
| 6022 | 3.1 | 92 | 6816 | 1.9 | 96 | 6849 | 2 | 20 |
| 8750 | 3.1 | 92 | 9301 | 1.9 | 96 | 9863 | 2 | 20 |
| 14040 | 3.1 | 92 | 18899 | 1.9 | 96 | | | |
| ω Cen | | | | | | | | |
| 10123 | 3.1 | 92 | C521 | 1.9 | 96 | BC77702 | 4 | 20 |
| D16003 | 3.1 | 92 | | | | | | |
| NGC 6752 | | | | | | | | |
| S3616 | 3.0 | 92 | S23768 | 2.2 | 92 | S3936 | 2.0 | 96 |
| S3422 | 2.5 | 92 | S23665 | 2.0 | 96 | S24268 | 2.0 | 96 |
| S31695 | 3.0 | 92 | S23407 | 5.0 | 75 | S5610 | 4.5 | 92 |
| S30963 | 3.2 | 92 | S12087 | 7.0 | 58 | S23975 | 25 | 8 |
| S3008 | 2.8 | 92 | S11517 | 3.9 | 92 | S5719 | 14 | 25 |
| S29988 | 3.0 | 92 | S9135 | 3.0 | 92 | S27622 | 3.8 | 92 |
| S29704 | 2.2 | 92 | S7935 | 3.0 | 92 | S6224 | 3.3 | 92 |
| S28234 | 3.5 | 92 | S7860 | 4.3 | 92 | S28073 | 2.0 | 92 |

resolved, but typically appears close to 8 mma in nightly runs that do not resolve the pulsations. Therefore, we examined our own observations of known sdBV stars, as well as those of the literature to estimate pulsation amplitudes of known sdBV stars from 2 hour data runs. This provides two detection limits:

(1) the 4σ limit, and

(2) a “likelihood” that we would detect pulsations. The percentage of known pulsators that would be detected at our 4σ limit from a 2 hour data run (of 24 known sdBV stars). These values are given in Table 1 and show that we are far more likely to have detected pulsations, were they occurring, than to have missed them for the majority of our targets.

2. RESULTS

Though this is a work-in-progress, we have already made significant progress and achieved some success. We have observed more than half of our goal of 100 stars, but have yet to ensure that all targets have appropriate temperatures and gravities for EC 14026-type pulsators. We have also not completed our photometry and analysis, yet are already aware that some stars will not have useful detection limits. During the 2004 January SAAO observing run, we became aware that

NGC 2808 was too faint for the seeing conditions and scampered for back-up targets. These stars were chosen on the basis of color, so should be EHB stars, but may not be sdB stars. In contrast, during our 2004 July SAAO observing run, the seeing was excellent and we obtained useful limits for nearly every target star on our list.

At this point in our analysis, we have not detected any pulsating stars, but it is too early to determine how significant our non-detection is. Yet we can state with some certainty that previously suspected open cluster pulsators B5 and D702 (Yong et al. 1998; Baily 1998) do not pulsate. We also examined our data for PG 1716-type pulsations. However, our observing runs were typically too short to discern, with any accuracy, whether or not such variations exist. In no case did we detect long period variations, even though the star B4 is known to vary with a period near 19 hours; far too long for us to detect. (However, for contrast we refer readers to the paper by Kilkenny et al. (2006) where a PG 1716-type pulsator *was* detected with just 2 hours of data!)

Our efforts have been somewhat hampered by the fact that most of our targets are in the Southern Hemisphere, yet telescope time is very difficult to obtain there. The SAAO 1.9 m, though readily available and an excellent telescope, is a bit too small for most clusters while 4 m telescopes either lack appropriate instrumentation (CTIO) or are heavily constrained by queue schedules and allocation procedures (ESO).

ACKNOWLEDGMENTS. The Authors gratefully acknowledge Dr. Sabine Moehler for her finding charts for nearly all of our targets. This material is based upon work supported by the National Science Foundation under Grant No. 0307480. Any opinions, findings, and conclusions or recommendations expressed in this material are those of the author(s) and do not necessarily reflect the views of the National Science Foundation.

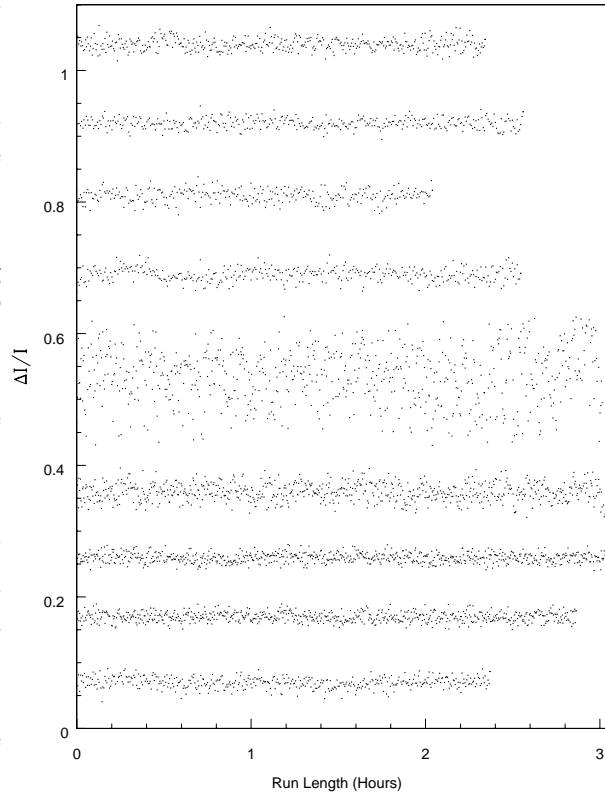


Fig. 1. Sample light curves for nine stars in NGC 6752 observed from SAAO.

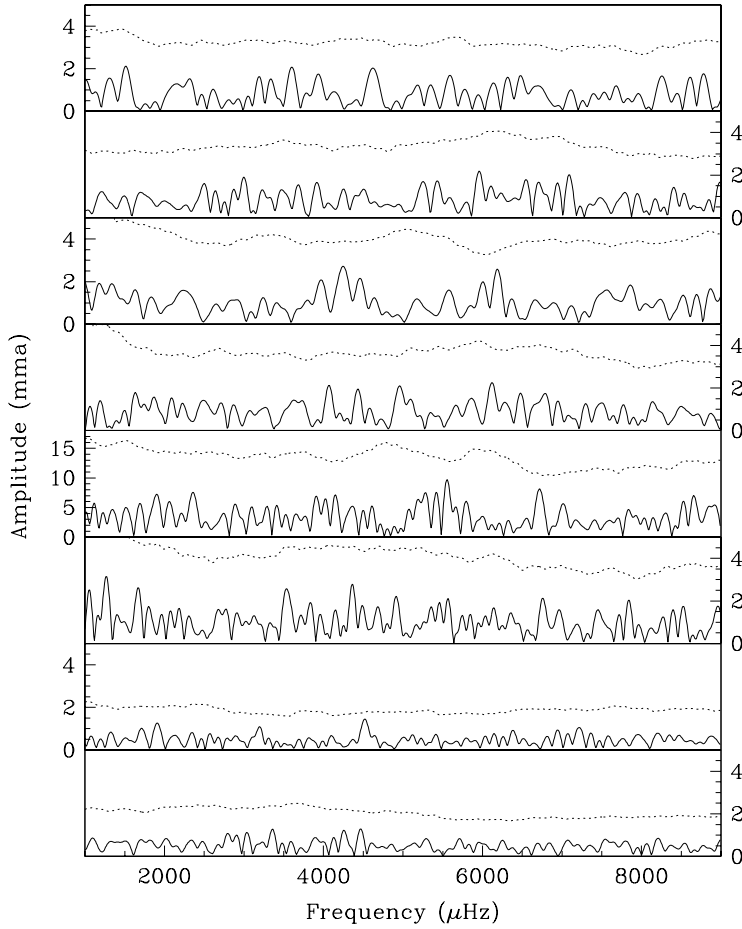


Fig. 2. Fourier transforms of the light curves in Fig. 1. Dashed lines are the 4σ detection limit.

REFERENCES

- Bailyn C. D. 1998, private communication
 Breger M., Ostermann W. M., Shi-Yang J. 1994, *A&A*, 289, 162
 Howell S. B. 1992, in *Astronomical CCD Observing and Reduction Techniques*, ed. S. B. Howell, ASP Conf. Ser., 23, 105
 Kilkenney D., O'Donoghue D., Reed M. D. et al. 2006, *Baltic Astronomy*, 15, 317 (these proceedings)
 Kjeldsen H., Frandsen S. 1992, *PASP*, 104, 413
 Yong H., Bailyn C. D., Demarque P. 1998, *BAAS*, 193.6403

HOT SUBDWARFS FROM LOW-DISPERSION SURVEYS – METHODS OF EXTRACTION AND AUTOMATIC ANALYSIS

C. Winter, C. S. Jeffery, A. Ahmad and D. R. Morgan
Armagh Observatory, College Hill, Armagh BT61 9DG, Northern Ireland

Received 2005 August 1

Abstract. We present our first attempts to construct an automatic system for extracting and analysing hot subdwarf spectra from a large set of unknown, low-resolution spectra. The first element in this system is a filtering technique, based on Principal Components Analysis (PCA), which is used to extract hot subdwarf candidates from the unknown data. We field-test the PCA filter on a test data set obtained from the SDSS, and initial results are illuminating. The second element in the system is an automatic pipeline for providing spectral classification and parameterisation of hot subdwarf candidates. Classification is carried out by an artificial neural network, and parameterisation by a χ^2 minimiser over a set of LTE model atmospheres. We combine both elements to extract and analyse a set of 282 hot subdwarf candidates obtained from the SDSS. As such, this work is the first step toward constructing a fully automated tool for analysing large data sets.

Key words: methods: data analysis – methods: numerical – stars: fundamental parameters – stars: subdwarfs – stars: Hertzsprung-Russell (HR) and C-M diagrams

1. INTRODUCTION

Modern digital sky surveys, such as the Sloan Digital Sky Survey (SDSS), are able to produce extremely large data sets which contain observations of millions of objects. To extract and process data of relevance to a particular line of research in a time-efficient manner requires the astronomer to employ automated methods to help sift through the soup of objects not necessarily of interest and then analyse any resulting candidate objects.

As such, we are attempting to construct an automated filtering tool to assist in locating hot subdwarf candidates from any set of low-dispersion spectra. These will then be submitted to an automated analysis pipeline from which classifications and physical parameterisations are derived.

The filtering tool is based around the multivariate statistical technique called Principal Components Analysis (PCA) which can be used to identify patterns in an N-dimensional data set. Our intention is to employ PCA as a coarse spectral classifier to distinguish between hot subdwarf-like objects, and objects/data of little interest, e.g., white dwarfs, QSOs, incomplete or low SNR exemplars. As a test, we apply the tool to a sample of spectra obtained from the SDSS.

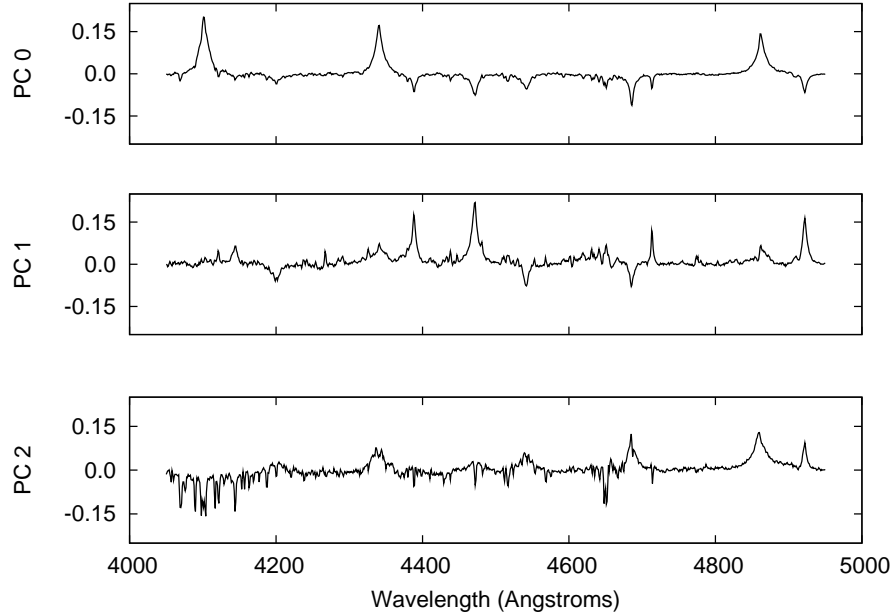


Fig. 2. First three principal components. Eigenfluxes are plotted against wavelength.

The automated analysis pipeline will allow us to gain insight into large volumes of spectra in a short amount of time. At present, the pipeline accepts a quantity of spectra, prepares them for analysis, and simultaneously feeds them to an artificial neural network (ANN), which has been trained to perform classifications using the Drilling et al. (2005) system, and a spectral optimisation toolkit which determines physical parameters by fitting each spectrum to a grid of LTE model atmospheres. Herein, we present the first application of the automated pipeline to a collection of 282 hot subdwarf candidates extracted from the SDSS with the aid of the PCA filter.

2. PRINCIPAL COMPONENTS ANALYSIS FILTER

2.1. Background

The basic idea behind PCA is to describe the variation of an N-dimensional data set in terms of a set of uncorrelated variables, each of which is a mutually-orthogonal linear combination of the original variables. Geometrically speaking, PCA is a rotation and scaling of a data set onto a new set of orthonormal vectors. The vectors (principal components) represent the directions of greatest variance in the data, and are a natural means for classifying the data set. If the first few vectors account for most of the variance in the original data, then they can be used to summarise the data with little loss of information – thus a reduction in dimensionality is achieved.

Technically, the principal components (PCs) are found by calculating the eigen-

vectors of the covariance matrix of an N -dimensional data set. A complete derivation of the technique can be found in, e.g., Murtagh & Heck (1987).

PCA has been applied on several occasions to the classification of astronomical spectra. Deeming (1964) applied the technique to stellar spectral classification, Connolly et al. (1995) used it to classify galaxy spectra, and Francis et al. (1992) applied it to the classification of quasar spectra. The dimensionality reduction capabilities of PCA have been used in conjunction with artificial neural networks, for example, Storrie-Lombardi et al. (1994).

2.2. Filter construction

We construct our PCA-based filter from the set of hot standards used in the classification system of Drilling et al. (2005). The spectra, which are at a resolution of 2.5 \AA , were velocity corrected and resampled onto a uniform wavelength grid of $4050\text{--}4950 \text{ \AA}$ at a dispersion of 1 \AA per pixel before performing the PCA. The first three of the derived PCs are shown in Figure 1. One can immediately notice that the first PC (PC 0) distinguishes between H and He lines. The second PC (PC 1) differentiates between He I and He II. This reification makes sense as it is the hydrogen and helium lines which vary most across all of the Drilling et al. (2005) spectra. Weaker lines, and uncorrelated features, such as noise, are distributed across the remaining less significant PCs. The first three derived PCs account for 69% of the variance present in the set of hot standards, and we use them to summarise the data set and to construct our filter.

If we consider the $(3 \times n)$ matrix, \mathbf{E} , of these eigenvectors, we can find the 3-dimensional projection vector, \mathbf{p} , of a spectrum projected onto the PCs by,

$$\mathbf{p} = \mathbf{x} \cdot \mathbf{E}, \quad (1)$$

where \mathbf{x} is a vector of fluxes of dimension n .

Using the projection vector, we can then derive a reconstructed version of the original spectrum, \mathbf{x}_{rec} by,

$$\mathbf{x}_{\text{rec}} = \sum_{k=1}^{k=3} p_k \mathbf{e}_k, \quad (2)$$

where p_k is the k^{th} element of the projection vector, \mathbf{p} , and \mathbf{e}_k is the k^{th} eigenvector stored in matrix \mathbf{E} . The RMS error between \mathbf{x} and \mathbf{x}_{rec} can be used to differentiate between unknown stars which are most like the Drilling et al. (2005) hot standards, and those objects which we wish to discard.

2.3. Test application

We have applied the PCA filter to a test sample of ~ 4600 spectra from the SDSS Data Release 3 database. Our selection criteria naively rely upon the classifications assigned automatically by the SDSS reduction pipeline. The SQL query used is as follows:

```
SELECT s.plate, s.mjd,s.fiberid
FROM BESTDR3.SpecPhotoAll as s
WHERE s.specClass = dbo.fSpecClass('STAR')
AND (s.primTarget & (dbo.fPrimTarget('TARGET_STAR_BHB')
+ dbo.fPrimTarget('TARGET_STAR_SUB_DWARF')) > 0)
AND (s.objType = 2)
```

Each spectrum was velocity corrected using the redshift as derived by the SDSS spectroscopic processing pipeline and stored in the FITS file header, and subsequently resampled onto the same wavelength grid as the Drilling et al. (2005) hot standards before being reconstructed by the PCA filter.

At present, the reconstruction filter is successful in filtering out objects with spectroscopic features that differ significantly from those of the hot subdwarfs, e.g., the white dwarfs in our test sample, or incomplete spectra.

The filter also allows a SNR threshold to be determined beyond which all samples can be discarded on the principle that they are too noisy for further analysis. Unfortunately, the filter does not readily allow the extraction of objects that are spectroscopically similar to subdwarfs but which contain small, yet important, differences that set them apart somehow. For instance, the test data sample, because it was selected based on the automatic classifications given by the SDSS (which are not very precise), contained many A- and F-type BHB stars which were clearly not subdwarfs because of very strong Balmer lines and the appearance of metal lines, and also other objects with weaker Balmer lines but containing the molecular G-band.

In calculating the reconstruction error of such spectra, the simple RMS error measure is not sensitive enough to allow small differences to influence the final error value in any meaningful way. The error calculation could be enhanced perhaps by introducing a weighting scheme, however, although these stars may have much in common with subdwarfs spectroscopically, they are very dissimilar photometrically and can be avoided easily by searching the SDSS by color.

3. AUTOMATED ANALYSIS PIPELINE

3.1. Outline

The input for our analysis pipeline comes from the PCA filter described in the previous section. The filter does still admit a number of false positives at this stage, so a manual inspection of the data is necessary.

Candidate spectra are subjected to a data preparation stage. The SDSS continuum fitting procedure does not do a great job in most cases, so we renormalise the calibrated spectra using a cubic spline fitting algorithm. The normalised spectra are then resampled onto a uniform wavelength grid of 4050–4950 Å, at a dispersion of 1 Å per pixel, ready for further analysis.

Classification is performed by an artificial neural network (ANN) which has been trained to classify onto the system defined by Drilling et al. (2005). This is an MK-like system which extends and refines the earlier work of Drilling (1996) and Jeffery et al. (1997) – it defines a spectral type (analogous to MK spectral classes), luminosity class and a helium class based on H, He I and He II line strengths. The ANN can classify onto this system with approximate errors (1σ) of ± 2 subtypes for spectral type, ± 1 subclass for luminosity class, and ± 4 subclasses for the helium class.

Physical parameters (T_{eff} , $\log g$, $\log(n\text{He}/n\text{H})$) are derived from candidate spectra by χ^2 fitting to a grid of LTE model atmospheres. This is performed automatically by our spectrum optimisation toolkit, SFIT2 (Jeffery et al. 2001). To accommodate the physical diversity of the hot subdwarfs, our grid of model atmospheres coarsely covers the parameter space T_{eff} : 15 000–50 000; $\log g$: 3–6; $n\text{He}$:

0.001–0.999.

3.2. SDSS data samples

We selected two samples of spectra from the SDSS Data Release 3 database. The first sample consists of all the hot standard stars used for SDSS spectrophotometric calibrations.

Our second sample was selected based on photometric colors. Although the SDSS spectroscopic processing pipeline does make an attempt to classify stellar spectra, we learned in section 2.3 that it does not do so in any great detail, so we cannot rely upon the SDSS classifications to accurately extract a complete sample of subdwarf candidates from the database. Our selection criteria are summarised in the following SQL query:

```
SELECT s.fiberID,s.mjd,s.plate
FROM BESTDR3.SpecPhotoAll as s
WHERE s.psfMag_u < 21
AND (s.psfMag_u - s.psfMag_g) < 0.7
AND (s.psfMag_g - s.psfMag_r) < -0.1
AND s.specClass <> dbo.fSpecClass( QS0 )
```

After passing all the retrieved spectra through our PCA filter, manually extracting any false positives and removing samples occurring in both data sets, we obtained a final sample of 282 hot subdwarf candidates. A summary of data set statistics is given in Table 1.

Table 1. With the combination of our PCA filter and visual selection, we were able to extract 282 unique subdwarf candidates from a total of 8171 spectra retrieved from the SDSS.

| Data set | Spectra retrieved | Candidates extracted |
|---------------|-------------------|----------------------|
| Hot standards | 1417 | 152 |
| Color-color | 6754 | 249 |
| Total | 8171 | 401 (282 Unique) |

3.3. Results

Classification and parameterisation results for the 282 SDSS spectra are presented in Figure 2. The analogues between the classification parameters and physical parameters can be clearly seen by comparing the left-hand plots with the right-hand plots in Figure 2.

We note the patterns visible in the $\log g$ vs. T_{eff} plot: the gap at approximately $T_{\text{eff}} \approx 20,000\text{K}$, $\log g \approx 4.5$; and the line extending leftwards at $\log g \approx 5.0$. We are unsure as to their nature, but the work of Green et al. (2006) discovered similar patterns from an analysis of an independent set of subdwarf stars.

An example of the model atmosphere fits and corresponding ANN classification of four stars from the sample are presented in Figure 3.

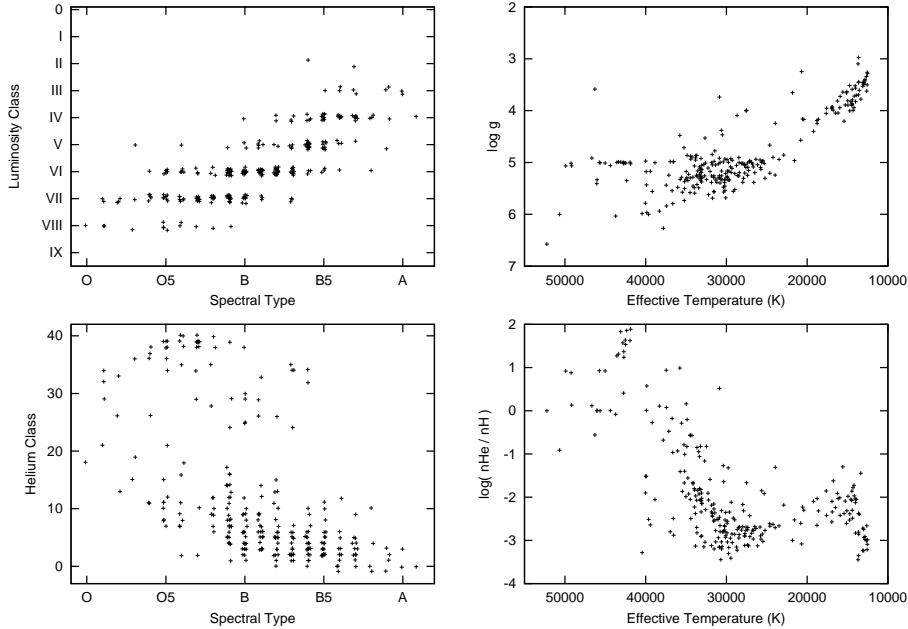


Fig. 2. Results of classifying and parameterising the 282 hot subdwarf candidates extracted from the SDSS. Classifications are presented in the two left-hand plots, with parameterisations presented in the two right-hand plots. The analogues between classification parameters and physical parameters is clearly evident.

4. FUTURE DIRECTIONS

The automatic filtering and analysis pipeline presented here is a part of what will be a more extensive system for automatic spectral analysis (see Jeffery 2003).

Given the nature of the hot subdwarfs, our use of LTE model atmospheres represents a problem for the analysis of very hot stars wherein NLTE effects become more apparent. However, our analysis pipeline can be easily extended to incorporate third-party model atmosphere codes that will allow us to address this issue in future work. We have used this study to help us refine our analysis pipeline and uncover the main hazards in dealing with large quantities of data. As we work to further improve the system, we must also tackle a number of issues, such as:

- **Data management.** Keeping track of different data sets, selection criteria, extracted candidates, their classifications and parameterisations, and maintaining general order when working with large quantities of spectra is an important task. Doing it manually is time-consuming, prone to user-forgetfulness, and can result in unfortunate industrial accidents (`rm -fr *`)¹.

- **Visualisation and interaction.** Analysing large data sets presents the problem of how to visualise thousands of spectra in a meaningful way. Also, when results have been obtained, the user must be able to produce plots and interact

¹ This is the Unix shell incantation which wipes clean the files in a user's current working directory and all its sub-directories.

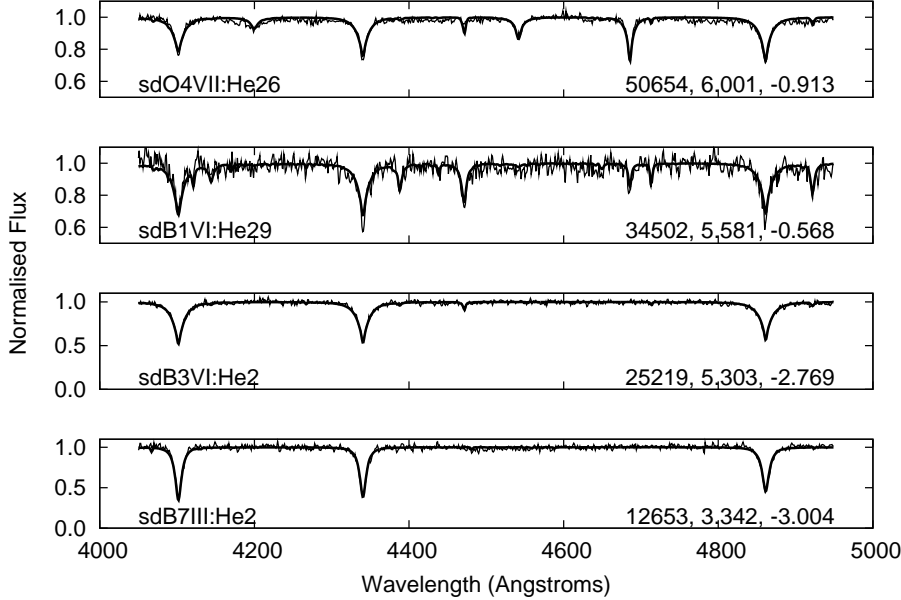


Fig. 3. A selection of stars from the set of 282 subdwarf candidates. The bottom-left of each plot details that star's spectral type as determined by the ANN, and the derived physical parameters are given at the bottom-right (T_{eff} , $\log g$, $\log(n\text{He}/n\text{H})$). The thicker line in each plot is the best-fit model determined by SFIT2.

with them such that objects of interest can be displayed, allowing the data to be explored and connections to be made.

ACKNOWLEDGEMENTS. This work was carried out as part of the Cosmo-Grid project, funded under the Programme for Research in Third Level Institutions (PRTLII) administered by the Irish Higher Education Authority under the National Development Plan and with partial support from the European Regional Development Fund.

REFERENCES

- Connolly A. J., Szalay A. S., Bershady M. A., Kinney A. L., Calzetti D. 1995, *AJ*, 110, 1071
- Deeming T. J. 1964, *MNRAS*, 127, 493
- Drilling J. S. 1996, in *Hydrogen Deficient Stars*, eds. C. S. Jeffery & U. Heber, ASP Conf. Ser., 96, 461
- Drilling J. S., Jeffery C. S., Moehler S., Heber U., Napiwotzki R. 2005, in preparation
- Francis P. J., Hewett P. C., Foltz C. B., Chaffee F. H. 1992, *ApJ*, 398, 476
- Green E. M., Fontaine G., Hyde E. A., Charpinet S., Chayer P. 2006, *Baltic*

Astronomy, 15, 167

Jeffery C. S. 2003, in *Stellar Atmosphere Modeling*, eds. I. Hubeny, D. Mihalas & K. Werner, ASP Conf. Ser., 288, 137

Jeffery C. S., Drilling J. S., Harrison P. M., Heber U., Moehler S. 1997, *A&AS*, 125, 501

Jeffery C. S., Woolf V. M., Pollacco D. L. 2001, *A&A*, 376, 497

Murtagh F., Heck A., 1987, *Multivariate Data Analysis*, Reidel, Dordrecht

Storrie-Lombardi M. C., Irwin M. J., von Hippel T., Storrie-Lombardi L. J. 1994, *Vistas in Astronomy*, 38, 331

A SPECTROSCOPIC SEARCH FOR NEW SDB STARS FROM THE GALEX SURVEY

J. Rhee^{1,2}, M. Seibert¹, R. H. Østensen³, S. K. Yi⁴, S.-C. Rey⁵, R. M. Rich⁶,
L. Bianchi⁷ and Y.-W. Lee²

¹ *Space Astrophysics Laboratory, California Institute of Technology, MC 405-47,
1200 East California Boulevard, Pasadena, CA 91125, U.S.A.*

² *Center for Space Astrophysics, Yonsei University, Seoul 120-749, S. Korea*

³ *Isaac Newton Group, E-37800 Santa Cruz de La Palma, Canary Islands, Spain*

⁴ *Department of Physics, University of Oxford, Keble Road, Oxford OX1 3RH,
U.K.*

⁵ *Department of Astronomy and Space Sciences, Chungnam National University,
Daejeon 305-764, S. Korea*

⁶ *Department of Physics and Astronomy, University of California at Los Angeles,
Los Angeles, CA 90095, U.S.A.*

⁷ *Department of Physics and Astronomy, Johns Hopkins University, Baltimore,
MD 21218, U.S.A.*

Received 2005 August 1

Abstract. We have recently initiated a systematic search for the UV-bright, subdwarf B (sdB) stars in the Milky Way. The sdB stars are core He-burning stars with very thin H envelopes and are known to be immediate progenitors of white dwarfs, but their formation mechanism is still enigmatic. For instance, it is not clear whether such objects are born as single stars or can form only in binary systems. The number ratio of sdB stars in each Galactic stellar population (i.e., thin disk, thick disk and halo) may give a clue to which of the suggested formation mechanisms dominates: the binary scenario or the RGB-peel-off scheme. This approach was hampered by the lack of identified sdB stars belonging to the thin disk and halo. Thus, it is of primary importance to find new sdB stars that are faint (halo) and lie at lower Galactic latitudes (thin disk). In this contribution, we will describe the motivation and plan for our spectroscopic survey and preliminary results based on pilot observations for 34 sdB star candidates from the GALEX All-sky Imaging Survey.

Key words: stars: early-type – stars: subdwarfs – surveys

1. INTRODUCTION

The UV bright, hot subdwarf B (sdB) stars are considered to be core He-burning stars of $0.5 M_{\odot}$ with very thin H envelopes of $M_{\text{env}} \leq 0.02 M_{\odot}$ (Heber 1986). In the Galactic field, they are characterized by H-dominated atmospheres with $T_{\text{eff}} \approx 24\,000\text{--}30\,000$ K and $\log g > 5$. Their counterparts in globular clusters are generally recognized to be extended horizontal-branch (EHB) stars found as the faint and blue tail of the horizontal-branch (HB) in clusters such as NGC 6752 and M 13. These observations suggest that the UV-bright stars might be populous

enough to account for much of the UV upturn phenomenon observed in elliptical galaxies and spiral galaxy bulges (Greggio & Renzini 1990; O’Connell 1999; Yi et al. 1999). The sdB stars are known to be immediate progenitors of low mass white dwarfs (WDs), although they consist of only a small fraction of whole sample of WD progenitors (Saffer et al. 1994). In their past, sdB stars must have experienced a core He flash and substantial mass-loss during or after the red giant branch (RGB) phase. But, it is still a mystery how the mass-loss mechanism in the sdB star’s progenitor manages to remove all but a tiny fraction of the H envelope exactly at the same time when the He core has attained the canonical sdB mass of $0.5 M_{\odot}$ required for the He flash. This project aims to study the sdB population in the Galaxy, which may shed light on their still enigmatic formation process.

2. WHY LOOK FOR “NEW” SDB STARS?

Major formation channels of sdB stars can be divided into two scenarios: (1) single sdB stars are created from the enhancement of stellar wind near the RGB tip which strips off the H envelope (D’Cruz et al. 1996), and (2) sdB stars are formed from close binary evolution with strong mass transfer by a companion (Mengel et al. 1976). Previous observational results are not in contradiction with either scenario (Maxted et al. 2001; Altmann et al. 2004). The RGB-peel-off models predict a depletion of the HB stars in the middle temperature range (HBA stars) as metallicity increases, while stars at the hot and cold ends of HB (sdB and Red HB stars) should be abundant at all metallicities. Thus, as proposed by Altmann et al. (2004), the number ratio of sdB stars in each stellar population may provide a clue to answer which formation mechanism can be dominating. If the binary scenario is the most significant process, the number ratio of sdB stars in the thin disk, thick disk and halo would be similar to that of other evolved, low-mass stars. In the RGB-peel-off scheme, sdB stars would be more dominant over HBA stars in the thin disk. Unlike the known case of HBA stars (e.g., Altmann & de Boer 2000), this approach was hampered by the lack of identified sdB stars belonging to the thin disk and halo. Therefore, it is particularly important to increase the number of identified sdB stars with faint magnitudes (halo) and at lower Galactic latitudes (thin disk), and GALEX can provide useful targets for it.

It has lately been confirmed that large He abundance variations (ΔY) among stars can not only naturally reproduce the EHB stars in ω Cen, but can also explain the large spread of FUV magnitude for the EHB stars in NGC 2808 (Lee et al. 2005). They have suggested He abundance being a third parameter which influences HB morphology of such clusters, other than metallicity and age. Spectroscopic distances of these field sdB stars will be derived from stellar radii and angular diameters: the former is based on the surface gravity measured from the spectra and a canonical mass of $0.5 M_{\odot}$, and the latter is obtained from comparing model atmosphere flux with dereddened NUV photometry. We then expect to be able to determine absolute M_{FUV} of sdB stars at an accuracy of 0.2 magnitude owing to the spectroscopic distances and GALEX FUV photometry, and thus reasonable ΔY among the sdB stars by the comparison of, if any, observed M_{FUV} spread and the predictions derived from isochrones. This would permit us to systematically obtain ΔY of sdB stars as a function of stellar population in order to study the global third parameter effect of the Galaxy.

It has been known that sdO stars have a larger scale height (≥ 1.0 kpc, Thejll et al. 1994) than sdB stars (~ 0.5 kpc, Villeneuve et al. 1995), which is inconsistent

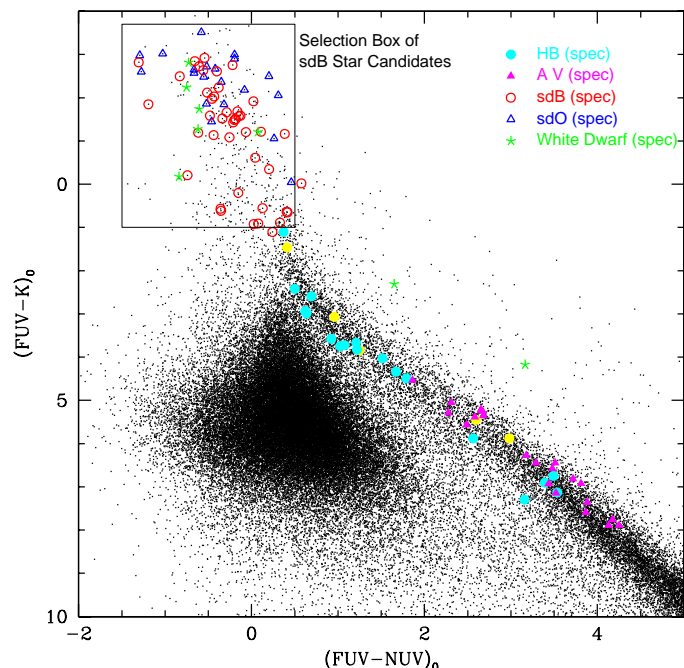


Fig. 1. GALEX AIS objects from about 1000 fields in GR1, also matched in 2MASS. Spectroscopically known *sdB/O*, WD, HB and A V stars are marked by different symbols. The *sdB* and *sdO* stars are clearly separated.

with an evolutionary connection between *sdB* and *sdO* stars. But, a larger scale height of 0.9 kpc has recently been obtained including “fainter” (but still $B \leq 16$) *sdB* stars (Altmann et al. 2004). This implies that a correct scale height can only be obtained with a sample without limiting magnitude bias.

3. CANDIDATE SELECTION

The public GALEX Release (GR1) of All-sky Imaging Survey (AIS) data was made in 2004 December. We performed cross-matching of the GALEX and 2MASS catalogs for some 3000 AIS fields ($\sim 3500 \text{ deg}^2$). As seen in Figure 1, two-color diagram efficiently separates *sdB/O* stars because the FUV-NUV color provides relatively long temperature baseline (spectral type) for hot stars, while the FUV- K_S color is useful for classification between stellar and non-stellar objects. Our empirical comparison with spectroscopically known *sdB/O* stars agrees well with the above expectation. It should be pointed out that replacing 2MASS K_S with SDSS i or USNO-B I gives a similar result, so our *sdB* candidate stars should reach apparent magnitude $\text{NUV} \approx 20$ ($B \approx 20$), four magnitudes fainter than for the Palomar Green survey (Green et al. 1986) which was one of the most extensive surveys for *sdB* star in the past. Using this method, we have selected a sample of some 1000 *sdB* star candidates over a range of depths and sky-coverages.

4. OBSERVATIONS, RESULTS AND PLANS

We have performed pilot spectroscopic observations for 34 *sdB* star candidates with the KPNO 2.1 m telescope and GoldCam, McDonald 2.7 m telescope and LCS and Lick 3.0 m telescope and KAST between 2004 June and 2005 May. Based

on the visual inspection of spectra and measurements of $D_{0.2}$ (average width of $H\gamma$ and $H\delta$ lines at 20% below continuum) and R_c (average depth of $H\gamma$ and $H\delta$ lines) employed in Beers et al. (1992), the medium-resolution (1–3 Å) spectroscopy has revealed that the sample consists of 14 sdB, 5 narrow-lined B, 8 WD, 4 HBB with He lines and 3 normal B stars. Based on the preliminary detection rate of sdB stars (14/34) and the number of our sdB star candidates ($N \geq 1000$), we expect to “newly” confirm more than 400 *bona fide* sdB stars in the halo and thin disk as well as in the thick disk. In the future, more sophisticated methods will be employed to determine stellar parameters ($\log g$, T_{eff} , and He abundance) accurately. Using observing time awarded at the CTIO 4.0 m, KPNO 2.1 m and Lick 3.0 m telescopes, we plan to complete a spectroscopic survey of some 1000 sdB star candidates by early 2006. Radial velocities determined from our spectroscopy, combined with proper motions from astrometric surveys such as UCAC2 (Zacharias et al. 2004), USNO-B (Monet et al. 2003) and future space missions (Gaia and SIM), will provide us with full space motions and thus allow us to assign population membership for the sdB stars. Indeed, this huge data set of GALEX sdB stars, which reach the entire UV visible Milky Way, will eventually help us broaden our understanding about their formation/evolution mechanism and Galactic structure.

ACKNOWLEDGMENTS. We are grateful to the referee, Sabine Moehler, for her careful review of the paper and a number of thoughtful suggestions. We gratefully acknowledge support for this work from NASA grant GALEX GI 04-0000-0096. J. R. and Y.-W. L. appreciate partial support by the Korean Ministry of Science and Technology through the Creative Research Initiative Program.

REFERENCES

- Altmann M., de Boer K. S. 2000, A&A, 353, 135
 Altmann M., Edelmann H., de Boer K. S. 2004, A&A, 414, 181
 Beers T. C., Doinidis S. P., Griffin K. E., Preston G. W., Shectman S. A. 1992, AJ, 103, 267
 D’Cruz N. L., Dorman B., Rood R. T., O’Connell R. W. 1996, ApJ, 466, 359
 Green R. F., Schmidt M., Liebert J. 1986, ApJS, 61, 305
 Greggio L., Renzini A. 1990, ApJ, 364, 35
 Heber U. 1986, A&A, 155, 33
 Lee Y.-W., Joo S.-J., Han S.-I. et al. 2005, ApJ, 621, L57
 Maxted P. F. L., Heber U., Marsh T. R., North R. C. 2001, MNRAS, 326, 1391
 Mengel J. G., Norris J., Gross P. G. 1976, ApJ, 204, 488
 Monet D. G., Levine S. E., Canzian B. et al. 2003, AJ, 125, 984
 O’Connell R. W. 1999, ARA&A, 37, 603
 Saffer R. A., Bergeron P., Koester D., Liebert J. 1994, ApJ, 432, 351
 Thejll P., Bauer F., Saffer R. et al. 1994, ApJ, 433, 819
 Villeneuve B., Wesemael F., Fontaine G., Carignan C., Green R. F. 1995, ApJ, 446, 646
 Yi S., Lee Y.-W., Woo J.-H. et al. 1999, ApJ, 513, 128
 Zacharias N., Urban S. E., Zacharias M. I. et al. 2004, AJ, 127, 3043

SEARCHING FOR THE “MISSING” PG HOT SUBDWARFS IN SDSS AND GALEX DATA

R. A. Wade¹, M. A. Stark¹, R. F. Green² and P. R. Durrell³

¹ *Department of Astronomy & Astrophysics, Pennsylvania State University, 525 Davey Lab., University Park, PA 16802, U.S.A.*

² *NOAO, P.O. Box 26732, Tucson, AZ 85726-6732, U.S.A.*

³ *Department of Physics and Astronomy, Youngstown State University, Youngstown, OH 44555-2001, U.S.A.*

Received 2005 July 28

Abstract. Many EHB stars have been found in short-period binaries, where the companions in these post-common envelope systems are either white dwarfs or dM stars; these systems are catalogued as hot subdwarfs because the subdwarf is the more luminous component. Hypothesized Roche-lobe overflow systems (with more massive companions) may largely be uncatalogued, since the G band or Ca II K line from the companion may have caused them to be overlooked or discarded. In particular, many candidate objects were excluded from the PG catalog because of such spectroscopic indicators. Could these rejects include large numbers of “missing” hot subdwarfs? We have examined 2MASS, SDSS and GALEX archival data for large subsets of these rejected stars and conclude that only a handful (about 3%) show indications of binarity; most are consistent with (single) metal-poor F stars, as was originally supposed.

Key words: binaries: close – stars: horizontal-branch – ultraviolet: stars

1. HYPOTHETICAL “MISSING sdB” STARS

Binary population synthesis (BPS) models suggest that many core-helium burning, thin hydrogen envelope objects (“sdB stars”) are not yet discovered, hidden in binary systems with luminous (non-degenerate) relatively cool companions. The existing catalogs of sdB stars would therefore be significantly biased, and a clear picture of the true situation regarding formation and current population of sdB stars is lacking. It is desirable to learn whether these proposed hidden populations of sdB stars actually exist.

It has been suggested (Han et al. 2002, 2003) that the stars that were rejected from the Palomar-Green (PG: Green, Schmidt & Liebert 1986, GSL86) survey for ultraviolet-excess (UVX) objects are a potential rich source for some types of these. During the PG survey, candidate UVX objects were those with (transformed) $U-B < -0.46$. Because of the large errors in $U-B$, $\sigma \approx 0.38$, the color selection was supplemented by classification spectroscopy, for more accurate temperature information. Many candidate UVX targets were indeed excluded from the final

PG catalog, because their spectra showed the CaII K line (or the G band) in absorption. These rejected K-line stars were inferred to be metal-poor subdwarf F or G stars that crept into the candidate list owing to a combination of low metal-line blanketing and photometric errors.

In the alternative BPS view, these “PG-rejects” could be binaries containing sdB or sdO stars. The cool star would contribute a K line and make the blended $U-B$ color marginal for the PG color criterion, giving a result similar to a metal-poor subdwarf. In this interpretation, therefore, the PG-rejects actually belong in the PG catalog, and moreover would constitute important evidence in favor of certain binary formation channels for sdBs.

2. THE SAMPLE OF REJECTED (K-LINE) STARS

Here we use broad-band photometry over extended wavelength ranges to assess two large subsamples from the list of PG rejects. This allows the spectral energy distribution of a composite hot+cool system to be distinguished from that of a single star. From the master catalog of 1125 PG-rejects (RW & RFG, in preparation), we found 291 stars that are present in both the Two-Micron All-Sky Survey (2MASS) Point Source Catalog and the Sloan Digital Sky Survey (SDSS) DR2 survey region, and we identified 103 stars that have GALEX observations accessible in the first Data Release. These samples are almost completely non-overlapping.

3. THE SDSS/2MASS DATASET: COLOR-COLOR DIAGRAMS

Of the 291 K-line stars that overlap 2MASS/SDSS, we consider here the 173 stars with Sloan r magnitudes in the range 14.00 to 16.00 (median $r = 14.86$) that have non-flagged (unsaturated) magnitudes in at least 4 of the 5 passbands of the SDSS ($ugriz$) photometric system (136 have all 5 optical magnitudes). All of these 173 stars have detections in the 2MASS J , H and K_s bands.

We plotted the 173 K-line stars in both $g-r$ vs. $u-g$ and $r-K_s$ vs. $g-r$ diagrams, along with 199 PG stars that have been classified as hot subdwarfs. We compared these with loci for the Population I main sequence, metal-poor main sequence and metal-poor giants (representing horizontal branch stars). We also considered three sequences of composite (binary) models. These combine the light from a hot subdwarf star ($T_{\text{eff}} = 25\,000$ K, $30\,000$ K and $35\,000$ K; M_V derived from the zero-age EHB calculations of Caloi 1972) with the light from a cool main-sequence (MS) companion. These sequences emerge from the hot end of the stellar locus (faintest, coolest companions at this end), loop away from the single-star locus, and then loop back to meet the stellar locus at a (single-star) $T_{\text{eff}} \approx 10\,000$ K. At this end, the ‘cool’ (A or F star) companion dominates.

In these diagrams, the recognized PG hot subdwarfs and the K-line PG-rejects are very different groups of stars. In this sense, the spectroscopy carried out by GSL86 succeeded in improving on the photographic $U-B$ color selection. Some catalogued PG hot subdwarfs clearly are composite objects (Stark & Wade 2003; Reed & Stiening 2004). Most PG-reject stars, however, are consistent with being single stars, just as they were interpreted to be by GSL86. Except for a few outliers, they are not EHB+MS binary systems.

4. FITTING THE PG-REJECT STARS AS SINGLE STARS

We fitted the observed magnitudes for the 173 stars with model magnitudes, derived from the synthetic photometry done by the Padova group (Girardi et al. 2002, 2004). We considered all Padova models with T_{eff} in the range 4000–50 000 K, $4.0 < \log g < 5.0$ and metallicities between solar and $[M/H] = -2.5$.

For each of the 173 stars, we scaled each model in brightness to find the best fit. We chose as the best overall model, the one that gave the smallest reduced chi-square statistic, χ_{ν}^2 . Seven outliers have either large χ_{ν}^2 or unusual T_{eff} or $\log g$. All of the remaining 166 PG-rejects can be fitted as single stars with T_{eff} in the range 5000–7100 K. The χ_{ν}^2 values for these 166 non-outliers are acceptably small, given our present understanding of the SDSS error estimates, our neglect of interstellar reddening, etc. Most of these stars (136 of 166) are preferably fitted with low-metallicity models, $[M/H] = -1.0$ or below, consistent with the GSL86 interpretation that these are metal-poor F and G subdwarfs.

Two of the outliers have SDSS spectra. They show Mg Ib, Na D and Ca II infrared triplet absorption, but the continua are blue. Both stars lie among the composite models in the color-color diagrams. A plausible model for the first is a 30 000–35 000 K hot subdwarf plus a $T_{\text{eff}} \approx 6000$ K MS star. A plausible model for the second outlier is a $\sim 30\,000$ K hot subdwarf plus a $T_{\text{eff}} \sim 7500$ K MS star. The other outliers lie either close to the hot single-star locus or the sequences of composite models; one may be a blue horizontal branch star.

5. THE GALEX DATASET

The GALEX photometry is in two bands, far- and near-ultraviolet (F and N), with $\lambda_{\text{eff}} = 1528 \text{ \AA}$ and 2271 \AA . Figure 1 is a two-color diagram, with models of single and composite stars shown (synthetic photometry from Kurucz models). At the hot (upper left) end we show the observed colors of six known EHB stars (three of these are in binary systems, based on their 2MASS colors). We also found GALEX observations for a number of well-observed ($V \sim 9$) metal-poor single stars near $T_{\text{eff}} = 6000$ K, and thus determined that the locus for such stars actually lies higher than the model line shows, by about 1–2 mag in $F-N$.

Of the 103 PG-rejects that were observed by GALEX, only twelve were detected in both FUV and NUV bands. We derived limits on $F-N$ for the rest (assuming $F > F_{\text{lim}} = 19.9$). We plot 24 limits in Figure 1; the other 67 systems have similar locations in the figure and are omitted to reduce confusion. Only three of the 103 stars show far-UV flux consistent with the presence of a hot star; the rest are consistent, given the errors and limits, with single cool stars. All of the “hot” detections have red $J-K_s$ colors from 2MASS, so these stars are composite. (One of the three “hot” cases, at $N-V \approx 5.1$ and $F-N = 3.0$ is not an EHB+MS binary but can be modeled as a $T_{\text{eff}} \approx 30$ kK WD+dG system.)

6. SUMMARY

A few objects ($\sim 3\%$) in our sample of PG-reject stars may plausibly be binary systems that include a hot subdwarf star as a member. The vast majority of the PG-reject stars, however, are sufficiently modeled as single stars, consistent with their being the metal-poor sdF and sdG contaminants that GSL86 were guarding against. The color-color sequences of sdB + cool (MS) star binaries are

well separated from the observed colors of the PG-reject stars in both the optical vs.infrared plane and the optical vs. ultraviolet plane. There is no compelling evidence for large numbers of additional hot subdwarf stars hiding in binaries that were rejected from the PG catalog.

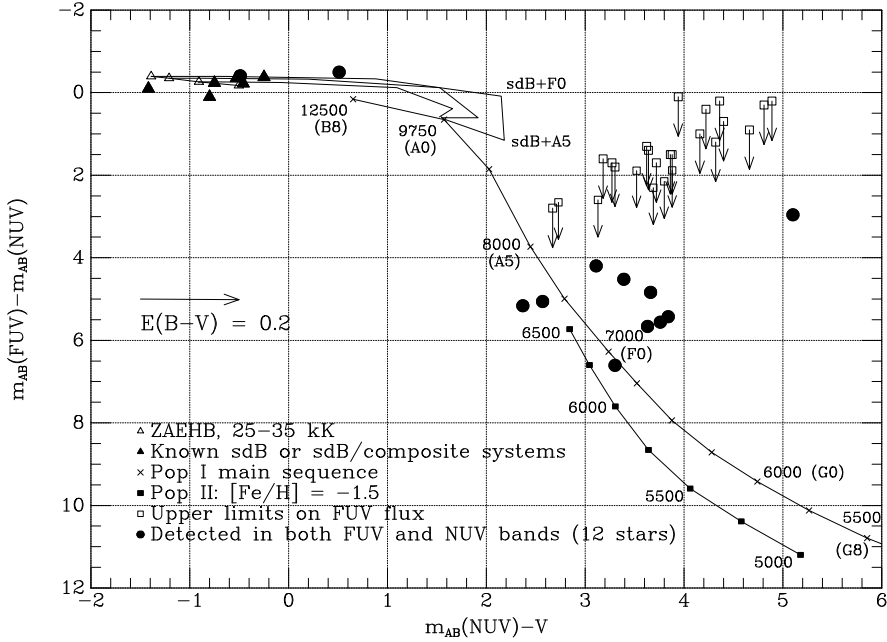


Fig. 1. GALEX and visible two-color diagram.

ACKNOWLEDGMENTS. We made use of SDSS Data Release 2, the 2MASS, GALEX Data Release 1, the USNO-A2 catalog, and SIMBAD. Supported in part by Sigma Xi, NASA grants NAG5-9586 and NGT5-50399, and the Pennsylvania Space Grant Consortium.

REFERENCES

- Caloi V. 1972, *A&A*, 20, 357
 Girardi L. et al. 2002, *A&A*, 391, 195
 Girardi L, Grebel E. K., Odenkirchen M., Chiosi C. 2004, *A&A*, 422, 205
 Green R. F., Schmidt M., Liebert J. 1986, *ApJS*, 61, 305 (GSL86)
 Han Z., Podsiadlowski Ph., Maxted P. F. L., Marsh T. R., Ivanova N. 2002, *MNRAS*, 336, 448
 Han Z., Podsiadlowski Ph., Maxted P. F. L., Marsh T. R. 2004, *MNRAS*, 341, 669
 Reed M. D., Stiening R. 2004, *PASP*, 116, 506
 Stark M. A., Wade R. A. 2003, *AJ*, 126, 1455

THE SUBDWARF DATABASE: RELEASED

R. H. Østensen

Isaac Newton Group, Apartado 321, E-38700 Santa Cruz de La Palma, Spain

Received 2005 August 15

Abstract. The work on the Subdwarf Database, presented at the previous meeting, has been completed, and the tool is now publicly available. The first release contains data from close to 240 different literature sources, but more still awaits entry. The database interface includes advanced search capabilities in coordinate, magnitude and color space. Output tables can be generated in HTML with hyperlinks to automatically generated finding charts, the Aladin viewer and a detailed data sheet that displays all registered data for each target, including physical data such as temperature, gravity and helium abundance, together with a finding chart. Search results can be visualized automatically as interactive position, magnitude or color diagrams.

Key words: stars: hot subdwarfs – catalogs – surveys

1. INTRODUCTION

As presented at the last subdwarf meeting (Østensen 2004) a database has been designed and implemented based on the data in The Catalogue of Spectroscopically Identified Hot Subdwarf Stars (or the Subdwarf Catalogue, for short: Kilkenny et al. 1988) and its updates. This list contains more than 2300 unique hot subdwarf stars.

The database runs under MySQL¹ with interfaces in Perl for uploading and linking together the database entries. The WWW interface uses HTML forms and PHP².

2. WHAT'S NEW

In the past year the whole database has been completely redesigned. The first implementation was merely a searchable version of the original electronic table, but it soon became evident that there was a major problem with this simple solution. For instance, the table allows space for a small number of different classifications and several photometry entries, but there was no way to distinguish between the quality of two measurements of the same object. This applies both to photometric data, classifications and physical data.

¹ MySQL (www.mysql.com) is an open source database.

² PHP (www.php.net) is a script language can produce HTML documents. The PHP code is interpreted when a page is requested, allowing the server to generate HTML in real time.

Fig. 1. The Subdwarf Database Search Form.

Obviously, if a particular object is observed and classified by several different authors, the reliability of the respective classifications will depend on the quality of the observations. If a classification entry was accompanied by a quality indicator, the system would be able to automatically adopt the classification with the highest quality flag, and thus vastly improve the reliability of the entries in the database. Thus, a scheme was implemented where a quality indicator of 1 signifies a photometric classification, a 2 signifies a classification based on a low resolution photographic spectrum, a 3 signifies a low to intermediate resolution spectrum (3–15 Å) – typically a photoelectric scan, a 4 signifies an intermediate resolution spectrum (1–3 Å) – typically a CCD observation in the blue part, and so on.

With this scheme in place it is easy to distinguish between reliably classified objects, and objects with dubious classifications. Also, for the photometric data in the database, it was decided that all entries must be accompanied by an error bar – either a one sigma error estimate provided by the observer, or at the very least a crude estimate based on the technique applied. Furthermore, the system is now able to convert magnitudes from photometric systems like the *Strömgren* system or *SDSS* magnitudes to Johnson *UBVRIZ* with reasonable precision and while maintaining realistic error estimates. It will then load the *UBVRIZ* magnitudes with the lowest error estimates available into the searchable database, regardless if this is an observed or derived magnitude. The database also contains *Strömgren*, *SDSS* and 2MASS *JHK* magnitudes, but these are never derived by conversion.

Your query matches 27 stars.

| Name | RA | Dec | Class | Q | U | B | V | R | I | Z | b-y | c1 | m1 |
|--|-------------|--------------|------------|---|-------|-------|-------|-------|-------|---|--------|--------|--------|
| <input type="checkbox"/> PG 0044+097 | 00:47:29.21 | 09:58:55.70 | sdB | 4 | 9.16 | 10.03 | 10.27 | 10.40 | 10.52 | - | -0.092 | 0.092 | 0.118 |
| <input type="checkbox"/> BD+37 442 | 01:58:33.43 | 38:34:23.82 | sdO | 2 | 8.55 | 9.70 | 9.98 | - | - | - | - | - | - |
| <input type="checkbox"/> PHL 1532 | 03:25:35.92 | -20:20:03.54 | sdB? | 1 | 9.27 | 10.00 | 10.34 | - | - | - | -0.072 | 0.185 | 0.122 |
| <input type="checkbox"/> HDE 283048 | 03:53:13.71 | 25:45:21.84 | sdO+F? | 3 | - | - | 10.30 | - | - | - | - | - | - |
| <input type="checkbox"/> CD-44 2920 | 06:48:04.69 | -44:18:58.49 | sdO | 3 | 6.83 | 7.99 | 8.28 | 8.39 | 8.54 | - | -0.139 | -0.220 | 0.067 |
| <input type="checkbox"/> CD-23 4585 | 06:55:18.22 | -23:32:16.58 | sdB | 3 | 8.64 | 9.20 | 9.52 | - | - | - | -0.059 | 0.416 | 0.112 |
| <input type="checkbox"/> BD+34 1543 | 07:10:07.68 | 34:24:54.29 | sdB+F | 3 | - | - | 9.40 | - | - | - | - | - | - |
| <input type="checkbox"/> BD-3 2179 | 08:02:14.88 | -03:58:16.20 | sdO | 5 | 8.86 | 10.00 | 10.36 | - | - | - | -0.132 | -0.184 | 0.057 |
| <input type="checkbox"/> FB 49 | 08:10:49.47 | 74:57:57.80 | He-sdO | 4 | 7.26 | 8.47 | 8.90 | - | - | - | -0.158 | -0.233 | 0.048 |
| <input type="checkbox"/> CD-45 5068 | 09:20:34.00 | -45:35:20.29 | sdB | 3 | 9.35 | 9.59 | 9.62 | 9.62 | 9.63 | - | 0.007 | 0.759 | 0.113 |
| <input type="checkbox"/> BD+37 1977 | 09:24:26.38 | 36:42:53.29 | sdO | 3 | - | - | 9.20 | - | - | - | - | - | - |
| <input type="checkbox"/> HD 100340 | 11:32:49.93 | 05:16:36.20 | sdB? | 1 | 8.83 | 9.77 | 10.13 | - | - | - | -0.100 | -0.017 | 0.088 |
| <input type="checkbox"/> BD+10 2357 | 11:55:56.65 | 09:50:49.09 | sdO+A | 3 | 8.22 | 8.81 | 8.87 | - | - | - | 0.078 | 0.146 | 0.097 |
| <input type="checkbox"/> BD+49.2226 | 13:33:59.29 | 48:46:07.51 | sdB | 3 | - | - | 10.28 | - | - | - | 0.010 | - | - |
| <input type="checkbox"/> EC 14295-2226 | 14:32:21.49 | -22:39:25.59 | sdO | 3 | 8.58 | 9.76 | 10.03 | 10.14 | 10.31 | - | -0.113 | -0.206 | 0.050 |
| <input type="checkbox"/> BD+19 2824 | 14:35:15.78 | 19:12:54.50 | sdO+G | 4 | 7.90 | 8.75 | 8.54 | - | - | - | - | - | - |
| <input type="checkbox"/> PG 1631-039 | 16:34:23.32 | -04:00:51.99 | sdOB | 4 | 7.58 | 8.66 | 8.94 | 9.06 | 9.20 | - | -0.137 | -0.150 | 0.088 |
| <input type="checkbox"/> BD+39 3226 | 17:46:31.90 | 39:19:09.09 | He-sdO | 3 | 8.71 | 9.92 | 10.21 | - | - | - | - | - | - |
| <input type="checkbox"/> CD-23 14002 | 18:09:51.62 | -23:36:51.32 | sdB? | 1 | 9.51 | 10.13 | 9.87 | - | - | - | 0.223 | -0.008 | -0.001 |
| <input type="checkbox"/> CD-23 14565 | 18:37:56.68 | -23:11:35.19 | sdB | 4 | 8.54 | 9.49 | 9.86 | - | - | - | -0.100 | -0.036 | 0.091 |
| <input type="checkbox"/> BD-06 5221 | 19:39:38.81 | -06:03:49.44 | sdB+K0III | 4 | - | - | 8.10 | - | - | - | - | - | - |
| <input type="checkbox"/> CD-28 16258 | 19:54:31.39 | -28:20:20.90 | sdB+? | 4 | 9.19 | 9.99 | 10.18 | 10.27 | 10.39 | - | -0.101 | 0.090 | 0.129 |
| <input type="checkbox"/> Saturn Nebula | 21:04:10.83 | -11:21:48.49 | sd | 1 | 8.99 | 9.30 | 8.84 | 10.01 | 10.84 | - | - | - | - |
| <input type="checkbox"/> FB 178 | 21:39:10.60 | -46:05:51.50 | sdB | 4 | 9.01 | 9.95 | 10.18 | 10.30 | 10.43 | - | -0.114 | 0.016 | 0.090 |
| <input type="checkbox"/> FB 179 | 21:59:42.00 | 26:25:57.78 | sdO | 2 | 8.27 | 9.43 | 9.69 | - | - | - | -0.125 | -0.176 | 0.040 |
| <input type="checkbox"/> BD-3 5357 | 22:00:36.40 | -02:44:26.80 | sdOB+G8III | 3 | 10.12 | 9.98 | 9.33 | 8.95 | 8.57 | - | - | - | - |
| <input type="checkbox"/> FB 180 | 22:34:04.57 | -12:09:29.59 | sdB | 2 | 8.44 | 8.91 | 9.03 | - | - | - | -0.031 | 0.558 | 0.084 |

Check All Uncheck All Re-tabulate Plot Show details

Done

Fig. 2. Sample output from a magnitude limited search in the Subdwarf Database.

3. A FLEXIBLE INPUT FORMAT

Instead of the old system where the database merely reflected the entries in an electronic table with a fixed number of columns, the new system allows free format tables. Each data file under the new scheme contains information from one (or a related set of) publications with standardized tags to identify authors, title and a reference code. After a valid reference is given, each line contains data on one object in a format that specifies a list of names identifying the object followed by a colon and a list of data entries. The data entries are given in the form of a comma separated list of tag-value associations. Errors or quality flags are provided either on a separate line for all entries in the file, or as a number in brackets after each data value.

When the database is initialized, each data file is parsed and the data loaded

Subdwarf DB: Data sheet - Mozilla Firefox

File Edit View Go Bookmarks Tools Help

http://www.ing.iac.es/~roy/sdbs/catent.php

Subdwarf Database: Data sheet

DB Name: PG 0900+400

Simbad Name: PG 0900+400

Class: HeB+G

Coordinates (J2000): 09:03:19.45 +39:51:00.42

UBVRI Photometry: U=12.140 B=13.100 V=12.870
R=- I=12.290 Z=-

Strömgren Photometry: Not available

2MASS IR Photometry: Not available

SDSS Photometry: Not available

Aliases: BPS BS 16468-13, FBS 0900+401, PG 0900+401, FBS B 59, BI Lyn, V* BI Lyn, PG 0900+400



Show Aliases Photometry Classifications Physical data

Photometry for PG 0900+400:

| Data | Value | Error | Reference |
|------|--------|--------|---------------------|
| m_pg | 12.800 | ±0.500 | 1990Afz....32...29A |
| VI | 0.580 | ±0.030 | 1984ApJ...287..320F |
| BV | 0.230 | ±0.030 | 1984ApJ...287..320F |
| UB | -0.960 | ±0.030 | 1984ApJ...287..320F |
| V | 12.870 | ±0.100 | 1984ApJ...287..320F |
| m_pg | 12.840 | ±0.290 | 1986ApJS...61..305G |

Classifications for PG 0900+400:

| Class | Quality | Reference |
|--------|--|---------------------|
| HeB+G | 5 = Spectroscopic class, 0.8-2 AA res, blue and red | 2001A&A...378..936J |
| sdB+K | 4 = Spectroscopic class, 1-3 AA res, blue part | 2001A&A...368..994A |
| CV | 2 = Spectroscopic class, photographic (low res) | 1990Afz....32...29A |
| sdB+K3 | 4 = Spectroscopic class, 1-3 AA res, blue part | 1984ApJ...287..320F |
| Bin | 3 = Spectroscopic class, photoelectric scan (3-15AA res) | 1986ApJS...61..305G |

Physical data for PG 0900+400:

| Data | Value | Error | Reference |
|------|-------|---------|---------------------|
| logg | 3.6 | +/-0.1 | 2001A&A...378..936J |
| Teff | 28600 | +/-1000 | 2001A&A...378..936J |
| logg | 5 | +/-0.3 | 2001A&A...368..994A |
| Teff | 25000 | +/-925 | 2001A&A...368..994A |
| Teff | 31000 | +/-5000 | 1984ApJ...287..320F |

Done

Fig. 3. Sample data sheet from the Subdwarf Database. Different observers have given many different classifications for this composite system.

into a number of database tables. The list of object names are loaded into one table, and coordinates, classifications, references and physical data are loaded into separate tables. Each entry is associated with its reference code, and there is no longer any limit on the number of entries for the same object.

After all available data files have been loaded into the set of database tables,

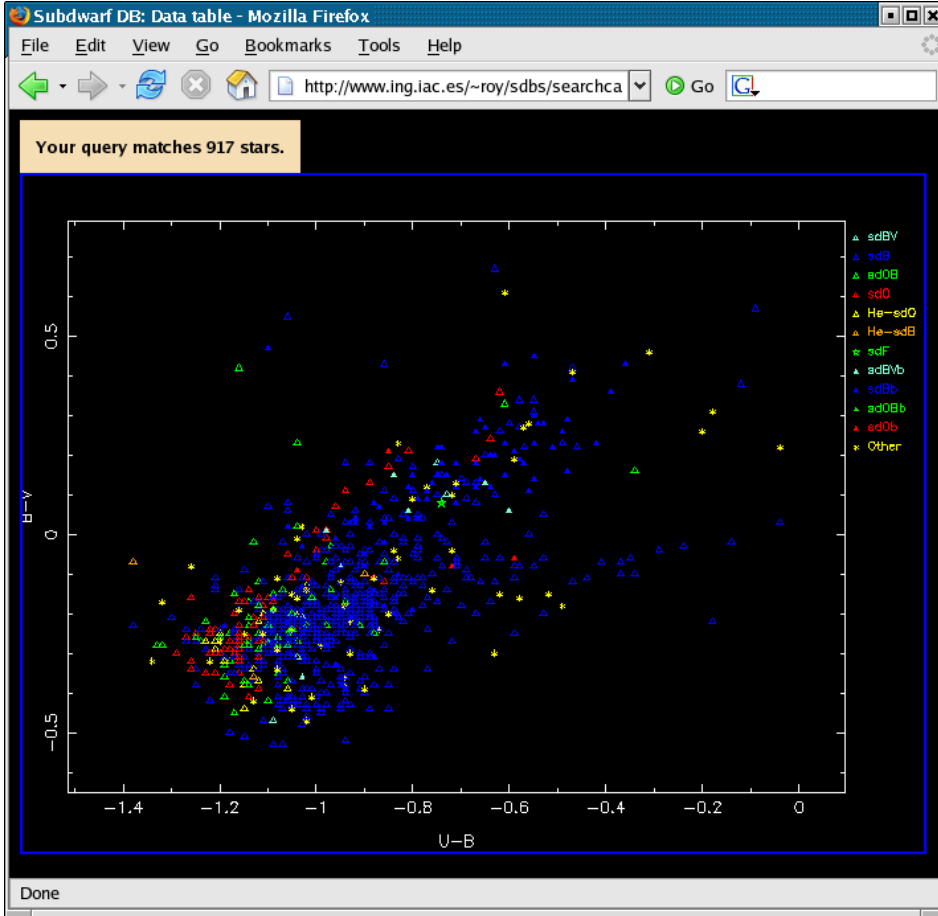


Fig. 4. A color-color plot auto-generated from the database with set limits on photometric quality. The plot is interactive in the sense that moving the pointer over a symbol will show the name of the star, and clicking on a symbol will produce the data sheet for that object.

a table containing compiled data is constructed. The script that does this job searches the table of classifications for entries of hot subdwarf stars. This list is then cross-checked so that each entry has a pair of valid coordinates associated with it. For each entry, all classifications and photometric data are loaded from the respective tables, derived magnitudes are computed, and only the best values are loaded into the compiled database. The entry that is created may actually not be that of a subdwarf star. All stars that have at one time been classified as a hot subdwarf star will be registered in the database, but the classification recognized is the one with the highest quality flag (e.g., Figure 3).

4. TO DO

The released database contains all the 146 references from the original Subdwarf Catalogue, with the exception of a few references that I have not been able to

access. About 100 additional sources have been added to this collection, but this is still far away from exhausting the available sources. Many more papers still need to be recognized, and their data must be entered into tables. This is a work that can hardly ever be completed, and in order for the situation to improve, I will have to rely on people sending me notifications of old papers that have been missed as well as new papers being released. It would also be a great help if authors could provide electronic tables of their data that I can convert to the database format, thereby avoiding introducing further typing errors to the collection of discrepancies that already exist. If you spot any, please let me know.

The database is currently hosted at <http://www.ing.iac.es/~roy/sdbs/>. A more permanent home is being sought.

REFERENCES

- Kilkenny D., Heber U., Drilling J. S. 1988, SAAOC, 12, 1, with updated electronic edition (1992)
Østensen R. H. 2004, Ap&SS, 291, 263

SUBLUMINOUS O STARS

U. Heber¹, H. Hirsch¹, A. Ströer¹, S. O’Toole¹, S. Haas¹ and S. Dreizler²

¹ *Remeis-Sternwarte Bamberg, Astronomisches Institut der Universität Erlangen-Nürnberg, Sternwartstrasse 7, D-96049 Bamberg, Germany*

² *Institut für Astrophysik, Georg-August-Universität Göttingen, Friedrich-Hund-Platz 1, D-37077 Göttingen, Germany*

Received 2005 August 1

Abstract. We report results of spectral analyses of sdO stars selected from the Supernova Ia Progenitor Survey, the Hamburg Quasar Survey and the Sloan Digital Sky Survey and based on state-of-the-art NLTE model atmospheres. By combining the sdO with the sdB samples we discuss trends of the atmospheric parameters in order to search for evidence for possible evolutionary linkage. The He-sdO stars are found to cluster near $T_{\text{eff}} = 45\,000$ K, $\log g = 5.5$, whereas the number of sdO stars in this area is very small. The “cooler” sdO stars seem to form an extension to the sdB sequences. A couple of sdO stars are obviously evolved from the extended horizontal branch and reach temperatures as high as 80 000 K. We conjecture that the He-sdO stars and sdO/sdB stars have a different evolutionary origin. This is corroborated by the much lower binary frequency of the former. Strong enrichments of iron group elements are discovered for hydrogen-rich sdO stars as well as for sdB stars from high resolution UV spectra and have severe implications for the temperature scale. We finally highlight the discovery of a hyper-velocity He-sdO star with a radial velocity of 708 km s^{-1} unbound to the Galaxy.

Key words: stars: hot subdwarfs – stars: helium – stars: atmospheres

1. INTRODUCTION

Ever since the field has been introduced by Greenstein & Sargent (1974), the helium-rich sdO stars were believed to be linked to the evolution of the hydrogen-rich subluminoous B stars. Any evolutionary link between subluminoous B and O stars, however, is difficult to explain since the physical processes driving a transformation of a hydrogen-rich star into a helium-rich one remain obscure. The convective transformation has been explored by Wesemael et al. (1984) as well as by Groth, Kudritzki & Heber (1985). While the former found helium convection to occur even at subsolar helium abundances which mixes helium from deeper layers into the photosphere, the latter concluded that a helium driven convection zone develops only in helium-rich atmospheres. If the latter is true, convective transformation would not work.

Several evolutionary scenarios for subluminoous O stars have been suggested: invoking either a delayed helium core flash or merging of white dwarfs. In the *late hot flasher scenario* the core helium flash occurs when the star has already left the RGB and is approaching the white dwarf cooling sequence (delayed He core flash). During the flash, He and C are dredged-up to the surface (Sweigart 1997).

The merger scenario is favored by binary population synthesis models and has met with some success to explain the origin of subluminescent B stars. Merging of two helium core white dwarfs will result in helium main sequence stars with masses between $0.3 M_{\odot}$ and $0.9 M_{\odot}$. It has been proposed that some of the subluminescent O and B stars may form through this channel (Webbink 1984). Recently detailed population synthesis models have been calculated by Han et al. (2003) which demonstrate, that a significant fraction of sdB stars can indeed form either through mass exchange or through merging of two Helium white dwarfs. The first mass exchange episode (on the RGB) results in sdB stars with a main sequence companion, while after the second mass exchange a white dwarf companion forms. After correcting for selection effects birthrates are predicted. The models predict rather high birth rates for mergers, which in some case even exceed the birthrate of sdB-white dwarf binaries.

Whether or not the merger scenario is applicable to subluminescent O stars as well is yet unclear. The situation is more complicated than for the sdB stars since the sdO stars form a much less homogenous class than the sdB stars (cf. Heber 1992). They have to be divided into at least three subclasses. Most of the sdO stars are enriched in helium, from mild cases (helium abundance slightly above solar) to extreme cases (no hydrogen detectable which translates into enrichments of at least several hundred times solar). The helium richness is accompanied by peculiar C and N line spectra. In addition the sdO stars have to be subdivided according to their luminosity. The most luminous sdO stars are very similar to some central stars of planetary nebulae and can be explained by post-AGB evolution which strongly suggest an evolutionary linkage to the helium giants (extreme helium stars and RCrB stars). Amongst the less luminous sdO stars again two spectroscopic subclasses differing in chemical composition must be distinguished. The first one, which we shall name He-sdO, does not show any trace of hydrogen but strong nitrogen and/or carbon lines. The second subclass, which we shall term simply sdO from now on, has hydrogen in quite different amounts. The evolutionary link between these two subgroups on the one hand and the sdB stars on the other is not yet clear.

Detailed quantitative spectral analyses are available for the subluminescent B stars but only a few have been carried out for the sdO class because of the complexity of their spectra. In addition deviations from local thermodynamic equilibrium (NLTE) have to be taken into account, because of their high effective temperatures. However, only few quantitative spectral analyses have been published (Dreizler 1993; Dreizler et al. 1990; Thejll et al. 1994; Bauer & Husfeld 1995; Haas et al. 1996; Lanz et al. 1997), with some conflicting results becoming apparent. This is probably due to shortcomings in the early NLTE models used. Therefore we construct a new grid of atmospheric models and synthetic spectra using a state-of-the-art NLTE model atmosphere code.

2. MODEL ATMOSPHERES

An extensive grid of NLTE atmosphere models was calculated using the latest version of the PRO2 code (Werner & Dreizler 1999) that employs a new temperature correction technique (Dreizler 2003). A new detailed model atom for helium appropriate for the sdO temperature regime was constructed. 2700 partially line blanketed NLTE model atmospheres consisting of hydrogen and helium were calculated resulting in a grid of unprecedented coverage and resolution, extending

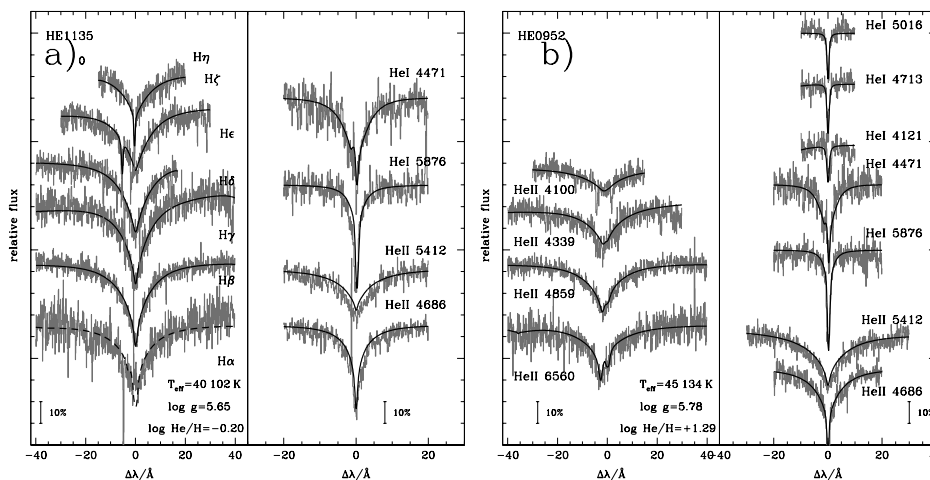


Fig. 1. Line profile fits for a H-sdO (left panel) and a He-sdO (right panel).

from 30 000 K to 100 000 K in T_{eff} , from 4.0 to 6.4 in $\log g$ and from -4 to $+3$ in helium abundance, i.e., $\log(N_{\text{He}}/N_{\text{H}})$, in order to match the diversity of observed spectra (see Ströer et al. 2005).

We have used this model grid to analyze spectra of sdO stars from the ESO SPY-survey (Ströer et al. 2005), the Hamburg Quasar Survey (HQS, Ströer 2004) and the Sloan Digital Sky Survey (SDSS).

3. SDO STARS FROM THE SPY, HQS AND SDSS SURVEYS

SPY. The ESO Supernova Progenitor Survey (SPY) has identified 137 hot subluminous stars. 79 of them were classified as hydrogen rich subluminous B stars, 58 of them were classified as subluminous O stars. The spectra of the subluminous B/OB stars have been analyzed by Lisker et al. (2005).

High resolution spectra of sdO stars covering the spectral range from 3300 Å to 6650 Å at a resolution of 0.36 Å have been obtained with the UVES spectrograph at the ESO-VLT. In the course of spectral classification we distinguished He-sdO (30) from sdO stars (28) by the absence of Balmer line absorption in the former. Napiwotzki et al. (2004) searched for radial velocity variables amongst the SPY sdB and sdO stars and found a large fraction ($\sim 40\%$) amongst the sdB stars as well as amongst the sdO stars but only one He-sdO star turned out to be radial velocity variable. This star is unique amongst the SPY-subdwarfs as it turns out to be a double sdO (Lisker et al. 2004).

Effective temperatures (T_{eff}), surface gravities ($\log g$), and helium abundances ($N_{\text{He}}/N_{\text{H}}$) for 49 stars were determined by fitting simultaneously hydrogen and helium lines to our synthetic model spectra, using a χ^2 procedure (Napiwotzki 1999). Resulting temperatures range from 36 000 K to 78 000 K, gravities from $\log g = 4.9$ to 6.4 and helium abundances from $\log(N_{\text{He}}/N_{\text{H}}) = -3$ to $+3$. Four stars have temperatures in excess of 60 000 K and are probably post-AGB stars and will not be discussed further. Figure 1 gives two examples, one for each spectral subclass.

HQS. During our follow-up observations of blue stars from the Hamburg

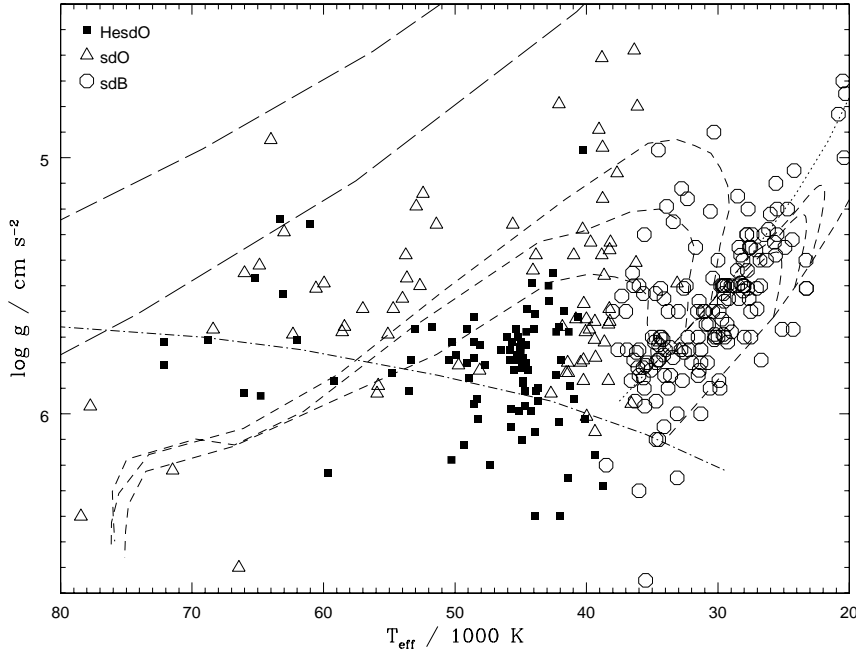


Fig. 2. Distribution of sdB, sdO and He-sdO stars (combined sample) in the T_{eff} vs. $\log g$ plane. Also shown are evolutionary tracks for post-EHB and post-AGB evolution.

Quasar Survey we have discovered many hot subdwarf stars. The analysis based on medium to low resolution spectra of the more than 100 HQS sdB stars has been presented by Edelmann et al. (2003).

In addition several sdO stars have been found. Due to insufficient S/N some of the spectra could not be analyzed. We also had to exclude the lowest resolution spectra because the results had errors too large to be useful. This left us with 14 hydrogen-rich sdO stars and 23 He-sdOs analyzed from spectra of 3.5 \AA resolution.

SDSS. The ongoing Sloan Digital Sky Survey is a rich source of hot subluminoous O stars. Candidates were found photometrically by selecting all stars with $u - g < 0.2$, $g - r < 0.1$. Inspection of their spectra yielded 40 sdO and 43 He-sdO stars, which were analyzed as described above.

Combined SPY, HQS & SDSS sample. In Figures 2 and 3 we combine the results of the spectral analyses of all three samples including the sdB stars. Figure 2 displays the distribution in the T_{eff} vs. $\log g$ plane. A strong concentration of the He-sdO stars near $T_{\text{eff}} = 45\,000 \text{ K}$, $\log g = 5.5$ is obvious. Some of the sdO stars lie in between the sdB star domain and the He-sdO stars, while others are of lower gravity than the sdB stars. It is worthwhile to note that a gap in the sdO sequence becomes apparent. There are very few sdO stars in the T_{eff} range from 40 000 to 50 000 K, where most of the He-sdOs are found.

Edelmann et al. (2003) noticed a trend of increasing helium abundances with increasing T_{eff} for sdB stars. They also pointed out that two distinct sequences exist. The “cooler” sdO stars nicely match the sdB sequences (see Figure 3) and extend the trend to higher T_{eff} ($\approx 40\,000 \text{ K}$).

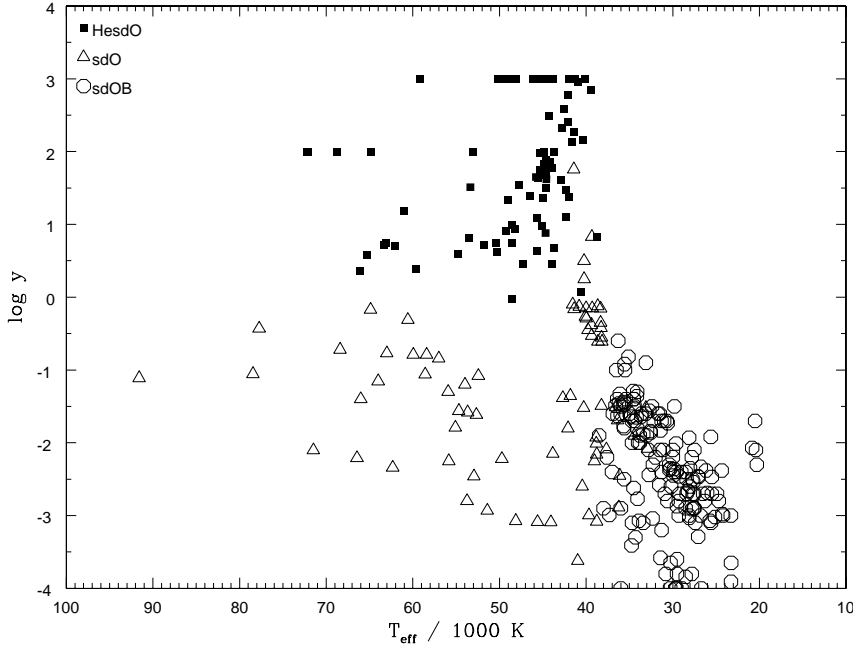


Fig. 3. Distribution of sdB, sdO and He-sdO stars (combined sample) in the T_{eff} vs. $\log y$ plane ($y = N_{\text{He}}/N_{\text{H}}$). For stars with $\log y > +3$ lower limits are given.

4. METAL ABUNDANCES

While metal abundances of several dozens of sdB stars have been derived using LTE techniques from optical spectra (see Edelmann et al. 2006) very few detailed abundance analyses are available for sdO stars. A self-consistent spectral analysis is available for BD+75 325 only (Lanz et al. 1997). Abundances of Fe and Ni have been determined in a few sdO and He-sdO stars. Haas (1997) finds strong enrichments of Fe (10 times solar) and Ni (70 times solar) in the hot hydrogen-rich sdO stars Feige 34, Feige 67 and LS II+18 9. These high abundances cause strong backwarming and the temperatures derived from the Fe/Ni ionization equilibria (60 000 K) is much lower than the one (75 000 K) obtained from optical Balmer and He II lines using metal free NLTE model atmospheres.

Recently, O'Toole & Heber (2006) analyzed high resolution ultraviolet spectra of five sdB stars from HST/STIS. Many heavy elements (up to lead) become accessible to a detailed quantitative analysis. Abundance of 23 metals were derived. While the cooler sdB stars ($T_{\text{eff}} < 30\,000$ K) show abundances of the iron group elements similar to the sun. The hotter ones ($T_{\text{eff}} \approx 35\,000$ K) have near solar iron abundances as well, but strong enrichments (100 times) of other elements are found. The high Ni abundances are very similar to those found by Haas (1997) for the hydrogen-rich sdO stars.

As has been noted by Heber, Reid & Werner (2000) in their quantitative spectral analysis of pulsating sdB stars, there is a discrepancy between temperatures derived from Balmer line fitting and helium ionization equilibrium. For PG 1219+534, the difference in T_{eff} was found to be as large as 2000 K.

After the initial discovery of strongly super-solar abundances of heavy metals in three sdB stars (Feige 66, CD $-24^{\circ}731$ and PG 1219+534), we investigated how this affects the determination of the atmospheric parameters. Using LTE atmospheres with metals scaled by a factor of 10 ($[M/H] = 1.0$), we have recalculated both our abundances and stellar parameters (T_{eff} , $\log g$). There are currently no opacity distribution functions with higher metallicities.

In Figure 4 we show a fit with these models to the optical spectrum of the pulsating sdB star PG 1219+534. The Balmer lines and the He II can now be matched simultaneously. The parameters we derive with our metal-enhanced models is closest to those found by fitting the Balmer lines only with a solar-metallicity model. Hence the discrepancy between Balmer and He-ionization can be traced back to a metallicity effect. Unfortunately, however, the heavy metal abundances can be derived from UV spectra, only. Opacity sampling techniques (see Behara & Jeffery 2006) are required to account for the different enrichment of individual heavy elements.

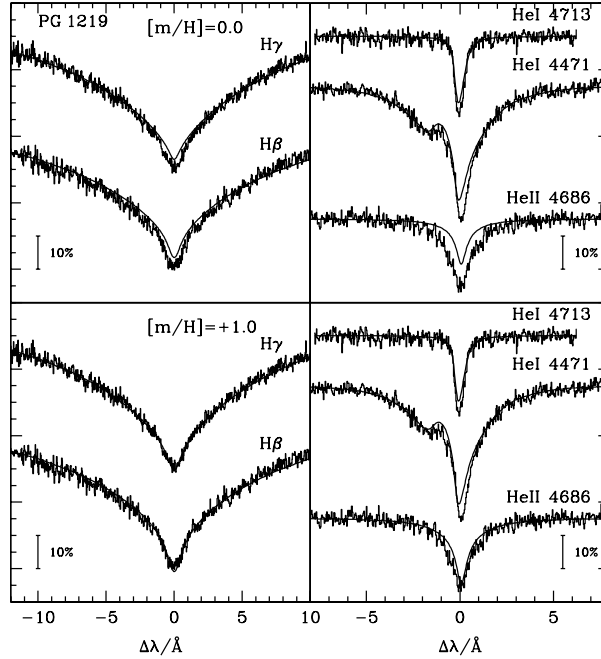


Fig. 4. Line profile fit for PG 1219+534 using solar metallicity models (top panel) and metal-rich models (10 times solar, bottom panels). The Balmer lines and He II at 4686 Å match simultaneously when using the metal-rich models.

5. A HYPER-VELOCITY SDO STAR

While all the hot subluminous stars studied by us have low radial velocities (system velocities in case of close binary stars), one object sticks out. In the sample of sdO stars selected from the SDDS we found the faint He-sdO US 708 ($g = 18.75$) to have a radial velocity of more than 700 km s^{-1} . To improve this measurement and to check for radial velocity variations, we observed the star with the Low Resolution Imaging Spectrometer LRIS at the KECK I telescope and obtained spectra of 5 \AA and 4.4 \AA resolution in the blue and red channels, respectively, with much better S/N than the SDSS spectrum (see Figure 5). The heliocentric radial velocity of $708 \pm 20 \text{ km s}^{-1}$ is consistent with that from the SDSS spectrum, and we conclude that the high radial velocity is due to a very large space motion. Its radial velocity corresponds to a minimum Galactic rest frame velocity of 750 km s^{-1} exceeding the Galactic escape velocity at the position of the star. Hence the US 708 is unbound to the Galaxy. A spectral analysis of the LRIS spectrum is

performed and the preliminary result is $T_{\text{eff}} = 45\,500$ K, $\log g = 5.2$ and $\text{He}/\text{H} = 10$, typical for He-sdO stars. Assuming a mass of $0.5 M_{\odot}$ this places US 708 at a distance of almost 20 kpc.

Two so-called hyper-velocity stars have recently been discovered with radial velocities of 853 km s^{-1} (Brown et al. 2005) and 723 km s^{-1} (Edelmann et al. 2005). The corresponding minimum Galactic rest frame velocities are 709 km s^{-1} and 563 km s^{-1} , respectively. Proper motions are unavailable but their measurement probably has to await future space missions, such as *Gaia* as they are probably very small given the large distances of the stars. Unlike US 708, the two hyper-velocity stars are young massive B stars at distances of 60 kpc. It is generally believed that interaction with the massive black hole in the Galactic center can accelerate stars to such high velocities. Hills (1988) investigated the tidal break-up of binary stars by a massive black hole and found ejection velocities, indeed, to be as high as 4000 km s^{-1} . Some kinematical experiments are presently being carried out to check whether a Galactic center origin is feasible for US 708.

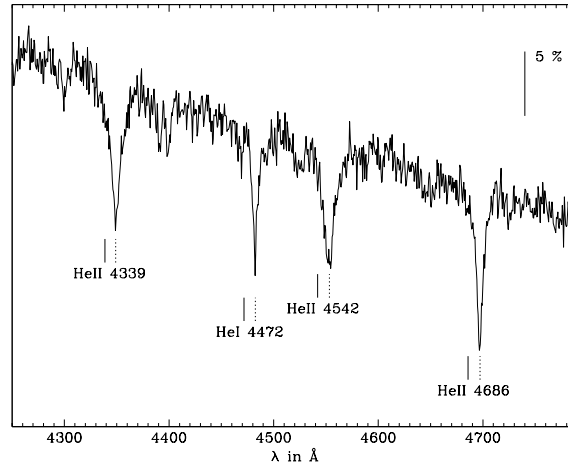


Fig. 5. Keck/LRIS spectrum of the He-sdO US 708 in the blue channel showing the typical He I and He II lines shifted by 708 km s^{-1} .

6. CONCLUSION

Recent spectral analyses of sdO stars have paved the way to discuss the evolutionary status of these stars as well as their linkage to sdB stars. The Supernova Ia Progenitor Survey has provided a set of high resolution spectra of sdO stars. The most important result is a separation of the subluminous O stars into at least two groups, the He-sdOs and the sdOs. The sdO stars form an extension of the sdB stars to higher temperatures and higher helium abundances. A couple of sdO stars are obviously evolved from the extended horizontal branch and reach temperatures as high as $80\,000$ K. The He-sdO stars, however, cluster near $T_{\text{eff}} = 45\,000$ K, $\log g = 5.5$. The second important result from SPY is that the binary fraction of sdO stars is similar to that of the sdB stars, while it is very low for He-sdO stars. Therefore we conclude that the two types of subluminous stars have different evolutionary origin. Recently, many sdO stars have been analyzed from low-resolution spectra from the HQS follow-up project and the SDSS spectral database. The results strength the conclusions drawn from the SPY set substantially and suggest the presence of a gap in the distribution of sdO stars at the position of He-sdO cluster in the T_{eff} vs. $\log g$ plane.

From high resolution UV spectra strong enrichments of iron group elements are discovered for hydrogen-rich sdO stars as well as for sdB stars and have severe implications for the temperature scale.

We finally highlighted the discovery of a hyper-velocity (HVS) He-sdO star with a radial velocity of 708 km s^{-1} unbound to the galaxy. While the two known HVS stars are main-sequence stars, this is the first highly-evolved HVS. The star is probably ejected by the supermassive black hole in the Galactic center.

REFERENCES

- Bauer F., Husfeld D. 1995, *A&A*, 300, 481
 Behara N. T., Jeffery C. S. 2006, *Baltic Astronomy*, 15, 115 (these proceedings)
 Brown W. R., Geller M. J., Kenyon S. J., Kurtz M. J., 2005, *ApJ*, 622, L33
 Dreizler S. 1993, *A&A*, 273, 212
 Dreizler S. 2003, in *Stellar Atmosphere Modeling*, eds. I. Hubeny et al., ASP Conf. Ser., 288, 69
 Dreizler S., Heber U., Werner K., Moehler S., de Boer K. S. 1990, *A&A*, 235, 235
 Edelmann H., Heber U., Hagen H.-J., Lemke M., Dreizler S., Napiwotzki R., Engels D. 2003, *A&A*, 400, 939
 Edelmann H., Napiwotzki R., Heber U., Christlieb N., Reimers D. 2005, *ApJ* (submitted)
 Edelmann H., Heber U., Napiwotzki R. 2006, *Baltic Astronomy*, 15, 103 (these proceedings)
 Greenstein J. L., Sargent, A. I. 1974, *ApJS*, 28, 157
 Groth H. G., Kudritzki R. P., Heber U. 1985, *A&A*, 152, 107
 Haas S. 1997, PhD Thesis, University of Erlangen-Nürnberg
 Haas S., Dreizler S., Heber U., Jeffery C. S., Werner K. 1996, *A&A*, 311, 669
 Han, Z., Podsiadlowski P., Maxted P. F. L., Marsh T. R. 2003, *MNRAS*, 341, 669
 Heber U. 1992, in *The Atmospheres of Early-Type Stars*, Lecture Notes in Physics, Springer-Verlag, 401, 233
 Heber U., Reid I. N., Werner K. 2000, *A&A*, 363, 198
 Hills J. G. 1988, *Nature*, 331, 687
 Lanz T., Hubeny I., Heap S. R. 1997, *ApJ*, 485, 843
 Lisker T., Heber U., Napiwotzki R., Christlieb N., Reimers D., Homeier D. 2004, *Ap&SS*, 291, 351
 Lisker T., Heber U., Napiwotzki R. et al. 2005, *A&A*, 430, 223
 Maxted P. F. L., Heber U., Marsh T. R., North R. C. 2001, *MNRAS*, 326, 1391
 Napiwotzki R., Karl C. A., Lisker T., Heber U. et al. 2004, *Ap&SS*, 291, 321
 O'Toole S., Heber U. 2006, *A&A* (submitted)
 Ströer A., Heber U., Lisker T., Napiwotzki R., Dreizler S. 2005, in *14th European Workshop on White Dwarfs*, eds. D. Koester & S. Moehler, ASP Conf. Ser., 334, 309
 Ströer A. 2004, Diploma Thesis, University of Erlangen-Nürnberg
 Sweigart A. 1997, in *Third Conference on Faint Blue Stars*, eds. A. G. D. Philip, J. Liebert & R. A. Saffer, L. Davis Press, Schenectady, NY, p. 3
 Thejll P., Bauer F., Saffer R. et al. 2004, *ApJ*, 433, 819
 Webbink R. F. 1984, *ApJ*, 277, 252
 Wesemael F., Winget D. E., Cabot W., van Horn H. M., Fontaine G. 1981, *ApJ*, 254, 221
 Werner K., Dreizler S. 1999, *J. Comp. and Appl. Mathematics*, 109, 65

ANALYSIS OF THE FUSE SPECTRA OF THE HE-POOR SDO STAR MCT 0019–2441

M. Fontaine¹, P. Chayer^{2,3}, F. Wesemael¹, G. Fontaine¹ and R. Lamontagne¹

¹ *Département de Physique, Université de Montréal, Montréal, H3C 3J7, Canada*

² *Bloomberg Center for Physics and Astronomy, The Johns Hopkins University, Baltimore, MD 21218, U.S.A.*

³ *Department of Physics and Astronomy, University of Victoria, Victoria, BC, V8W 3P6, Canada*

Received 2005 August 1

Abstract. We present a preliminary analysis of the FUSE spectra of MCT 0019–2441, a relatively He-poor sdO star. Among the handful of absorption features of photospheric origin present in the ultraviolet, we identify the OVI doublet at 1031.9 and 1037.6 Å, the S VI doublet at 933.4 and 944.5 Å, the Si IV triplet at 1122.5 and 1128.3 Å and some NIV lines. While synthetic spectra based on NLTE line blanketed model atmospheres can reproduce most line profiles, they fail to reproduce the OVI line profiles in a satisfactory manner. Possible solutions to this puzzle are considered.

Key words: stars: hot subdwarfs – stars: abundances – stars: individual (MCT 0019–2441)

1. INTRODUCTION

The hot subdwarf MCT 0019–2441 ($V = 14.48$) was observed with the FUSE Observatory as a part of an ongoing effort at mapping the atmospheric chemical composition of a relatively large sample of sdB and sdOB stars (see, e.g., Fontaine et al. 2005). The main objective of this work is to understand better the physical processes that determine the chemical composition of subdwarf atmospheres. However, at $T_{\text{eff}} = 58\,350$ K and $\log g = 5.6$, MCT 0019–2441 turned out to be a “cool” sdO star with a low helium abundance ($n_{\text{He}}/n_{\text{H}} = 0.08$). Since its FUSE spectra do not show the myriad of lines that are present in the spectra of most other hot subdwarf stars, MCT 0019–2441 is well suited for a complete spectral analysis, as the continuum level is clearly defined and most photospheric absorption features can be identified. A first look at the unusual FUSE spectra of this object was provided by Lamontagne et al. (2003), and we present here the first quantitative analysis of its abundance pattern.

2. OBSERVATIONAL MATERIAL AND MODEL ATMOSPHERES

The FUSE data on MCT 0019–2441 (dataset B0541001) are similar to those presented by Lamontagne et al. (2003) and consist of four exposures, for a total of 9.2 ksec. In parallel, a medium-resolution optical spectrum of MCT 0019–2441 was secured by M. Billères at the NTT, while two IUE low-dispersion observations

were recovered from the MAST archives (images SWP 26277 and LWP 06290).

To carry out our analysis of the spectra, we use TLUSTY 200 and SYNSPEC 48 (Hubeny 1988; Hubeny & Lanz 1995) respectively for the computation of model atmospheres and synthetic spectra. These codes are used to generate grids of NLTE, homogeneous, plane-parallel models that include blanketing by the hydrogen and helium lines. A first grid, used to derive the atmospheric parameters, is devoid of heavy elements. Our fits to the hydrogen and helium lines yield $T_{\text{eff}} = 58\,350$ K, $\log g = 5.6$ and $n_{\text{He}}/n_{\text{H}} = 0.08$. The corresponding reddening-free energy distribution shows good agreement with the composite energy distribution built from FUSE, IUE and optical data.

With these atmospheric parameters, grids of model atmospheres were generated that include detailed atomic models for O III through O VI and for Si IV through Si VI. Not only does this allow line blanketing by O and S to be accounted for, but NLTE populations of O and S can also be calculated and used in the computation of synthetic spectra. For other heavy elements (C, N, Si, P and Fe), we currently use a line blanketed model with $\log(\text{O}/\text{H}) = -5$ and $\log(\text{S}/\text{H}) = -7$ for the computation of synthetic spectra in which these elements are added as traces and treated in LTE. The atomic data for the lines is taken from the compilations of Kurucz¹.

3. ABUNDANCE ANALYSES

The ultraviolet line spectrum of MCT 0019–2441, although far simpler than that of the vast majority of hot subdwarfs, provides interesting challenges when confronted to detailed abundance analyses. Some features, like the Si IV 1128 Å lines, can be fit with the help of a χ^2 minimizing procedure that simultaneously optimizes the abundance and the level of the continuum. For the O VI lines the procedure does not work well, because the lines appear too strong to be entirely photospheric. In many cases, the absence of absorption features in the FUSE spectra led to upper limits on the abun-

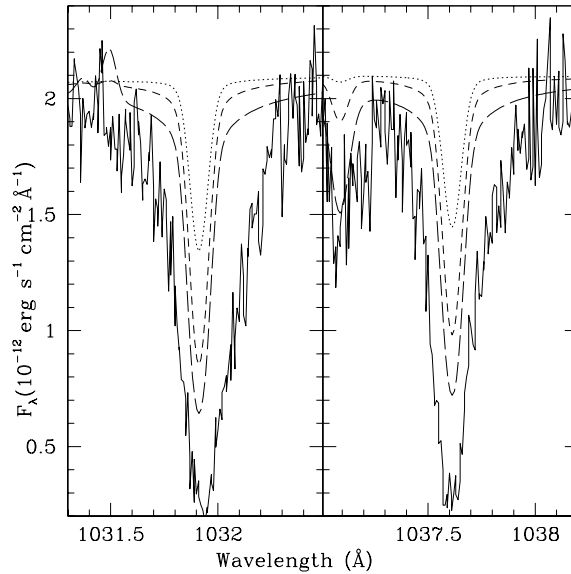


Fig. 1. Synthetic spectra with $\log(\text{O}/\text{H}) = -5$ (dots), -4 (short dash) and -3 (long dash) compared to the FUSE data.

¹ see <http://cfa-www.harvard.edu/amdata/ampdata/kurucz23/sekur.html>

dance of the element considered. We now comment on specific elements.

Oxygen. We observe strong O VI resonance lines at 1031.9 and 1037.6 Å, with respective equivalent widths of ~ 275 and ~ 190 mÅ. They have the same velocity as the Lyman lines within the instrumental resolution (about 15 km s^{-1}). At the same time, there is negligible absorption from O IV throughout the FUSE spectral range. The only O IV lines detected in the FUSE spectra (1067.768 and 1067.832 Å) indicate $\log(\text{O}/\text{H}) < -4.8$, an abundance too low by orders of magnitude to reproduce the O VI equivalent widths, not to mention the line profiles (see Figure 1). This situation is addressed in the next section.

Sulfur. The S VI 933 and 944 Å lines are detected and have equivalent widths of 67.6 and 62.4 mÅ, respectively. The fit to the S VI 933 Å line yields an abundance of $\log(\text{S}/\text{H}) = -7.9$, while the 944 Å line is best matched for $\log(\text{S}/\text{H}) = -7.6$. In the latter case, the core of the line is still poorly matched.

Carbon. The C III 1175 Å multiplet is absent, while the C III 977 Å resonance line is strong. This indicates that C III absorption occurs in the ISM, as the 1175 Å multiplet arises from an excited state. Unfortunately, there are no additional constraints to be extracted from the IUE spectra, since the C IV resonance lines are absent. From the absence of absorption features near 1175 Å, we derive an upper limit to the photospheric carbon abundance of $\log(\text{C}/\text{H}) < -7.0$.

Nitrogen. The N IV lines around 922–955 Å are all compatible with an abundance of $\log(\text{N}/\text{H}) = -7.6 \pm 0.3$, but there are minor discrepancies between the shape of the observed continuum and the synthetic spectrum in this spectral interval. This may perhaps be due to small errors in the values of the atmospheric parameters we determined or to problems with the flux calibration of the FUSE data at such short wavelength.

Silicon. The Si IV 1128 Å lines are well matched by our automated χ^2 procedure, yielding $\log(\text{Si}/\text{H}) = -7.4$. The 1122 Å line is blended with a Fe III ISM line, but the observed feature is compatible with the derived abundance.

Phosphorus. The absence of the P V resonance lines at 1118.0 and 1128.0 Å yields an upper limit of $\log(\text{P}/\text{H}) < -9.6$. The atmosphere of MCT 0019–2441 appears to be completely devoid of phosphorus, an element observed in most hot subdwarfs.

Iron. The FUSE spectra have been inspected for evidence of Fe V or Fe VI lines or both. Their non-detection implies an upper limit of $\log(\text{Fe}/\text{H}) < -5.0$ under LTE assumption. We stress that NLTE effects play an important role in the ionization and excitation balance of iron under such atmospheric conditions and are not accounted for in this preliminary analysis.

4. DISCUSSION

Many lines routinely seen in hot subdwarfs are absent from the ultraviolet spectrum of MCT 0019–2441; we nevertheless have some difficulty in accounting for the strongest features, those of O VI, observed in the spectrum. While small errors in the atmospheric parameters (T_{eff} and $\log g$) could play some role in explaining these difficulties, we note that the parameters we derive reproduce satisfactorily both the optical spectrum and the overall energy distribution; the only disagreement appears in the predicted continuum in the 910–950 Å region. We also remark that, while our calculations for the Stark broadening of the O VI and S VI lines make use of the latest semi-classical damping constants of Dimitrijević & Sahal-

Bréchet (1992, 1993), there are still no fully quantum-mechanical calculations of the broadening of these lines.

In addition to these obvious possibilities, other scenarios should perhaps also be considered to account for the strength of the O VI lines. The first possibility is that their strength reflects an inhomogeneous equilibrium distribution of heavy elements. A stratification of this type might be disrupted by a weak stellar wind, however. In MCT 0019–2441, the O VI lines do show asymmetric profiles that may be related to the presence of such a wind. It appears therefore unlikely that stratification can be invoked to solve the puzzle of the O VI lines.

Another possibility is a contribution to the observed profile from diffuse O VI absorption in the local ISM. This is considered unlikely, on the basis of the recent analysis by Oegerle et al. (2005) of 25 lines of sight to nearby ($d < 250$ pc) white dwarfs. They report equivalent widths of O VI lines less than 22 mÅ. Situated ~ 1.7 kpc away, however, MCT 0019–2441 is significantly beyond the distance sampled by Oegerle et al. On a much longer line of sight ($d = 10.2$ kpc), Howk et al. (2003) present an analysis of vZ 1128, a post-AGB star located in the globular cluster M 3, which shows an ultraviolet spectrum similar to that of MCT 0019–2441. They suggest that the O VI absorption, with equivalent widths of 260 mÅ and 150 mÅ respectively, arises at the interfaces between the hot and warm phases of the ISM. While the line strengths are compatible with those observed in MCT 0019–2441, the distance is significantly larger than that to our target.

A final possibility is that circumstellar material might contribute to the observed O VI absorption. In the case of vZ 1128, Howk et al. (2003) argue that this is unlikely given the absence of high-velocity material. The same argument could be made for MCT 0019–2441, but the issue could be settled by a direct observation of the surroundings of that star. For instance, Otte et al. (2004) report the detection of a O VI-emitting nebula around the hot white dwarf KPD 0005+5106 ($T_{\text{eff}} = 120\,000$ K, $\log g = 7.0$), a hot PG 1159 star known to show O VI absorption in the optical (Sion et al. 1985).

ACKNOWLEDGMENTS: This work was supported in part by the NSERC Canada, by the Fund FQRNT (Québec) and by NASA contract NAS5-32985.

REFERENCES

- Dimitrijević M. S., Sahal-Bréchet S. 1992, *A&AS*, 93, 359
 Dimitrijević M. S., Sahal-Bréchet S. 1993, *A&AS*, 100, 91
 Fontaine M., Chayer P., Wesemael F. et al. 2005, in *Astrophysics in the Ultraviolet*, eds. G. Sonneborn, H. W. Moos & B.-G. Andersson, in press
 Howk J. C., Sembach K. R., Savage B. D. 2003, *ApJ*, 586, 249
 Hubeny I. 1988, *Computer Physics Comm.*, 52, 103
 Hubeny I., Lanz T. 1995, *ApJ*, 439, 875
 Lamontagne R., Chayer P. et al. 2003, in *White Dwarfs*, eds D. de Martino, R. Silvotti, J.-E. Solheim & R. Kalytis, NATO Science Series II, 105, 159
 Oegerle W. R. et al. 2005, *ApJ*, 622, 377
 Sion E.M., Liebert J., Starrfield S. G. 1985, *ApJ*, 292, 471

METAL ABUNDANCES OF SDB STARS

H. Edelmann¹, U. Heber¹ and R. Napiwotzki²

¹ *Remeis-Sternwarte Bamberg, Astronomisches Institut der Universität Erlangen-Nürnberg, Sternwartstrasse 7, D-96049 Bamberg, Germany*

² *Centre for Astrophysics Research, University of Hertfordshire, College Lane, Hatfield AL10 9AB, U. K.*

Received 2005 August 1

Abstract. The surface abundance patterns of four dozen bright sdB stars have been determined from high resolution, high S/N optical spectra. As typical in early B stars, the metal lines are few and weak. We searched for trends of the metal abundance patterns with the atmospheric parameters (effective temperature and gravity). It is remarkable that almost all metal abundances of sdBs with $T_{\text{eff}} < 32\,000$ K stay at similar values, virtually independent of stellar parameters. The only exceptions are He and C which vary considerably from star to star. The hottest EHB stars lack O, Mg, Al and Si. Furthermore, all stars are rotating very slowly or not at all.

Key words: stars: abundances – stars: horizontal-branch – stars: rotation – hot subdwarfs

1. INTRODUCTION

The atmospheres of hot subdwarfs represent a huge puzzle in stellar physics: some chemical elements (such as helium) are highly depleted, whereas other elements (e.g., iron group elements) are enriched by factors up to a few 10 000 (Edelmann et al. 2001). Although these anomalies can probably be understood in terms of chemical layering processes in stellar envelopes (gravitational settling, radiative levitation and mass-loss), current models fail to explain the observed abundance patterns by orders of magnitudes. Also, the available sample of stars with well determined abundances is far too small to constrain diffusion theory. We present here the analysis for 49 sdB stars to determine their surface metal abundance patterns. This analysis has increased drastically (factor of ten) the number of detailed metal abundance analyses of sdB stars done so far.

2. OBSERVATIONS

Optical echelle spectra with high S/N were obtained at the German-Spanish Astronomical Center (DSAZ) on Calar Alto, Spain, with the 2.2 m telescope equipped with the FOCES spectrograph and at the ESO 1.5 m and 2.2 m telescopes equipped with the FEROS spectrograph. The observational dataset is homogeneous due to similar spectral resolutions (0.14Å at DSAZ and 0.09Å at ESO) and spectral coverage (3900 Å–6900 Å at DSAZ and 3600Å–8900Å at ESO) of all observed sdBs.

3. ANALYSIS

The atmospheric parameters (effective temperature, gravity and helium abundance) of all sdB's were derived simultaneously from the spectra by means of a χ^2 fit using fully line blanketed LTE model atmospheres (updated version of the code of Heber 1986). The results for all program stars are shown in Figure 1 in a theoretical (T_{eff} vs. $\log g$) diagram.

LTE abundances were derived for all metals from measured equivalent widths using the classical curve-of-growth method. We generated model atmospheres, using the atmospheric parameters and solar metal abundances with the ATLAS9 code of Kurucz (1992). From these models we calculated curves-of-growth for the observed metal lines, from which abundances were derived. Blends from different ions were omitted from the analysis. Finally, the abundances were determined from a detailed spectrum synthesis for all lines measured before. The atomic data for the analysis were taken from the list of Wiese et al. (1996) for the CNO elements, from Kurucz (1992) and Ekberg (1993) for Fe and for all other elements from the table of Hirata & Horaguchi (1995).

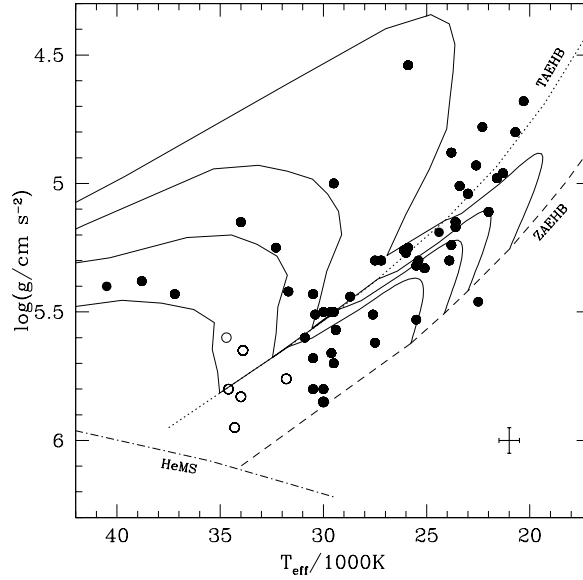


Fig. 1. Program stars in the T_{eff} vs. $\log(g)$ plane (stars denoted by open symbols lack of O, Mg, Al and Si).

4. TRENDS WITH ATMOSPHERIC PARAMETERS?

The chemical abundances observed in the atmospheres of sdB stars are very puzzling. There is now general consensus, that the peculiar abundance patterns are due to *diffusion*. Diffusion denotes the interplay between radiative acceleration (directly proportional to T_{eff}^4) which levitates particles into upper regions, and the gravity which settles heavier particles into lower regions inside the envelope of stars. Therefore, we tried to identify possible trends of the chemical composition with T_{eff} , $\log g$ and the luminosity (expressed in terms of the Eddington luminosity L_e).

Figure 2 shows the results for helium and for some (five) of the analyzed metal ions. Binarity and pulsations may influence the metal abundance patterns. Therefore we indicate known short period binaries (triangles) and pulsators (circles) in Figure 2. However, their metal abundance do not differ from those of apparently single, non-pulsating sdB stars (squares). Surprisingly, the abundances for most analyzed metal ions (especially for N II and Fe III) are constant irrespective of the

stellar parameters. Only for S II and also for N III there seem to be a direct correlation with the stellar parameters: the larger the temperature and/or gravity, the larger the abundance for S II, and the lower the abundance for N III. However, this is most likely due to NLTE effects because the dominant ionization stages (N II and S III) do not show such trends.

For most of our program stars hotter than $\sim 32\,000$ K no absorption lines due to O, Mg, Al and Si can be detected in the optical wavelength range. This indicates that for the majority of sdB stars the abundances of O, Mg, Al and Si drop suddenly from a slightly subsolar value below $\sim 32\,000$ K to larger depletion for T_{eff} exceeding $32\,000$ K (see Figure 2). There are a few exceptions, though.

Those hot stars ($T_{\text{eff}} > 32\,000$ K) that do show O, Mg, Al and Si are all of low gravity and, therefore, have evolved off the EHB. None of the hot sdB stars on or near the EHB show O, Mg, Al and Si lines (see Figure 1).

Furthermore, three of those more luminous stars show a supersolar helium abundance (indicated by thick open symbols in Figure 2) and metal abundances which are almost solar or even higher in the case of N and Ar, which are enriched each by a factor or 3–10.

In a previous analysis of a large sample of low resolution spectra of sdB stars drawn from the Hamburg Quasar survey (Edelmann et al. 2003) we found a general trend of the helium abundances to increase with increasing T_{eff} . Actually, sdB stars were found to separate into two distinct sequences. A small fraction (1/6) have much lower helium abundances at the same temperatures than the bulk of sdB stars. For the program stars presented here, we find also two distinct sequences with exactly the same fraction of stars (1/6) to show a helium “underabundance” (indicated by filled symbols in Figure 2). The metal abundances of these helium underabundant sdB stars, however, do not differ from those of the others.

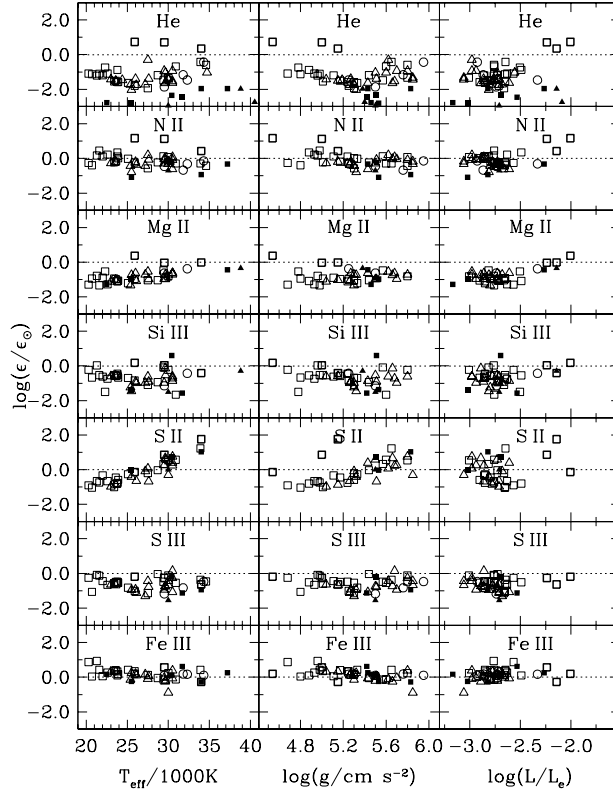


Fig. 2. Sample LTE abundances for all analyzed sdB stars relative to the solar values (dashed horizontal lines) versus T_{eff} , $\log g$ and L/L_{\odot} (different symbols, see text).

5. ROTATION

The projected rotational velocity can be measured by comparing synthetic line profiles, calculated for the given atmospheric parameters (T_{eff} , $\log g$, element abundance) of a star folded with an adopted rotational velocity, with the observed line profiles. The MgII doublet at 4481.13 Å and 4481.33 Å is most suitable for this purpose. The lines are very narrow and closely separated, and therefore very sensitive to rotational broadening. If the doublet is resolved into two components, the projected rotation velocity has to be very small. Only sdB stars that are known to be in short period binary systems show significant rotation. All others are slow rotators ($v_{\text{rot}} \sin(i) < 3 \text{ km s}^{-1}$) or do not rotate at all (unless seen pole-on).

6. CONCLUSION

With this work, the number of detailed metal abundance analyses of sdB stars has increased drastically (by a factor of ten). We have selected sdB stars for the abundance analysis covering a wide range of parameter space, which allowed us to search for trends of the metal abundances with these parameters. It is remarkable that for all program stars the abundances for many metals which are common in the atmospheres of sdB stars (C, N, S, Ar and Fe), are similar all over the parameter space. The same holds for O, Mg, Al and Si, but, only for stars with $T_{\text{eff}} < 32000 \text{ K}$. These metals practically vanish from the surface of most sdB stars with higher temperatures. Only for luminous (i.e., post-EHB) sdB stars the abundances of O, Mg, Al and Si are “normal”, or become even larger than in the cooler EHB stars. No obvious differences for the abundances of pulsating or non-pulsating, and radial velocity variable or non-variable sdB stars became apparent. Our results represent a challenge for a theoretical interpretation.

REFERENCES

- Ekberg J. O. 1993, A&AS, 101, 1
 Edelmann H., Heber U., Napiwotzki R. 2001, Astron. Nachr., 322, 401
 Edelmann H., Heber U., Hagen H.-J., Lemke M., Dreizler S., Napiwotzki R., Engels D. 2003, A&A, 400, 939
 Heber U. 1986, A&A, 155, 33
 Hirata R., Horaguchi T. 1995, *Atomic Spectral Line List*, Department of Astronomy, Faculty of Science, Kyoto University, and National Science Museum, 3-23-1 Hyakunin-cho, Shinjuku-ku, Tokyo
 Kurucz R. L. 1992, in *The Stellar Populations of Galaxies*, IAU Coll. 149, eds. B. Barbuy & A. Renzini, Kluwer Academic Publishers, Dordrecht, p. 225
 Wiese W. L., Fuhr J. R., Deters T. M. 1996, in *Atomic Transition Probabilities of Carbon, Nitrogen and Oxygen: a Critical Data Compilation*, eds. W. L. Wiese, J. R. Fuhr & T. M. Deters, American Chemical Society ... for the National Institute of Standards and Technology (NIST), Washington, QC 453 W53

NLTE ANALYSES OF SDB STARS: PROGRESS AND PROSPECTS

N. Przybilla¹, M. F. Nieva^{1,2} and H. Edelmann¹

¹ *Remeis-Sternwarte Bamberg, Sternwartstrasse 7, D-96049 Bamberg, Germany*

² *Observatório Nacional, R. Gal. José Cristino 77, 20921-400, São Cristóvão, Rio de Janeiro, RJ, Brasil*

Received 2005 July 31

Abstract. We report on preliminary results of a hybrid non-LTE analysis of high-resolution, high- S/N spectra of the helium-rich subdwarf B star Feige 49 and the helium-poor sdB HD 205805. Non-LTE effects are found to have a notable impact on the stellar parameter and abundance determination. In particular the He I lines show significant deviations from detailed balance, with the computed equivalent widths strengthened by up to $\sim 35\%$. Non-LTE abundance corrections for the metals (C, N, O, Mg, S) are of the order ~ 0.05 – 0.25 dex on the mean, while corrections of up to ~ 0.7 dex are derived for individual transitions. The non-LTE approach reduces systematic trends and the statistical uncertainties in the abundance determination. Consequently, non-LTE analyses of a larger sample of objects have the potential to put much tighter constraints on the formation history of the different sdB populations than currently discussed.

Key words: line: formation – stars: abundances – stars: atmospheres – stars: fundamental parameters – stars: evolution – hot subdwarfs

1. INTRODUCTION

Astrophysics faces the general difficulty that almost all relevant information cannot be directly inferred from observation. One has to rely on the interpretation of the radiation from a light-emitting plasma and its interaction with matter. Accurate physical modeling is crucial, with systematic uncertainties often dominating the error budget at present. In the case of subdwarf B (sdB) stars quantitative spectroscopy is well established, relying on grids of either line-blanketed LTE or metal-free non-LTE model atmospheres (e.g., Heber & Edelmann 2004 and references therein). Here we investigate what improvements on sdB analyses can be expected from a hybrid non-LTE method, which avoids the weaknesses of both traditional approaches by combining metal line-blanketed model atmospheres with non-LTE line formation. The impact on the stellar parameter determination is of special interest, as this provides the basis for all further interpretation. Then, in the second part, non-LTE metal abundances are determined from observations in the visual spectral range for the first time. More accurate stellar parameter and abundance determinations can be expected to shed further light on the formation mechanisms of sdB stars that have been debated over the last decades.

2. MODEL CALCULATIONS AND OBSERVATIONAL DATA

The model calculations are carried out in a hybrid approach, thus solving the (so-called) restricted non-LTE problem. Hydrostatic, plane-parallel and line-blanketed – via an opacity sampling (OS) technique – LTE model atmospheres are computed with the ATLAS12 code (Kurucz 1996), which is in particular suited for the analysis of chemically peculiar stars. Then, non-LTE line formation is performed on the resulting model stratifications. The coupled radiative transfer and statistical equilibrium equations are solved, and spectrum synthesis with refined line-broadening theories is performed using DETAIL and SURFACE (Giddings 1981; Butler & Giddings 1985). Both codes have undergone major revisions and improvements over the past few years. State-of-the-art non-LTE model atoms (see Table 1) are utilized for the stellar parameter and abundance determination.

The model atoms are largely based on data from quantum-mechanical *ab-initio* computations using the *R*-matrix method in the close-coupling approximation, which typically have uncertainties of the order ~ 10 – 20 %. Data sources comprise the astrophysically motivated Opacity and IRON Project, but also the vast physics literature, see the original publications for details. This allows for a realistic treatment not only of the (non-local) radiative processes, which drive the departures from detailed balance. Also the thermalizing collisions are accurately represented for the relevant transitions, in contrast to the usual approach of applying simple approximation formulae, which can be in error by orders of magnitude. Finally, state-of-the-art line-broadening theories are accounted for, like the data of Stehlé & Hutcheon (1999) for the Stark broadening of the hydrogen lines.

Spectra of HD 205805 and Feige 49 were taken with FEROS (Kaufer et al. 1999) on the ESO 1.52 m and 2.2 m telescopes, respectively. The Echelle spectra were reduced using standard procedures, giving complete wavelength coverage of the entire visual spectral region at high S/N (> 100) and high resolution ($R \simeq 48\,000$).

3. STELLAR PARAMETERS

Standard methods are used for the stellar parameter determination, by simultaneous fitting the hydrogen Balmer and helium line profiles, and when possible utilizing the He I/II ionization balance. We deviate from the usual approach based on χ^2 -fitting on grids of synthetic spectra, because of the largely increased computational expenses for OS model atmospheres and non-LTE line formation. For

Table 1. Non-LTE model atoms.

| Ion | Source |
|----------|---|
| H | Przybilla & Butler (2004) |
| He I/II | Przybilla (2005) |
| C II/III | Nieva & Przybilla (in prep.) |
| N II/III | Przybilla & Butler (2001), with extensions |
| O II | Becker & Butler (1988) |
| Mg II | Przybilla et al. (2001) |
| S II/III | Vrancken et al. (1996), with updated atomic data |

Table 2. Stellar parameters.

| | HD 205805 | Feige 49 |
|----------------------|-----------|----------|
| T_{eff} (K) | 25 000 | 35 000 |
| $\log g$ (cgs) | 5.00 | 5.25 |
| ξ (km/s) | 0 | 2 |
| y | 0.01 | 0.15 |
| $v \sin i$ (km/s) | 0 | 0 |

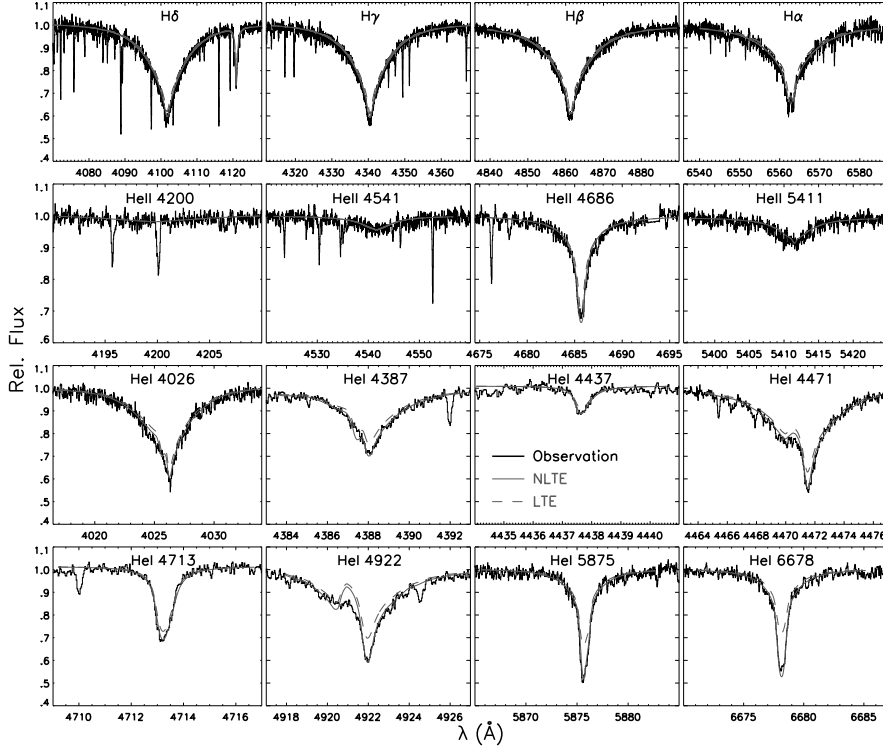


Fig. 1. Fits to H and He lines in the helium-rich sdB Feige 49.

the moment, the fits are done by eye. The resulting stellar parameters, effective temperature T_{eff} , surface gravity $\log g$, microturbulence ξ , helium abundance y (by number) and projected rotational velocity $v \sin i$, are summarized in Table 2.

Examples for the quality of the modeling achievements are displayed in Figures 1 and 2, where our spectrum synthesis for several diagnostic features (grey lines) is compared to observation (histogram) for the two sample stars. Obviously, non-LTE line formation (full lines) improves enormously on the LTE spectrum synthesis for identical stellar parameters (dashed lines), resulting in a practically perfect match of theory and observation (except for the forbidden component of He I at 4922 Å).

The largest discrepancies between non-LTE and LTE results occur for some He I lines. Non-LTE equivalent widths are larger by up to $\sim 35\%$ in particular for the strong features in the red. Both, line wings and cores can be affected. This is because the lower levels of the transitions (for principal quantum number $n=2$) are overpopulated relative to states at higher excitation energy that couple closely to the He II ground state, which is in detailed balance. Among the He II lines only the He II 4686 Å line gets slightly strengthened by non-LTE effects. A similar situation as with the He I lines occurs with the hydrogen Balmer lines because of an analogous non-LTE overpopulation of the $n=2$ level, which also can affect the line wings (most notable for H α in Feige 49). The non-LTE effects get reduced with decreasing temperature. In HD 205805 only the line cores are affected.

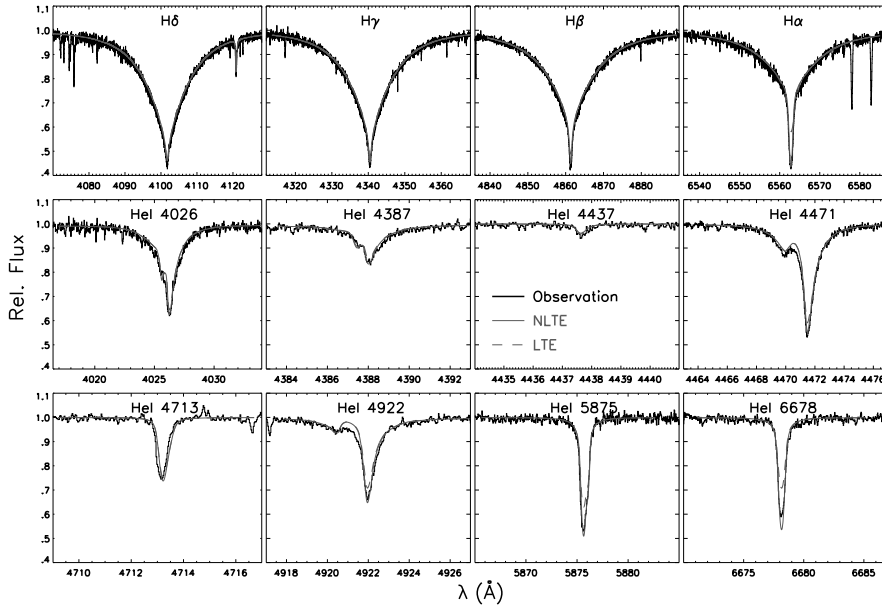


Fig. 2. Fits to H and He lines in the helium-poor sdB HD 205805.

It is obvious that the overall differences in the fitting process will impact the stellar parameter determination. In the present case this transfers into a ΔT_{eff} of +1000 and +1200 K and a $\Delta \log g$ of +0.10 and +0.12 dex for Feige 49 and HD 205805 relative to the LTE results of Edelmann et al. (2006). These *systematic* shifts are slightly larger than the typically attributed uncertainties of sdB analyses. Further refinements can be expected from the use of (multiple) non-LTE ionization equilibria of metals which are even more sensitive to stellar parameter changes than the hydrogen and helium lines. So far, only the S II/III ionization equilibrium has been used to verify the parameter determination for HD 205805 from H and He line profile fits (see below).

4. ELEMENTAL ABUNDANCES

Besides unbiased stellar parameters, which are a prerequisite for meaningful comparisons with stellar evolution computations, also the surface abundances of the heavier elements bear important information. They allow to put observational constraints on formation/evolution scenarios of the stars and on transport processes (in particular diffusion for sdBs) in stellar atmospheres.

For the time being, non-LTE abundances are determined only for H, He, C, N, O and the α -elements Mg and S because we lack realistic non-LTE model atoms for the other chemical species. The lighter elements are of interest because of their involvement in fusion reactions, either as catalysts or as burning products, thus giving clues on the nature of the sdB progenitors. The α -process elements on the other hand can be used as tracers for the stellar metallicity. All the present-day abundances may be of course subject to diffusion. We intend to extend the study to Al, Si and Fe in the near future. Work on this is in progress.

Elemental abundances are derived from line-profile fits, using a χ^2 -minimization

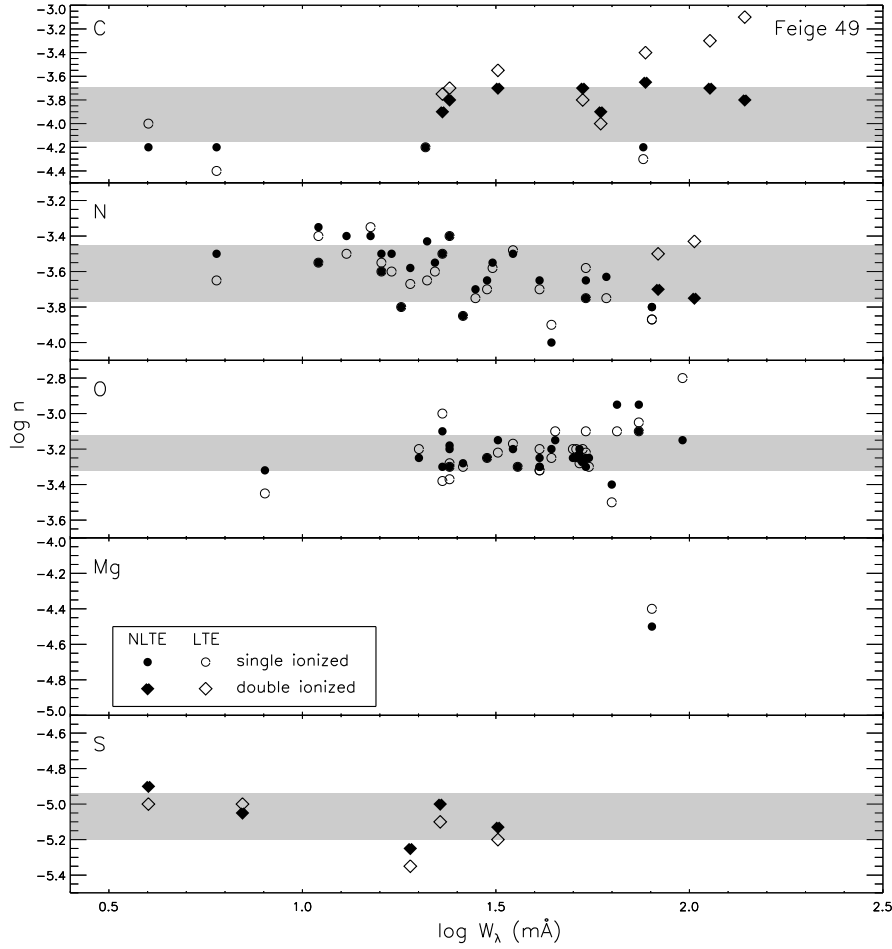


Fig. 3. Elemental abundances in Feige 49 from individual spectral lines.

technique based on small grids of synthetic spectra with varying abundances for given stellar parameters. This puts tighter constraints than the standard equivalent-width analysis. Abundances (by number) from individual spectral lines as a function of equivalent width are displayed in Figures 3 and 4. Non-LTE abundances are denoted by full and LTE results by open symbols; circles mark single-ionized and diamonds double-ionized species. The grey bands indicate the 1σ -uncertainty range of the resulting abundances for the chemical species.

The results have to be viewed as preliminary, as abundances from the different ionization stages of the elements – in particular C II/III and N II/III – indicate a need to improve on the stellar parameters. Metal ionization equilibria react much more sensitively to changes than the hydrogen and helium lines, such that the necessary fine-adjustments will barely impact the fit quality of the latter. However, already now the advantages of non-LTE computations become apparent: a tendency towards a reduced statistical scatter relative to LTE and a reduction of systematic trends, like for N II in HD 205805. The aim is to push the statistical 1σ -

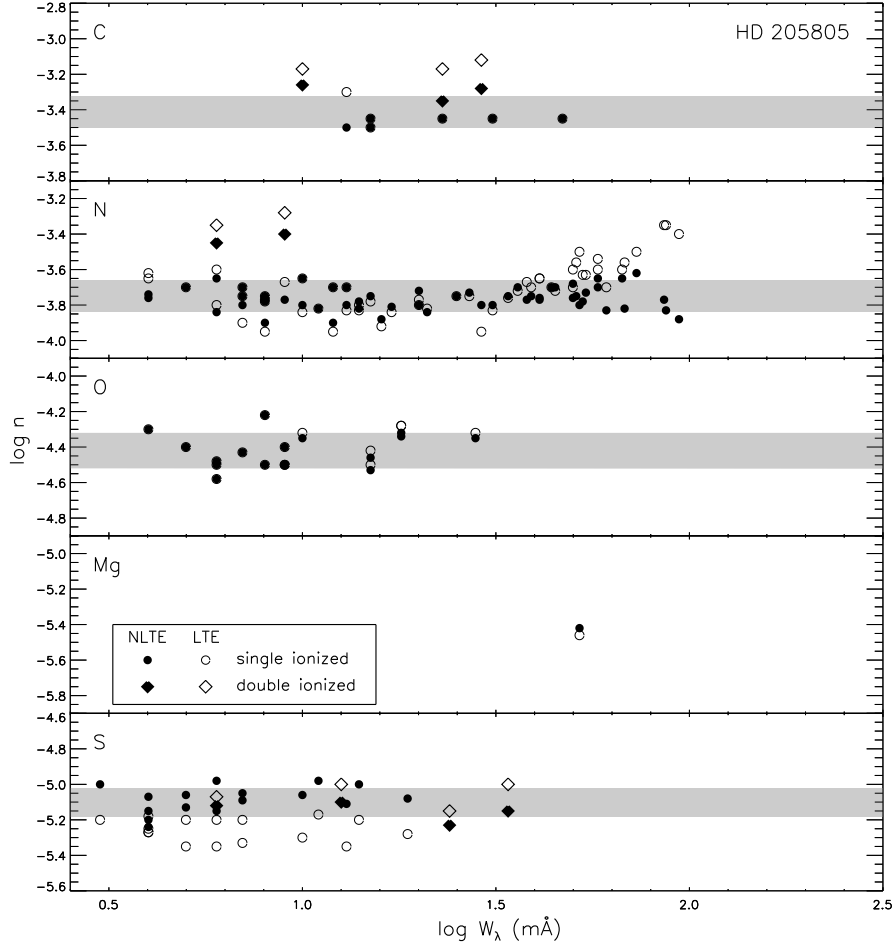


Fig. 4. Elemental abundances in HD 205805 from individual spectral lines.

Table 3. Metal abundances in the sample stars, relative to the solar standard (Grevesse & Sauval 1998): $[\log n] = \log n_{\star} - \log n_{\odot}$.

| | | C II | C III | N II | N III | O II | Mg II | S II | S III |
|-----------|------|-------|-------|-------|-------|-------|-------|-------|-------|
| Feige 49 | NLTE | -0.72 | -0.29 | +0.48 | +0.35 | -0.05 | -0.08 | ... | -0.27 |
| | | ... | 0.10 | 0.16 | 0.04 | 0.10 | ... | ... | 0.13 |
| | LTE | -0.75 | -0.10 | +0.44 | +0.61 | -0.06 | +0.02 | ... | -0.33 |
| | | 0.17 | 0.30 | 0.15 | 0.05 | 0.14 | ... | ... | 0.15 |
| HD 205805 | NLTE | +0.01 | +0.18 | +0.32 | +0.65 | -1.25 | -1.00 | -0.28 | -0.35 |
| | | 0.03 | 0.05 | 0.06 | 0.04 | 0.10 | ... | 0.08 | 0.06 |
| | LTE | +0.05 | +0.33 | +0.38 | +0.77 | -1.24 | -1.04 | -0.46 | -0.25 |
| | | 0.07 | 0.03 | 0.14 | 0.05 | 0.10 | ... | 0.07 | 0.07 |

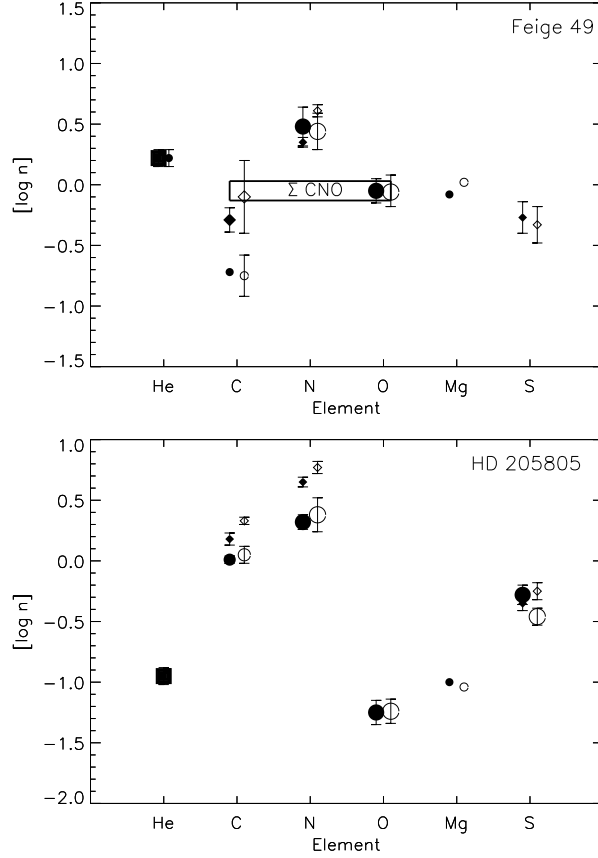


Fig. 5. Elemental abundances in the two sample sdBs (symbols as in Fig. 4).

uncertainties below 0.1 dex, like in similar computations for BA-type supergiants (Przybilla 2002) and B-type main-sequence stars (Nieva & Przybilla, in prep.). The systematic uncertainties need to be determined, but they can be expected to be of the order ~ 0.1 dex on the mean, as in the other cases.

The metal abundances of the sample stars relative to the solar standard are summarized in Table 3. For each ionic species non-LTE and LTE results with uncertainties derived from the line-to-line scatter are given. The data is also displayed in Figure 5, using the same symbols as in the figures before, with the symbol size encoding the number of lines used for the abundance determination.

The abundance pattern for Feige 49 indicates mixing of the surface layers with CNO-processed material: He and N are enriched and C is depleted. Oxygen appears to be unchanged relative to the other α -elements, which indicate approximately solar metallicity for this star. Note that the sum of the CNO abundances also gives a value close to solar, emphasizing the catalyst role of these species. The pattern is unusual for a sdB star. On the other hand, HD 205805 shows an abundance pattern more typical for sdB stars, indicating that diffusion processes have been active.

5. CONCLUSIONS AND PROSPECTS

Hybrid non-LTE analyses of two sdB stars demonstrate that non-LTE effects have to be accounted for in the stellar parameter and abundance determination, resulting in excellent fits of *all* the diagnostic spectral features. Systematic shifts in the basic parameters T_{eff} and $\log g$ are implied and non-LTE abundance corrections on the order of ~ 0.05 – 0.25 dex on the mean. The latter are similar to corrections of metal abundances in (less-luminous) BA-type *supergiants* (Przybilla 2002).

The next steps in the refinements of the method will include the necessary fine-adjustments in the stellar parameter determination in order to meet the constraints imposed by various metal ionization equilibria. The uncertainties in the metal abundances can then be expected to drop below 0.1 dex, as experience tells us from analyses of objects in other parts of the Hertzsprung-Russell diagram. Additional non-LTE model atoms are required for a few other important diagnostic chemical species, like aluminum (an element with odd neutron number), silicon (another α -element, highly valuable for stellar parameter estimations) and iron (to cover iron group abundances).

Similar analyses of a larger sample of sdB stars, and an extension towards the sdO regime, will allow for unbiased positioning in the T_{eff} vs. $\log g$ plane. This will help to delineate the different populations of subluminous stars with unprecedented accuracy and may provide the crucial clues for uncovering their formation history (single vs. binary star evolution channels). A stellar sample with highly accurate parameter and abundance determinations will hereby also put tight observational constraints on the stellar evolution computations. These can be used for an empirical calibration of the parametrization of complex (hydrodynamical) phenomena involved in the stellar evolution calculations, thus leading to an improved modeling.

REFERENCES

- Becker S. R., Butler K. 1988, A&A, 201, 232
 Butler K., Giddings J. R. 1985, in Newsletter on Analysis of Astronomical Spectra, No. 9, Univ. London
 Edelmann H., Heber U., Napiwotzki R. 2006, Baltic Astronomy, 15, 103 (these proceedings)
 Giddings J. R. 1981, Ph. D. thesis, Univ. London
 Grevesse N., Sauval A. J. 1998, Space Sci. Rev., 85, 161
 Heber U., Edelmann H. 2004, Ap&SS, 291, 341
 Kaufer A., Stahl O., Tubbesing S. et al. 1999, ESO Messenger, 95, 8
 Kurucz R. L. 1996, in *Model Atmospheres and Spectrum Synthesis*, eds. S. J. Adelman, F. Kupka & W. W. Weiss, ASP Conf. Ser., 108, 160
 Przybilla N. 2002, Ph. D. thesis, Univ. Munich
 Przybilla N. 2005, A&A, 443, 293
 Przybilla N., Butler K. 2001, A&A, 379, 955
 Przybilla N., Butler K. 2004, ApJ, 609, 1181
 Przybilla N., Butler K., Becker S. R., Kudritzki R. P. 2001, A&A, 369, 1009
 Stehlé C., Hutcheon R. 1999, A&AS, 140, 93
 Vrancken M., Butler K., Becker S. R. 1996, A&A, 311, 661

NEW MODEL ATMOSPHERES FOR HYDROGEN-DEFICIENT STARS: CONTINUOUS AND LINE OPACITIES

N. T. Behara and C. S. Jeffery

Armagh Observatory, College Hill, Armagh BT61 9DG, N. Ireland

Received 2005 August 1

Abstract. The model atmosphere code STERNE has evolved considerably over the years. Most recently, attention has turned to revising the treatment of both continuous and line opacities. Opacity Project photoionization cross-sections have been incorporated and an opacity sampling technique has been implemented. The new opacities and methods are described, while the principal consequences for the models are presented. In studying the application of these new models to atmospheres with extreme chemical compositions, we find the new opacity treatment increases the temperature in the line forming region by 1000–3000 K for extremely hydrogen-poor stars with T_{eff} around 30 000 K. This implies cooler effective temperature measurements for stars of this type.

Key words: stars: atmospheres – stars: chemically peculiar

1. INTRODUCTION

Hydrogen deficiency is a wide spread phenomenon occurring in a variety of stellar objects such as extreme helium stars, hydrogen-deficient binaries, helium-rich subdwarfs, Wolf-Rayet stars, R CrB stars and helium white dwarfs. These hydrogen-deficient systems are believed to evolve by very different processes. R CrB and extreme helium stars evolve by binary merger or late thermal pulse evolution from the white dwarf phase, hydrogen-deficient binary stars through a sequence of mass exchange phases, and helium-rich subdwarfs evolve possibly through white dwarf mergers, late helium flash or common envelope evolution.

Stellar atmosphere models are an essential tool used in the derivation of fundamental stellar parameters, such as effective temperature, surface gravity and overall metallicity, as well as determining individual element abundances. The accuracy of the atmospheric structure obtained from our models is inherently dependent on the quality of the atomic data used and the methods by which they are incorporated into the models, especially in the case of hydrogen-deficient atmospheres.

Because neutral helium is a poor absorber, the effect of continuous and line opacity is of greater importance in hydrogen-deficient stars, shown in Figure 1. The figure on the left shows the emergent flux distribution of hydrogen-rich atmospheres and on the right for hydrogen-deficient atmospheres with $(T_{\text{eff}}, \log g) = (10\,000, 1.0), (11\,000, 1.0), (12\,000, 1.0), (13\,000, 1.5)$ and $(14\,000, 1.5)$. Continuum-only models are shown by dotted lines and line-blanketed models by

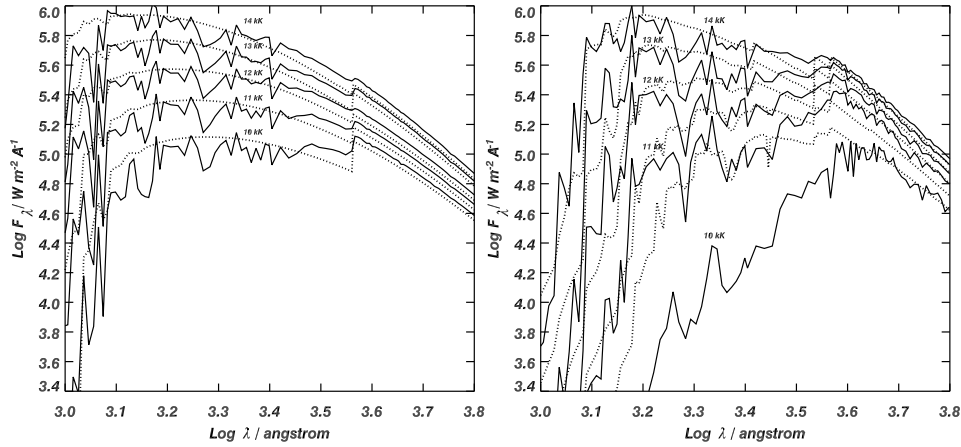


Fig. 1. Importance of line blanketing in hydrogen-rich atmospheres (left panel) and hydrogen-deficient atmospheres (right panel). The figure on the left is from Dudley & Jeffery (1993).

solid lines labeled with effective temperature. The effects of line blanketing on the flux distribution are extremely marked for stars with effective temperatures below 14 000 K.

The entire spectrum of hydrogen-deficient stars comprises an inhomogeneous mix of chemical abundances. For example, in the case of extreme helium stars the hydrogen abundance is roughly 1 part in 10^4 , and carbon dominates the opacity at many wavelengths. As a consequence, the carbon abundance greatly influences the atmospheric structure. However, hydrogen-deficient binaries are carbon-poor and nitrogen-rich, while for a few hot R CrB stars n_{H} may be as high as 0.1. In order to model these atmospheres correctly, we should adapt the composition of our models to the composition of stars.

Theoretical work in recent years has provided superior calculations of continuous opacities, and the contribution of absorption lines to the overall opacity has also been an area of progress since *STERNE* was originally written. We discuss the recent revisions to *STERNE* and compare some results of the new updated version to the last published version of the code (Jeffery & Heber 1992).

1.1. *STERNE* – model atmosphere program

The LTE model atmosphere code *STERNE* was originally developed to study hydrogen-deficient stars. The code is optimized for stars with effective temperatures between 10 000 K and 35 000 K, and extreme compositions dominated by helium, carbon and nitrogen (Schönberner & Wolf 1974; Jeffery & Heber 1992). The model assumes hydrostatic, radiative and local thermodynamic equilibrium, as well as plane-parallel geometry. The radiative transfer equation is solved using Feautrier’s scheme, and the temperature correction follows the Unsöld-Lucy procedure.

From 1990 to 2003 the treatment of the continuous opacities followed Kurucz (1979), with the addition of carbon and nitrogen opacities from Peach (1970). The line opacities were calculated using opacity distribution functions (ODF) computed for hydrogen-deficient mixtures from the Kurucz & Peytremann (1975) list of 265 000 lines.

Table 1. Opacity Project photoionization cross-sections used in the continuous opacity calculations.

| Element | Ionization stage | Number of states |
|---------|------------------|------------------|
| H | I | 55 |
| He | I, II | 13, 55 |
| Li | I, II, III | 25, 53, 55 |
| Be | I, II, III, IV | 55, 25, 54, 55 |
| B | I, II, III, IV | 55, 55, 26, 53 |
| C | I, II, III, IV | 50, 21, 38, 24 |
| N | I, II, III, IV | 36, 50, 32, 39 |
| O | I, II, III, IV | 50, 29, 25, 36 |
| F | I, II, III, IV | 50, 50, 50, 50 |
| Ne | I, II, III, IV | 50, 50, 50, 50 |
| Na | I, II, III, IV | 32, 50, 50, 50 |
| Mg | I, II, III, IV | 50, 32, 50, 50 |
| Al | I, II, III, IV | 41, 50, 31, 50 |
| Si | I, II, III, IV | 50, 51, 50, 31 |
| S | I, II, III, IV | 50, 50, 50, 50 |
| Ar | I, II, III, IV | 50, 50, 50, 50 |
| Ca | I, II, III, IV | 50, 17, 50, 50 |
| Fe | III, IV, V, VI | 50, 50, 50, 50 |

2. METHODS

2.1. Continuous opacities

We focus the discussion on the continuous opacities due to bound-free transitions only, as the treatment of free-free absorption and scattering is preserved from the previous version of STERNE.

The Opacity Project (OP, The Opacity Project Team 1995, 1997) data used in the opacity calculations is shown in Table 1. The individual cross-sections must first be resampled on the model wavelength grid before the opacity calculations are carried out, and as a consequence the photoexcitation of the core (PEC) resonances of the cross-sections are not fully resolved. The resampling preserves the cross-sections to within an error of 10%.

The way in which the OP data are included in the model atmosphere code is sufficiently general that any combination of ions may be selected, once the necessary cross-sections have been downloaded from TOPbase (Cunto et al. 1993). Additional cross-sections may be added as they become available.

2.2. Line opacities

We have devised a procedure, loosely based on Sneden et al. (1976) to sample the line opacity directly at each wavelength grid point for all layers in a model atmosphere. Relevant lines are selected from a master list of atomic lines based on the temperature, pressures and abundances of the model at each wavelength and depth point. Approximately 500 000 lines are selected. For each grid point, the

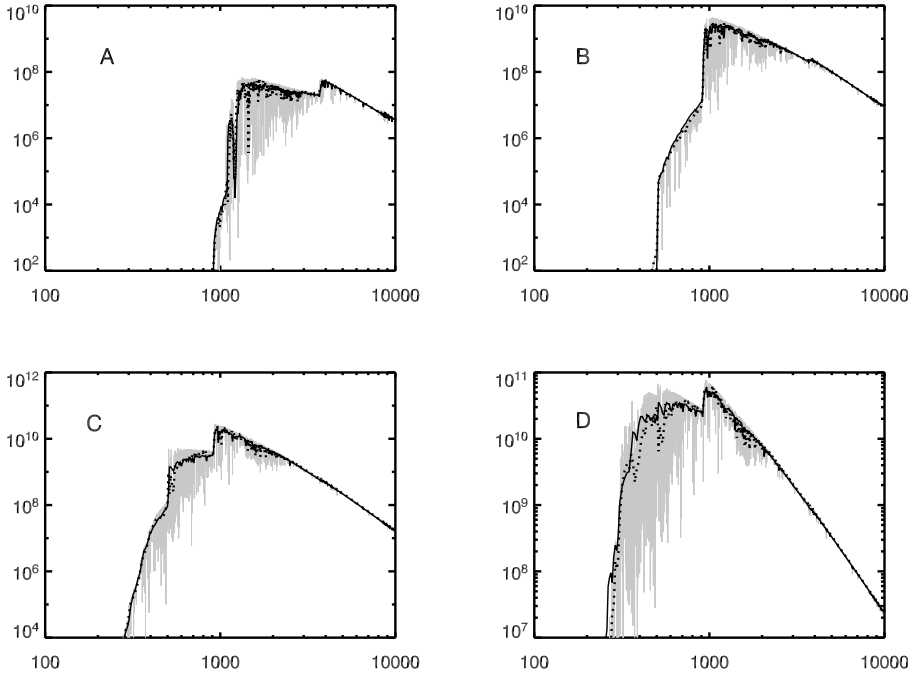


Fig. 2. Solar composition comparisons of the STERNE opacity sampled models to Kurucz's ATLAS9 models. The ATLAS9 models are shown by the black lines. The STERNE models are represented by the grey lines, and also shown resampled on the ATLAS9 grid by the dotted lines. The emergent flux is plotted as a function of wavelength for four T_{eff} , $\log g$ pairs (see text).

contributions of all selected lines within prescribed search windows are included in the line opacity calculation. The line opacity is calculated using detailed line profiles for each selected spectral line. Computed in this fashion, the opacity sampling (OS) method is able to account for the depth dependence of the variation with wavelength of the line opacities. Lines are selected from the atomic line list compiled by Kurucz & Bell (1995).

2.3. Model verification

A comparison of the STERNE models with Kurucz's ATLAS9 models has been carried out using a solar composition and four effective temperature and gravity pairs. The results are shown in Figure 2.

The emergent flux is plotted as a function of wavelength for A: $T_{\text{eff}} = 10\,000$ K, $\log g = 3.0$, B: $T_{\text{eff}} = 20\,000$ K, $\log g = 3.0$, C: $T_{\text{eff}} = 30\,000$ K, $\log g = 3.5$ and D: $T_{\text{eff}} = 40\,000$ K, $\log g = 4.5$. The STERNE model has been resampled on the ATLAS9 grid to allow for comparison. Differences in the models can be accounted for by the different solar abundances used, and differences in the treatment of continuous and line opacities, which alter the model structure. We use the solar abundances of Grevesse & Sauval (1998), while Kurucz uses the abundances by Anders & Grevesse (1989).

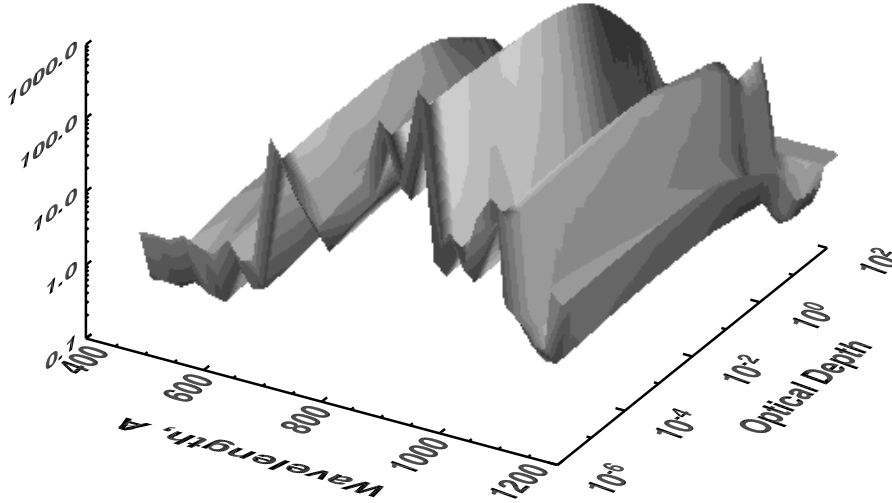


Fig. 3. The ratio of the OP CII continuous opacity to the Peach opacity in a model atmosphere with $T_{\text{eff}} = 20\,000$ K and $\log g = 3.0$.

3. RESULTS

We have compared hydrogen-rich and helium-rich models of the opacity sampled version of STERNE with new continuous opacities to the models computed using the ODF version of STERNE. Models have been computed with and without line opacity in order to compare the effect of changing the continuous opacities alone.

Looking at continuum-only models, we find general agreement between the models in the hydrogen-rich case. However, when comparing helium-rich models, we have found that the new opacities produce significant changes in the emergent flux distribution of the atmosphere, particularly in the region $500 \text{ \AA} < \lambda < 1000 \text{ \AA}$. The primary cause is the CII continuous opacity.

An increase in the opacity when using the OP cross-sections leads to an increase in the continuum opacity at $\lambda < 1000 \text{ \AA}$, resulting in more UV flux with a steeper continuum at $\lambda > 1200 \text{ \AA}$. A comparison of the CII opacity computed in both models is shown in Figure 3. The ratio of the opacity computed with the OP cross-sections to the opacity computed using the Peach tables (1970) is plotted as a function of optical depth in the atmosphere and as a function of wavelength.

When comparing continuum plus line models, we find that differences in the flux and temperature distributions are far more drastic for the helium-rich case than the hydrogen-rich case.

The plot on the left of Figure 4 shows the effects of the new opacities on the flux distribution of a hydrogen-rich atmosphere and the figure on the right for a helium-rich atmosphere with $T_{\text{eff}} = 30\,000$ K and $\log g = 5.0$. The ODF model is shown by the solid line, the OS model by the grey line and the OS model resampled on the ODF wavelength grid by the dotted line. The plots have been cropped to show regions of interest, the integral over the flux remains the same for both models.

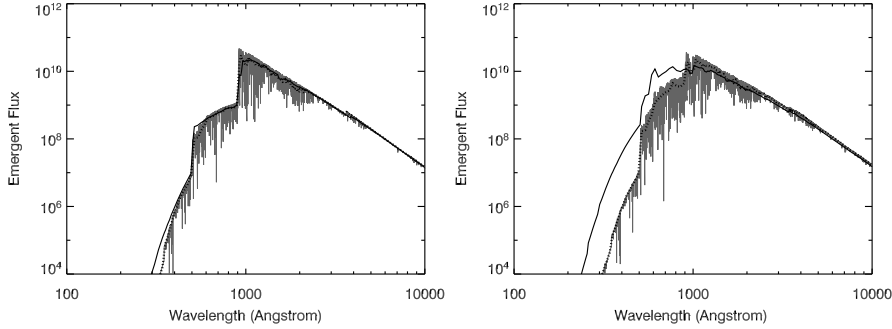


Fig. 4. Flux distributions of hydrogen-rich and helium-rich model atmospheres. The solid line represents the ODF model, and the grey line represents the new OS model, also shown resampled on the ODF grid (dotted line). Model parameters on the left: $T_{\text{eff}} = 30\,000\text{ K}$, $\log g = 5.0$, $n_{\text{H}} = 0.911$ and $n_{\text{He}} = 0.089$. Model parameters on the right: $T_{\text{eff}} = 30\,000\text{ K}$, $\log g = 5.0$, $n_{\text{H}} = 0.0001$ and $n_{\text{He}} = 0.99$, $n_{\text{C}} = 0.0099$ and solar metallicity.

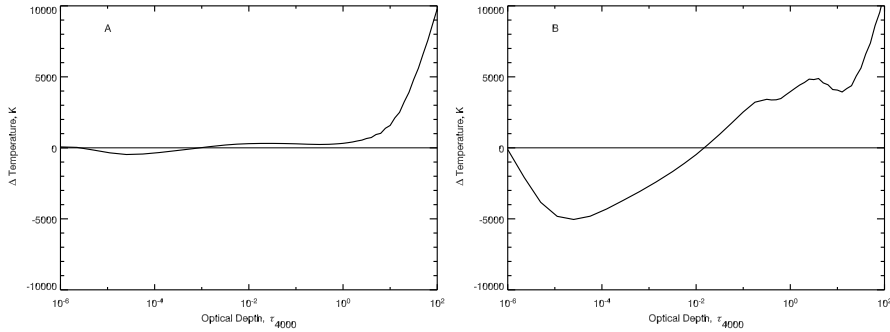


Fig. 5. Differences ($T_{\text{OS}} - T_{\text{ODF}}$) in the temperature distribution for the models as a function of optical depth. A – hydrogen-rich models from the left plot of Fig. 4, B – helium-rich models from the right plot of Fig. 4.

The effect of the new opacities on the temperature distribution of the atmosphere is shown in Figure 5. The temperature differences ($T_{\text{OS}} - T_{\text{ODF}}$), are plotted as a function of optical depth for both compositions. The differences in the temperature distribution translate into an approximate increase of up to 3000 K in the line forming region of the atmosphere for a hydrogen-deficient star with $T_{\text{eff}} = 30\,000\text{ K}$. In the hydrogen-rich case we expect an increase of approximately 300 K.

Figure 6 shows the range of the approximate increase in temperature across the line forming region of both helium-rich and hydrogen-rich high-gravity stars at several effective temperatures. These results show that the new treatment of opacity will have implications in the effective temperature measurements of stars of all compositions and temperatures.

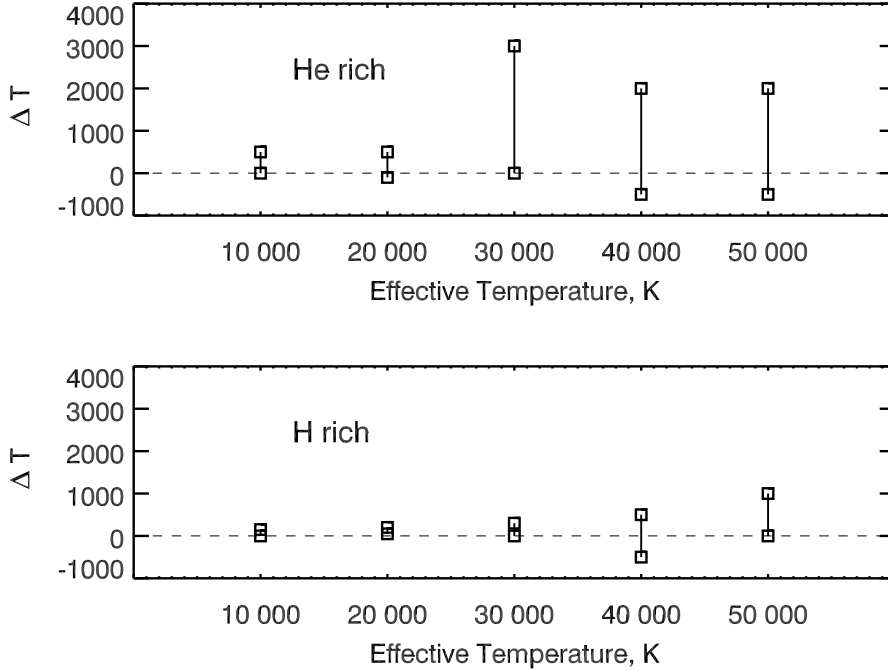


Fig. 6. Differences ($T_{\text{OS}} - T_{\text{ODF}}$) in the line forming region of the temperature distribution of helium-rich and hydrogen-rich model atmospheres with $(T_{\text{eff}}, \log g) = (10\,000, 3.0), (20\,000, 4.0), (30\,000, 5.0), (40\,000, 6.0), (50\,000, 6.0)$. The line forming region has been approximated as the range in optical depth 10^{-2} to 10^0 .

4. SUMMARY

The treatments of continuous and line opacity in the model atmosphere code STERNE have been revised. Opacity Project cross-sections have been incorporated and an opacity sampling method has been implemented. Results show significant differences for chemically peculiar stars when compared to model atmospheres computed using Kurucz and Peach continuous opacities and an ODF treatment for line opacity. The principal results are that the C II continuous opacity computed using OP cross-sections substantially modifies the flux distribution of hydrogen-deficient atmospheres at $\lambda \sim 1000 \text{ \AA}$, and the new line opacity treatment significantly modifies the temperature distribution of these stars. Effects in the temperature distribution of hydrogen-rich stars of up to 300 K are also seen. These results will have consequences in the effective temperature measurements of stars of all compositions.

Several applications exist for these models. We intend to examine extreme helium stars, helium-rich sdB stars, chemically peculiar subdwarf B stars and hydrogen-deficient binaries.

ACKNOWLEDGMENTS. Research at Armagh Observatory is funded by the Department of Culture, Arts and Leisure, Northern Ireland.

REFERENCES

- Anders E., Grevesse N. 1989, *Geochim. Cosmochim. Acta*, 53, 197
- Cunto W., Mendoza C., Ochsenbein F., Zeippen C. J. 1993, *A&A*, 275, L5
- Dudley R. E., Jeffery C. S. 1993, *MNRAS*, 262, 945
- Grevesse N., Sauval A. J. 1998, *Space Sci. Rev.*, 85, 161
- Jeffery C. S., Heber U. 1992, *A&A*, 260, 133
- Kurucz R. L. 1979, *ApJS*, 40, 1
- Kurucz R. L., Bell B. 1995, *Kurucz CD-ROM 23*, Cambridge, SAO
- Kurucz R. L., Peytremann E. 1975, *SAOSR*, 326, 1
- Peach G. 1970, *MNRAS*, 73, 1
- Schönberner D., Wolf R. 1974, *A&A*, 37, 87
- Snedden C., Johnson H. R., Krupp B. M. 1976, *ApJ*, 204, 281
- The Opacity Project Team. 1995 in *The Opacity Project*, Vol. 1, Institute of Physics Publishing, Bristol
- The Opacity Project Team. 1997 in *The Opacity Project*, Vol. 2, Institute of Physics Publishing, Bristol

ATMOSPHERIC PARAMETERS FOR SUBDWARF B STARS: A CONSISTENCY CHECK BETWEEN THE BALMER LINES AND THE FAR-ULTRAVIOLET SPECTRUM

C. Pereira, F. Wesemael and P. Bergeron

Département de Physique, Université de Montréal, C.P. 6128, Succ. Centre-Ville, Montréal, Québec H3C 3J7, Canada; e-mail: pereira@astro.umontreal.ca

Received 2005 August 1

Abstract. The use of Balmer line profiles to determine atmospheric parameters of subdwarf B stars is a well-established method that relies on a comparison of spectroscopic observations with synthetic spectra generated from model atmospheres. This method allows us to determine parameters such as the effective temperature, surface gravity and photospheric helium abundance. The self-consistency of these parameters can be investigated by examining the Lyman lines covered by current far-ultraviolet observations. We discuss the results of a preliminary analysis of a sample of ten subdwarf B stars for which both optical and far-ultraviolet spectra were secured. At temperatures below 30 000 K we find good consistency between optical and ultraviolet spectra when some allowance is made for the metal-line blanketing present in the ultraviolet region. At higher effective temperatures, however, the consistency is not as satisfactory. Possible solutions to this puzzle are considered.

Key words: stars: atmospheres, subdwarfs

1. INTRODUCTION

The atmospheric parameters which characterize the subdwarf B (or sdB) stars are now routinely obtained from simultaneous fits to the Balmer line profiles with synthetic spectra generated from model atmospheres (see, e.g., Saffer et al. 1994). Over the years, this method has proved quite reliable, although systematic effects between various grids of models may still be present. The method can, in principle, be extended to the Lyman region of the spectrum, just as it has been for the DA (Barstow et al. 2001, 2003) and DAO white dwarfs (Good et al. 2004). However, in the case of the hot B subdwarfs, it is expected that the interpretation of the fits to the Lyman lines might be more complicated, since the far ultraviolet spectra of sdB stars are known to include hundreds of transitions from heavy elements (see, e.g., Ohl et al. 2000). The blocking effect of these numerous lines would have to be considered in any fit purporting to match the ultraviolet continuum level of hot B subdwarfs. This problem could be solved by fitting the ultraviolet continuum with fully blanketed synthetic spectra; however, this cannot be accomplished in a routine manner yet, as the abundance patterns of heavy elements which characterize sdB stars are still being documented (Edelmann et al. 2006; Fontaine et al.

2005). Thus, at this stage, it might be more appropriate to (i) determine the atmospheric parameters of hot B subdwarfs on the basis of optical spectroscopy and synthetic spectra as sophisticated as possible; (ii) calculate the ultraviolet continuum predicted at the values of T_{eff} , $\log g$ and He/H derived in the optical; and (iii) investigate to what extent the predicted ultraviolet continuum is consistent with that observed with the FUSE satellite. We have undertaken such an exploratory study on a small sample of hot B subdwarfs and present here preliminary results from this investigation.

2. OBSERVATIONS, MODELS AND BALMER LINE FITS

Ten subdwarf B stars were selected for this analysis. The optical spectra were secured using the 2.3 m telescope at Steward Observatory, while the far-ultraviolet spectra were obtained through the FUSE satellite archives. We computed pure hydrogen and mixed helium and hydrogen ($\log \text{He}/\text{H} = -2.5$), NLTE model atmospheres using version 200 of TLUSTY (Hubeny 1988) and the corresponding synthetic spectra using version 48 of SYNSPEC (Hubeny & Lanz 1995) with the Stark broadening tables of Lemke (1997). Our model grid extends over the following parameters: $T_{\text{eff}} = 20\,000$ to $60\,000$ K spaced by 2000 K and $\log g = 5.0$ to 6.5 spaced by 0.25 dex. We emphasize that our grid includes no heavy elements.

The technique used to fit the Balmer lines is standard and can be summarized as follows: the observed and theoretical Balmer line profiles (H β -H9) are normalized to a linear continuum set to unity. The observations are then compared to synthetic spectra and a chi-squared minimization technique is then applied until a best fit is achieved between the calculated model and the observations (see, e.g., Bergeron et al. 1992). All in all, the pure hydrogen models fit the optical spectra of our target stars quite satisfactorily.

3. THE FAR-ULTRAVIOLET CONTINUUM OF sdB STARS

As we emphasized earlier, a fit to the Lyman lines carried out in the same manner as the fit to the Balmer lines is not possible: while the optical spectra show few features besides the H I and He I lines, the FUSE observations reveal numerous lines of heavy elements that mar the ultraviolet spectrum. This prevents us from clearly determining the placement of the continuum, a crucial step in the standard fitting procedure. Thus, to verify the consistency of the parameters, we adopt the following approach. With the atmospheric parameters derived from the optical spectrum, we calculate the theoretical flux at 5458.7 \AA associated with each star and, on the basis of existing Strömgren photometry, fix the solid angle. This allows us to normalize the emergent flux from our model atmospheres, and to predict the ultraviolet flux received at the Earth. For all but one star in our sample, no interstellar reddening was included, although the presence of small amounts of reddening cannot be excluded. In the case of PG 0823+466, however, reddening was required, and the color excess we determine, $E_{B-V} = 0.10$, is not unusual even for high-latitude PG stars. Unfortunately, there are no archival IUE observation of this object which would have provided a check on this measurement.

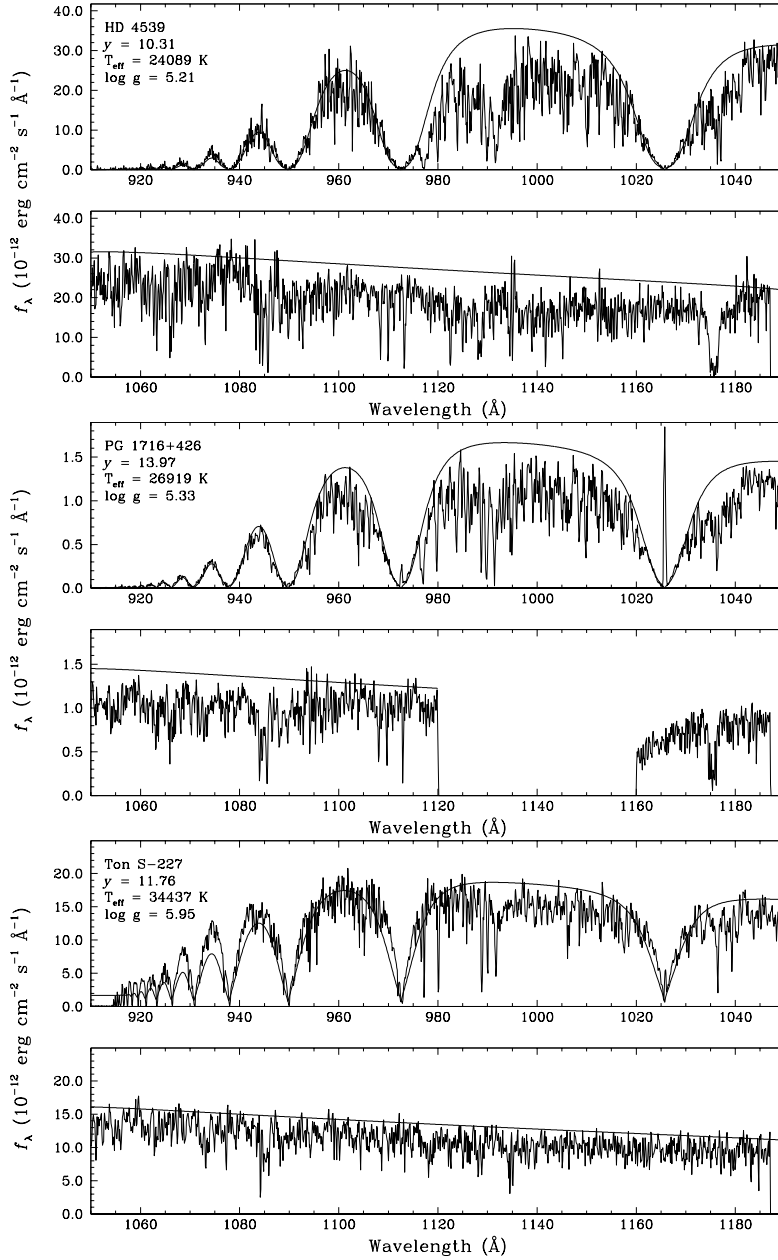


Fig. 1. Synthetic spectra calculated for three objects using the parameters derived from their optical spectrum (values are indicated in the top lefthand corner). These are superimposed onto the FUSE observations and are not fits, but rather provide a check on the consistency between the optical and ultraviolet ranges. The synthetic spectra are normalized using the y magnitude, as described in the text.

Our predictions of the ultraviolet flux are compared to the absolute flux measured by the FUSE satellite in Figure 1 for three objects in our sample. These include HD 4539, a cool and bright sdB star, PG 1716+426, the prototypical long-period sdB variable and Ton S-227, a well-studied sdB star at a somewhat higher effective temperature. The predicted fluxes are calculated on the basis of pure hydrogen or mixed hydrogen/helium models which do not include any heavy elements. For objects with $T_{\text{eff}} < 30\,000$ K, our comparisons at ultraviolet wavelengths yield satisfactory results in the sense that, when some allowance is made for metal line blanketing, the synthetic spectra reproduce in a satisfactory manner the general shape of the continuum as well as the Lyman line profiles. This is shown in Figure 1 for HD 4539 and PG 1716+426. Interestingly, our procedure may provide us with a way to decide where the continuum level should be set in abundance analyses of FUSE spectra.

For objects with $T_{\text{eff}} > 30\,000$ K, however, there appears to be a systematic discrepancy between the synthetic spectra derived from the optically determined parameters and the observed ultraviolet spectra. Ton S-227 provides us with a clear illustration of this situation: the predicted Lyman lines appear too wide, as if the surface gravity determined in the optical were too large, while the flux level in the interline region appears too low, in contrast to what it should be if line-blocking were the only significant omission in our models. Because some heavy elements are more abundant in hotter objects than in cooler ones, while the reverse is true for other elements, it is not possible, at this stage, to connect simply and unambiguously the trend we observe at high effective temperatures with the abundance of heavy elements. Moreover, it should be noted that Barstow et al. (2001, 2003) encountered similar discrepancies for DAs with $T_{\text{eff}} > 50\,000$ K.

We are currently exploring other alternatives to account for the systematic discrepancy observed in the hotter sdB stars. Interstellar reddening, stratified H/He atmospheres, as well as homogeneous atmospheres incorporating large abundances (up to solar) of heavy elements, such as those considered by Heber (2006) and Behara & Jeffery (2006) at this conference, are currently being considered.

ACKNOWLEDGMENTS. We thank P. Chayer for useful discussions pertaining to this project. This work was supported in part by the NSERC Canada and by the Fund FQRNT (Québec)

REFERENCES

- Barstow M. B., Good S. A., Burleigh M. R. et al. 2003, MNRAS, 334, 562
 Barstow M. B., Holberg J. B., Hubeny I. et al. 2001, MNRAS, 328, 211
 Bergeron P., Saffer R. A., Liebert J. 1992, ApJ, 394, 228
 Fontaine M., Chayer P., Wesemael F. et al. 2005, in *Astrophysics in the Ultraviolet*, eds. G. Sonneborn, H. W. Moos & B.-G. Andersson, in press
 Edelmann H., Heber U., Napiwotzki R. 2006, Baltic Astronomy, 15, 103 (these Proceedings)
 Good S. A., Barstow M. B., Holberg J. B. et al. 2004, MNRAS, 355, 1031
 Hubeny I. 1988, Computer Physics Comm., 52, 103
 Hubeny I., Lanz T. 1995, ApJ, 439, 875
 Lemke M. 1997, A&AS, 122, 285
 Ohl R. G., Chayer P., Moos H. W. 2000, ApJ, 538, 950
 Saffer R. A., Bergeron P., Koester D., Liebert J. 1994, ApJ, 432, 351

IMPROVED HELIUM LINE FORMATION FOR EXTREME HELIUM STARS

N. Przybilla¹ K. Butler² U. Heber¹ and C. S. Jeffery³

¹ *Remeis-Sternwarte Bamberg, Sternwartstr. 7, D-96049 Bamberg, Germany*

² *Universitätssternwarte München, Scheinerstr. 1, D-81679 München, Germany*

³ *Armagh Observatory, College Hill, Armagh BT61 9DG, Northern Ireland*

Received 2005 July 31

Abstract. Quantitative analyses of extreme helium stars to date face the difficulty that theory fails to reproduce the observed helium lines in their entirety, wings *and* line cores. Here, we demonstrate how the issues can be resolved using state-of-the-art non-LTE line formation for these chemically peculiar objects. Two unique B-type objects are discussed in detail, the pulsating variable V652 Her and the metal-poor star HD 144941. The improved non-LTE computations for helium show that analyses assuming LTE or based on older non-LTE model atoms can predict equivalent widths, for the He I 10 830 Å transition in particular, in error by up to a factor ~ 3 . Our modeling approach also succeeds in largely resolving the general mismatch for effective temperatures of EHe stars derived from ionization equilibria and from spectral energy distributions.

Key words: line: formation – stars: atmospheres – stars: fundamental parameters – stars: individual (V 652 Her, HD 144941)

1. INTRODUCTION

Extreme helium stars (EHes) are a rare class of low-mass H-deficient objects with spectral characteristics of B-giants. Most of the two dozen known EHes could be explained by post-AGB evolution, linking R CrB stars to Wolf-Rayet type central stars of planetary nebulae, see Heber (1986) and Jeffery (1996) for reviews.

LTE spectral analyses encounter two difficulties for EHe stars: (i) synthetic spectra have so far not succeeded in matching the observed helium lines in their entirety, and (ii) spectroscopic and spectrophotometric temperatures differ systematically. As inadequacies in the basic parameter determination can potentially hamper any further interpretation, the issue needs to be resolved. The necessary steps for improving the modeling will be discussed in the following for two test cases, V652 Her and HD 144941. Here, extreme helium stars turn out to be important testbeds for stellar atmosphere modeling. In particular, non-LTE model atoms for helium can be tested in more detail than in any other type of star, since all predicted transitions – including all forbidden components – can be measured. The sample stars are unique among the class members in several aspects. Both objects have gravities too large for post-AGB evolution and they show atypical surface abundances.

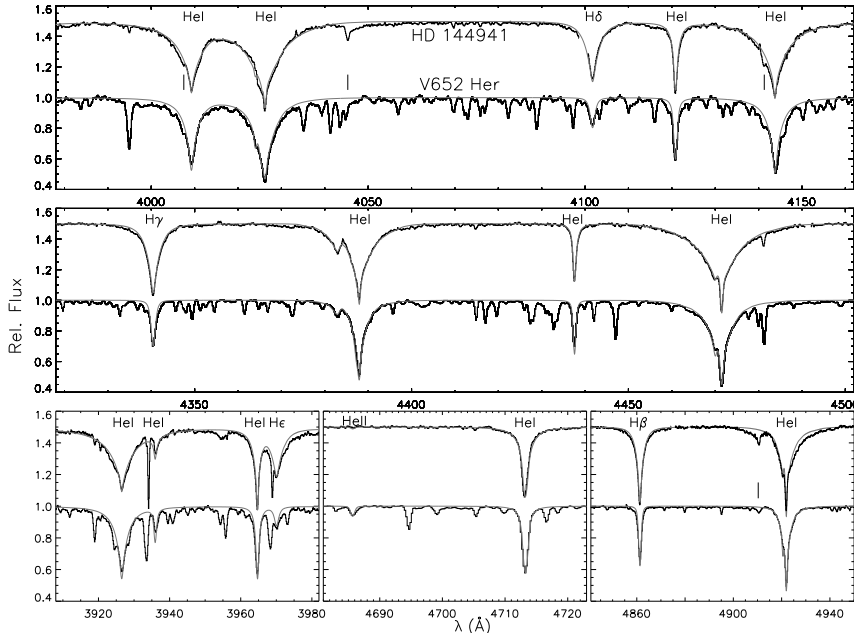


Fig. 1. Fits to He and H lines in the two sample stars.

2. MODEL CALCULATIONS AND OBSERVATIONAL DATA

The model calculations are carried out in analogy to the hybrid non-LTE approach chosen for sdB star analyses (Przybilla et al. 2006), but see also Przybilla et al. (2005) for further details. In brief, the atmospheric structure computations are carried out using the Atlas12 code (Kurucz 1996). Note that we have replaced the photoionization data for He I levels with principal quantum number $n = 2$ as used by Kurucz with data from the Opacity Project (Fernley et al. 1987). In particular the cross-sections for the $2p^3P^\circ$ level are increased by a factor ~ 2 at the threshold, thus improving the fits of computed energy distributions with observation. Then, the restricted non-LTE problem is solved. State-of-the-art model atoms for He (Przybilla 2005) and H (Przybilla & Butler 2004) are utilised, and detailed line-broadening is accounted for in the spectrum synthesis (Barnard et al. 1969, 1974; Dimitrijević & Sahal-Bréchet 1990; Stehlé & Hutcheon 1999). For comparison, additional calculations are made using the He model atom of Husfeld et al. (1989). Details of the observations and the data reduction have been published elsewhere (Jeffery et al. 2001; Harrison & Jeffery 1997).

3. DISCUSSION

The stellar parameters are derived in a standard manner, using the He I/II ionization balance as T_{eff} and the Stark-broadened He I lines as $\log g$ indicators. Data for the final models (with estimated uncertainties) are summarised in Table 1, including microturbulence ξ and also H abundance $n_{\text{H}}^{\text{NLTE}}$ (by number). For V652 Her the atmospheric parameters agree very well with those found by Jeffery

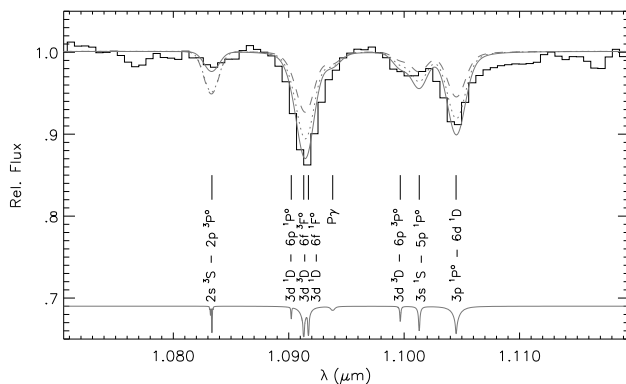


Fig. 2. Modeling of the J -band spectrum of V 652 Her.

Table 1. Stellar parameters.

| | V652 Her (R_{\max}) | HD 144941 |
|------------------------------|-------------------------|--------------------|
| T_{eff} (K) | $22\,000 \pm 500$ | $22\,000 \pm 1000$ |
| $\log g$ | 3.20 ± 0.10 | 4.15 ± 0.10 |
| ξ (km/s) | 4 ± 1 | 8 ± 2 |
| $n_{\text{H}}^{\text{NLTE}}$ | 0.005 ± 0.0005 | 0.035 ± 0.005 |

– wings *and* line cores – is found. The great improvement achieved becomes obvious when comparing Figure 1 to Figure 2 of Harrison & Jeffery (1997) and Figure 5 of Jeffery et al. (2001). This resolves one of the most persistent inconsistencies in quantitative analyses of extreme helium stars. A few forbidden components of He I lines missing in our modeling are indicated by short vertical marks. The appropriate broadening data are unavailable to us.

The He I lines in the visual experience non-LTE strengthening, facilitated by the overpopulation of the $n=2$ states relative to the levels of higher principal quantum number. This overpopulation occurs because of recombinations to levels of He I at higher excitation energies and subsequent de-excitation via downward cascades to the (pseudo-)metastable $2s$ states (the singlet resonance lines are close to detailed balance). Singlet lines are in general subject to larger non-LTE effects than the triplet lines. The level populations deviate by only a few percent from detailed equilibrium at the formation depths of the continua, indicating that the assumption of LTE for the model atmosphere computations is appropriate.

Analyses in the near-IR range are highly useful for constraining the atomic data input for the non-LTE computations because of amplified non-LTE effects in the Rayleigh-Jeans tail of the spectral energy distribution. The comparison of model calculations with the current He model (full grey line) and an old model by Husfeld et al. (1989, dotted line) with observation (histogram) for the He I 10 830 Å feature in Figure 2 demonstrates the superiority of the former. The old model predicts the line to be ~ 3 times stronger than observed, showing little deviation from detailed balance (dashed line). This success is facilitated by making use of accurate photoionization cross-sections in particular for the $2s\ ^3S$ state and a proper account of line blocking. Note that the line broadening is dominated by

et al. (2001), except for the hydrogen abundance, which is reduced by a factor ~ 2 because of non-LTE strengthening of the Balmer lines. For HD 144941, however, the resulting parameters differ significantly from previous work of Harrison & Jeffery (1997), implying a reduction in T_{eff} by 1200 K and an increase in surface gravity by a factor ~ 2 . The reduction in the hydrogen abundance is less pronounced in this star.

A comparison of our non-LTE spectrum synthesis for He and H (grey lines) with the observed spectra of V 652 Her and HD 144941 (histograms) is made in Figure 1. Excellent agreement for the entire line profiles

instrumental effects.

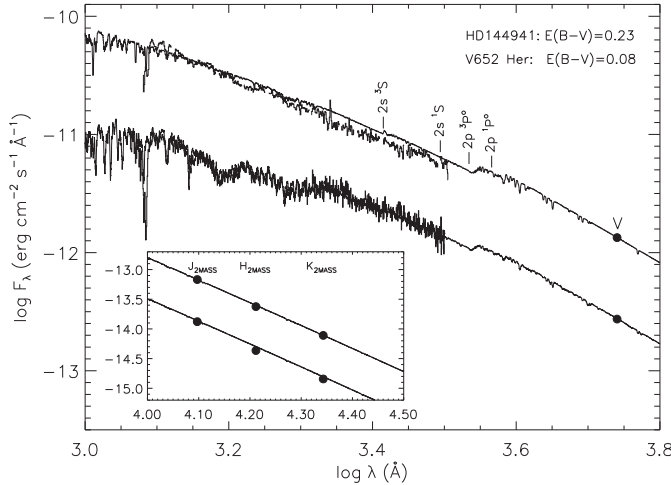


Fig. 3. SED fits for the sample stars.

He I/II ionization equilibria (see Table 1) with IUE spectrophotometry and visual and near-IR photometry (black histograms and dots) is made in Figure 3. Excellent agreement is found for V 652 Her, and a reasonable match for HD 144941 when interstellar reddening is accounted for. We conclude that the hybrid non-LTE approach based on state-of-the-art model atoms as discussed here succeeds in solving the most persistent problems in the quantitative spectroscopy of extreme helium stars.

REFERENCES

- Barnard A. J., Cooper L., Shamey L. J. 1969, *A&A*, 1, 28
 Barnard A. J., Cooper L., Smith E. W. 1974, *J. Quant. Spec. Rad. Transf.*, 14, 1025
 Dimitrijević M. S., Sahal-Bréchet S. 1990, *A&AS*, 82, 519
 Fernley J. A., Taylor K. T., Seaton M. J. 1987, *J. Phys. B*, 20, 6457
 Harrison P. M., Jeffery C. S. 1997, *A&A*, 323, 177
 Heber U. 1986, in *Hydrogen Deficient Stars and Related Objects*, eds. K. Hunger, D. Schönberner & N. Kameswara Rao, Reidel Publ. Co., Dordrecht, p. 33
 Husfeld D., Butler K., Heber U., Drilling J. S. 1989, *A&A*, 222, 150
 Jeffery C. S. 1996, in *Hydrogen-Deficient Stars*, eds. C. S. Jeffery & U. Heber, ASP Conf. Ser., 96, 152
 Jeffery C. S., Woolf V. M., Pollacco D. L. 2001, *A&A*, 376, 497
 Kurucz R. L. 1996, in *Model Atmospheres and Spectrum Synthesis*, eds. S. J. Adelman, F. Kupka & W. W. Weiss, ASP Conf. Ser., 108, 160
 Przybilla N. 2005, *A&A*, 443, 293
 Przybilla N., Butler K. 2004, *ApJ*, 609, 1181
 Przybilla N., Butler K., Heber U., Jeffery C. S. 2005, *A&A*, 443, L25
 Przybilla N., Nieva M. F., Edelmann H. 2006, *Baltic Astronomy*, 15, 107 (these proceedings)
 Stehlé C., Hutcheon R. 1999, *A&AS*, 140, 93

High-resolution observations would be highly desirable for constraining the modeling even further.

The second major difficulty in the modeling of extreme helium stars is a general mismatch of effective temperatures derived from ionization equilibria and spectrophotometry. A comparison of the Atlas12 model fluxes (grey lines) for stellar parameters derived from the

FUSE OBSERVATIONS OF GERMANIUM, ZIRCONIUM AND LEAD IN SDB STARS

P. Chayer^{1,2}, M. Fontaine³, G. Fontaine³, F. Wesemael³ and J. Dupuis¹

¹ *Department of Physics and Astronomy, The Johns Hopkins University, 3400 N. Charles St., Baltimore, MD 21218, U.S.A.*

² *Primary affiliation: Department of Physics and Astronomy, University of Victoria, P.O. Box 3055, Victoria, BC, V8W 3P6, Canada*

³ *Département de Physique, Université de Montréal, CP6128, Station Centre-ville, Montréal, QC H3C 3J7, Canada*

Received 2005 August 1

Abstract. We report the detection of the Ge III, Zr IV, Pb III and Pb IV resonance lines in Far Ultraviolet Spectroscopic Explorer (*FUSE*) spectra of hot subdwarf B stars (sdB). We analyze 18 stars that cover the effective temperature domain for this class of stars. We carry out an abundance analysis and demonstrate that Ge, Zr and Pb abundances are higher than the ones observed in the Sun's photosphere in almost every star. We perform radiative levitation calculations on Ge, Zr and Pb, and show that the theory predicts higher Ge and Zr abundances than the observations. Moreover, the large scatter of observed abundances cannot be explained by the radiative levitation alone. This suggests that other mechanisms must be taken into account for explaining the abundances of Ge, Zr and Pb in the atmospheres of sdB stars.

Key words: diffusion – spectroscopy – stars: abundances – subdwarfs

1. INTRODUCTION

The recent discovery of elements beyond the iron group in the atmospheres of hot subdwarf B stars (sdB) by O'Toole (2004) adds new pieces to the abundance anomaly puzzle observed at the surface of these relatively high gravity stars. O'Toole (2004) reported the detection of strong resonance lines of Ga III, Ge IV, Sn IV and Pb IV in the STIS and IUE spectra of many sdB and sdOB stars that cover a wide range of effective temperatures. Strong resonance lines of Ge III, Zr IV, Pb III and Pb IV are also formed in the far ultraviolet wavelength range. This is one of the last unexplored spectral windows in the study of sdB atmospheres. The Far Ultraviolet Spectroscopic Explorer (*FUSE*), which covers a spectral wavelength range of 905–1187 Å with a resolution of $R = \lambda/\Delta\lambda \simeq 18\,000$, is exploring in great details this important waveband. In this paper we present the results of an abundance analysis for the elements Ge, Zr and Pb observed in the atmospheres of 18 sdB stars. We also present results of radiative levitation calculations on Ge, Zr and Pb based on an approach developed by Michaud et al. (1976).

2. *FUSE* OBSERVATIONS

We retrieved the *FUSE* spectra from the Multimission Archive at STScI. All stars were observed through large apertures with exposure times of about 6000 s on average. The data were reduced using the program CALFUSE that processes the raw data into wavelength and flux calibrated 1-d spectra. Because each observation consists of several exposures, we co-added the individual exposures by cross-correlating them in order to remove any wavelength shifts. Figure 1 illustrates an example of merged *FUSE* spectra of the bright and cool sdB star HD 205805. The strongest lines observed in the spectrum are the hydrogen lines from Ly β to the series limit, the He II 1084 and 992 Å lines, the C III 977 Å line and the C III 1175 Å multiplet.

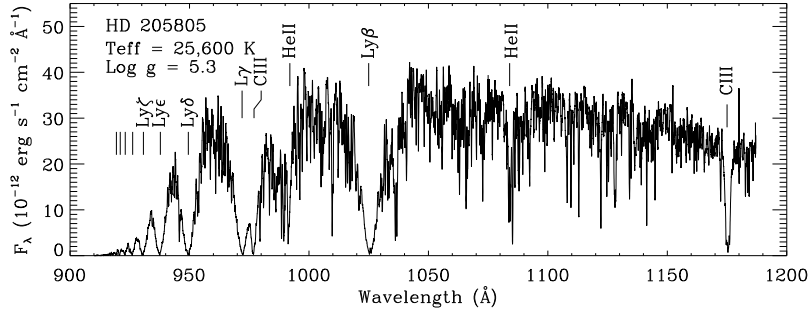


Fig. 1. *FUSE* spectrum of HD 205805.

The spectrum in Figure 1 seems noisy at this scale. In fact, this apparent noise is due to the huge number of photospheric and interstellar absorption lines that are observed in the *FUSE* spectra of almost all sdB stars. Interstellar lines such as H₂, C II, C III, N I, O I, Si II, P II and Fe II are observed along the lines of sight of many sdB stars. Photospheric lines come from elements such as C, N, O, Si, P, S, Cl and elements from the iron group such as V, Cr, Mn, Fe, Co and Ni. In addition to these elements, the *FUSE* wavelength range contains lines that are produced by elements beyond the iron group. Resonance lines from ions such as Ge III, Zr IV, Pb III and Pb IV are observed in the *FUSE* spectra of almost all sdB stars. Lines coming from excited levels of Pb III are also observed in a few stars. Table 1 summarizes the atomic properties of the Ge III, Zr IV, Pb III and Pb IV lines observed in the *FUSE* band.

Table 1. Atomic data for Ge, Zr and Pb.

| Ion | Z | Wavelength (Å) | $\log gf$ | g_l | E_l (cm ⁻¹) |
|--------|-----|-------------------|-----------|-------|------------------------------|
| Ge III | 32 | 1088.463 | 0.264 | 1.0 | 0.0 |
| Zr IV | 40 | 1183.973 | 0.000 | 4.0 | 0.0 |
| Pb III | 82 | 1048.877 | 0.114 | 1.0 | 0.0 |
| Pb IV | 82 | 1028.611 | 0.086 | 2.0 | 0.0 |

3. ABUNDANCE ANALYSIS

We computed a set of LTE atmosphere models with the atmospheric parameters listed in Table 2 (the atmospheric parameters were derived by E. M. Green et al. 2006, in preparation; Edelmann 2003; M. Fontaine et al. 2006, in preparation; Kilkeny et al. 1987; Heber et al. 2002; Allard 1986 and Saffer et al. 1994). These models were computed for a hydrogen/helium chemical composition. We used two methods for determining the abundances of Ge, Zr and Pb. For stars that do not have numerous absorption lines and have a well defined continuum, we fitted each line by using a χ^2 minimization technique for which the

abundance and a scaling factor are the free parameters. In this case we computed grids of LTE synthetic spectra by considering Ge, Zr and Pb as trace elements. The lines of Ge III, Zr IV, Pb III and Pb IV were computed for abundances ranging from $\log N(X)/N(H) = -10.4$ to -6.0 in steps of 0.4 dex by assuming no microturbulent velocity. The calculations were performed by using the programs TLUSTY (Hubeny & Lanz 1995) and SYNSPEC (I. Hubeny 2004, private communication). The partition functions for the neutral, +1 and +2 ionization stages of Ge, Zr and Pb are calculated in the same manner as in the Kurucz's ATLAS9 code (Kurucz 1993; Proffitt et al. 2001). For the +4 ionization stage of Zr and Pb we adopted the ground-state statistical weights for the partition functions. The sdB star Feige 87 is a good example of a low-metallicity star for which this method gives excellent results (see Figures 2 and 3).

We cannot apply the χ^2 fitting technique for stars like the one illustrated in Figure 1 (see also Figure 1 of Blanchette et al. 2006). Instead we used the IDL (Interactive Data Language) program SYNPLLOT developed by I. Hubeny. SYNPLLOT is an interactive program that calculates and plots synthetic spectra using the program SYNSPEC. We can then overplot the observed spectrum and compare it to the model. If the model does not reproduce the observation, we can change the abundance and repeat the operation until the fit is acceptable, i.e., the comparison between the model and the observation is satisfactory. This is what we call fitting a spectrum by eye. The main difficulty encountered when fitting spectra with this method is the placement of the continuum. For instance, Pereira et al. (2006) showed that LTE hydrogen-rich synthetic spectra computed in the *FUSE* band yielded continuum above the observed continuum. In their calculations they used T_{eff} and $\log g$ from a Balmer line analysis and normalized the synthetic spectra to the y magnitude. Their results indicate that the placement of the continuum may be one of the main sources of systematic error. When fitting a small portion of the spectrum we have a tendency to put the continuum close to what we believe is the real continuum. The study of Pereira et al. (2006) shows, however, that the continuum may be well above the one that we set for determining the abundances. Consequently, we may underestimate the abundances when fitting

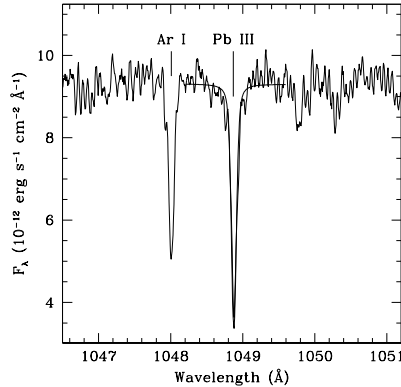


Fig. 2. *FUSE* spectrum of Feige 87 showing the Pb III 1048 Å line and our best fit.

spectra that contain numerous absorption lines.

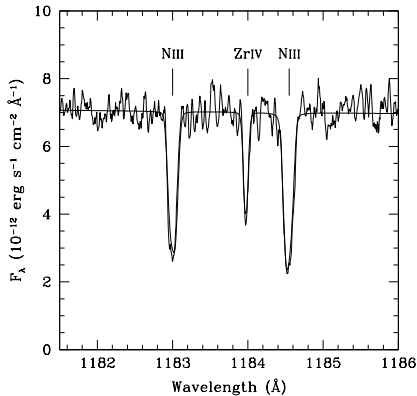


Fig. 3. *FUSE* spectrum of Feige 87 showing the Zr IV 1184 Å and N III 1183 and 1184 Å lines and our best fit.

to obtain the best fit for this line. This best gf value is given in Table 1. Because the Zr IV 1012 Å line is blended with the S III resonance line at 1012.498 Å, we only used the Zr IV 1184 Å line to estimate the Zr abundance. Figure 3 illustrates the best fit of the Zr IV 1184 Å and N III 1184 Å lines for the star Feige 87.

In order to measure the zirconium abundance, we estimated the oscillator strength of the Zr IV 1184 Å line empirically, because no oscillator strength was available from the literature. We measured the Zr abundance in the atmosphere of the sdB star Feige 48 by using its ultraviolet spectrum obtained by the Space Telescope Imaging Spectrograph onboard HST (O’Toole et al. 2004). We analyzed the Zr III lines at 1790.113 Å, 1793.523 Å and 1798.048 Å and measured an abundance of $\log N(\text{Zr})/N(\text{H}) = -8.0$. Keeping this abundance constant, we fitted the Zr IV 1184 Å line observed in the *FUSE* spectrum by maximizing the oscillator strength gf in order

4. RESULTS

Table 2 summarizes the abundances for Ge, Zr and Pb observed in the atmospheres of our program stars. The first column is the name of the star. The second and third columns give the effective temperature in ascending order and the gravity, respectively. Columns 4, 6 and 8 are the measured abundances or upper limits ($\log[N(\text{X})/N(\text{H})]_{\star} : \star$ symbol). Columns 5, 7, and 9 are the observed abundances reported relative to the abundances in the Sun ($\log[N(\text{X})/N(\text{H})]_{\star} - \log[N(\text{X})/N(\text{H})]_{\odot} : \star - \odot$ symbol). The Ge, Zr and Pb abundances in the atmosphere of the Sun are -8.42 , -9.41 and -10.00 , respectively. They are taken from the review of Asplund et al. (2005). We estimate that the uncertainties (statistical and systematic) associated with the measured abundances vary from 0.1 dex to 0.3 dex. Table 2 shows that Ge, Zr and Pb are present in the atmospheres of almost all sdB stars. Although the average abundances relative to hydrogen are about the same for these three elements with a value of about $\log[N(\text{X})/N(\text{H})] \simeq -7.8$ and a dispersion of about 1.0 dex, the Ge, Zr and Pb abundances relative to the solar abundances are 0.62, 1.61 and 2.20 dex, respectively. The difference in the abundances relative to solar is due to the fact that

$$\log[N(\text{Pb})/N(\text{H})]_{\odot} < \log[N(\text{Zr})/N(\text{H})]_{\odot} < \log[N(\text{Ge})/N(\text{H})]_{\odot}. \quad (1)$$

Figure 4 illustrates the Ge, Zr and Pb abundances by number relative to hydrogen as a function of effective temperature. Filled circles and downward-pointing arrows correspond to abundances and upper limits. The horizontal dotted line in each panel is the solar abundance according to Asplund et al. (2005). The figure

Table 2. Abundance of Ge, Zr and Pb in the atmospheres of sdB stars compared to the Sun

| Star | T_{eff} (10^3 K) | $\log g$ (cm s^{-2}) | Ge | | Zr | | Pb | |
|--------------|---------------------------------|------------------------------------|-------|-------|-------|-------|-------|-------|
| | | | ★ | ★ - ☉ | ★ | ★ - ☉ | ★ | ★ - ☉ |
| HD 4539 | 23.9 | 5.2 | -7.7 | 0.7 | -7.7 | 1.7 | -8.1 | 1.9 |
| JL 36 | 24.5 | 5.6 | -7.8 | 0.6 | -8.0 | 1.4 | -7.7 | 2.3 |
| HD 205805 | 25.6 | 5.3 | -8.0 | 0.4 | -7.4 | 2.0 | -8.7 | 1.3 |
| LB 1516 | 26.1 | 5.4 | -8.0 | 0.4 | -8.0 | 1.4 | -8.7 | 1.3 |
| Feige 48 | 29.6 | 5.5 | -8.0 | 0.4 | -8.0 | 1.4 | -8.5 | 1.5 |
| Feige 87 | 29.9 | 5.4 | -10.3 | -1.9 | -8.4 | 1.0 | -7.3 | 2.7 |
| JL 236 | 29.9 | 5.7 | -7.6 | 0.8 | -7.5 | 1.9 | -8.1 | 1.9 |
| PG 0823+465 | 29.9 | 5.8 | -9.0 | -0.6 | -7.4 | 2.0 | <-9.0 | <1.0 |
| PG 1710+490 | 30.3 | 5.7 | -7.9 | 0.5 | -7.1 | 2.3 | <-9.5 | <0.5 |
| PG 1206+165 | 30.5 | 5.6 | -9.3 | -0.9 | -9.3 | 0.1 | -6.7 | 3.3 |
| PG 1610+529 | 31.0 | 5.8 | -7.6 | 0.8 | -7.1 | 2.3 | -7.7 | 2.3 |
| PG 1032+406 | 31.3 | 5.9 | -6.7 | 1.7 | -7.3 | 2.1 | -7.1 | 2.9 |
| Feige 91 | 31.3 | 6.0 | -6.5 | 1.9 | -7.3 | 2.1 | -7.0 | 3.0 |
| KPD2109+4401 | 31.4 | 5.6 | -7.5 | 0.9 | <-9.0 | <0.4 | -7.3 | 2.7 |
| PG 1619+522 | 33.0 | 5.8 | -6.7 | 1.7 | -7.3 | 2.1 | -7.2 | 2.8 |
| PG 1538+401 | 33.5 | 5.9 | -8.0 | 0.5 | -8.8 | 0.6 | -9.0 | 1.0 |
| PG 1219+534 | 33.6 | 5.8 | -6.6 | 1.8 | -8.3 | 1.1 | -7.0 | 3.0 |
| PG 1255+547 | 33.9 | 5.8 | -6.4 | 2.0 | -7.1 | 2.3 | -6.8 | 3.2 |

shows that the abundances are higher than the solar abundances in almost every star, and that these overabundances can reach 3 orders of magnitude in a few cases. The analysis of several stars provides the opportunity to uncover some trends in the abundance patterns. Can we observe such trends with the data that we have in hand? There may be a slight increase in the abundance as the temperature increases. The large scatter of the abundances, however, is really the most striking result. For instance, stars with $T_{\text{eff}} \geq 29\,500$ K show a scatter of the abundances on a scale of 2 to 3 orders of magnitude for the three elements.

Three stars in our sample are EC 14026 pulsators: Feige 48, KPD 2109+4401 and PG 1219+534. The Ge, Zr and Pb abundances in Feige 48 are about the same and are close to the cooler stars. KPD 2109+4401 and PG 1219+534 display the same abundance pattern. Although they show relatively high Ge and Pb abundances, their Zr abundance is much lower. By comparison with other stars in general, the pulsators do not show any abundance enhancement. Two stars in our sample are out of the ordinary: Feige 87 and PG 1206+165. The two stars show low Ge and Zr abundances but high Pb abundance. Moreover, their *FUSE* spectra show very low abundances of iron peak elements, although their C, N and O abundances are relatively high. The hot PG1538+401 star is another interesting object. Its Ge, Zr and Pb abundances are systematically lower than the other hot stars.

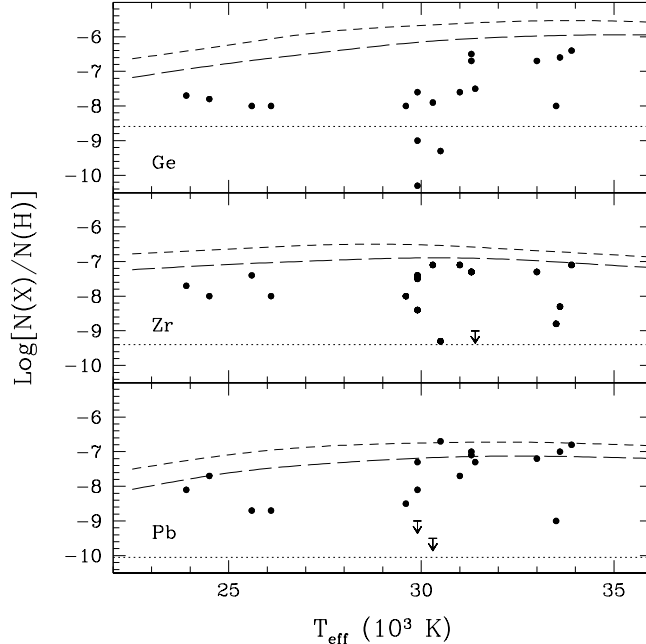


Fig. 4. Ge, Zr and Pb abundances (*filled circles*) and upper limits (*downward-pointing arrows*) observed in the *FUSE* spectra of sdB stars. The dotted line in each panel is the solar abundance according to Asplund et al. (2005). The dashed and long-dashed lines are predicted abundances computed within the framework of the radiative levitation theory according to Michaud et al. (1976) for models with $\log g = 5.5$ and 6.0 , respectively.

5. RADIATIVE LEVITATION

In order to confirm the role of the radiative levitation for maintaining traces of heavy elements, we carried out radiative levitation calculations on Ge, Zr and Pb. Figure 4 illustrates radiative equilibrium abundances computed at $\tau_R = \frac{2}{3}$ for models with $\log g = 5.5$ (dashed lines) and 6.0 (long-dashed lines). Because of lack of atomic data for Ge, Zr and Pb, we used the approximate method developed by Michaud et al. (1976) to compute the equilibrium abundances illustrated in Figure 4. Bergeron et al. (1988) showed that the approach of Michaud et al. (1976) yields good agreement with more detailed radiative levitation calculations carried out in sdB models for C, N and Si. Bergeron et al. (1988) added that this approximate formalism overestimates the radiative acceleration by no more than a factor of ~ 3 in the line-forming regions, and concluded that this method could be applied to other elements. Following the findings of Bergeron et al. (1988) and in order to better match the observed abundances, we reduced the radiative acceleration on Ge, Zr and Pb by a factor of 3. Figure 4 shows that the radiative levitation provides more than enough support for our elements of interest.

The predicted abundances are in general greater than the observed abundances. In a few cases the predictions are consistent with the observations. It is difficult to explain, however, the large scatter of the observed abundances. For instance,

stars with $T_{\text{eff}} \geq 29\,500$ K show abundances that vary over two to three orders of magnitude. According to the parameter-free diffusion model, which consists of a strict equilibrium between the gravitational and radiative accelerations, stars with similar atmospheric parameters should show similar abundances. The large scatter of the abundances for $T_{\text{eff}} \geq 29\,500$ K cannot be interpreted only in terms of the atmospheric parameters.

6. DISCUSSION AND CONCLUSION

A weak stellar wind at the surface of sdB stars is one of the mechanisms that was proposed for opposing gravitational settling and at the same time affecting the equilibrium abundances predicted by the radiative levitation. Although the proposed mass loss rates are too low to be detected directly, their effect on the surface abundances may be quite important. Michaud et al. (1985) and Bergeron et al. (1988) put forward the wind hypothesis to explain the Si underabundance observed in a handful of sdB stars. Bergeron et al. (1988) demonstrated that detailed radiative levitation calculations predicted large Si abundances, even though observations showed that Si was underabundant as much as five orders of magnitude in stars with $T_{\text{eff}} \geq 27\,000$ K. Michaud et al. (1985) suggested that an outward velocity field produced by a weak stellar wind could decrease the Si abundance at the surface of a sdB star.

By trying to explain the He underabundance in sdB stars, Michaud et al. (1989) demonstrated that the radiative forces were in fact too small to support the observed He abundance. This result prompted Fontaine & Chayer (1997) and Unglaub & Bues (1998) to compute time dependent diffusion calculations that included mass loss. Both groups showed that mass loss rates of the order of 10^{-13} to $10^{-14} M_{\odot} \text{yr}^{-1}$ could maintain He abundances similar to those observed in the atmospheres of sdB stars. The wind hypothesis was also assumed by Chayer et al. (2004) to explain the presence of EC 14026 pulsators and non-pulsators in the empirical instability region. Chayer et al. (2004) showed that weak stellar winds could disrupt the Fe reservoir, which is responsible for driving the pulsations in EC 14026 stars, and explain why a star pulsates while another does not.

All the diffusion calculations that we have just reviewed involve weak stellar winds that assume an outward velocity that is provided by the continuity equation. This velocity depends on the mass loss rate, the density of matter, and the position where the velocity is calculated. This means that at a given radius all elements have the same outward velocity. This velocity is low in the deeper layers of the atmosphere, and is large in the upper layers. O'Toole (2004) proposed that this velocity could be different for elements with different atomic mass. He suggested that a fractionated wind could explain the Si underabundance and the presence of Ge, Sn and Pb in the atmospheres of sdB stars. O'Toole (2004) argued that Si, Ge, Sn and Pb should have similar susceptibility to absorb radiative momentum given that they occupy the same column of the periodic table and should have in principle similar atomic properties. He added that the atomic mass should be the parameter that could be involved in the separation of the elements in the wind. Consequently, a light element such as Si could be removed preferentially from the atmospheres of sdB stars in a fractionated stellar wind, while the heavier elements Ge, Sn and Pb should lag behind.

This interesting hypothesis can be tested by comparing the abundances of Si, Ge, Sn and Pb in a sample of stars with atmospheric parameters that cover the

whole range of possible values for sdB stars. The present study is the first step in this direction. The *FUSE* observations provide the spectral window to identify not only Ge and Pb, but also Si. We are in the process of completing the Si abundance analysis and hope to test the hypothesis of the fractionated wind put forward by O'Toole (2004).

ACKNOWLEDGMENTS. P.C. is supported by CSA under a PWGSC contract. G.F. acknowledges the contribution of the Canada Research Chair Program. This work was supported in part by NASA grant NAG510647.

REFERENCES

- Allard F. 1986, Master Thesis, Univ. Montréal
- Asplund M., Grevesse N., Sauval A. J. 2005, in *Cosmic Abundances as Records of Stellar Evolution and Nucleosynthesis*, eds. F. N. Bash & T. G. Barnes, ASP Conf. Ser., in press (astro-ph/0410214)
- Bergeron P., Wesemael F., Michaud G., Fontaine G. 1988, *ApJ*, 332, 964
- Blanchette J. P. et al. 2006, *Baltic Astronomy*, 15, 301 (these proceedings)
- Chayer P. et al. 2004, *Ap&SS*, 291, 359
- Edelmann H. 2003, Ph.D. Thesis Universität Erlangen-Nürnberg
- Fontaine G., Chayer P. 1997, in *Third Conf. on Faint Blue Stars*, eds. A. G. D. Philip, J. Liebert & R. Saffer, Schenectady, L. Davis Press, p. 169
- Heber U., Moehler S., Napiwotzki R., Thejll P., Green E. M. 2002, *A&A*, 383, 938
- Hubeny I., Lanz T. 1995, *ApJ*, 439, 875
- Kilkenny D., Heber U., Drilling J. S. 1987, in *Second Conf. on Faint Blue Stars*, IAU Colloq. 95, eds. A. G. D. Philip, D. S. Hayes & J. W. Liebert, L. Davis Press, p. 731
- Kurucz R. L. 1993, CD-ROM 13, ATLAS9 Stellar Atmospheres Program and 2 km/s Grid, SAO, Cambridge
- Michaud G., Bergeron P., Heber U., Wesemael F. 1989, *ApJ*, 338, 417
- Michaud G., Bergeron P., Wesemael F., Fontaine G. 1985, *ApJ*, 299, 741
- Michaud G., Charland Y., Vauclair S., Vauclair G. 1976, *ApJ*, 210, 447
- Pereira C., Wesemael F., Bergeron P. 2006, *Baltic Astronomy*, 15, 123 (these proceedings)
- Proffitt C. R., Sansonetti C. J., Reader J. 2001, *ApJ*, 557, 320
- Saffer R. A., Bergeron P., Koester D., Liebert J. 1994, *ApJ*, 432, 351
- O'Toole S. J. 2004, *A&A*, 423, L25
- O'Toole S. J., Heber U., Chayer P., Fontaine G., O'Donoghue D., Charpinet S. 2004, *Ap&SS*, 291, 427
- Unglaub K., Bues I. 1998, *A&A*, 338, 75

CHEMICAL ABUNDANCES OF HELIUM-RICH SUBDWARF B STARS

A. Ahmad and C. S. Jeffery

Armagh Observatory, College Hill, Armagh BT61 9DG, U.K.

Received 2005 August 17

Abstract. Helium-rich subdwarf B (He-sdB) stars represent a small fraction of the population of hot subdwarfs. We report recent results of our spectral analysis of He-sdB stars including surface chemical abundance measurements of a bright He-sdB star – JL 87 – measured from its high-resolution optical spectrum using line-blanketed LTE model atmospheres. These measurements provide further insight into the formation mechanism(s) of these rare faint blue stars.

Key words: stars: chemically peculiar – stars: early-type - subdwarfs – stars: fundamental parameters – stars: abundances

1. INTRODUCTION

A very small fraction ($\leq 5\%$) of the subdwarf population comprises the so called helium-rich subdwarf B (He-sdB) stars. These are “cooler” subdwarfs with strong neutral helium lines in their optical spectrum. They are found in the field of our Galaxy (Green et al. 1986) and also in some globular clusters (Moehler et al. 1997, 2002, 2004).

He-sdB stars were originally identified as sdOD in the Palomar Green survey (Green et al. 1986) as subdwarfs showing strong He I lines plus weak He II lines but with no detectable hydrogen Balmer lines. From this spectral definition one would expect all sdOD stars to be extremely helium-rich and cooler than sdO stars. However, this is not the case as our spectral analysis (Ahmad & Jeffery 2003) showed that He-sdB stars exhibit a wide range in helium abundance and temperatures similar to both sdB and sdO stars.

Since “helium-rich” can be interpreted differently by different authors, it is vital that the label “He-sdB” is used homogeneously. The new MK-type classification scheme being developed by Drilling et al. (2000) would address this issue. For now we would use the He-sdB label for all subdwarfs that have previously been identified as such by other authors.

Two evolutionary models have been proposed for the formation of these He-sdB stars. The first, by Iben & Tutukov (1986), involves the merger of two white dwarfs (WD) to form a He-sdB star. The second, by Lanz et al. (2004), involves convective flash mixing of the atmosphere of a star on the white dwarf cooling track which has previously undergone high mass-loss.

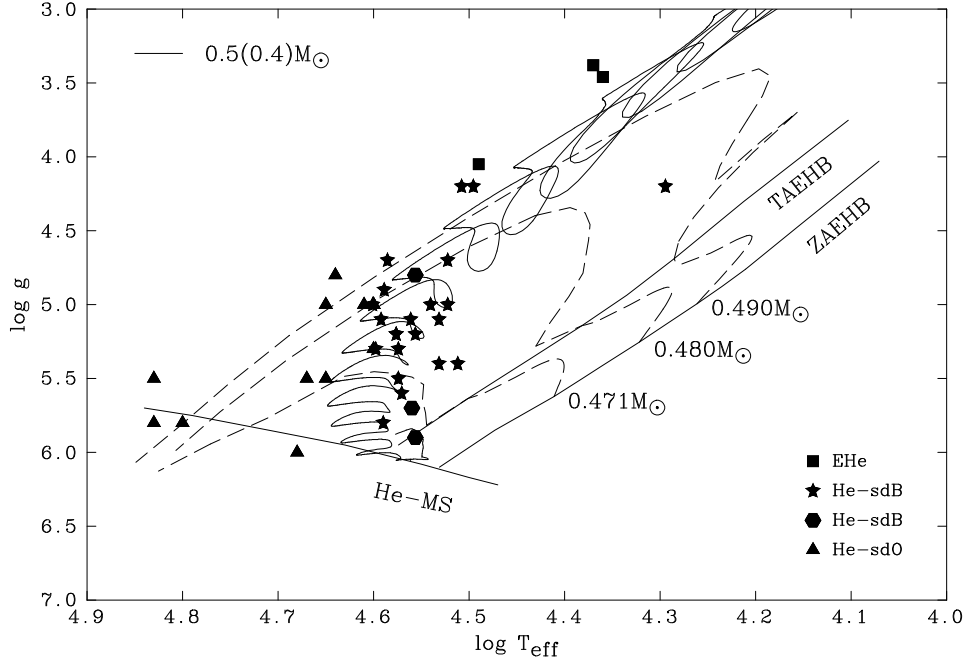


Fig. 1. Helium-rich stars on the T_{eff} vs. $\log g$ diagram plotted with evolutionary tracks. He-sdB stars from this study are plotted using the filled star symbol. He-sdB stars found in globular clusters (Moehler et al. 1997, 2002, 2004) are plotted with filled hexagonal symbol. Single star evolutionary tracks (dashed lines) are taken from Dorman et al. (1993) and merged He+He WD tracks (solid lines) are taken from Saio & Jeffery (2000). Adapted from Ahmad (2004).

Our aim is to establish whether either or both these models fit the observed properties of He-sdB stars. In this paper, we present physical parameters of additional He-sdB stars, new observations of the double-lined spectroscopic binary PG 1544+488, discuss preliminary abundance measurements of a He-sdB star JL 87, and discuss their possible evolution.

2. PHYSICAL PARAMETERS

In order to understand the evolution of He-sdB stars our first study involved determining the position of these stars on the T_{eff} vs. $\log g$ diagram. We measured atmospheric physical parameters of 22 He-sdB stars using LTE model atmospheres and the χ^2 fitting program SFIT2 (cf. Ahmad & Jeffery 2003) and plotted them on the T_{eff} vs. $\log g$ plane (Figure 1). In general, the effective temperatures (T_{eff}) of He-sdB stars lie in the range 30 000–40 000 K, surface gravities ($\log g$) in the range 4.5–6.0 and helium abundance (by number, n_{He}) in the range 0.10–0.99. Ten additional He-sdB stars appear to be hotter than 40 000 K. Since NLTE effects become increasingly important at such high temperature, these stars were not analyzed.

We have also divided our sample of He-sdB stars into carbon-rich and carbon-poor. Carbon-rich He-sdB stars show strong C II/III lines in their optical spectra

and CIII/IV lines in their ultraviolet (UV) spectra. It is likely that these two groups are produced by different evolutionary channels. To get some estimate of the carbon abundance in carbon-rich He-sdB stars we calculated a number of models with different carbon abundances and tried to match the strength of the carbon lines in the UV spectra. Preliminary results suggest that $n_C \leq 0.01$ in carbon-rich He-sdB stars.

3. ABUNDANCES

The surface chemical abundances of a star provides further clues about its prior evolution. In our next study we carried out high-resolution spectroscopy of He-sdB stars to measure these abundances. Two bright ($V \sim 12$) He-sdB stars – PG 1544+488 and JL 87 – were selected for this study.

3.1. PG 1544+488

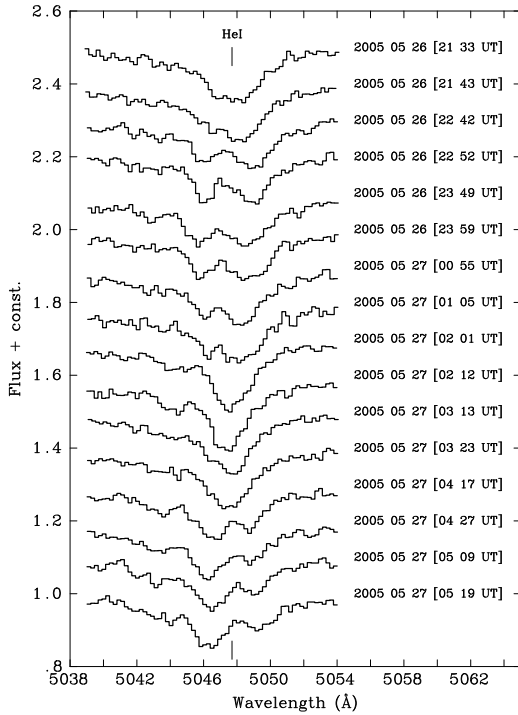


Fig. 2. One night’s data from the 2005 WHT run of PG 1544+488 showing line profile variations in the He I 5047 Å absorption line.

In this mode, both the position and time of each photon event on the detector is recorded and therefore it was possible to re-extract the archival data and split them into short time-resolved spectra (~ 900 s).

We then measured radial velocities from the WHT and FUSE spectra (for details, see Ahmad et al. 2004). The FUSE data showed similar velocity variations as the optical WHT data. We then combined the radial velocities from the FUSE

We obtained optical blue spectra of the prototype PG 1544+488 with the William Herschel Telescope (WHT) in 2003 April. In total, seven spectra were obtained over two consecutive nights. While carrying out the spectral analysis we noticed that some of the neutral helium line profiles had an unusual shape seen here in Figure 2. On closer examination it became evident that this was due to line-doubling. It was suspected to be due to binarity. However to confirm this hypothesis, more data were required.

Coincidentally, PG 1544+488 had been observed twice with the Far Ultraviolet Spectroscopic Explorer (FUSE) satellite (PI: T.M. Brown) in 2002. At first, it was observed in 2002 March but since one of the detectors on FUSE failed during the observations it was re-observed in 2002 July. The FUSE observations were made in the time-tag (TTAG) mode. In this

spectra with those obtained from the WHT spectra and solved for the orbit. From the orbital solution we were able to demonstrate that PG 1544+488 is a short period binary with a period of ~ 0.48 day, comprising two helium-rich hot subdwarfs and likely to be a product of close-binary evolution (cf. Ahmad et al. 2004). Some recent observations of PG 1544+88 from the 2005 WHT run are shown in Fig. 2.

No abundances could be measured for PG 1544+488 as line-doubling makes it impossible to measure the equivalent widths of the spectral lines. However in future, with better data it might be possible to deconvolve the spectra of the two components of the binary and measure their individual chemical abundances.

3.2. JL 87

A high-resolution optical spectrum of JL 87 was obtained at the Anglo-Australian Telescope (AAT) with the University College London Echelle Spectrograph (UCLES) in 1996. The spectrum was reduced using standard IRAF routines. Physical parameters of the star were measured from the optical spectrum using SFIT2 as described in section 2, and indicates that $T_{\text{eff}} = 24\,000$ K and $\log g = 4.5$. Lanz et al. (2004) have measured $T_{\text{eff}} = 29\,000$ K and $\log g = 5.5$ for JL 87 using far-ultraviolet spectrum of the star obtained with FUSE and NLTE model atmospheres. There is significant disagreement between the atmospheric parameters derived from the optical and far-ultraviolet spectra which cannot just be accounted for by NLTE effects.

Using our derived physical parameters, we measured the atmospheric chemical abundance listed in Table 1. There is some agreement between our preliminary measurement of hydrogen, helium and nitrogen abundances with those of Lanz et al. (2004).

There is a significant amount of hydrogen in the atmosphere of JL 87 ($n_{\text{H}} \sim 0.80$). This is also evident from the strong hydrogen Balmer lines in the optical spectrum (Figure 3). Such a high hydrogen abundance is not typical for most He-sdB stars ($n_{\text{H}} \leq 0.10$). Nitrogen is enriched while oxygen is depleted in JL 87 suggesting CNO processing. However carbon, which is destroyed in CNO cycle, is also enriched. The metal lines in the optical spectrum are quite sharp and can be reproduced with $v \sin i \leq 5 \text{ km s}^{-1}$.

Table 1. Chemical abundances in JL 87 in mass fraction compared to Lanz et al. (2004) – L04 and solar values.

| Element | this work | L04 | Sun |
|---------|-----------|-------------|--------|
| H | 0.5636 | 0.56 – 0.77 | 0.7054 |
| He | 0.4198 | 0.43 – 0.28 | 0.2758 |
| C | 0.0056 | 0.0140 | 0.0031 |
| N | 0.0031 | 0.0040 | 0.0011 |
| O | 0.0023 | – | 0.0096 |
| Si | 0.0003 | 0.0007 | 0.0007 |
| S | 0.0001 | – | 0.0004 |
| Fe | 0.0024 | 0.0013 | 0.0012 |

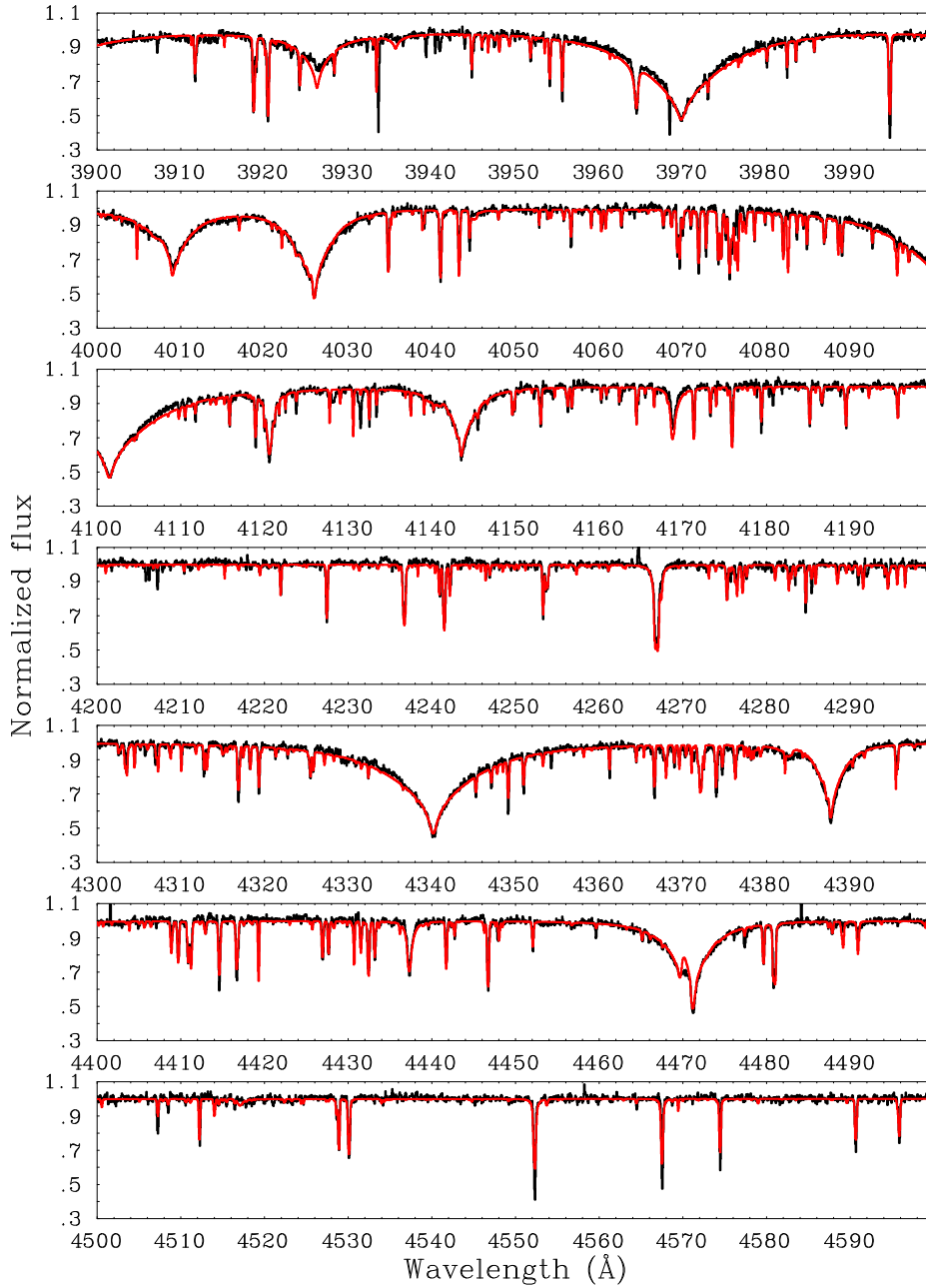


Fig. 3. A section (3900–4600 Å) of the high-resolution optical spectrum (3900–5000 Å) of JL 87 (dark line) along with best fit model.

It seems unlikely that JL 87 is the product of a white dwarf merger in which any remaining hydrogen is converted to helium resulting in an extremely helium-rich surface. It has been suggested that JL 87 is a product of shallow mixing (Lanz et al. 2004) as it can satisfactorily explain the surface abundances. However, our surface gravity measurement indicates that the star is too luminous to have been flash mixed. The atmospheric parameters and helium abundance of JL 87 are similar to those of chemically peculiar massive helium-rich stars known as intermediate helium stars (e.g., Zboril & North 1999). However, carbon is underabundant in these stars.

4. EVOLUTION

4.1. Late flash mixing model

It has been proposed by Lanz et al. (2004) that stars evolving with high mass-loss on the red giant branch undergo a late helium core flash on the white dwarf cooling track, leading to convective “flash mixing” of the envelope which then forms a helium and carbon rich hot subdwarf. All hot subdwarfs produced by this channel show carbon enrichment. Their recent analysis of the FUSE spectra of two He-sdB stars provide support for this evolutionary scenario.

4.2. Binary merger model

Iben & Tutukov (1986) on the other hand have suggested that the merger of two white dwarfs (WD) can produce a hot subdwarf with a depleted hydrogen atmosphere. More recently this has been modeled by Saio & Jeffery (2000) to explain the origin of extreme helium (EHe) stars. Some of these EHe stars are thought to evolve into He-sdB stars. The binary merger model can explain both carbon-rich and carbon-poor He-sdB stars. A merger of two helium WDs can produce a carbon-poor He-sdB star. A low-mass CO+He WD merger might produce a star which resembles a carbon-rich He-sdB during its evolution to the WD track. The analysis presented in section 2 (Ahmad & Jeffery 2003) and Fig. 1 lends general support to the white dwarf merger model for the formation of He-sdB stars.

4.3. Binary evolution

Both the existing evolutionary models for He-sdB stars assume a “single” star. The discovery that the prototype PG 1544+488 is a binary containing *two* He-sdB stars poses a challenge for both models. It is therefore likely that a close-binary evolution channel might be responsible for the formation of some He-sdB stars (see discussion in Ahmad et al. 2004).

4.4. Wind and magnetic field

None of the models discussed above satisfactorily accounts for all the observed parameters of JL 87. However, the observed properties of JL 87 are very similar to those of intermediate helium stars. These are massive young stars with stellar winds and magnetic fields. In normal B-type star atmospheres (assuming no wind), diffusion cannot lead to helium enrichment. However, it was shown by Vauclair (1975) that in the presence of stellar winds, diffusion can lead to helium overabundance. The intermediate helium stars normally show typical CNO abundances. However, peculiar CNO abundances patterns can also be produced depending on several parameters like magnetic field configuration and effective temperature. It

is therefore possible that luminous He-sdB stars showing some helium enrichment like JL 87 are in fact intermediate helium stars.

5. SUMMARY

Spectral analysis of He-sdB stars shows that they are a very inhomogeneous group of hot subdwarfs. A fraction of these stars are misclassified (or cool) He-sdO stars. Their evolution is still under much debate. We have discovered that the prototype, PG 1544+488, is a short-period binary containing two low-mass hot helium subdwarfs which demonstrates that close binary evolution also plays an important role in their formation. The observed atmospheric parameters and abundances in JL 87 are similar to those of intermediate helium stars which are chemically peculiar massive young stars.

REFERENCES

- Ahmad A., Jeffery C. S. 2003, *A&A*, 402, 335
Ahmad A., Jeffery C. S., Fullerton A. W. 2004, *A&A*, 418, 275
Ahmad A. 2004, Ph.D. thesis, Queens University, Belfast
Dorman B., Rood R. T., O'Connell R. W. 1993, *ApJ*, 419, 596
Drilling J. S., Moehler S., Jeffery C. S., Heber U., Napiwotzki R. 2000, in *The Kth Reunion*, ed. A. G. Davis Philip, p. 49
Green R. F., Schmidt M., Liebert J. 1986, *ApJS*, 61, 304
Iben I. J., Tutukov A. V. 1986, *ApJ*, 311, 742
Lanz T., Brown T. M., Sweigart A. V., Hubeny I., Landsman, W. B. 2004, *ApJ*, 602, 342
Moehler S., Heber U., Durrell P. R. 1997, *A&A*, 317, L83
Moehler S., Sweigart A. V., Landsman W. B., Dreizler S. 2002, *A&A*, 395, 37
Moehler S., Sweigart A. V., Landsman W. B., Hammer N. J. Dreizler S. 2004, *A&A*, 415, 313
Saio H., Jeffery C. S. 2000, *MNRAS*, 313, 671
Vauclair S. 1975, *A&A*, 45, 233
Zboril M., North P. 1999, *A&A*, 345, 244

MULTICOMPONENT WINDS IN SDB STARS?

K. Unglaub

Remeis Sternwarte Bamberg, Sternwartstrasse 7, D-96049 Bamberg, Germany

Received 2005 July 14

Abstract. In previous diffusion calculations with mass-loss a steady outflow of all elements has been assumed. However, the existence of a chemically homogeneous wind requires an efficient momentum transfer via Coulomb interactions from the heavy elements to hydrogen and helium. For the example $T_{\text{eff}} = 35\,000$ K and $\log g = 6.0$ it will be shown that hydrogen and helium would fall back onto the star if the mass-loss rate is below about $10^{-12} M_{\odot}/\text{yr}$. This effect may change the predicted surface compositions.

Key words: stars: hot subdwarfs – stars: mass-loss – stars: winds, outflow – stars: diffusion

1. INTRODUCTION

In previous papers (Unglaub & Bues 2001 and Unglaub 2005) it has been shown that the effects of diffusion and weak winds with mass-loss rates $\dot{M} \approx 10^{-13} M_{\odot}/\text{yr}$ may explain the helium abundances in sdB stars with number fractions H/He between about solar and 10^{-4} . However, the abundance anomalies of heavy elements can hardly be explained simultaneously, at least if a solar initial composition is assumed. In contrast to many observational results helium should always be more deficient than each of the elements C, N and O. A possible reason for this discrepancy may be the decoupling of metals on the one hand and H+He on the other hand in the wind region. This may happen if the momentum redistribution via Coulomb interactions between H, He and the metals is not sufficiently effective.

Vink & Cassisi (2002) calculated mass-loss rates for sdB stars with the assumption of a fixed velocity law. For “luminous” sdB stars with $5.0 \leq \log g \leq 5.5$ they obtain $10^{-11} M_{\odot}/\text{yr} \leq \dot{M} \leq 10^{-10} M_{\odot}/\text{yr}$ for solar composition and, for example, $\dot{M} \approx 10^{-12} M_{\odot}/\text{yr}$ for $T_{\text{eff}} = 35\,000$ K and $\log g = 6.0$. Our own hydrodynamical calculations, which will be published elsewhere (A&A, in preparation), are in good agreement with these results (within a factor of two). For the “compact” sdB stars with $\log g > 5.5$, however, \dot{M} may be clearly lower especially if the CNO elements are deficient.

Possible wind signatures (H α lines with a central line emission) have been detected by Heber et al. (2003) in four of the more luminous sdB stars. The spectral synthesis of H α by Vink (2004) with $\dot{M} \approx 10^{-11} M_{\odot}/\text{yr}$ showed a similar behavior of the line core. Insofar theoretical predictions seem to be in agreement with observational results. In the present paper, for the example $T_{\text{eff}} = 35\,000$ K, $\log g = 6.0$ and a stellar mass $M_{\star} = 0.5 M_{\odot}$ it will be investigated for which mass-loss rates a one component wind solution may be consistent.

2. METHOD OF ANALYSIS

In the following the elements H and He, for which the radiative acceleration is assumed to be zero, will be denoted as “element” 1, whereas the metals are denoted as “element” 2. As in the supersonic region the gradient of the gas pressure can be neglected, the momentum equation for “element” 1 (H+He) reads:

$$g_{\text{coll}} = g_{(r)} + v_1 \frac{dv_1}{dr}, \quad (1)$$

g_{coll} is the collisional acceleration on H and He due to Coulomb interactions with the metals and $g_{(r)}$ is the gravitational acceleration as a function of radius. The existence of a supersonic wind with increasing velocity in outward direction requires that the acceleration term $v_1 dv_1/dr$ is larger than zero. Thus this equation can only be valid if:

$$g_{\text{coll}} > g_{(r)}. \quad (2)$$

H and He cannot be accelerated if this condition is violated. Then the assumption of a steady outflow of all elements is inconsistent. As derived by Burgers (1969) g_{coll} can be written as:

$$g_{\text{coll}} = \frac{\rho_2}{m_1 m_2} \frac{4\pi q_1^2 q_2^2}{kT} (\ln \Lambda) G_{(x)}, \quad (3)$$

m_1 and m_2 are the mean masses of “elements” 1 and 2, respectively, and $\ln \Lambda = -1/2 + \ln(3kTR_D/(q_1 q_2))$, where R_D is the Debye radius. From Eq. (3) it can be seen that (apart from the weak dependence via $\ln \Lambda$) g_{coll} is proportional to the squares of the mean charges q_1 and q_2 of both “elements” and to the inverse of the temperature T . As g_{coll} is proportional to the density ρ_2 of the metals, it decreases if the metal abundances in the wind region are reduced.

In order to accelerate H and He via collisions with the heavy elements, the mean velocity in radial direction of the metals must be larger than the one for H and He. If this velocity difference is denoted with Δv , then x is defined as

$$x = \frac{\Delta v}{\alpha}, \quad (4)$$

where $\alpha = \sqrt{2kT/\mu}$ if μ is the reduced mass of both “elements”. For $T = 35\,000$ K it is $\alpha = 22$ km/s. The Chandrasekhar function $G_{(x)}$ is defined as in Krtićka et al. (2003) and as it is plotted, e.g., in Krtićka & Kubát (2005). The important point is that $G_{(x)}$ increases with x for $x < 1$, reaches a maximum value for $x \approx 1$ and decreases for $x > 1$. Thus for given temperature, mean charges of the elements and density of the metals, g_{coll} cannot exceed some maximum value. If this maximum value is smaller than the gravitational acceleration, no velocity difference exists for which condition (2) is fulfilled.

The density of the metals (“element” 2) as a function of radius and velocity can be obtained from the equation of continuity $\eta_2 \dot{M} = 4\pi r^2 \rho_2 v_2$ where η_2 is the mass fraction of the metals. From this equation ρ_2 can be inserted into Eq. (3) so that

$$g_{\text{coll}} = \frac{1}{m_1 m_2} \frac{\eta_2 \dot{M}}{4\pi r^2 v_2} \frac{4\pi q_1^2 q_2^2}{kT} (\ln \Lambda) G_{(x)} \quad (5)$$

As both g_{coll} and $g_{(r)}$ scale with r^{-2} , we calculate g_{coll} for $r = R_*$ and compare this with the surface gravity of the star. For the velocity of the metals $v_2 = 1000$ km/s is assumed, which is of the same order of magnitude as the surface escape velocity of 1260 km/s. If with these values condition (2) is violated for all values of x , H and He decouple from the metals before the wind is accelerated to the surface escape velocity.

3. RESULTS

The collisional acceleration on H and He is calculated for solar abundances of the metals (represented by the CNO elements). So we obtain mean masses $m_1 = 2.13 \times 10^{-24}$ g for H and He and $m_2 = 2.44 \times 10^{-23}$ g for the heavy elements. The mass fraction of the metals is $\eta_2 = 0.0133$. To maximize g_{coll} , the maximum value of $G_{(x)}$ at $x \approx 1$ is inserted, it is $G_{(1)} = 0.214$. The mean charges have been calculated with the LTE assumption for $T = 35\,000$ K and an electron density $n_e = 5 \times 10^{14}$ cm $^{-3}$. We obtain $q_1 = 1.0q_p$ (where q_p is the proton charge) for H and He and $q_2 = 2.6q_p$ for the CNO elements. As in the outer parts of the wind region the electron density is much lower, the mean charge of the metals may be larger. Thus the results for $q_2 = 5.0q_p$ are presented in addition.

Table 1. $g_{\text{coll}}^{\text{max}}$ for several values of mass-loss rates, mean charges q_2/q_p (q_p = proton charge) of the metals and temperatures.

| $\log \dot{M}$ [M_\odot/yr] | -11.0 | | | -12.0 | | | -13.0 | | |
|---|-------|-----|-----|-------|-----|-----|-------|-----|-----|
| q_2/q_p | 2.6 | 5.0 | 5.0 | 2.6 | 5.0 | 5.0 | 2.6 | 5.0 | 5.0 |
| T [kK] | 35 | 35 | 350 | 35 | 35 | 350 | 35 | 35 | 350 |
| $\log g_{\text{coll}}^{\text{max}}$ [cgs] | 6.7 | 7.3 | 6.4 | 5.7 | 6.3 | 5.4 | 4.8 | 5.3 | 4.4 |

In Table 1 the maximum values of g_{coll} (denoted with $g_{\text{coll}}^{\text{max}}$) are given for several mass-loss rates, temperatures and mean charges of the metals. $g_{\text{coll}}^{\text{max}}$ may be compared with the surface gravity of the star ($\log g = 6.0$).

For $\log \dot{M} = -11.0$ it is $g_{\text{coll}}^{\text{max}} > g$ in all cases. Thus for this mass-loss rate a steady outflow of all elements may exist.

For $\log \dot{M} = -12.0$ the situation is less clear. For $T = 35\,000$ K and $q_2 = 2.6q_p$ it is $\log g_{\text{coll}}^{\text{max}} = 5.7$ only. Thus H and He would fall back onto the star so that a one component wind solution is inconsistent. For $q_2 = 5.0q_p$ and the same temperature we obtain $\log g_{\text{coll}}^{\text{max}} = 6.3$, which is larger than the surface gravity. In this case the elements could be coupled. If, however, frictional heating (due to the velocity difference of the elements) increases the temperature, then the elements could decouple again. For $T = 350$ kK (instead of $T = 35$ kK) it is $\log g_{\text{coll}}^{\text{max}} = 5.4$ only. Thus for $\log \dot{M} = -12.0$ more detailed calculations are necessary.

Finally, for $\log \dot{M} = -13.0$ in all cases $g_{\text{coll}}^{\text{max}}$ is lower than $\log g$ by a factor of the order of ten at a distance where the velocity is 1000 km/s. This means that metals decouple from H and He clearly before the wind is accelerated to the surface escape velocity.

4. CONCLUSIONS

For the case $T_{\text{eff}} = 35\,000$ K and $\log g = 6.0$ it has been shown that a one component description of winds is clearly inconsistent for a mass-loss rate of the order

$10^{-13}M_{\odot}/\text{yr}$ as required from diffusion theory to explain the helium abundances. The Coulomb coupling between H, He and the metals in the supersonic region of the wind is not sufficient to accelerate or at least to levitate H and He. Thus these elements would fall back onto the star. This result is in agreement with the predictions of Krtićka & Kubát (2005).

The decoupling of elements in the wind region probably will lead to surface compositions which are different from those predicted with the assumption of chemically homogeneous winds. So it seems to be possible that fractionated winds exist and lead to the large deficiencies of Si in some sdB stars as suggested by O'Toole (2004). Fontaine et al. (2006) suggested that weak winds of the order $10^{-15}M_{\odot}/\text{yr}$ are responsible for the coexistence of pulsating and non-pulsating sdB stars with the same stellar parameters. As the actual mass-loss rate in a multicomponent wind is unclear, this may be a viable explanation.

ACKNOWLEDGMENTS. I thank I. Bues for careful reading of the manuscript and for financial support.

REFERENCES

- Burgers J. M. 1969, *Flow Equations for Composite Gases*, Academic Press, New York
- Fontaine G., Green E. M., Chayer P. et al. 2006, *Baltic Astronomy*, 15, 211 (these proceedings)
- Heber U., Maxted P. F. L., Marsh T. R., Knigge C., Drew J. E. 2003, in *Stellar Atmospheres Modeling*, eds. I. Hubeny, D. Mihalas & K. Werner, ASP Conf. Ser., 288, 251
- Krtićka J., Owocki S. P., Kubát J., Galloway R. K., Brown J. C. 2003, *A&A*, 402, 713
- Krtićka J., Kubát J. 2005, in *14th European Workshop on White Dwarfs*, eds. D. Koester & S. Moehler, ASP Conf. Ser., 334, 337
- O'Toole S. 2004, *A&A*, 423, L25
- Unglaub K. 2005, in *14th European Workshop on White Dwarfs*, eds. D. Koester & S. Moehler, ASP Conf. Ser., 334, 297
- Unglaub K., Bues I. 2001, *A&A*, 374, 570
- Vink J. S. 2004, in *Extreme Horizontal Branch Stars and Related Objects*, Ap&SS, 291, 239
- Vink J. S., Cassisi S. 2002, *A&A*, 392, 553

SPECTROSCOPIC ANALYSIS OF SDB BINARIES FROM THE SPY PROJECT

C. Karl¹, U. Heber¹, R. Napiwotzki² and S. Geier¹

¹ *Remeis-Sternwarte, Sternwartstrasse 7, D-96049 Bamberg, Germany*

² *Centre for Astrophysics Research, University of Hertfordshire, College Lane, Hatfield AL10 9AB, U.K.*

Received 2005 September 6

Abstract. In the course of our search for double degenerate binaries as potential progenitors of type Ia supernovae with the ESO VLT several new subdwarf B (sdB) binaries were discovered. In this paper, we present detailed analysis of six radial velocity variable sdB stars. Radial velocity curves have been measured. From the mass functions we derive lower limits to the masses of the unseen companions and discuss their nature. In addition, effective temperatures, surface gravities, helium abundances and metal abundances were determined.

Key words: binaries: spectroscopic – stars: atmospheres – stars: hot subdwarfs

1. INTRODUCTION

There is a general consensus that the precursors of type Ia supernovae (SN Ia) are white dwarfs in close binary systems. These white dwarfs accrete matter from their companions until a critical mass limit is reached. The two scenarios for SN Ia formation differ in the nature of the companion. This is a main-sequence or red giant star in the so-called 'single degenerate' scenario, and is another white dwarf in the 'double degenerate' scenario.

The purpose of the 'Supernova Ia progenitor survey' (SPY) was to check the double degenerate scenario by observational means. Thus, we observed more than 1000 WDs over the course of four years at the ESO VLT equipped with UVES in order to check the objects for radial velocity (RV) variations (cf. Napiwotzki et al. 2003). Follow-up observations of promising objects were performed in order to derive system parameters like periods (P) and RV semi-amplitudes (K). In combination with quantitative spectral analyses we computed the systems' total masses and merging times. A very promising SN Ia precursor candidate was discovered by Napiwotzki et al. (2005) in the course of our project.

Due to mis-classification in the input catalogue the SPY sample also contains a number of subdwarf B stars (sdBs; Lisker et al. 2005). Since these objects are immediate precursors of white dwarfs, they are also promising objects with respect to the search for SN Ia progenitors. For example, Maxted et al. (2000) and Geier et al. (2006) found the sdB binary KPD 1930+2752 to be a SN Ia

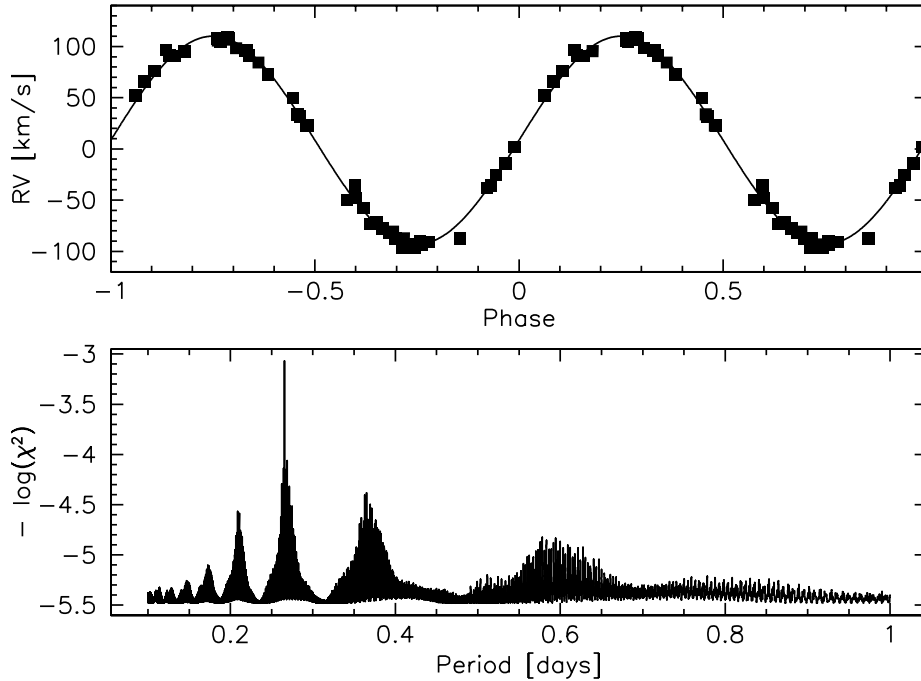


Fig. 1. Sample best fit RV curve and power spectrum for the visible sdB star in the HE 0532-4503 system. Upper panel: measured radial velocities as a function of orbital phase and fitted sine curve. Lower panel: power spectrum.

precursor candidate. Thus promising RV variable sdB stars were included in our follow-up observations as well.

In this paper we present the results of an analysis of six sdB binaries discovered by SPY.

2. OBSERVATIONS AND RADIAL VELOCITY CURVES

All program stars were observed at least twice in the course of the SPY project at the ESO VLT. Additional observations were made during follow-up campaigns at the ESO NTT (equipped with EMMI), the ESO VLT (UVES), the Calar Alto Observatory 3.5 m telescope (TWIN) and the 4 m WHT (ISIS) at La Palma.

Radial velocities of the individual observations are determined by calculating the shifts of the measured wavelengths relative to their laboratory values. Since the S/N ratio was of the order of 15 to 30, most of the narrow metal lines were hardly visible in our individual spectra. We therefore focussed on all available He I lines and on the observed $H\alpha$ line profile because of its sharp and well-defined non-LTE line core. We performed a simultaneous fit of a set of mathematical functions to the observed line profiles using the ESO MIDAS package. A linear function was used to reproduce the overall spectral trend and a Gaussian for the innermost line core. In order to fit the $H\alpha$ profile we used an additional Lorentzian to model the broad line wings. The central wavelength of the Lorentzian was fixed to that of the Gaussian for physical reasons.

The period search was carried out by means of a periodogram based on the ‘Singular Value Decomposition’ method. For a large range of periods the best fitting sine-shaped RV curve was computed (see Napiwotzki et al. 2001). The difference between the observed radial velocities and the best fitting theoretical RV curve for each phase set was evaluated in terms of the logarithm of the sum of the squared residuals (χ^2) as a function of period. This method finally results in the data-set’s power spectrum which allows to determine the most probable period of variability (see Lorenz et al. 1998).

From the best fit RV curve corresponding to the most probable period, the ephemeris, the system’s velocity and the semi-amplitude were derived. As an example, Figure 1 displays the resulting power spectrum and best-fit sine curve for HE 0532–4503. The ephemerides for all program stars, are given in Table 1, as well as the semi-amplitudes (K) and the derived system velocities (γ).

3. QUANTITATIVE SPECTRAL ANALYSIS

Prior to quantitative spectral analysis the spectra were corrected for the measured RV and coadded in order to increase the S/N ratio. Effective temperatures (T_{eff}), surface gravities ($\log g$) and helium abundances ($\log [n_{\text{He}}/n_{\text{H}}]$) were determined by fitting simultaneously each observed hydrogen and helium line with a grid of metal-line blanketed LTE model spectra. The procedure used is described in detail in Napiwotzki et al. (1999). Because of its sensitivity to non-LTE effects, the $\text{H}\alpha$ line was excluded from this analysis. Results are displayed in Table 2, and a sample fit is shown in Figure 2.

In addition, LTE metal abundances were derived for the program stars from measured equivalent widths using the classical curve-of-growth method. Some stars show very rich abundance patterns with many species above the detection threshold (e.g., HE 2135–3749), while others like HE 1448–0510 are extremely metal poor (see also Edelmann 2003). In order to derive upper limits to elemental abundances in these cases, we assumed the detection limit for metal lines to be equal to the S/N level (in terms of equivalent width). Results of our metal abundance analysis are given in Table 3.

4. NATURE OF THE UNSEEN COMPANION

Table 1. System parameters: ephemeris, RV semi-amplitudes K and system velocities γ for all the sdB stars discussed.

| System | Ephemeris [hel.JD ₀ –2 450 000] | K [km s ^{–1}] | γ [km s ^{–1}] |
|--------------|---|------------------------------|-----------------------------------|
| WD 0048–202 | $3\,097.5596 \pm 7.4436 \times E$ | 47.9 ± 0.4 | -26.5 ± 0.4 |
| HE 0532–4503 | $3\,099.9975 \pm 0.2656 \times E$ | 101.5 ± 0.2 | 8.5 ± 0.1 |
| HE 0929–0424 | $3\,100.0585 \pm 0.4400 \times E$ | 114.3 ± 1.4 | 41.4 ± 1.0 |
| HE 1448–0510 | $3\,097.0703 \pm 7.1588 \times E$ | 53.7 ± 1.1 | -45.5 ± 0.8 |
| HE 2135–3749 | $3\,099.6520 \pm 0.9240 \times E$ | 90.5 ± 0.6 | 45.0 ± 0.5 |
| HE 2150–0238 | $3\,100.6081 \pm 1.3209 \times E$ | 96.3 ± 1.4 | -32.5 ± 0.9 |

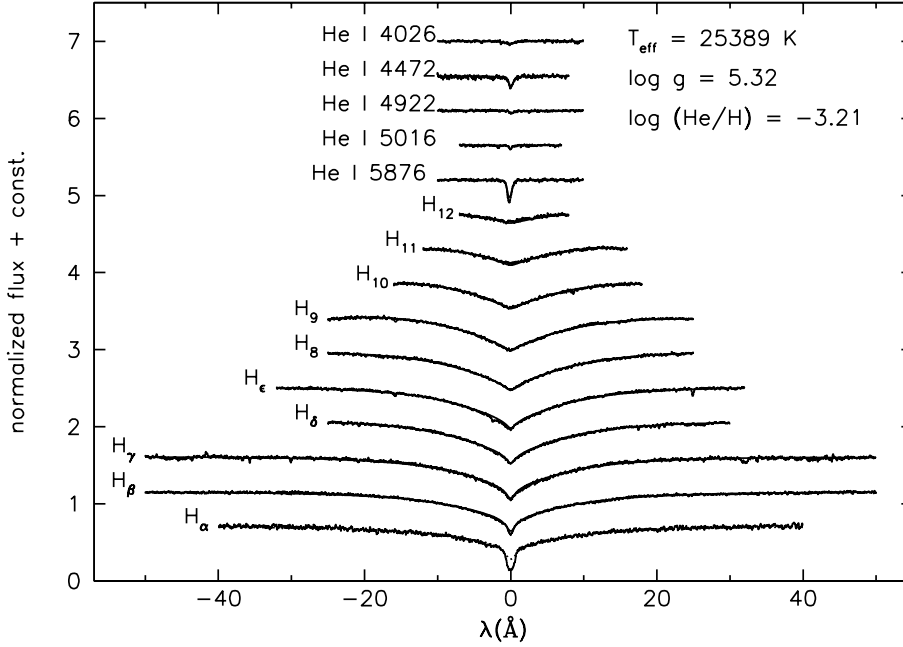


Fig. 2. Sample model fit for an sdB star (HE 0532-4503) based on 47 UVES spectra.

Since the spectra of the program stars are single-lined, they reveal no information about the orbital motion of the sdBs' companions, and thus we can only compute their mass functions

$$f_m = \frac{M_{\text{comp}}^3 \sin^3 i}{(M_{\text{comp}} + M_{\text{sdB}})^2} = \frac{PK^3}{2\pi G}. \quad (1)$$

Although the RV semi-amplitude K and the period P are determined by the

Table 2. Stellar parameters: effective temperatures, surface gravities and helium abundances of the visible components. Typical error margins for T_{eff} , $\log g$ and $\log [n_{\text{He}}/n_{\text{H}}]$ are 235 K, 0.03 dex and 0.15 dex, respectively.

| System | T_{eff} [K] | $\log g$ [cms^{-2}] | $\log [n_{\text{He}}/n_{\text{H}}]$ |
|--------------|-------------------------|-----------------------------------|-------------------------------------|
| WD 0048–202 | 29 960 | 5.50 | ≤ -4.00 |
| HE 0532–4503 | 25 390 | 5.32 | -3.21 |
| HE 0929–0424 | 29 470 | 5.71 | -1.99 |
| HE 1448–0510 | 34 690 | 5.59 | -3.06 |
| HE 2135–3749 | 30 000 | 5.84 | -2.54 |
| HE 2150–0238 | 30 200 | 5.83 | -2.44 |

Table 3. Metal abundance patterns of the program stars (relative to solar values).

| System | Abundances ϵ | | | | | |
|--------------|-------------------------|------------------------|-------------------------|----------------|------------------|------------------|
| | C II Si IV Ti III | N II S II Fe III | O II S III Zn III | Mg II Ar II | Al III Ar III | Si III Ca III |
| WD 0048–202 | — | −0.67 | −1.38 | −1.00 | −0.71 | −1.50 |
| | −1.98 | — | −1.41 | — | — | — |
| | +1.84 | −0.27 | — | — | — | — |
| HE 0532–4503 | −2.29 | −0.79 | −1.17 | −0.72 | — | −1.22 |
| | — | −0.28 | −0.82 | — | — | — |
| | — | 0.16 | — | — | — | — |
| HE 0929–0424 | −1.81 | −0.14 | −1.07 | −0.80 | −0.53 | −0.93 |
| | — | — | −0.80 | +0.79 | — | — |
| | — | 0.00 | — | — | — | — |
| HE 1448–0510 | ≤ -2.17 | ≤ -1.24 | ≤ -2.17 | −0.59 | ≤ -0.93 | — |
| | — | — | $\leq +0.80$ | $\leq +0.67$ | — | — |
| | — | ≤ -0.46 | — | — | — | — |
| HE 2135–3749 | — | −0.36 | — | — | — | — |
| | — | −0.12 | −0.58 | +0.74 | +0.50 | +1.89 |
| | +1.61 | −0.87 | +1.94 | — | — | — |
| HE 2150–0238 | — | −0.25 | ≤ -2.17 | ≤ -1.53 | ≤ -1.18 | ≤ -2.00 |
| | — | — | −0.26 | +0.92 | — | — |
| | — | ≤ -0.71 | — | — | — | — |

RV curve, M_{sdb} , M_{comp} and $\sin^3 i$ remain free parameters. Binary population synthesis models (Han et al. 2003) indicate a most likely mass of $M_{\text{sdb}} = 0.47 M_{\odot}$ for sdB stars, which we adopt for the following analysis. Assuming $i = 90^\circ$ we are able to compute the companions' minimum masses from Equation 1. The statistically most probable inclination angle is $i = 52^\circ$ which yields the most likely masses for the companions. Our results are summarized in Table 4.

Table 4. Mass functions, and masses (minimum mass $M_{\text{comp}}^{90^\circ}$ and most probable mass $M_{\text{comp}}^{52^\circ}$) of the unseen companions.

| System | f_{m} [M_{\odot}] | $M_{\text{comp}}^{90^\circ}$ [M_{\odot}] | $M_{\text{comp}}^{52^\circ}$ [M_{\odot}] |
|--------------|-----------------------------------|---|---|
| WD 0048–202 | 0.085 | 0.47 | 0.57 |
| HE 0532–4503 | 0.029 | 0.25 | 0.37 |
| HE 0929–0424 | 0.068 | 0.36 | 0.51 |
| HE 1448–0510 | 0.115 | 0.56 | 0.68 |
| HE 2135–3749 | 0.071 | 0.36 | 0.51 |
| HE 2150–0238 | 0.122 | 0.48 | 0.70 |

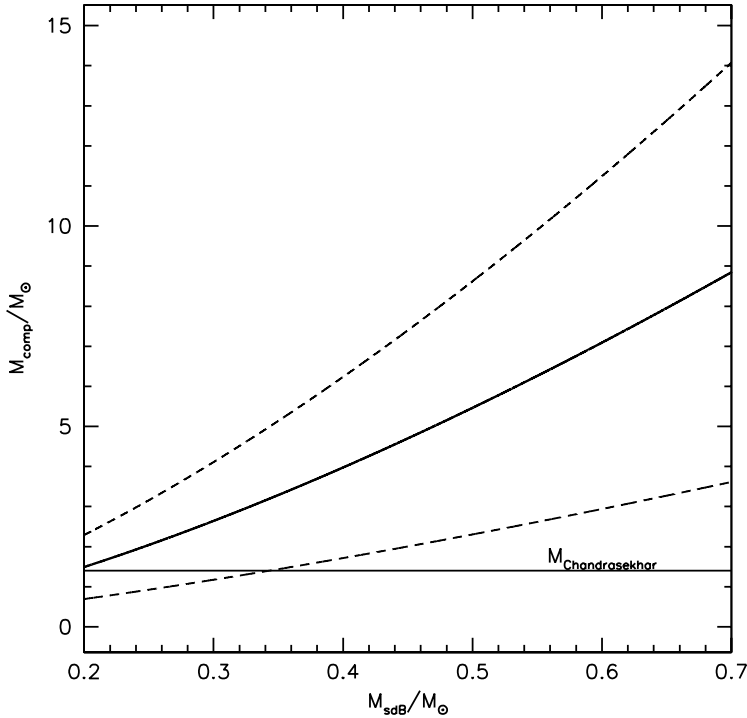


Fig. 3. Determination of the mass of the unseen companion for the system HE 0532-4503. The solid line marks the mean mass for the unseen companion, while the dashed lines indicate the error margins.

5. TIDALLY LOCKED ROTATION?

For close binary systems, rotational velocities of the components may be tidally locked to their orbital motions (see, e.g., Napiwotzki et al. 2001), which means

$$v_{\text{rot}} = \frac{2\pi R_{\star}}{P}. \quad (2)$$

Measurement of the projected rotational velocities $v_{\text{rot}} \sin i$ would therefore allow to determine inclination angles of the systems, i . In order to derive $v_{\text{rot}} \sin i$, we compared the observed spectra with rotationally broadened synthetic line profiles. The latter ones were computed for the stellar parameters given in Tables 2 and 3. Since sharp metal lines are much more sensitive to rotational broadening than Balmer or helium lines, we concentrated on strong N II lines between 5000 and 5008 Å.

Table 5 displays the resulting projected rotational velocities $v_{\text{rot}} \sin i$, as well as the deduced inclination angles i and corresponding masses M_{comp} . No rotation velocity could be determined for HE 1448-0510 due to the lack of suitable metal lines, the remaining five stars are slow rotators with projected rotational velocities below 10 km s^{-1} . For the short period systems HE 0532-4503, HE 0929-0424 and HE 2135-3749 we deduce inclination angles between 11° and 32° . The analyses of WD 0048-202 and HE 2150-0238, however, yield unreasonable values $\sin i > 1$.

Table 5. Periods and projected rotational velocities, as well as inclination angles and masses of the unseen companion computed for tidally locked rotation.

| System | P [d] | R_{sdB} [R_{\odot}] | v_{rot} [km/s] | $v_{\text{rot}} \sin i$ [km/s] | i [deg] | M_{comp} [M_{\odot}] |
|--------------|---------------------|-------------------------------------|----------------------------|-----------------------------------|--------------|--------------------------------------|
| HE 0532–4503 | 0.2656 ± 0.0001 | 0.25 | 47 | 9 ± 2 | 11 ± 3 | 5.0 ± 3.0 |
| HE 0929–0424 | 0.4400 ± 0.0002 | 0.16 | 18 | 6 ± 2 | 19 ± 7 | 2.7 ± 2.0 |
| HE 2135–3749 | 0.9240 ± 0.0003 | 0.14 | 7 | 4 ± 2 | 32 ± 20 | 1.1 ± 0.7 |
| HE 2150–0238 | 1.3209 ± 0.0050 | 0.14 | — | 8 ± 2 | $\sin i > 1$ | — |
| HE 1448–0510 | 7.1588 ± 0.0130 | 0.18 | — | — | — | — |
| WD 0048–202 | 7.4436 ± 0.0150 | 0.20 | — | ≤ 5 | $\sin i > 1$ | — |

A possible explanation is, that the latter systems are *not* tidally locked, which is plausible because they have rather long periods.

The masses deduced for the companions of the short-period systems are quite large, as can be seen from Table 5. For the HE 2135–3749 system, the sdB companion’s mass is $1 M_{\odot}$ which indicates a massive white dwarf. The companion of HE 0929–0424 is even more massive, but the large error in mass prevents us from drawing conclusions. For HE 0532–4503 the companion mass is larger than the Chandrasekhar mass, even if we allow for the large error and adopt the canonical mass for the sdB, indicating that it might possibly be a black hole. As can be seen from Figure 3, the companion mass could be sub-Chandrasekhar only if the sdB is of very low mass ($M_{\text{sdB}} < 0.34 M_{\odot}$). As indicated by some tests, it will be possible to reduce the uncertainty in $v_{\text{rot}} \sin i$ if we include more lines. This will be done in the near future.

Black holes are rare objects and it is therefore very unlikely that our small sample of six RV variable sdBs contain two of them. But stellar rotation and orbital motion may also be locked in a period-ratio that differs from unity (like Mercury, for which the ratio is $3/2$).

Since the projected rotational velocities are small, the crucial parameter for the measurement of $v_{\text{rot}} \sin i$ and subsequently for M_{comp} is the spectral resolution of the instrument. Our spectra, however, have been measured through rather wide slits. Their spectral resolution is therefore seeing dependent. We used information from the seeing monitor to determine the instrumental profile during these observations. When coadding the spectra we discarded those (few) taken in poor conditions and used only those taken under similar seeing conditions $\sim 1''$. This procedure may have led to an underestimation of the width of the instrumental profile which could have led to an overestimation of the system inclination. A lower inclination means even higher masses. Only if we should still have overestimated the width of the instrumental profile, the companion masses could be lower. To obtain more accurate values for $v_{\text{rot}} \sin i$, we need additional observations. These will have to be taken using a small slit so that the instrumental profile is well defined. For the time being the resulting high companion masses have to be taken with a pinch of salt.

REFERENCES

- Edelmann H. 2003, Ph.D. thesis, University of Erlangen-Nuremberg
- Geier S., Heber U., Przybilla N., Kudritzki R. P. 2006, *Baltic Astronomy*, 15, 243
(these proceedings)
- Han Z., Podsiadlowski P., Maxted P. F. L., Marsh T. R. 2003, *MNRAS*, 341, 669
- Lisker T., Heber U., Napiwotzki R. et al. 2005, *A&A*, 430, 223
- Lorenz L., Mayer P., Drechsel H. 1998, *A&A*, 332, 909
- Maxted P. F. L., Marsh T. R., North R. C. 2000, *MNRAS*, 317, L41
- Napiwotzki R., Christlieb N., Drechsel H. et al. 2003, *ESO Messenger*, 112, 25
- Napiwotzki R., Edelmann H., Heber U. et al. 2001, *A&A*, 378, L17
- Napiwotzki R., Green P. J., Saffer R. A. 1999, *ApJ*, 517, 399
- Napiwotzki R., Karl C., Nelemans G. et al. 2005, in *14th European Workshop on White Dwarfs*, eds. D. Koester & S. Moehler, *ASP Conf. Ser.*, 334, 375

SPECTRAL ANALYSIS OF sdB-He STARS FROM THE SDSS

A. Ahmad, C. Winter and C. S. Jeffery

Armagh Observatory, College Hill, Armagh BT61 9DG, North Ireland

Received 2005 July 28

Abstract. We present spectral classification and physical parameters of a sample of “helium-rich” sdB-He stars from spectra obtained from the SDSS archive. The spectral classification was carried out using an automated neural network, and the physical parameters were derived using LTE model atmospheres. The results indicate that most of these stars are not typical He-sdB stars but rather are normal sdB stars with slight helium enrichment. This is most likely a result of the use of a different definition of “helium-rich” in the initial SDSS classification to that used more widely in the field.

Key words: stars: chemically peculiar – early-type, subdwarfs, fundamental parameters

1. INTRODUCTION

Subluminous B stars form the dominant population of faint blue stars in our Galaxy down to a limiting magnitude of $B \approx 16$ mag. These so-called subdwarf B (sdB) stars are thought to be low-mass core helium burning stars with a thin hydrogen envelope. The surfaces of sdB stars are predominantly helium-deficient due to diffusion and gravitational settling. However, a small number have extremely helium-rich atmospheres. The evolution of these “helium-rich subdwarf B” (He-sdB) stars has recently been the subject of much debate involving both single and binary star evolution.

Only a very small fraction ($\sim 5\%$) of sdB stars identified in previous surveys of faint blue stars like the Palomar Green survey (Green et al. 1986) and the Edinburgh Cape survey (Kilkenny et al. 1997) are helium-rich. A small number of stars discovered amongst the many thousand hot subdwarfs in the recent Quasar survey – the Sloan Digital Sky Survey (SDSS) have been reported to show strong helium lines and labelled ‘sdB-He’ (Harris et al. 2003).

In this study we used an artificial neural network (ANN) to classify spectra of sdB-He stars from the SDSS and to derive fundamental atmospheric parameters. The aim was to determine whether sdB-He stars are similar to He-sdB stars. This would increase the number of known helium-rich subdwarfs for further studies.

2. DATA MINING

Where available, reduced spectra were manually extracted from the SDSS Data Release server using coordinates listed in Harris et al. (2003). The spectra were then normalized using the continuum provided in the fits file. The normalized spectra were then classified and parameterised. It should be noted that the spectra analysed here are moderate resolution ($\sim 3 \text{ \AA}$) and have a typical signal-to-noise (S/N) ratio of ~ 40 .

3. CLASSIFICATION

We have classified the SDSS sdB-He sample onto the MK-like system defined by Drilling et al. (2000). As the hot subdwarfs do not fall within the scope of the original MK system, Drilling et al. (2000) have extended and refined the earlier work of Drilling (1996) and Jeffery et al. (1997) to construct a three-dimensional MK-like classification scale for these stars.

Table 1. Classifications of the SDSS sdB-He sample as determined by the ANN. Error estimates are ~ 2 subtypes for spectral type, ~ 1 subclass for luminosity, and ~ 4 subclasses for the helium class.

| Name [SDSS J+] | n_{He} | ANN classification |
|----------------------|-----------------|--------------------|
| 09 40 44.08+00 47 59 | 0.16 | sdB0 VIII:He23 |
| 11 38 40.69-00 35 31 | 0.01 | sdB3 V:He1 |
| 12 43 46.38+00 25 34 | 0.05 | sdB1 V:He23 |
| 12 54 10.86-01 04 08 | 0.01 | sdB3 III:He5 |
| 13 17 45.80+01 04 50 | 0.01 | sdB0 VI:He3 |
| 13 45 45.24-00 06 41 | 0.15 | sdO9 VII:He21 |
| 13 46 35.68-00 18 04 | 0.09 | sdA2 IV:He0 |
| 13 57 07.35+01 04 54 | 0.36 | sdO6 VII:He30 |
| 14 15 56.68-00 58 14 | 0.21 | sdB8 VI:He14 |
| 14 39 17.64+01 02 51 | 0.01 | sdB6 V:He3 |
| 14 45 14.93+00 02 49 | 0.02 | sdB1 VII:He11 |
| 15 27 08.31+00 33 08 | 0.45 | sdO9 VIII:He35 |
| 15 29 05.62+00 21 37 | 0.06 | sdO9 VII:He10 |
| 15 42 38.43-00 37 58 | 0.07 | sdA2 III:He2 |

(ANN) to perform classifications onto the Drilling et al. (2000) scale. The ANN is a feed-forward back propagation network with an input layer of 901 nodes, two hidden layers of 5 nodes each, and an output layer of 3 nodes from which is obtained the spectral type, luminosity class, and helium class values determined by the network. The ANN was trained for 700 iterations on the same set of hot standards used by Drilling et al. (2000), with the spectra having been velocity corrected and resampled onto a uniform wavelength grid of 4050–4950 \AA at a dispersion of 1 \AA per pixel.

This scale is based upon a sample of spectra from a number of sources, covering the wavelength region 4050–4900 \AA at a resolution of 2.5 \AA . It defines a spectral type running from sdO1 to sdA, analogous to MK spectral classes, and uses luminosity classes IV–VIII, where most hot subdwarfs have a luminosity class \sim VII. A helium class has been introduced, which runs from ‘He0’ to ‘He40’, based on H, He I and He II line strengths.

As our intention is to classify large quantities of spectra obtained from digital sky surveys such as the SDSS, we have trained an artificial neural network

The results of applying the ANN to our sdB-He sample are presented in Table 1. Each spectrum was velocity corrected and resampled onto the same wavelength grid as was used for training the ANN. Error estimates (1σ) for each of the parameters determined by the ANN are ~ 2 subtypes for spectral type, ~ 1 subclass for luminosity, and ~ 4 subclasses for the helium class.

The spectra from Ahmad & Jeffery (2003) were also classified with the ANN to check for consistency as these have previously been manually classified by J. S. Drilling. The ANN classification with the manual classification, within the above errors.

4. SPECTRAL ANALYSIS

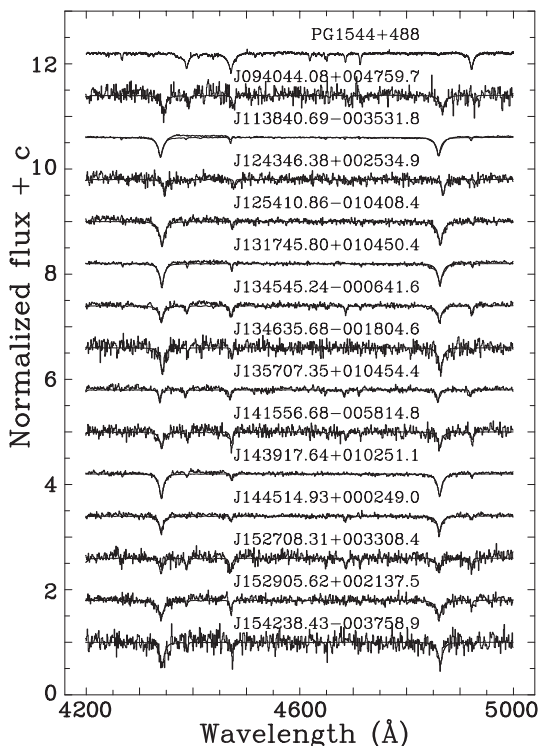


Fig. 1. Optical spectra of sdB-He stars (thick line) along with best fit model. The spectrum of the He-sdB star prototype – PG1544+488 is plotted on the top for comparison.

The physical parameters effective temperature (T_{eff}), surface gravity ($\log g$) and helium abundance (n_{He}) were measured from the optical blue (4200–5000 Å) spectra (Figure 1) using the latest version of the spectral fitting code SFIT2 and grid of high-gravity LTE models (cf. Ahmad & Jeffery 2003).

Note that the blue ends of the SDSS spectra are incorrectly normalized when corrected using the continuum provided by the SDSS therefore the region from 3900–4200 Å was not considered in the model fit. Given the low quality of the SDSS spectra the errors in T_{eff} are ± 1000 K, in $\log g$ are ± 0.4 and n_{He} are ± 0.05 .

The sdB-He stars are plotted on the T_{eff} vs. $\log g$ diagram using the derived parameters in Figure 2. The respective helium abundances are listed in Table 1 as number fraction. From their position on the T_{eff} vs. $\log g$ diagram (Figure 2), half of our sdB-He stars are too luminous to be subdwarfs, the others have a distribution typical of He-sdB stars.

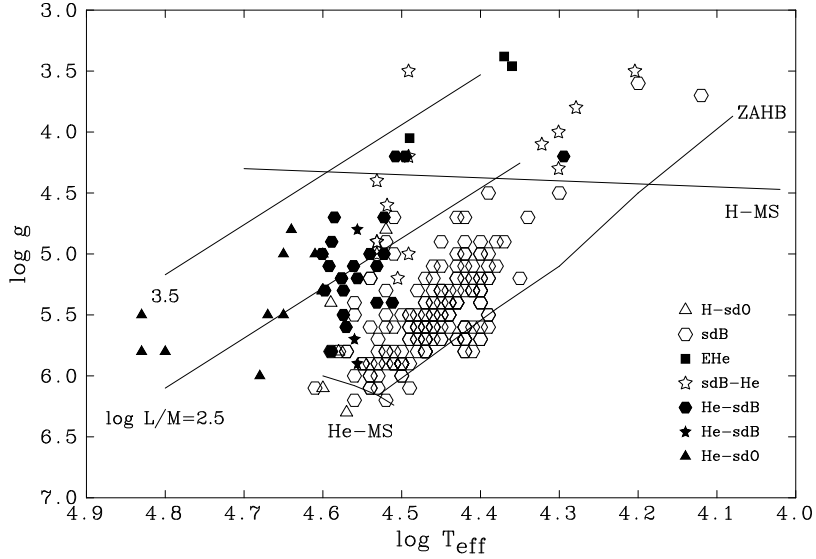


Fig. 2. Position of sdB-He stars on the T_{eff} vs. $\log g$ diagram shown with open star symbol. Other helium-rich objects like extreme helium (EHe) stars and He-sdO stars are shown with filled symbols. He-sdB stars from other work are shown by filled star symbol. For references see Ahmad & Jeffery (2003).

5. CONCLUSIONS

We have classified and parameterised a set of spectra of stars identified as sdB-He in the SDSS. It is clear from both spectral classification as well as parameterization that most of these stars show very little helium enrichment. Half of the stars in our sample have surface gravities too low to be subdwarfs. Out of the remaining subdwarfs only a handful are helium-rich (i.e. having $n_{\text{He}} \geq 0.10$ or He class > 20), again pointing out the need for a homogeneous classification scheme for hot subdwarfs.

REFERENCES

- Ahmad A., Jeffery C. S. 2003, *A&A*, 402, 335
 Drilling J. S. 1996, in *Hydrogen Deficient Stars*, eds. C. S. Jeffery & U. Heber, ASP Conf. Ser., 96, p. 461
 Drilling J. S., Moehler S., Jeffery C. S., Heber U., Napiwotzki R. 2000, in *The Kth Reunion*, ed. A. G. D. Philip, L. Davis Press, Schenectady, N.Y., p. 49
 Green R. F., Schmidt M., Liebert J. 1986, *ApJS*, 61, 304
 Harris H. C., Liebert J., Kleinman S. J. et al. 2003, *AJ*, 126, 1023
 Jeffery C. S., Drilling J. S., Harrison P. M., Heber U., Moehler S. 1997, *A&AS*, 125, 501
 Kilkeny D., O'Donoghue D., Koen C., Stobie R. S., Chen A. 1997, *MNRAS*, 287, 867

NON-LTE METAL ABUNDANCES IN V652 HER AND HD 144941

N. Przybilla¹, M. F. Nieva^{1,2}, U. Heber¹ and C. S. Jeffery³

¹ *Remeis-Sternwarte Bamberg, Sternwartstrasse 7, D-96049 Bamberg, Germany*

² *Observatório Nacional, R. Gal. José Cristino 77, 20921-400, São Cristóvão, Rio de Janeiro, RJ, Brasil*

³ *Armagh Observatory, College Hill, Armagh BT61 9DG, Northern Ireland*

Received 2005 July 31

Abstract. Two evolutionary scenarios are proposed for the formation of extreme helium stars: a post-AGB star suffering from a late thermal pulse, or the merger of two white dwarfs. An identification of the evolutionary channel for individual objects has to rely on surface abundances. We present preliminary results from a non-LTE analysis of CNO, Mg and S for two unique objects, V652 Her and HD 144941. Non-LTE abundance corrections for these elements range from negligible values to ~ 0.7 dex. Non-LTE effects typically lead to systematic shifts in the abundances relative to LTE and reduce the uncertainties.

Key words: line: formation – stars: abundances – stars: atmospheres – stars: evolution – stars: individual (V652 Her, HD 144941)

1. INTRODUCTION

Extreme helium stars (EHes) are a rare class of low-mass H-deficient objects with spectral characteristics similar to those of B-giants. Most of the two dozen known EHes could be explained by post-AGB evolution, linking R CrB stars to Wolf-Rayet type central stars of planetary nebulae, see Heber (1986) and Jeffery (1996) for reviews. The two stars studied here, V652 Her and HD 144941, are unique among the class members because of surface gravities too high for post-AGB evolution and atypical surface abundances. A merger of two He white dwarfs was suggested for the evolutionary origin of V652 Her (Saio & Jeffery 2000). The chemical composition puts important observational constraints on evolutionary scenarios. However, all elemental abundance analyses of EHes to date are based on the *assumption* of local thermodynamic equilibrium (LTE), therefore being subject to potential systematic uncertainties. We investigate here which improvements can be expected from a state-of-the-art non-LTE abundance analysis.

2. MODELS, OBSERVATIONS AND STELLAR PARAMETERS

The model calculations are carried out in a hybrid non-LTE approach, see Przybilla et al. (2005) for details. In brief, the atmospheric structure computations are performed using ATLAS12 (Kurucz 1996) for an appropriate chemical mixture.

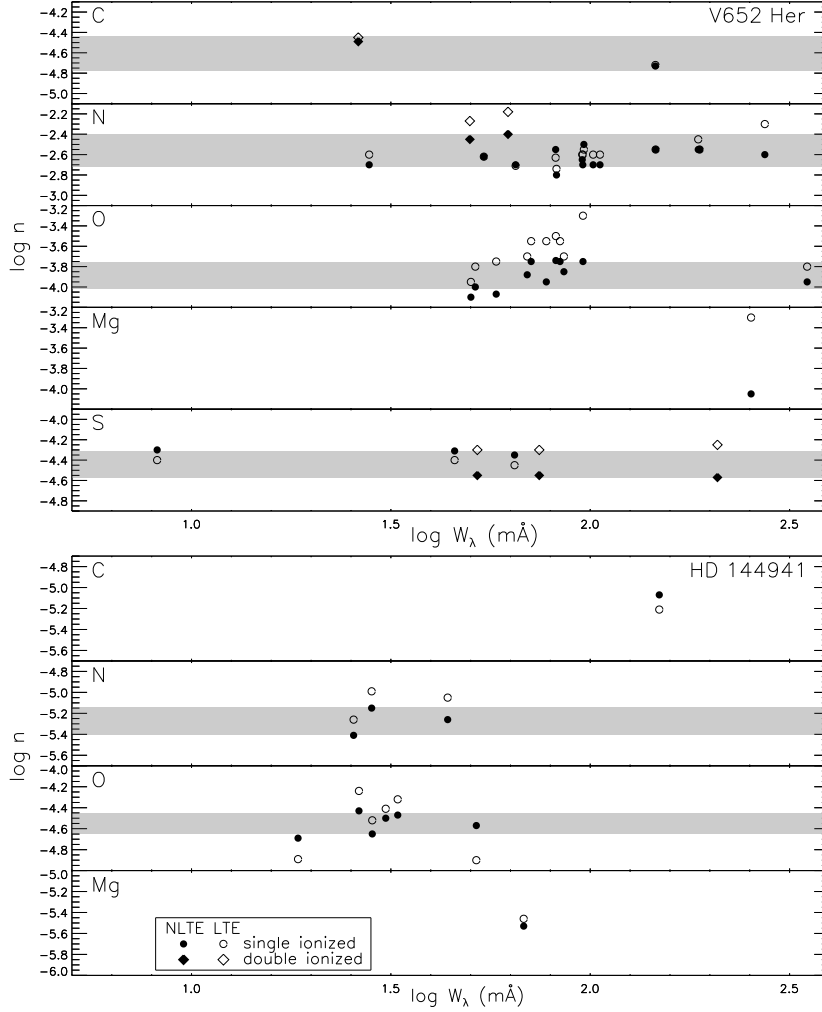


Fig. 1. Elemental abundances in the sample EHes from individual spectral lines

Table 1. Non-LTE model atoms.

| Ion | Source |
|----------|---|
| H | Przybilla & Butler (2004) |
| He I/II | Przybilla (2005) |
| C II/III | Nieva & Przybilla (in prep.) |
| N II/III | Przybilla & Butler (2001), with extensions |
| O II | Becker & Butler (1988) |
| Mg II | Przybilla et al. (2001) |
| S II/III | Vrancken et al. (1996), with updated atomic data |

Table 2. Stellar parameters.

| | V652 Her (R_{\max}) | HD 144941 |
|------------------------------|-------------------------|--------------|
| T_{eff} (K) | 22 000±500 | 22 000±1 000 |
| log g | 3.20±0.10 | 4.15±0.10 |
| ξ (km/s) | 4±1 | 8±2 |
| $n_{\text{H}}^{\text{NLTE}}$ | 0.005±0.0005 | 0.035±0.005 |

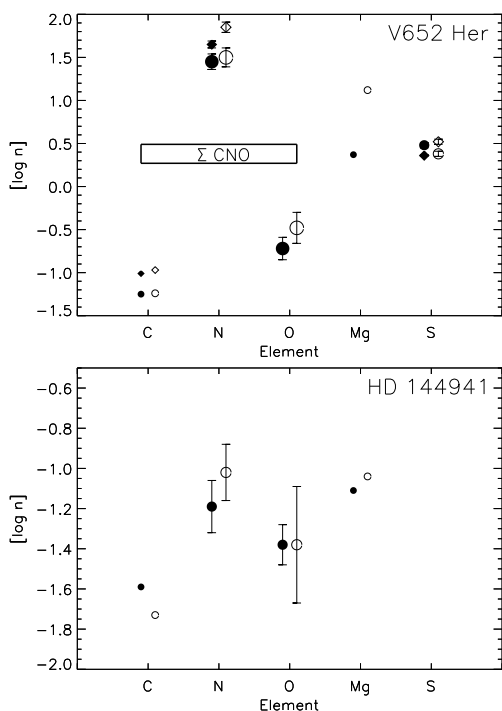


Fig. 2. Metal abundances in the sample EHeS (symbols as in Fig. 1)

Note that metal bound-free opacities are of minor importance for the two objects. Then, non-LTE line-formation is carried out on the resulting model stratifications. Updated and improved versions of DETAIL and SURFACE (Giddings 1981; Butler & Giddings 1985) are used for this, in combination with state-of-the-art non-LTE model atoms, see Table 1. High-resolution spectra at high- S/N are adopted for the analysis. Details on observations and data reduction are discussed by Jeffery et al. (2001) and Harrison & Jeffery (1997). The final model parameters are summarized in Table 2, including microturbulence ξ and H abundance $n_{\text{H}}^{\text{NLTE}}$ (by number). They are derived from the He I/II ionization equilibrium, Stark-broadened He I lines and H Balmer line strengths, using state-of-the-art model atoms.

3. NON-LTE ABUNDANCES

Elemental abundances are derived from line-profile fits, using a χ^2 -minimization technique based on small grids of synthetic spectra with varying metal abundances for given stellar parameters. This puts tighter constraints than the standard equivalent-width analysis. Abundances (by number) from individual spectral lines as a function of equivalent width W_λ are displayed in Figure 1. The grey bands indicate the 1σ -uncertainty range of the resulting abundances for the chemical species.

The non-LTE analysis reveals: (i) a reduction of systematic trends of abundance with W_λ , (ii) systematic shifts in the abundances relative to LTE, implying a downward revision in most cases and (iii) a potential for reducing the statistical scatter by a significant amount, e.g., for O II in HD 144941. Non-LTE abundance corrections for individual lines can be as large as ~ 0.7 dex (Mg II at 4481 Å in V652 Her), but usually they are (much) smaller. Note that the available spectra cover only a restricted wavelength range, such that the analysis has to rely on a rather small number of metal lines. Consequently, we view our results as preliminary, also because of residual uncertainties in the stellar parameter determination, which are indicated by a slight mismatch in the metal ionization equilibria in V652 Her. The situation is more aggravated in HD 144941 because of its strong metal-deficiency that is larger than in any other EHe star. The only metal ionization equilibrium available for an independent verification of the stellar parameter determination is that of silicon, for which we lack a reliable non-LTE model atom at present (the

model atom of Becker & Butler (1990) is too rudimentary in Si II).

The abundance patterns in the sample stars relative to the solar standard (Grevesse & Sauval 1998) are discussed in Figure 2. For each ionic species non-LTE and LTE results with uncertainties derived from the line-to-line scatter are displayed, using the same symbols as in Figure 1. The symbol size encodes the number of lines used for the abundance determination.

Both stars exhibit CNO-processed material in their atmospheres. For V652 Her the sum of CNO-abundances correlates well with the super-solar metallicity as indicated by the magnesium and sulphur abundances. Note the large non-LTE correction for magnesium, by a factor ~ 5 . Enhanced magnesium abundances as derived from LTE analyses of several EHe stars have been controversial because they cannot be consistently explained by nucleosynthesis (Jeffery 1996). The current findings indicate a solution of this issue. No further conclusions can be drawn for HD 144941 at present. We intend to extend the non-LTE study to aluminum, silicon and iron in the near future in order to complete the diagnostic inventory.

The preliminary non-LTE analysis of the two unique hydrogen-deficient, high-gravity objects V652 Her and HD 144941 does not drastically change our view of their evolutionary origin as constrained from surface abundances. While the non-LTE abundance corrections are small in most cases, they can be highly important in other cases. Accounting for non-LTE effects improves on the significance of abundance studies of extreme helium stars.

REFERENCES

- Becker S. R., Butler K. 1988, *A&A*, 201, 232
 Becker S. R., Butler K. 1990, *A&A*, 235, 326
 Butler K., Giddings J. R. 1985, in *Newsletter on Analysis of Astronomical Spectra*, No. 9, Univ. London
 Giddings J. R. 1981, Ph.D. thesis, Univ. London
 Grevesse N., Sauval A. J. 1998, *Space Sci. Rev.*, 85, 161
 Harrison P. M., Jeffery C. S. 1997, *A&A*, 323, 177
 Heber U. 1986, in *Hydrogen-Deficient Stars and Related Objects*, eds. K. Hunger, D. Schönberner & N. Kameswara Rao, Reidel Publ. Co., Dordrecht, p. 33
 Jeffery C. S. 1996, in *Hydrogen-Deficient Stars*, eds. C. S. Jeffery & U. Heber, ASP Conf. Ser., 96, 152
 Jeffery C. S., Woolf V. M., Pollacco D. L. 2001, *A&A*, 376, 497
 Kurucz R. L. 1996, in *Model Atmospheres and Spectrum Synthesis*, eds. S. J. Adelman, F. Kupka & W. W. Weiss, ASP Conf. Ser., 108, 160
 Przybilla N. 2005, *A&A*, 443, 293
 Przybilla N., Butler K. 2001, *A&A*, 379, 955
 Przybilla N., Butler K. 2004, *ApJ*, 609, 1181
 Przybilla N., Butler K., Becker S. R., Kudritzki R. P. 2001, *A&A*, 369, 1009
 Przybilla N., Butler K., Heber U., Jeffery C. S. 2005, *A&A*, 443, L25
 Saio H., Jeffery C. S. 2000, *MNRAS*, 313, 671
 Vrancken M., Butler K., Becker S. R. 1996, *A&A*, 311, 661

SUBDWARF B STAR EVOLUTIONARY SYSTEMATICS, CONUNDRUMS AND CAUTIONARY REMARKS *

E. M. Green¹, G. Fontaine², E. A. Hyde¹, S. Charpinet³ and P. Chayer⁴

¹ *Steward Observatory, University of Arizona, Tucson, AZ 85721, U.S.A.*

² *Département de Physique, Université de Montréal, C.P. 6128, Succ. Centre-Ville, Montréal, Québec, H3C 3J7, Canada*

³ *Observatoire Midi-Pyrénées, 14 Av. E. Belin, F-31400 Toulouse, France*

⁴ *Bloomberg Center for Physics and Astronomy, The Johns Hopkins University, Baltimore, MD 21218-2686, U.S.A.*

Received 2005 August 1

Abstract. We examine some of the systematics of different types of subdwarf B stars – short-period sdB+WD binaries, short period sdB+MS binaries, composite spectrum systems and apparently single stars – using recent results from our ongoing spectroscopic surveys and from asteroseismology, 2MASS photometry and open cluster color-magnitude diagrams. There are a wide variety of puzzles still remaining to be solved before we understand all the details of subdwarf B star formation and evolution.

Key words: binaries: close – stars: fundamental parameters – stars: EHB and post-EHB – stars: subdwarfs

1. INTRODUCTION

For several years, we have been collecting homogeneous stellar spectra of bright ($V \lesssim 14.4$) sdB stars using both the MMT blue spectrograph and Steward Observatory's 2.3 m Bok telescope. Accurate radial velocities derived from individual MMT spectra (1 Å resolution, 4000–4950 Å) are used to identify sdB binaries and determine precise orbital parameters (Green, For & Hyde 2005). We also shift multiple spectra for the same star to the rest velocity and combine them into a single high-S/N MMT spectrum for optical abundance analysis (see Fontaine et al. 2006). Our 2.3 m survey has much lower resolution (~ 9 Å, 3615–6900 Å) and was originally intended solely for identification and homogeneous classification of sdO and sdB candidates. However, when we recently compared the effective temperatures, gravities and helium abundances derived from combined MMT spectra vs. similarly combined 2.3 m spectra for the same stars, we found no systematic differences, given sufficient S/N for both (~ 200 –300).

We now have homogeneous parameters for 115 sdB and sdOB stars from MMT spectra, and we will soon have comparable parameters derived from 2.3 m spectra

*Observations reported here were obtained at the MMT Observatory, a joint facility of the University of Arizona and the Smithsonian Institution.

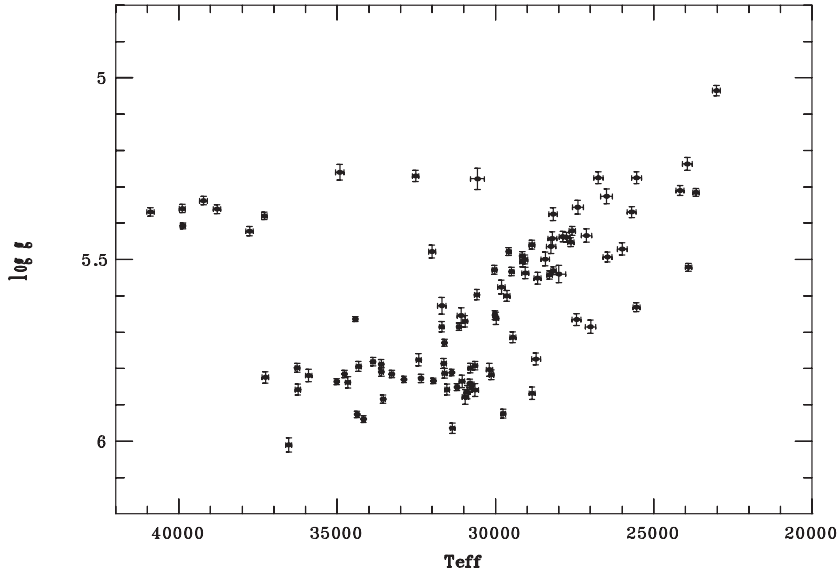


Fig. 1. The $\log g$ vs. T_{eff} diagram derived for 100 homogeneous, single-lined sdB stars in our MMT sample. The error bars are twice the formal errors of the fit.

for an overlapping sample of more than 200 stars. In sections 2 and 3, we will use the temperatures and gravities derived for our current MMT sample to show how such information can eventually help illuminate our ideas about sdB formation and evolution, particularly when combined with the new results just beginning to be uncovered by asteroseismology.

In section 4, we use 2MASS* photometry in combination with optical photometry to highlight another puzzle involving the distribution of low-mass main-sequence secondaries in sdB binaries. Finally, we reconsider the problem of representative samples of disk EHB stars in section 5. Using an infrared-selected (2MASS) hot star sample plus evidence from the color-magnitude diagrams of the old open clusters NGC 6791 and NGC 188, we investigate the cool end of the EHB region, which presents its own problems.

2. TEMPERATURE VS. GRAVITY RESULTS

Figure 1 shows the gravity vs. effective temperature diagram for stars in our MMT sample that do not have composite spectra. Fifteen sdB stars (mostly pulsators) fainter than our original magnitude limit were excluded in an effort to make this sample more representative. To the extent that this diagram truly is representative, the nonuniform distribution of stars must be reflecting significant details about their evolution. Additional data, e.g., stellar masses, will be needed before we can fully understand why these stars are distributed the way they are.

The nonuniformity shouldn't be too surprising, since we already know that several different scenarios can produce sdB stars. In fact, Figures 2 and 3 show, for the first time, that the distribution of apparently single sdB stars appears to

* <http://www.ipac.caltech.edu/2mass>

Table 1. Results from asteroseismology.

| Pulsator | T_{eff} | $\log g$ | Mass |
|-------------|------------------|-------------------|-------------------|
| PG 0014+067 | 34126 ± 165 | 5.769 ± 0.030 | 0.490 ± 0.019 |
| PG 1047+003 | 34768 ± 112 | 5.815 ± 0.019 | 0.490 ± 0.014 |
| PG 1219+534 | 33604 ± 125 | 5.809 ± 0.024 | 0.457 ± 0.012 |
| Feige 48 | 29582 ± 135 | 5.478 ± 0.023 | 0.460 ± 0.008 |

be somewhat different from that of short-period binary sdB stars. For example, 30% of the single sdB stars lie in a relatively dense “foot” between $5.75 < \log g < 5.90$ for $T_{\text{eff}} > 33\,000$ K, that is almost entirely missing in the binary distribution. However, the rest of the single stars are widely scattered over all the regions where the binaries occur. Another interesting feature is that short-period binaries with main sequence companions occupy only a small area in the middle of the range of sdB+WD binaries (except for one hot outlier, HS 2333+3927, which Heber et al. (2004) suggested might have an unusually small mass for an sdB star). It will be interesting to see if this holds up when larger samples are available, since there is no obvious reason why it should be so.

3. ASTEROSEISMOLOGICAL MASSES

Both single star evolution with enhanced mass-loss and binary mass transfer followed by common envelope ejection are expected to produce 0.46 to $0.49 M_{\odot}$ sdB stars, since that is the mass range near the first red giant tip where helium can ignite in stripped stellar cores. In contrast, mergers of He-core white dwarfs are expected to produce single sdB stars with a much wider range of masses. Asteroseismology is just beginning to provide an independent check of this crucial parameter. Recent results from Charpinet and collaborators (Brassard et al. 2001; Charpinet, Fontaine & Brassard 2003; Charpinet et al. 2005a; Charpinet et al. 2005b) are listed in Table 1. Radial velocities were derived from multi-epoch spectra for each of the four objects, with a typical precision of $\sim 2 \text{ km s}^{-1}$. The velocities indicate that PG 0014+067, PG 1047+003 and PG 1219+534 are single stars, consistent with other similar stars in Figure 2, while Feige 48 is a binary, as previously discovered by O’Toole, Heber & Benjamin (2004).

All four asteroseismological masses are consistent with a He core flash at, or during evolution away from, the tip of the first red giant branch. This is particularly gratifying in the case of the binary, since this is the only known way that such a binary could have formed. The values for the single stars do not, by themselves, rule out the merger theory, particularly since all three refer to essentially the same point in the $\log g$ vs. T_{eff} diagram. However, Figure 2 shows a distinct lack of stars scattered above and below the horizontal sequence of hot stars at $\log g \sim 5.8$, that would correspond to higher and lower masses. Therefore, it seems that mergers cannot be an important evolutionary channel for sdB stars hotter than $T_{\text{eff}} = 32\,000$ K. It will be very interesting for the merger theory to see what asteroseismology can tell us about the masses of single stars on the right side of Figure 2!

4. A SURPRISING RESULT FROM 2MASS PHOTOMETRY

So far, we have only discussed sdB stars with non-composite spectra, i.e., those whose optical spectra show no absorption lines from a cool companion. Stark

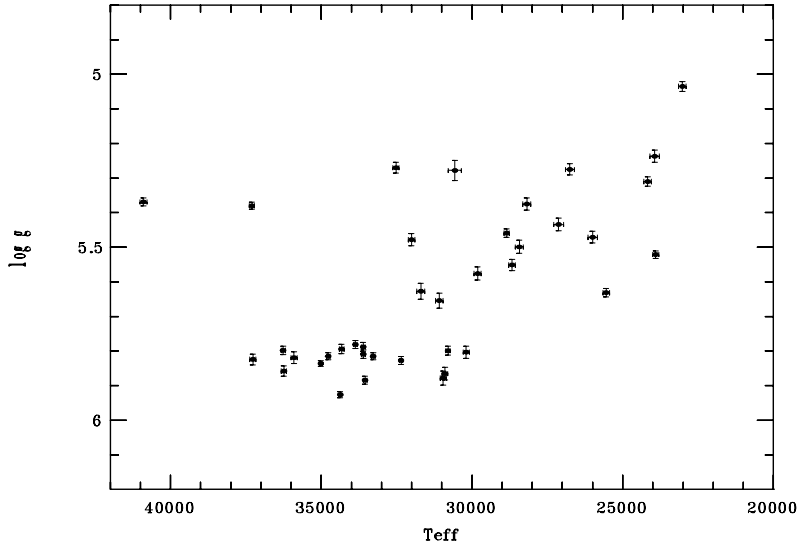


Fig. 2. The $\log g$ vs. T_{eff} diagram for the subsample of apparently single stars in Figure 1, i.e. those which show no significant radial velocity variations, reflection effects, absorption lines or detectable IR flux from a cool companion.

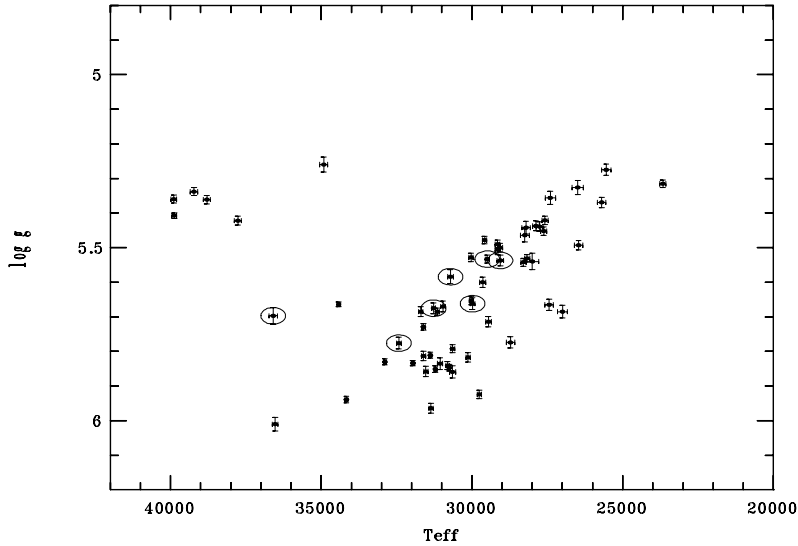


Fig. 3. The same as Figure 2, except only known short-period binary stars from Figure 1 are plotted. The seven circled objects have main-sequence secondaries, while nearly all the rest are believed to have white dwarf companions.

& Wade (2003) demonstrated that about 1/3 of sdB stars have main-sequence companions of type F, G or K, that are easily detected using a combination of optical and 2MASS infrared photometry. More recently, Green, For & Hyde (2005) showed that there is a surprising dichotomy in the $V-J$ vs. $J-H$ two-color plot

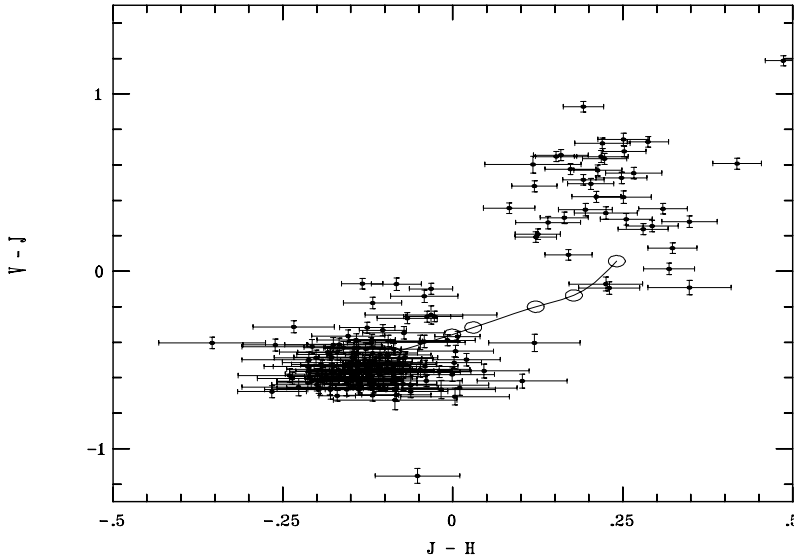


Fig. 4. $V-J$ vs. $J-H$ plot of spectroscopically confirmed sdB stars with $V < 14.4$ and $E_{B-V} \leq 0.05$. The curve between the two clumps illustrates how the color of a typical composite sdB star would vary with the mass of the main-sequence secondary; the open circles mark (from upper right to lower left) companion masses of 0.70, 0.60, 0.54, 0.37, 0.26 and 0.18 M_{\odot} (see text).

between sdB+MS binaries whose secondaries are detectable in optical spectra and all the rest (single stars and short-period binaries with invisible companions).

We have updated this result in Figure 4, having added several more stars, and the conclusions remain the same: (1) there is a significant color gap between the composite spectrum sdB stars in the upper right and all the other sdB stars at the lower left, that cannot be explained by selection effects, (2) none of the composite spectrum stars investigated so far have orbital periods shorter than many months to several years and (3) all of the sdB binaries with periods of the order of a few hours to several days fall in the lower left of Figure 4 along with the apparently single sdB stars, including the seven known sdB binaries with dwarf M3–M6 companions.

To determine the size of the gap between sdB stars with mid-M companions (in the lower left group) and those with companions of spectral types F, G or K (in the upper right), we calculated expected colors for composite stars over a range of secondary masses. Starting with a typical sdB primary having $M_V = 4.5$, $V-J = -0.50$ and $J-H = -0.12$, we used observed colors and magnitudes corresponding to empirically derived lower main-sequence masses from K8 to M6 (Kirkpatrick & McCarthy 1994; Henry & McCarthy 1993), to compute the combined colors (open circles). The results show that the color gap corresponds to a mass gap of about 0.3 M_{\odot} . Does this mean that nearly all sdB progenitors with main-sequence companions originally more massive than about 0.35 M_{\odot} were able to achieve a stable mass transfer of more than 0.4 M_{\odot} to their companions? Once again, the systematics of a large sample of sdB stars have provided a powerful clue for the formation and evolution of these stars.

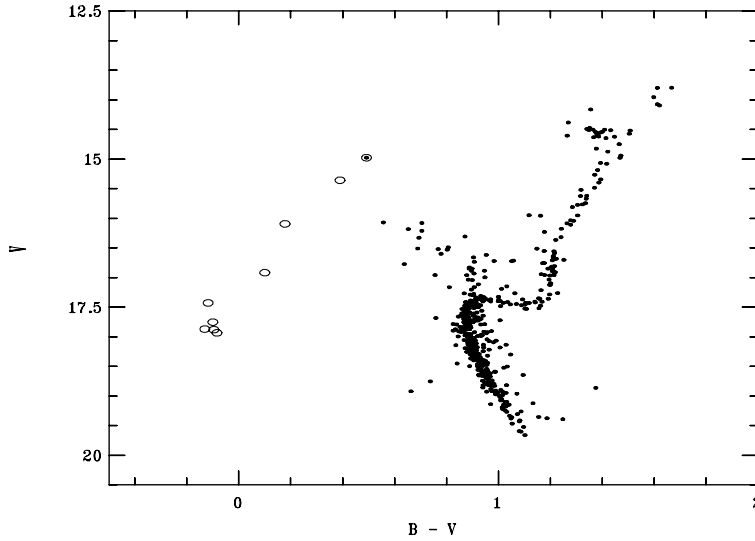


Fig. 5. NGC 6791 CMD for proper motion members (filled dots: Cudworth 1994 and private communication) and radial velocity members (open circles: Green et al., in preparation), with photometry by Kałuzny & Rucinski (1995).

5. REPRESENTATIVE SAMPLES OF EHB/SDB STARS

Detailed conclusions concerning the evolutionary histories of sdB stars will not be possible in the absence of large, homogeneous, precise and *representative* samples of EHB stars. We attempted to make Figure 1 more representative by requiring a magnitude-limited sample. We will soon achieve an improved sample, following the completion of our homogeneous, low resolution survey of every known sdB brighter than $V = 14.4$. But it is doubtful that even this sample will be truly representative, because of selection effects in the identification of known sdB stars. SdB stars are often chosen spectroscopically, which discriminates against composite sdB stars with brighter F, A, or even B main-sequence companions (as is well known). Selection effects should be more straightforward for a sample of sdB stars and composite sdB stars chosen by their UV flux, but this method requires complex follow-up to separate the sdB stars from sdO, main sequence B, post-AGB, BHB stars, etc., and it does not solve a key problem: a representative sample of sdB stars (canonical spectroscopic definition) won't necessarily help us understand all about EHB stars. What we really need are representative EHB samples including sdB, sdOB and other related hot stars, i.e., all those that are produced by processes similar to those that create sdB stars. However, there is no good definition of the hot and the cool limits for disk EHB stars.

Uli Heber (2006) has provided evidence that a number of cooler sdO stars should more properly be identified with EHB stars than with post-AGB stars. For a relatively unbiased look at the opposite end of the sdB sequence, consider the color-magnitude diagram for the old, metal-rich open cluster NGC 6791.

NGC 6791 and the similar cluster NGC 188 (not shown) are the only two disk clusters known to contain sdB stars. Both clusters also contain more luminous stars extending towards cooler temperatures along an apparent blue horizontal branch, as seen in Figure 5. All of the cluster BHB stars are proper motion and/or

radial velocity members, and therefore must surely be related to the sdB stars. Yet many of these cooler stars were not detected by the UIT surveys that found all the cluster sdB and sdO stars (Landsman et al. 1998). This means that even UV-selected samples will be affected by selection effects, if the goal is to find all of the relatives of sdB stars, determine their relative proportions and understand how they are related.

Another noteworthy point concerns the total distribution of the hot stars in these two disk clusters. About half are located in a small clump in the EHB region, while the other half are scattered thinly all along the BHB. This is quite different from what is found in globular clusters, where there are typically hundreds of stars along the upper horizontal branch (either the red horizontal branch, RR Lyrae strip, BHB, or some combination), but never more than a handful of EHB stars, if indeed, there exist any at all. We believe that the very different distributions between disk and halo EHB/BHB stars very likely indicate different formation histories.

In an effort to get a different perspective on the true proportions of hot EHB stars, one of us (E.M.G.) has experimented with a 2MASS-selected sample. Of the 62 197 2MASS point sources with $J < 14.6$, $-0.35 < J-H < 0.00$ and $-0.5 < J-K < -0.05$, there are 1550 with declinations north of -5° , galactic latitudes greater than 30° and $E_{B-V}(\text{max}) < 0.10$, including a number of previously known sdO and B stars. Spectra for 78 new objects have now been obtained in combination with our 2.3 m low resolution survey (section 2). This pilot study turned up 16 new sdB/sdOB stars, 3 sdO stars, 22 main-sequence B stars and 37 BHB stars between about 22 000K and 10 000K. We presume that most of the BHB stars are halo objects since their distribution along the BHB resembles that in globular clusters, but the old open clusters prove that at least a few of the BHB stars could be disk objects. This means that we cannot define a cutoff temperature for the cool end of the disk EHB at 22 000 K, or 20 000 K, or even 16 000 K, without excluding a number of related metal-rich BHB stars. (Of course, it will be tedious to identify them in the field, as they will be far outnumbered by halo BHB stars in most data sets).

Winter (2006) has found a very similar EHB/BHB distribution from his analysis of photometrically-selected SDSS spectra; he also finds the density of stars thins out at the cool end of the sdB sequence, but then rises again as the EHB merges into the tail of what appears to be the halo BHB. The distributions in both our 2MASS sample and Winter's SDSS sample confirm Newell's (1973) results for blue field stars, including the same low density region near 21 400 K that was identified as the second of the two famous "Newell gaps".

6. CONCLUSIONS

We conclude that precise, homogeneous, representative surveys of the fundamental parameters of EHB stars contain important information about the evolutionary histories of sdB stars. At a minimum, it will be necessary to understand the significance of the patterns in the $\log g$ vs. T_{eff} diagram for each different type of sdB star. For another example, we showed how precise temperatures plus asteroseismological gravities and masses appear to rule out mergers as an important formation channel for at least the hotter sdB stars.

We further conclude that the unexpected color gap between very short period sdB stars with mid-M type main-sequence secondaries, and the much longer pe-

riod systems with F, G or K type secondaries, corresponds to a mass gap in the approximate range between 0.35 and 0.65 M_{\odot} , although the significance of the gap is not yet clear.

Using the color magnitude diagram for members of the old disk cluster NGC 6791, and also a 2MASS-selected sample of hot stars, we have revisited the problem of obtaining representative samples of disk EHB stars. Although it will be difficult, we suggest that stars both hotter and cooler than those in typical “sdB” samples need to be included in future investigations, in order to get a clearer picture of EHB evolution. Lastly, we caution against assuming that halo EHB stars are produced by the same formation mechanisms as their disk counterparts, since the two types of horizontal branches have such widely different luminosity and temperature distributions.

REFERENCES

- Brassard P., Fontaine G., Billères M., Charpinet S., Liebert J., Saffer R. A. 2001, *ApJ*, 563, 1013
- Charpinet S., Fontaine G., Brassard P. 2003, in *White Dwarfs*, NATO Science Series, eds. D. de Martino, R. Silvotti, J.-E. Solheim, & R. Kalytis, Kluwer Academic Publishers, Dordrecht, 105, 69
- Charpinet S., Fontaine G., Brassard P., Billères M., Chayer P., Green E. M. 2005a, *A&A*, 443, 251
- Charpinet S., Fontaine G., Brassard P., Green E. M., Chayer P. 2005b, *A&A*, 437, 575
- Cudworth K. M. 1994, *BAAS*, 25, 1454
- Green E. M., Fontaine G., Reed M. D., Callera K., et al. 2003, *ApJ*, 583, L31
- Green E. M., For B.-Q., Hyde E. A. 2005, in *14th European Workshop on White Dwarfs*, eds. D. Koester & S. Moehler, ASP Conf. Ser., 334, 363
- Heber U., Drechsel H., Østensen R., et al. 2004, *A&A*, 420, 251
- Heber U., Hirsch H., Ströer A., O’Toole S., Haas S., Dreizler S. 2006, *Baltic Astronomy*, 15, 91 (these proceedings)
- Henry T. J., McCarthy D. W. 1993, *AJ*, 106, 773
- Kałużny J., Rucinski S. M. 1995, *A&AS*, 114, 1
- Landsman W., Bolin R. C., Neff S. G., O’Connell R. W., Roberts M. S., Smith A. M., Stecher T. P. 1998, *AJ*, 116, 789
- Kirkpatrick J. D., McCarthy D. W. 1994, *AJ*, 107, 333
- Lisker T., Heber U., Napiwotski R., Christlieb N., Han Z., Homeier D., Reimers D. 2005, *A&A*, 430, 223
- Newell E. B. 1973, *ApJS*, 26, 37
- O’Toole S. J., Heber U., Benjamin R. A. 2004, *A&A*, 422, 1053
- Peterson R. C., Green E. M. 1998, *ApJ*, 502, L39
- Saffer R., Green E. M., Bowers T. 2001, in *12th European Workshop on White Dwarfs*, eds. J. L. Provencal, H. L. Shipman, J. MacDonald & S. Goodchild, ASP Conf. Ser., 226, 408
- Stark M. A., Wade R. A. 2003, *AJ*, 126, 1455
- Winter C., Jeffery C. S., Ahmad A., Morgan D. R. 2006, *Baltic Astronomy*, 15, 69 (these proceedings)

THE NATURE OF LATE-TYPE COMPANIONS IN HOT SUBDWARF COMPOSITE-SPECTRUM BINARIES

M. A. Stark^{1,2} and R. A. Wade¹

¹ *Department of Astronomy and Astrophysics, Pennsylvania State University, 525 Davey Lab., University Park, PA 16802, U.S.A.*

² *Department of Physics and Astronomy, University of Wyoming, Dept. 3905, 1000 East University Avenue, Laramie, WY 82071, U.S.A.*

Received 2005 August 1

Abstract. We present the results of a study of late-type companions in hot subdwarf composite spectrum binaries. The exact nature of these late-type companions has been disputed in the literature – some argue that they are main-sequence stars, and others have claimed they are subgiants. To determine the properties of the late-type companions, we first conducted a survey utilizing the Two Micron All Sky Survey (2MASS) All-Sky Data Release Catalog to identify composite-colored binaries in the *Catalogue of Spectroscopically Identified Hot Subdwarfs* (Kilkenny et al. 1988, 1992). We then conducted a spectroscopic study of a sub-sample of the 2MASS composite-colored hot subdwarfs. The sample consists of photometrically and spectroscopically single and composite hot subdwarfs (14 single and 51 composite). We also obtained spectra of 59 single late-type stars with Hipparcos parallaxes for calibration. We used measured equivalent width (EW) indices from the composite systems to estimate the temperature and gravity of the late-type star, taking into account the dilution of its spectral features by light from the hot subdwarf. Results from combining the spectroscopic data with model energy distributions indicate that the late-type companions in composite-spectrum systems are best described by main-sequence companions overall.

Key words: binaries: spectroscopic – stars: horizontal-branch

1. DEFINING THE SAMPLE

For this investigation we studied hot subdwarf stars listed in the *Catalogue of Spectroscopically Identified Hot Subdwarfs* (Kilkenny, Heber & Drilling 1988, KHD) as updated and expanded in an electronic version by D. Kilkenny in 1992. While the KHD catalog contains all varieties of hot subdwarfs, we primarily focused on the more numerous sdB stars. The sdB are understood to be relatively homogeneous and probably have a common evolution history from the zero-age extended horizontal branch (ZAEHB), while sdO stars likely follow multiple evolutionary pathways and might be expected to be less homogeneous and to have less simply explained properties.

To make a comparison of the KHD data with existing databases (such as 2MASS) or to obtain new observations of the correct star, accurate coordinates on

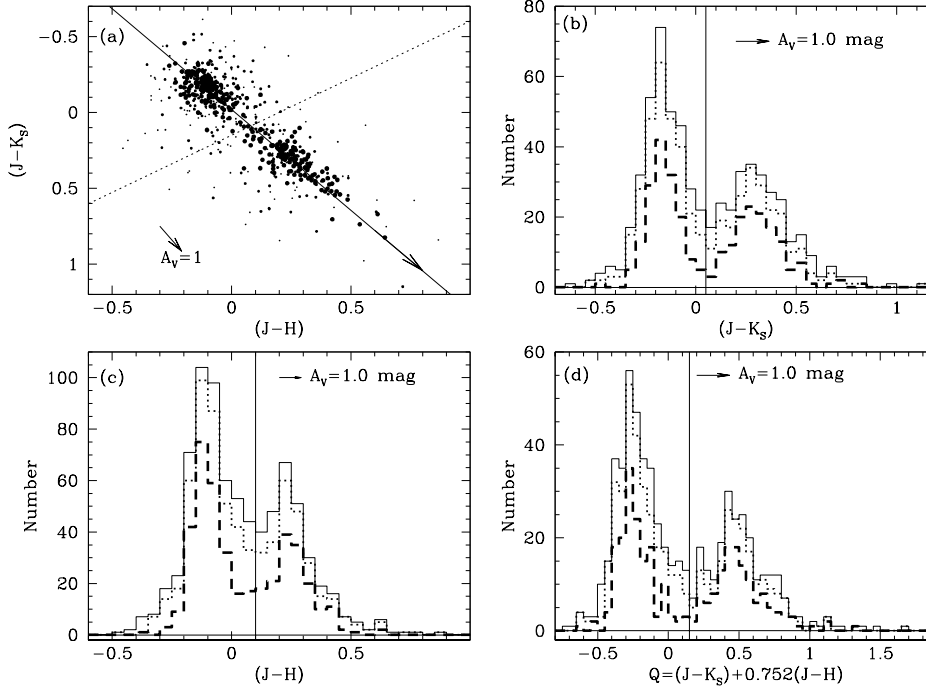


Fig. 1. Panel a. Two color plot for 2MASS colors of sdBs only with a linear fit to the points shown as the solid line, the parameter Q increases along this line as indicated. The dashed line is mathematically perpendicular to the linear fit line, and demonstrates a contour of constant Q (the two lines cross at $Q = +0.15$). All other panels contain histograms (bin sizes 0.05) of 2MASS color indices: $J - K_S$ (panel b), $J - H$ (panel c) and Q (panel d). In the three histograms (panels b–d), the solid line is for all sdB, the dotted line is for sdB with both $\sigma(J - K_S)$ and $\sigma(J - H) < 0.2$ the dashed line is for sdB with both $\sigma(J - K_S)$ and $\sigma(J - H) < 0.1$. Single sdBs fall in the left peak ($Q < 0.15$), composites fall in the right peak ($Q \geq 0.15$). The effect of 1 mag of extinction ($A_V = 1$) is indicated.

a consistent system are required. For each entry the object’s position was verified by referring whenever possible to original published finding charts or by contacting knowledgeable observers, then locating the object on a chart prepared from the USNO A2.0 Catalog (Monet 1998, see also Stark & Wade 2003).

2. 2MASS RESULTS

We collected readily available visible and near-IR flux measurements of hot subdwarfs from the 2MASS All-Sky Data Release (ASDR) Catalog and identified those whose colors indicate the presence of a late type companion (for more information see Stark & Wade 2003; Stark et al. 2005). We thus determined the fraction of hot subdwarfs that exist in composite spectrum binaries ($\sim 40\%$ of sdBs from KHD are composite in a magnitude limited sample). We defined an approxi-

mately volume limited sample of hot subdwarfs from KHD for statistical purposes (see Stark & Wade 2003; Stark et al. 2005), and found that $\sim 25\%$ of sdBs are composite in a volume limited sample (VLS).

We defined the color parameter $Q = 0.752(J-H) + (J-K_S)$, which gives the clearest separation between composite and single hot subdwarfs based on 2MASS photometry alone. We compared the distributions in $J-K_S$, $J-H$ and Q , and found them all to show a bimodally distributed population (Figure 1). In a histogram of the IR color indices $J-K_S$ and Q , the two peaks of the bimodal distribution can be understood as single stars (blue peak at $J-K_S = -0.170$, $Q \approx -0.275$) and composite systems (red peak at $J-K_S = +0.289$, $Q \approx +0.500$). This bimodal distribution is also present in the approximately VLS, again with the two peaks at $J-K_S = -0.167$ and $+0.248$ and $Q \approx -0.275$ and $+0.475$.

There are no (or very few) F or dM companions of the hot subdwarfs in the KHD catalog. This is evident from the bimodal distribution in 2MASS colors (Q , $J-K_S$ and $J-H$). Were there a large population of F or dM companions, their composite colors would have filled in the gap between the two bimodal peaks. However, the distribution in 2MASS colors can be described by only a very small (or no) spread in the colors of the late-type companions. In the case of F-type and earlier companions, should they actually exist, it is likely that most of them were never identified as containing a hot subdwarf. The F-type star would dominate the light at visual wavelengths, and the combined light would look spectroscopically like a metal-poor Population II star (the metal lines of the Population I star being diluted by the hot subdwarf so they look like a metal-deficient star). So, it is understandable that there are very few of these objects in the current KHD catalog. The dM stars on the other hand, have no obvious reason to be selected against in surveys that have identified hot subdwarfs. The dM is significantly fainter than the hot subdwarf, so that it should be basically undiscernible in the visible (both photometrically and spectroscopically). So, the fact that there are no (or very few) dM companions in the KHD sample represents a true trend in the hot subdwarf population (as opposed to a possible selection bias as in the case of the F-type and earlier stars).

The observed distribution of hot subdwarfs in 2MASS colors can be reproduced equally well by either assuming main-sequence companions with $M_V(\text{sdB}) \approx 4.5\text{--}5.0$ mag, or by assuming subgiant companions with more luminous sdB stars ($M_V(\text{sdB}) \approx 2.5\text{--}3.0$ mag) – photometric data alone cannot distinguish between these two possibilities.

3. SPECTROSCOPY OF COMPOSITE HOT SUBDWARFS

Spectroscopy of a sub-sample of the 2MASS composite-colored hot subdwarfs was obtained to break the degeneracy between main-sequence and subgiant companions present in the 2MASS and visual photometry alone. Observations were made primarily at the Kitt Peak National Observatory (KPNO) 2.1 m telescope using the GoldCam spectrograph, but some additional observations came from the McDonald Observatory 2.7 m telescope with LCS. Both sets of observations cover roughly 4500–9000 Å with ~ 3.3 Å resolution (~ 1.3 Å/pix) using two spectrograph settings. This wavelength region covers H β , Mg I b, He I 5875 Å, Na I D, H α , He I 6678 Å and the Ca II IR Triplet (CaT). The sample of observed stars consists of photometrically and spectroscopically single and composite hot subdwarfs (14 single and 51 composite). We also obtained spectra of 59 single late-type stars from

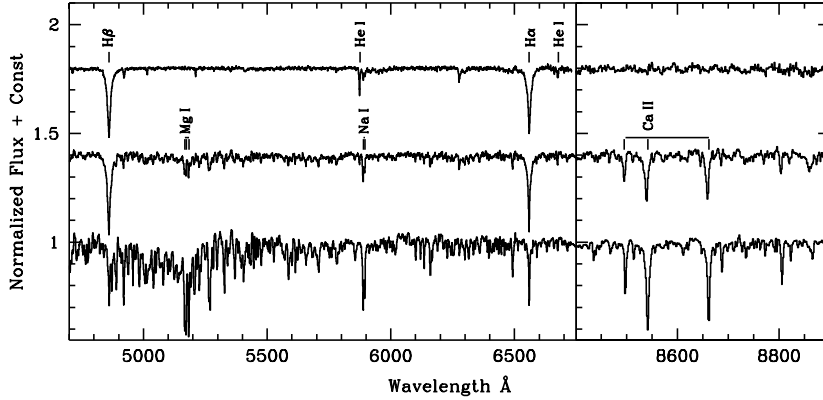


Fig. 2. Normalized spectra for a “typical” single hot subdwarf (top, LSIV+00°21), a composite hot subdwarf (middle, PB 6107), and a single HIP standard star (bottom, HIP 13081). Left panel shows the region from H β to H α , right panel shows the CaT. Prominent spectral features are labelled.

both the main sequence and subgiant branch with Hipparcos (HIP) parallaxes for calibration. Example spectra from KPNO GoldCam (of a single, composite, and standard star) are shown in Figure 2. Our analysis focused on Mg Ib, Na I D and CaT equivalent widths (EWs). Each of these lines has a very different behavior with T_{eff} and $\log g$, so they are useful for constraining the dilution by the hot subdwarf, as well as T_{eff} and M_V of the late-type companion, thus breaking the main sequence-subgiant degeneracy present in the 2MASS and visual photometry alone.

The observations (2MASS and visual photometry combined with EWs) for each composite hot subdwarf were compared with diluted models based on HIP standard star observations, models of ZAEHB stars (Caloi 1972), terminal-age EHB (TAEHB) stars (Dorman et al. 1993), and Kurucz (1998) spectral energy distributions, in order to determine the combination of sdB+late-type star that best explained all observations. In most cases the actual fit was driven primarily by the measured EWs, and secondarily by $J-K_S$ color (this agrees with the previous determination that photometry alone cannot distinguish between main-sequence and subgiant companions in these cases). With a few exceptions, it was found that the late-type companions in composite-spectrum systems are best identified as main sequence. The majority of the well constrained main-sequence companions have $0.5 \lesssim (B-V)_{\text{comp}} \lesssim 1.1$ (spectral types \sim F6–K5, see Figure 3). The spectra and identifications of four composite subdwarfs are compared in Figures 4 and 5.

There are some interesting objects identified through our spectroscopy. These include:

- Two new emission line objects, LSIV–08°03 (possible X-ray binary) and PB 5333 (NLTE emission in the core of H α). One possible new NLTE core emission object, TON 264.
- Nine objects that are best fit with subgiant companions (assuming ZAEHB or TAEHB hot subdwarfs), with an additional six best fit with subgiants assuming

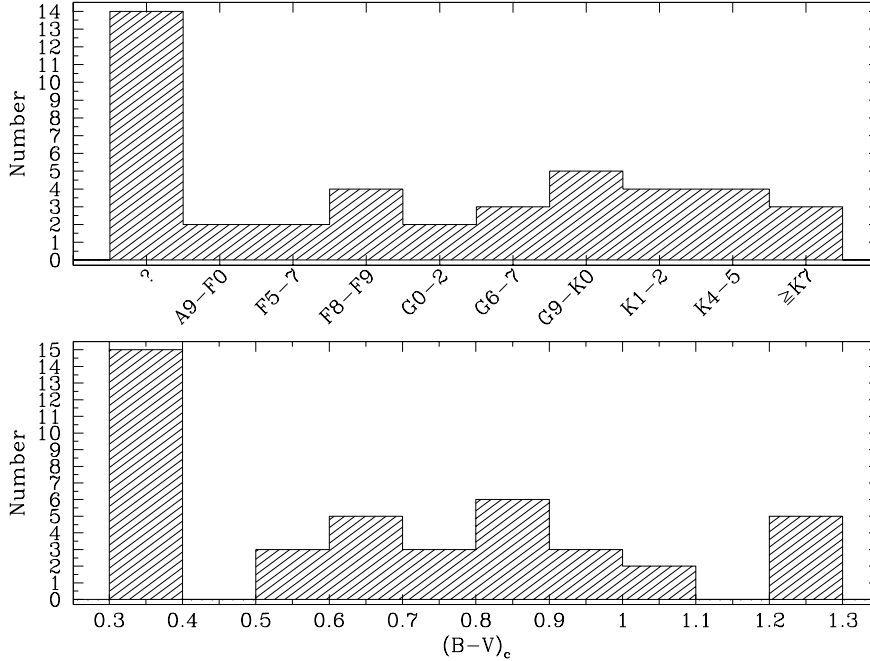


Fig. 3. Histogram showing the distribution of late-type companions in $B-V$ (bottom) and approximate Spectral Type (top). Objects in the last bins on either end of the histograms are upper or lower limits and either (1) have problems with their fits or (2) belong outside the range of parameters examined (see discussion at the end of §3). PG 0232+095 and those stars fitted with subgiant companions (assuming ZAEHB hot subdwarfs) have been excluded from this plot.

TAEHB hot subdwarfs. PG 0232+095's late-type companion seems to show molecular features indicative of a giant star (e.g., possible CN-red molecular bands), but the CaT appears too weak for a giant star – this object requires further study.

- A possible *resolved* visual double sdB+sdB (or sdB+HBB), HZ 18 (Figure 6), which may also contain an inner short-period binary (based on the velocity difference between the spectra for the two stars).

There were 18 cases in which the late-type companion was poorly fitted by our models (namely the best-fit parameters fell right at or near the edge of our model grid). The EWs in some of these objects may be erroneous due to an interstellar contribution. Additional refinement of the models, extension of the models to include a larger temperature range in both the late-type stars (by obtaining more observations of standards) and the hot subdwarfs (more models over a larger temperature range), or adjustments to correct for interstellar contributions, are needed to accurately fit these objects.

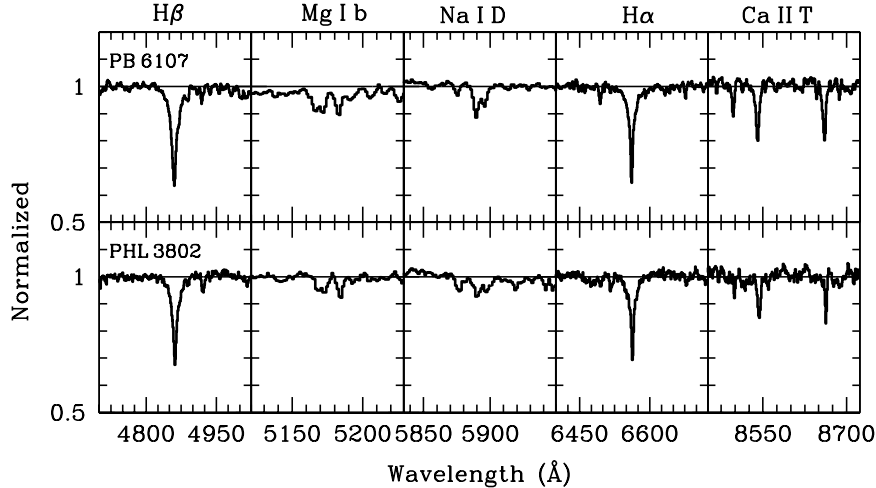


Fig. 4. Comparison of the major spectral features in the spectra of PB 6107 and PHL 3802. Panels from left to right show: $H\beta$, Mg I b, Na I D, $H\alpha$ and Ca II T. These two stars were both fit with similar hot subdwarfs ($B-V = -0.246$ & -0.233 and $M_V = 4.43$ & 4.22 for PB 6107 and PHL 3802 respectively) and companions (G9V–K0V), so their spectra look similar. (Continuum fits shown were *not* used for the calculation of EWs.)

4. LIMITATIONS AND DIRECTIONS FOR FUTURE WORK

Our modeling procedure is limited in the range of both hot subdwarf and late-type stars included. These models could be greatly improved by including a greater range in temperatures for both the companion and particularly for the hot subdwarf. Specifically we have trouble identifying and coping with the hottest sdBs and the sdOs. We are also using the assumption that the hot member is in fact a true sdB-type star; if it is in fact a HBB or post-EHB star, then the modeling breaks down, giving bogus fits. Additional information to help constrain the properties of hot subdwarf would be of value (including whether it is sdB, sdO, post-EHB, or HBB). This additional information could include UV observations or spectra with coverage farther to the blue. Also, including additional late-type spectral features from our spectra would help better constrain the fits.

Future work related to, or stemming from, this project includes:

1. Classification of more composite hot subdwarfs.
2. Long-term RV studies of composite spectrum systems to determine periods (or at least set lower limits on the periods).
3. Follow-up observations of “unusual” objects identified, including (for example): PG 0232+095, TON 264, HZ 18 and the emission-line objects.
4. Further observations of the resolved visual doubles, including proper motions, and better classifications of the companions (particularly HZ 18, which may be a resolved sdB+sdB or sdB+HBB system).

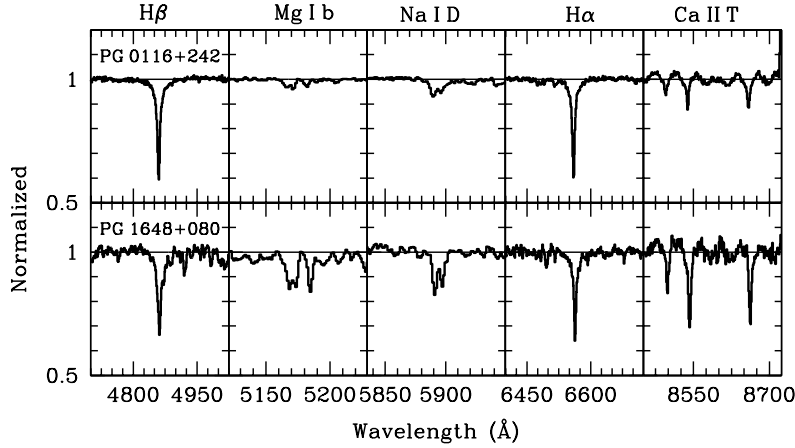


Fig. 5. Comparison of the major spectral features in the spectra of PG 0116+242 and PG 1648+080. Panels from left to right show: $H\beta$, Mg I b, Na I D, $H\alpha$ and Ca II T. These two stars were fit with similar companions (G0 IV) but different hot subdwarfs (PG 1648+080 was fit with a hotter, fainter hot subdwarf, while PG 0116+242 was fit with a cooler, brighter hot subdwarf). In PG 1648+080, the late-type companion dominates over the hot subdwarf so its lines appear much stronger in the combined spectra, while in PG 0116+242, the brighter hot subdwarf washes out the features from the late-type star making them appear much weaker. (Continuum fits shown were *not* used for the calculation of EWs.)

5. IMPLICATIONS

Han et al. (2002, 2003) predict that for companions that are later than $\sim G$, all companions in short-period systems are main-sequence stars (in post-CE binaries) and all companions in long-period systems ($P > 40$ days) are subgiant or giant stars (in post-Roche lobe overflow binaries). RV studies of composite spectrum hot subdwarfs with FGK-type companions (i.e., Orosz et al. 1997; Maxted et al. 2001; Saffer et al. 2001), have found that the orbital periods must be long, many months to years or more. In the Han et al. scenario this would imply that they contain subgiant or giant companions. Han et al., however, assume that hot subdwarfs with subgiant and giant companions, i.e., these same long-period systems, were excluded from surveys for hot subdwarfs. Indeed, in our study, the majority of composite companions are consistent with main-sequence stars (although we have identified some subgiant companions, so this exclusion is not complete).

If the GK-type companions are main-sequence stars, why do they seem to be in long-period binaries? At face value, there is something incorrect or incomplete in the Han et al. binary formation scenario or its interpretation as applied to existing samples of hot subdwarfs. It may be that aspects of the Han et al. study (binary evolution model, or mapping onto observables) are at the heart of the matter; or perhaps the apparent contradictions can be resolved via discovering some subtlety of different sample selection for the RV studies reported so far and our present spectroscopic analysis. (The latter possibility can be assessed, for example, by an RV study of the composite binaries in our study.)

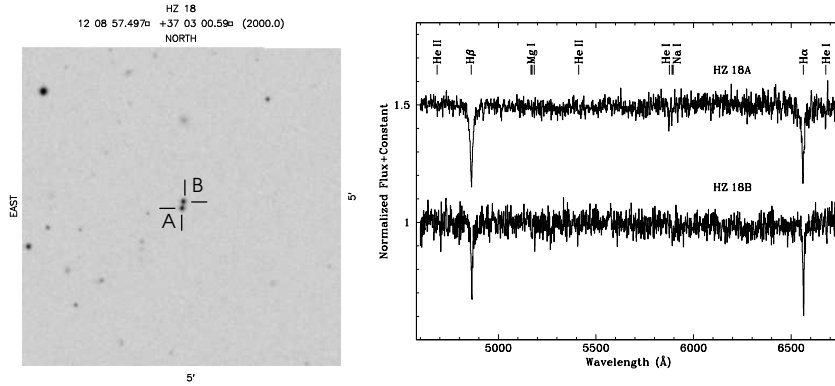


Fig. 6. Finding chart and spectra for the two components of HZ 18 (=A).

ACKNOWLEDGMENTS. This research has been supported in part by: NASA grant NAG5-9586, NASA GSRP grant NGT5-50399, Zaccheus Daniel Fund for astronomy research, Sigma Xi Grant-in-Aid of Research, NOAO Thesis Travel Support and a NASA Space Grant Fellowship through the Pennsylvania Space Grant Consortium. This research has made use of: data products from the Two Micron All Sky Survey (2MASS), the SIMBAD database, the Digitized Sky Surveys and the NASA/IPAC Extragalactic Database (NED).

REFERENCES

- Caloi V. 1972, *A&A*, 20, 357
- Dorman B., Rood R. T., O'Connell R. W. 1993, *ApJ*, 419, 596
- Han Z., Podsiadlowski P., Maxted P. F. L., Marsh T. R. 2003, *MNRAS*, 341, 669
- Han Z., Podsiadlowski P., Maxted P. F. L., Marsh T. R., Ivanova N. 2002, *MNRAS*, 336, 449
- Kilkenny D., Heber U., Drilling J. S. 1988, *South African AO Circular*, 12, 1
- Kurucz R. 1998, *Solar Abundance Model Atmospheres for 0, 1, 2, 4, 8 km/s.*, Smithsonian Astrophys. Obs., <http://kurucz.harvard.edu/>
- Maxted P. F. L., Heber U., Marsh T. R., North R. C. 2001, *MNRAS*, 326, 1391
- Monet D. B. A., Canzian B., Dahn C., Guetter H., Harris H. et al. 1998, *The USNO-A2.0 Catalogue*, U.S. Naval Observatory Flagstaff Station [USNOFS] and Universities Space Research Association stationed at USNOFS)
- Orosz J., Wade R. A., Harlow J. J. B. 1997, *AJ*, 114, 317
- Saffer R. A., Green E. M., Bowers T. 2001, in *12th European Workshop on White Dwarfs*, ASP Conf. Ser., 226, 408
- Stark M. A., Wade R. A. 2003, *AJ*, 126, 1455
- Stark M. A., Wade R. A., Berriman G. B. 2004, *Ap&SS*, 291, 333

MONTE CARLO SIMULATIONS OF POST-COMMON ENVELOPE SDB STAR PLUS WHITE DWARF BINARIES

B.-Q. For and E. M. Green

Steward Observatory, University of Arizona, Tucson, AZ 85721, U.S.A.

Received 2005 August 1

Abstract. We present first results from Monte Carlo simulations of short-period sdB plus white dwarf binaries, with various possible distributions of orbital separation and secondary mass. We compare these results with our observed distributions and discuss the implications for the common envelope evolution.

Key words: binaries: close – methods: numerical – stars: hot subdwarfs – white dwarfs

1. INTRODUCTION

Radial velocity surveys show that a large fraction of sdB stars are in post-common envelope binaries with orbital periods between a few hours and several days (Green et al. 1997; Morales-Rueda et al. 2003, 2004; Green et al. 2005). Such short orbital periods suggest that they must have evolved via binary mass transfer and common envelope evolution. The vast majority of short-period sdB secondaries are not detectable from optical spectra or 2MASS fluxes, nor do they show reflection effects. Therefore, given their mass functions, nearly all such companions must be white dwarfs. Since sdB stars are relatively bright and numerous, they provide an extremely useful sample for studying interacting binary evolution.

2. SIMULATIONS

We used Monte Carlo simulations to investigate which distributions of orbital separation and minimum secondary mass are most compatible with the observed periods, radial velocity semi-amplitudes and minimum masses in a small, but representative, sample of sdB plus white dwarf binaries (Green et al. 2005). We assumed circular orbits and sdB masses of $0.49 M_{\odot}$, in agreement with Saffer et al. (1994) and with recent asteroseismological results for four pulsating sdB stars (see the contribution by Green et al. 2006). The number of trials in each simulation is 50 000.

For our initial attempt, we assumed the simplest case of flat distributions for both the companion masses, m_2 , and the orbital separations, a . Guided by the periods and minimum masses, $m_2(\text{min})$, derived from our observed sample, we randomly chose secondary masses and orbital separations independently of each

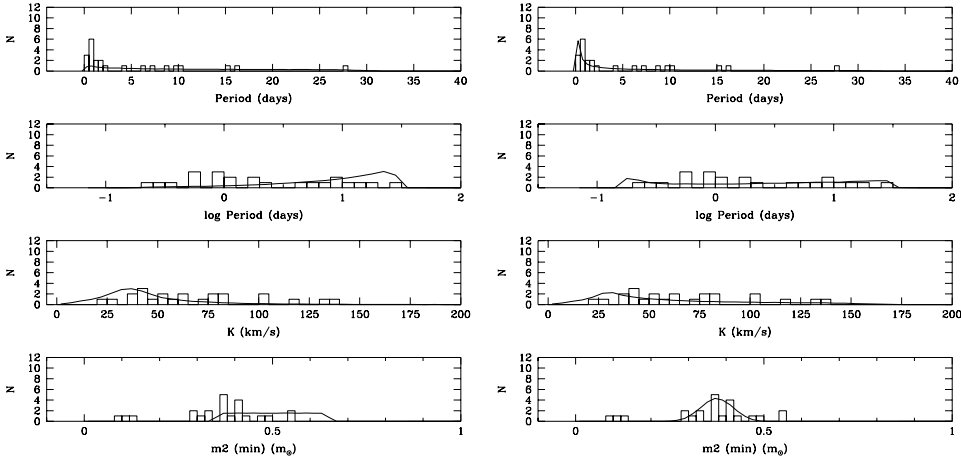


Fig. 1. Panel (a). Flat distributions for m_2 and a with $0.35 < m_2 < 0.65 M_\odot$ and $1.3 < a < 40 R_\odot$, respectively. Panel (b). A Gaussian distribution in the range m_2 with $0.25 < m_2 < 0.50 M_\odot$, plus an exponential distribution for a .

other in the ranges $0.35 < m_2(\text{total}) < 0.65 M_\odot$ and $1.3 < a < 40 R_\odot$, respectively. We calculated the period and velocity amplitude for each simulated system using Kepler's law.

Another parameter needed to compare with the observed distributions is the orbital inclination. In each case, we selected the direction of the orbital axis of rotation by generating random values for x , y and z between 0 and 1, discarding any with $r > \sqrt{x^2 + y^2 + z^2}$ so that all orientations would occur with equal probability. $\cos i = x/r$ for an observer looking along the x -axis. The probability of seeing a particular inclination is proportional to $\sin i$, resulting in a mean observed inclination from a large number of trials equal to 57.3° (1 radian), in agreement with theoretical expectation.

3. RESULTS

The following plots show the results of our Monte Carlo simulations (curves) compared to the observed histograms (boxes). We have adjusted the assumed parameters in each case to get the best fits. From top to bottom, the four panels display the comparisons as functions of the period, log period, observed velocity amplitude (K), and $m_2(\text{min})$.

Figure 1a shows that the best flat distributions are still a poor fit to the observed data: the periods and minimum masses are overestimated, while the velocity amplitudes are too small. Figure 1b shows an acceptable fit using a Gaussian mass distribution and an exponential distribution for the orbital separation, although the mass range is not quite large enough to include all the data points.

Although Fig. 1b matches the observations surprisingly well with uncorrelated secondary masses and orbital separations, theory suggests that a more massive secondary should eject its common envelope at a larger separation, while a less massive one would need to spiral inwards to a smaller separation. In fact, observed

sdB binaries generally do tend to have larger $m_2(\text{min})$ at longer periods. We constructed a simple empirical relation using the upper envelope in a plot of observed minimum mass vs. log period (Figure 2), which also fits two eclipsing sdB+WD systems. (Two other, apparently rare, eclipsing sdB+WD systems with extremely short periods have secondary masses $>0.50 M_\odot$, and do not fit any picture with correlated m_2 and a . They must result from a different evolutionary path, and are not considered further in these simulations.) Figure 3 shows the results of using this dashed curve to derive m_2 from the period. An upper mass limit of $0.65 M_\odot$ (Fig. 3a) produced too few longer period binaries, but a similar curve with an upper limit of $0.75 M_\odot$ (Fig. 3b) fit the observations quite well.

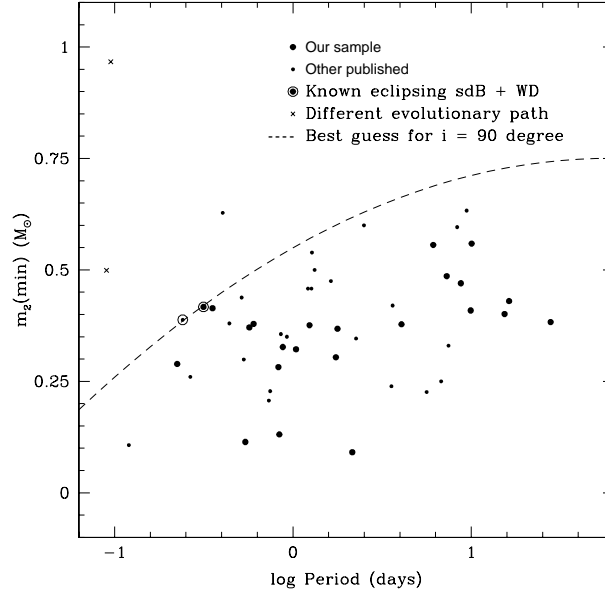


Fig. 2. The adopted relation between m_2 and orbital period (dashed curve). Orbital inclinations less than 90° scatter the observed points down from this curve.

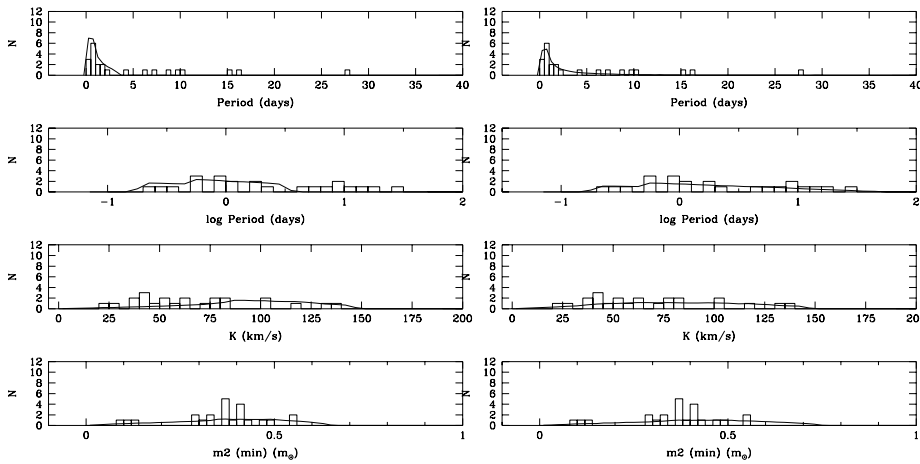


Fig. 3. Panel (a). Flat distributions over the ranges $0.35 < m_2 < 0.475 M_\odot$ ($N = 15\,000$) and $0.475 < m_2 < 0.65 M_\odot$ ($N = 35\,000$). Panel (b). Flat distributions for $0.35 < m_2 < 0.475 M_\odot$ ($N = 10\,000$) and $0.475 < m_2 < 0.75 M_\odot$ ($N = 40\,000$).

We also tried Gaussian mass distributions instead of the flat distributions in Figure 3, but they produced two discrete humps as a function of orbital period, which are not seen in the data. Eliminating the humps required such large spreads in the Gaussians that the distributions approached the flat case.

4. CONCLUSIONS

Our two most successful simulations are shown in Fig. 1b, for uncorrelated m_2 and a , and in Fig. 3b, where we attempted a supposedly more realistic correlated scenario. While Fig. 3b shows a seemingly better fit, it also requires that 80% of the white dwarf companions have masses greater than the He core flash value, which is difficult to believe. If most of the WD's in sdB+WD binaries were to experience their initial mass transfer on the AGB, then the subsequent separations would be too large to allow a second mass transfer at the first red giant branch tip, which is needed to produce a sdB star. The better-looking fits in Fig. 3b, compared to Fig. 1b, are most likely due to a larger number of free parameters. Given the small number of observed data points, an upper mass limit of $0.65 M_{\odot}$ in Fig. 1b would produce a fit that is nearly as successful, with a much more reasonable distribution of companion masses. Thus the most believable results so far suggest that white dwarf companion masses might not be correlated with their orbital separation after all.

While these initial efforts are interesting, it is obvious that we need to obtain orbital parameters for a larger complete sample in order to better constrain future Monte Carlo investigations.

REFERENCES

- Green E. M., Fontaine G., Hyde E. A. et al. 2006, *Baltic Astronomy*, 14, 167 (these proceedings)
- Green E. M., For B.-Q., Hyde E. A. 2005, in *14th European Workshop on White Dwarfs*, eds. D. Koester & S. Moehler, ASP Conf. Ser., 334, 363
- Green E. M., Liebert J., Saffer R. A. 1997, in *Third Conference on Faint Blue Stars*, eds. A. G. D. Philip, J. Liebert, R. Saffer & D. S. Hayes, L. Davis Press, Schenectady, p. 417
- Morales-Rueda L., Maxted P. F. L., Marsh T. R. 2004, *Ap&SS*, 291, 299
- Morales-Rueda L., Maxted P. F. L., Marsh T. R., North R. C., Heber U. 2003, *MNRAS*, 338, 752
- Saffer R. A., Bergeron P., Koester D., Liebert J. 1994, *ApJ*, 432, 351

SUBDWARF B BINARIES IN THE EDINBURGH-CAPE SURVEY

L. Morales-Rueda¹, P.F.L. Maxted², T. R. Marsh³, D. Kilkeny⁴ and D. O'Donoghue⁴

¹ *IMAPP, Department of Astrophysics, Radboud University Nijmegen, The Netherlands*

² *School of Chemistry and Physics, Keele University, United Kingdom*

³ *Department of Physics, Warwick University, United Kingdom*

⁴ *South African Astronomical Observatory, South Africa*

Received 2005 July 27

Abstract. We give an update of the results of a campaign to obtain orbital solutions of subdwarf B stars from the Edinburgh-Cape survey (Stobie et al. 1997). To date we have obtained blue spectra of 40 subdwarf B stars from the Edinburgh-Cape catalogue using the grating spectrograph at the 1.9 m Radcliffe telescope at the South African Astronomical Observatory. We find that 17 out of these 40 are certain binaries with a few other objects showing radial velocity variations of small amplitude. The binary fraction found in our sample, after correcting for our binary detection efficiency, is 48%. We have secured the orbital parameters for 4 of the 17 systems and narrowed down the orbits of another 7 to a small range of periods.

Out of the four subdwarf B binaries for which we have determined the orbital solution, three have orbital periods that, according to population synthesis studies by Han et al. (2003), suggest they have been formed via a common envelope ejection channel. The masses of the companions, assuming a canonical mass of $0.5 M_{\odot}$ for the subdwarf B star, suggest that they are probably white dwarfs. We observed the shortest period binary (3 h) of the three, to search for indications of modulation in the lightcurve due to irradiation of the companion by the subdwarf B star. No indications of reflection effect were found confirming that the companion is indeed a white dwarf. The fourth system with measured orbital parameters shows an orbital period that could correspond to a subdwarf B binary formed either via the common envelope ejection channel or the stable Roche Lobe overflow channel.

The aim of this study: to obtain an independent, statistically significant sample of subdwarf B binaries, with solved orbits, based purely upon the Edinburgh-Cape survey to avoid the uncertain biases of the Palomar-Green and other surveys, is underway.

Key words: subdwarfs – binaries: close – binaries: spectroscopic

1. THE BINARY FRACTION OF SUBDWARF B STARS

Maxted et al. (2001) find that $69\pm 9\%$ of the subdwarf B (sdB) stars in their observed sample are in binary systems. Napiwotzki et al. (2004) find a binary fraction of 40% in their SPY (Supernova type Ia Progenitor Survey) sample.

Radial velocity measurements of a sample of 40 sdBs from the Edinburgh-Cape (EC) survey yield 17 certain spectroscopic binaries. Radial velocities were measured by fitting a model line profile to $H\beta$ and $H\gamma$ simultaneously (Morales-Rueda et al. 2004). To determine the true binary fraction in our sample we need to compute our detection efficiency, i.e., the probability of detecting (or not detecting) a binary at a certain orbital period due to the sampling of the data and the accuracy of the radial velocity measurements. These probabilities were calculated in a similar way to those by Maxted et al. (2001) and are shown in Fig. 1 (solid line). For comparison

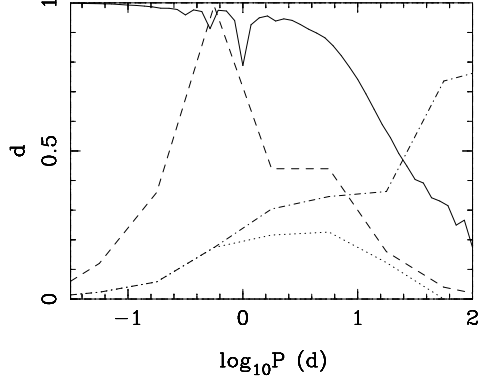


Fig. 1. Detection efficiency as a function of orbital period.

we are also plotting in Fig. 1 the observed orbital period distribution (dashed line) and the theoretical distribution, considering both the common envelope (CE) ejection and the Roche lobe overflow (RLOF) channels (dash-dotted line) and only the CE ejection channel (dotted line). These distributions will be discussed again in Section 3. We find that for orbital periods up to 1 day our average detection efficiency is 87% which gives a binary fraction for our sample of $49\pm 8\%$. The observed distribution peaks at $\log_{10} P = -0.1$ and the theoretical distribution (only considering binaries formed through the CE ejection channel) peaks at $\log_{10} P = 0.6$ where the detection efficiency is 90% in which case the binary fraction of our sample is $47\pm 8\%$. We find that this number agrees better with the binary fraction found by Napiwotzki et al. (2004) than with that found by Maxted et al. (2001).

Napiwotzki et al. (2004) suggested that this discrepancy in binary fraction could be due to the fact that the SPY sdB sample belongs mainly to the thick disk and the halo, whereas the PG sample studied by Maxted et al. (2001) comes from the thin disk. In the case of our EC sample, we expect most of the sdBs to belong to the thin disk population which indicates that the reason for the discrepancy in binary fraction is due to something else, probably to low number statistics.

It is also worth noticing how our detection probability decreases with longer period systems (less than 50% above 25 days). A longer time baseline is one of the requirements to increase our sensitivity in this period range.

2. ORBITAL SOLUTIONS

We find the orbital solutions for four of the systems observed, EC 00404–4429, EC 02200–2338, EC 12327–1338 and EC 12408–1427. The orbital solutions for EC 00404–4429 and EC 02200–2338 were already presented by Morales-Rueda et

al. (2005) and are given in parenthesis in the following paragraphs. The orbital solutions for EC 12327–1338 and EC 12408–1427 are given in Table 1.

EC 00404–4429 ($P = 0.12834(4)$ d, $M_2(\text{min}) = 0.32 M_\odot$). Its orbital period places it in the group of sdB binaries formed via the CE ejection channel (see right panel of Fig. 2). The minimum mass of the companion, assuming the canonical mass of $0.5 M_\odot$ for the sdB, indicates that the companion is probably a white dwarf. We have looked for indications of a reflection effect on the companion of this system as it is the shortest period binary of our sample and found no significant reflection effect. This confirms that the companion is a white dwarf. The system must have formed therefore via the second CE ejection channel (Han et al. 2003)

EC 02200–2338 ($P = 0.8022(7)$ d, $M_2(\text{min}) = 0.39 M_\odot$) & **EC 12327–1338**. Their orbital periods place them in the group of sdB binaries formed via the CE ejection channel. The minimum masses of the companions, assuming the canonical mass for the sdB star, indicate that the companions are probably white dwarfs.

EC 12408–1427. The orbital period of this sdB binary is consistent with the binary having been formed either via the CE ejection channel or via the RLOF channel. The minimum mass of the companion is compatible with both a white dwarf or a main sequence star.

Table 1. Orbital solution for two sdB binaries. γ is the systemic velocity, K is the radial velocity semiamplitude, and the 1 and 10 percent rows give the probability that the true period lies further than 1 and 10 per cent (respectively) from the given value. The numbers given are the \log_{10} of the probabilities.

| | EC 12327-1338 | EC 12408-1427 |
|--|-------------------|-------------------|
| Period (d) | 0.363221(1) | 0.90243(1) |
| HJD ₀ (d) | 2452728.153(1) | 2452732.068(5) |
| γ (km s ⁻¹) | -6.44 ± 1.74 | -52.02 ± 1.19 |
| K (km s ⁻¹) | 124.30 ± 2.55 | 58.90 ± 1.55 |
| $M_2(\text{min}) (M_\odot)$ | 0.38 | 0.21 |
| χ^2_{reduced} | 1.9 | 0.8 |
| 2nd best alias (d) | 0.369281(1) | 9.493(1) |
| $\Delta\chi^2$ | 33 | 38 |
| n | 15 | 29 |
| 1 percent | -7.34 | -6.89 |
| 10 percent | -11.58 | -6.96 |
| Systematic error (km s ⁻¹) | 2 | 2 |

3. ORBITAL PERIOD DISTRIBUTION

Theory predicts that most sdB stars should be in long period binaries (Han et al. 2003). They would have formed via a stable Roche Lobe overflow channel (dashed line in right panel of Fig. 2) and have main sequence companions. This long period population is missing from the observations shown in the left panel of Fig. 2. At present only two long period sdBs candidates are known. This is probably caused by biases in the observed sample: (1) early type companions will swamp the light of the sdB star, (2) long period binaries will show smaller amplitude radial velocities thus higher resolution spectra is needed to find them,

(3) longer time baselines are required to measure periods of a few hundred days.

Biases numbers 2 and 3 affect directly the binary detection efficiency curves presented in Section 1. This explains the differences between the observed and the predicted orbital period distributions at long orbital periods.

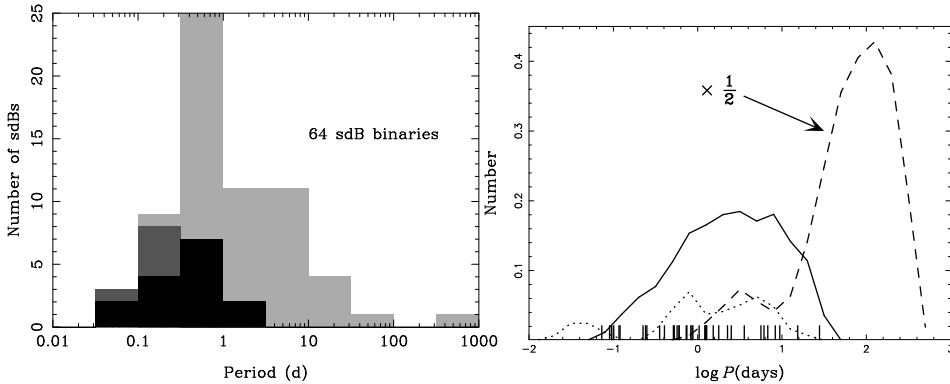


Fig. 2. Left panel: Observed orbital period distribution of sdB binaries. Light grey: unknown companion type, dark grey: main-sequence companions, black: white dwarf companions. Right panel: theoretical orbital period distribution taken from Han et al. (2003). Dotted line: CE channel sdBs with white dwarf companions, solid line: CE channel sdBs with main-sequence companions, dashed line: stable Roche Lobe overflow channel sdBs with main-sequence companions.

With 40 EC sdBs observed and 17 binaries found, this study is well on its way. More observations are required to obtain the statistically significant sample, based only on EC sdBs, that we seek.

ACKNOWLEDGMENTS. This paper uses observations made at the South African Astronomical Observatory (SAAO). LMR is supported by NWO-VIDI grant 639.042.201 to P. J. Groot. The authors would like to thank the Leids Kerkhoven-Bosscha Fonds for providing funding to attend this meeting.

REFERENCES

- Han Z., Podsiadlowski Ph., Maxted P. F. L., Marsh T. R. 2003, MNRAS, 341, 669
 Maxted P. F. L., Heber U., Marsh T. R., North R. C. 2001, MNRAS, 326, 1391
 Morales-Rueda L., Maxted P. F. L., Marsh T. R. 2004, Ap&SS, 291, 299
 Morales-Rueda L., Maxted P. F. L., Marsh T. R. et al. 2005, *14th European Workshop on White Dwarfs*, eds. D. Koester & S. Moehler, ASP Conf. Ser., 334, 333
 Napiwotzki R. et al. 2004, Ap&SS, 291, 321
 Stobie R. S. et al. 1997, MNRAS, 287, 848

DISCOVERY OF 4 RADIAL VELOCITY VARIABLE SDB STARS WITH ECCENTRIC ORBITS

H. Edelmann¹, M. Altmann² and U. Heber¹

¹ *Remeis-Sternwarte Bamberg, Astronomisches Institut der Universität Erlangen-Nürnberg, Sternwartstrasse 7, D-96049 Bamberg, Germany*

² *Departamento de Astronomia de la Universidad de Chile, Casilla 36D, Correo Central, Santiago, Chile*

Received 2005 July 29

Abstract. Radial velocity curves for 14 bright subdwarf B close binary systems have been measured using high precision radial velocity measurements from high S/N optical high-resolution spectra. The companions for all systems are unseen. The periods range from about 0.18 days up to about 6 days. The radial velocity semi-amplitudes are found to lie between 15 and 130 km s^{-1} . The invisible companions for three of our program stars are undoubtedly white dwarfs. In the other cases they could be either white dwarfs or main-sequence stars. For two stars the secondaries could possibly be brown dwarfs. The orbits for most observed systems are circular. However, small periodic deviations of the measured radial velocity points from the adopted theoretical sine curve are discovered for four program stars. These deviations can be perfectly matched assuming slightly eccentric orbits with small eccentricities of $e = 0.02\text{--}0.06$. Possibly, this is the first time that non-circular orbits have been detected in sdB binaries.

Key words: stars: hot subdwarfs – stars: horizontal branch – stars: mass function – binaries: close

1. INTRODUCTION

The origin of subdwarf B (sdB) stars has been under discussion for years. Since many apparently single sdB stars show variable Doppler line shifts resulting from orbital motion (e.g., Green, Liebert & Saffer 2001; Maxted et al. 2001), close binary interaction appears to be important for the evolution of sdB stars. From a theoretical point of view, Han et al. (2002, 2003) elucidated in detail three channels that can produce sdB stars from close binary systems: (i) the common envelope ejection channel, (ii) the stable Roche lobe overflow channel and (iii) the merger channel. Adopting these three channels in principle all sdB stars, i.e., also single sdB stars (as mergers), could be produced by close binary evolution.

Surveys keep going on to find radial velocity variable sdB stars and the number of sdB binaries for which the orbits have been measured is steadily increasing (see, e.g., Morales-Rueda et al. 2006) and has now risen to more than five dozen.

The unseen companions can only be white dwarfs or low mass main-sequence

stars. Some of such systems may qualify as type Ia Supernova progenitors as exemplified by the subdwarf B star KPD 1930+2752, for which Maxted, Marsh & North (2000) found a massive WD companion ($M \geq 0.95 M_{\odot}$) and the system mass to exceed the Chandrasekhar mass limit (see also Geier et al. 2006). The typical mass for WDs is about $0.6 M_{\odot}$, thus it is not very likely to find a system like KPD 1930+2752, i.e., exceeding the mass limit. Nevertheless, in the context of evolutionary theory for close binaries, systems with lower masses are also very interesting, because they went through a common envelope phase (or two such phases if the companion is a white dwarf). The physics of common envelope evolution is still unclear, but very important for the future evolution of binary stars in general.

The observational results agree reasonably well with the theoretical predictions of Han et al (2003). However, the observations suffer from one main bias: almost all studies were based on sdB stars drawn from surveys for UV excess objects (e.g., Palomar Green, PG, Green et al. 1986, or Hamburg ESO, HE, Wisotzki, Reimers & Wamsteker 1991). These stars are mostly rather faint ($B > 13$ mag), and therefore most likely at larger distances. Some bright sdB stars ($B = 10 - 12$ mag) certainly have been overlooked, because they are not listed in the PG or HE catalogs or misidentified due to saturation effects of photographic survey plates.

The *Catalogue of Spectroscopically Identified Hot Subdwarf Stars* (Kilkenny, Heber & Drilling 1988; Østensen 1996) contains more than 2300 such objects. Several (~ 200) of them are brighter than 13th mag and some as bright as 10th magnitude. These bright stars are ideally suited for detailed spectroscopic studies¹. Hence we select a sdB sample mostly brighter than $B = 13$ mag, which should contain stars much closer from us than in the samples of Maxted et al. (2001) and Napiwotzki et al. (2004).

Here, we present the results of 14 bright ($B \leq 13$ mag), short period radial velocity (RV) variable sdB systems.

2. OBSERVATIONS AND ANALYSIS

We obtained optical echelle spectra with high S/N at the German-Spanish Astronomical Center (DSAZ) on Calar Alto, Spain, with the 2.2 m telescope equipped with the Fiber-Optics Cassegrain Echelle Spectrograph (FOCES), and at the European Southern Observatory (ESO) on La Silla, Chile, with the Fiber-fed Extended Range Optical Spectrograph (FEROS) mounted until 2002 October on the 1.52 m ESO telescope, and afterwards on the 2.2 m telescope. The spectra have a nominal resolution of $\lambda/\Delta\lambda = 30\,000$ (DSAZ) and 48 000 (ESO), and cover the wavelengths from 3900 Å to 6900 Å (DSAZ) and 3600 Å to 8900 Å (ESO).

The radial velocities are determined by calculating the shifts of the measured wavelengths of Balmer H α , He I 5876 Å, and all clearly identified metal lines (typically more than 30 lines due to N II, O II and Si III) to laboratory wavelengths. Gaussian curves are fitted to the absorption lines in order to determine their central wavelengths. After the measurement, all values were corrected to heliocentric values.

¹ Our aim is not only to discover new radial velocity variable sdB stars, but also to determine their atmospheric parameters, metal abundances, isotopic anomalies and rotation velocities (Edelmann, Heber & Napiwotzki 2001; Edelmann et al. 2006).

Table 1. Orbital parameters for our program stars, ordered by increasing periods from the top to the bottom. Given are the periods P , the system velocities γ_0 , the RV semi-amplitudes K , the minimum masses of the system components M_{comp} , and the nature of the unseen companions due to their determined masses (bd = brown dwarf, ms = main-sequence star, wd = white dwarf). All numbers in parentheses give the uncertainty of the last given digit.

| Star | P days | γ_0 [km s $^{-1}$] | K [km s $^{-1}$] | M_{comp} [M_{\odot}] | Nature comp. |
|----------------|-------------|-------------------------------|------------------------|--------------------------------------|-----------------|
| 22169–0001 | 0.1780(3) | 2.8 ± 0.3 | 14.9 ± 0.4 | 0.03 | bd/ms/wd |
| CPD –64° 481 | 0.2772(5) | 94.1 ± 0.3 | 23.8 ± 0.4 | 0.05 | bd/ms/wd |
| PG 1232–136 | 0.3630(3) | 4.1 ± 0.3 | 129.6 ± 0.4 | 0.41 | ms/wd |
| [CW83] 1419–09 | 0.4178(2) | 42.3 ± 0.3 | 109.6 ± 0.4 | 0.34 | ms/wd |
| HE 0230–4323 | 0.4515(2) | 16.6 ± 1.0 | 62.4 ± 1.6 | 0.17 | ms/wd |
| PG 0001+275 | 0.529842(5) | -44.7 ± 0.5 | 92.8 ± 0.7 | 0.29 | ms/wd |
| JL 82 | 0.7371(5) | -1.6 ± 0.8 | 34.6 ± 1.0 | 0.10 | ms/wd |
| Ton S 183 | 0.8277(2) | 50.5 ± 0.8 | 84.8 ± 1.0 | 0.32 | ms/wd |
| PG 0133+114 | 1.23787(3) | -0.3 ± 0.2 | 82.0 ± 0.3 | 0.36 | ms/wd |
| [CW83] 1735+22 | 1.280(6) | 20.6 ± 0.4 | 104.6 ± 0.5 | 0.53 | wd |
| HD 171858 | 1.63280(5) | 62.5 ± 0.1 | 87.8 ± 0.2 | 0.46 | wd |
| PB 7352 | 3.62166(5) | -2.1 ± 0.3 | 60.8 ± 0.3 | 0.40 | ms/wd |
| Ton S 135 | 4.122(8) | -3.7 ± 1.1 | 41.4 ± 1.5 | 0.26 | ms/wd |
| CD –24° 731 | 5.85(30) | 20 ± 5 | 63 ± 3 | 0.55 | wd |

The errors for the given RV values which are derived from the measurements of single lines are unrealistically small (typically $\sim 0.1 \text{ km s}^{-1}$). To estimate the dominating systematic errors that arise from the observations (placement of the stars disc on the slit, S/N), and from the data reduction (e.g., wavelength calibration), we plotted the RVs for all measured absorption lines versus the corresponding wavelength positions for all single spectra (shown for one spectrum in Figure 1). From each plot the mean RV value together with its corresponding error limit (mostly 1–2 km s^{-1}) can be determined. No wavelength dependent trend for the obtained RV values could be found for any of our observations.

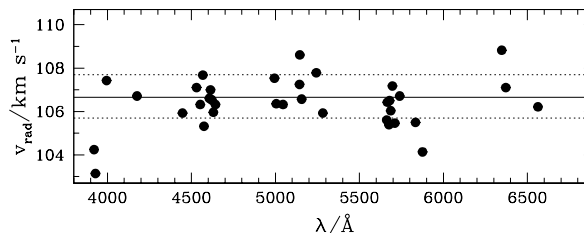


Fig. 1. Radial velocity determination for one spectrum of CPD–64 481. The dots denote the radial velocities determined for all measured lines. Note the very good consistency irrespective of the wavelength. The straight line indicates the mean value, and the dashed lines the 1σ error limit.

The period search was carried out by means of a periodogram analysis based on the Singular Value Decomposition (SVD) method. A sine-shaped RV curve is fitted to the observations for a multitude of phases which are calculated as a function of period (see Napiwotzki et al. 2001). The difference between the observed radial velocities and the best fitting theoretical RV curve for each phase set is evaluated in terms of the logarithm of the sum of squared residuals (χ^2) as a function of period, yielding the power spectrum of the data set which allows to determine the most probable period of variability (see, e.g., Lorenz, Mayer & Drechsel 1998). Table 1 summarizes the orbital parameters (period, systemic velocity and semi-amplitude) for all analyzed stars.

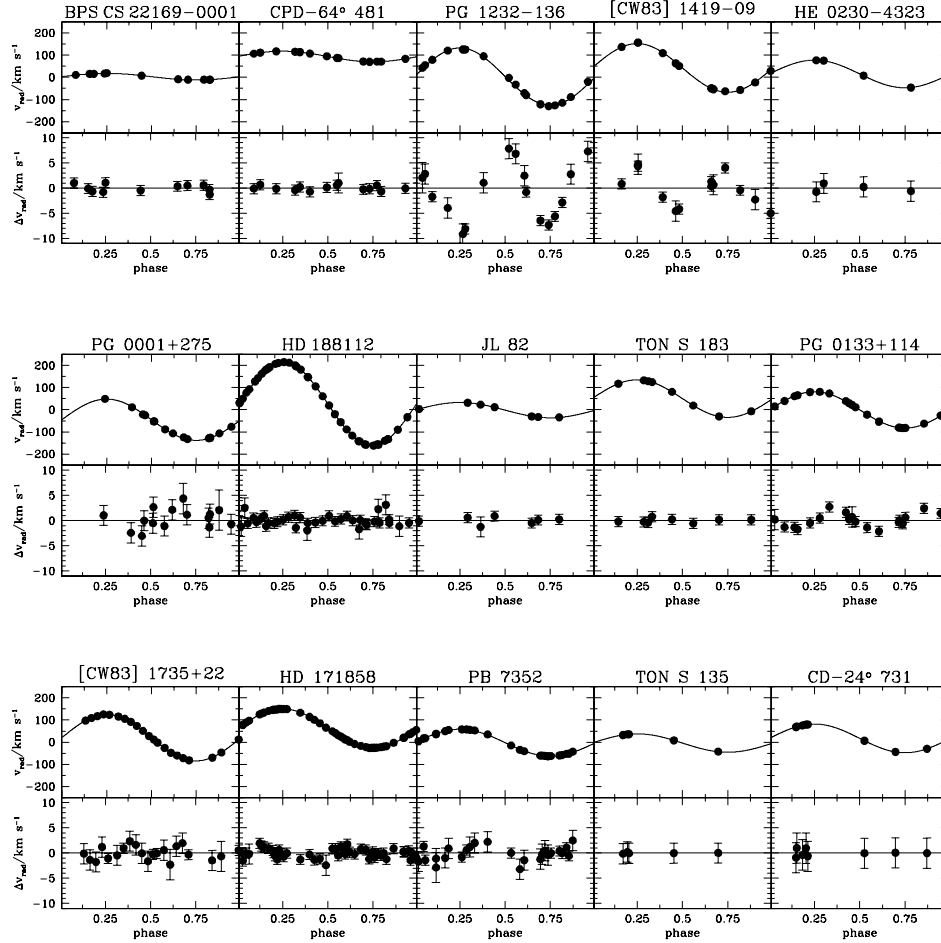


Fig. 2. Measured radial velocities as a function of orbital phase and fitted sine curves, together with the residuals ($\Delta v_{\text{rad}} = v_{\text{obs}} - v_{\text{sine}}$) to the sine fits including error bars for all program stars (ordered by increasing periods: from top left to bottom right).

3. ECCENTRIC ORBITS?

In Figure 2 the residuals to the sine fits are plotted. One can see that the RV values for most of our program stars are well reproduced by sinusoidal curves (semi-amplitudes of possible periodic deviations of the residuals $\leq 2 \text{ km s}^{-1}$, i.e., our detection limit²). This means the orbits for the majority of our analyzed stars are most likely circular.

However, for three stars (PG 1232–136, [CW83] 1419–09 and PG 0133+114), and potentially also for PB 7352, periodic deviations of the residuals can be seen. There are some possibilities to explain such periodic deviations:

² A semi-amplitude of 2 km s^{-1} for the periodic deviations of the residuals for a system with a semi-amplitude of 100 km s^{-1} is equivalent to an eccentricity of $e = 0.02$.

(i) Triple systems. This can be ruled out on a very high confidence level. Because the time-span of the observations for all four systems were within a few weeks and the period of the remaining residuals are exactly one half of the binary orbital period, respectively. However, the influence of a third light might play a role.

(ii) Observational or analytical effects. These are also not very likely. Especially for the most significant cases PG 1232–136 and [CW83] 1419–09, all RV measurements are from one observing run. For both stars, during all nights the setup has not been changed, nor has the data reduction, or analysis method. PG 0133+114 also clearly shows periodic deviations of the residuals. Its observations were carried out during different observing runs but at the same observatory. For comparison, [CW83] 1735+22 does not show any sign of a periodic deviation of the residuals at all, although it has almost the same period as PG 0133+114 and was observed mainly during the same observing runs as PG 0133+114.

(iii) A somewhat eccentric orbit. To test this we took the best fitting sinusoidal for each star, calculated a set of theoretical RV curves with varying eccentricities and periastron angles Ω , and fit these curves to the observed RV values. Another attempt was made by applying a program (Mayer, priv. comm.) which fits all parameters, including eccentricity and periastron angles, simultaneously to the observed data points. Both methods give exactly the same results: the observed RV points for three stars can be reproduced best assuming a non-circular orbit (see Figure 3). For PG 1232–136 we determined an eccentricity of $e = 0.060 \pm 0.005$ and a periastron angle of $\Omega = 162.5^\circ \pm 0.5^\circ$, for [CW83] 1419–09 the points match best by applying an eccentricity of $e = 0.039 \pm 0.005$ together with a periastron angle of $\Omega = 355.6^\circ \pm 0.5^\circ$, and for PG 0133+114 the observed RV points are fitted almost perfectly by using an eccentricity of $e = 0.025 \pm 0.005$ and a periastron angle of $\Omega = 101.5^\circ \pm 0.5^\circ$. The data points for PB 7352 can also be matched better for a non-zero eccentricity than assuming a circular orbit (see Figure 3), however, by a very much lower significance level. An eccentricity of $e = 0.024 \pm 0.01$ and a periastron angle of $\Omega = 85.8^\circ \pm 1.0^\circ$ result.

We have also checked whether the small eccentricities are actually significant using the standard test of Lucy & Sweeney (1971). All four systems passed the test and lie well below the $p = 0.05$ level (PG 1232–136: $p = 6 \times 10^{-9}$, [CW83] 1419–09: $p = 3 \times 10^{-5}$, PG 0133+114: $p = 6 \times 10^{-7}$ and PB 7352: $p = 2 \times 10^{-4}$). The random distribution of periastron angles of those four stars supports our conclusion that eccentric orbits are the cause for the periodic deviations.

(iv) Gravitational deformation of the sdB primary due to tidal forces in a bound rotating system (like seen for KPD 1930+2752). This can also be ruled out. From the lack of the broadening of the spectral lines we have been able to exclude tidally locked rotation, e.g., for PG 1232–136 which shows the largest periodic deviations.

As the circularization time-scale strongly depends on the period ($t_{\text{cir}} \sim P^{49/12}$, Tassoul & Tassoul 1992) one would expect that the eccentricity would be correlated with the period. However, for our four stars this is not the case; i.e., the star with the longest period (PB 7352) does not have the largest eccentricity, nor does the star with the shortest period (PG 1232–136) have the smallest eccentricity. Surprisingly, the opposite is the case!

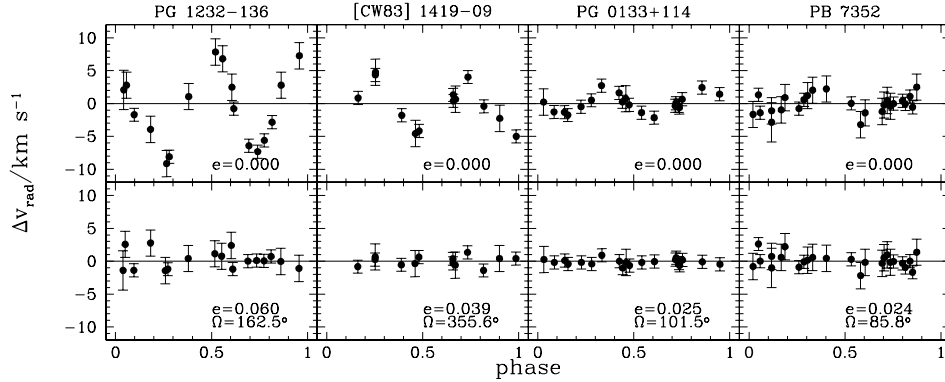


Fig. 3. Residuals to the fits including error bars for PG 1232–136, [CW83] 1419–09, PG 0133+114, PB 7352 and PG 0001+275 for two different eccentricities. Upper panel: fits using vanishing eccentricities, lower part: best matching fits.

However, lacking a better explanation, we suggest that the orbits of four of our program stars are probably not circular, making these close binaries the first for which eccentric orbits are detected

4. NATURE OF THE UNSEEN COMPANIONS

The lower limits to the companion masses of the unseen companions, resulting from the mass function by adopting the canonical mass of the sdB star of $M = 0.5 M_{\odot}$ (Heber 1986), are given in Table 1.

The companions are most likely either white dwarfs or late type main-sequence stars. Spectral signatures of degenerate companions would not be detectable at optical wavelength due to the faintness of the white dwarfs. On the other hand, assuming the star is sufficiently bright, spectral features arising from a late-type main-sequence star could be seen. Therefore we searched for lines which are prominent in cool stars, e.g., the Ca II H and K lines, the G-band, the Mg I triplet at 5167 Å, 5173 Å and 5184 Å, or the Ca II triplet (CaT) at 8498 Å, 8542 Å and 8662 Å (cf. Jeffery & Pollacco 1998). None are found.

We estimate that any cool main-sequence star that contributes more than 10% of light in the *I* band should be detectable via the CaT search. Even at a spectral type as late as M1 the CaT lines are strong with equivalent width larger than 1 Å (Jones, Alloin & Jones 1984). Adopting $M(I) = 4.6$ mag for the sdB star this corresponds to a companion spectral type of \approx M1 or a mass of $\approx 0.45 M_{\odot}$ (Drilling & Landolt 2000).

Accordingly we classify the companion as a white dwarf if its minimum mass exceeds $0.45 M_{\odot}$. This is the case for CD–24 731, [CW83] 1735+22 and HD 171858. In all other cases the companion type can not be constrained further from our observations, they could be either main sequence stars or white dwarfs. The minimum companion masses for BPS CS 22169–0001 and CPD –64° 481 are so small ($0.03 M_{\odot}$ and $0.05 M_{\odot}$, respectively) that they may be brown dwarfs if the inclination is larger than 20° and 38° , respectively.

Table 1 summarizes the probable nature for all companions to our program stars.

5. DISCUSSION

The unseen companions of three stars are white dwarfs whereas in the other cases they are either low mass main sequence stars or white dwarfs. The periods are in almost all cases shorter than ten days (dictated by our search strategy). This indicates that all observed RV variable sdB stars have evolved through at least one common envelope phase, consistent with the theoretical prediction of Han et al. (2003). After such a common envelope phase the orbit of the resulting close binary system should be circular, irrespective of a possible former eccentric orbit, as found for all former observed close hot subdwarf or white dwarf binary systems. Also, most of our radial velocity curves can be reproduced best by assuming a circular orbit. However, for four systems (which comprise one fourth of our sample) we detected periodic deviations from fitted sinusoidal curves. These deviations can be removed almost perfectly for PG 1232–136, [CW83] 1419–09 and PG 0133+114 by introducing small eccentricities of $\epsilon = 0.025 - 0.06$. Also for PB 7352 the observed data points can be matched better assuming a very small eccentricity of $\epsilon \approx 0.02$.

Unfortunately, for all four stars it is unclear whether their companions are main-sequence stars or white dwarfs, i.e., we do not know whether the stars have evolved during one or two common envelope phases. If their companions are white dwarfs, it is really hard to believe that the orbits of the stars remain eccentric although the systems have undergone two common envelope phases.

Another point arises concerning the common envelope itself. Terman, Taam & Hernquist (1994) show that during the common envelope phase the initial spiral-in of the companion is very eccentric, but their modeling shows also that the orbit circularizes very quickly. Did the common envelope phase for sdB stars in eccentric orbits last shorter and are they younger than “normal” sdB binaries?

6. SUMMARY AND CONCLUSION

We have determined the orbital parameters for 14 bright binary subdwarf B systems using high precision radial velocity measurements from high S/N optical high-resolution spectra. The companions are unseen in the spectra.

For most systems the orbits are circular. However, for four sdB stars we discovered that their orbits are probably non-circular with small eccentricities of $e = 0.022-0.060$. These close binaries are probably the first for which eccentric orbits have been detected.

Using the canonical mass for the sdB primary of $M = 0.5 M_{\odot}$ and the mass function, the nature of the invisible secondaries for all program stars could be constrained. Three systems consist of a sdB star and a white dwarf because the companion mass exceeds $\sim 0.45 M_{\odot}$. The companions of two systems are possibly brown dwarfs. For all other systems the nature of the unseen companions remain unclear; they could either be main-sequence stars or white dwarfs.

Important questions remain to be answered. Are the periodic deviations from fitted sine shaped RV curves really due to eccentric orbits? If so, are the radial velocity curves of all other close binary sdB systems, which have been determined by other groups really consistent with circular orbits or were the observations performed so far simply too inaccurate to detect such small eccentricities? To verify or clarify the nature of the invisible companions more high-precision measurements of radial velocity variable sdB systems and further photometric observations are necessary to search for eclipses or reflection effects.

REFERENCES

- Drilling J. S., Landolt A. U. 2000, in *Allen's Astrophysical Quantities*, eds. A. N. Cox, Springer, p. 381
- Edelmann H., Heber U., Napiwotzki R. 2001, *Astron. Nachr.* 322, 401
- Edelmann H., Heber U., Napiwotzki R. 2006, *Baltic Astronomy*, 15, 103 (these proceedings)
- Geier S., Heber U., Przybilla N., Kudritzki R.-P. 2006, *Baltic Astronomy*, 15, 243 (these proceedings)
- Green R. F., Schmidt M., Liebert J. 1986, *ApJS*, 61, 305
- Green E. M., Liebert J., Saffer S. A. 2001, in *12th European Workshop on White Dwarfs*, eds. J. L. Provencal et al., ASP Conf. Ser., 226, 192
- Han Z., Podsiadlowski P., Maxted P. F. L., Marsh T. R. Ivanova, N. 2002, *MNRAS*, 336, 449
- Han Z., Podsiadlowski P., Maxted P. F. L., Marsh T. R. 2003, *MNRAS*, 341, 669
- Heber U. 1986, *A&A*, 155, 33
- Jeffery C. S., Pollacco D. L. 1998, *MNRAS*, 298, 179
- Jones J. E., Alloin D. M., Jones B. J. T. 1984, *ApJ* 283, 457
- Kilkenny D., Heber U., Drilling J. S. 1988, *SAAO Circular*, 12, 1
- Lorenz L., Mayer P., Drechsel H. 1998, *A&A*, 332, 909
- Lucy L. B., Sweeney M. A. 1971, *AJ*, 76, 544
- Maxted P. F. L., Marsh T. R., North R. C. 2000, *MNRAS*, 317, L41
- Maxted P. F. L., Heber U., Marsh T. R., North R. C. 2001, *MNRAS*, 326, 1391
- Morales-Rueda L., Maxted P. F. L., Marsh T. R. et al. 2006, *Baltic Astronomy*, 15, 187 (these proceedings)
- Napiwotzki R., Edelmann H., Heber U., Karl C., Drechsel H. et al. 2001, *A&A*, 378, L17
- Napiwotzki R., Karl C. A., Lisker T., Heber U., Christlieb N. et al. 2004, *Ap&SS*, 291, 321
- Østensen R. H. 2006, *Baltic Astronomy*, 15, 85 (these proceedings)
- O'Toole S. J., Heber U., Benjamin R. A. 2004, *A&A*, 422, 1053
- Tassoul J.-L., Tassoul M. 1992, *ApJ*, 395, 259
- Terman J. L., Taam R. E., Hernquist L. 1994, *ApJ*, 422, 729
- Wisotzki L., Reimers D., Wamsteker W. 1991, *A&A*, 247, L17

PHOTOMETRIC PERIOD VARIATION OF V 1379 AQL

E. Sipahi, S. Evren, G. Taş and C. İbanoğlu

Ege University Observatory, 35100, Bornova, İzmir, Turkey

Received 2005 August 1

Abstract. V 1379 Aql is an eclipsing binary consisting a hot subdwarf (sdB) and a red giant star (K0 III/IV). According to the brightness variation outside of eclipses, the giant component is a chromospherically active star. The dark and cool active structures on this component and their evolution cause the variation of the total light of the system. Photometric observations spanning 16 years yield the variations of the photometric period and the mean brightness. There is a correlation between them. We suggest that the photometric period decreases as the latitude of the active region moves toward the equator.

Key words: stars: hot subdwarfs – stars: variables – stars: individual (V 1379 Aql)

1. INTRODUCTION

V 1379 Aql is a binary system composed of a red giant star (K0 III/IV) and a hot subdwarf star (sdB). The first indication of chromospheric activity on the giant star came from the detection of CaII H&K emission by Bidelman & MacConnell (1973). Photometric variations with an amplitude of about $0^m.2$ were first observed by Henry et al. (1982). The presence of a hot companion was noticed by Fekel & Simon (1985) in ultraviolet IUE spectra. They suggested that the hot companion was a B subdwarf. Balona et al. (1987) discovered the eclipse of the subdwarf from a variation of about $0^m.12$ of the color index $U-B$. The system is asynchronous, the rotational period of 25.4 days found by Balona et al. (1987) and Lloyd et al. (1987) being longer than the orbital period of 20.7 days determined from radial velocity measurements by Balona (1987) and Fekel et al. (1993). Jeffery et al. (1992) determined the mass ratio from UV radial velocity measurements which, together with a light curve analysis, gave the masses. Hooten & Hall (1990) determined a photometric period of about 26 days with an amplitude of $0^m.20-0^m.25$ in the V passband. Fekel et al. (1993) improved the orbital elements and the spectroscopic ephemeris from a new radial velocity curve. Jeffery & Simon (1997) analyzed the UV eclipse. They defined the eclipse duration and the light curve profile. UBV photometry and $H\alpha$ spectroscopy of the system in 1995 was presented and discussed by Frasca et al. (1998).

Starspots in a photosphere induce quasi-periodic brightness variations due to the star's axial rotation. Therefore, the modulation period marks the angular velocity of the mean latitude at which they are centered. By analogy with the solar case, the year-to-year variations of the rotational period can be attributed to the migration of stellar activity centers towards latitudes possessing different

Table 1. The subsets of V photometry of V 1379 Aql.

| Datasets | Mean epoch | Time range | N_{obs} | Source |
|----------|------------|-------------|-----------|--------|
| 88A | 1988.48 | 47276–47329 | 60 | 1 |
| 88B | 1988.86 | 47415–47483 | 41 | 1 |
| 89A | 1989.44 | 47615–47702 | 100 | 1 |
| 89B | 1989.88 | 47779–47853 | 37 | 1 |
| 90A | 1990.47 | 47987–48067 | 42 | 1 |
| 90B | 1990.93 | 48185–48212 | 12 | 1 |
| 91A | 1991.46 | 48354–48428 | 32 | 1 |
| 92A | 1992.46 | 48702–48809 | 31 | 1 |
| 92B | 1992.88 | 48874–48957 | 42 | 1 |
| 93A | 1993.47 | 49081–49165 | 58 | 1 |
| 93B | 1993.88 | 49236–49322 | 29 | 1 |
| 94A | 1994.45 | 49428–49545 | 59 | 1 |
| 94B | 1994.93 | 49643–49688 | 22 | 1 |
| 95A | 1995.46 | 49791–49909 | 72 | 1 |
| 95B | 1995.90 | 49982–50053 | 47 | 1 |
| 96A | 1996.44 | 50160–50261 | 57 | 1 |
| 96B | 1996.96 | 50392–50421 | 16 | 1 |
| 97A | 1997.44 | 50515–50642 | 61 | 1 |
| 97B | 1997.89 | 50713–50777 | 31 | 1 |
| 98A | 1998.41 | 50881–50992 | 53 | 1 |
| 98B | 1998.91 | 51089–51148 | 33 | 1 |
| 99A | 1999.44 | 51257–51353 | 56 | 1 |
| 99B | 1999.90 | 51447–51510 | 51 | 1 |
| 00A | 2000.42 | 51615–51712 | 50 | 1 |
| 00B | 2000.89 | 51805–51873 | 23 | 1 |
| 01A | 2001.44 | 51979–52092 | 44 | 1 |
| 01B | 2001.90 | 52181–52229 | 11 | 1 |
| 02A | 2002.47 | 52354–52459 | 54 | 1 |
| 02B | 2002.89 | 52535–52603 | 38 | 1-2 |
| 03A | 2003.65 | 52809–52914 | 32 | 2 |
| 04A | 2004.64 | 53177–53264 | 28 | 2 |

1. Henry (2002) 2. This study

angular velocity. The long-term photometric monitoring of active stars provides a powerful tool to derive relevant parameters of stellar surface activity (Rodono et al. 2000; Messina & Guinan 2003). In this paper we investigate the presence of the photometric period variation and its connection with the mean brightness variation. The analysis of extended time-series of broad-band photometric observations of V 1379 Aql showed the existence of periodic variations of the seasonal mean brightness level and periodic variations of its photometric period. The second section of this paper contains B and V photometry obtained between 1998 and 2004 and the variations which appeared in the light (V) and color ($B-V$) curves. In the third section we present the seasonal rotational periods obtained by means of a periodogram analysis. The existence of the photometric period variation is discussed in Section 4.

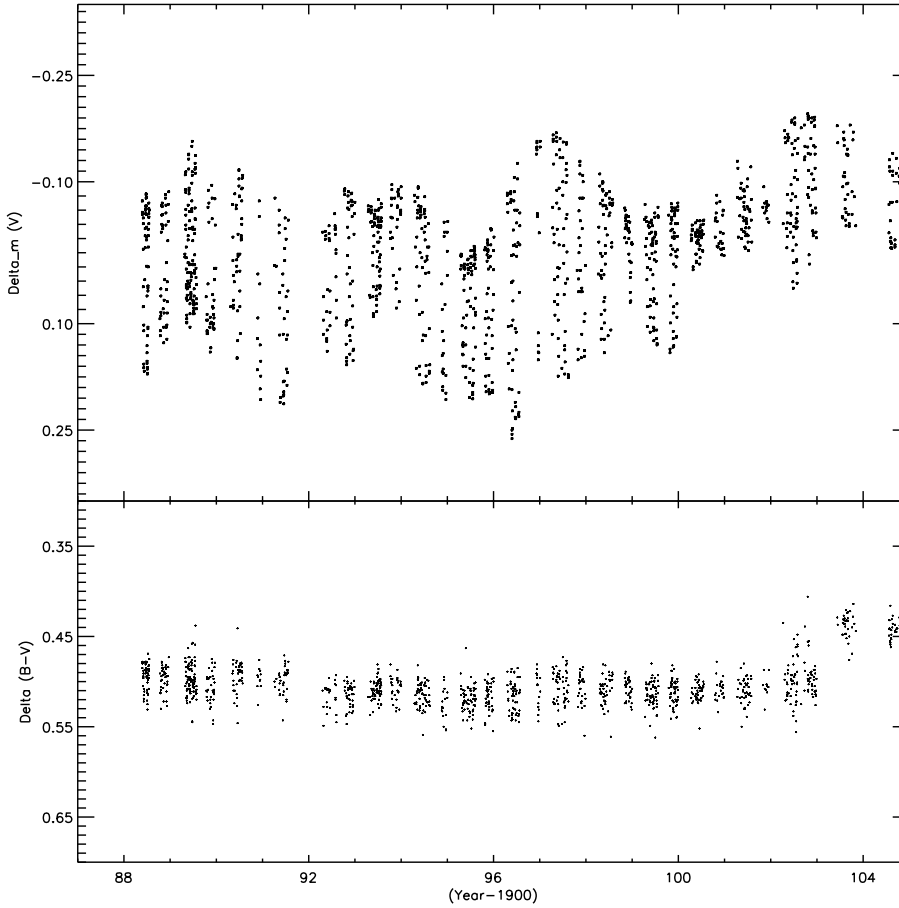


Fig. 1. The light (V) and color ($B-V$) variations of V 1379 Aql plotted against years.

2. OBSERVATIONS AND THE LIGHT CURVES

The observations of V 1379 Aql were obtained with two telescopes at two observatories. The differential BV photometry of the system was carried out between 1988 and 2002 with the Vanderbilt-Tennessee State 40 cm Automated Photoelectric Telescope (APT) and between 2002 and 2004 with the 48 cm Cassegrain telescope at Ege University Observatory. HD 185567 and HD 185587 were used as comparison and check stars, respectively. The comparison and check stars were found to be constant in brightness during the period of observations. All the differential magnitudes were corrected for the atmospheric extinction. Each observation was a mean of four or five measurements. A total of 1338 and 1364 average points in B and V filters, respectively, were obtained during 1307 nights.

Since the mean magnitude and amplitude of the light curve vary with time, B and V data of V 1379 Aql obtained between 1988 and 2004 are separated into 31 subsets. The V -band datasets are listed in Table 1. The columns of Table 1 show

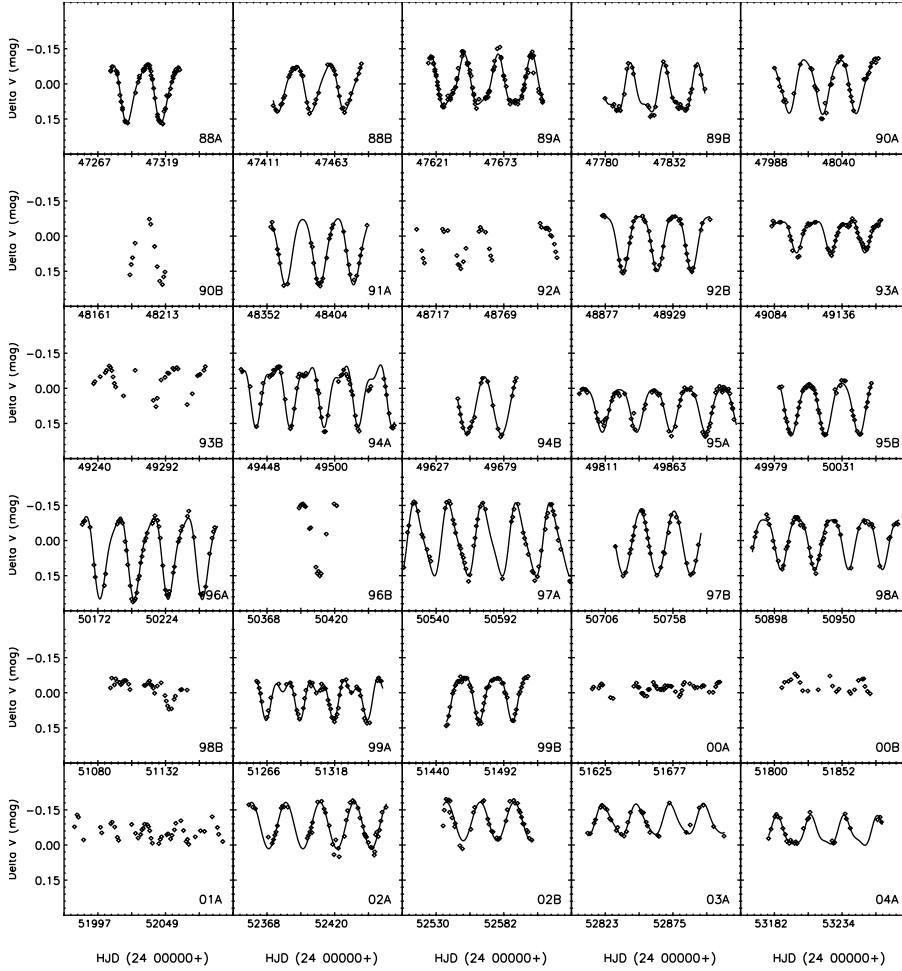


Fig. 2. The V light variation of V 1379 Aql for each year. The synthetic curves calculated by the periodogram analysis are also plotted. The observing seasons are listed in boxes at the top and left of the figure.

the data subsets, the mean epoch, the observing time range (HJD–24 00000) and the number of average observing points in each data subset. B and V photometry of the system obtained in 1988–2004 is shown in Figure 1.

We show the light variation for each observing season in Figure 2. As can be seen, the shape of the light curves is quite different in all observing seasons. The scales of the axes in this figure are the same for each data set. The amplitudes, as well as the minimum and maximum brightness vary during the years depending on the evolution of the activity structures on the cool component. The shape of the light curves is more complex in some years and therefore more difficult to analyze (e.g., 90B), while they have a descriptive shape allowing the period analysis in some observing seasons (e.g., 91A).

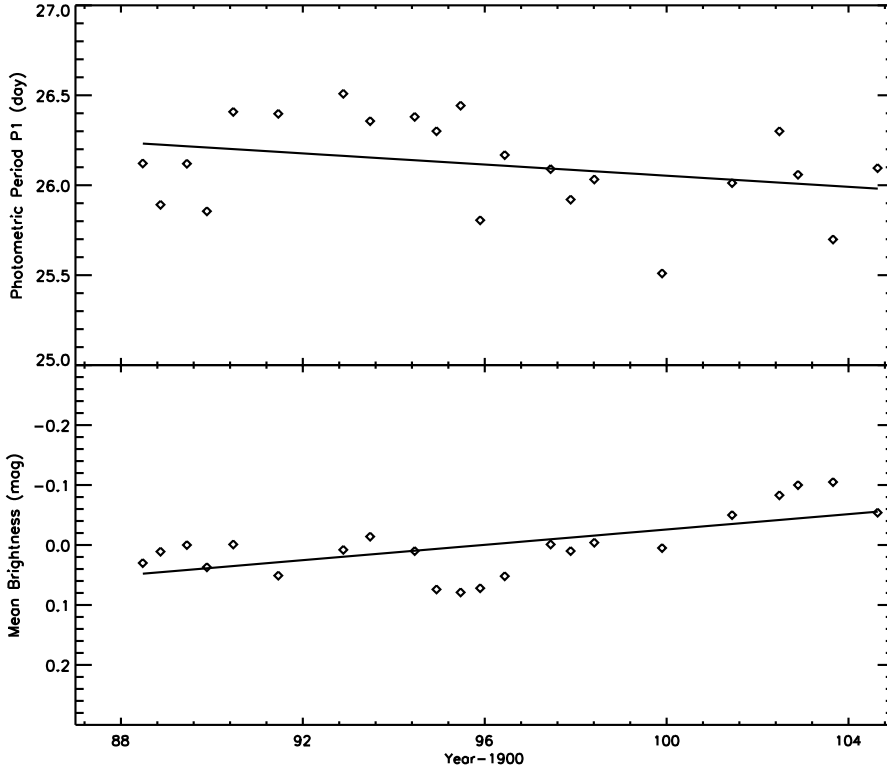


Fig. 3. Variations of the fundamental photometric period (P_1) and the mean brightness.

3. PHOTOMETRIC PERIOD VARIATION

In this study we used a periodogram analysis (Scargle 1982) to look for the period of the photometric rotational modulation and the stellar surface differential rotation. The datasets given in Table 1 have been analyzed by applying the program PERIOD04 (Lenz & Breger 2005). The photometric period, the amplitude and the mean brightness of the light variations are calculated from each dataset. A search for secondary periodicities was also performed by filtering the primary frequency modulation from the data and recomputing the periodogram for the residual data. The periodogram analysis detected the presence of a secondary rotation period in several datasets. The two rotational periods are believed to be due to the presence of two long-lived active regions at different latitudes having different angular velocities due to differential rotation (Messina & Guinan 2003). No periodicity was detected in some sets. The lack of periodicity was presumed to be caused by a rather uniform longitudinal distribution of spot centers that could not produce a rotational modulation.

The results are listed in Table 2. In it we give datasets and the mean epochs (year-1900) to which the photometric periods refer, the photometric periods (P_1 , P_2) and their uncertainty, the amplitudes of the sinusoids resulting from the periodogram analysis (A_1 , A_2) and the mean brightnesses (ZP) of the light curves. The agreement of the sinusoids obtained from the periodogram analysis with the

Table 2. The results of the photometric period analysis for V datasets.

| Data Sets | Mean Epoch | P_1 (day) | σ | P_2 (day) | σ | A_1 (mag) | σ | A_2 (mag) | σ | ZP (mag) | σ |
|-----------|------------|----------------|----------|----------------|----------|----------------|----------|----------------|----------|-------------|----------|
| 88A | 1988.48 | 26.1214 | 0.0002 | 26.1293 | 0.0007 | 0.236 | 0.002 | 0.052 | 0.002 | 0.030 | 0.002 |
| 88B | 1988.87 | 25.8916 | 0.0002 | 25.0722 | 0.0011 | 0.195 | 0.002 | 0.031 | 0.002 | 0.011 | 0.001 |
| 89A | 1989.45 | 26.1197 | 0.0001 | 25.6051 | 0.0005 | 0.204 | 0.003 | 0.053 | 0.002 | 0.000 | 0.002 |
| 89B | 1989.89 | 25.8555 | 0.0002 | 25.7881 | 0.0006 | 0.187 | 0.003 | 0.071 | 0.003 | 0.037 | 0.002 |
| 90A | 1990.47 | 26.4082 | 0.0002 | | | 0.227 | 0.004 | | | -0.001 | 0.003 |
| 90B | 1990.93 | | | | | | | | | | |
| 91A | 1991.46 | 26.3973 | 0.0001 | 25.5825 | 0.0014 | 0.281 | 0.004 | 0.036 | 0.003 | 0.051 | 0.003 |
| 92A | 1992.46 | | | | | | | | | | |
| 92B | 1992.89 | 26.5087 | 0.0001 | 26.2948 | 0.0004 | 0.233 | 0.002 | 0.053 | 0.002 | 0.008 | 0.001 |
| 93A | 1993.48 | 26.3565 | 0.0002 | 26.1758 | 0.0006 | 0.126 | 0.002 | 0.045 | 0.002 | -0.014 | 0.002 |
| 93B | 1993.89 | | | | | | | | | | |
| 94A | 1994.46 | 26.3804 | 0.0002 | 26.0821 | 0.0004 | 0.223 | 0.004 | 0.096 | 0.004 | 0.010 | 0.003 |
| 94B | 1994.94 | 26.3007 | 0.0003 | | | 0.246 | 0.003 | | | 0.074 | 0.002 |
| 95A | 1995.47 | 26.4427 | 0.0001 | 26.4814 | 0.0006 | 0.182 | 0.002 | 0.036 | 0.003 | 0.079 | 0.002 |
| 95B | 1995.90 | 25.8054 | 0.0001 | 26.5692 | 0.0009 | 0.223 | 0.002 | 0.037 | 0.002 | 0.072 | 0.001 |
| 96A | 1996.44 | 26.1680 | 0.0001 | 26.2992 | 0.0005 | 0.332 | 0.003 | 0.076 | 0.003 | 0.052 | 0.002 |
| 96B | 1996.96 | | | | | | | | | | |
| 97A | 1997.45 | 26.0902 | 0.0000 | 26.0591 | 0.0004 | 0.292 | 0.003 | 0.060 | 0.003 | -0.001 | 0.002 |
| 97B | 1997.89 | 25.9204 | 0.0002 | | | 0.271 | 0.003 | | | 0.010 | 0.002 |
| 98A | 1998.41 | 26.0323 | 0.0001 | 25.9106 | 0.0006 | 0.212 | 0.002 | 0.043 | 0.002 | -0.004 | 0.002 |
| 98B | 1998.92 | | | | | | | | | | |
| 99A | 1999.44 | | | | | | | | | | |
| 99B | 1999.90 | 25.5102 | 0.0002 | 25.6521 | 0.0006 | 0.181 | 0.002 | 0.057 | 0.002 | 0.005 | 0.001 |
| 00A | 2000.43 | | | | | | | | | | |
| 00B | 2000.90 | | | | | | | | | | |
| 01A | 2001.44 | 26.0124 | 0.0004 | 26.4932 | 0.0004 | 0.065 | 0.003 | 0.066 | 0.003 | -0.050 | 0.002 |
| 01B | 2001.90 | | | | | | | | | | |
| 02A | 2002.48 | 26.3002 | 0.0002 | | | 0.198 | 0.004 | | | -0.083 | 0.003 |
| 02B | 2002.89 | 26.0589 | 0.0005 | | | 0.165 | 0.005 | | | -0.100 | 0.004 |
| 03A | 2003.66 | 25.6987 | 0.0003 | 26.2197 | 0.0015 | 0.126 | 0.003 | 0.021 | 0.003 | -0.105 | 0.002 |
| 04A | 2004.64 | 26.0954 | 0.0003 | | | 0.117 | 0.002 | | | -0.054 | 0.002 |

observed data are shown in Figure 2. The connection between the fundamental photometric period (P_1) and the mean brightness is shown in Figure 3. In 1988–2004 the mean brightness of the system increases when the photometric period decreases.

4. RESULTS

Measurements of stellar surface differential rotation are obtained in different ways. One of these is Fourier analysis of broad-band photometric data. In this paper, using 16 years of continuous V -band data of V 1379 Aql, we found a photometric period variation consistent with a solar-type differential rotation. As seen in Fig. 2, the shape of light curve varies for each dataset. The continual redistribution of spots as a result of stellar differential rotation accounts for much of the

changing shape and amplitude of the light curve on rotational timescales. The observed asymmetries in the light curve clearly demonstrate that spot groups are present at multiple longitudes. As seen in Fig. 3, the photometric period (P_1) of the system varies between 26.5 and 25.5 days. We suggest that the latitude of spot activity center moves toward the equator, i.e., toward faster rotating latitudes during an activity cycle, producing a decrease in the photometric period. V 1379 Aql displays a solar-like behavior. As the active regions reach the equator, the activity cycle ends. The spots start to decay, and the system becomes brighter. The mean period of the system was reduced by ~ 0.25 d in 16 years, but the mean light brightened by about $0^m.2$ in the same time interval. We consider that the evolution of the active regions affected the variations of the photometric period and the mean brightness. There is an interesting correlation between them. Photometric observations of V 1379 Aql are continuing.

ACKNOWLEDGMENTS. This research was mostly based on observations obtained using the Vanderbilt-Tennessee State Automated Photoelectric Telescope. We would like to thank Dr. G. W. Henry for sending his unpublished photometric data. We are grateful to Dr. S. Jeffery for useful discussions and the referee for comments that improved the paper. One author (E. Sipahi) sends special thanks to Erol Turan for financial support.

REFERENCES

- Balona L. 1987, South African Astron. Obs. Circ., 11, 1
Balona L., Lloyd Evans T., Simon T., Sonneborn G. 1987, IBVS, 3601
Bidelman W. P., MacConnell D. J. 1973, AJ, 78, 687
Collier Cameron A., Donati J. F., Semel M. 2002, MNRAS, 330, 699
Donati J. F., Mengel M. Carter B. D. et al. 2000, MNRAS, 316, 699
Fekel F. C., Henry G. W., Busby M. R., Eitter J. J. 1993, AJ, 106, 2370
Fekel F. C., Simon T. 1985, AJ, 90, 812
Frasca A., Marilli E., Catalano S. 1998, A&A, 333, 205
Henry G. W., Murray S., Hall D. S. 1982, IBVS, 2215
Henry G. W. 2002, private communication
Hooten J. T., Hall D. S. 1990, ApJS, 74, 225
Jeffery C. S., Simon T., Lloyd Evans T. 1992, MNRAS, 258, 64
Jeffery C. S., Simon T. 1997, MNRAS, 286, 487
Lenz P., Breger M. 2005, Comm. in Asteroseismology, 146, 53
Lloyd Evans T., Koen M. C. J. 1987, South African Astron. Obs. Circ., 11, 21
Messina S., Guinan E. F. 2003, A&A, 409, 1017
Reiners A., Schmitt J. H. M. M. 2002, A&A, 384, 155
Rodono M., Messina S., Lanza A. F., Cutispoto G., Teriaca L. 2000, A&A, 358, 624
Scargle J. D. 1982, ApJ, 263, 835
Vogt S. S., Penrod G. P. 1983, PASP, 95, 565

HELIUM, CARBON AND SILICON ABUNDANCES IN THE HW VIRGINIS ECLIPSING BINARY SUBDWARF-B PRIMARY

A. N. Mortimore and A. E. Lynas-Gray

*Department of Physics, University of Oxford, Denys Wilkinson Building, Keble
Road, Oxford OX1 3RH, U.K.*

Received 2005 August 15

Abstract. Light curve solutions show HW Vir and PG 1336-018 to be remarkably similar eclipsing binaries. The subdwarf-B (sdB) primary of PG 1336-018 is a pulsator but pulsation is not detected in the sdB primary of HW Vir. Ultraviolet spectra were used to obtain carbon and silicon abundances in the sdB primary of HW Vir; in due course these should be compared with those in the sdB primary of PG 1336-018 to see if pulsation in the latter could be explained by the κ -mechanism, arising from higher metal abundances and microscopic diffusion.

Key words: stars: hot subdwarfs – stars: abundances – stars: individual (HW Vir)

1. INTRODUCTION

HW Vir (BD–073477) is reported by Menzies & Marang (1986) to be an eclipsing binary with an orbital period of 0.1161 days, the primary being a sdB star. Much subsequent work is concerned with an interpretation of the period change, first identified as a decrease by Kilkenny et al. (1994). İbanoğlu et al. (2004) find a sinusoidal variation in residuals between observed and calculated times of mid-eclipse which they suggest is due to a third body in the system; a brown dwarf orbiting with a period of 18.8 years, and having a mass between $0.022 M_{\odot}$ and $0.07 M_{\odot}$ depending on the inclination of its orbit.

Kilkenny et al. (1998) discover NY Vir (PG 1336-018) to also be an eclipsing binary with a remarkable resemblance to HW Vir; the essential difference is the pulsation in the sdB primary of PG 1336-018, and the non-detection of change in the binary orbital period (Kilkenny 2005). The similarity between HW Vir and PG 1336-018 is indicative of the absence of a clear separation between pulsating and non-pulsating sdB stars in the T_{eff} vs. $\log g$ diagram (Koen et al. 1999). Charpinet (2001) reviews earlier theoretical work which explains sdB star pulsation as being driven by a metal ionization zone, its required overabundance of metals being provided by microscopic diffusion from outer layers.

A comparison of photospheric abundances in HW Vir and PG 1336-018 could serve as a verification of our understanding of sdB star pulsation. As a first step, metal abundances were determined for HW Vir from International Ultraviolet

Explorer (IUE) spectra. Different T_{eff} and $\log g$ values are obtained from light curve solutions (Kiss et al. 2000) and Balmer line fits (Wood & Saffer 1999), prompting a new determination with ultraviolet spectroscopy.

2. OBSERVATIONS

HW Vir was observed with IUE on 1984 May 10 and 11. On May 10 a series of low dispersion spectra were obtained using the Long Wavelength Prime (LWP) camera. While reading the LWP camera, a high dispersion spectrum was accumulated in the Short Wavelength Prime (SWP) camera and only read once an adequate exposure had been achieved. During May 11 the role of the two cameras was reversed, leading to a series of low dispersion SWP spectra and accumulation of LWP high dispersion spectra while reading the SWP camera. Images were reprocessed (Nichols & Linsky 1996) and spectra extracted.

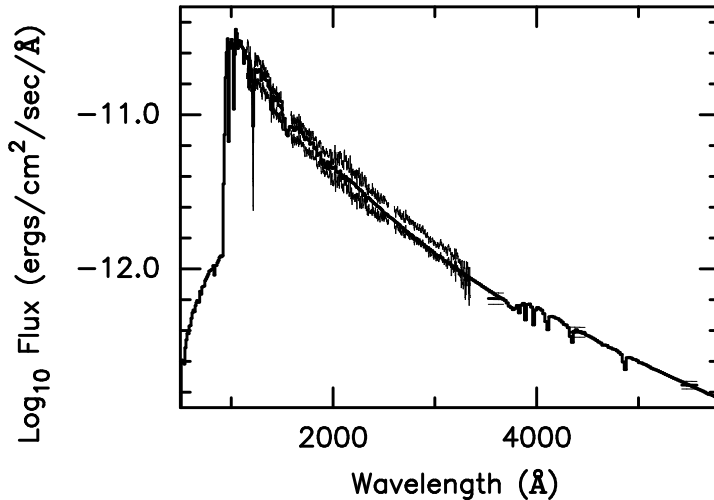


Fig. 1. The energy distribution of HW Vir.

3. EFFECTIVE TEMPERATURE AND ANGULAR RADIUS

The energy distribution of HW Vir is based on IUE images SWP 22985, SWP 22986, LWP 03322 and LWP 03323; these are supplemented by fluxes in U , B and V passbands derived from photometry by Menzies et al. (1990). SWP 22984 was obtained during primary eclipse and not therefore included. Other low resolution SWP and LWP spectra obtained at various orbital phases give flux densities which agree within error limits, indicating the absence of an ultraviolet reflection effect. Remie & Lamers (1982) iteration was used for T_{eff} determination with trial reddening estimates in the range $0.00 \leq E_{B-V} \leq 0.04$, calculated following Seaton (1979), which attempt to remove the 2200 Å feature.

Thin lines in Figure 1 are dereddened UBV flux densities and merged IUE low resolution spectra for $E_{B-V} = 0.00$ and $E_{B-V} = 0.04$. UBV flux densities for $E_{B-V} = 0.02$ are similarly shown as thick lines. The remaining thick line in Figure 1 is the flux density at the top of the Earth's atmosphere estimated

from the adopted model stellar atmosphere, computed following Kurucz (1992), normalized at V for $E_{B-V} = 0.02$. Reddening along the line of sight to HW Vir is therefore $E_{B-V} = 0.02 \pm 0.02$ and $T_{\text{eff}} = 29\,400 \pm 700$ K with a corresponding angular radius $\alpha = (2.03 \pm 0.06) \times 10^{-11}$ radians. Upper and lower T_{eff} and α limits correspond to the uncertainty in E_{B-V} .

4. SURFACE GRAVITY AND ABUNDANCES

High dispersion spectra from images SWP 22971, SWP 22972 and SWP 22973 were corrected for relative velocity shifts and merged. Abundances and surface gravity were determined by comparison with synthetic spectra computed with SYN-SPEC (Hubeny & Lanz 2003) assuming local thermodynamic equilibrium (LTE), using model stellar atmospheres computed with ATLAS9 (Kurucz 1992). The version of SYN-SPEC used differed from the public domain version in that He I line Stark broadening was computed using tables by Dimitrijević & Sahal-Bréchet (1984, 1990) as appropriate. Synthetic spectra were broadened to allow for orbital motion and rotation of the sdB, assuming the binary is tidally locked.

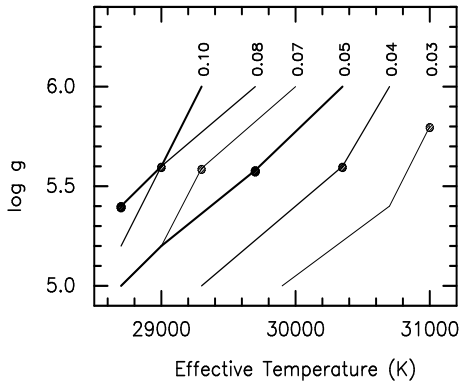


Fig. 2. Loci of fits to He II at 1640 Å.

Determination of surface gravity and helium abundance was based on the He II 1640 Å line. Loci of fits in the T_{eff} vs. $\log g$ diagram are shown in Figure 2 as lines of differing thickness annotated by helium abundances (by number) relative to the Sun. Large filled circles show the best fit obtained for each helium abundance.

Allowing for error limits on the derived T_{eff} , Figure 2 shows the helium abundance (by numbers) to lie between 0.04 and 0.10 of the solar helium abundance and $\log g$ to lie between 5.4 and 5.8. The derived helium abundance by numbers for sdB primary of HW Vir was therefore $n(\text{He}) = 0.07 \pm 0.03$ of the solar value; its surface gravity was similarly, $\log g = 5.6 \pm 0.2$.

Few metal lines were readily identified in high dispersion spectra though lines of Si III, Si IV, C III and C IV could be used for abundance determinations by direct comparison with synthetic spectra. Abundances by number, relative to the Sun, obtained for several assumed T_{eff} and $\log g$ values are presented in Table 1. Abundances obtained appear to be ionization stage dependent; synthetic spectrum calculations in non-LTE do not explain the apparent discrepancies.

In the case of carbon, abundances from C III and C IV lines do not appear to

Table 1. Carbon and silicon abundances.

| T_{eff} (K) | $\log g$ | Si IV | Si III | C IV | C III |
|----------------------|----------|-------------------------------|-----------------------|-------------------------------|-----------------------|
| | | λ (Å) 1394 1403 | λ (Å) 1299 | λ (Å) 1548 1551 | λ (Å) 1247 |
| 28700 | 5.0 | 0.06 | 0.21 | 0.008 | 0.030 |
| | 5.6 | 0.07 | 0.16 | 0.014 | 0.030 |
| | 6.0 | 0.08 | 0.13 | 0.023 | 0.030 |
| 29350 | 5.0 | 0.06 | 0.28 | 0.006 | 0.027 |
| | 5.6 | 0.07 | 0.21 | 0.011 | 0.030 |
| | 6.0 | 0.08 | 0.16 | 0.017 | 0.032 |
| 30100 | 5.0 | 0.06 | 0.39 | 0.005 | 0.029 |
| | 5.6 | 0.07 | 0.29 | 0.008 | 0.030 |
| | 6.0 | 0.08 | 0.21 | 0.033 | 0.033 |

be significantly different in view of uncertainties in T_{eff} and $\log g$ and weakness of the CIV, all are formed at similar depths in the atmosphere. Silicon abundances are better determined because the lines are stronger and the difference between Si IV and Si III appears to be real; this could arise because of stratification in the atmosphere because the Si IV and Si III lines are formed at Rosseland mean depths of 4×10^{-7} and 10^{-3} , respectively.

5. CONCLUSIONS

The T_{eff} lower limit is just above the Wood & Saffer (1999) upper limit but the derived helium abundance and surface gravity were in good agreement. Both silicon and carbon are depleted relative to the Sun. The difference between silicon abundances derived from Si IV and Si III lines suggests a stratified atmosphere caused by microscopic diffusion, though further work on abundance gradients would be needed for confirmation.

Hipparcos parallax measurements indicate, at 68% confidence, a distance to HW Vir of not less than 264 pc. The angular radius lower limit derived in this paper then suggests a HW Vir sdB primary radius of not less than $0.22 R_{\odot}$. Light curve solutions (see Kiss et al. 2000) indicate $0.22 R_{\odot}$ as an upper limit for the radius of the sdB primary, which suggests a discrepancy unless $E_{B-V} = 0.0$ in which case T_{eff} is close to the lower limit suggested by the ultraviolet energy distribution and in agreement with Wood & Saffer's (1999) result.

REFERENCES

- Charpinet S. 2001, *Astron. Nachr.*, 322, 387
 Dimitrijević M. S., Sahal-Bréchet S. 1984, *JQRST*, 31, 301
 Dimitrijević M. S., Sahal-Bréchet S. 1990, *A&AS*, 82, 519
 Hubeny I., Lanz T. 2003, <http://tlusty.gsfc.nasa.gov/Synspec43/synspec.html>
 İbanoğlu C., Çakırlı Ö., Taş G., Evren S. 2004, *A&A*, 414, 1043
 Kilkenny D. 2005, private communication
 Kilkenny D., Marang F., Menzies J. W. 1994, *MNRAS*, 267, 535
 Kilkenny D., O'Donoghue D., Koen C., Lynas-Gray A. E., Van Wyk F. 1998, *MNRAS*, 296, 329
 Kiss L. L., Csák B., Sztatmáry K., Fűrész G., Sziládi K. 2000, *A&A*, 364, 199
 Koen C., O'Donoghue D., Kilkenny D., Stobie R. S., Saffer R. A., 1999, *MNRAS*, 306, 213
 Kurucz R. L. 1992, in *The Stellar Populations of Galaxies*, IAU Symp. 149, eds. B. Barbuy & A. Renzini, Reidel Publ. Company, Dordrecht, p. 225
 Menzies J. W., Marang F. 1986, in *Instrument and Research Programmes for Small Telescopes*, IAU Symp. 118, eds. J. B. Hearnshaw & P. L. Cottrell, Reidel Publ. Company, Dordrecht, p. 305
 Menzies J. W., Marang F., Westerhuys J. E. 1990, *SAAO Circ.* 14, 1
 Nichols J. S., Linsky J. L. 1996, *AJ*, 111, 517
 Remie H., Lamers H. J. G. L. M. 1982, *A&A*, 105, 85
 Seaton M. J. 1979, *MNRAS*, 187, 73p
 Wood J. H., Saffer R. 1999, *MNRAS*, 305, 820

ON THE EMPIRICAL INSTABILITY DOMAINS FOR PULSATING SUBDWARF B STARS

G. Fontaine¹, E. M. Green², P. Chayer³, P. Brassard¹, S. Charpinet⁴ and
S. K. Randall¹

¹ *Département de Physique, Université de Montréal, C.P. 6128,
Succ. Centre-Ville, Montréal, Québec H3C 3J7, Canada*

² *Steward Observatory, University of Arizona, Tucson, AZ 85721, U.S.A.*

³ *Bloomberg Center for Physics and Astronomy, The Johns Hopkins University,
Baltimore, MD 21218-2686, U.S.A.*

⁴ *Observatoire Midi-Pyrénées, 14 Av. E. Belin, F-31400 Toulouse, France*

Received 2005 August 1

Abstract. We present some of the results of an ongoing spectroscopic survey to derive reliable atmospheric parameters for the known pulsating sdB stars as well as several known constant stars. This survey involves high S/N ratio optical observations in conjunction with detailed NLTE model atmospheres. The homogeneity of our approach allows us, for the first time, to discuss with some confidence the locations of the empirical instability regions for the short-period pulsating EC 14026 stars and for the long-period PG 1716 stars in the surface gravity-effective temperature plane. We also briefly address the question of the influence of a weak stellar wind on these pulsators.

Key words: stars: hot subdwarfs – stars: oscillations

1. INTRODUCTION

It is now well established that stellar pulsations are a common phenomenon among hot B subdwarf (sdB) stars. A first type of pulsating sdB stars, called EC 14026 stars after the prototype EC 14026–2647, was discovered some years ago (Kilkenny et al. 1997), while the existence of a second type, the PG 1716 stars (after the prototype PG 1716+426), was reported only recently (Green et al. 2003). The relatively short pulsation periods observed in the EC 14026 stars – typically in the range 100–200 s – are attributed to *p*-mode oscillations, while the much longer periods detected in the PG 1716 stars – from 3000 s to upward of 8000 s – are attributed to *g*-mode pulsations (see, e.g., Fontaine et al. 2003).

In order to fully understand the properties of the pulsating sdB stars, it is necessary to have, among other things, a reliable description of the instability regions in the log *g* vs. T_{eff} diagram. The most recent discussion of the empirical instability strips for pulsating sdB stars was presented by Fontaine et al. (2004). However, that discussion remained limited because the estimates of the atmospheric parameters for pulsating sdB stars available at the time came from various mixed sources,

potentially sporting significant systematic differences. As a consequence, only a somewhat blurred view of the empirical instability regions in the $\log g$ vs. T_{eff} plane could be provided.

Since then, we have worked hard to improve the situation by pursuing a spectroscopic program which emphasizes high S/N ratio observations and homogeneity of approach. We have now determined the atmospheric parameters of almost all known pulsating sdB stars accessible from Arizona, as well as many known constant stars for comparison purposes. We report here on the preliminary results of that ongoing program.

2. AN HOMOGENEOUS APPROACH THROUGH SPECTROSCOPY

Our approach has been part of a global optical spectroscopy program designed to improve on the characterizing of sdB stars. So far, we have gathered medium resolution ($\sim 1 \text{ \AA}$), high signal-to-noise ratio ($\langle S/N \rangle \sim 170$) spectra for 115 stars with the blue spectrograph at the new 6.5 m Multiple Mirror Telescope (MMT). Those spectra cover the range from $\sim 4000 \text{ \AA}$ to $\sim 4950 \text{ \AA}$. Most of these stars have been searched by one of us (E.M.G.) for long-period photometric activity of the PG 1716 type. Several have also been searched by Billères et al. (2002) for short-period pulsations and found to be constant. In addition, we also gathered low resolution ($\sim 9 \text{ \AA}$) spectra of even higher sensitivity ($\langle S/N \rangle \sim 273$) for a sample of 55 stars at the Steward Observatory 2.3 m telescope. Those latter spectra cover the range from $\sim 3615 \text{ \AA}$ to $\sim 6900 \text{ \AA}$ and all belong to pulsating sdB's, either of the EC 14026 type or PG 1716 category. A detailed comparison of the 38 objects in common in the two samples has allowed us to conclude that, in spite of different resolution and spectral coverage, there are no significant systematic differences in the inferred atmospheric parameters of stars belonging to either one of the two samples. We explain that in terms of sufficiently high S/N ratio.

An integral part of our program is the development of a bank of model atmospheres and synthetic spectra suitable for the analysis of the spectroscopic data. To this end, we have so far computed two detailed grids (one in LTE and the other in NLTE) with the help of the public codes TLUSTY and SYNSPEC (Hubeny & Lanz 1995; Lanz & Hubeny 1995). Each grid is defined in terms of 11 values of the effective temperature (from 20 000 K to 40 000 K in steps of 2000 K), 10 values of the surface gravity (from $\log g$ of 4.6 to 6.4, in steps of 0.2 dex) and 9 values of the helium-to-hydrogen number ratio (from $\log N(\text{He})/N(\text{H})$ of -4.0 to 0.0 , in steps of 0.5 dex). These grids were originally developed to analyze our MMT data and, therefore, our current synthetic spectra are limited to the range from 3500 \AA to 5800 \AA , but this can easily be widened as needed. We are planning to include metals in the near future. More details about these models will be found in Green, Fontaine & Chayer (in preparation).

We show in Figure 1 the results of our analysis for our current sample of 115 sdB stars with MMT spectroscopy. Those were obtained with the help of our NLTE grid of He/H models. The figure illustrates the three atmospheric parameters that were inferred: $\log g$, T_{eff} and the He/H number ratio. The size of each point is proportional to the logarithm of that latter quantity. In comparison to the normal (solar) He/H ratio (illustrated here by the open circle), all of the stars observed show helium deficiencies in their atmospheres. The observed pattern of He/H ratios is, however, rather complicated and defies simple explanations.

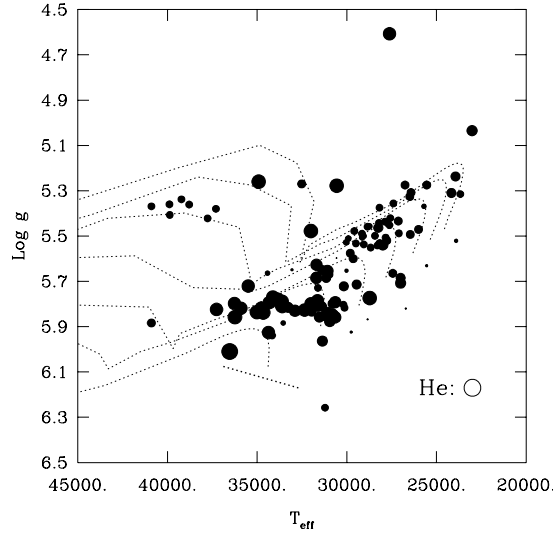


Fig. 1. Distribution of 115 sdB stars with MMT spectroscopy in the $\log g$ vs. T_{eff} diagram. The size of a circle gives a logarithmic measure of the inferred He/H number ratio. The thin dotted lines show some of Ben Dorman’s evolutionary tracks for models with a range of H envelope masses. The thick dotted line represents the zero-age He-burning main sequence for masses with $0.3\text{--}0.6 M_{\odot}$.

3. AN UPDATED VIEW OF THE EMPIRICAL INSTABILITY REGIONS

Figure 2 shows our updated view of the locations of the instability domains for pulsating sdB stars in the $\log g$ vs. T_{eff} plane as calculated from our He/H NLTE model atmospheres. It is possible, even probable, that the inclusion of metals will modify the picture somewhat. We are planning to investigate that point in the near future with the computations of NLTE models that would include metals along with H and He. For the time being, however, this is what we can offer. The built-in homogeneity of our approach is of central interest here; we show only stars for which we obtained spectra ourselves with the same instruments and that were analyzed in the same way.

All of the 30 known PG 1716 pulsators (except for one whose recent discovery was announced by Kilkenny et al. 2006) are plotted in Figure 2 and are shown as open circles. It can be seen that a typical PG 1716 star has a $\log g$ value of about 5.4 and an effective temperature of about 27 000 K. As indicated above, PG 1716 stars are long-period, high-order g -mode pulsators. In comparison, there are 34 known short-period, low-order p -mode pulsators of the EC 14026 type. The positions of 26 of these objects belonging to our homogeneous spectroscopic sample are plotted as filled circles in the figure. It is apparent that a typical EC 14026 star has a $\log g$ value of around 5.7 and an effective temperature of about 33 000 K, but there is some dispersion as well.

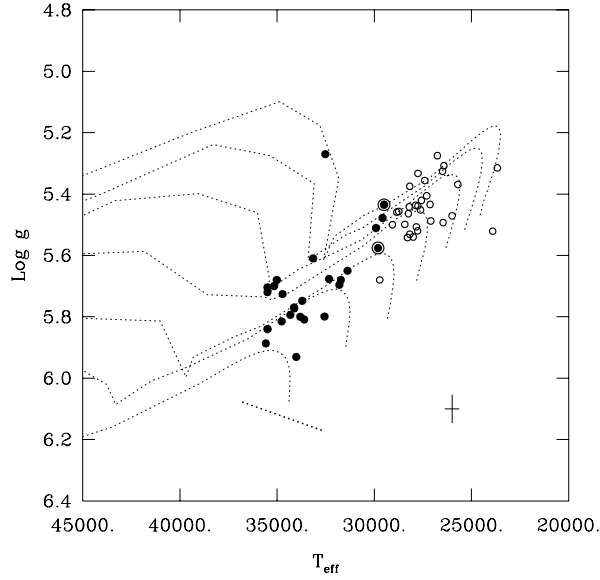


Fig. 2. Distribution of the pulsating sdB stars in the $\log g$ vs. T_{eff} diagram. The filled circles give the locations of 26 EC 14026 stars, while the open circles indicate those of 30 PG 1716 pulsators. The cross indicates typical uncertainties on the atmospheric parameters, while the curves are the same as in Fig. 1.

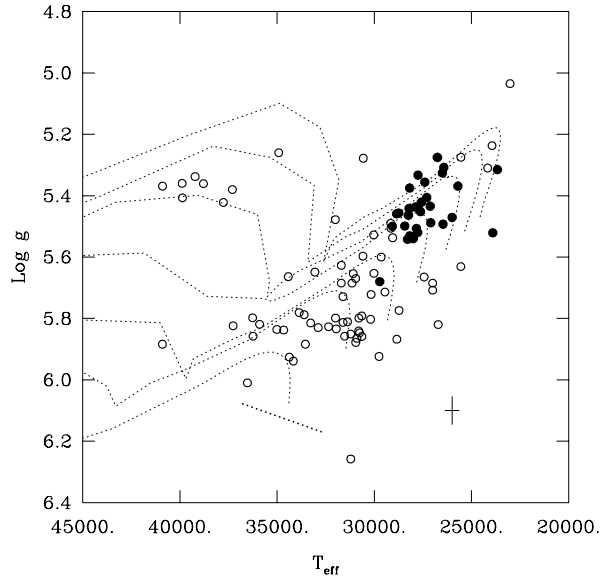


Fig. 3. Distribution of the sdB stars in the $\log g$ vs. T_{eff} diagram which have been searched for long-period photometric variations of the PG 1716 type. The filled circles give the locations of the 30 known PG 1716 pulsators, while the open circles indicate those of 70 constant stars. The other features in the figure are the same as in Fig. 2.

Figure 2 clearly shows that the two classes of pulsating sdB stars occupy different domains in the $\log g$ vs. T_{eff} plane, although the domains actually touch. As a matter of fact, two stars initially discovered as short-period pulsators have been reported to also exhibit long-period luminosity variations more characteristic of PG 1716 stars. These are HS 0702+6043 (Schuh et al. 2005) identified in the figure by the upper filled circle surrounded by a larger open circle and Balloon 090100001 (Oreiro et al. 2005; Baran et al. 2005) identified by the lower similar symbol. The positions of these two objects at the common boundary of the two classes of pulsating sdB stars are quite consistent with the suggestion that HS 0702+6043 and Balloon 090100001 are both EC 14026 and PG 1716 pulsators at the same time!

We show, in Figure 3, the distribution of the sdB stars which have been searched for long-period photometric activity of the PG 1716 type. The plot includes the locations of 30 (out of 31) known long-period pulsators (filled circles) and the locations of 70 constant stars (open circles). The latter are defined as stars with amplitude limits of less than ~ 1 mmag in the period range 400–15 000 s (E.M.G., unpublished). We note that all of the objects illustrated in the figure belong to our MMT sample, hence the figure does provide an homogeneous view of the PG 1716 phenomenon in the $\log g$ vs. T_{eff} plane.

We also cannot help but point out the strong concentration of PG 1716 stars on the low-gravity cool side of the sdB range. Actually, at least two of the four apparently constant stars in that region may show very low-amplitude variations, but we prefer to adopt a conservative selection criterion and declare them “constant” for the time being. More generally, we cannot exclude the possibility that *all* cool sdB stars of low gravity may be PG 1716 pulsators at this stage.

The corresponding homogeneous view of the EC 14026 phenomenon is shown in Figure 4. In that figure, we plotted the positions of the 26 EC 14026 stars (out of 34 currently known) and of the 33 constant stars for which we have spectroscopic measurements. The latter are defined as stars with amplitude limits of less than ~ 1 mmag in the period range 20–1 000 s (see Billères et al. 2002). As discussed by Charpinet et al. (2006), it is a remarkable fact that *all* of the known pulsators are found in the region of maximum p -mode instability as obtained through detailed nonadiabatic calculations using equilibrium models that include radiative levitation of iron. We take this as a strong observational proof of the basic validity of the driving mechanism based on radiative levitation as originally proposed by Charpinet et al. (1997) for EC 14026 stars.

At the same time, the possibility that variable and nonvariable stars may coexist in the EC 14026 instability domain was first hinted at by Billères et al. (1997) on the basis of early statistics. The homogeneous spectroscopy presented here confirms that this is indeed the case. Fig. 4 clearly reveals that sdB stars show a mixed population of variable and nonvariable stars inside the EC 14026 instability strip. The best contending mechanism to explain this phenomenon is the possibility that weak stellar winds significantly perturb the levitating reservoir of iron or iron-peak elements in some cases (see, e.g., Charpinet, Fontaine & Brassard 2001). We briefly discuss this possibility in the rest of this paper.

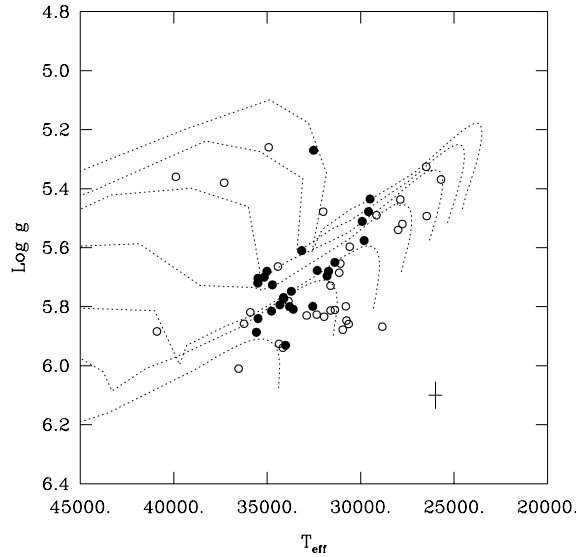


Fig. 4. Distribution of the sdB stars in the $\log g$ vs. T_{eff} diagram which have been searched for short-period photometric variations of the EC 14026 type, and which belong to our homogeneous spectroscopic sample. The filled circles give the locations of 26 EC 14026 pulsators, while the open circles indicate those of 33 constant stars. The other features in the figure are the same as in Fig. 2.

4. EFFECTS OF A STELLAR WIND ON THE SDB PULSATORS

The effects of a weak stellar wind on the levitating reservoir of iron in a typical model of a sdB star have already been discussed by Chayer et al. (2004). We have followed up on these calculations by integrating them into our equilibrium model building code and then analyzing the pulsational properties of such an evolving model with the help of our nonadiabatic pulsation code. We recall that the model considered by Chayer et al. (2004) is characterized by the values of $M = 0.5 M_{\odot}$, $\log g = 5.5$ and $T_{\text{eff}} = 30\,000$ K. Furthermore, it has been assumed that the model, in its initial configuration at time $t = 1$ yr, is a standard “second generation” model à la Charpinet et al. (1997) in which diffusive equilibrium between gravitational settling and radiative levitation of iron has been reached. A stellar wind is then turned on at a rate of $6 \times 10^{-15} M_{\odot}/\text{yr}$. The key question is then to find out when the model loses its capacity to drive pulsation modes.

Figure 5 illustrates some of our results. It shows the evolving distribution of Fe in the envelope of our representative model. The initial equilibrium distribution at the beginning of the simulation is the curve labelled “0.00” and highlighted, in part, by the heavy curve. We recall here that diffusive equilibrium is reached at a given shell when the outward radiative acceleration on an element can be equated to the downward effective gravitational acceleration. Because the radiative acceleration depends on the abundance of the element in question, the condition of equilibrium implies an abundance at a given depth which depends on the local conditions. Hence, the equilibrium abundance of a radiatively levitating element is a function of depth.

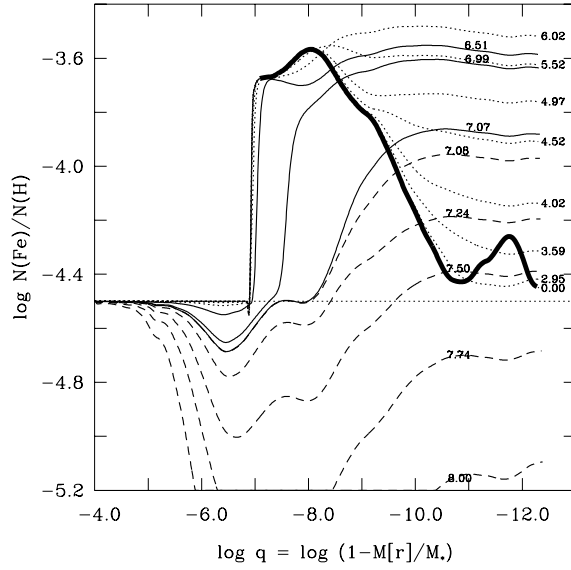


Fig. 5. Evolving distribution of iron in a representative sdB star model in the presence of a weak stellar wind. Only the envelope part of the stellar model is shown since the “action” is confined there. The heavy solid curve labelled “0.00” illustrates part of the initial distribution that is provided by the condition of diffusive equilibrium between gravitational settling and radiative levitation. Each curve is labelled by the logarithmic value of the time elapsed (in years) since the wind was turned on in the simulation. The dotted (solid) curves correspond to phases during which the Fe abundance in the driving region increases (decreases) while p -mode pulsations can be driven. The dashed curves, starting at an age of $10^{7.08}$ yrs, correspond to late phases when the Fe abundance in the driving region has dropped to values too small for pulsational driving to be possible.

As time goes by, the presence of a weak stellar wind progressively perturbs this equilibrium profile and, ultimately, the whole reservoir of levitating Fe is swept away. This is the case, for instance, for the profile labelled “8.00” that corresponds to the Fe distribution after 10^8 yrs of evolution. Thus, at the end of the simulation, the whole envelope becomes depleted of iron as compared to its normal value of $\log N(\text{Fe})/N(\text{He}) = -4.5$. On the other hand, there is an intermediate phase during which Fe pollution reaches its maximum across the outermost layers. This is shown by the profile obtained after $10^{6.02}$ yrs of evolution. After that phase, the abundance of Fe decreases monotonously throughout the envelope until the reservoir of levitating atoms is completely depleted.

In Fig. 5, the dotted and solid curves are associated with epochs when pulsational driving is possible. In fact, the model can drive a maximum number of modes precisely when Fe pollution is at a maximum in the driving region, i.e., after $10^{6.02}$ yrs of elapsed time in this particular simulation. After some $10^{7.08}$ yrs of evolution, however, the wind has done its damage and the model can no longer excite pulsation modes because the Fe abundance in the driving region has dipped below a critical level. The dashed curves thus correspond to epochs when the excitation of pulsation modes is no longer possible.

Fig. 5 also reveals the potential fate of the surface abundance of iron in a

sdB star in the context of a wind scenario. According to our simulation, pulsators should show some Fe enhancements in their atmospheres – but note that this is a strong function of $\log g$ and T_{eff} – while nonpulsators may show enhanced, normal, or depleted abundances depending on their age and the wind’s magnitude. This result has some important and unfortunate implications if the wind scenario that we have envisioned is realistic. Indeed, it may be difficult, if not impossible, to detect a spectroscopic signature that would discriminate between pulsating and nonpulsating sdB stars. This may be in line with the recent negative results reported from searches for a spectroscopic signature of pulsating sdB stars (e.g., Blanchette et al. (2006) and O’Toole et al., in preparation).

REFERENCES

- Baran A., Pigulski A., Kogiel D., Ogloza W., Silvotti R., Zola S. 2005, *MNRAS*, 360, 737
- Billères M., Fontaine G., Brassard P., Liebert J. 2002, *ApJ*, 578, 515
- Billères M., Fontaine G., Brassard P., Charpinet S., Liebert J., Saffer R. A., Vauclair G. 1997, *ApJ*, 487, L81
- Blanchette J.-P., Chayer P., Wesemael F. et al. 2006, *Baltic Astronomy*, 15, 301 (these proceedings)
- Charpinet S. 1999, Ph.D. thesis, Université de Montréal
- Charpinet S., Fontaine G., Brassard P. 2001, *PASP*, 113, 775
- Charpinet S., Fontaine G., Brassard P., Chayer P., Rogers F. J., Iglesias C. A., Dorman B. 1997, *ApJ*, 483, L123
- Charpinet S., Fontaine G., Brassard P. et al. 2006, *Baltic Astronomy*, 15, 305 (these proceedings)
- Chayer P., Fontaine G., Fontaine M., Lamontagne R., Wesemael F., Dupuis J., Heber U., Napiwotzki R., Moehler S. 2004, *Ap&SS*, 291, 359
- Fontaine G., Brassard P., Charpinet S., Green E. M., Chayer P., Billères M., Randall S. K. 2003, *ApJ*, 597, 518
- Fontaine G., Green E. M., Brassard P., Charpinet S., Chayer P., Billères M., Randall S. K, Dorman B. 2004, *Ap&SS*, 291, 379
- Green E. M., Fontaine G., Reed M. D., Callerame K., Seitzzahl I. R., White B. A., Hyde E. A., Østensen R., Cordes O., Brassard P., Falter S., Jeffery E. J., Dreizler S., Schuh S. L., Giovanni M., Edelmann H., Rigby J., Bronowska A. 2003, *ApJ*, 583, L31
- Hubeny I., Lanz T. 1995, *ApJ*, 439, 875
- Kilkenny D., Koen C., O’Donoghue D., Stobie R. S. 1997, *MNRAS*, 285, 640
- Kilkenny D., O’Donoghue D., Reed M. D. et al. 2006, *Baltic Astronomy*, 15, 317 (these proceedings)
- Lanz T., Hubeny Y. 1995, *ApJ*, 439, 905
- Oreiro R., Pérez Hernández F., Ulla A., Garrido R., Østensen R., MacDonald J. 2005, *A&A*, 438, 257
- Schuh S. L., Huber J., Green E. M., O’Toole S. J., Dreizler S., Heber U., Fontaine G. 2005, in 14th European Workshop on White Dwarfs, eds. D. Koester & S. Moehler, *ASP Conf. Ser.*, 334, 530

LINE-PROFILE VARIATIONS IN PULSATING SDB STARS AS A PULSATION MODE DIAGNOSTIC

C. Schoenaers and A. E. Lynas-Gray

Department of Physics, University of Oxford, Denys Wilkinson Building, Keble Road, Oxford OX1 3RH, U. K.

Received 2005 July 31

Abstract. In previous attempts to perform seismic modeling of pulsating subdwarf-B stars, various mode identification techniques are used with uncertain results. We investigated a method so far neglected in sdB stars, but very successful for main-sequence pulsators, i.e., mode identification from the line-profile variations caused by stellar pulsation. We report the calculation of time-resolved synthetic spectra for sdB stars pulsating with various combinations of pulsation modes; these calculations were carried out over appropriate ranges of effective temperature, surface gravity and helium abundances. Preliminary tests using these synthetic line-profile variations demonstrated their potential for mode identification by comparison with observations.

Key words: stars: hot subdwarfs – stars: oscillations

1. INTRODUCTION

Subdwarf B (sdB) stars are believed to be low-mass ($\sim 0.5M_{\odot}$) core helium burning objects belonging to the extreme horizontal branch (EHB) (Heber 1986). With thin and mostly inert hydrogen-rich residual envelopes, sdB stars remain hot ($20\,000 \leq T_{\text{eff}} \leq 40\,000$) and compact ($5 \leq \log g \leq 7$) throughout their EHB lifetime (Saffer et al. 1994); they eventually evolve towards the

white dwarf cooling sequence without experiencing the asymptotic giant branch and planetary nebula phases of evolution. While binary population synthesis calculations by Han et al. (2002, 2003) successfully demonstrate the formation of sdB stars through several possible channels, resulting models require further comparison with observation. As sdB stars are believed to be responsible for the ultraviolet-upturn seen in the energy distributions of elliptical galaxies and spiral galaxy bulges (Yi et al. 1997), understanding sdB star formation may provide an

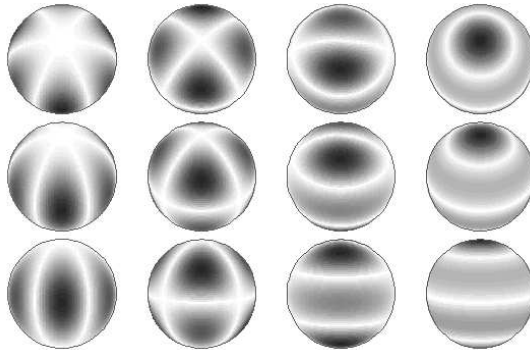


Fig. 1. $l = 3$ pulsation mode with m from 3 (left) to 0 (right) and i from 30° (top) to 90° (bottom) (GONG/NSO/AURA/NSF).

important diagnostic for studying galaxy evolution and formation.

The discovery (Kilkenny et al. 1997; Green et al. 2003) that some sdB stars are nonradial pulsators means asteroseismology could be used to discern their internal structure and so constrain evolution models. But before any seismic modeling can be reliably attempted one must identify pulsation modes which are excited.

Assuming radial and non-radial pulsations can be modeled by spherical harmonics Y_{nlm} , mode identification tries to assign values to the spherical wavenumbers n , l and m : n is related to the number of nodes of the radial displacement, l is the number of nodal lines on the stellar surface and m is the number of such lines passing through the rotation axis of the star, as shown in Figure 1.

2. THE PROBLEM OF MODE IDENTIFICATION IN SDB STARS

Mode identification in sdB stars is far from being trivial. Several methods which prove efficient for mode identification in pulsating main-sequence stars have limitations in the case of sdB stars. Nevertheless, these mode identification techniques, however uncertain, are used in meritorious attempts at seismic modeling of the most promising pulsating sdB stars.

2.1. Period fitting

The method entails fitting an observed period spectrum of a pulsating star to a theoretical period spectrum and is straightforward in principle. However, when considering pulsating sdB stars there is a major difficulty to overcome (Brassard et al. 2001): so far, most sdB stars (except for PG 1605+072 with more than 50 periods (Koen et al. 1998) and KPD 1930+2752 with at least 44 periods (Billères et al. 2000)) have a rather sparse period spectrum, possibly because lower amplitude frequencies are not yet observed. This makes it very difficult to match objectively observed periods with periods computed from a model, as the latter are much more numerous.

Despite the intrinsic difficulty of period fitting in sdB stars, Brassard et al. (2001) use this technique to model the pulsating sdB star PG 0014+067 and tentatively identify 23 distinct pulsation modes. They search a four-parameter space (T_{eff} , $\log g$, the mass of the star M_* and the mass of its H-rich envelope M_{env}) for a model whose theoretical period spectrum could account for the observed periods in PG 0014+067, using a “merit” function that is minimum for the best fit(s). In addition to the four parameters, they also deduce the rotation velocity of the star and other properties (see their Table 6). They claim a good agreement with previous spectroscopic determination of T_{eff} and $\log g$, but we note that in order to discriminate between equally good fits (several minima of their merit function) they use spectroscopic constraints. More recently, the same method is applied by Charpinet et al. (2005) to PG 1219+534.

2.2. Amplitude ratios

Yet another method in use for mode identification in pulsating main-sequence stars relies on multicolor photometry. This method, known as the amplitude ratio method (Heynderickx et al. 1994), relies on the fact that for non-radially pulsating stars the photometric pulsation amplitude depends on wavelength and on the spherical wavenumber l of the pulsation mode. Ramachandran et al. (2004) investigate this method for non-radially pulsating sdB stars and draw the following

conclusions.

- For EC 14026 stars, only the modes of high l (3 and 4) should be easy to disentangle, provided their amplitudes are large enough to observe. On the other hand, low degree modes are very difficult to distinguish, and this problem becomes worse as the period shortens.

- For “Betsy” stars, modes of spherical degree $l = 1$ may be difficult to distinguish from modes with $l > 1$ in the case of longer periods.

Using ULTRACAM multicolor photometry, Jeffery et al. (2004, 2006) use the amplitude ratio method to identify pulsation modes of three sdB stars, HS 0039+4302, KPD 2109+4401 and PG 0014+067. Their results are provisional, as only statistical errors are taken into account.

3. LINE-PROFILE VARIATIONS IN PULSATING SDB STARS

We saw in the previous section that current mode identification methods in sdB stars need improvement. However none of these techniques use spectroscopy to perform mode identification, although it has proved useful when modeling pulsating main-sequence stars (e.g., Aerts et al. 1992; Briquet & Aerts 2003). Our claim is that spectroscopy, and the pioneering detailed computation of line-profile variations (lpv) we perform, could provide a more reliable mode identification method. Indeed, lpv enable a complete reconstruction of the non-radial oscillations of a star, provided that a time-series of spectra are observed with a high enough S/N ratio, temporal and wavelength resolution.

3.1. Computation of synthetic line-profile variations

The method used for our computation of theoretical line-profile variations is quite straightforward. We combined three computer programs, BRUCE (Townsend 1997), SYNSPEC (Hubeny & Lanz 2000) and KYLIE (Townsend 1997), so as to compute a series of time-resolved spectra exhibiting line-profile variations.

BRUCE first divides the stellar surface into a large number of very small surface elements that are determined by the usual polar and azimuthal coordinate angles θ and φ and a step-size $\Delta\theta$ and $\Delta\varphi$. BRUCE then perturbs the stellar surface, assuming the pulsation is linear and adiabatic, with selected combinations of pulsation modes at selected time steps, giving for each surface element its temperature, surface gravity, orientation, projected radial velocity and projected area.

It is important to realize that, because of the pulsation, different points on the stellar surface not only have different radial velocity, but also different temperature, $\log g$ and orientation, meaning that the contributions of the different surface elements to the line-profile have different amplitudes and energy distributions. The line-profile variations do not only come from the Doppler shift in wavelength, but also from the complex temperature and $\log g$ behavior on the stellar surface.

The emergent monochromatic flux in wavelength interval $\Delta\lambda$, at some wavelength λ and time t is then given by

$$F_\lambda(t) = \sum_{i,j} I_\lambda(t)_{ij} \mu(t)_{ij} \sin \theta_i \Delta\theta_i \Delta\varphi_j, \quad (1)$$

where $I_\lambda(t)_{ij}$ is the specific intensity emergent from the tile at θ_i and φ_j in wavelength interval $\Delta\lambda$, at wavelength λ and time t , in the direction of the observer,

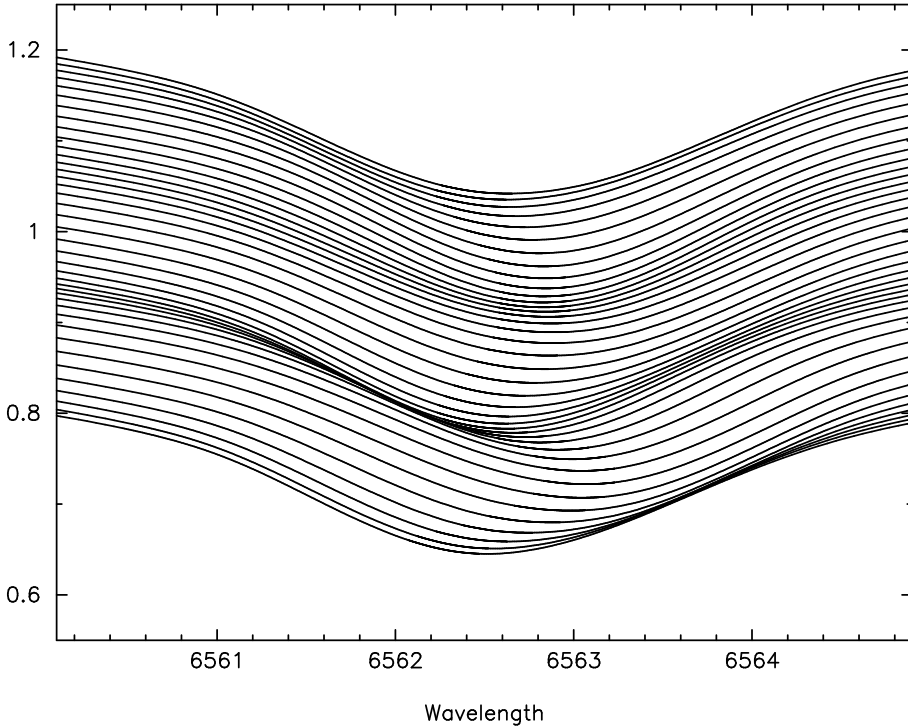


Fig. 2. Trial computation of H_α line-profile variations for the short-period pulsator PG 1605+072. Only the six highest-amplitude pulsation modes (out of more than 50) were taken into account in this computation in order to reduce computing time. The line-profiles have been shifted along the ordinate axis (normalized flux) for clarity.

as computed by our modified version of SYNSPEC. The quantity

$$\mu(t)_{ij} \equiv \vec{n}(t)_{ij} \cdot \vec{s}$$

accounts for the time-dependent orientation of each tile, $\vec{n}(t)_{ij}$ being the normal to the tile at some time t , and \vec{s} being the direction of propagation of the radiation.

This is then repeated for the desired number of time-steps using KYLIE, therefore producing series of time-resolved observer-directed spectra. Examples of line-profile variations computed with our codes are given for different modes in Figures 2 and 3.

3.2. Observation of line-profile variations in pulsating sdB stars

Observations of line-profile variations in sdB stars have been made by Telting & Østensen (2004) who observed PG 1325+101 with the 2.5 m NOT telescope. Their observations showed strong evidence for a dominant radial pulsation mode, but most importantly drew attention to the potential of spectroscopic mode identification. Similar observations were made of the bright sdB star Balloon 090100001 (Telting et al. 2006).

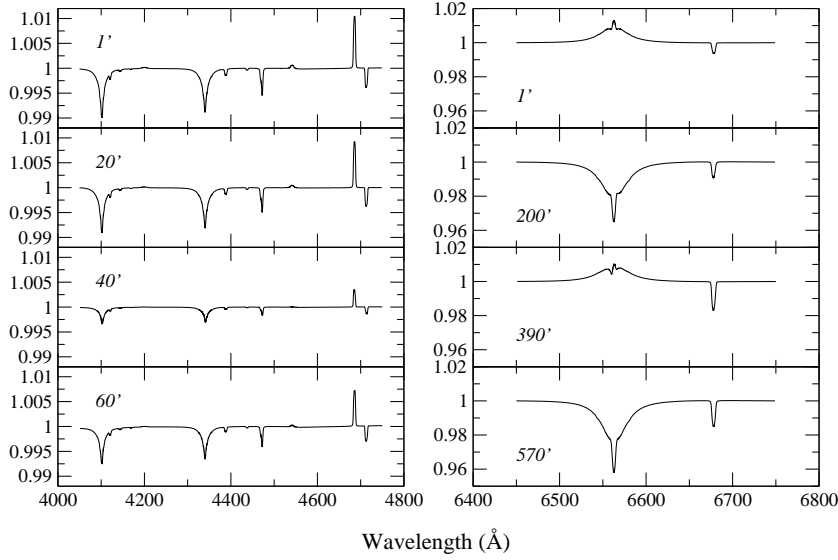


Fig. 3. A time series of 1 Å resolution synthetic spectrum ratios for PB 8783 (short-period pulsator) and EC 21324-1346 (long-period pulsator) in left and right frames respectively. Second and subsequent synthetic spectra in each time-series are divided by the first, the elapsed time being given in minutes. Time-series calculations were based on assumed pulsation modes ($l = 3, m = 0; l = 2, m = 0; l = 1, m = 0; l = 2, m = 1; l = 3, m = 0$) and velocity amplitudes from Jeffery & Pollacco (2000) for PB 8783 and on modes ($l = 1, m = 1; l = 2, m = 1; l = 3, m = 0$) and amplitudes to match photometric variations of EC 21324-1346.

4. THE MOMENT METHOD AND ITS APPLICATION TO SDB STARS

4.1. The moment method

Mode identification from line-profile variations could in principle be carried out by a direct comparison of observed and synthetic spectra, but we propose to adapt to pulsating sdB stars the so-called *moment method*. It was first introduced by Balona (1986a,b, 1987) and later refined and applied to main-sequence pulsators by Aerts et al. (1992), Aerts (1996) and Briquet & Aerts (2003).

In this method, an observed line-profile is replaced by its first few moments, and their time dependence studied to identify the pulsation modes. The n th moment of a line-profile $p(v)$ (where v is the line-of-sight velocity component corresponding to the displacement from the laboratory wavelength) is defined as

$$\langle v^n \rangle \equiv \frac{\int_{-\infty}^{+\infty} v^n p(v) dv}{\int_{-\infty}^{+\infty} p(v) dv}. \quad (2)$$

All the information contained in the line-profile can be reconstructed from the entire series of moments of n th order, but Briquet & Aerts (2003) showed that most of the information is contained in the first three moments:

- the first moment $\langle v \rangle$ is the centroid of the line-profile in a reference frame with origin at the stellar center;

- the second moment $\langle v^2 \rangle$ is related to the variance of the line-profile;
- the third moment $\langle v^3 \rangle$ relates to the skewness of the profile (see also Telting 2003).

Once the moments of the observed line-profile have been computed, their variations are compared with the time-dependence of theoretical moments (Aerts 1992). These depend on the wavenumbers l and m of the pulsation mode, but also on its amplitude v_p , on the inclination i of the star's axis of rotation to the observer, on its rotation velocity v_Ω and on the width σ of the intrinsic broadening profile, allowing a complete reconstruction of non-radial pulsation. One then selects the most likely set of parameters $(l, m, v_p, i, v_\Omega, \sigma)$ by minimizing a so-called discriminant (Briquet & Aerts 2003), which is a function that takes into account the quality of the fit between the theoretical and observed moments.

In Figure 4 we show the three normalized moments for a synthetic radial mode we computed. Even without computing the discriminant, the phase-dependence of the observed moments can provide some useful information. For instance

- the peak-to-peak amplitude of the first moment gives an idea about the overall velocity range due to the oscillation;
- if $\langle v^2 \rangle$ can be described by a single sine function with twice the frequency of the first moment it means that $m = 0$, while if the mode is sectoral ($|m| = l$) $\langle v^2 \rangle$ behaves sinusoidally with the same frequency as the frequency of the first moment.

4.2. Application to pulsating sdB stars

The major difficulty to overcome in order to apply the moment method to pulsating sdB stars comes from its current formulation (Briquet & Aerts 2003) in which the moment method neglects the variation of the specific intensity (i.e., $\delta I_\lambda(\theta_i, \varphi_j) = 0$) due to changes in T_{eff} and $\log g$ during the pulsation. This can be a good approximation when dealing with spectral lines that are not sensitive to temperature variations (such as silicon lines in β Cephei stars (Dupret et al. 2002 and De Ridder et al. 2002)) but in the case of sdB stars, temperature effects should not be neglected.

We tested the moment method in its current formulation on lpv of H α for various pulsation modes, but the identification was not always satisfactory. However it was extremely difficult to choose a suitable wavelength range over which the moments were to be computed. We are investigating a systematic way to make that

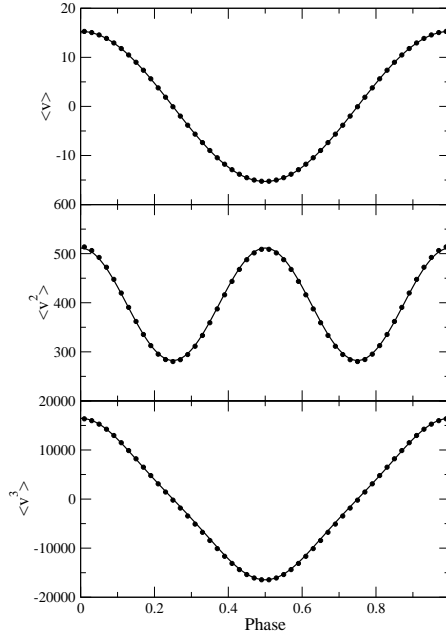


Fig. 4. First, second and third moments for the synthetic line profile of a radial mode computed using our codes.

choice, as well as whether the use of the narrower and much weaker helium lines might improve the mode identification. Another possibility is to take temperature effects into account using the higher-order moments, as Balona (1987) suggests.

5. FUTURE PROSPECTS

Our development of spectroscopic methods for pulsation mode identification in sdB stars was stimulated by the acquisition of observational data. A start on this was made in 2005 August using the South African Astronomical Observatory 1.9 m telescope to obtain time-resolved spectroscopy of “Betsy” stars (Schoenaers & Lynas-Gray 2006).

Furthermore, Kawaler & Hostler (2005) show internal rotation to be expected in sdB stars, the rate depending on distance from the stellar center. Mode splitting due to internal rotation cannot be identified using the usual formula applicable in the case of surface rotation and may have led to incorrect mode identification in previous works. Special attention therefore needs to be given to the modeling of this effect in pulsating sdB stars, even though the moment method should not be affected much by differential rotation, contrarily to period fitting.

However, mode identification in pulsating sdB stars is a real challenge with the methods discussed above. Other methods might prove worth investigating.

The so-called IPS method aims at comparing the observed amplitude and phase variations across the line-profile with the theoretical variations (Schrijvers et al. 1997 and Telting & Schrijvers 1997a, b). It was recently used by De Cat et al. (2005) to identify pulsation modes in monoprotic SPB (slowly pulsating B) stars, together with the method of photometric amplitude ratios and the moment method (with moments up to the sixth order).

Yet another mode identification method, Doppler Imaging, should be investigated. The method is based on the idea that line-profile variations of rapidly rotating stars are a sort of “doppler image” of the stellar surface within the line-profile. This method has been challenged because of its apparent lack of physical foundation, but Kochukhov (2004) claims a reliable recovery of the surface pulsation velocity structures can be achieved for all types of pulsation geometries accompanied by significant line-profile variations. It remains to be seen whether the line-profile variations in sdB stars are large enough.

To summarize, this paper presents several options for meeting the challenge presented by sdB star pulsation mode identification by spectroscopic methods. All appear to be worthy for further investigation, and the progress made to date is briefly summarized.

ACKNOWLEDGMENTS. The authors are indebted to Conny Aerts for a stimulating discussion, to John Telting for his valuable comments as referee and the University of Oxford, Department of Physics, for travel grants.

REFERENCES

- Aerts C. 1996, *A&A*, 314, 115
- Aerts C., de Pauw M., Waelkens C. 1992, *A&A*, 266, 294
- Balona L. A. 1986a, *MNRAS*, 219, 111
- Balona L. A. 1986b, *MNRAS*, 220, 647

- Balona L. A. 1987, MNRAS, 224, 41
- Billères M., Fontaine G., Brassard P. et al. 2000, ApJ, 530, 441
- Brassard P., Fontaine G., Billères M. et al. 2001, ApJ, 563, 1013
- Briquet M., Aerts C. 2003, A&A, 398, 687
- Charpinet S., Fontaine G., Brassard P., Green E., Chayer P. 2005, A&A, 437, 575
- De Cat P., Briquet M., Daszynska-Daszkiewicz J. et al. 2005, A&A, 432, 1013
- De Ridder J., Dupret M.-A., Neuforge C., Aerts C. 2002, A&A, 385, 572
- Dupret M.-A., De Ridder J., Neuforge C., Aerts C. 2002, A&A, 385, 563
- Green E. M., Fontaine G., Reed M. D. et al. 2003, ApJ, 583, L31
- Han Z., Podsiadlowski Ph., Maxted P. F. L., Marsh T. R. 2003, MNRAS, 341, 669
- Han Z., Podsiadlowski Ph., Maxted P. F. L., Marsh T. R., Ivanova N. 2002, MNRAS, 336, 449
- Heber U. 1986, A&A, 155, 33
- Heynderickx D., Waelkens C., Smeyers P. 1994, A&AS, 105, 447
- Hubeny I., Lanz T. 2000, <http://tlusty.gsfc.nasa.gov/Synspec43/synspec.html>
- Jeffery C. S., Aerts C., Dhillon V. S., Marsh T. R. 2006, Baltic Astronomy, 15, 259 (these proceedings)
- Jeffery C. S., Dhillon V. S., Marsh T. R., Ramachandran B. 2004, MNRAS, 352, 699
- Jeffery C. S., Pollacco D. 2000, MNRAS, 318, 974
- Kawaler S. D., Hostler S. R. 2005, ApJ, 621, 432
- Kilkenny D., Koen C., O'Donoghue D., Stobie R. S. 1997, MNRAS, 285, 640
- Kochukhov O. 2004, A&A, 423, 613
- Koen C., O'Donoghue D., Kilkenny D. et al. 1998, MNRAS, 296, 317
- Ramachandran B., Jeffery C. S., Townsend R. H. D. 2004, A&A, 428, 209
- Saffer R. A., Bergeron P., Koester D., Liebert J. 1994, ApJ, 432, 351
- Schoenaers C., Lynas-Gray A. E. 2006, MNRAS (in preparation)
- Schrijvers C., Telting J. H., Aerts C., Ruymaekers E., Henrichs H. F. 1997, A&AS, 121, 343
- Telting J. H. 2003, Ap&SS, 284, 85
- Telting J. H., Østensen R. H. 2004, A&A, 419, 685
- Telting J. H., Østensen R. H., Heber U., Augusteijn T. 2006, Baltic Astronomy, 15, 235 (these proceedings)
- Telting J. H., Schrijvers C. 1997a, A&A, 317, 723
- Telting J. H., Schrijvers C. 1997b, A&A, 317, 742
- Townsend R. H. D. 1997, *Ph. D. Thesis*, University College London
- Yi S., Demarque P., Oemler A. 1997, ApJ, 486, 201

BALLOON 090100001: A LINK BETWEEN THE TWO CLASSES OF PULSATING HOT SUBDWARFS

A. Baran^{1,2}, R. Oreiro^{3,4}, A. Pigulski⁵, F. Pérez Hernández^{3,4} and A. Ulla⁶

¹ *Mt. Suhora Observatory, Cracow, Poland*

² *Torun Centre for Astronomy, Torun, Poland*

³ *Instituto de Astrofísica de Canarias, Tenerife, Spain*

⁴ *Universidad de La Laguna, Tenerife, Spain*

⁵ *Instytut Astronomiczny, Uniwersytet Wrocławski, Poland*

⁶ *Departamento Física Aplicada, Universidad de Vigo, Spain*

Received 2005 July 29

Abstract. We present results of photometric observations of the high-amplitude EC 14026-type star, Balloon 090100001. The data were obtained in broad-band *B* filter and span over five weeks, consisting of about 150 hours of observations. Fourier analysis of these data led us to the detection of at least 50 modes of pulsation, out of which 37 are independent. The frequencies of 22 detected modes are in the region of pulsations of EC14026-type stars, theoretically attributed to *p*-modes, and cluster into four narrow ranges, around 2.8, 3.8, 4.7 and 5.5 mHz, where the radial fundamental mode, the first, second and third overtones are likely to occur. Surprisingly, we also detect 15 independent modes in the low-frequency domain, between 0.1 and 0.8 mHz. These modes are typically found in PG 1716+426-type stars, recently discovered among cool B-type subdwarfs, and theoretically attributed to high-order *g*-modes. As both kinds of oscillations are observed in Balloon 090100001, it represents a link between the two classes of pulsating hot subdwarfs. At present, it is probably the most suitable target for testing evolutionary scenarios and internal constitution models of these objects by means of asteroseismology. Three of the modes we detect form an equidistant frequency triplet which can be explained by invoking rotational splitting of an $\ell = 1$ mode.

Key words: stars: oscillations – stars: individual: Balloon 090100001

1. INTRODUCTION

Balloon 090100001 (BA09) was found to be an sdB star by Bixler et al. (1991). Although it is one of the brightest sdB stars its pulsational nature was discovered only recently by Oreiro et al. (2004). Owing to a very short run, the authors were able to extract only two independent modes and the first harmonic of the main mode. Beside these three peaks, they noted a small signal around 0.3 mHz, whose appearance was surprising for an EC14026 star. With a *B* magnitude of 11.8, periods around 300 s and amplitude up to 50 mmi for the main mode, this

EC14026 object turned out to be an excellent candidate for follow-up photometry.

2. OBSERVATIONS

BA09 was re-observed independently by two of us (A.B. and R.O.) in 2004 August and September. A.B. used a SBIG ST-10XME CCD camera attached to a 60 cm telescope at Mt. Suhora Observatory. Johnson-Cousins *UBVR* filters were used. R.O. employed the TCP instrument on the 80 cm IAC80 telescope. Only a *B* filter was used in this case, allowing a cycle time of 10 s. Results of the analysis of these data are published separately (Baran et al. 2005; Oreiro et al. 2005). Some time later, we combined our *B* filter data and made a common FT analysis. The light curve of our combined data is presented in Figure 1. In this way we improved the spectral window (Figure 2), but the difference is not significant since our sites are located at similar longitude, and the observations were not simultaneous.

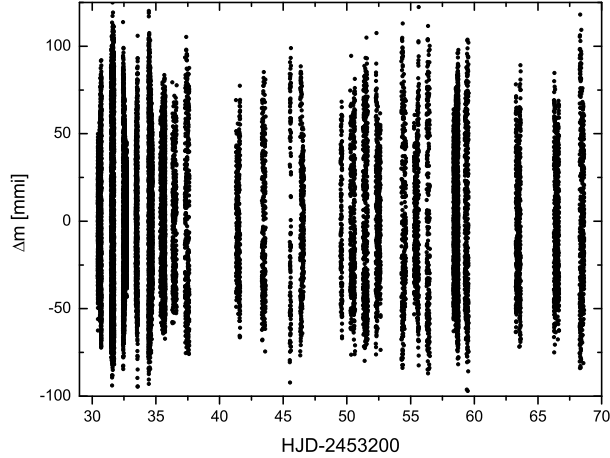


Fig. 1. Light curve from Tenerife and Poland.

3. PERIODOGRAM ANALYSIS

Figure 3 shows the Fourier spectrum for non prewhitened data. Note that the highest peak (with an amplitude of 53 mma) is truncated in order to better view the signal with lower amplitudes. At first look, seven groups of peaks can be distinguished (not all of them turned out to be real). Down to S/N about 7 we revealed 50 frequencies, which are listed in Table 1. Frequencies f_2 , f_3 , f_4 form an equally spaced triplet. If we assume they are due to rotational splitting of an $\ell = 1$ mode, with $C_{nl} = 1$ then a rotation period of 7.1 days is derived. Despite the large data set we still have an aliasing problem, and in a few cases we were not able to distinguish correctly between a real mode and its aliases. In

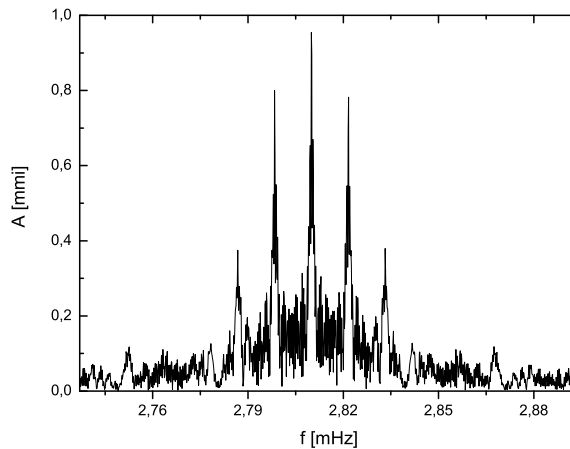


Fig. 2. Spectral window resulting from the Poland-Tenerife combined data.

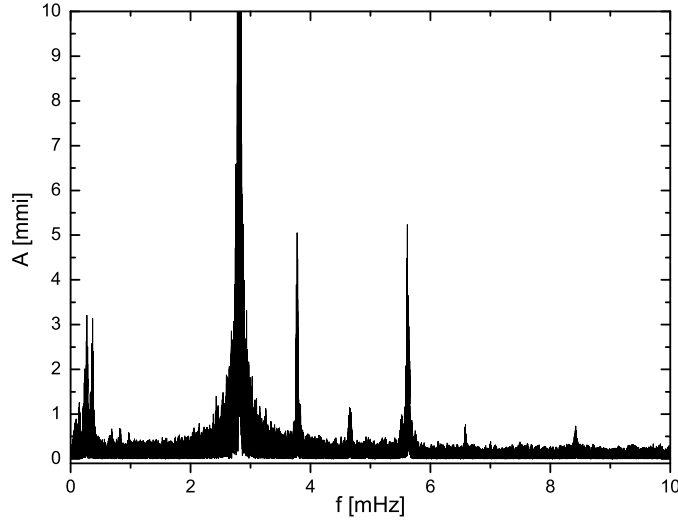


Fig. 3. Amplitude spectrum calculated on joined data.

Figure 4 residuals out of 50 frequencies subtracted are shown. As can be seen there are still many peaks that could be real, but this can be verified only with data of better quality.

4. 2005 CAMPAIGN

In order to get such a higher quality set of data, we are arranging for the summer of 2005 a simultaneous photometric and spectroscopic campaign on BA09. The official web page can be found at <http://webpages.uillinois.edu/users/raquelor>, where the relevant information on the campaign is posted. Some photometric and spectroscopic sites have already agreed to participate although for some of them the observing time has not yet been awarded. All observatories but one will use CCD cameras with a *B* filter. Two sites will use multicolor photometry, so we will be able to compare amplitudes from two seasons. With these new data we will also make an attempt to identify the pulsational modes in BA09. In particular, the method which uses spectroscopy and multicolor information, described in detail in Daszynska-Daszkiewicz (2003), will be used for that purpose.

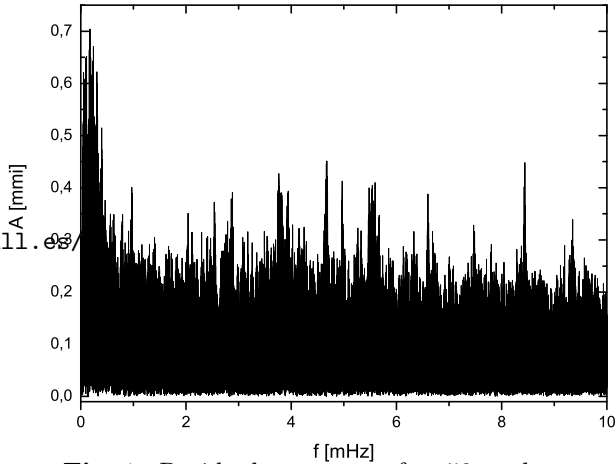


Fig. 4. Residual spectrum after 50 peaks subtracted.

Table 1. Frequencies, amplitudes and phases of the prewhitened peaks from the Poland–Tenerife combined data. Letter (number) subscripts refer to g-mode (p-mode) frequencies

| | Freq. (mHz) | Ampl. (mma) | Phase | | Freq. (mHz) | Ampl. (mma) | Phase |
|----------|----------------|----------------|-------|--------------|----------------|----------------|-------|
| f_A | 0.2724 | 2.886 | 2.646 | f_{11} | 3.7918 | 1.143 | 2.906 |
| f_B | 0.3658 | 2.708 | 2.843 | f_{12} | 3.7867 | 1.223 | 3.091 |
| f_C | 0.2400 | 1.848 | 1.228 | f_{13} | 3.8229 | 0.827 | 2.353 |
| f_D | 0.3257 | 1.092 | 4.600 | f_{14} | 4.6511 | 0.768 | 5.712 |
| f_E | 0.2463 | 0.970 | 3.013 | f_{15} | 4.6761 | 0.967 | 6.135 |
| f_F | 0.1451 | 0.874 | 5.569 | f_{16} | 4.6591 | 0.882 | 2.447 |
| f_G | 0.2110 | 0.987 | 4.646 | f_{17} | 4.6686 | 0.760 | 3.257 |
| f_H | 0.3312 | 1.067 | 5.106 | f_{18} | 4.6421 | 0.621 | 5.684 |
| f_I | 0.0904 | 0.888 | 5.794 | f_{19} | 4.6614 | 0.648 | 6.005 |
| f_J | 0.2989 | 0.822 | 6.040 | f_{20} | 5.5329 | 0.770 | 4.097 |
| f_K | 0.1356 | 0.828 | 0.479 | f_{21} | 5.4944 | 0.623 | 5.903 |
| f_L | 0.2480 | 0.815 | 4.578 | f_{22} | 5.5551 | 0.626 | 5.759 |
| f_M | 0.6844 | 0.702 | 5.466 | $f_1 - f_B$ | 2.4417 | 0.739 | 0.429 |
| f_N | 0.8331 | 0.623 | 4.416 | $f_1 - f_D$ | 2.4818 | 0.404 | 4.933 |
| f_O | 0.6311 | 0.492 | 0.568 | $f_1 + f_1$ | 5.6149 | 5.930 | 4.560 |
| f_1 | 2.8075 | 53.101 | 3.030 | $f_1 + f_2$ | 5.6307 | 4.496 | 4.609 |
| f_2 | 2.8232 | 20.539 | 3.061 | $f_1 + f_3$ | 5.6323 | 2.785 | 2.150 |
| f_3 | 2.8248 | 12.075 | 0.603 | $f_1 + f_4$ | 5.6338 | 0.970 | 3.695 |
| f_4 | 2.8264 | 4.800 | 2.069 | $f_2 + f_3$ | 5.6480 | 0.709 | 1.882 |
| f_5 | 2.8539 | 1.665 | 1.208 | $f_2 + f_2$ | 5.6465 | 0.719 | 4.458 |
| f_6 | 2.8557 | 1.212 | 4.244 | $f_2 + f_4$ | 5.6496 | 0.441 | 4.462 |
| f_7 | 2.8585 | 1.140 | 5.084 | $f_1 + f_9$ | 6.5835 | 0.684 | 4.891 |
| f_8 | 2.8250 | 0.901 | 2.605 | $2f_1 + f_1$ | 8.4224 | 0.846 | 0.031 |
| f_9 | 3.7761 | 4.572 | 3.694 | $2f_1 + f_2$ | 8.4381 | 0.523 | 6.051 |
| f_{10} | 3.7956 | 1.111 | 1.421 | $2f_1 + f_3$ | 8.4397 | 0.458 | 3.847 |

ACKNOWLEDGMENTS. R.O. acknowledges Gobierno de Canarias for its financial support. This work received financial support from the Spanish MCyT under grant AYA2003-09499.

REFERENCES

- Baran A. et al. 2005, MNRAS, 360, 737
 Bixler J. V., Bowyer S., Laget M. 1991, A&A, 250, 370
 Daszynska-Daszkiewicz J. et al. 2003, A&A, 407, 999
 Oreiro R. et al. 2004, A&A, 418, 243
 Oreiro R. et al. 2005, A&A, in press

MORE NEW SDB PULSATORS DISCOVERED WITH THE NORDIC OPTICAL TELESCOPE [†]

J.-E. Solheim¹ and R. Østensen²

¹ *Institutt for Teoretisk Astrofysikk, Box 1029 Blindern, N-0315 Oslo, Norway*

² *Isaac Newton Group, E-37800 Santa Cruz de La Palma, Canary Islands, Spain*

Received 2005 August 26

Abstract. We report briefly the results from a continuation of the NOT search program for pulsating sdB stars. During this period we have observed 45 candidates and found three new short period pulsating sdB stars. Two of the new pulsators were selected based on spectroscopy from the Sloan Digital Sky Survey, while the third is a PG object. All the stars have periods in the range 120–140 s, typical for short period subdwarf B pulsators, and the detected pulsation amplitudes are all relatively low, between 0.3 and 0.7 %.

Key words: stars: hot subdwarfs – stars: oscillations – stars: individual (PG 1419+081, SDSS J 1445+0002, SDSS J 1642+4252)

1. INTRODUCTION

A search program for new sdB pulsators was conducted with the Nordic Optical Telescope (NOT) in the years 1999–2001. In total ten pulsators were found among candidates selected from the HS, HE and PG surveys. Additionally, one pulsator was found in a small SDSS sample observed in 2002 October (Solheim et al. 2004). Here we report the results of a continuation of the NOT search program in 2004 and 2005. Candidates were selected from sdB stars with T_{eff} between 27 000 and 37 000 K, with preliminary T_{eff} determined from SDSS spectra or taken from literature sources.

2. OBSERVATIONS

The program was granted observing time 2004 June 4–9 and 2005 February 15–20. The first run had mostly clear weather, but the second was totally lost due to heavy snow at the observatory. In the 2004 run 45 candidates were observed and three new pulsators were detected. They are PG 1419+081 and two new sdB

[†]Based on observations made with the Nordic Optical Telescope, operated on the island of La Palma jointly by Denmark, Finland, Iceland, Norway and Sweden, in the Spanish Observatorio del Roque de los Muchachos of the Instituto de Astrofísica de Canarias. The data presented here have been taken using ALFOSC, which is owned by the Instituto de Astrofísica de Andalucía (IAA) and operated at the Nordic Optical Telescope under agreement between IAA and the NBIFAFG of the Astronomical Observatory of Copenhagen.

Table 1. Time series photometry. The length of each run is the number of cycles N times the cycle time.

| Object | Date (2004) | Observers | Start (UT) | N | Cycle (s) |
|---------------------------|----------------|--------------|---------------|-----|--------------|
| PG 1419+081 | June 8 | J.E.S., R.Ø. | 21:56 | 128 | 30 |
| SDSS J 144514.93+000249.0 | June 6 | J.E.S., R.Ø. | 00:27 | 137 | 30 |
| | June 7 | J.E.S., R.Ø. | 23:57 | 121 | 30 |
| SDSS J 164214.21+425234.0 | June 6 | J.E.S., R.Ø. | 02:22 | 220 | 20 |
| | June 9 | J.E.S. | 01:48 | 181 | 20 |

Table 2. Detected periods and amplitudes for the three new pulsators. The last column gives the one-sigma noise level found in the amplitude spectrum when avoiding the region between 7 and 9 mHz.

| Object | Date (2004) | P_1 | P_2 (s) | P_3 | A_1 | A_2 (mma) | A_3 | σ (mma) |
|-------------|----------------|-------|--------------|-------|-------|----------------|-------|-------------------|
| PG 1419+081 | June 8 | 144 | 136 | | 7.3 | 2.3 | | 0.7 |
| J 1445+0002 | June 6 | 119 | 124 | 142 | 7.7 | 6.2 | 4.8 | 0.9 |
| | June 7 | 118 | 126 | 142 | 5.7 | 4.5 | 4.4 | 0.8 |
| J 1642+4252 | June 6 | 138 | 130 | | 3.3 | 1.9 | | 0.4 |
| | June 9 | 138 | | | 3.4 | | | 0.5 |

stars from the SDSS survey, which we refer to as J 1445+0002 and J 1642+4252. The log of observations for these three stars is given in Table 1, together with the full designations for the two SDSS stars.

PG 1419+081 ($V = 15.1$) was classified as a subdwarf (sd) in the PG catalogue (Green et al. 1986) and as an sdB in the BPS catalogue (BPS CS 22883-25; Beers et al. 1992). The $\log(T_{\text{eff}}) = 4.53$ given in the BPS catalogue was based on UBV photometric observations only and has a large associated error (10%). No new spectroscopy has been obtained yet, but it is worth noting that 2MASS photometry indicates IR excess ($J-H = +0.28$), compatible with an F-G class main-sequence companion.

The SDSS stars have magnitudes $g' = 17.34$ for J 1445+0002 and $g' = 15.68$ for J 1642+4252. Both show IR excess from 2MASS photometry ($J-H = +0.15$ and $+0.19$, respectively), and their spectra also show signs of contamination from a cool companion (Ca II, Mg I and Na D lines). Model fits to the SDSS spectroscopy of these stars give effective temperatures of 37 650 and 33 900 K, respectively, but these fits are quite uncertain due to the contamination from the main-sequence companion. J 1445+0002 displays the He II 4686 Å line making it an sdOB star, which is consistent with the relatively high temperature, but we note that such a high temperature has not been seen in any other pulsating sdOB star yet, so it is probably an artifact introduced by the contamination, and we estimate that the true temperature could be lower by as much as 10%.

The time-series observations were all done with ALFOSC in the windowed readout mode as described in Solheim et al. (2004). The observing log for the new pulsating objects is shown in Table 1.

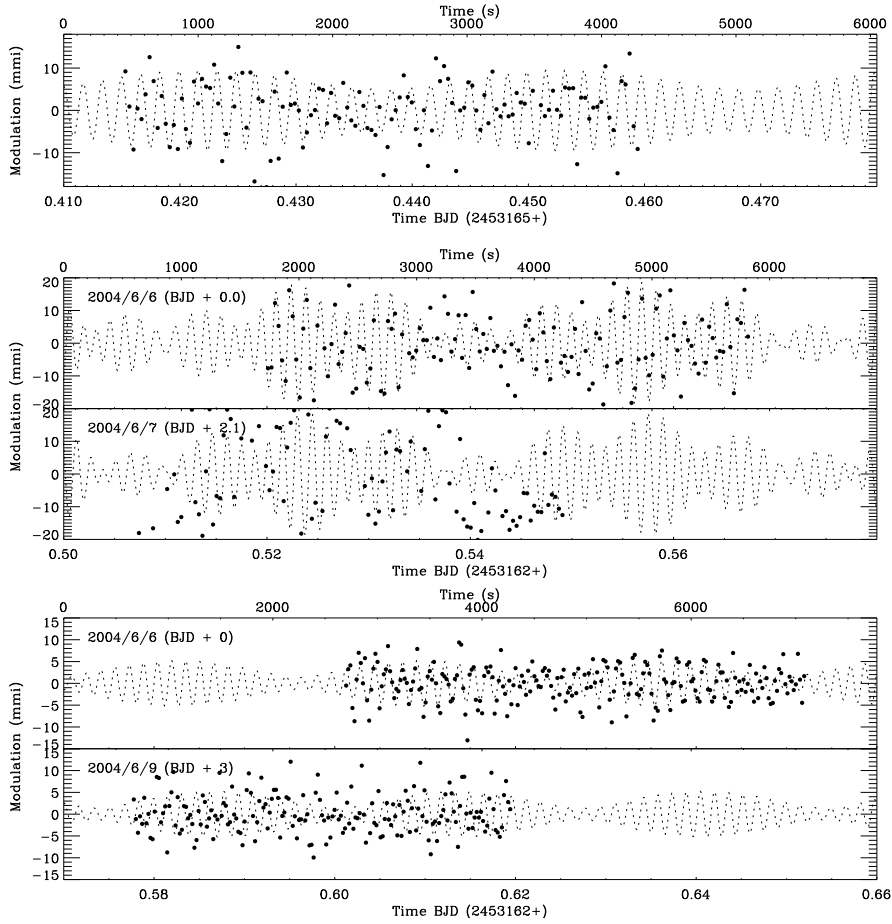


Fig. 1. The observed light-curves of the three new pulsators. Top panel: PG 1419+081; Middle panel: J 1445+0002; Lower panel: J 1642+4552. The dotted lines show the oscillations associated with the detected periods.

3. RESULTS

The three new pulsators show low amplitude pulsations with periods between 118 and 142 s, typical for most other known EC 14026 pulsators. The light-curves are shown in Figure 1, and their Fourier transforms in Figure 2.

For PG 1419+081 we have only one short run which shows one clear peak at 144 s and a second barely above the 3σ detection limit.

The Fourier transforms of the two light-curves of J 1445+0002 both show rich amplitude spectra with three clearly detected periods on the first night, all confirmed on the second run 46 hours later.

J 1642+4552 is the lowest amplitude pulsator, with the strongest peak at 138 s and an amplitude of 3.4 mma. The first night we detected also a second peak at 130 s, but this was below the detection limit the second run.

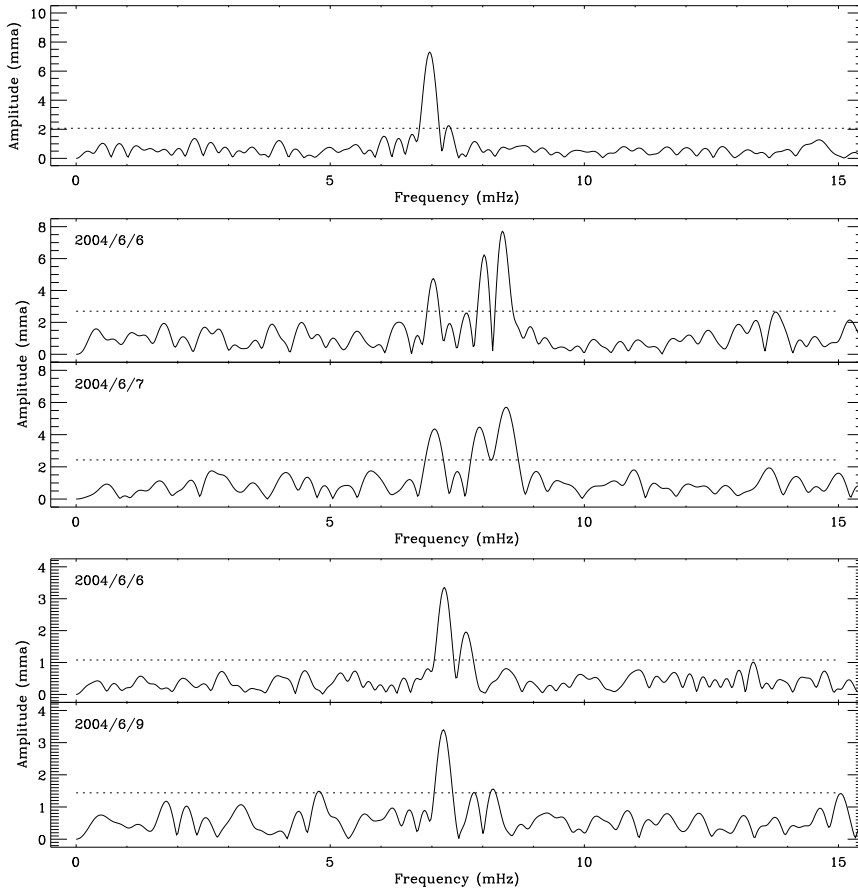


Fig. 2. The Fourier transforms of the light-curves of the three new pulsators. Top panel: PG 1419+081; Middle panel: J 1445+0002; Lower panel: J 1642+4552. The dotted lines indicate three times the noise level as given in Table 2.

4. CONCLUSIONS

We have presented the discovery data for three new short period sdB pulsators. With these three pulsators, the total no of EC 14026 pulsators has now reached 36. All these sdB stars show evidence of having a main-sequence companion, as has been seen with about half of all short period pulsators discovered to date.

REFERENCES

- Beers T. C., Preston G. W., Schectman S. A. et al. 1992, AJ, 103, 267
 Green R. F., Schmidt M., Liebert J. 1986, ApJS, 61, 305
 Solheim J.- E., Østensen R., Silvotti R., Heber U. 2004, Ap&SS, 291, 419

TIME-RESOLVED SPECTROSCOPY OF THE BRIGHT sdBV STAR BALLOON 090100001

J. H. Telting¹, R. H. Østensen², U. Heber³ and T. Augsteijn¹

¹ *Nordic Optical Telescope, Apartado 474, E-38700 Santa Cruz de La Palma, Spain*

² *Isaac Newton Group, Apartado 321, E-38700 Santa Cruz de La Palma, Spain*

³ *Remeis Sternwarte, Astronomisches Institut der Universität Erlangen-Nürnberg, Sternwartstr. 7, D-96049 Bamberg, Germany*

Received 2005 July 15

Abstract. We have obtained 2552 low-resolution spectra of the bright sdBV star Balloon 090100001, aiming to derive its pulsational characteristics. The data were obtained at the Nordic Optical Telescope during seven nights in 2004 August/September over a total time base of 38 nights. In this paper we present preliminary results obtained from frequency analyses and spectral modeling of phase-folded spectra. Additionally, we briefly discuss the prospect of mode-identification for the main modes in this star, using preliminary amplitude ratios derived from our spectra.

Key words: stars: subdwarfs – line: profiles – stars: early-type, oscillations – stars: variables: general – stars: individual: Balloon 090100001

1. INTRODUCTION

Oreiro et al. (2004) found high-amplitude photometric variability and labelled Balloon 090100001 as the brightest known pulsating subdwarf-B star ($B = 11.8$). Furthermore, Oreiro et al. (2004), Baran et al. (2005) and Baran et al. (2006) presented a rich p- and g-mode frequency spectrum, including a triplet close to the dominant frequency of 2.8075 mHz. The fact that both p- and g-modes have been discovered in this star shows that Balloon 090100001 is in essence part of both the slow and fast pulsating groups of subdwarf-B stars. Altogether, the brightness, the pulsational amplitude and the rich but seemingly non-randomly distributed frequency spectrum, make this star an excellent target for asteroseismological studies.

So far, several pulsating sdB stars have been studied using low-resolution spectrographs on intermediate-size telescopes, e.g., PB 8783 and KPD 1209+4401 (Jeffery & Pollacco 2000), PG 1605+072 (O’Toole et al. 2003), PG 1325+101 (Telting & Østensen 2004), as well as a few other studies in these proceedings. All these studies have shown that low-resolution spectroscopy gives additional information (with respect to photometric studies) regarding the fundamental parameters of the stars, and gives essential velocity information that characterises the pulsa-

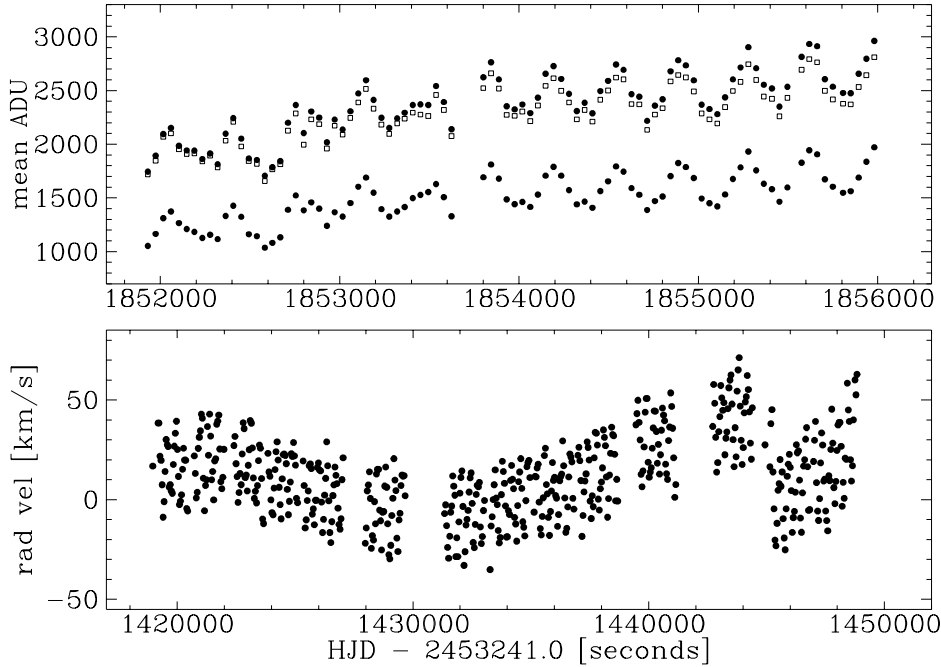


Fig. 1. Top: quasi-Strömrgren u (lowest), v and b (open squares) light curve for about 1 hour of data. Bottom: radial velocities derived from cross-correlation for one night of data. The short-period variations reflect the main pulsation mode; the long term drifts and sudden shifts are (largely) instrumental effects.

tional behavior of these stars.

In this paper we present preliminary results derived from our data set that was obtained with the aim to put constraints on the pulsational characteristics of the star Balloon090100001.

2. OBSERVATIONS

We observed the star during 7 nights in 2004 August/September over a total time-base of 38 nights. Our data set overlaps the photometric data set presented by Baran et al. (2006). We used the Andalucia Faint Object Spectrograph and Camera, ALFOSC, at the Nordic Optical Telescope on La Palma.

Our instrumental setup was: grism #16, CCD #8, and a long slit of $0''.8$ width. This setup samples the wavelength region of approximately $3500\text{--}5060\text{ \AA}$, and gives a FWHM spectral resolution of about 3 \AA corresponding to 54 km/s/pixel . We used an exposure time of 30 s, which hardly affects the amplitude of the main pulsation ($P = 356\text{ s}$) in terms of phase smearing. With appropriate binning and windowing in the spatial direction we achieved a cycle time of 43 seconds. Thorium-argon and helium arc-line spectra were made sandwiching 40 or less consecutive spectra.

The spectra were flatfielded and extracted using standard tasks within IRAF. The average signal to noise ratio of the individual extracted spectra is $S/N = 50$. A total of 2552 useful spectra were obtained.

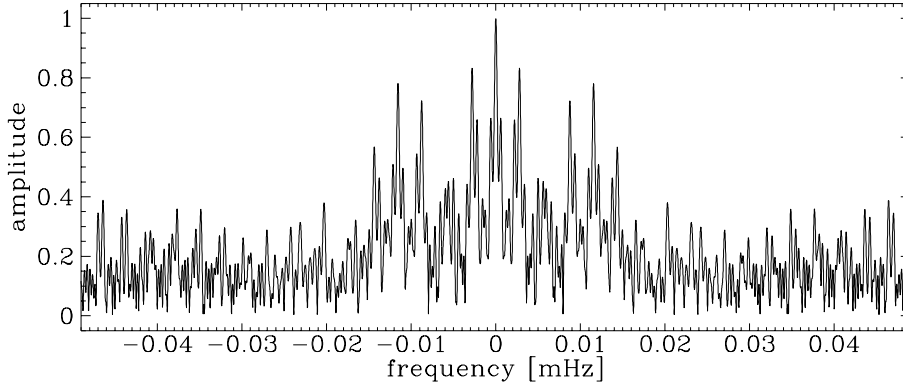


Fig. 2. The amplitude of the window function in Fourier space, showing strong 4-day and 1-day aliases.

3. RADIAL VELOCITIES AND SPECTROPHOTOMETRY

We used the cross-correlation routine FXCOR in IRAF using the mean spectrum as a template. The cross-correlation function (CCF) is dominated by the strong Balmer lines in the spectrum. We used the center of the CCF as a measure for the radial velocity of the star, and the FWHM of the CCF as a measure of the width of the Balmer lines, which in itself reflects the apparent surface gravity.

We used the average equivalent width (EW) of the H γ –H9 Balmer lines as a further observable. To beat the noise in the wings of the profiles, each point in the profile was weighted with its own depth with respect to the continuum, implying the following non-standard form $EW = \sqrt{\sum(1 - P(\lambda))^2} \times \Delta\lambda$, where $P(\lambda)$ is the line profile.

We also used our unnormalised spectra to obtain quasi-Strömgen *uvb* photometry from the mean count level in the following bands: 3515–3715 Å, 4000–4200 Å and 4600–4800 Å. For each band the mean count levels were put on a magnitude scale and were subsequently detrended as a function of time.

Figure 1 shows the radial-velocity measurements of one night of data, and a typical *uvb* light curve for about 1 hour of data. From the plot of the radial-velocity measurements it is clear that drifts in velocity and shifts due to recentering of the star on the slit. We have corrected for such instrumental/observational drifts and shifts by detrending appropriate chunks of radial-velocity data using first and second order polynomial fits. Note that such detrending can affect the amplitudes of low-frequency pulsational signal in the data.

4. FOURIER ANALYSES

We have analysed the quantities described above using a standard discrete Fourier transform. The distribution in time of the spectra results in strong 1-day and 4-day aliases (see the window function in Figure 2). Although the frequency resolution as obtained from the central window peak is on the order of 1 μ Hz, the severe aliasing pattern makes it difficult to separate real peaks from aliases.

Figure 3 shows the Fourier transforms of three of our observables, indicating the dominance of the main pulsation mode at 2.80749 mHz in the Fourier spectra.

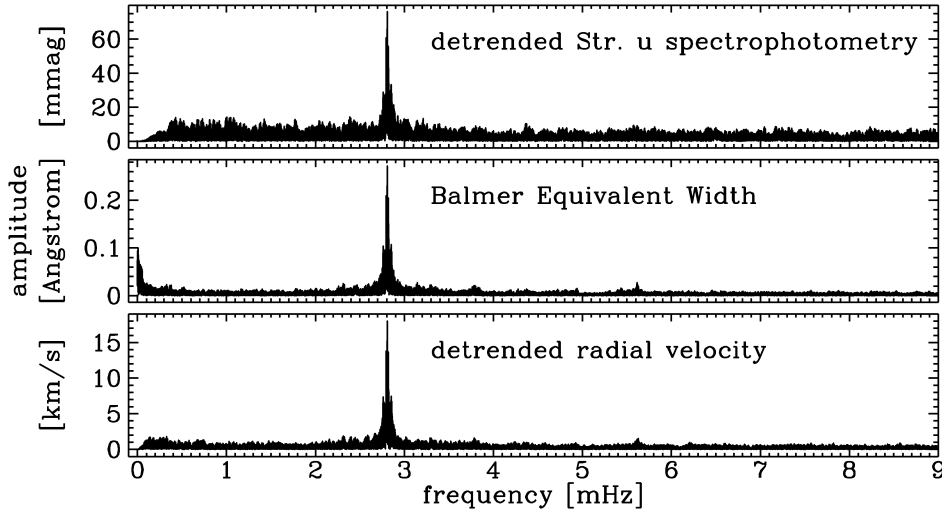


Fig. 3. Amplitude of Fourier transforms.

To estimate the errors on the amplitudes in Fourier space, we prewhitened the 25 strongest peaks and averaged the remaining amplitude spectrum between 0 and 15 mHz. The resulting error levels are 2.7 mmag for photometry amplitudes, and 0.24 km/s for the radial-velocity amplitude. The radial-velocity amplitude of the main pulsation mode is 18.0 km/s.

We have looked for the presence of other pulsation frequencies in the Fourier transforms of the observables. In Table 1 we list the pulsation frequencies from Baran et al. (2006), for which we find evidence in our data. Note that for some of these detections our data set alone would not suffice to label them as significant.

Table 1. Frequencies and B -mag amplitudes from Baran et al. (2006), for which we find evidence in our spectra. One asterisk denotes a corresponding peak, two asterisks denote a peak at an obvious alias.

| mHz | mmag | | mHz | mmag | |
|--------|------|----|--------|-------|------|
| 0.2724 | 2.89 | ** | 2.8075 | 53.10 | * |
| 0.3658 | 2.71 | * | 2.8232 | 20.53 | */** |
| 0.3257 | 1.09 | ** | 2.8248 | 12.08 | * |
| | | | 3.7761 | 4.57 | * |

5. PHASE-FOLDED SPECTRA

In order to investigate the pulsational characteristics of the dominant mode (2.8075 mHz), we have phase-folded and averaged our spectra into 20 phase bins, each bin containing more than 100 spectra. The phase binning and subsequent averaging increases the S/N to better than 500 for the resulting spectra, and significantly reduces the variations that may be present at other frequencies. Besides

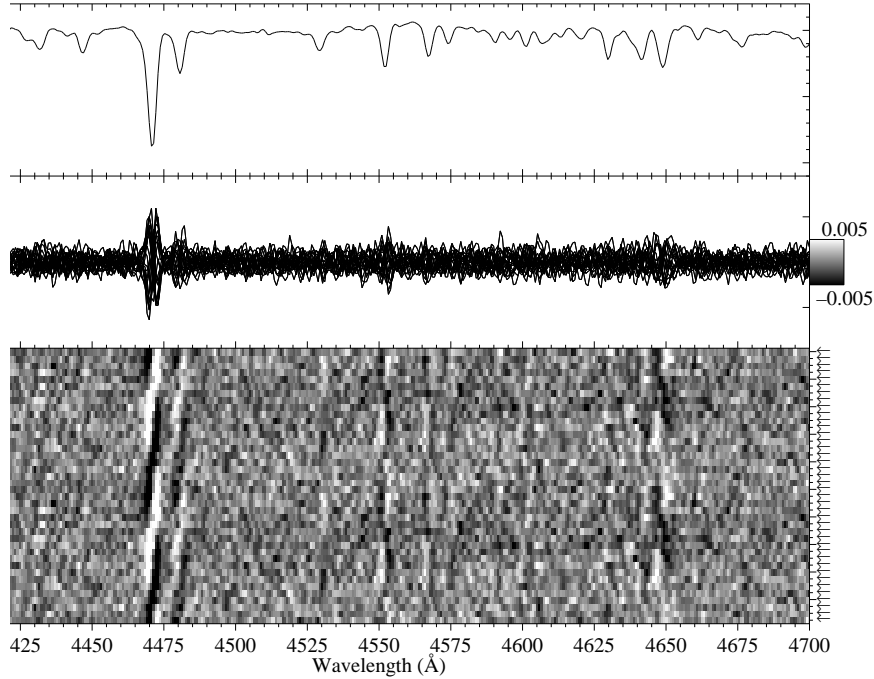


Fig. 4. Bottom panel: spectra folded to pulsational phase of the dominant mode (2.8075 mHz) and subsequently binned to 20 phase bins; the residual spectra are shown in grey-scale representation. Middle panel: overplot of the residual spectra. Top panel: average of all 2552 spectra. We show the wavelength region covering He I 4471 Å, Mg II 4481 Å, Si III 4552 Å, C III 4650 Å, to indicate the profile variations for these lines.

clear variations in the Balmer lines and He I lines, we detect pulsational variations in lines of heavier elements as well (see Figure 4).

We fitted the LTE spectral synthesis models of Heber et al. (2000) to each of the 20 phase-folded spectra to obtain values of the apparent effective temperature and apparent effective gravity. Both temperature and gravity show sinusoidal behaviour as a function of pulsation phase. The mean values are found to be $T_{\text{eff}} = 28\,700$ K, $\log g = 5.39$ dex, with a helium abundance $\log(n(\text{He})/n(\text{H})) = -2.75$ dex that does not vary with pulsation phase. The pulsational amplitudes of apparent surface temperature and gravity are $\Delta T_{\text{eff}} = 1250$ K, $\Delta \log g = 0.1$ dex. The pulsational track of Balloon 090100001 is plotted in the gravity versus temperature diagram in Figure 5.

It is noteworthy that the main cause of the large variations in $\log g$ is the pulsational acceleration, which alters the surface gravity an order of magnitude more than the pulsational radius change does. Consequently, any type of modeling of p-mode line-profile and brightness variations for stars like Balloon 090100001 should account for the effect that the pulsational acceleration has on the surface gravity.

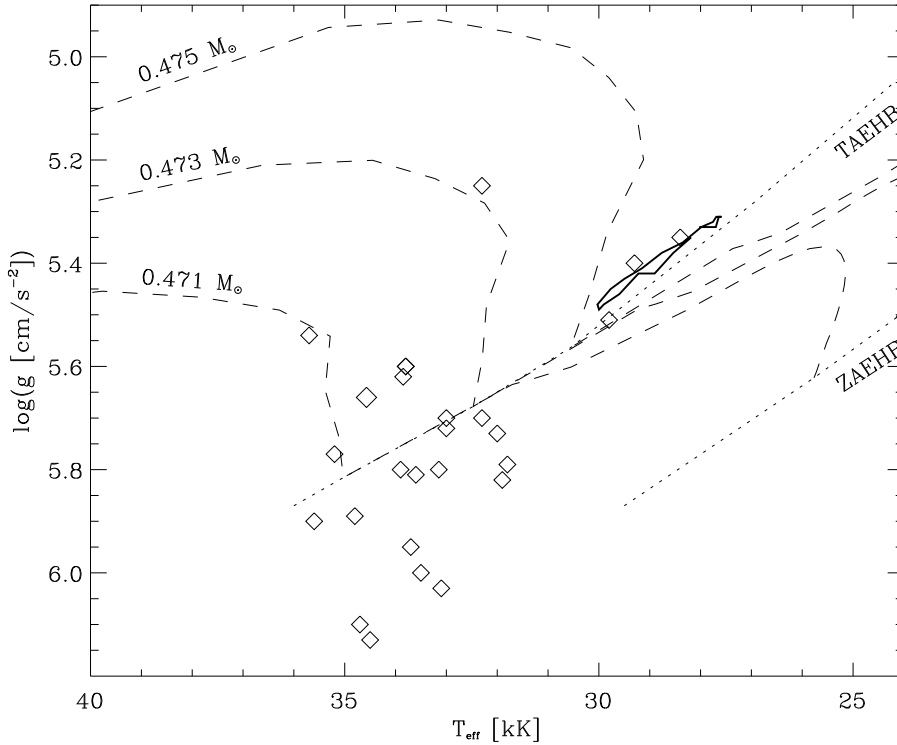


Fig. 5. Diagram of $\log g$ vs. T_{eff} , with three evolutionary tracks from Dorman et al. (1993). In only six minutes the star sweeps through the diagram along the indicated pulsational track (the ragged closed contour close to the TAEHB). The diamonds depict all other known p-mode sdB pulsators.

6. TOWARDS MODE IDENTIFICATION

We computed uvb amplitude ratios for the main pulsation mode (2.8075 mHz) and for the strongest (2.8232 mHz) of the three frequencies that were identified by Baran et al. (2006) to form an equidistant triplet. Because of the triplet structure, this latter frequency is likely due to an $\ell = 1$ mode. Given its very high amplitude, the main pulsation mode is likely to be of low degree nature: $\ell < 3$.

The amplitude ratios A_v/A_u and A_b/A_u are plotted as a function of wavelength in Figure 6, similar to the diagrams presented by Ramachandran et al. (2004). Note that the stellar and pulsational parameters of the models presented by Ramachandran et al. (2004) are not consistent with those of Balloon 090100001.

We find that there is a clear separation between the amplitude ratios of the two modes, which indicates that it is unlikely that the two modes have the same pulsational degree ℓ , leaving as likely identifications of the main mode $\ell = 0$ and $\ell = 2$.

We prefer the $\ell = 0$ identification of the main mode, because of the high observed amplitude of that mode. Nevertheless, we are convinced that detailed modeling of the amplitudes as a function of wavelength, in a similar fashion as presented by Randall et al. (2006), could provide further evidence to confirm our

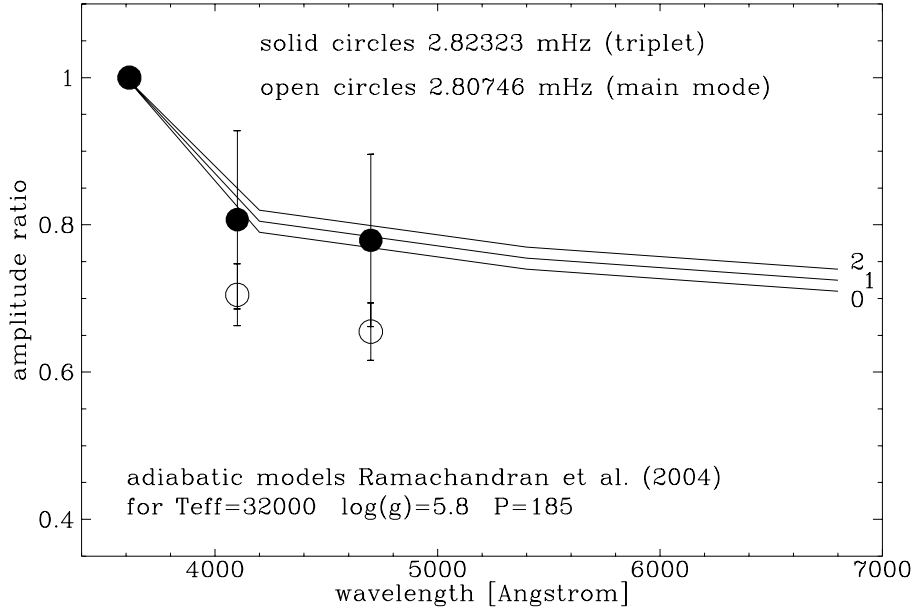


Fig. 6. Our uvb amplitude ratios compared with theoretical $UVBR$ ratios for a sdB star hotter and more compact than Balloon 090100001 (see Ramachandran et al. 2004). Unlike the theoretical curves, our amplitude ratios show clear separation for the two modes.

tentative identification of the main pulsation mode of Balloon 090100001.

7. SUMMARY AND PRELIMINARY CONCLUSIONS

We have obtained a large spectroscopic data set of Balloon 090100001, and find clear signatures of the main pulsation mode. In our Fourier periodograms we find further evidence for other previously known frequencies.

In the phase-folded spectra, as folded on the main pulsation period, we find clear pulsational variations in the Balmer and helium lines that are present in our spectra. Moreover, we find clear pulsational variations in lines of heavier elements as well.

The apparent pulsational variations of temperature and gravity, due to the main pulsation mode, are $\Delta T_{\text{eff}} = 1250$ K and $\Delta \log(g) = 0.1$ dex (semi amplitudes). The radial velocity amplitude of this mode is 18 km/s.

We show that the uvb amplitude ratios, derived from our spectra, of the main mode and of the strongest of the triplet modes are not the same, indicating that these modes may have a different ℓ value. We tentatively identify the main mode to be a radial mode.

ACKNOWLEDGMENTS. J.T. thanks Raquel Oreiro for an early copy of her poster on Balloon 090100001 that was presented at the meeting (Baran et al. 2006).

REFERENCES

- Baran A., Oreiro R. et al. 2006, *Baltic Astronomy*, 15, 227 (these proceedings)
- Baran A., Pigulski A., Koziel D., Ogłóza W., Silvotti R., Zola S. 2005, *MNRAS*, 360, 737
- Dorman B., O’Connell R. W., Rood R. T. 1993, *ApJ*, 419, 596
- Heber U., Reid I. N., Werner K. 2000, *A&A*, 363, 198
- Jeffery C. S., Pollacco D. 2000, *MNRAS*, 318, 974
- Oreiro R., Ulla A., Pérez Hernández F., Østensen R., Rodríguez López C., MacDonald J. 2004, *A&A*, 418, 243
- O’Toole S. J., Jørgensen M. S., Kjeldsen H., Bedding T. R., Dall T. H., Heber U. 2003, *MNRAS*, 340, 856
- Ramachandran B., Jeffery C. S., Townsend R. H. D. 2004, *A&A*, 428, 209
- Randall S. K., Fontaine G. et al. 2006, *Baltic Astronomy*, 15, 291 (these proceedings)
- Telting J. H., Østensen R. H. 2004, *A&A*, 419, 685

TIME-RESOLVED SPECTROSCOPY OF KPD 1930+2752

S. Geier¹, U. Heber¹, N. Przybilla¹ and R.-P. Kudritzki²

¹ *Remeis-Sternwarte, Universität Erlangen-Nürnberg, Sternwartstrasse 7, D-96049 Bamberg, Germany*

² *Institute for Astronomy, University of Hawaii, 2680 Woodlawn Drive, Honolulu, HI 96822, U.S.A.*

Received 2005 July 29

Abstract. We present the analysis of 200 high-resolution and 150 low-resolution spectra of the pulsating subdwarf close binary KPD 1930+2752 obtained with the Keck and the Calar Alto 2.2 m telescopes. Using metal-rich, line blanketed LTE model atmospheres the atmospheric parameters ($T_{\text{eff}} = 35\,500 \pm 500$ K), $\log g = 5.56 \pm 0.05$) and $\log \text{He}/\text{H} = -1.48 \pm 0.02$ were derived. The radial velocity curve was measured and combined with all available published and unpublished radial velocity data in order to get results of high accuracy: $K = 341 \pm 1$ km s⁻¹), $P = 0.0950933 \pm 0.0000015$ d). For the first time we measured the projected rotational velocity. The preliminary result is $v_{\text{rot}} \sin i = 97 \pm 9$ km s⁻¹ (3σ). Since the rotation of the sdB star is very likely tidally locked to the orbit, we can constrain the inclination of the system. Assuming the companion to be a white dwarf, the mass of the sdB is limited from $0.44 M_{\odot}$ to $0.63 M_{\odot}$ and the total mass range of the system is $1.3 M_{\odot}$ to $2.0 M_{\odot}$. It is very likely that the total mass exceeds the Chandrasekhar limit. Hence KPD 1930+2752 is a candidate for a progenitor of a Type Ia supernova. According to the derived limits for the inclination angle, eclipses are likely to occur.

Key words: binaries: spectroscopic – stars: atmospheres – stars: individual (KPD 1930+2752) – subdwarfs – supernovae: general

1. INTRODUCTION

KPD 1930+2752 was identified as a subdwarf B star in the Kitt Peak-Downes survey (Downes 1986). The parameters which were derived from spectroscopy by model atmosphere fits (Saffer & Liebert 1995) are consistent with the theoretical instability strip for pulsating sdB stars, which was predicted by Charpinet et al. (1996). After the first pulsating sdBs (EC 14026 stars) were discovered in 1997 (Kilkenny et al. 1997; Koen et al. 1997; Stobie et al. 1997), Billères et al. (2000) initiated a survey to search for these objects in the northern hemisphere. They selected KPD 1930+2752 from the list of Saffer & Liebert (1995) for their fast photometry program and detected multiperiodic variations with short periods and low amplitudes. In addition to 44 p -mode pulsations they found a strong variation at a much longer period of about 4100 s. This variation could be identified as

an ellipsoidal deformation of the sdB most likely caused by a massive companion. Billères et al. predicted the period of the binary to be two times the period of the brightness variation $P = 8217.8 \text{ s} = 0.095111 \text{ d}$.

This was proven by Maxted et al. (2000), who measured a radial velocity curve of KPD 1930+2752 which could be fitted with the proper period. The radial velocity amplitude $K = 349.3 \pm 2.7 \text{ km s}^{-1}$ combined with the assumption of the canonical mass for sdBs $M_{sdB} = 0.5 M_{\odot}$ led to a lower limit for the mass of the system derived from the mass function. This lower limit $M \geq 1.47 M_{\odot}$ exceeded the Chandrasekhar mass of $1.4 M_{\odot}$. Because there was no sign of a companion in the spectra, it was concluded that the unseen object must be a white dwarf. Putting all this together, Maxted et al. concluded that KPD 1930+2752 could be a good candidate for the progenitor of a Type Ia supernova.

Type Ia supernovae (SNe Ia) are the most important standard candles for extragalactic distance measurements and play an outstanding role in observational cosmology. The progenitors of SNe Ia as well as the dynamics of the explosions are still under debate. The thermonuclear explosion of a white dwarf turned out to be the most reasonable explanation. A white dwarf has to exceed the Chandrasekhar mass to explode in this way. In the single degenerate scenario the white dwarf accretes matter from a nearby non-degenerate companion star. Possible progenitor candidates are supersoft X-ray sources. Double degenerate systems consist of two white dwarfs in a short period system, which merge within a Hubble time due to gravitational wave radiation (Livio 2000). KPD 1930+2752 has a sufficiently short period and may have a sufficiently high total mass. The sdB can be expected to evolve to a white dwarf before the merger.

From the theoretical point of view Ergma et al. (2001) questioned the double degenerate scenario in the case of KPD 1930+2752. Their simulations based on the derived parameters of Maxted et al. suggested the formation of a single massive ONeMg white dwarf or a neutron star.

The main drawback of all previous investigations is the lack of information on the inclination angle and the assumption made on the sdB mass. We drop the latter assumption and derive constraints on the inclination for the first time by means of an accurate measurement of the projected rotational velocity and surface gravity. Because the rotation of the sdB star is tidally locked to the orbit, we can derive $\sin i$ as a function of the sdB mass from these two quantities.

2. OBSERVATIONS AND DATA REDUCTION

With the 10 m Keck telescope at the Mauna Kea Observatory two hundred high-resolution spectra were obtained by N. Przybilla in half a night in 2004 July, using the High Resolution Echelle Spectrometer (HIRES, Vogt et al. 1994). The spectra covered a wavelength range of 4200–6800 Å with a few small gaps at a resolution of 0.1 Å and exposure times of 20 s each. The data were reduced using the ESO-MIDAS package. Bias and flatfield corrections were applied and a wavelength calibration was done. All spectra were corrected to the heliocentric frame of reference.

Additional observations were obtained with the 2.2 m telescope at the Calar Alto Observatory in 2004 July. The Calar Alto Faint Object Spectrograph (CAFOS) was used to obtain 150 spectra covering a wavelength range of 3600–6200 Å with 5 Å resolution and an exposure time of 180 s each. The data were reduced in analogy to the HIRES spectra.

3. STELLAR PARAMETER DETERMINATION

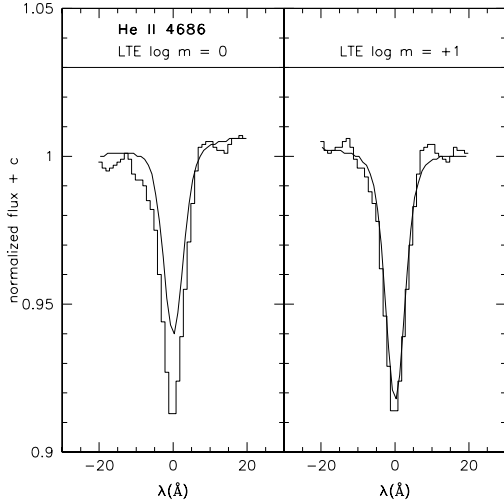


Fig. 1. LTE models with $\log m = +1$ solve the helium problem.

matching of the observed spectra was done with the FITPROF routine by the means of a χ^2 fit (Napiwotzki 1999). The results of the fits with different grids were consistent (see Table 1).

Table 1. Parameters of KPD 1930+2752.

| Model | T_{eff} K | $\log g$ | $\log \frac{n(\text{He})}{n(\text{H})}$ |
|-------------------|--------------------|-----------------|---|
| LTE $\log m = 0$ | 35 549 | 5.63 | -1.58 |
| LTE $\log m = +1$ | 35 183 | 5.56 | -1.48 |
| NLTE (PRO2) | 35 619 | 5.56 | -1.51 |
| NLTE (NGRT) | 35 516 | 5.53 | -1.45 |
| NLTE (lf) | 35 617 | 5.64 | -1.53 |
| Adopted | $35\,500 \pm 500$ | 5.56 ± 0.05 | -1.48 ± 0.02 |

NLTE effects played a minor role. In the first instance it was not possible to fit the hydrogen and some helium lines (He I 5876, He II 5412 and in particular He II 4686) simultaneously. This so called helium problem already occurred during other analyses of pulsating subdwarfs (Heber et al. 2000; Edelmann 2003). The analysis of HST-UV spectra of three sdB stars with similar T_{eff} as KPD 1930+2752 revealed supersolar abundances of the iron group elements (O’Toole & Heber 2005). Those stars also displayed the optical He ionization problem. Using more appropriate metal-rich models ($10 \times$ solar metallicity) the problem could be remedied (see also Heber 2006). The abundances of the iron group elements have not been measured for KPD 1930+2752. Because of the similarity of its atmospheric

The coadded CAFOS spectrum had a very smooth continuum, which made it very suitable for model atmosphere fits. Different LTE and NLTE model grids were used to fit 7 hydrogen and 8 He I and He II lines: a grid of metal-line blanketed LTE model atmospheres (Heber et al. 2000) with solar and ten times solar metallicity; a grid of partially line-blanketed NLTE model atmospheres without metal lines (Dreizler et al. 1990) based on the ALI method (PRO2); a grid calculated with a new version of PRO2 (so called NGRT) that employs a temperature correction scheme and uses more sophisticated model atoms; a small grid based on the LTE models with NLTE line formation (Przybilla et al. 2006). The

parameters to those of the stars studied by O’Toole and Heber (2005), we adopted high-metallicity models as well and, indeed, the fit improved (Figure 1). The derived temperature is about 2000 K higher than in prior analyses (Billères et al. 2000) irrespective of the choice of model atmosphere. With this KPD 1930+2752 is situated at the edge of the instability strip in the T_{eff} vs. $\log g$ diagram (Charpinet et al. 1996).

4. SPECTROSCOPIC ORBIT

Due to the low signal to noise ratio of the HIRES spectra only the H α and H β lines could be used for determining the radial velocity by χ^2 cross-correlation with a model spectrum at rest wavelength. To improve the accuracy, the resulting radial velocity curve was combined with all available radial velocity data of KPD 1930+2752 (Maxted et al. 2000; Woolf et al. 2002; Orosz 2000, priv. comm.) covering a timespan of four years. A sine curve was fitted to these 2900 data points using a χ^2 minimizing method and the power spectrum was generated (FITRV and FITPOW routines by H. Drechsel). The sine curve fit is excellent and no period change could be detected over the whole timebase (Figures 2). The orbital parameters were measured with unprecedented accuracy: $\gamma(\text{H}\alpha) = 5 \pm 1 \text{ km s}^{-1}$, $K = 341 \pm 1 \text{ km s}^{-1}$, $P = 0.0950933 \pm 0.0000015 \text{ d}$. No radial velocity variations due to pulsations could be found.

5. PROJECTED ROTATIONAL VELOCITY

The main aim of the high-resolution time-series spectroscopy was to obtain a high-precision measurement of the projected rotational velocity. For this purpose the 200 HIRES spectra were shifted to rest wavelength, and the median was calculated in order to filter cosmic rays. The projected rotational velocity was measured using a model spectrum with the derived atmospheric parameters fixed and performing a χ^2 fit. The lines He II 4686, He I 4922 and He I 5016 were used for this measurement. Furthermore one single high resolution spectrum obtained with the ESO Very Large Telescope (VLT) at the Paranal Observatory and the Ultraviolet and Visual Spectrograph (UVES) was available. The rotational velocity was measured in the same way for the helium lines. The still preliminary results were consistent (see Figure 3) and yield: $v_{\text{rot}} \sin i = 97 \pm 9 \text{ km s}^{-1} (3\sigma)$

6. MASS AND INCLINATION

KPD 1930+2752 is obviously affected by the gravitational forces of the companion, demonstrated by its ellipsoidal deformation. Since the period of the photometric variations are exactly half the period of the radial velocity curve the rotation of the sdB star is very likely tidally locked to the orbit. In addition to the mass function two more equations set additional constraints on the problem with only M_{sdB} remaining as free parameter.

$$\sin i = \frac{v_{\text{rot}} \sin i P}{2\pi R} \quad ; \quad R = \sqrt{\frac{M_{\text{sdB}} G}{g}} \quad (1)$$

With $\log g$, P and $v_{\text{rot}} \sin i$ measured and the fact that $\sin i$ cannot exceed unity a lower limit for the mass of the sdB of $0.44 M_{\odot}$ is derived. As can be seen in Figure

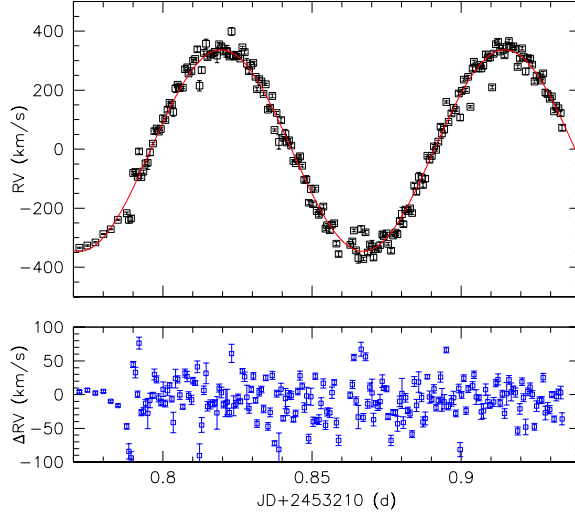


Fig. 2. Radial velocity curve. The data points are from the new HIRES spectra, the solid line is from the fit of all data points over a timespan of four years. The residuals in the lower part show no signs of eccentricity.

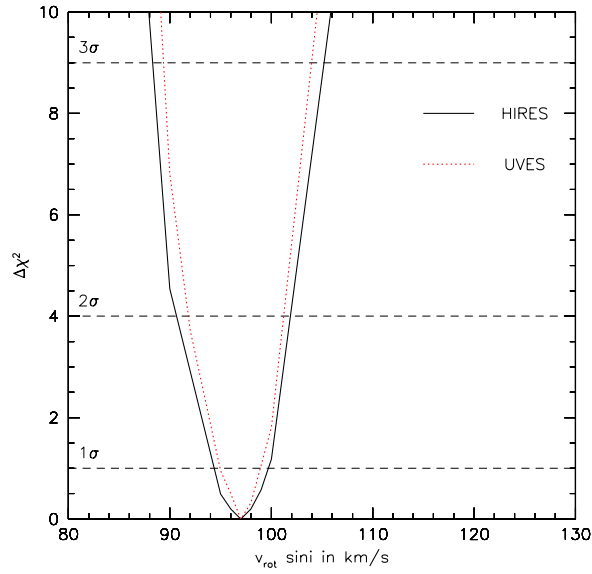


Fig. 3. Reduced χ^2 as a function of $v_{\text{rot}} \sin i$ from fits to the HIRES and UVES data. The minimum of the two curves indicates the most probable value. The dashed horizontal lines mark the confidence levels of the errors.

4, the total mass of the system exceeds the Chandrasekhar limit for all reasonable assumptions of M_{sdB} . If the companion is a white dwarf, its mass has to be lower than the Chandrasekhar limit. This implies an upper limit $M_{\text{sdB}} \leq 0.63 M_{\odot}$ and a possible total mass range of $M_{\text{sdB+WD}} = 1.3 \pm 0.1 - 2.0 \pm 0.2 M_{\odot}$ (Figure 5). Although a more massive companion cannot be ruled out completely, the object would probably be a bright X-ray source in this case. No such source is known at these coordinates.

The inclination angle of the system (Figure 4) in the lower mass range is very close to 90° . KPD 1930+2752 could be an eclipsing binary (cf. the very similar binary KPD 0422+5421, Orosz and Wade 1999), as some features in the light curve already indicated (Maxted et al. 2000).

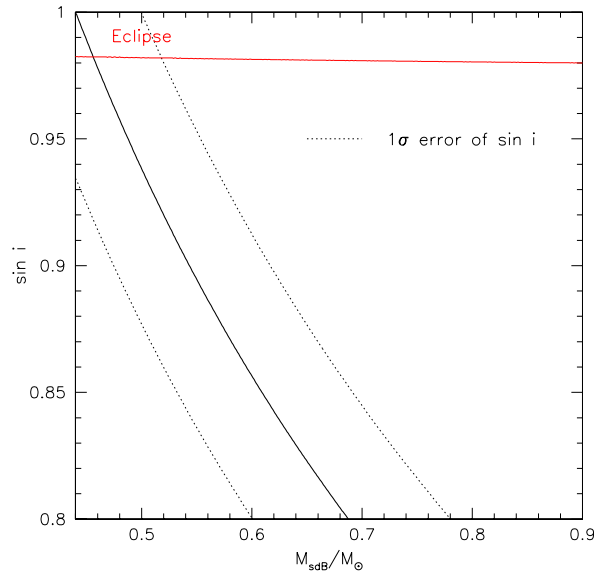


Fig. 4. Inclination with 1σ error (dotted line) versus mass of the sdB. The upper curve indicates the minimum inclination for an eclipse.

7. CONCLUSION

The combination of an extensive set of 350 spectra and 2700 radial velocity data points from prior observations made it possible to determine the parameters of KPD 1930+2752 with very high accuracy. The tidally locked rotation together with a white dwarf companion implies a mass range for the sdB without any evolutionary model considerations. KPD 1930+2752 is the first subdwarf, whose mass could be constrained in this way. The total mass and the merging time of the binary indicate that it is a very good candidate for a SN Ia progenitor. KPD 1930+2752 is one of only three known double degenerate systems, which fulfill these requirements (Napiwotzki et al. 2003a; Karl 2004). While it fits into the DD scenario, KPD 1930+2752 might also evolve into a SN Ia via the SD scenario. Since time for merging due to gravitational wave radiation is of the same order as the EHB life time, Roche lobe overflow could occur well before the

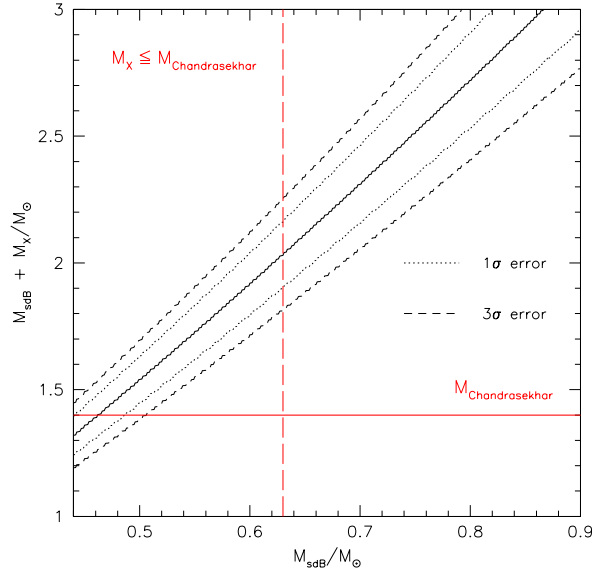


Fig. 5. Total mass of the binary as a function of the sdB mass. The dashed vertical line marks the point where the companion mass equals the Chandrasekhar mass.

sdB becomes a white dwarf due to the shrinkage of the orbit. Recent calculations by Han and Podsiadlowski (priv. comm.) indicate that the mass transfer would be stable. Follow-up observations should be undertaken to measure an improved light curve and search for signs of an eclipse. If detected all system parameters will be determined. An alternative promising option is asteroseismology, which could tightly constrain the sdB mass.

REFERENCES

- Billères M., Fontaine G., Brassard P., Charpinet S., Liebert J., Saffer R. A. 2000, *ApJ*, 530, 441
- Charpinet S., Fontaine G., Brassard P., Dorman B. 1996, *ApJ*, 471, L103
- Downes R. A. 1986, *ApJS*, 61, 569
- Edelmann H. 2003, PhD-thesis, Friedrich Alexander Universität Erlangen-Nürnberg
- Eggleton P. P. 1982, *ApJ*, 268, 368
- Ergma E., Fedorova A. V., Yungelson L. R. 2001, *A&A*, 376, L9
- Han Z., Podsiadlowski P., Maxted P. F. L., Marsh T. R., Ivanova N. 2002, *MNRAS*, 336, 449
- Han Z., Podsiadlowski P., Maxted P. F. L., Marsh T. R., Ivanova N. 2003, *MNRAS*, 341, 669
- Heber U. 1986, *A&A*, 155, 33
- Heber U., Reid I. N., Werner K. 2000, *A&A*, 363, 198

- Heber U., Hirsh H., Ströer A. et al. 2006, *Baltic Astronomy*, 15, 91
- Karl C. 2004, PhD-thesis, Friedrich Alexander Universität Erlangen-Nürnberg
- Kilkenny D., Koen C., O'Donoghue D., Stobie R. S. 1997, *MNRAS*, 285, 640
- Koen C., Kilkenny D., O'Donoghue D., Van Wyk F., Stobie R. S. 1997, *MNRAS*, 285, 645
- Livio M. 2000, in *Type Ia Supernovae: Theory and Cosmology*, eds. J. C. Niemeyer & J. W. Truran, Cambridge Univ. Press, p. 33
- Maxted P. F. L., Marsh T. R., North R. C. 2000, *MNRAS*, 317, L41
- Napiwotzki R. 1999, *A&A*, 350, 101
- Napiwotzki R., Christlieb N., Drechsel H. et al. 2003a, *ESO Messenger*, No. 112, 25
- Orosz J. A., Wade R. A. 1999, *MNRAS*, 310, 773
- O'Toole S., Heber U. 2005, *A&A*, submitted
- Przybilla N., Nieva M. F., Edelmann H. 2006, *Baltic Astronomy*, 15, 107
- Saffer R. A., Liebert J. 1995, in *Proc. 9th European Workshop on White Dwarfs*, eds. D. Koester & K. Werner, Springer Verlag, p. 221
- Stobie R. S., Kawaler S. D., Kilkenny D., O'Donoghue D., Koen C. 1997, *MNRAS*, 285, 651
- Vogt S. et al. 1994, *Proc SPIE*, 2198, 362
- Wolf V. M., Jeffery C. S., Pollacco D. L. 2002, *MNRAS*, 332, 34

TIME-SERIES SPECTROSCOPY AND PHOTOMETRY OF PG 1219+534

S. L. Harms¹, M. D. Reed¹ and S. J. O’Toole²

¹ *Missouri State University, Springfield, MO 65804, U.S.A.*

² *Remeis-Sternwarte, Astronomisches Institut der Universität
Erlangen-Nürnberg, Sternwartstrasse 7, Bamberg, D-96049, Germany*

Received 2005 August 1

Abstract. We present a preliminary report of time-series spectroscopic data obtained on a sdB star PG 1219+534. An analysis of three years of photometric observations is also included.

Key words: stars: hot subdwarfs – stars: oscillations – stars: individual (PG 1219+534)

1. INTRODUCTION

In order for asteroseismology to determine the structure and evolution of subdwarf B stars, we must first determine their modes of pulsation using spherical harmonics. Although time-series photometry is sufficient to detect frequencies of pulsation, time-series spectroscopy shows more promise for uniquely determining modes of pulsation (O’Toole et al. 2000; Telting & Østensen 2004). Spectroscopy is particularly sensitive to higher ℓ -modes which have lower photometric amplitudes. This is because the surface cancellation that affects photometry does not have the same affect on spectroscopy, which focuses on velocity and line-profile measurements.

The sdB star PG 1219+534 (hereafter PG 1219) is an ideal candidate for simultaneous time-series spectroscopy and photometry. Since PG 1219 was discovered to be an sdB pulsator (Koen et al. 1999), its $\log g$ and T have been constrained (Heber et al. 2000), and its pulsation spectrum has been studied (Charpinet et al. 2005). Unlike other sdB pulsators, photometry has revealed a simple pulsation spectrum of four stable frequencies with occasional low-amplitude interlopers. As long as the pulsations are not all the same mode (which is highly unlikely), PG 1219 should serve as a baseline to understand the relationship between time-series spectroscopy and models. Then other similar, but more complicated stars may be understood as well.

2. PHOTOMETRY

Photometric data of PG 1219 has been collected during 2003, 2004 and 2005 (Reed et al. 2005). Dates of observations are shown in Table 1. Although most observations were conducted at Baker Observatory, some were also done at Mc-

Table 1. List of observations of PG 1219.

| Year | Inclusive dates | Hours observed |
|------|-----------------------|----------------|
| 2003 | May 13 – June 4 | 48.6 |
| 2004 | March 9 – 15 | 21.5 |
| 2005 | February 25 – March 2 | 23.8 |

Table 2. Periods, frequencies, and amplitudes of PG 1219 over three years. Formal least-squares errors in parenthesis.

| Period (s) | Frequency (μHz) | Amplitudes (mma) | | |
|---------------|---------------------------------|---------------------|----------|----------|
| | | 2003 | 2004 | 2005 |
| 122.4165(26) | 8168.832(174) | – | 1.24(22) | – |
| 128.0775(5) | 7807.754(9) | 5.13(11) | 7.35(22) | 9.78(37) |
| 133.5106(2) | 7490.037(10) | 4.36(11) | 5.66(22) | 6.81(37) |
| 135.1614(54) | 7398.558(298) | – | 0.72(22) | – |
| 143.6495(1) | 6961.386(7) | 6.48(11) | 6.62(22) | 7.11(37) |
| 148.7761(3) | 6721.508(14) | 3.34(11) | 3.93(22) | 2.22(37) |

Donald Observatory in 2003. Images were taken with a red cutoff filter. The list of periods, frequencies and amplitudes of each year are provided in Table 2 and the Fourier transform (FT) of each year is shown in Fig. 1.

Pulsations were detected in PG 1219 over the range of 122 to 149 seconds. There are four stable frequencies in all three years whose amplitudes vary from year to year as seen in both Table 2 and Figure 1. The frequency that has the highest amplitude varies as well. Two low-amplitude frequencies appeared in 2004 that were not detected in the 2003 or 2005 data. These frequencies were not prewhitened in Fig. 1 and they are indicated by the arrows. In the prewhitened FT of 2003 (Fig. 1), the residual signal near 7490 μHz is due to short-term amplitude variations of that pulsation frequency within that data set. The lower amplitude of this same residual peak in 2004 is due to the shorter length of the 2004 run than the 2003 run.

3. SPECTROSCOPY

Spectroscopic observations of PG 1219 were obtained at the Mayall 4 m telescope at Kitt Peak National Observatory. Although four nights were requested and granted, both weather and telescope mirror support problems led to observing only on 2005 February 24 for a duration of 1.5 hours and a total of 154 spectra. Images were taken with the F3KB blue sensitive CCD camera, RC spectrograph and KPC007 dispersion grating at a spectral resolution $\sim 2.5 \text{ \AA}$ and a wavelength range of ~ 3400 to 5500 \AA . Exposure times ranged from 15 to 20 s for a duty cycle of 28 to 34 s, respectively, providing at least four measurements per pulsation period.

The length of the run gives a pulsation resolution of 187.5 μHz , which is just barely enough to resolve the pulsations in PG 1219. Velocities were derived by cross correlating individual spectra with the mean spectra with the IRAF task *fxcor*,

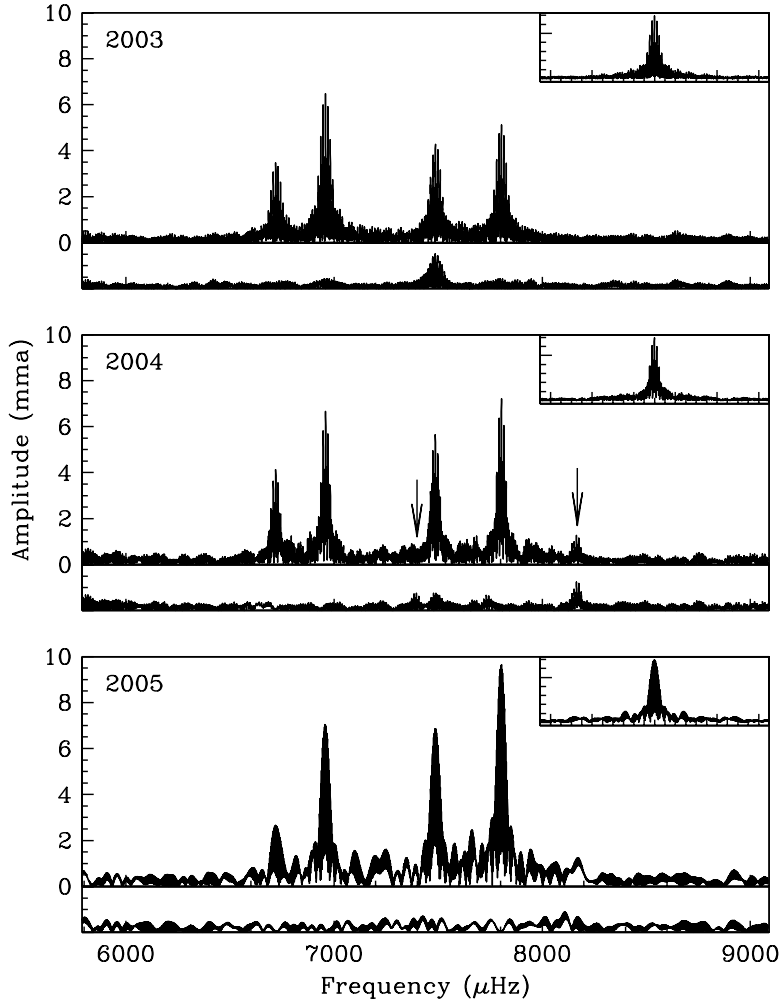


Fig. 1. The temporal pulsation spectra (FTs) for PG 1219 for three consecutive years. Each set prewhitened by four frequencies is shown below the FT. The window function for each year is shown in the inset of each panel. Arrows indicate the two low amplitude interlopers in 2004, which were not prewhitened.

then a Fourier transform was calculated for the velocities. Fourier transforms are sensitive to coherent signals while noise cancels out when many spectra are collected over a long time span. It follows that the noise level of the FT is still too high to detect any modes clearly, as there were too few measurements in this ill-fated short run. So even though the highest peak in the FT of the velocity curve (shown in Figure 2) corresponds to the highest amplitude photometric frequency, peaks of this amplitude were easily reproducible in a randomized dataset. Hence, our detection of this peak was not significant.

We still reach the conclusion that time-series spectroscopy on PG 1219 and similar stars is feasible using this instrumentation. The spectral resolution and

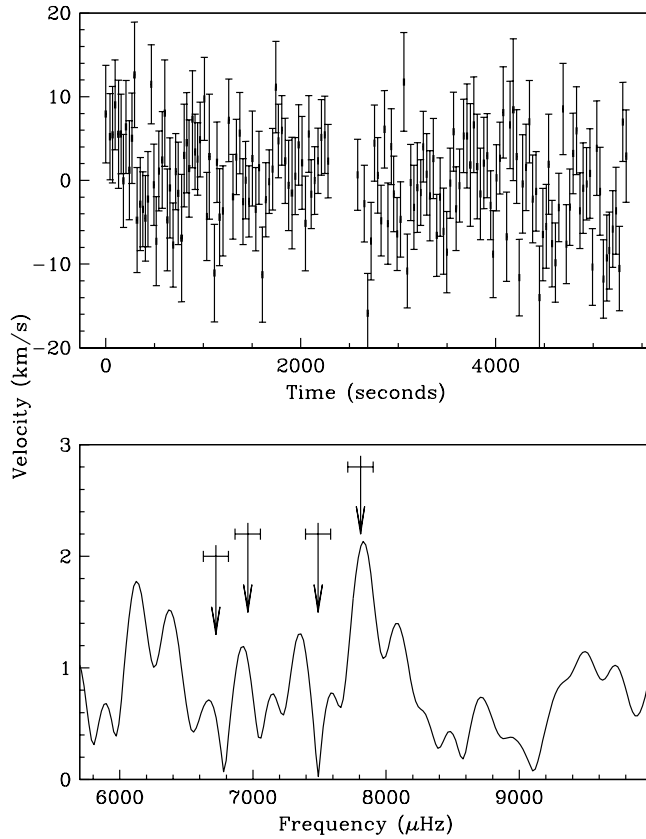


Fig. 2. Top panel: the velocity curve for PG 1219+534. Bottom panel: the Fourier transform of the velocity curve. Arrows indicate photometric frequencies with error bars from the temporal resolution of the spectroscopic data set.

integrations per period were sufficient, so had the run been longer, pulsation velocities could have been measured.

ACKNOWLEDGMENTS. This material is based in part upon work supported by the National Science Foundation under Grant Nos. AST007480 and AST9876655. Any opinions, findings and conclusions or recommendations expressed in this material are those of the author(s) and do not necessarily reflect the views of the National Science Foundation.

REFERENCES

- Charpinet S. et al. 2005, *A&A*, 437, 575
 Heber U. et al. 2000, *A&A*, 363, 198
 Koen C. et al. 1999, *MNRAS*, 305, 28
 O'Toole S. J. et al. 2000, *ApJ*, 537, L53
 Telting J. H., Østensen R. H. 2004, *A&A*, 419, 685
 Reed M. D. et al. 2005, in preparation

FOUR RAPIDLY PULSATING SDB STARS REVISITED

D. Kilkeny¹, J. P. Kotze², E. Jurua³, M. Brownstone² and H. A. Babiker²

¹ *South African Astronomical Observatory, PO Box 9, Observatory 7935, South Africa*

² *University of Cape Town, Rondebosch 7701, Cape Town, South Africa*

³ *University of the Free State, P.O. Box 339, Bloemfontein 9300, South Africa*

Received 2005 August 1

Abstract. We have re-observed four rapidly-pulsating sdB stars during 2003 and 2004 and compared the results to earlier observations. The class prototype, EC 14026–2647 (=V361 Hya), had a weak frequency which has apparently disappeared, whilst a new frequency has appeared. In EC 20338–1925, the strongest frequency (6806 μHz ; ampl. 0.026 mag) has reduced to about 0.004 mag, and weaker frequencies have come and gone. Between 1997 and 2004, the complex pulsator, PG 1605+072 (=V338 Ser), has had its strongest frequency (f_1) halve in amplitude, f_3 and f_4 double in amplitude, whilst f_2 has remained essentially constant. Finally, HS 2149+0847 (=V384 Peg) shows no significant change between 2003 and 2004, but we have increased the number of known frequencies from two to six.

Key words: stars: oscillations – stars: horizontal-branch

1. INTRODUCTION

The existence of a new class of variable star – the rapidly pulsating sdB stars – was reported by Kilkeny et al. (1997). These stars have been called EC 14026 stars, after the prototype, though they are also referred to as sdBV stars and the prototype is now designated V361 Hya. They pulsate with very short periods (typically ~ 2 to 3 minutes); they usually have several oscillation frequencies; they have surface temperatures around $28\,000 < T_{\text{eff}} < 35\,000$ K and surface gravities $5.2 < \log g < 6.1$. Reviews of pulsating sdB stars have been given by Kilkeny (2002) and Charpinet, Fontaine & Brassard (2001) for example.

The EC 14026 stars provide potential for examination of the internal structure of hot subdwarfs via the identification of pulsation modes. In addition, it is clear that the rapidly pulsating sdB stars can undergo quite significant changes in their pulsational behavior. A comparison of the 1996 data for PG 1336–018 (=NY Vir, with the 1999 data from the “Whole Earth Telescope” campaign (XCov17), shows that the main pulsation frequencies in that star had changed substantially – and were changing from day to day (see Figures 7–9 of Kilkeny et al. 2003)

The South African Astronomical Observatory (SAAO), in collaboration with several South African Universities, has set up a program – the National Astro-

physics and Space Science Programme (NASSP) – to provide training at graduate level in astronomy and astrophysics for students from Africa. Part of the honors course is a practical project and some students opt to do this at the Sutherland site of the SAAO. So far, students have carried out observational projects on four pulsating sdB stars, obtaining data sets with baselines up to 14 days – comparable in length to a “WET” campaign but with only one site. Some results are presented below and compared to earlier data.

2. OBSERVATIONS

Observations were made with the University of Cape Town’s frame-transfer CCD on the 1.9 m and 1.0 m telescopes at the Sutherland site of the SAAO. Where possible, target stars were differentially corrected using other stars on each frame. The frequency analyses described in this paper were all carried out using software which produces periodogram analysis following the Fourier transform method of Deeming (1975).

3. RESULTS

3.1. *EC 14026–2647 (=V361 Hya)*

EC 14026–2647 is the class prototype, but is somewhat atypical. It is dominated by a single frequency and appears at times to show only that frequency. Periodograms from the discovery paper (Kilkenny et al. 1997) reveal a frequency at 6930 μHz (144.3 s) with an amplitude of ~ 0.012 mag but, on a few nights, a clear frequency at 7485 μHz (133.6 s; 0.004 mag) is also visible.

The more recent data (2003 July) again shows the 144 s variation, except that the amplitude is only about 0.007 mag – half that previously seen – and two nights show a frequency near 7265 μHz ($P \sim 137.6$ s). The previously seen frequency near 7485 μHz is not detected.

3.2. *EC 20338–1925*

EC 20338–1925 was discovered to be a pulsator in 1998 (paper in preparation). At that time, the variability was dominated by a very strong frequency near 6806 μHz (146.9 s, 0.026 mag) but four other much weaker frequencies were clearly present. The same five frequencies were found from data obtained in 1998 July and September, although there is some indication of changes in amplitude in some frequencies.

In 2003 July, two runs of just over six hours each were obtained on successive nights. The most obvious change is that the very strong frequency near 6806 μHz has decreased in amplitude from 0.026 mag to 0.004 mag. It is also apparent that a frequency near 7425 μHz (135 s, 0.002 mag) has disappeared in the 2003 data and a new frequency near 7913 μHz (126 s, 0.004 mag) has appeared.

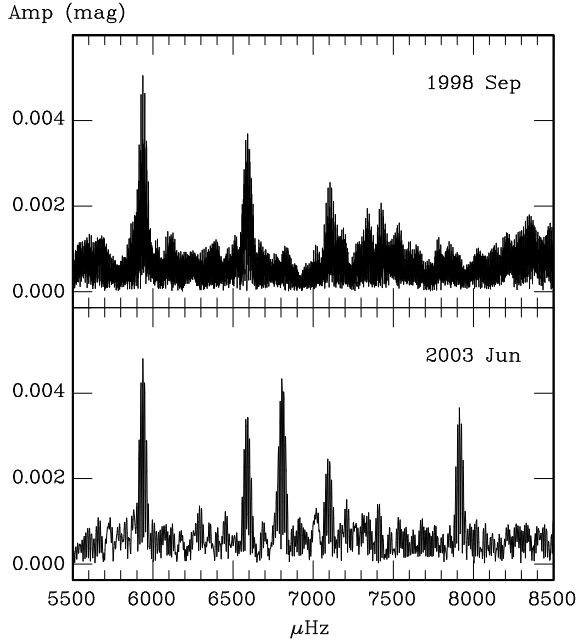


Fig. 1. Periodograms for EC 20338-1925 for 1998 September and 2003 July. The strong frequency (0.026 mag) near 6805 μHz has been removed from the 1998 September data to allow other frequencies to be seen. The most dramatic difference between 1998 and 2003 is that this frequency has dropped to an amplitude of 0.004 mag in 2003. The frequency near 7425 μHz has disappeared from the 2003 data and a completely new frequency near 7913 μHz has appeared.

3.3. HS 2149+0847 (=V384 Peg)

HS 2149+0847 was discovered to be a pulsating sdB star by Østensen et al. (2001). Two short runs showed two clear frequencies near 6.3 mHz (0.011 mag) and 7.1 mHz (0.007 mag) with a possible third frequency near 6.7 mHz (0.002 mag). We obtained four runs on HS 2149+0847 during 2003 July and ten runs during 2004 June. In both sets of data, we find the same six frequencies (see Figure 2) and there seems little evidence for any significant changes in the amplitudes between the two dates.

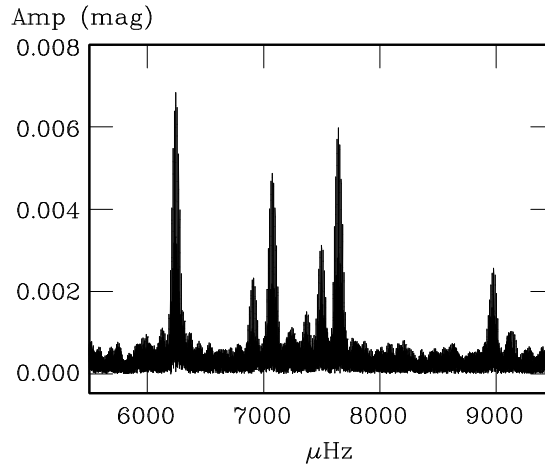


Fig. 2. Periodogram for HS 2149+0847 for 2004 June (10 nights).

3.4. PG 1605+072 (=V338 Ser)

PG 1605+072 was discovered to be an sdB pulsator by Koen et al. (1998). It is the largest amplitude sdB pulsator known and has a remarkable number of frequencies resolved (> 40) as was shown in both the discovery paper and in 1997 by Kilkenny et al. (1999). It is also unusual in that most of its pulsation modes are of rather longer period than in the other rapidly pulsating sdB stars (350–550 s) – probably due to the lower surface gravity.

During the 2004 NASSP student project, PG 1605+072 was observed on twelve nights out of two weeks. The 1997 data – split into two separate weeks – seem consistent between the two weeks, but significant changes are obvious between the two weeks in 2004 and between 2004 and 1997. Such changes are not unexpected – they were noted between the discovery data of Koen et al. (1998) and the campaign reported by Kilkenny et al. (1999).

Between 1997 and 2004, the four strongest frequencies are still the strongest, but their “rank” is reversed. Using the Kilkenny et al. (1999) nomenclature, f_3 and f_4 have more than doubled in amplitude; f_1 has more than halved, while f_2 is about the same. Many of the strongest remaining frequencies from 1997 are still found in the top twenty, though f_7 is absent and a number of “new” frequencies have appeared.

4. CONCLUSIONS

The phenomenon described above is not new – several authors have noted changing amplitudes – but these raise some questions:

- Are these changes related to the growth and decay of normal modes? This seems likely, but why does this happen?
- On what sort of time scale(s) are the changes happening?
- If these are normal modes, will repeated observation of the stars enable us to map out a more substantial frequency set for analysis?

REFERENCES

- Charpinet S., Fontaine G., Brassard P. 2001, PASP, 113, 775
- Deeming T. J. 1975, Ap&SS, 36, 137
- Kilkenny D. 2002, in *Radial and Non-Radial Pulsations as Probes of Stellar Physics*, eds. C. Aerts, T. R. Bedding, J. Christensen-Dalsgaard, ASP Conf. Ser., 259, 356
- Kilkenny D., Koen C., O’Donoghue D., Stobie R. S. 1997, MNRAS, 285, 640
- Kilkenny D. et al. 1999, MNRAS, 303, 525
- Kilkenny D. et al. 2003, MNRAS, 345, 834
- Koen C., O’Donoghue D., Kilkenny D., Lynas-Gray A. E., Marang F., van Wyk F. 1998, MNRAS, 296, 317
- Østensen R., Solheim J.-E., Heber U., Silvotti R., Dreizler S., Edelmann H. 2001, A&A, 368, 175

ULTRACAM PHOTOMETRY OF PULSATING SUBDWARF B STARS

C. S. Jeffery¹, C. Aerts^{2,3}, V. S. Dhillon⁴ and T. R. Marsh⁵

¹ *Armagh Observatory, College Hill, Armagh BT61 9DG, U.K.*

² *Institute of Astronomy, Catholic University of Leuven, Celestijnenlaan 200 B, B-3001 Leuven, Belgium*

³ *Department of Astrophysics, Radboud University Nijmegen, PO Box 9010, 6500 GL Nijmegen, The Netherlands*

⁴ *Department of Physics and Astronomy, University of Sheffield, Sheffield S3 7RH, U.K.*

⁵ *Department of Physics, University of Warwick, Coventry CV4 7AL, U.K.*

Received 2005 September 29

Abstract. High-speed multicolor photometry with ULTRACAM promises to revolutionize the study of pulsating subdwarf B stars. As well as providing high S/N light curves with excellent temporal resolution, color amplitude ratios may be used to discriminate between different pulsation modes. In this paper we review the methods for mode determination developed for KPD 2109+4401 and HS 0039+4302 since the 2003 workshop. We also present a new dataset obtained over 6 nights in 2004 August for PG 0014+067. This was the first sdB star to be subjected to a detailed asteroseismological analysis. It was also the subject of the WET campaign in 2004 October/November (XCov24). We discuss the implications of our new observations for mode identification and rotation.

Key words: stars: hot subdwarfs – stars: oscillations

1. INTRODUCTION

The discovery of pulsations in subdwarf B (sdB) stars has provided a vital key for measuring their global properties and for exploring their internal structure. Such information allows us to test theories of stellar physics, the structure of horizontal-branch stars and the origin of sdB stars. Many aspects of sdB star astronomy are described elsewhere in this volume; here we describe our application of high-speed multicolor photometry to the asteroseismology of sdB stars.

2. NON-RADIAL OSCILLATIONS

Nonradial oscillations (*nro*'s) are waves travelling through the interior of a star. They may manifest as surface displacements characterized by a spherical harmonic:

$$s = s_0 Y_{\ell,m}(\theta, \phi) \cos(2\pi\nu t) \quad (1)$$

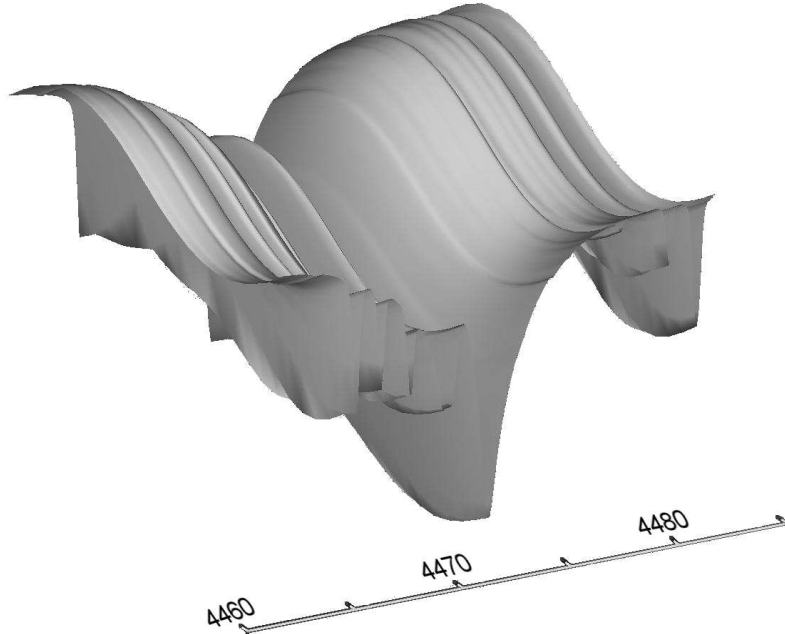


Fig. 1. Spectral variation near He I 4471 Å due to one cycle of a radial mode ($\ell, m = 0, 0$) in a pulsating sdB star. Scales are arbitrary.

where ν represents the frequency of the oscillation, ℓ : the degree of the spherical harmonic or the number of lines of nodes on a spherical surface and m : the azimuthal number or the number of lines of nodes passing through the polar axis ($|m| \leq \ell$). Besides these surface nodal line identifications, n (or k) denotes the order of the oscillation eigenfunction. In the linear adiabatic approximation this is equivalent to the number of nodes along the radial direction.

Such oscillations are probably excited at some level in a very large fraction of all stars. Many hundreds of modes have been identified in the Sun. However, because of superposition and cancellation, *nro*'s are generally manifest only when they are both of sufficiently low degree *and* of significant amplitude. They become observable principally as variations in total light, color, radial velocity or absorption line profile. The effects of low-degree oscillations on a stellar spectrum are illustrated in Figures 1 and 2. Fig. 1 shows the flux as a function of wavelength and time through one cycle of a radial pulsation with a simulated velocity amplitude of 10 km s^{-1} . The top panel in Fig. 2 shows the average spectrum of a star in the region of $\text{H}\gamma$. Below are shown grey-scale representations of residual time series (e.g., the average spectrum subtracted from the time-varying spectrum) for three non-radial modes (amplitudes = 10 km s^{-1}). The horizontal shading shows how the total flux varies through the pulsation cycle. The s-waves running through the vertical bands demonstrate how the disk-averaged radial motion of the stellar surface modifies the profiles of the absorption lines.

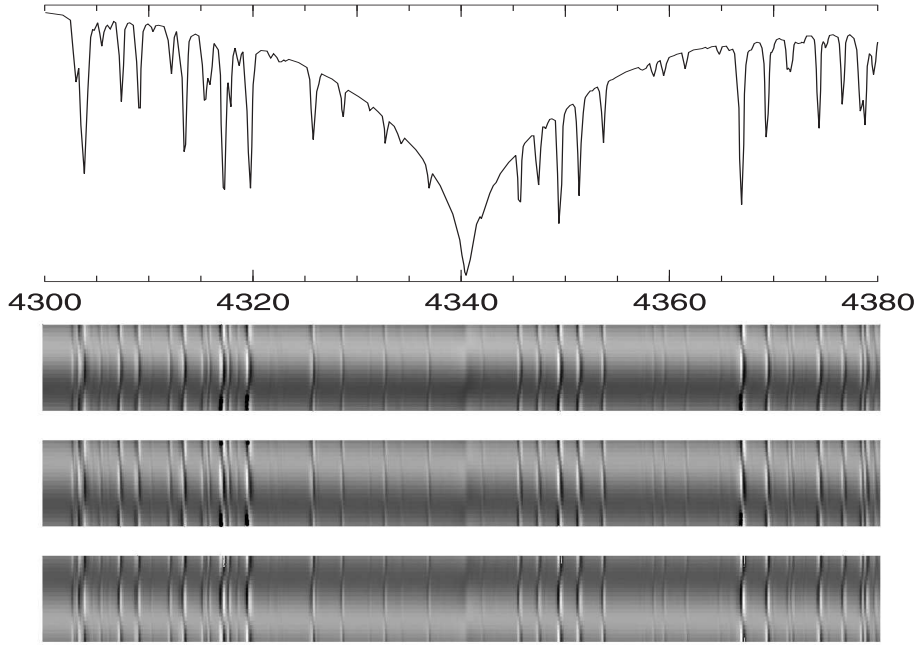


Fig. 2. Mean and trailed residual spectra for modes $l, m = (0, 0), (2, 0)$ and $(2, 2)$ (top to bottom).

Because *nro*'s propagate through the stellar interior, they provide indirect information about stellar structure. The best example is provided by the Sun, where *nro*'s have been used to measure the internal density profile, internal rotation speed, structure of the tachocline, and the presence of sunspots on the invisible hemisphere. In stars, internal structure is inferred by finding the best match between observed oscillation frequencies and frequencies computed from families of stellar interior models. Generally, only frequencies are used, principally because these can be measured from a single-channel light curve. In the best cases, such methods may yield n from the frequencies if the stellar radius is known and m from frequency splitting if rotation lifts the azimuthal degeneracy. l is harder to identify, but can generally be assumed to be small.

We have attempted various approaches to identify l in the *nro*'s of pulsating sdB stars. One result is particularly apposite (Heynderickx et al. 1994). For a given mode, the ratio of photometric amplitude at different wavelengths is independent of the inclination of the pulsation axis i to the observer and to m , but is sensitive to l . In principal, this allows us to identify l from multicolor photometry or spectrophotometry, and thereafter by elimination to identify n . With n and l derived empirically, the comparison with theoretical models is much more tightly constrained. We may also be able to learn something about rotation by identifying multiplets, i.e., oscillations at different frequencies with the same n, l but different m .

We have therefore obtained high-speed multicolor photometry for a number of sdB stars using 4 m telescopes and developed the necessary diagnostic tools in an effort to identify n and l for comparison with models.

Table 1. Codes for spectroscopy and photometry simulations.

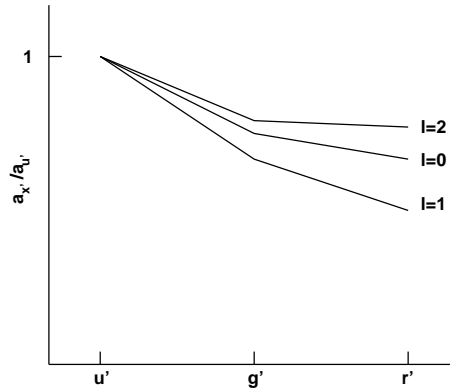
| |
|---|
| STERNE: LTE line-blanketed model atmospheres |
| IN: $T_{\text{eff}} = 25 - 35$ kK, $\log g = 4 - 6$, X_i |
| OUT: model grid: T_τ, P_τ |
| SPECTRUM: LTE specific intensities |
| IN: STERNE models, $X_i, v_{\text{turb}}, \langle \mu \rangle, \langle \lambda \rangle$ |
| OUT: intensity grid: $I_{\mu\lambda}$ |
| BRUCE: surface description of <i>nro</i> 's |
| IN: $M, T_{\text{eff}}, R_{\text{eq}}, i, v_{\text{rot}}, \langle \ell, m, P, v \rangle, n_t, t_n$ |
| OUT: $T_{\theta\phi}, g_{\theta\phi}, \mu_{\theta\phi}, a_{\theta\phi} \sin i, v_{\theta\phi} \sin i$ |
| KYLIE: apparent fluxes |
| IN: BRUCE models, $I_{\mu\lambda}, \langle \lambda \rangle, \delta\lambda$ |
| OUT: $F_{\lambda t}$ |
| FAST: Fourier analysis of spectroscopic time-series |
| IN: $F_{\lambda t}$ |
| OUT: ν, ϕ, a |

3. THEORETICAL PHOTOMETRY

The color-amplitude ratio method involves measuring the amplitude a of an oscillation in light measured in two or more wavelength intervals. The principle is illustrated schematically in Figure 3. In order to determine the value of ℓ responsible for an observed curve in this figure, it is first necessary to derive theoretical amplitude ratios from model atmospheres and pulsation theory. For consistency we will refer to the pass bands u', g' and r' of the Sloan Digital Sky Survey (Fukugita et al. 1996).

A summary of the codes used, with their principal inputs and outputs, is given in Table 1. The same codes, models and methods may of course be used to compute amplitude ratios for broad-band photometry and for spectrophotometry, as well as for detailed modelling of line-profile and radial velocity variations (cf., Figs. 1 and 2).

Ramachandran et al. (2004) have predicted amplitude ratios for examples of both short and long-period sdBVs (EC 14026-2647 or V 361 Hya and PG 1716+426 variables). These are based on a grid of LTE model atmospheres and synthetic spectra computed (using programs STERNE and SPECTRUM) over a range of effective temperatures T_{eff} , surface gravities g and wavelengths λ , with appropriate values for composition X_i and microturbulent velocity v_{turb} (Jeffery et al. 2001). We calculate intensity spectra $I_{\mu\lambda}$, including continuum intensities, over a range

**Fig. 3.** Schematic amplitude ratios.

of cosine angles μ in order to have an explicit description of what is known as the effective “limb darkening” at all wavelengths and, notably, in all lines.

Using program KYLIE (Townsend 1997), these intensity spectra are folded into a description of the moving surface provided by program BRUCE (*ibid.*), which calculates the surface geometry due to an adiabatic non-radial pulsation. This description includes the local T_{eff} , g , projected velocity, surface area and inclination on a finely spaced grid covering the visible hemisphere.

The result is a time series of spectra, both line and continuum fluxes $F_{\lambda t}$, $F_{c\lambda t}$ for any specified temporal resolution and duration and for any desired spectral resolution and range, for a star pulsating in one or more non-radial modes, each with a specified period and amplitude.

This time series may be analyzed in a number of ways. For application of the amplitude ratio method, we convolved each spectrum $F_{\lambda t}$ with photometric filter transmission functions (SDSS $u'g'r'$ and Johnson $UBVRI$) and converted to magnitudes. We then fitted one or more sine functions to determine the amplitude (and phase) of each oscillation in each filter ($a_{u'}$, $a_{g'}$, $a_{r'}$) from which ratios were trivial to compute.

To find disk integrated and projected velocity amplitudes and line profile behavior, we identified a template spectrum $A_{\lambda 0} - 1$ and computed the cross-correlation function (ccf) for each residual spectrum $A_{\lambda t} - 1$. The projected radial velocity v_t is measured by locating the peak of each ccf; higher order moments of the ccf are also computed. Sine functions are again fitted to each oscillation in order to measure amplitudes and phases. This work is done with the program FAST (Fourier Analysis of Spectroscopic Time Series).

This procedure may be further refined by choosing the wavelength region to include either a single line profile, many absorption lines or the entire UV/optical spectrum. Our goal is to choose a series of procedures which effectively mimic the observations as closely as possible.

4. ULTRACAM PHOTOMETRY

ULTRACAM is a high-speed 3-channel CCD camera (Dhillon & Marsh 2001, Figures 4 and 5). Dichroics split the light into ultraviolet, visual and red wavebands which are simultaneously imaged with frame transfer CCDs, each having a $5' \times 5'$ (1024×1024 pixels) imaging area. These CCDs use a masked area into which exposures are shunted rapidly from the imaging area, and which can then be read out while the next exposure is running. Mounted on the 4.2 m William Herschel Telescope, the combination of high throughput and high time resolution provides

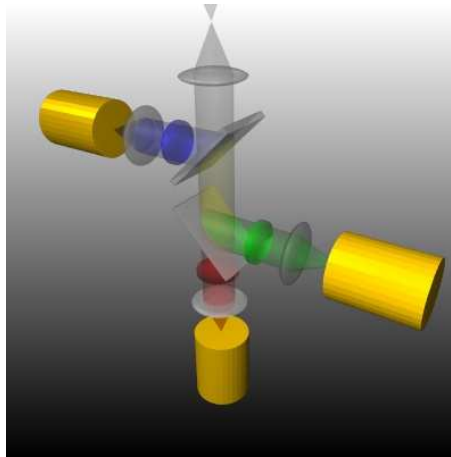


Fig. 5. ULTRACAM design.

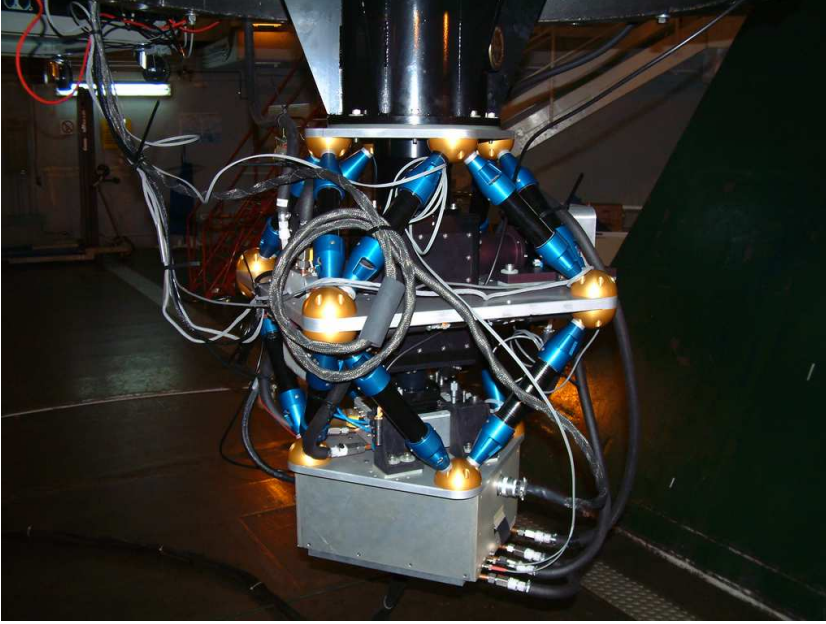


Fig. 4. ULTRACAM on the WHT.

an outstanding tool with which to explore pulsating sdB stars. It is equipped with filters u' , g' , r' , i' and z' in the system designed for the Sloan Digital Sky survey (Fukugita et al. 1996), where the r' , i' and z' may be interchanged in the red channel. By a judicious choice of windows on the CCD, frame rates of $\sim 10^3$ Hz can be achieved. In our observations of sdBVs, frame rates of 0.1–10 Hz are more typical, primarily dictated by the pulsation frequencies ($\sim 5 - 8$ mHz) and, for the brightest targets, the need to avoid CCD saturation.

4.1. 2002 WHT campaign

First observations were obtained in 2002 September for the targets KPD 2109+4401 and HS 0039+4302. A portion of the light curves for each of these targets is shown in Figure 6. From amplitude spectra obtained with these light curves, the amplitudes of several modes were measured in each of the three ULTRACAM channels, being u' , g' and r' of the SDSS system. The ratios $a_{g'}/a_{u'}$ and $a_{r'}/a_{u'}$ were computed and are shown in Figure 7. Meanwhile, theoretical models of the color amplitude ratios expected for non-radial oscillations of different spherical degree in sdBVs were computed by Ramachandran et al. (2004).

From Fig. 7 it was clear that at least one oscillation in each target had to be a relatively high-degree ($\ell = 4$) mode. Predicted ratios for low-degree modes ($\ell = 0, 1, 2$) lie close together, so it is not possible to identify the degree of the observed modes so easily. There were no modes identified with $\ell = 3$. Assuming the observed frequencies belong to modes with unique k, ℓ values (i.e., there is no rotational splitting), an additional constraint can be used. For a given degree ℓ , modes of successive radial order k must be well-spaced in frequency, so modes of similar frequency cannot have the same ℓ . By imposing such a constraint and

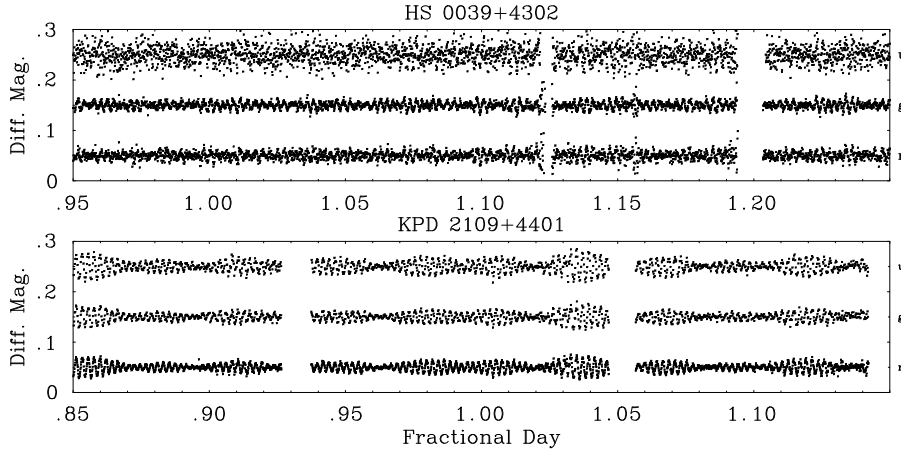


Fig. 6. Partial ULTRACAM light curves in u' , g' and r' for sdBVs KPD 2109+4401 and HS 0039+3202 (adapted from Jeffery et al. 2004). Gaps are due to clouds.

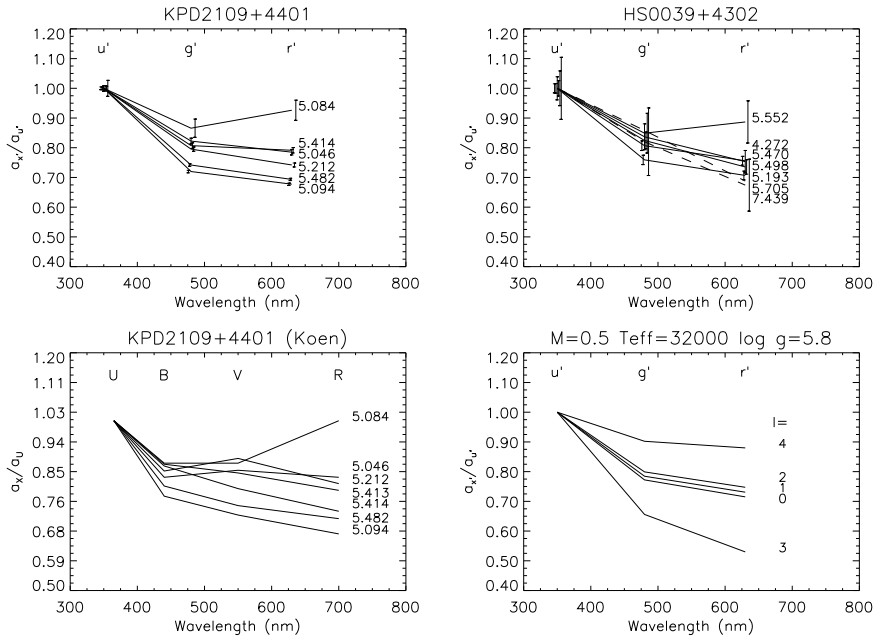


Fig. 7. Observed amplitude ratios for KPD 2109+4401 and HS 0039+4302 (top). Modes with $a_{u'} < 1.4$ mmag shown as dashed lines. Lower panels show previous photometry of KPD 2109+4401 (left, Koen 1998) and a set of theoretical color-amplitude ratios $\ell = 0, \dots, 4$ (right, Ramachandran et al. 2004). From Jeffery et al. (2004).

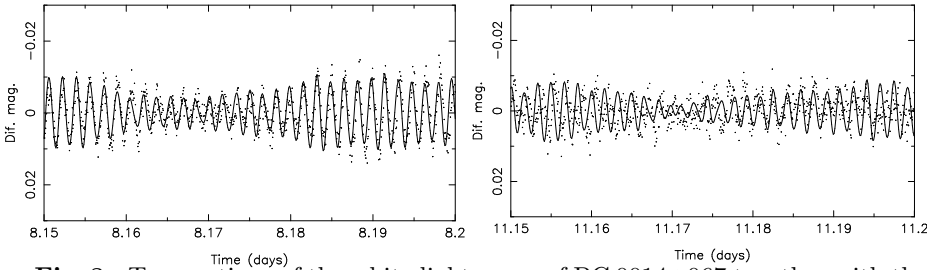


Fig. 8. Two sections of the white light curve of PG 0014+067 together with the 19-frequency solution. Time (t) is JD-2453230. From Jeffery et al. (2005).

by comparing the color-amplitude ratios, it is possible to assign k and ℓ values with some confidence. It is then possible to compare the observed frequency spectrum with theoretical models for non-radial oscillations in extended horizontal-branch stars (cf. Charpinet et al. 2002), and hence to select which models best represent the star observed in terms of total mass, envelope mass, age and other characteristics. A full description of the observations and the identification of the modes in these two stars is given by Jeffery et al. (2004).

4.2. 2004 WHT campaign

A second ULTRACAM run to observe pulsating sdBVs was executed in 2004 September. Observations of a secondary target, the 17th mag sdB SDSS J171722.08 +58055.8, are presented by Aerts et al. (2006).

The primary target was the magnitude 16.5 star PG 0014+067, previously the subject of successful asteroseismological studies by Brassard et al. (2001) and Charpinet et al. (2005). This star showed ~ 20 independent frequencies in its white light curve with frequencies between 5.7 and 12.9 mHz. Our aim was to check mode identifications deduced from the theoretical model that best fitted the fre-

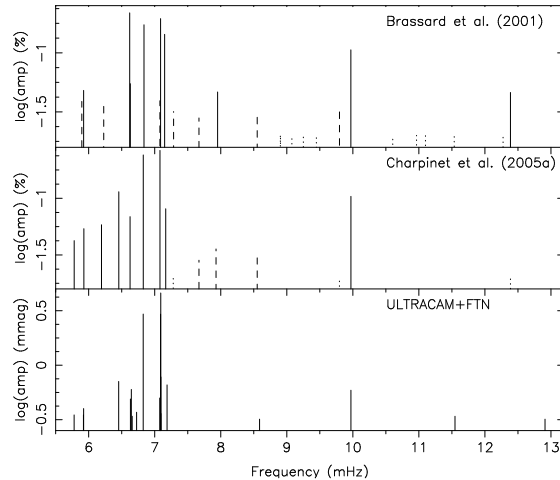


Fig. 9. Comparison of three independent frequency amplitude spectra for PG 0014+067. Solid lines are 4σ detections, dashed lines 3σ , and dotted lines are observed frequencies coincident with frequencies in best fit models. From Jeffery et al. (2005).

quency spectrum, and also to support a subsequent Whole Earth Telescope campaign to improve the overall frequency resolution. Although a much more challenging target than the 2002 targets, it was possible to observe this object with the WHT for ~ 6 hours on each of 6 successive nights. These observations were supported with data from Faulkes Telescope North, located on the Hawaiian island

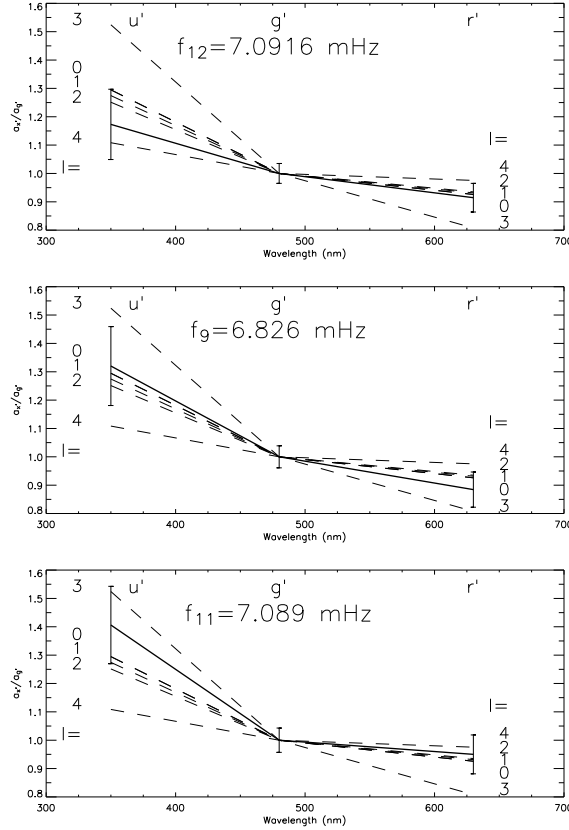


Fig. 10. Amplitude ratios for the three largest amplitude modes in PG 0014+067 (solid) and from theory (Ramachandran et al. 2004, dashed lines). From Jeffery et al. (2005).

of Maui. ~ 8 hours data obtained over five nights proved invaluable for improving the window function and enabling us to identify 19 frequencies correctly.

Two segments of the “white light” curve, obtained by combining the 3-channel ULTRACAM data with data from the Faulkes telescope, together with the 19-frequency solution, are shown in Figure 8. One important goal was to verify previous frequency analyses (Figure 9). Most major frequencies identified previously were confirmed, differences are probably due to cycle d^{-1} aliases.

In terms of mode identification, the results were less conclusive than for the targets observed in 2004. However it was possible to show that the two dominant modes must be $\ell = 0, 1$ or 2 (Figure 10), and to find evidence that the rotational period should be nearer to 4 d than to the 1.35 d reported previously. The first result is significant because it contradicts the best seismic models (Charpinet et al. 2005, Brassard et al. 2001), in which the dominant mode has $\ell = 3$.

Full details of this analysis have been published by Jeffery et al. (2005). Preliminary results of the 2004 WET campaign on PG 0014+067 are presented by Kawaler et al. (2006).

5. THE FUTURE

ULTRACAM has proved to be a powerful instrument for the interpretation of, to date, four pulsating sdB stars. There are three ways in which it will make a significant impact in the future. Mounted on an 8 m class telescope, such as the VLT, it can provide outstanding multicolor light curves for short-duration events, such as eclipses in those HW Vir systems which contain a pulsating sdB star. In conjunction with other 4 m telescopes, multi-site campaigns covering four to seven days and multicolor photometry of stars brighter than 15th mag. will allow identification of both frequencies and ℓ values for modes with amplitudes 0.5 mmag or less. Finally, the prospect that ULTRACAM may be available for more extended periods on a 2.5 m class telescope offers the prospect of extending mode identifications to a much larger sample of sdBVs than has been possible so far.

REFERENCES

- Aerts C., Jeffery C. S., Dhillon V. S. et al. 2006, *Baltic Astronomy*, 15, 275 (these proceedings)
- Brassard P., Fontaine G., Billères et al., 2001, *ApJ*, 563, 1013
- Charpinet S., Fontaine G., Brassard P., Dorman B. 2002, *ApJS*, 140, 469
- Dhillon V., Marsh T. R. 2001, *New Astr. Rev.*, 45, 91
- Fukugita M., Ichikawa T., Gunn J. E., Doi M. 1996, *AJ*, 111, 1748
- Heynderickx D., Waelkens C., Smeyers P. 1994, *A&AS*, 105, 447
- Jeffery C. S., Dhillon V. S., Marsh T. R., Ramachandran B. 2004, *MNRAS*, 352, 699
- Jeffery C. S., Aerts C., Dhillon V. S., Marsh T. R., Gänsicke B. 2005, *MNRAS*, 362, 66
- Kawaler S. 2006, *Baltic Astronomy*, 15, 283 (these proceedings)
- Koen C. 1998, *MNRAS*, 300, 567
- Ramachandran B., Jeffery C. S., Townsend R. H. D. 2004, *A&A*, 428, 209
- Townsend R. H. D. 1997, Ph. D. Thesis, University College London

SEARCHING FOR OBSERVATIONAL EVIDENCE OF TIDALLY INCLINED PULSATIONS

M. D. Reed¹ and the Whole Earth Telescope Xcov 21 and 23 collaborations²

¹ *Missouri State University, Springfield, MO 65804, U.S.A.*

² *Complete lists of participants available at wet.physics.iastate.edu*

Received 2005 August 1

Abstract. We attempt to interpret frequencies detected in KPD 1930+2752 with those of a pulsator in which the pulsation axis is influenced by tidal forces and continually points toward the companion. KPD 1930+2752 is in a close binary with a period of about 2 hours. It was observed by the Whole Earth Telescope in the summer of 2003.

Key words: stars: post-AGB – stars: oscillations – stars: individual (KPD 1930+2752)

1. INTRODUCTION

In order for asteroseismology to discern the internal conditions of variable stars, the pulsation “mode” as represented mathematically by spherical harmonics with quantum numbers n (sometimes designated k), ℓ and m , must be identified. For nonradial, multimode pulsating stars, pulsation periods, frequencies and/or the spacings between them are used to discern the spherical harmonics (see for example Winget et al. 1991). These *known* modes are then matched to models that are additionally constrained by non-asteroseismic observations; typically T_{eff} and $\log g$ from spectroscopy. Within such constraints, the model that most closely reproduces the observed pulsation periods (or period spacing) for the proper modes is inferred to be the correct one. Occasionally, such models can be confirmed by independent measurements (Reed et al. 2004; Reed, Kawaler & O’Brien 2000; Kawaler 1999). Unfortunately, more often than not, it is impossible to uniquely identify the spherical harmonics and asteroseismology cannot be applied to obtain a unique conclusion.

Several methods are being pursued to observationally constrain the spherical harmonics including time-series spectroscopy (see Telting et al. 2006, Aerts et al. 2006, Harms et al. 2006, Schoenaers & Lynas-Gray 2006 and Geier et al. 2006 in these proceedings) and multicolor photometry (see Jeffery et al. 2006). Our contribution is to use tidal forces in close binaries.

Analogous to the oblique pulsator model described by Kurtz (1992), that has been successfully applied to roAp stars, tidal forces may impact pulsations by inclining the spherical harmonics towards the companion along the tidal force. KPD 1930+2752 (hereafter KPD 1930) was discovered to be an sdBV star with a massive white dwarf companion in a 2.5 hour binary (Billères et al. 2001). In this

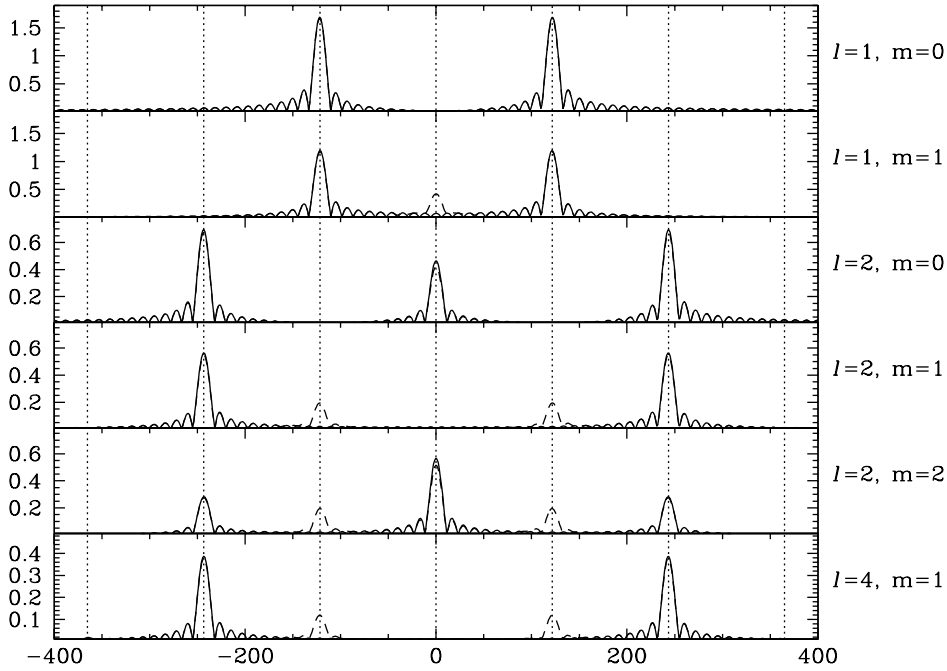


Fig. 1. Temporal spectra (Fourier transform, FT) of simulations for KPD 1930 assuming a tidally induced pulsation axis. The solid lines are simulations for an orbital axis of 90° and the dashed lines are for an orbital axis of 80° . The dotted lines indicate the input frequency (at 0) and orbital splittings.

case the tidal force is strong enough to slightly distort the sdB star but no eclipses have been positively detected. As the pulsation geometry should align with the strongest force, a measure of the likelihood of the pulsation axis to point at the companion is the ratio of the tidal to centrifugal acceleration. For KPD 1930 this ratio is 1.7:1, making it the best candidate known at this point.

2. WHAT DO WE EXPECT TO SEE?

We have previously discussed our simulations to determine the impact on pulsations for a pulsation axis that points at the companion and precesses with the orbital period (Reed, Brondel & Kawaler 2005; Reed et al. 2001). For KPD 1930 we can specifically ask what we expect to see. Our simulations calculate the relative brightness for a grid of 10 000 points on the observable surface of the star (one half of the entire spherical surface with the line-of-sight remaining constant). A modest amount of limb darkening was included using limb darkening coefficients from van Hamme (1993) for a model with $T_{\text{eff}} = 29\,000$ K and $\log g = 5.0$ for the square root law at $\lambda = 5000$ Å. For the simulations in this paper, we used pulsation and orbital periods appropriate for KPD 1930, assuming that the tidal force causes the pulsation axis to point directly at the companion and tested two orbital (rotational) axis inclinations of 80° and 90° . Figure 1 shows the results of these

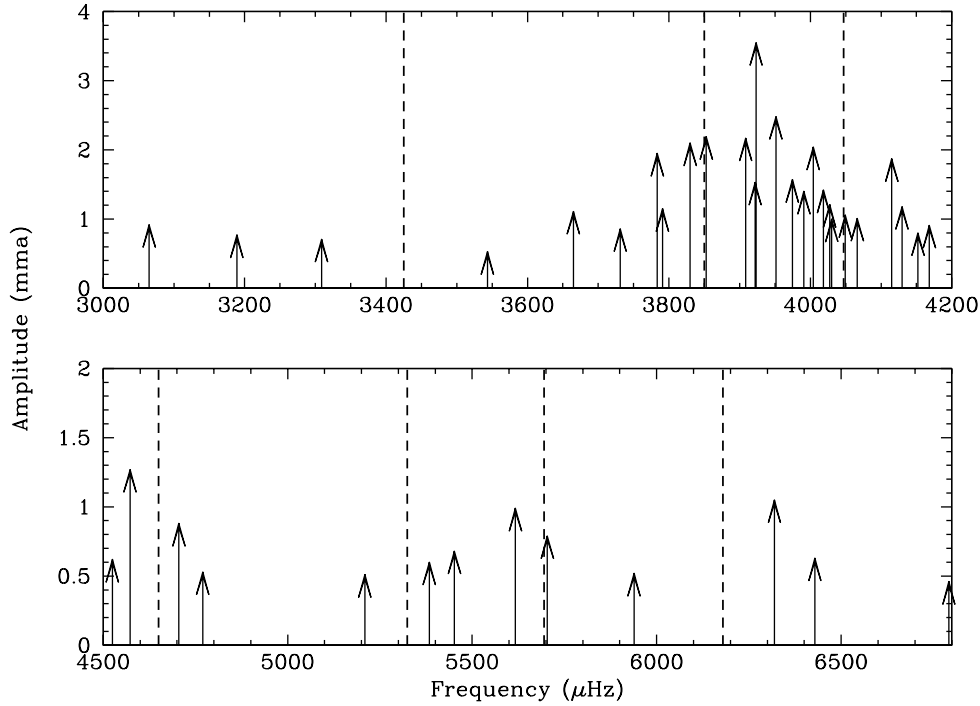


Fig. 2. Representation of the temporal spectrum (FT) for KPD 1930. Arrows indicate frequencies detected with the height indicating the observed amplitude. Dashed lines indicate frequencies we anticipate to detect once the data are divided into phases appropriate for various modes.

simulations for several pulsation modes. For each panel of the figure, we input a single frequency (at 0 μHz) and then, using 10 s time steps, integrated the light curve over about 10 orbital cycles (about a day). This has been done for two inclinations for the binary/rotation axis: 80° (dashed lines in the figure) and 90° . As the dashed 80° lines are nearly indistinguishable from the solid 90° lines, we can conclude that small changes in the binary/rotation axis will not change the results. Note that in four of the six modes shown, the original, input frequency is not detected. This is because the phase of pulsation changes over the orbital period as we “look” at opposite sides of the star. These opposite phases serve to cancel the input frequency in many cases. If the light curve is properly divided into regions of like phase for an individual pulsation mode, the central, input frequency is recovered. So even though both of the m values for $\ell = 1$ look the same, the data are divided differently to recover the input frequency. As such, different m values are easily distinguishable.

2.1. The pulsation content of KPD 1930

The next step is to examine the observed frequency content of KPD 1930 in the complete data set to look for multiplets matching those in Figure 1. An examination of the complete frequency content of KPD 1930 is beyond the scope (and

Table 1. Pulsation frequencies split by a multiple of the rotation/orbital frequency. The pulsation frequencies are in descending order and the number in parentheses indicates the multiple of the rotation/orbital frequency between itself and the previously listed frequency.

| | |
|---------|---|
| 6791.9: | 6428.9 (3), 5938.6 (4), 5451.8 (4), 5208.9 (2) |
| 5383.8: | 4769.8 (5), 4524.8 (2) |
| 4705.2: | 3974.5 (6), 3852.7 (1), 3731.1 (1) |
| 4168.1: | 4049.2 (1), 3923.2 (1) |
| 4152.1: | 4030.2 (1), 3908.5 (1), 3783.4 (1), 3664.9 (1), 3543.2 (1), 3308.8 (2), |
| cont. | 3188.9 (1), 3064.9 (1) |
| 4129.6: | 4004.0 (1) |
| 4115.0: | 3990.8 (1) |
| 4066.4: | 3951.2 (1), 3829.9 (1) |
| 3921.9: | 3790.9 (1) |

space) of this paper, but 39 frequencies have been detected with some confidence in the Xcov 23 data. Table 1 lists those frequencies which form multiplets near the orbital/rotational frequency splitting. The pulsation frequencies are listed in descended order (an arbitrary choice) with the multiple of the splitting between that frequency and the previously listed one in parentheses.

Anytime we see a splitting of $2 \times f_{\text{orb}}$, it is an indication of a tipped $\ell = 1$ mode, while splittings of $4 \times f_{\text{orb}}$ indicate either an $\ell m = 2, 1$ or $4, 1$ mode. Figure 2 shows arrows representing frequencies detected in the Xcov 23 data, and the dashed lines indicate where we would expect new peaks to appear when the data are phase-separated for individual modes.

3. WHAT DO WE REALLY SEE?

Now that we know what to potentially look for from the simulations, and where to look for new peaks from the complete data set, it is time to separate the data into regions of like phases for various pulsation modes and see what appears. Pulsations modes that would change phases during an orbital cycle are separated so that all the data for each phase forms a data set. Then we can fit and prewhiten them in the usual manner, without influence from the complete data set (that is, reduce them as per normal without assuming any a priori frequencies). Frequencies that match between the two phase sets are then examined to see if they (1) are detected in the complete data or are only in the phased data, (2) at a frequency expected (dashed lines in Figure 2) if not in the complete data, and/or (3) differ in phase as expected. Figures 3 and 4 show data phase-separated for several different pulsation modes.

4. RESULTS

We have examined data from Xcov 23 to look for indications of tidally modified pulsations. As can be seen from Figures 3 and 4, we have failed to detect any. No new frequency peaks appear where we would expect them to. Though KPD 1930 is the best candidate for such inclined pulsations to occur, our efforts have been thwarted by an incredibly rich and complex pulsation spectrum. KPD 1930 has at least 39 independent pulsation frequencies, perhaps many more,

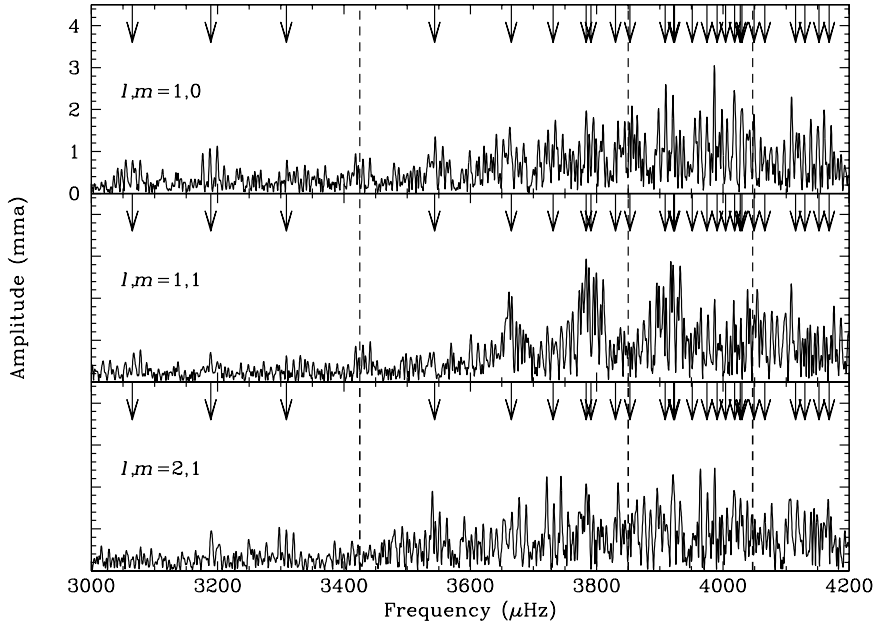


Fig. 3. Temporal spectra of Xcov 23 data separated appropriately for phase for the given mode. Only one of the phases is shown. The arrows and dashed lines are the same as in Fig. 2 except the arrows are inverted.

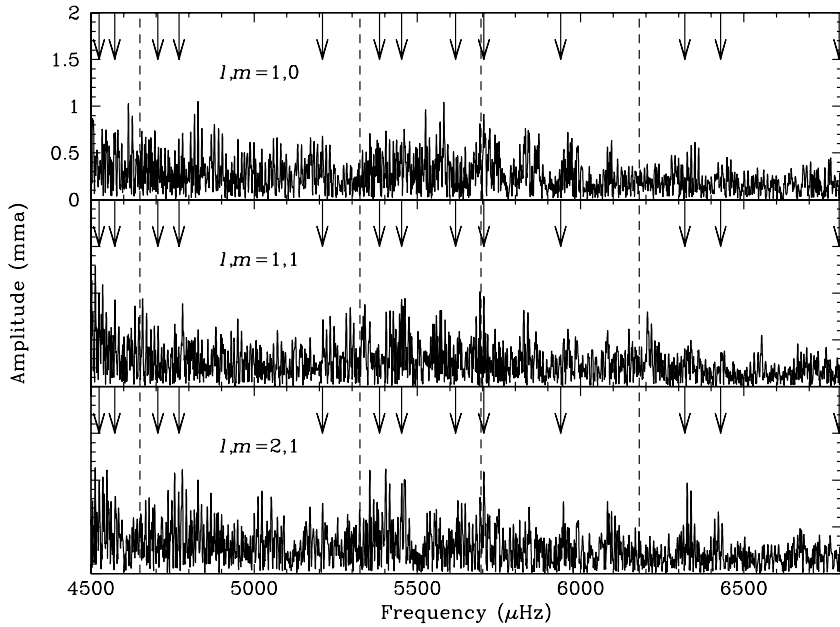


Fig. 4. The same as Fig. 3 for the higher frequency range.

with the amplitudes changing over just a few days. As such, it is incredibly difficult to interpret. If the data are divided such that amplitudes of pulsations are roughly constant, then most of the frequencies are unresolved. If the data are long enough to resolve the pulsations, then the amplitudes have changed significantly within the data set, perhaps even disappearing altogether. It seems that if it is at all possible to understand the pulsation nature of KPD 1930, it will require constant, single-instrument observations over several weeks. Satellites such as MONS (which will not observe KPD 1930) would be the tool of choice. For such a complex pulsator, any additional complications, such as those from multiple and multiply-sensitive instruments, or aliasing caused by gaps in the data, make the temporal spectrum impossible to decipher.

ACKNOWLEDGMENTS. This material is based in part upon work supported by the National Science Foundation under Grant Numbers AST 007480 and AST 9876655. Any opinions, findings and conclusions or recommendations expressed in this material are those of the author(s) and do not necessarily reflect the views of the National Science Foundation.

REFERENCES

- Aerts C., Jeffery C. S., Dhillon V. S. et al. 2006, *Baltic Astronomy*, 15, 275 (these proceedings)
- Billères M., Fontaine G., Brassard P., Charpinet S., Liebert J., Saffer R. A., Bergeron P., Vauclair G. 1998, *ApJ*, 494, L75
- Geier S., Heber U., Przybilla N., Kudritzki R.-P. 2006, *Baltic Astronomy*, 15, 243 (these proceedings)
- Harms S., Reed M. D., O'Toole S. J. 2006, *Baltic Astronomy*, 15, 251
- Jeffery C. S., Aerts C., Dhillon V. S., Marsh T. R. 2006, *Baltic Astronomy*, 15, 259 (these proceedings)
- Jeffery C. S., Pollacco D. 2000, *MNRAS*, 318, 974
- Kawaler S. D. 1999, in *The 11th European White Dwarf Workshop*, ed. J.-E. Solheim, ASP Conf. Ser., 158, 169
- Kurtz D. W. 1992, *MNRAS*, 259, 701
- Reed M. D., Brondel B. J., Kawaler S. D. 2005, *ApJ*, 634, 602
- Reed M. D. et al. 2004, *MNRAS*, 348, 1164
- Reed M. D., Kawaler S. D., O'Brien M.S. 2000, *ApJ*, 545, 429
- Reed M. D., Kawaler S. D., Kleinman S. J. 2001, in *12th European Workshop on White Dwarfs*, eds. J. L. Provencal, H. L. Shipman, J. MacDonald & S. Goodchild, ASP Conf. Ser. 226, 181
- Schoenaers C., Lynas-Gray A. E. 2006, *Baltic Astronomy*, 15, 219 (these proceedings)
- Telting J., Østensen R. H., Heber U., Augusteijn T. 2006, *Baltic Astronomy*, 15, 235 (these proceedings)
- van Hamme W. 1993, *AJ*, 106, 2096
- Winget D. E. et al. 1991, *ApJ*, 378, 326

HIGH-SPEED ULTRACAM COLORIMETRY OF THE SUBDWARF B STAR SDSS J171722.08+58055.8

C. Aerts^{1,2} C. S. Jeffery³ V. S. Dhillon⁴ T. R. Marsh⁵ and P. Groot²

¹ *Institute of Astronomy, University of Leuven, Celestijnenlaan 200B, B-3001 Leuven, Belgium*

² *Department of Astrophysics, Radboud University Nijmegen, P.O. Box 9010, The Netherlands*

³ *Armagh Observatory, Armagh BT61 9DG, U.K.*

⁴ *Department of Physics and Astronomy, University of Sheffield, Sheffield S3 7RH, U.K.*

⁵ *Department of Physics, University of Warwick, Coventry CV4 7AL, U.K.*

Received 2005 August 1

Abstract. We present high-speed multicolour photometry of the faint subdwarf B star SDSS J171722.08+58055.8 ($m_B = 16.7$ mag), which was recently discovered to be pulsating. The data were obtained during two consecutive nights in 2004 August using the three-channel photometer ULTRACAM attached to the 4.2 m William Herschel Telescope. We confirm the star to be oscillating and we refine the dominant frequency to 6.960 mHz. A second new frequency of 7.267 mHz was discovered. Both frequencies are significant in all three colors at level $> 5\sigma$ and vary in phase in the three colors. We attempted mode identification for the strongest mode from its amplitude ratios but did not succeed.

Key words: stars: subdwarfs – stars: variables – stars: oscillations – stars: individual (SDSS J171722.08+58055.8)

1. INTRODUCTION

Of the 33 sdB stars with p-mode oscillations known to date, few have been modelled seismically so far (Charpinet et al. 2006). These modeling efforts result in mode identification based on frequency matching from the theoretical predictions, by means of a procedure that gives equal probability to spherical degrees $\ell = 0, 1, 2, 3$. It is therefore clear that a great need for empirical mode identification, i.e., identification obtained independently of the details of the theoretical models, emerges. The easiest way to achieve such empirical identification is from multicolor high-precision photometry (Jeffery et al. 2006).

In this poster, we present ULTRACAM multicolor photometry of the sdB star SDSS J171722.08+58055.8 (hereafter abbreviated as SDSS 1717). This is an sdB star of B magnitude 16.7 in which Solheim et al. (2004) discovered oscillations from white-light data gathered with the Nordic Optical Telescope (NOT). The NOT data revealed a frequency of 7.03 mHz and a variable amplitude ranging

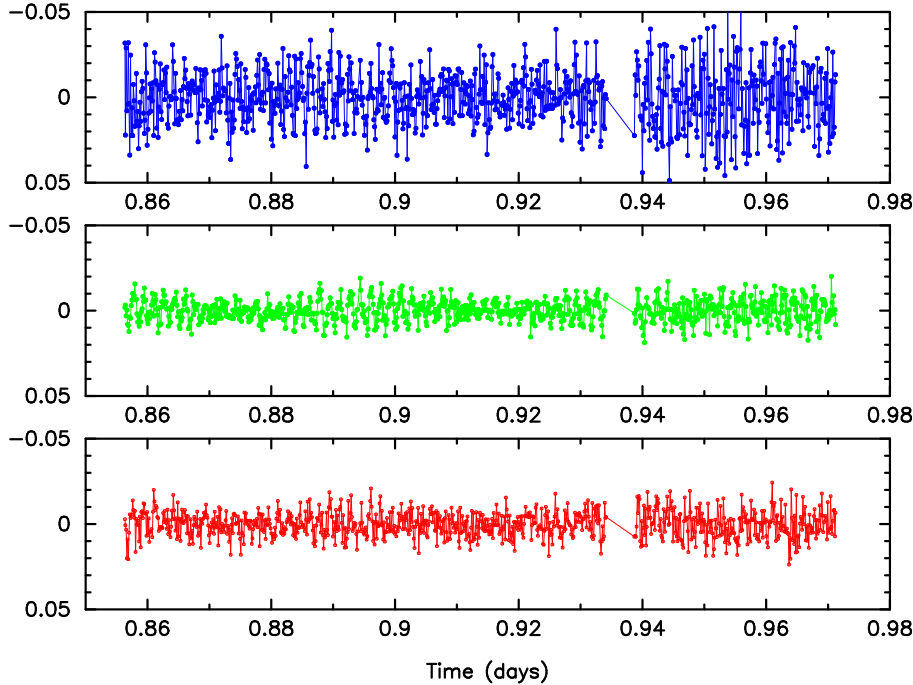


Fig. 1. ULTRACAM light curves for SDSS 1717 on 2004 August 24.

from 4.4 to 6.2 mmag, most likely due to multimode beating. Our data confirm this result and prove the multiperiodicity.

2. DATA DESCRIPTION

Jeffery et al. (2005) recently reported on the outcome of a six nights ULTRACAM run with the 4.2 m William Herschel Telescope dedicated to the sdB star PG 0014+067 performed in 2004 August. The main target was not yet visible during the first 2.5 hours of each of these nights. Two such blocks of 2.5 h on two consecutive nights were devoted to SDSS 1717 ($\alpha_{2000} = 17:17:22.0$, $\delta_{2000} = +58:05:59$) together with several comparison stars. We adopted an integration time of 10 s which samples the dominant 140 s pulsation well.

The reduction of the data frames was performed in the same manner as for PG 0014+067, which was already described in much detail in Jeffery et al. (2005). We hence refer the reader to that paper for information. Different comparison stars were considered to compute the differential magnitudes in the three channels (u' , g' , r'). The final results of the frequency analysis is independent of the different choices of the comparison stars. The details of the light curve computation will be presented elsewhere (Aerts et al., in preparation), but the final result for one night is shown in Figure 1. A beat pattern is readily seen in the g' light curve, pointing towards multiperiodicity as already suspected by Solheim et al. (2004).

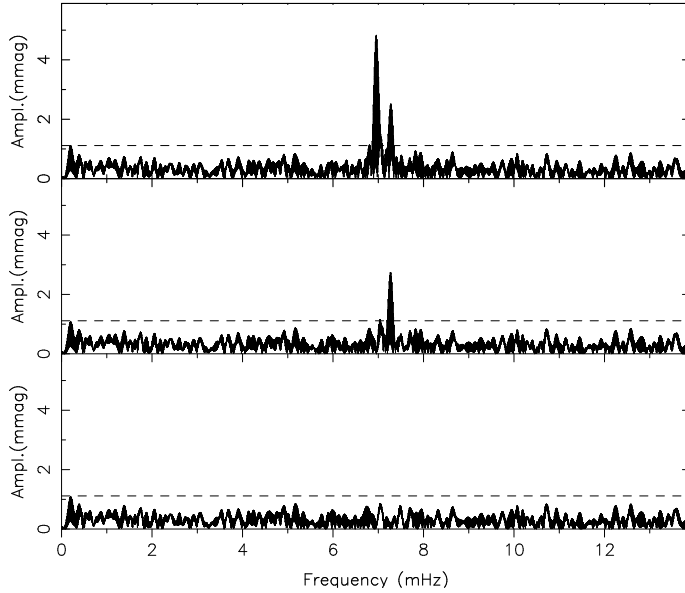


Fig. 2. Lomb-Scargle periodograms at subsequent stages of prewhitening for the g' light curve. The dashed line indicates the 4σ level after prewhitening with f_1 and f_2 determined within the interval 17–23 mHz.

3. FREQUENCY ANALYSIS

As in Jeffery et al. (2005), we computed Lomb-Scargle periodograms (Scargle 1982) over the frequency range $[0 \div 14]$ mHz in steps of $0.1 \mu\text{Hz}$ for each of the light curves and adopted a prewhitening procedure. The results for the g' filter are shown in Figure 2. We find one dominant frequency of $f_1 = 6.960(2)$ mHz with amplitudes of 5.8(8), 5.0(3) and 3.7(4) mmag for respectively u' , g' and r' . This result is entirely compatible with the one of Solheim et al. (2004). After prewhitening with f_1 , we find a second very significant frequency in all three residual light curves (middle panel of Fig. 2): $f_2 = 7.267(3)$ mHz. This new second frequency has amplitudes 3.8(7), 2.8(3) and 2.0(3) mmag in respectively u' , g' and r' . The periodograms following the second prewhitening stage reveal no further significant frequencies (see bottom panel in Fig. 2). The dashed lines in Fig. 2 indicate the 4σ level which we adopted as a stop criterion. In conclusion, we have found two independent oscillation frequencies in SDSS 1717, of which the second one was not known so far. All three light curves are in phase with each other for both f_1 and f_2 .

4. MODE IDENTIFICATION

We show the amplitude ratios with respect to the g' filter for f_1 and f_2 in Figure 3. The 1σ confidence interval is shown only for f_1 . The theoretical predictions in the adiabatic approximation are taken from Ramachandran et al. (2004, their Fig.4 top panel) for the temperature and gravity of SDSS 1717 (Solheim et al. 2004). It is impossible to identify the modes from this plot. For f_1 , the ratio u'/g' behaves according to $\ell \neq 3$, while the r'/g' ratio is only compatible with

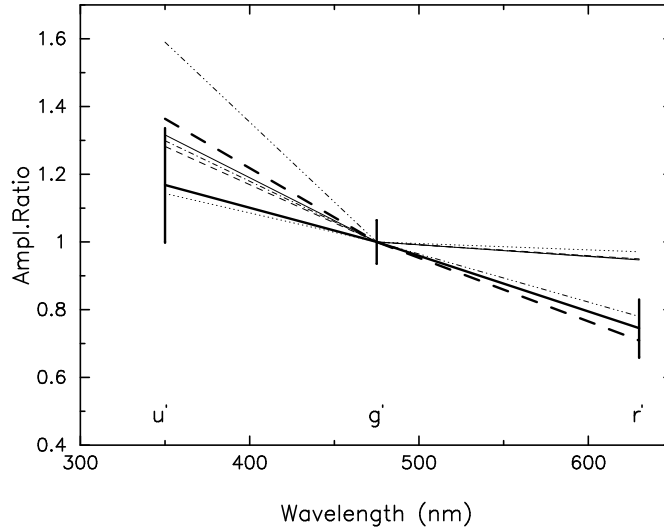


Fig. 3. Observed amplitude ratios for f_1 (thick full line) and f_2 (thick dashed line). The 1σ confidence interval is shown only for f_1 . The thin lines are theoretical predictions taken from Ramachandran et al. (2004): dashed-dot-dot-dot: $\ell = 3$, full: $\ell = 0$, dashed-dot: $\ell = 1$, dashed: $\ell = 2$, dotted: $\ell = 4$.

$\ell = 3$. We are currently investigating whether the non-adiabatic approximation (Fontaine 2006) leads to better results. It may also be that unresolved beating affects the observed amplitude ratios and makes them deviate from the theoretical predictions. The error bars for f_2 (not shown) are too large to draw conclusions.

ACKNOWLEDGMENTS. CA was supported for this work by the “Stichting Nijmeegs Universiteits Fonds” and by NOVA. Research at the Armagh Observatory is funded by the Northern Ireland Department of Culture, Arts and Leisure and by PPARC grant PPA/G/S/2002/00546. ULTRACAM operations are currently funded by PPARC under grant PPA/G/S/2002/00092. The authors are much indebted to the ULTRACAM team from Sheffield for their support at the telescope.

REFERENCES

- Charpinet S., Fontaine G., Brassard P. et al. 2006, *Baltic Astronomy*, 15, 305 (these proceedings)
- Fontaine G., Chayer P., Wesemael F. et al. 2006, *Baltic Astronomy*, 15, 99 (these proceedings)
- Jeffery C. S. et al. 2005, *MNRAS*, 362, 66
- Jeffery C. S. et al. 2006, *Baltic Astronomy*, 15, 259 (these proceedings)
- Ramachandran B., Jeffery C. S., Townsend R. H. D. 2004, *A&A*, 428, 209
- Scargle J. D. 1982, *ApJ*, 263, 835
- Solheim J.-E., Østensen R., Silvotti R., Heber U. 2004, *Ap&SS*, 291, 419

FOLLOW-UP OBSERVATIONS OF KNOWN EC 14026-TYPE PULSATORS

G. W. Wolf¹, M. D. Reed¹, A.-Y. Zhou¹, D. M. Terndrup², S. L. Harms¹, D. An², C.-W. Chen³, H.-C. Lin³, S. Zola⁴, A. Baran⁴, W. Ogloza⁴, M. Siwak⁴, K. D. Gazeas⁵, P. G. Niarchos⁵ and D. Kilkenny⁶

¹ *Missouri State University, Springfield, MO 65804, U.S.A.*

² *The Ohio State University, 140 W. 18th Avenue, Columbus, OH 43210, U.S.A.*

³ *Graduate Institute of Astronomy, National Central University, Chung-Li, Taiwan*

⁴ *Mt. Suhora Observatory of the Pedagogical University, ul. Podchorążych 2, PL-30-084 Cracow, Poland*

⁵ *Department of Astrophysics, Astronomy and Mechanics, Faculty of Physics, University of Athens, GR 157 84, Zografos, Athens, Greece*

⁶ *South African Astronomical Observatory, Cape Town, South Africa*

Received 2005 August 1

Abstract. We present follow-up observations of pulsating sdB stars as part of our efforts to resolve the pulsation spectra for use in asteroseismological analyses. This paper reports on our overall efforts, but specifically on our results for the pulsating sdB stars KPD 2109+4401 and PG 0154+182.

Key words: stars: hot subdwarfs – stars: oscillations – stars: individual (PG 0154+182, KPD 2109+4401)

1. INTRODUCTION

The scientific goal of this observational study is to resolve the pulsation structure of pulsating sdB stars by combining limited amounts of data from larger telescopes with data from smaller (~ 0.5 m) telescopes. This combination allows us a long time base sufficient to resolve closely spaced pulsations and the increased signal-to-noise of the larger telescopes allows us to detect pulsations with low amplitudes. Table 1 lists stars we have observed and observatories from which we have obtained data. Though the majority of our data is from Baker, MDM and McDonald observatories, we routinely participate in multisite collaborations, including the Whole Earth Telescope.

2. OBSERVATIONS AND ANALYSES

KPD 2109+4401. Our dataset for KPD 2109+4401 (hereafter KPD 2109) consists of 29 data runs with a total length of 182.6 hours over 31 days. The temporal resolution is $0.4 \mu\text{Hz}$ with a detection limit of 0.3 mma (milli-modulation amplitudes). We detect eight pulsation frequencies extending from 4701 to $8375 \mu\text{Hz}$, corresponding to periods of 119.4 to 212.7 s. Table 2 lists the frequencies we

Table 1. List of observations of pulsating sdB stars.

| Target | Inclusive dates | Hours observed | Sites [†] |
|---------------|------------------------|-----------------------|--------------------|
| EC 05217-3914 | 1999 Nov. 6 – 15 | 59 | 1, 2 |
| PG 1336-018 | 2001 Apr. 14 – May 1 | 288 | 13 |
| HS 2201+2610 | 2000 Sep. 17 – Oct. 4 | 95.0 | 3, 14 |
| Feige 48 | 1999 Mar. 6 – Apr 13 | 63.6 | 7, 8, 13 |
| | 1999 Dec. 10 – 16 | 17.5 | 3 |
| | 2000 Feb. 8 – Mar. 05 | 42.4 | 3, 7, 8 |
| | 2000 Nov. 2 – Dec. 22 | 45.7 | 3, 9, 12 |
| | 2001 Jan. 18 – Feb. 1 | 55.0 | 3 |
| | 2001 Apr. 19 – 30 | 52.0 | 13 |
| | 2002 Apr. 5 – 21 | 56.8 | 13 |
| | KPD 1930+2752 | 2003 Aug. 15 – Sep. 9 | 246.5 |
| KPD 2109+4401 | 2004 Sep. 12 – Oct. 14 | 182.6 | 4, 5, 7, 9, 11 |
| PG 0154+182 | 2004 Oct. 6 – 14 | 28.4 | 5 |
| PG 1325+101 | 2003 Mar. 3 – Apr. 3 | 264 | 4, 14 |
| PG 1219+534 | 2003 May 13 – Jun. 4 | 48.6 | 4, 7 |
| | 2004 Mar. 9 – 15 | 21.5 | 4 |
| | 2005 Feb. 25 – Mar. 2 | 23.8 | 4 |
| PG 0014+067 | 2004 Oct. 8 – Oct. 20 | 142 | 5, 13 |
| PG 1618+563 | 2005 Mar. 17 – May 1 | 200.5 | 4, 6, 7, 9, 10 |
| HS 1824+5745 | 2005 May 24 – July 11 | Unknown | 6 |

[†] Observing sites: (1) CTIO 1.5 m, (2) SAAO 1.9 m, (3) Fick 0.6 m, (4) Baker 0.4 m, (5) MDM 1.3 m, (6) MDM 2.4 m, (7) McDonald 2.1 m, (8) McDonald 0.9 m, (9) Suhora 0.6 m, (10) Lulin 1.0 m, (11) Greece 0.4 m, (12) Beijing 0.85 m, (13) Whole Earth Telescope Campaign, (14) Other campaign (non-PI)

Table 2. Periods, frequencies and amplitudes for KPD 2109. Formal least-square errors in parentheses.

| Period (s) | Frequency (μ Hz) | Ampl. (mma) | Period (s) | Frequency (μ Hz) | Ampl. (mma) |
|---------------|--------------------------|----------------|----------------------------|--------------------------|----------------|
| 182.42120(8) | 5481.819(3) | 6.13(9) | 196.31012(10) | 5093.981(2) | 6.44(9) |
| 184.71248(23) | 5413.819(6) | 2.63(10) | 198.19774(30) | 5045.466(8) | 2.03(9) |
| 184.74037(25) | 5413.002(7) | 2.32(10) | 209.14104(20) [†] | 4781.462(45) | 0.35(9) |
| 191.84271(36) | 5212.604(10) | 1.63(9) | 212.71520(22) [†] | 4701.122(49) | 0.32(9) |

[†] These frequencies are only above the detection threshold in the MDM data.

detected and Figure 1 shows temporal spectra of the complete data set as well as successive prewhitening steps.

We confirm five of the known frequencies previously identified by both Koen (1998; hereafter K98) and Billères et al. (1998), but do not detect the 5084 μ Hz frequency detected by K98. We resolve a doublet that was suspected by K98, but at 0.8 μ Hz, was not resolvable in his data. Furthermore, our high signal-to-noise datasets detect the feature at 4781 μ Hz, which was suspected by K98 and marginally detect another frequency at 4701 μ Hz. The peak around 4781 μ Hz was also marginally detected in the spectroscopic analysis by Jeffery & Pollacco (2000).

PG 0154+182. PG 0154+182 (hereafter PG 0154) was observed as a sec-

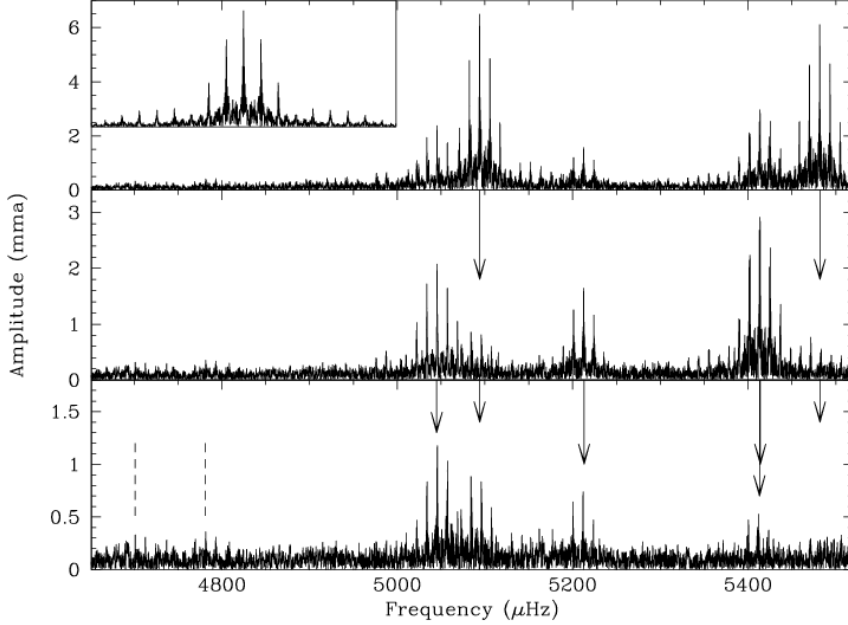


Fig. 1. Temporal spectra (FT) for KPD 2109 showing the original data (top) and prewhitening by 2 and 6 frequencies, respectively. Arrows indicate prewhitened frequencies and the dashed lines indicate low-amplitude frequencies not prewhitened in this figure. Inset is the data window.

ondary star at MDM observatory during our KPD 2109 run. It was observed for 4 hours (on average) over 9 consecutive nights. The discovery data only detected a single frequency (Koen et al. 2004), whereas we clearly detected 6 frequencies, one of which is likely an unresolved doublet. Figure 2 shows an FT of the original data (window function is inset), prewhitened data (arrows indicate frequencies removed) and the amplitude of the 6785.20 μHz frequency over the course of our run. The smooth, roughly sinusoidal appearance of the 6785.20 μHz amplitude leads us to believe this frequency is in fact two with a splitting of $\sim 1.5\mu\text{Hz}$, or a beat period slightly longer than our run.

Table 3. Periods, frequencies and amplitudes for PG 0154. Formal least-squares errors in parentheses.

| Period | Frequency | Amplitude | Period | Frequency | Amplitude |
|--------------|-------------|-----------|--------------|-------------|------------|
| 110.9280(15) | 9014.85(12) | 1.13(22) | 142.2137(7) | 7031.67(3) | 3.88(23) |
| 119.5830(19) | 8362.39(13) | 1.04(23) | 147.3795(30) | 6785.20(14) | 3.58(1.27) |
| 130.2638(11) | 7676.72(6) | 2.15(24) | 164.2108(3) | 6089.73(1) | 9.46(23) |

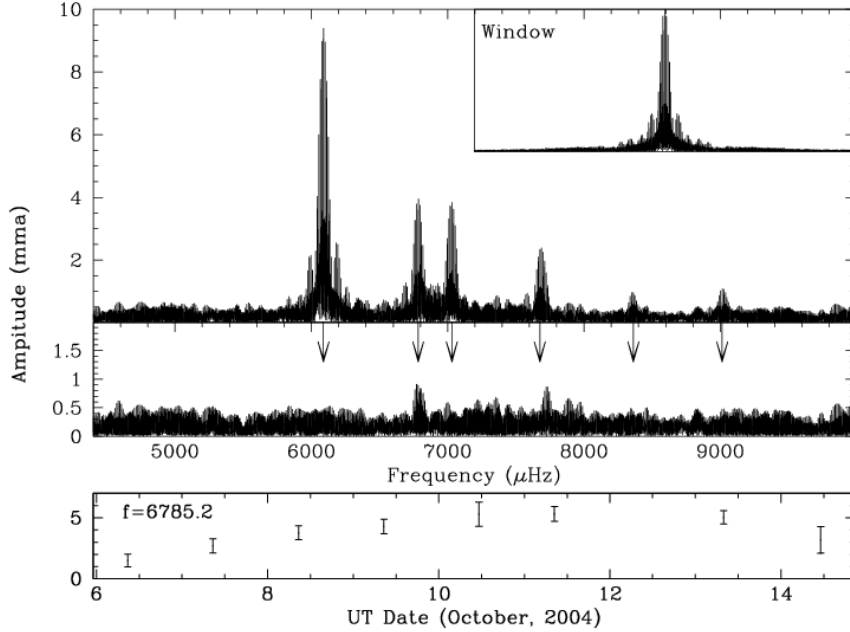


Fig. 2. Temporal spectra (FT) for PG 0154 showing the original data (top) and prewhitening by 6 frequencies. Arrows indicate prewhitened frequencies. Inset is the data window and bottom panel shows the amplitude of the 6785 μHz frequency over the course of our run.

ACKNOWLEDGMENTS. This material is based in part upon work supported by the National Science Foundation under grant nos. AST 007480 and AST 9876655. Any opinions, findings and conclusions or recommendations expressed in this material are those of the authors and do not necessarily reflect the views of the National Science Foundation. SLH was supported by the Missouri Space Grant Consortium which is funded by NASA.

REFERENCES

- Billères M., Fontaine G., Brassard P., Charpinet S., Liebert J., Saffer R. A., Bergeron P., Vauclair G. 1998, *ApJ*, 494, L75
 Jeffery C. S., Pollacco D. 2000, *MNRAS*, 318, 974
 Koen C. 1998, *MNRAS*, 300, 567
 Koen C., O'Donoghue D., Kilkeny D., Pollacco D. L. 2004, *NewA*, 9, 565

PG 0014+067: WET OBSERVATIONS AND A NEW TWIST TO THE SDB STAR PUZZLE

S. Kawaler M. Vučković and the WET collaboration
*Department of Physics and Astronomy, Iowa State University, Ames, IA 50011,
U.S.A.*

Received 2015 September 27

Abstract. In the Whole Earth Telescope (WET) observations of the sdBV PG 0014+067, made in 2004 October, we found a peculiar regularity of the pulsation frequencies reminiscent of asymptotic p -mode pulsation along with rotational splitting. This finding was amplified by adding additional modes found by observations with the WHT earlier in the year. To determine if this was a peculiarity of that star, we examined other sdBV stars that have extended-longitude coverage, and found a similar pattern in all of them. High-order p -mode pulsations (such as seen in the Sun and roAp stars) should not be present if our models of these stars and their pulsations are any guide to reality. The reasons behind this pattern are currently unknown.

Key words: stars: oscillations – stars: evolution – subdwarfs

1. INTRODUCTION

The pulsation frequencies seen in pulsating subdwarf (sdBV) stars show frequencies that are of the same order as the radial fundamental frequency. However, these stars generally show multiperiodic pulsation, with many modes seen within a relatively narrow frequency range. Correctly identifying the reason for this rich mode spectrum should reveal some fundamental features of the stars themselves. The leading candidate explanation is that we are seeing nonradial modes with degree ℓ ranging from 0 to 3 or 4; Brassard et al. (2001) demonstrate this for the star PG 0014+067 (hereafter PG 0014), while Kilkenney et al. (2002) follow a similar prescription for PG 1047+003. An alternate explanation is that we are seeing rotational splits of $\ell = 0$ –2 modes in stars with rapidly rotating cores, which in turn are a consequence of differential rotation that develops on the red giant branch (Kawaler & Hostler 2005).

PG 0014, as one of the richest pulsators among the short period sdBV stars (i.e., the EC 14026 stars) is an excellent candidate to try to distinguish between these two possibilities. While Brassard et al. (2001) did demonstrate that this star is a rich pulsator, the data they used were single-site data and therefore could suffer from 1 c/d aliases. We observed PG 0014 in a massive multi-longitude run with the Whole Earth Telescope in 2004 October. The results of that run, combined with data from the William Herschel Telescope taken two months earlier (Jeffery et al. 2005) allow us to present a detailed frequency list with assurance that all are real periodicities and no daily aliases are present.

What we found is that, while the frequencies might be describable in terms of

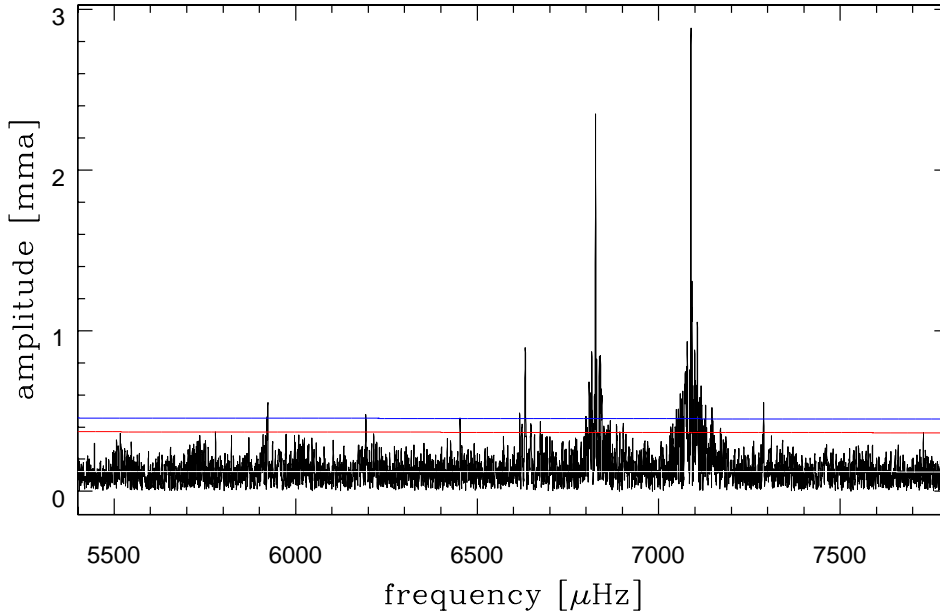


Fig. 1. Fourier transform of the WET data on PG 0014; the horizontal lines show noise levels of 3σ (lower) and 3.7σ (upper).

higher-than-usual values of ℓ or rapid internal rotation, they show a pattern that looks more like asymptotic p -mode pulsation. A similar pattern has been found in the other well-studied pulsating sdBV stars. Unfortunately, the models demand that these stars are displaying low-order p -mode pulsations, which show no such asymptotic patterns.

2. PG 0014 FREQUENCIES FROM WET AND ULTRACAM/WHT

The results of the WET run on PG 0014 will appear elsewhere (Vučković et al. 2005). We show the amplitude spectrum of the main region of interest in the WET data in Figure 1; the signal-to-noise level is sufficient to reveal peaks with amplitudes above about 0.45 mma. For possible lower-amplitude modes, we include in our analysis the frequencies found by Jeffery et al. (2005) in multicolor photometry of PG 0014 using Ultracam on the WHT; the merged frequency list is shown in Table 1. In creating this list, we used the WET data as the primary source, and added lower-frequency modes identified by Jeffery et al. (2005). Even though the Jeffery et al. (2005) data are mostly single-site, we are confident in their frequency identifications. This confidence comes from their identification of all modes that they have in common with the WET data, without a single instance of selection of a 1 c/d alias in their analysis. In Table 1, the Ultracam peaks are indicated in the Notes column, with the symbol (w) indicating that the mode was seen only in the combined Ultracam data (all colors).

The frequency list of PG 0014 displays some suggestive systematics; concentrating on the second column of Table 1 we see several modes with separations of approximately integral multiples of $90 \mu\text{Hz}$. Other separations of nearly $100 \mu\text{Hz}$

Table 1. Frequencies present in PG 0014 and a “model”.

| # | Freq. [μHz] | Amp. [mma] | Note | i | j | Model | Difference |
|----|--------------------------|------------|----------------|-----|-----|--------|------------|
| 2 | 5923.4 | 0.54 | fine structure | 0 | 0 | 5923.2 | 0.2 |
| 3 | 6193.5 | 0.44 | | 3 | 0 | 5194.1 | -0.6 |
| 4 | 6452.9 | 0.45 | | 7 | -1 | 6454.1 | -1.2 |
| 5 | 6632.8 | 0.65 | fine structure | 9 | -1 | 6634.6 | -1.8 |
| 6 | 6646.5 | 0.60 | UltraCam | 8 | 0 | 6645.6 | 0.9 |
| 7 | 6659.9 | 0.34 | UltraCam (w) | 7 | 1 | 6656.5 | -3.4 |
| 8 | 6726.8 | 0.37 | UltraCam (w) | 10 | -1 | 6724.9 | 1.9 |
| 9 | 6826.1 | 2.38 | | 10 | 0 | 6826.1 | 0.0 |
| 10 | 7088.7 | 2.98 | fine structure | 14 | -1 | 7086.1 | 2.6 |
| 11 | 7187.5 | 0.66 | UltraCam | 14 | 0 | 7187.3 | 0.2 |
| 12 | 7289.0 | 0.65 | | 14 | 1 | 7288.5 | 0.5 |

are apparent as well. Our initial inclination was to try to identify the 100 μHz splitting as a rotational splitting. While this large splitting could be caused by rotation, the implied rotation rate (if solid-body rotation) would be much larger than upper limits based on spectroscopic study of line profiles. On the other hand Kawaler & Hostler (2005) suggest that rapid internal rotation could produce large splits in a star with a slow surface rotation rate, but their predictions suggest that the splits of different modes should not show the same value.

3. A PHENOMENOLOGICAL MODEL

With two apparent splits present, we decided to explore an entirely phenomenological parametrization that could then be used to make an empirical fit to the observed frequencies. We chose a form reminiscent of asymptotic p -mode pulsation with a constant rotation frequency:

$$f(i, j) = f_o + i \times \delta + j \times \Delta, \quad (1)$$

where δ represents a small spacing (and i can range from 0 upwards) and Δ represents a large spacing (with j initially limited to being either -1, 0 or 1). In the equation above, f_o represents a zero-point for the fit with $i = j = 0$.

In the general case of fitting a set of frequencies, we perform a two-dimensional χ^2 minimization to find best-fit values for δ and Δ . Clearly, there is an aliasing problem when the combinations of i , j , δ and Δ produce commensurate spacings, so the χ^2 surface shows multiple minima. We break that degeneracy (when possible) by choosing the (δ, Δ) pair for which we have at least two modes with the same value of i but different j . In practice, we make the further requirement that the fit must include at least two different pairs of modes (i.e., modes with the same value of i) that show the same Δ ; i.e., the fit must contain modes with (i_1, j_1) , (i_1, j_2) , (i_2, j_3) and (i_2, j_4) . In a subsequent paper, we will show that enforcing these additional conditions on the fit criteria restrict the aliasing problem and greatly statistical significance of the fit.

For PG 0014 this procedure yields values of $\delta = 90.37$, $\Delta = 101.22$ and $f_o = 5923.24$ (all in μHz). Using these values in Equation 1, we find the model frequencies listed in Table 1. Note that the fit is extremely good – the 11 modes

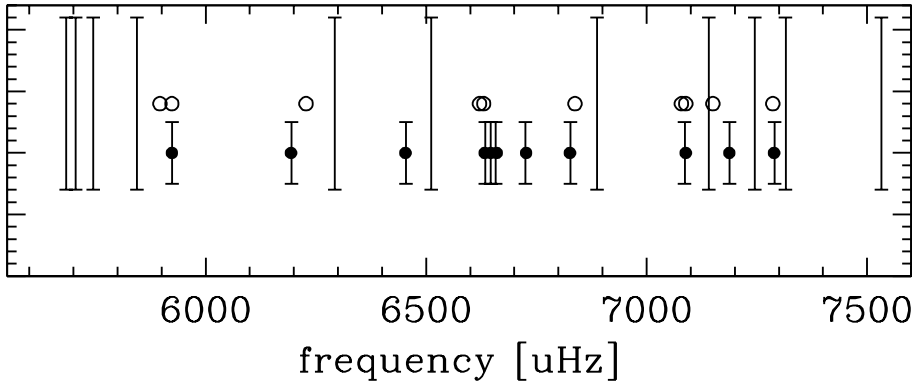


Fig. 2. Schematic diagram of the frequencies of PG 0014. The open circles are the frequencies in Brassard et al. (2001) and the long vertical lines are the frequencies of their best-fit stellar model. Closed circles represent the frequencies from the WET+UltraCam data (Table 1) and short lines give the fit to those frequencies using Equation (1) and the derived values for δ and Δ .

identified in the table are all fit to within 0.05 %, with an RMS difference of 0.013 δ . Figure 2 displays the closeness of the fit in comparison with the data, and with the fit frequencies from Brassard et al. (2001).

To estimate the statistical significance of this fit, we performed sets of 1000 trials with randomly chosen frequencies that span the same frequency interval. In each set of trials, the best fit (as judged by the RMS difference between the best model and the random frequency set) was tabulated. This procedure helped us determine the statistical significance of the star’s fit by the model. In the case of PG 0014, the star departs from a random frequency distribution at the 4σ level.

Is this asymptotic pulsation? After all, high-order p -modes show a more-or-less constant frequency spacing; such sequences are seen in helioseismical data and in the rapidly oscillating Ap stars (see Kurtz et al. 2005).

The sequence of modes split by integral multiples of δ cannot be asymptotic p -mode behavior. Models of PG 0014, and sdBV pulsators in general, indicate that the radial fundamental frequency in the models is usually close (in frequency) to the observed mode frequencies. Asymptotic relations, such as Equation (1), are usually valid (at the few-percent level) only for values of $n \gg \ell$, or more generally for large values of n . Even so, the computed frequency separation for p -modes in sdBV models yields values of several hundred μHz – a factor of 10 or more larger than what PG 0014 shows.

4. IS PG 0014 A FREAK? NO...

To see if PG 0014 is just a strange star, we examined published frequency lists for other sdBV stars that are known to be rich pulsators and which have extended longitude coverage that ensures correct separation of true frequencies from diurnal aliases.

Table 3 shows that nearly all sdBV stars with extended-longitude coverage show similar splits across their temporal spectra. As an example, in Table 2 we show the frequency list for PG 1336-018 (from Kilkenney et al. 2003) along with the best-fit model using values of δ and Δ derived from the observed frequencies

Table 2. Frequencies present in PG 1336-018 and a “model”.

| # | Freq. [μHz] | Note | i | j | Model | Difference |
|----|--------------------------|---------|-----|-----|---------|------------|
| 1 | 4885.1 | | 0 | 0 | 4886.7 | 1.5 |
| 2 | 5219.0 | | 13 | -1 | 5218.7 | -0.3 |
| 7 | 5444.3 | | 13 | 1 | 5447.6 | 3.3 |
| 3 | 5356.5 | | 17 | -1 | 5356.0, | -0.4 |
| 8 | 5470.9 | | 17 | 0 | 5470.5 | -0.4 |
| 11 | 5585.7 | | 17 | 1 | 5585.0 | -0.7 |
| 4 | 5369.4 | no fit | - | - | - | - |
| 12 | 5598.5 | no fit | - | - | - | - |
| 5 | 5392.2 | | 18 | -1 | 5390.4 | -1.8 |
| 9 | 5505.6 | | 18 | 0 | 5504.8 | -0.8 |
| 13 | 5621.2 | | 18 | 1 | 5619.3 | -1.7 |
| 6 | 5435.4 | doublet | 16 | 0 | 5436.2 | 0.7 |
| 10 | 5516.7 | | 15 | 1 | 5516.3 | -0.5 |
| 14 | 5757.3 | doublet | 22 | 1 | 5756.7 | -0.6 |
| 15 | 5891.5 | | 26 | 1 | 5894.1 | 2.6 |
| 16 | 5916.3 | | 30 | 0 | 5917.0 | 0.7 |

alone. We note that the value of Δ is precisely equal to the orbital frequency of this close binary, which is also (presumably) the rotation frequency of both stars if the system is tidally locked.

Another way to show the regularity to these patterns is through an echelle diagram (similar to those used in helioseismology and seismological observations of solar-type stars). Figure 3 shows such diagrams for PG 0014 and PG 1336-019.

5. AND SO, A MYSTERY

We stress that what we have done is to make a purely empirical fit to the observed frequencies – this is, essentially, simple numerology with NO known physics involved. While we have no explanation at all for why this works, there are several points that may be important.

Feige 48 has the lowest gravity of the bunch; the five frequencies from Reed et al. (2004) show a small splitting that is the smallest of the ensemble, but show no evidence of a second large spacing (Δ). Aside from PG 0014, there appears to be some correlation between $\log g$ and δ . Two stars show spectra that are completely

Table 3. Splittings found in pulsating sdBV stars.

| Star | $\log g$ | f_o [μHz] | δ [μHz] | Δ [μHz] | Significance |
|----------|----------|--------------------------|-----------------------------|-----------------------------|--------------|
| PG 0014 | 5.8 | 5923 | 90.4 | 101.2 | 4.0 σ |
| PG 1219 | 5.85 | 5812 | 60.5 | - | 3.7 σ |
| PG 8783 | >5.6 | 7193 | 58.1 | 138.9 | 3.9 σ |
| PG 1047 | 5.9 | 6310 | 55.9 | 186.5 | 4.2 σ |
| PG 1336 | 5.7 | 4886 | 34.4 | 114.5 | 6.0 σ |
| Feige 48 | 5.5 | 2642 | 13.9 | - | - |

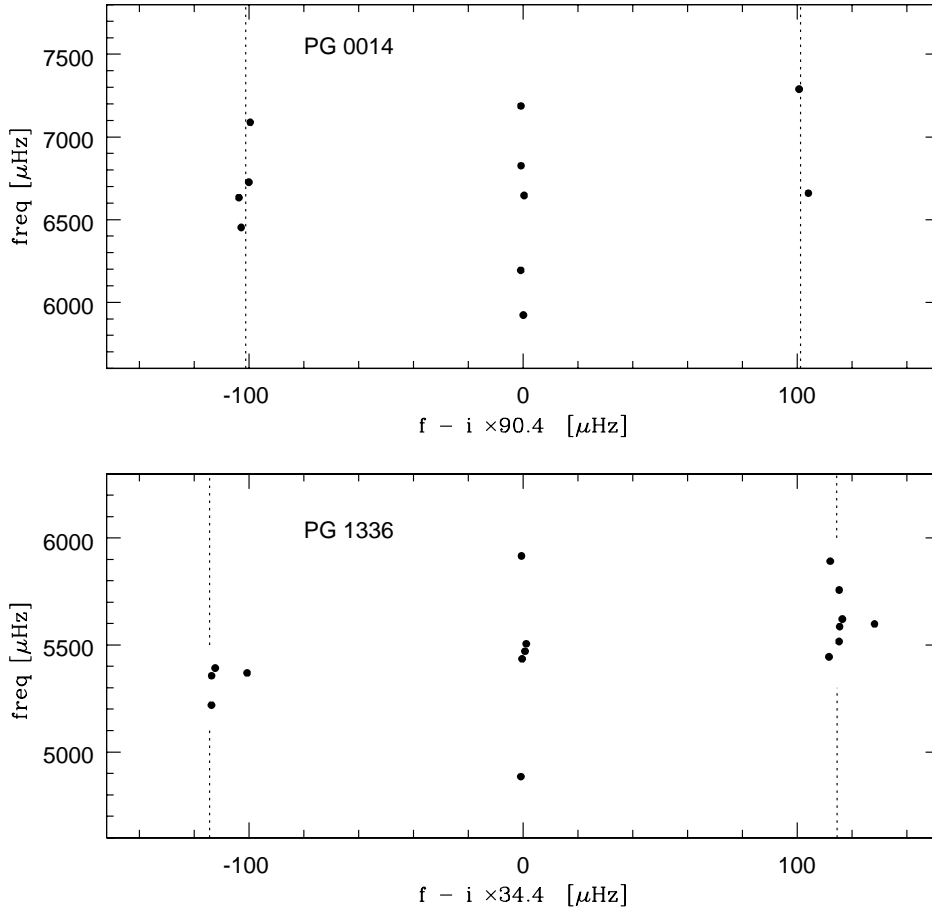


Fig. 3. “Echelle” diagrams of the frequencies in PG 0014 (top) and PG 1336 (bottom); the frequencies have been folded on the small spacing δ and stacked, showing the uniformity of the frequency spacings within the main band and the two side bands separated from the main band by the large spacing Δ .

described without the need of a large spacing. And, PG 1336 is a member of a close binary. The large spacing we identify is precisely equal to the orbital frequency. If we can assume that the stars in this system are tidally locked and therefore in synchronous rotation, then in this system at least the large spacing Δ can be identified with the stellar rotation rate. Reed (private communication) points out that the two modes, for which the spacing model fails, are those that display a pulsation geometry aligned not with the orbital plane, but pointing from the primary to the secondary.

ACKNOWLEDGMENTS. Financial support for this work came from the U.S. National Science Foundation, through grant AST20205983 to Iowa State University.

REFERENCES

- Brassard P., Fontaine G., Billères M., Charpinet S., Lieber J., Saffer R. A. 2001, *ApJ*, 331, 1013
- Kilkenny D., Billères M., Stobie R. S., Fontaine G., Shobbrook R., O'Donoghue D., Brassard P., Sullivan D. J., Burleigh M. R., Barstow M. 2002, *MNRAS*, 331, 399
- Kilkenny D. et al. (the WET collaboration) 2003, *MNRAS*, 345, 834
- Jeffery C., Dhillon V., Aerts C., Marsh T., Gänsicke B. 2005, *MNRAS*, 362, 66
- Kawaler S. D., Hostler S. R. 2005, *ApJ*, 621, 432
- Kurtz D. et al. (the WET collaboration) 2005, *MNRAS*, 358, 651
- Kilkenny D. et al. (the WET collaboration) 2003, *MNRAS*, 345, 834
- Reed M. D. et al. (the WET collaboration) 2004, *MNRAS*, 348, 1164
- Vučković M. et al. (the WET collaboration) 2005, in preparation

LONG-PERIOD VARIABLE SUBDWARF B STARS: PROSPECTS FOR ASTEROSEISMOLOGY

S. K. Randall¹, G. Fontaine¹, E. M. Green², P. Brassard¹ and D. M. Terndrup³

¹ *Département de Physique, Université de Montréal, C.P. 6128, Succ. Centre-Ville, Montréal, Québec, H3C 3J7, Canada*

² *Steward Observatory, University of Arizona, Tucson, AZ 85721, U.S.A.*

³ *Department of Astronomy, Ohio State University, 140 West 18th Avenue, Columbus, OH 43210, U.S.A.*

Received 2005 August 1

Abstract. We summarize the results of an extensive study aimed at quantitatively interpreting the oscillations detected in long-period variable subdwarf B stars. Our analysis is based on between 300 and 400 hours of time-series photometry obtained for each of three representative targets: PG 1627+017, PG 1338+481 and PG 0101+039. The former two were the subjects of extensive multi-site campaigns led from the 1.52 m Steward Observatory telescope on Mt. Bigelow, Arizona, while the latter was observed with the 0.15 m Canadian space telescope MOST. We find that, unlike the short-period oscillators, where asteroseismology has been successful in some instances, our understanding of the slow pulsators is somewhat limited due to both observational and conceptual challenges. In particular, the period spectra measured to date are much sparser than those anticipated from models, implying that the indices of the modes observed must be constrained from the outset if asteroseismology is to be achieved. One promising idea is the exploitation of a mode's color-amplitude dependence on its degree index ℓ through multicolor photometry. Applying that method to the PG 1338+481 data together with other constraints suggests the excitation of $\ell = 1$ modes. If confirmed, this would point to a discrepancy between the observed and predicted long-period variable subdwarf B star instability strips of around 7000 K on the blue side, although some of it could be due to incorrect spectroscopic determinations of the effective temperatures of cool sdB stars.

Key words: stars: EHB and post-EHB, variable: general – stars: subdwarfs

1. INTRODUCTION

Pulsating subdwarf B (sdB) stars can be divided into two groups: the rapidly oscillating EC 14026 stars (Kilkenny et al. 1997) and the long-period variable PG 1716 stars (Green et al. 2003). At effective temperatures between 29 000 K and 36 000 K, the rapid oscillators correspond to the hotter of the two classes and excite both radial and low-degree non-radial pressure modes with typical periods in the 80–500 s range. Their instabilities are thought to be driven by a classical

kappa mechanism associated with a local overabundance of iron, which in turn depends on the competitive actions of gravitational settling and radiative levitation (Charpinet et al. 1996). Indeed, models taking into account diffusion processes and the resulting non-uniform iron abundance profile have been very successful at predicting the observed EC 14026 instability strip on the HR diagram as well as the range of periods excited for a given object (see Fontaine et al. 2006 for details). Beyond this, quantitative period matches leading to mode identification and asteroseismological estimates of key stellar parameters have been possible in a few instances (see Charpinet et al. (2006) for details).

In comparison, the study of the long-period variables is still in its infancy. Found at cooler temperatures in the 22 000 K to 29 000 K range, these stars exhibit brightness variations on a typical timescale of 1–2 hours, immediately implying high radial order gravity modes. While the driving mechanism is believed to be the same as for the EC 14026 stars (Fontaine et al. 2003), the vast majority of current PG 1716 models can excite only modes with degree indices $\ell \geq 3$, the observability of which is controversial due to cancellation effects when integrating over the visible disk of the star. However, discrepancies between the observed and predicted instability strips have been difficult to quantify due to a lack of data. Unlike the EC 14026 stars, where just a few nights of photometry can be sufficient to identify enough periods for asteroseismology, the long-period variables need to be monitored over the course of weeks or even months to yield a comparable number of periodicities. Extracting the observed frequency spectrum is further complicated by severe aliasing effects and the fact that atmospheric variations occur on a similar timescale as the stellar oscillations. These observational challenges notwithstanding, the detailed study of long-period variable subdwarf B stars could prove invaluable to our understanding of post-main sequence stellar evolution. In contrast to the shallow pressure modes observed in the EC 14026 pulsators, the slow oscillators' gravity modes probe deep within the star and are sensitive to the exact composition of the CO/He core. Successful asteroseismology of the latter would thus hold implications for the core helium burning phase not only of subdwarfs, but of other evolved stars as well.

In what follows, we present the results of an ambitious observational campaign aimed at measuring and quantitatively interpreting the period spectra of three representative slowly oscillating subdwarf B stars. We begin with an account of the observing runs and the frequencies extracted before comparing our findings to qualitative non-adiabatic and quantitative adiabatic predictions. We then outline the steps taken towards asteroseismical modeling and note the implications of our preliminary results.

2. OBSERVATIONAL PROGRAM

2.1. *PG 1627+017*

At atmospheric parameters $T_{\text{eff}} \sim 23\,700$ K and $\log g \sim 5.32$ (Green, Fontaine and Chayer, in preparation), PG 1627+017 is one of the coolest subdwarf B stars known. It was chosen as a first observational target because of its brightness ($V \sim 12.9$), relatively high-amplitude pulsations, and an equatorial location vital to the success of our multi-site collaboration. While the majority of the data were gathered at the 1.52 m Steward Observatory telescope on Mt. Bigelow, Arizona, between 2003 May 9 and 2003 June 11, the time coverage and baseline

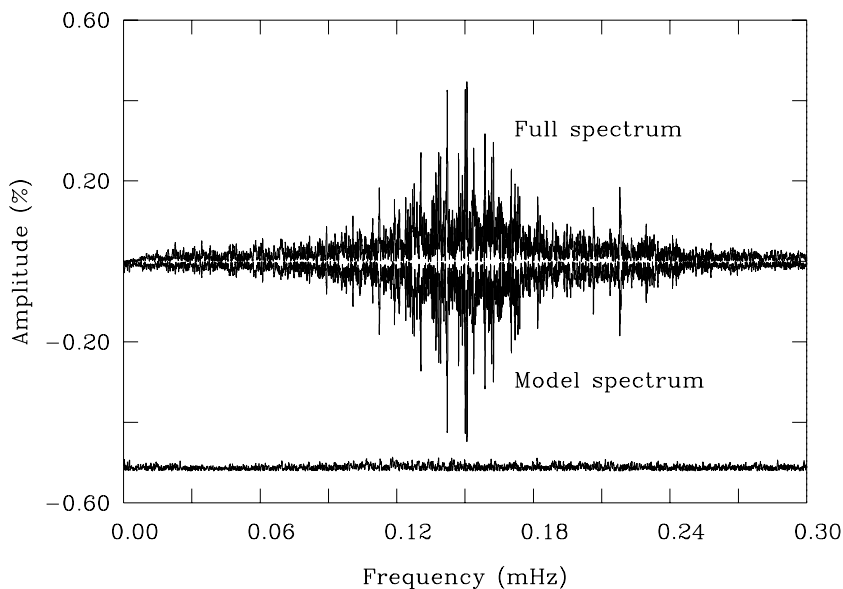


Fig. 1. Fourier transform for PG 1627+017.

were improved by simultaneous observing time granted on the 1 m telescope of the South African Astronomical Observatory and the 2.3 m telescope of the Siding Spring Observatory (Australia), as well as by weekend runs at Mt. Bigelow in the weeks leading up to the main campaign. Our efforts yielded a total of 303 hours of useful *R*-band photometry with a duty cycle of 33% over the five week period. Some spectroscopy was also obtained with the aim of recovering the main peaks from radial velocity shifts (see For et al. 2006 for details). The Fourier transform of the entire photometry light curve is shown in Figure 1, mirrored by a model spectrum (upside down) constructed on the basis of 23 extracted periodicities with amplitudes of at least three times the noise level. The residual between the observed and modeled spectra is displayed at the bottom of the figure.

All 23 periods detected in the light curve of PG 1627+017 lie in the 4500-9000 s range and have *R*-band amplitudes between 0.3 and 0.5 % of the star's mean brightness. Note that their distribution in frequency space is non-uniform, with the most powerful oscillations clustering between 6300–7050 s and several very closely spaced doublets and triplets occurring throughout the period spectrum. The latter may partially be explained by rotational splitting. PG 1627+017 forms part of a close binary system and, assuming a binary-synchronous rotation rate, spins on its axis with a period of $P_{\text{rot}} = P_{\text{bin}} \sim 0.83$ days (Morales-Rueda et al. 2003). The resulting break in spherical symmetry lifts the $(2\ell + 1)$ -fold degeneracy of a mode with given radial order k and degree index ℓ , introducing a dependence on the azimuthal index m . To first order, the components of a (k, ℓ) mode with adjacent values of m are then separated by a frequency spacing $\Delta f = (1 - C_{k\ell})/P_{\text{rot}}$, where for the high radial order gravity modes encountered in PG 1716 stars $C_{k\ell} \sim 1/(\ell(\ell + 1))$. These equations imply that, in theory, rotational splitting can be exploited to determine the degree indices of the modes observed. However, in the case of PG 1627+017 the frequency spectrum uncovered is too dense to allow the unambiguous identification of a given peak, as is shown in Figure 2. While

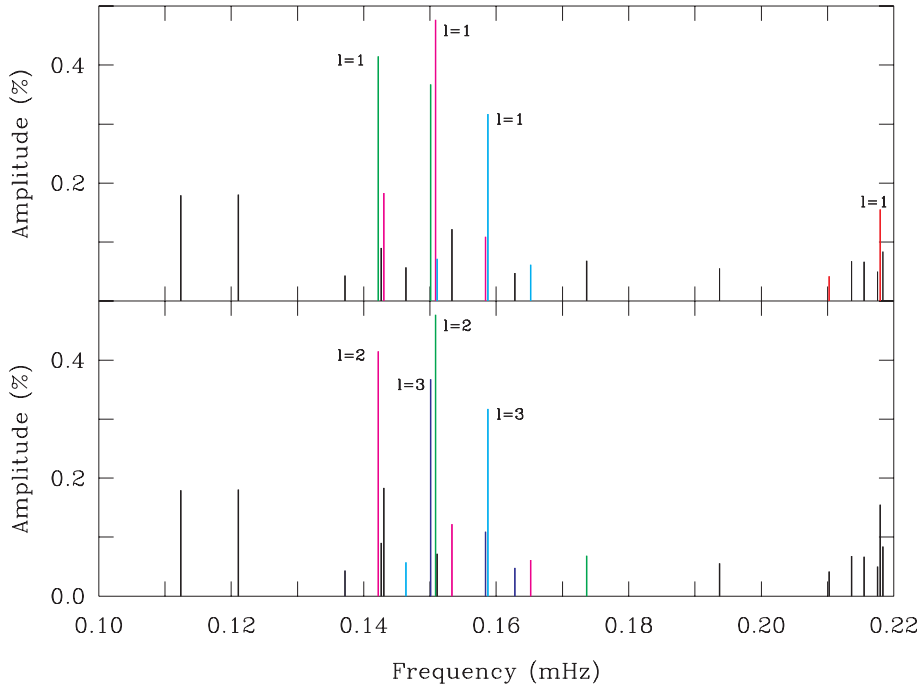


Fig. 2. Two possible manifestations of rotational splitting for PG 1627+017, depending on the degree indices invoked. Peaks illustrated in the same color refer to modes with the same values of ℓ and k but different m . The values of ℓ shown are derived from the frequency spacing between split components.

the scenario invoking modes with $\ell = 1$ (upper panel) seems more convincing, the possibility of explaining the observed period distribution in terms of $\ell = 2$ and $\ell = 3$ modes (lower panel) cannot be ruled out. It is thus unclear not only what degree indices the modes observed are associated with, but also which of the peaks detected are independent stellar pulsations, and which are rotational in nature. This makes asteroseismology and mode identification challenging, if not impossible.

2.2. PG 1338+481

Our second target, PG 1338+481 ($V \sim 13.6$), is a much more typical long-period variable in terms of atmospheric parameters at $T_{\text{eff}} \sim 28\,400$ K and $\log g \sim 5.40$ (Green, Fontaine and Chayer, in preparation). It was chosen for its representative qualities as well as the fact that it is a single, and thus probably slowly rotating, star. Observational efforts were conducted between 2004 March 15 and May 3 and focussed on just two sites: the 1.52 m Steward Observatory telescope employed during the previous campaign and the 1.3 m MDM telescope at Kitt Peak. In total, we obtained ~ 250 hours of simultaneous U - and R -band photometry, as well as an additional ~ 70 hours of R -band data. The resulting Fourier transforms are displayed in Figure 3 for both the U (blue) and the R (red) light curves. It is evident that, while the amplitudes in the U are significantly higher than those in the R , the oscillations are locked in frequency and phase. This

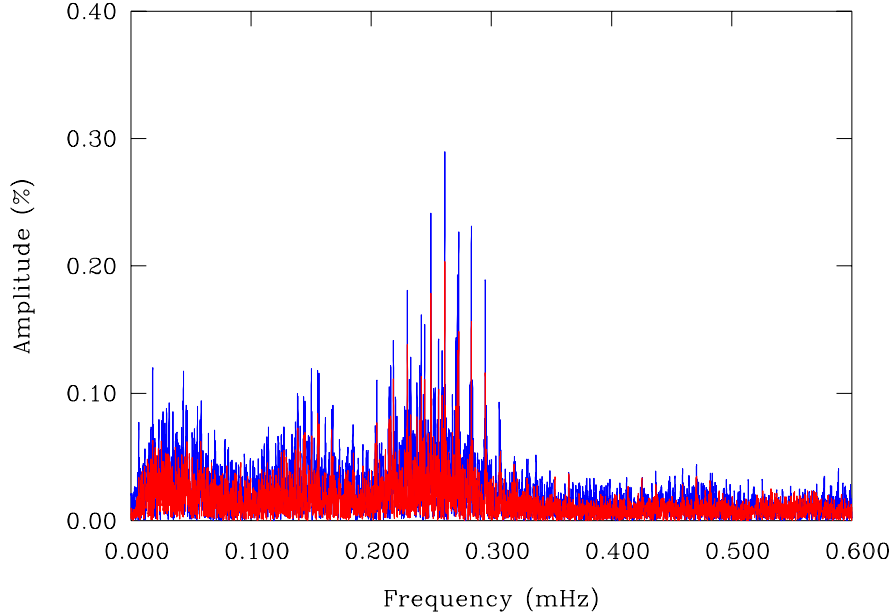


Fig. 3. U (blue) and R (red) band Fourier transforms for PG 1338+481.

is confirmed during the pre-whitening process, where the periods determined in the two colors are generally found to lie within 0.5 s of each other. Adopting a threshold of three times the local noise level, we were able to extract 13 periods in the 2100 s to 7200 s range with amplitudes up to 0.3 % and 0.2 % of the mean brightness in the U and R passbands respectively.

The decision to observe PG 1338+481 in two wavebands was based on a theoretical study exploiting the dependence of a mode's color-amplitude behavior on its degree index ℓ (Randall et al. 2005). Put simply, the ratio of a pulsation peak's amplitudes as measured in two well-separated passbands can be used to directly infer the associated mode's degree index provided the star's atmospheric parameters are known. We list, in Table 1, the U/R amplitude ratios for

Table 1. U/R amplitude ratios for the five dominant peaks detected in the light curves of PG 1338+481.

| Period (s) | U/R amplitude |
|------------|-----------------|
| 3530 | 1.49 ± 0.29 |
| 3828 | 1.42 ± 0.22 |
| 4090 | 1.39 ± 0.40 |
| 4347 | 1.27 ± 0.30 |
| 4625 | 1.55 ± 0.51 |

the five most convincing periodicities extracted from the data. Note that these all correspond to peaks with amplitudes of at least four times the local noise level. It is obvious from the table that the amplitude ratios of all five peaks are consistent within the error margins, which may imply that the corresponding modes have the same degree index. That possibility is supported by the fact that the oscillations are relatively evenly spaced in period, neighboring peaks being separated by $257 \text{ s} \leq \Delta P \leq 298 \text{ s}$. According to asymptotic theory, this is precisely what would be expected for high radial order modes with consecutive values of k and constant degree index ℓ . While the matter remains to be investigated in more detail, the

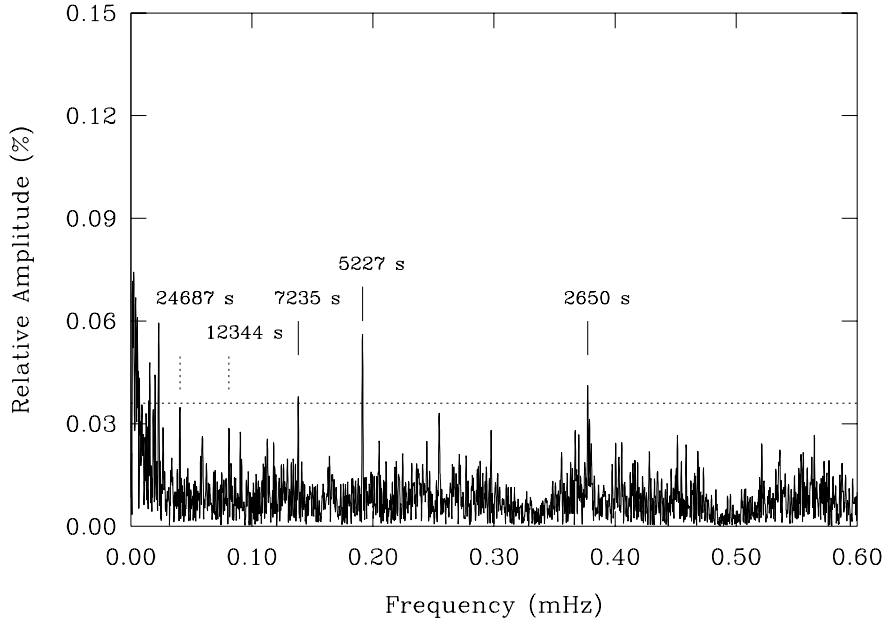


Fig. 4. Fourier transform for PG 0101+039.

resulting constraint on mode identification makes PG 1338+481 a prime target for asteroseismological studies.

2.3. PG 0101+039

PG 0101+039 was observed with the Canadian space telescope MOST (Walker et al. 2003) from 2004 September 28 to October 15 in a trial run for potential future missions. Since the effects of daily aliasing and atmospheric variation had undermined the extraction of periodicities for both of the previously studied targets, we had concluded that the successful asteroseismology of long-period variable subdwarf B stars would be facilitated by space-based observations. However, it was not clear from the outset whether the 15 cm aperture MOST telescope, currently the only satellite dedicated to asteroseismology, would be able to achieve sufficient precision for detecting pulsations in the relatively faint subdwarfs. It was therefore imperative to select a bright target like PG 0101+039 ($V \sim 12.1$), regardless of its other characteristics such as atmospheric parameters ($T_{\text{eff}} \sim 28\,300$ K and $\log g \sim 5.52$ according to Green, Fontaine and Chayer, in preparation), or the fact that it forms part of a short-period binary system ($P_{\text{bin}} \sim 0.57$ days from Moran et al. 1999).

The ~ 400 hours of broad-band photometry gathered by MOST boast a duty cycle of 96.5% and a noise level similar to that achieved for PG 1338+481 after seven weeks of ground-based observations. It is thus beyond doubt that, given the appropriate observing time, data from MOST can surpass anything obtainable from the ground in terms of time coverage. And indeed, the Fourier transform illustrated in Figure 4 shows no visible signs of aliasing. Adopting a threshold of four times the mean noise level, we were able to extract three convincing periodicities attributed to stellar oscillation (continuous line segments). Note that

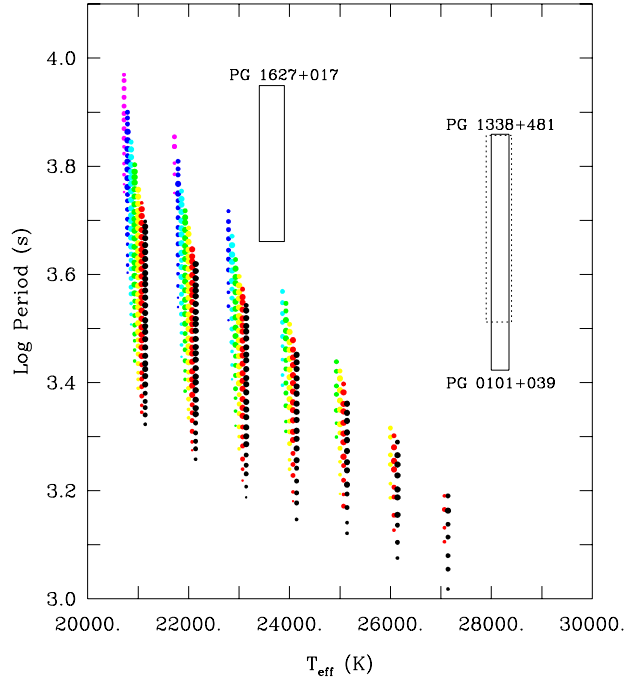


Fig. 5. Comparison between the range of periods predicted from a sequence of PG 1716 models (color-coded dots) and those observed for PG 1627+017, PG 1338+481 and PG 0101+039 (boxes). See text for further details.

their amplitudes are significantly lower than those detected for either of the previous targets, which could well be due to PG 0101+039's higher surface gravity. In addition, we found two lower amplitude peaks (dotted line segments) that are probably caused by an ellipsoidal deformation of the subdwarf due to the gravitational pull of its companion, and would imply a binary-synchronous rotation rate. Unfortunately, the fact that only three pulsations were identified makes this star unsuitable for asteroseismology for the time being.

3. QUALITATIVE COMPARISON WITH NON-ADIABATIC THEORY

In order to compare the ranges of periods observed for PG 1627+017, PG 1338+481 and PG 0101+019 to those predicted by non-adiabatic theory, we computed a short sequence of sdB models in the appropriate temperature range. Constituting an updated version of the numerical tools employed by Charpinet et al. (1996) to explain the EC 14026 phenomenon, these models incorporate radiative levitation and are characterized by five free parameters: effective temperature T_{eff} , surface gravity $\log g$, total stellar mass M_* , logarithmic depth of the transition between the hydrogen-rich envelope and the helium core $\log q(\text{H})$, and logarithmic depth of the extent of the inner carbon-oxygen core $\log q(\text{He})$. Note that, while M_* and $\log q(\text{He})$ were kept at constant representative values over the entire sequence, $\log q(\text{H})$ and $\log g$ were changed with T_{eff} so as to keep all of the structures parallel to the zero-age extreme horizontal branch (for precise values see Randall et al.

2005). Each model was then subjected to adiabatic and non-adiabatic pulsation calculations, the former estimating the periods of modes present, and the latter computing their stability. Figure 5 illustrates the periodicities predicted to be excited over the sequence for modes with $\ell = 2$ (magenta), $\ell = 3$ (blue), $\ell = 4$ (cyan), $\ell = 5$ (green), $\ell = 6$ (yellow), $\ell = 7$ (red) and $\ell = 8$ (black). Superposed on this theoretical instability strip are the ranges of periods observed for our three targets. It can be seen that the general trend of the unstable period range decreasing with increasing temperature is recovered by the models, however on an absolute scale the periods observed are longer than those predicted. Moreover, the modes excited by models hotter than 23 000 K are associated with degree indices $\ell \geq 4$, and the structure representative of PG 1338+481 and PG 0101+039 at $T_{\text{eff}} = 28\,000$ K drives no modes with $\ell \leq 8$ whatsoever. It is thus clear that our models are subject to important deficiencies that have yet to be determined and addressed. Given the similarities that exist between the theoretical instability strip and that observed, we nevertheless believe that the driving mechanism identified for the long-period variable subdwarfs lies at the origin of the oscillations detected and will be able to account for them quantitatively when more realistic models become available.

4. QUANTITATIVE COMPARISON WITH ADIABATIC THEORY

In a first attempt to quantitatively explain the period spectra uncovered in long-period variable subdwarf B stars we focus primarily on PG 1338+481, the most promising object observed so far. One thing that the photometry for all our targets have in common is a strong deficiency in periodicities observed compared to those predicted in the same range. While this could be partly alleviated by more sensitive measurements, it is obvious that asteroseismology will only be achieved if there is some constraint on mode identification from the outset. Possible methods of determining the degree index ℓ of a mode observed include the exploitation of rotational splitting (e.g., Charpinet et al. 2005), line-profile variations from time-series spectroscopy (see Schoenaers & Lynas-Gray 2006) and multicolor photometry (e.g., Randall et al. 2005). Since our observations do not include high-resolution spectroscopy and rotational

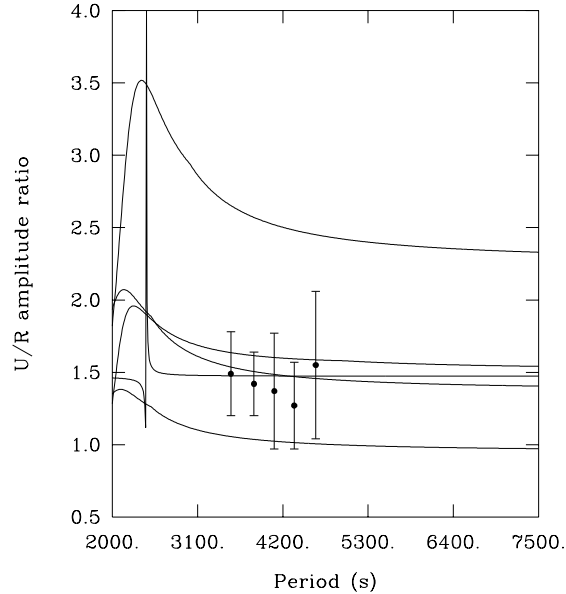


Fig. 6. U/R amplitude ratios predicted for a representative PG 1338+481 model for degree indices $\ell = 3, 2, 1, 4$ and 5 from top to bottom on the right-hand side. The amplitude ratios measured for PG 1338+481 are also indicated.

Since our observations do not include high-resolution spectroscopy and rotational

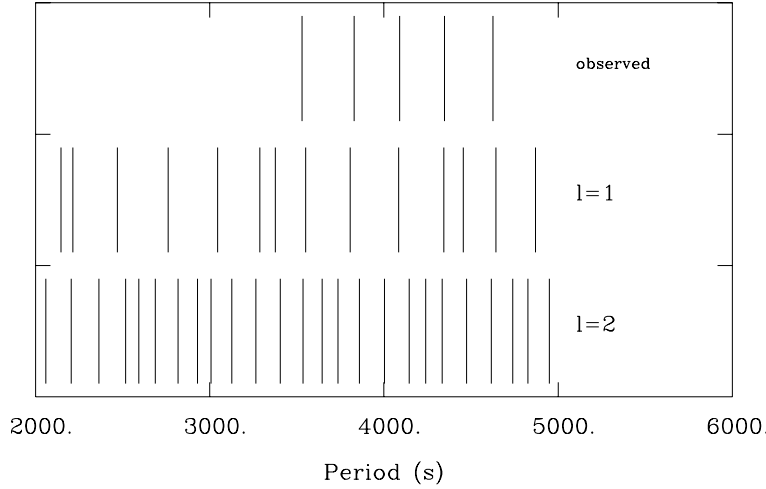


Fig. 7. Period spectrum predicted for a model with $T_{\text{eff}} = 28\,600$ K, $\log g = 5.22$, $M_* = 0.45 M_{\odot}$, $\log q(\text{H}) = -2.68$ and $\log q(\text{He}) = -0.24$. The five highest amplitude periodicities observed for PG 1338+481 are also illustrated.

splitting was found to yield ambiguous results when it was detected (see section 2.1), the simultaneous U/R photometry of PG 1338+481 is our best option. Figure 6 illustrates the period-dependent U/R amplitude ratios calculated from a model with $T_{\text{eff}} = 28\,200$ K and $\log g = 5.38$ for degree indices $\ell = 3, 2, 1, 4$ and 5 (from top to bottom on the right-hand side). Superposed on this are the amplitude ratios observed for the five dominant pulsations of PG 1338+481 (see Table 1). Considering the measurement errors, only modes with $\ell = 3$ and $\ell = 5$ can be excluded with any confidence, although the $\ell = 1$ and $\ell = 4$ curves do represent better matches to the data than that for $\ell = 2$.

Another feature that makes the PG 1338+481 data stand out is the nearly equal period spacing of the five highest amplitude pulsations. As discussed in section 2.2, this could well imply that they are all associated with the same degree index, which in light of the multicolor findings would correspond to $\ell = 1, 4$ or possibly 2 . Since the brightness variation caused by an oscillation of given intrinsic amplitude strongly decreases with increasing ℓ -value when integrating over the visible disk of a star, the detection of $\ell = 1$ or 2 modes is naturally favored compared to that of $\ell = 4$ modes. Indeed, all main sequence g-mode pulsators with good empirical mode identification show $\ell = 1$ modes only. A similar scenario holds true for white dwarfs, which do exhibit the occasional $\ell = 2$ mode, but primarily excite dipole modes. As subdwarf B stars lie in between the two regimes, we would expect their case to be no different. In addition to this, the average period spacing between the five peaks ($\langle \Delta P \rangle \simeq 274$ s) is very close to that expected for $\ell = 1$ modes in a representative PG 1338+481 model, as can be seen in Figure 7. $\langle \Delta P \rangle$ decreases significantly with increasing degree index, implying that the observed period spectrum could be matched to that predicted for $\ell = 2$ or higher only if a significant fraction of the theoretical periodicities were not excited to appreciable amplitudes. Since we find no convincing reason why this should be the case, we believe these modes to have degree indices of $\ell = 1$.

5. CONCLUSION

The observational campaign described in these Proceedings constitutes the first serious attempt at quantitatively interpreting the period spectra excited in long-period variable subdwarf B stars. It has revealed that even the most sensitive measurements available yield an observed period spectrum far sparser than that expected from theory. Consequently, mode identification must be constrained from the outset if asteroseismology is to be possible. One way of doing this is the exploitation of multicolor photometry, which we attempted for the case of PG 1338+481. Together with mode visibility and period spacing considerations, the results point to the excitation of $\ell = 1$ modes in that star. If confirmed, this would aggravate the discrepancy between the computed and the observed instability strip compared to the detection of $\ell = 3$ or 4 modes. Indeed, none of the models shown in Figure 5 are able to excite dipole modes. These are predicted only for models cooler than 21 000 K, implying a difference of 7000 K between the theoretical and observed blue edge. While this clearly indicates shortcomings in our models that have yet to be addressed (the spectroscopic determinations may also be partly at fault), qualitative similarities between the observed and predicted instability strips nevertheless point to the identification of the correct driving mechanism. Beyond this, we feel that the constraints placed on the mode identification for PG 1338+481 have opened this star up to asteroseismology, a possibility we are still in the process of investigating.

ACKNOWLEDGMENTS. We would like to thank for their contribution to the observations: T. Bedding, N. Brown, O. Cordes, L. Crause, A. Daane, M. Fontaine, B.-Q. For, A. Jacob, D. Kilkenny, L. Kiss, R. Kuschnig, J. Matthews, S. O’Toole, P.-O. Quirion, J. Rowe and P. Zacharias.

REFERENCES

- Charpinet S., Fontaine G., Brassard P., Billères M., Green E. M., Chayer P. 2005, *A&A*, 443, 251
- Charpinet S., Fontaine G., Brassard P., Dorman B. 1996, *ApJ*, 471, L103
- Charpinet S., Fontaine G., Brassard P. et al. 2006, *Baltic Astronomy*, 15, 305 (these proceedings)
- Fontaine G., Brassard P., Charpinet S., Green E. M., Chayer P., Billères M., Randall S. K. 2003, *ApJ*, 597, 518
- Fontaine G., Green E. M., Chayer P. et al. 2006, *Baltic Astronomy*, 15, 211 (these proceedings)
- For B.-Q., Green E. M. 2006, *Baltic Astronomy*, 15, 183 (these proceedings)
- Green E. M., Fontaine G., Reed M. D. et al. 2003, *ApJ*, 583, L31
- Kilkenny D., Koen C., O’Donoghue D., Stobie R. S. 1997, *MNRAS*, 285, 640
- Morales-Rueda L., Maxted P. F. L, Marsh T. R., North R.C., Heber U. 2003, *MNRAS*, 338, 752
- Moran C., Maxted P., Marsh T. R., Saffer R. A., Livio M. 1999, *MNRAS*, 304, 535
- Randall, S.K., Fontaine, G., Brassard, P., Bergeron, P. 2005, *ApJS*, 161, 456
- Schoenaers C., Lynas-Gray A. E. 2006, *Baltic Astronomy*, 15, 219 (these proceedings)
- Walker G. A. H., Matthews J. M., Kuschnig R. et al. 2003, *PASP*, 115, 1023

FUSE DETERMINATION OF THE ABUNDANCES OF IRON-PEAK ELEMENTS IN THE PG 1716+426 STARS

J.-P. Blanchette¹, P. Chayer^{2,3}, F. Wesemael¹, G. Fontaine¹, M. Fontaine¹,
J. Dupuis², J. W. Kruk² and E. M. Green⁴

¹ *Département de Physique, Université de Montréal, Montréal, Québec H3C 3J7, Canada*

² *Bloomberg Center for Physics and Astronomy, The Johns Hopkins University, Baltimore, MD 21218, U.S.A.*

³ *Department of Physics and Astronomy, University of Victoria, Victoria, BC V8W 3P6, Canada*

⁴ *Steward Observatory, University of Arizona, Tucson, AZ 85721, U.S.A.*

Received 2005 August 1

Abstract. We present preliminary analysis of the FUSE spectra of five PG 1716+426 stars, the subgroup of sdB stars that exhibit very low amplitude, long-period multiperiodic luminosity variations. Our aim is to investigate whether these stars display abundances of iron-peak elements which differ from those observed in the shorter-period EC 14026 stars and in non-variable sdB stars. Our preliminary results suggest that the abundances of Fe, Mn, Co and Ni in PG 1716+426 stars do not differ appreciably from those measured in our reference samples. The implications of these findings for non-adiabatic calculations which link the driving of both the long- and short-period pulsations to an opacity bump associated with a local enhancement of the abundance of iron and iron-peak elements in the envelope are briefly discussed.

Key words: stars: hot subdwarfs – stars: abundances – stars: oscillations – techniques: spectroscopic – stars: individual (PG 1716+426, PG 1627+017, PG 1338+481, PG 0101+039, PHL 457)

1. INTRODUCTION

The PG 1716+426 stars are pulsating subdwarf B stars that exhibit very low amplitude (≤ 5 mmag), long-period (2000–8000 s), multiperiodic luminosity variations. These variations are associated with high radial order g -modes. In the PG 1716+426 stars, which cluster between 20 000 and 28 000 K, the κ driving mechanism is currently thought to be similar to that which is relevant to the hotter (28 000–36 000 K), shorter-period (100–500 s) EC 14026 stars. In both classes, it has been suggested that the driving is linked to an opacity bump associated with a local enhancement of the abundance of iron and, presumably, other iron-peak elements in the envelope (Charpinet et al. 1997; Fontaine et al. 2003). This enhancement could be brought about by radiative element support, as argued by Chayer et al. (2004). Analyses of element abundances in sdB stars could be of some help in constraining current non-adiabatic models, since the mean photospheric

abundances of iron-peak elements in both classes of pulsating stars might differ from those which characterize the constant sdB stars. Furthermore, the relative importance of a stellar wind might differ when one considers the sample of cool PG 1716+426 stars instead of the hotter EC 14026 stars. On that basis, it might be possible to distinguish between various groups of B-subdwarfs on the basis of the abundance of iron-peak elements.

Motivated by these considerations, we have undertaken a systematic analysis of the abundances of iron-peak elements in the PG 1716+426 stars and present here preliminary results of this work.

2. ANALYSIS AND RESULTS

Our analysis is based on high-resolution FUSE observations of a sample of five sdB stars that comprises all the PG 1716+426 observed up to now with FUSE. The basic atmospheric parameters of our target stars, as determined within the extensive analysis of the MMT sample being carried out by Chayer et al. (2003), are summarized in Table 1. For comparison purposes, we are also redetermining abundances for a sample of constant sdB stars (PG 0749+658, HD 4539, Feige 87, JL 236 and PG 1710+490, all located between 24 600 and 30 700 K), as well as for one EC 14026 star, Feige 48 ($T_{\text{eff}} = 29\,600$ K). The abundances of heavy elements are determined on the basis of analyses carried out with version 201 of TLUSTY and version 48 of SYNSPEC (Hubeny & Lanz 1995; I. Hubeny 2004, private communication). In order to facilitate the comparison with our own reference samples of constant and EC 14026 stars, analyzed in LTE (e.g., Chayer et al. 2004), we use the same approximation here and treat various heavy elements as traces. The turbulent velocity is neglected and, as is standard in this type of analysis, the local continuum level is set by eye in each wavelength region.

The main results of our preliminary analysis can be summarized as follows. The PG 1716+426 stars appear to form a very homogenous group in terms of their abundances of iron-peak elements (Figure 1); the abundances by number we determine for Mn, Fe, Co and Ni are similar for our five objects and differ at most by 0.4 dex. They cluster around $\log(\text{Mn}/\text{H}) = -6.6$, $\log(\text{Fe}/\text{H}) = -4.6$, $\log(\text{Co}/\text{H}) = -7.4$ and $\log(\text{Ni}/\text{H}) = -5.8$, with typical errors of the order of 0.4 dex.

The abundances in the cooler star, PG 1627+017, are quite similar to those obtained in the slightly hotter stars of the sample. Furthermore, the lines of heavy elements in PHL 457 appear to be broader than those observed in the other stars in our sample. This suggests that some additional rotational broadening might be present. We note, in this context, that Edelman et al. (2006a) report that PHL 457 is a member of a binary system.

Table 1. Adopted atmospheric parameters.

| Star | $T_{\text{eff}}/10^3$ (K) | $\log g$ | $\log(\text{He}/\text{H})$ |
|-------------|---------------------------|----------|----------------------------|
| PG 1627+017 | 23.7 | 5.3 | -2.9 |
| PG 1716+426 | 27.6 | 5.5 | -2.9 |
| PG 0101+039 | 28.1 | 5.5 | -2.8 |
| PG 1338+481 | 28.1 | 5.4 | -2.9 |
| PHL 457 | 28.2 | 5.5 | -2.5 |

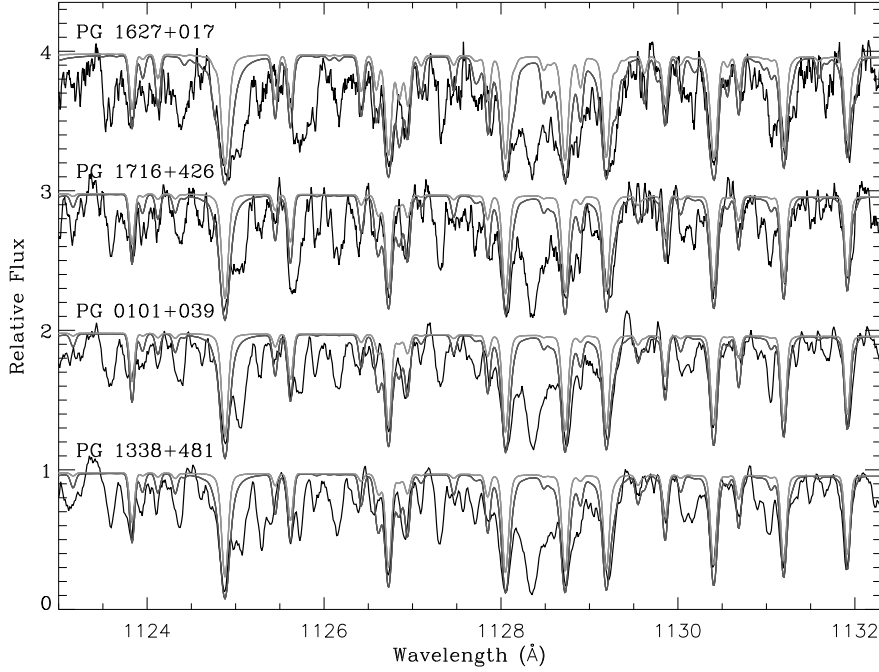


Fig. 1. Comparison between FUSE spectra of four of our program stars from 1123 to 1132 Å with synthetic spectra containing only Fe lines. This spectral region shows strong Fe III lines that correspond to transitions from the ground state $3d^6\ ^5D$ to the $3d^54p\ ^5P^o$ state. The synthetic spectra are calculated for two Fe abundances: $\log(\text{Fe}/\text{H}) = -4.2$ (lower curve) and -5.0 (upper curve). The final Fe abundances are derived on the basis of several such regions and give a larger weight to regions with little contamination by lines of other ions.

We also carried out a comparison with the reference stars (EC 14026 and constant stars) we reanalyzed. A comparison of the four long-period variables hotter than 27 500 K with Feige 48, the EC 14026 star with similar parameters, shows that the abundances of Fe and Ni are quite similar, but that the abundances of Mn and Co appear somewhat lower (by roughly 0.4 dex) in the EC 14026 star.

A comparison of the long-period variables with the non-variables in the same temperature range shows that the abundances Fe, Mn, Co and Ni are similar in both groups. In Feige 87, recognized as a constant star with low abundances of heavy elements, there are no traces of Co and Ni, as well as lower abundances of Fe and Mn than in the PG 1716+426 stars.

As is often the case with analyses in the far-ultraviolet, the placement of the continuum represents a source of systematic error. For example, Pereira et al. (2006) have recently shown that, in the far-ultraviolet range the continuum level obtained by using a theoretical energy distribution (i) normalized at the Strömgren y magnitude and (ii) calculated at the values of T_{eff} and $\log g$ determined from the Balmer lines, could well lie above that used in abundance analyses. Fortunately, the impact of this work appears somewhat blunted here, since our

analysis relies principally on relative, rather than absolute, abundances between various subgroups of hot B-subdwarfs.

What, then, can be said at this stage of the agreement with the abundances expected in the PG 1716+426 stars? Fontaine et al. (2006) present the first predictions of the time-dependence of the abundance of heavy elements expected in hot B-subdwarfs in the combined presence of radiative support and of a weak stellar wind. Their preliminary results suggest that there is a complex dependence of the surface abundance of heavy elements on the age; the abundance of selected heavy elements might thus not be the reliable indicator of pulsation instability it was once believed to be. While this makes the interpretation of abundances analyses such as ours and that of Edelman et al. (2006b) less straightforward, it also suggests that abundance analyses will continue to play an important role in the near future: they will undoubtedly contribute to sorting out the interplay of the various physical processes taking place in the photospheres of hot B-subdwarfs.

ACKNOWLEDGMENTS. This work was supported in part by the NSERC Canada, by the Fund FQRNT (Québec) and by the FUSE Project funded by NASA contract NAS5-32985.

REFERENCES

- Charpinet S., Fontaine G., Brassard P., Chayer P., Rogers F. J., Iglesias C. A., Dorman B. 1997, *ApJ*, 483, L123
- Chayer P., Green E. M., Fontaine G., Saffer R. A. 2003, in *White Dwarfs*, eds. D. de Martino, R. Silvotti, J.-E. Solheim and R. Kalytis, NATO Science Series II, 105, 85
- Chayer P., Fontaine G., Fontaine M., Lamontagne R., Wesemael F., Dupuis J., Heber U., Napiwotzki R., Moehler S. 2004, in *Extreme Horizontal Branch Stars and Related Objects*, ed. P. F. L. Maxted, *Ap&SS*, 291, 359
- Edelman H., Altmann M., Heber U. 2006a, *Baltic Astronomy*, 15, 191 (these proceedings)
- Edelman H., Heber U., Napiwotzki R. 2006b, *Baltic Astronomy*, 15, 103 (these proceedings)
- Fontaine G., Brassard P., Charpinet S., Green E. M., Chayer P., Billières M., Randall S. K. 2003, *ApJ*, 597, 518
- Fontaine G., Green E. M., Chayer P., Brassard P., Charpinet S., Randall S. K. 2006, *Baltic Astronomy*, 15, 211 (these proceedings)
- Hubeny I., Lanz T. 1995, *ApJ*, 439, 875
- Pereira C., Wesemael F., Bergeron P. 2006, *Baltic Astronomy*, 15, 123 (these proceedings)

THE STRUCTURE OF SUBDWARF B STARS AS REVEALED BY ASTEROSEISMOLOGY

S. Charpinet¹, G. Fontaine², P. Brassard², P. Chayer^{3,4} and E. M. Green⁵

¹ *UMR 5572, Université Paul Sabatier et CNRS, Observatoire Midi-Pyrénées, 14 Av. Edouard Belin, F-31400 Toulouse, France*

² *Département de Physique, Université de Montréal, C.P. 6128, Succursale Centre-Ville, Montréal, QC, H3C 3J7, Canada*

³ *Department of Physics and Astronomy, Johns Hopkins University, 3400 North Charles Street, Baltimore, MD 21218-2686, U.S.A.*

⁴ *Primary affiliation: Department of Physics and Astronomy, University of Victoria, P.O. Box 3055, Victoria, BC V8W 3P6, Canada*

⁵ *Steward Observatory, University of Arizona, 933 North Cherry Avenue, Tucson, AZ 85721, U.S.A.*

Received 2005 April 1

Abstract. The rapid p -mode oscillations observed in EC 14026 stars offer interesting opportunities to constrain, with the tools of asteroseismology, the main parameters that define their internal structure. We present the structural properties of sdB stars that are emerging from our detailed asteroseismic studies. We find, in particular, that these properties seem to follow (and thus confirm) expectations from standard EHB stellar evolution. We also show that asteroseismology of EC 14026 stars should play a crucial role in solving the long-standing puzzle of the evolution mechanisms that lead to the formation of extreme horizontal branch stars.

Key words: stars: interiors – stars: oscillations – stars: asteroseismology – stars: hot subdwarfs

1. FROM MODE DRIVING TO ASTEROSEISMOLOGY OF EC 14026 STARS

Since the first discovery of rapid oscillations in hot subdwarf B stars (these are referred to as the EC 14026 stars from the name of the prototype; Kilkenney et al. 1997) and the identification of an efficient driving mechanism to explain this phenomenon (Charpinet et al. 1996, 1997), substantial observational efforts from various groups (see the reviews of Charpinet 2001 and Kilkenney 2002) have raised significantly the number of known EC 14026 pulsators (34 at the time of this writing). The driving mechanism is a κ -effect triggered by the region of partial ionization of heavy elements, especially iron, in the envelope of the star. It can reach sufficient efficiency to destabilize modes because of the accumulation of iron in the driving region due to microscopic diffusion processes.

It was quickly recognized by us that an adequate modeling of the EC 14026

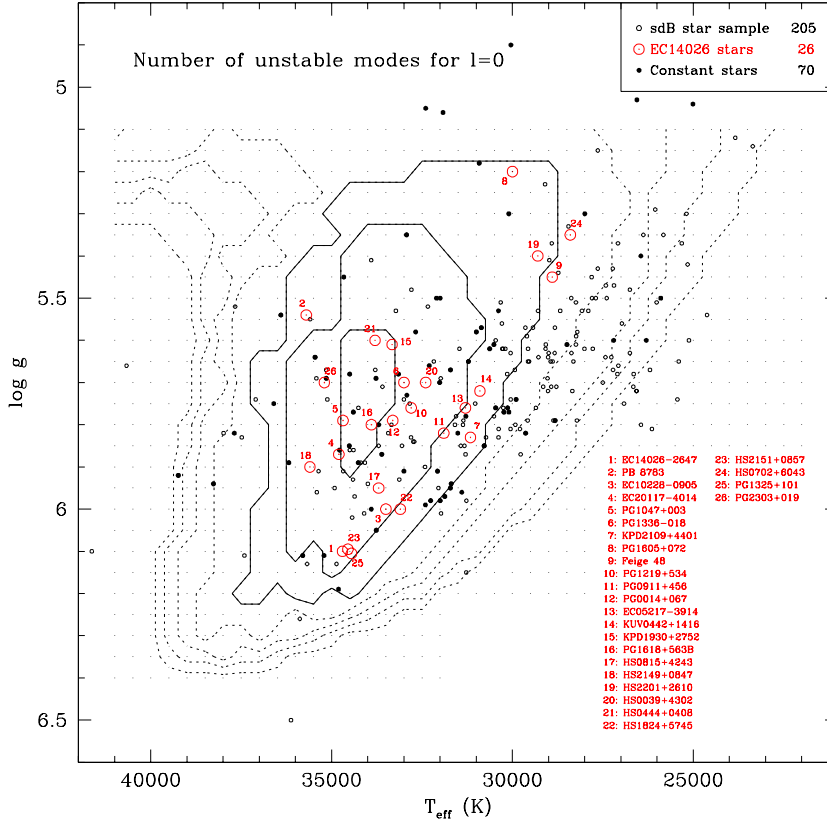


Fig. 1. Global comparison: the observed and predicted instability domain.

phenomenon would require special attention to such diffusion processes. This led to the development of our so-called “2nd generation” models described in Charpinet et al. (1997, 2001) that implement the nonuniform profiles of iron (i.e., the main contributor to the opacity bump) predicted by the condition of diffusive equilibrium between gravitational settling and radiative levitation. With such models, global theoretical properties of the EC 14026 pulsators could be derived and, of course, confronted to the observed properties emerging from the evergrowing sample of known pulsators. To date, with almost three dozen known EC 14026 variables, such comparisons continue to show remarkable similarities between the global properties of the modelled and observed pulsators, thus strongly suggesting that the basic ideas and physics behind the driving of pulsations in these stars are sound. We illustrate below two aspects of these model/observation comparisons.

1.1. The theoretical instability region

Figure 1 represents the $\log g$ vs. T_{eff} plane where are positioned 26 (out of the 34 known) EC 14026 stars which have spectroscopic estimates of their atmospheric parameters available (shown as red dot-circles in the figure). Filled circles represent the 70 sdB stars observed with fast-photometry and found constant by Billères et

al. (2002). As an illustration of the extent of the region where sdB stars are found, the sample of Saffer et al. (1994) is also shown as open circles. In addition, contours derived from full, non-adiabatic pulsation calculations based on the 2nd generation models are superimposed to the observations. These contours indicate the number of excited, $\ell = 0$ modes found in the models – a tracer of the efficiency of the driving mechanism – as a function of $\log g$ and T_{eff} . Remarkably, *all* the 26 EC 14026 stars represented in this diagram are found within or slightly outside the three highest contours (shown as plain lines in Figure 1), i.e., where the driving is most efficient. Of course, this is precisely where one would expect to find the pulsators based on theory. Also, a closer look at Figure 1 indicates that the theoretical instability domain is wider than observed and that non-pulsators cohabitate with pulsators in the same $\log g$ vs. T_{eff} region, a property not expected from the 2nd generation models as they currently stand. Some of these issues, however, may be solved with further refinements in the modeling of the diffusion processes in sdB stars (see Fontaine et al. 2006).

1.2. The driven pulsation modes

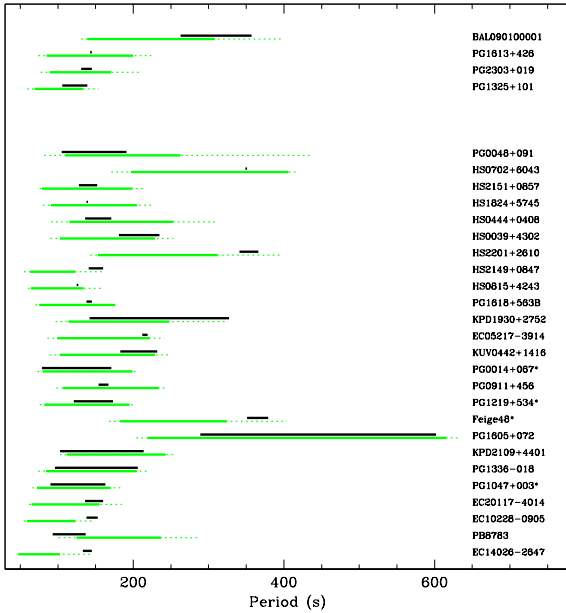


Fig. 2. Global comparison: the observed and predicted period ranges

PG 1605+072 or Feige 48 which have much lower surface gravities and longer periods than the other known pulsators, show periods that are within the expected range according to theory.

These basic observations underline the fact that a very strong overall consistency exists between the predicted properties of EC 14026 stars from the current 2nd generation models and the observed properties of the real pulsators.

Figure 2 provides a comparison between the observed period range (black segments) and the theoretical period range of the driven modes (green segments) for the EC 14026 stars with spectroscopic $\log g$ and T_{eff} measurements available. These were taken at face value to compute a representative 2nd generation model of each star from where the non-adiabatic pulsation properties could be derived. Considering the (sometimes large) uncertainties associated with the spectroscopic evaluations of the atmospheric parameters (which, in terms of the driven periods, translate into the dotted extensions of the green segments), we find that, so far, *all* EC 14026 stars, including outliers like

2. DETAILED ASTEROSEISMIC STUDIES

The excellent global correspondence uncovered between theory and observation has strongly encouraged us to attempt modeling individual EC 14026 pulsators in detail. The ambition was: (1) to fully and accurately reproduce the observed pulsation period spectra based on the 2nd generation models, thus leading to a complete mode identification, and (2) to isolate the most accurate (or best-fitting) model (or family of models) that correspond to the star under study, hence bringing, for the first time, asteroseismic constraints to the stellar structure of Extreme Horizontal Branch (EHB) stars.

2.1. A global approach to asteroseismology

In the recent years, we have set up a new global approach to the problem of asteroseismology of EC 14026 pulsators. Inspired by the well known forward method, which simply consists of comparing directly theoretical periods from a model to the observed periods of a given star, our global optimization technique allows us to exhaustively and efficiently explore the vast model parameter space in order to isolate the model(s) that can best-match the period spectrum of the EC 14026 pulsator under study. Developed mainly in the context of interpreting white light fast-photometric data for which no a priori information on the mode identification exists, our procedure is a “double-optimization” scheme that simultaneously searches for the optimal combination of observed and computed periods (for a model with given parameters) and for the optimal set of model parameters. This method leads objectively to the best match of the observed periods, providing estimates of the structural parameters of the star and a complete mode identification (i.e., the ℓ and k indices) of the observed periods. More details on this method can be found in the pioneering paper of Brassard et al. (2001) and, more recently, in Charpinet et al. (2005a).

2.2. Asteroseismic analyses of EC 14026 stars

The global optimization technique has been applied to a handful of rapid pulsating sdB stars, so far. This includes the analysis of PG 0014+067 from the early work of Brassard et al. (2001), the analysis of PG 1047+003 (Charpinet et al. 2003), of PG 1219+534 (Charpinet et al. 2005a) and most recently of Feige 48 (Charpinet et al. 2005b). These studies were all based on high signal-to-noise white light photometry specifically gathered at the Canada-France-Hawaii 3.6 m telescope (CFHT) with the fast-photometer *Lapoune*. In addition, precise medium-resolution, high signal-to-noise spectroscopy from the MMT coupled with detailed atmospheric modeling has proved essential to isolate a unique best-fit model solution. In each case, it was possible to achieve a simultaneous fit of *all* the observed periods to $\sim 0.8\%$ and better. Moreover, in each case, the asteroseismic solutions appear fully consistent with expectations from non-adiabatic pulsation theory (all observed periods are assigned to modes predicted to be unstable), and the parameters derived for the best-fit model are entirely consistent with the spectroscopic values.

It is an important result that, for at least four stars analyzed in detail with asteroseismology so far, solutions could be achieved which can accommodate three different aspects of the modeling of rapid pulsating sdB stars, namely the pulsation period distribution, the excitation of the modes through the driving mechanism, and detailed model atmospheres. This was certainly not guaranteed at the outset

and this provides strong additional support to the underlying ideas that explain the pulsations in EC 14026 stars, considering that we find that, so far, high consistency between models and observations is preserved even in the details.

3. LINKS TO EVOLUTION AND FORMATION THEORIES

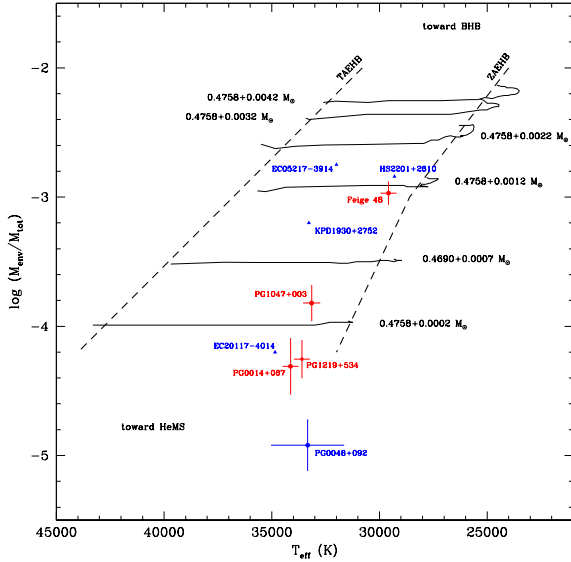


Fig. 3. T_{eff} vs. $\log[M_{\text{env}}/M_{\star}]$ diagram. Evolutionary tracks are from Ben Dorman (1995, priv. comm.).

The two latter parameters in particular, i.e., the total mass and the mass of the H-rich envelope, are quantities that cannot be measured directly with techniques other than asteroseismology (except in some rare cases for the parameter M_{\star} in binary systems). Yet, their importance in the context of EHB stellar evolution and formation theories is crucial. Hence, systematic asteroseismic studies of EC 14026 star are bound to bring new insight on these specific domains. Two interesting links with EHB stellar evolution and formation are illustrated below, based on current asteroseismic results.

3.1. A link to extreme horizontal branch stellar evolution

Figure 3 shows representative evolutionary tracks of extreme horizontal branch stars with various H-rich envelope masses (see figure for details) in a T_{eff} vs. $\log[M_{\text{env}}/M_{\star}]$ diagram. The ZAEHB and TAEHB are indicated by dashed-lines (at low and high T_{eff} , respectively). These sequences illustrate a well known property of evolutionary models near the ZAEHB which tend to have higher (lower) effective temperatures with thinner (thicker) H-rich envelopes, as the mostly inert envelope acts as an isolating layer between the helium core and the stellar surface. Asteroseismic measurements of the envelope mass should now allow us to check if this property, indeed, exists in real subdwarf B stars. Remarkably, this trend seems to be confirmed by the four EC 14026 pulsators analyzed in detail

Asteroseismic analyses of EC 14026 stars using the global optimization technique lead to determinations of the structural parameters of the stars under study. Four fundamental parameters are required to specify the internal structure of hot B subdwarf stars with the 2nd generation models. These are the effective temperature T_{eff} , the surface gravity $\log g$, the total mass of the star M_{\star} , and the logarithmic fractional mass depth of the hydrogen rich envelope $\log q(H) \equiv \log[M(H)/M_{\star}] \simeq \log[M_{\text{env}}/M_{\star}]$, where M_{env} corresponds to the total mass of the H-rich envelope of the star (a more familiar parameter used in stellar evolution theory). The two

(PG 0014+067, PG 1047+003, PG 1219+534, Feige 48; shown as red circles with error bars in Figure 3). Preliminary (and thus still insecure) analyses of additional EC 14026 stars (HS 2201+2610, EC 05217-3914, KPD 1930+2752, EC 20117-4014, and PG 0048+092; blue triangles and circle with error bars) tend to confirm this conclusion. Nonetheless, more precise and additional asteroseismic measurements will be necessary to allow for a definitive conclusion on this issue.

3.2. A link to subdwarf B star formation scenarios

Figure 4 shows the distribution of the asteroseismic masses (with uncertainties) obtained for the four well studied EC 14026 stars. A value derived for PG 0048+092 is also given, although it should be considered as preliminary at this stage. Among the various channels (from single and binary stellar evolution) proposed to form extreme horizontal branch stars, some are expected to produce broader mass distributions than originally believed, with masses that could be as low as $\sim 0.30 M_{\odot}$ and as high as $0.7 M_{\odot}$ (see, e.g., Han et al. 2002, 2003, 2006). Quite interestingly, all the asteroseismically measured masses, so far, have values in the range $0.45\text{--}0.49 M_{\odot}$, i.e., close to the canonical mass for extreme horizontal branch stars ($\sim 0.47 M_{\odot}$; see, e.g., Dorman et al. 1993) with a very small dispersion. Also of interest, one of the channels likely to form “low-mass” or “high-mass” EHB stars is the merger of two helium white dwarfs, which would also contribute to produce isolated sdB stars (as opposed to sdB’s in binary systems). Three of the four EC 14026 stars analyzed in detail (namely, PG 1047+003, PG 0014+067, PG 1219+534), indeed, are very likely single sdB stars. Their masses remain, however, close to the canonical mass. This result might suggest that the merger scenario is not the dominant channel that forms single sdB stars. However, the mass distribution from the merger channel, although it spans a broader range, still has a dominant peak close to the canonical value. Hence, considering that the statistics are still very uncertain due to the small number involved, it is not yet possible to draw firm conclusions on this particular topic. Nonetheless, the potential of asteroseismology in solving such issues is obviously very high and asteroseismic mass measurements for more EC 14026 stars will certainly bring interesting insight in this field.

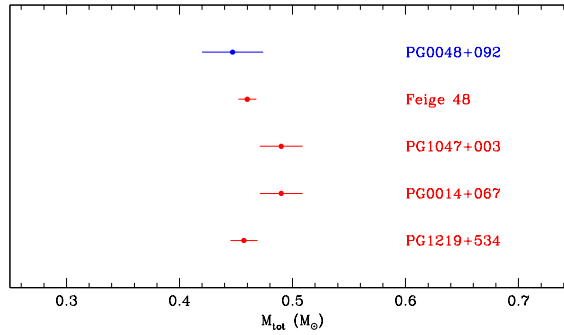


Fig. 4. Distribution of EC 14026 star masses measured by asteroseismology.

4. CONCLUSIONS AND PROSPECTS

4.1. The future of asteroseismology of EC 14026 stars

For more than two decades, major efforts have been pursued in the community of stellar pulsations in order to reach the ultimate goal of asteroseismology, which is to exploit the information that is contained in the vibrations of pulsating

stars to extract new information on the inner structure, physics, and evolution of stellar objects. This goal is about to be achieved for EHB stars, as the detailed study of rapid sdB pulsators has begun to reveal new fundamental elements of the structure of these objects that, so far, were known only through modeling based on standard stellar evolution theory. As illustrated in this paper, systematic asteroseismic analyses of EC 14026 stars, among other applications, open new opportunities to test the validity of stellar evolution theory applied to the helium core burning phase, and propose new ways of constraining the various scenarios that are envisioned to form extreme horizontal branch objects (a problem of stellar evolution theory that still needs to be solved). Hence, as surely as, yesterday, the advent of precise spectroscopy and model atmospheres have revolutionized our understanding of subdwarf B stars and have become, nowadays, essential tools to study the properties of these stars, asteroseismology of EC 14026 stars will, tomorrow, constitute an essential instrument to improve further our knowledge of EHB stars. The technique of asteroseismology applied to rapid sdB pulsators is still in its infancy and more work is certainly needed to improve and check the models, the method and its predictions (the mode identification, for instance). Clearly, however, the high consistency of the solutions that could be achieved in the seismic analyses conducted so far indicate that the most basic ingredients of the models are correct and that the asteroseismic results obtained should be robust.

4.2. The prospect of multicolor fast-photometry

One of the most promising avenues for future independent tests of the asteroseismic predictions resides in multicolor fast-photometry from which one has, in principle, the ability to identify the ℓ index of the pulsation modes from their amplitude ratios at different wavelengths. Theoretical efforts have been pursued recently (see Ramachandran et al. 2004; Randall et al. 2005) to accurately interpret multicolor data in the context of sdB pulsators. In parallel, a growing amount of effort is being devoted to multicolor observations (see, e.g., Jeffery et al. 2004). Such partial identification of the geometry of the modes would, of course, be extremely valuable to check, and possibly improve, the complete mode identification derived from the global optimization techniques. Along this line, we initiated several projects to carry out high S/N ratio UBV photometry of EC 14026 pulsators using the Canada-France-Hawaii Telescope in conjunction with the fast-photometer *Lapoune*. In addition, a project is underway to use the Far UV Spectroscopic Explorer (FUSE) as a fast photometer (a possibility offered by the so-called “Time-Tag” mode of the instrument) that would provide a light curve of the sdB pulsator PG 1219+534 in the FUV ($\sim 1000 \text{ \AA}$) passband. Combined with nearly simultaneous ground based observations in the optical, this project should lead to strong independent constraints on the ℓ value of the modes seen in PG 1219+534, from which the predicted mode identification will be checked.

ACKNOWLEDGMENTS. This work was based in part on observations gathered at the Canada-France-Hawaii Telescope, operated by the National Research Council of Canada, the Centre National de la Recherche Scientifique of France and the University of Hawaii, and observations obtained at the MMT Observatory, a joint facility of the University of Arizona and the Smithsonian Institution. This study made extensive use of the computing facilities offered by the Calcul en Midi-Pyrénées (CALMIP) project (France). This work was supported in part by the

NSERC of Canada and by the Fund FQRNT (Québec). G.F. also acknowledges the contribution of the Canada Research Chair Program.

REFERENCES

- Billères M., Fontaine G., Brassard P., Liebert J. 2002, *ApJ*, 578, 515
- Brassard P., Fontaine G., Billères M., Charpinet S., Liebert J., Saffer R. A. 2001, *ApJ*, 563, 1013
- Charpinet S. 2001, *Astron. Nachr.*, 322, 387
- Charpinet S., Fontaine G., Brassard P., Dorman B. 1996, *ApJ*, 471, L103
- Charpinet S., Fontaine G., Brassard P., Chayer P., Rogers F. J., Iglesias C. A., Dorman B. 1997, *ApJ*, 483, L123
- Charpinet S., Fontaine G., Brassard P. 2001, *PASP*, 113, 775
- Charpinet S., Fontaine G., Brassard P. 2003, in *White Dwarfs*, eds. D. de Martino et al., Proc. Conf. at Capodimonte, Napoli, NATO Science Ser., Vol. 105, p. 69, Kluwer, Dordrecht
- Charpinet S., Fontaine G., Brassard P., Green E. M., Chayer P. 2005a, *A&A*, 437, 575
- Charpinet S., Fontaine G., Brassard P., Green E. M., Chayer P. 2005b, *A&A*, in press
- Dorman B., Rood R.T., O'Connell R.W. 1993, *ApJ*, 419, 596
- Fontaine G., Green E. M., Chayer P. et al. 2006, *Baltic Astronomy*, 14, 211 (these proceedings)
- Han Z., Podsiadlowski P., Lynas-Gray A. E. 2006, *Baltic Astronomy*, 14, 17 (these proceedings)
- Han Z., Podsiadlowski P., Maxted P. F. L., Marsh T. R., Ivanova N. 2002, *MNRAS*, 336, 449
- Han Z., Podsiadlowski P., Maxted P. F. L., Marsh T. R. 2003, *MNRAS*, 341, 669
- Jeffery C. S., Dhillon V. S., Marsh T. R., Ramachandran B. 2004, *MNRAS*, 352, 699
- Kilkenny D. 2002, in *Radial and Nonradial Pulsations as Probes of Stellar Physics*, IAU Colloq. 185, eds. C. Aerts, T. R. Bedding & J. Christensen-Dalsgaard, ASP Conf. Ser., 259, 356
- Kilkenny D., Koen C., O'Donoghue D., Stobie R. S. 1997, *MNRAS*, 285, 640
- Ramachandran B., Jeffery C. S., Townsend R. H. D. 2004, *A&A*, 428, 209
- Randall S. K., Fontaine P., Brassard P., Bergeron P. 2005, *ApJS*, 161, 456
- Saffer R. A., Bergeron P., Koester D., Liebert J. 1994, *ApJ*, 432, 351

AN APPROACH TO A STABILITY ANALYSIS OF AN SDO STAR

C. Rodríguez-López^{1,3}, A. Moya², R. Garrido³, J. MacDonald⁴, A. Ulla¹,
S. Dreizler⁵, S.D. Hügelmeyer⁵ and M. Manteiga⁶

¹ *Departamento de Física Aplicada, Universidade de Vigo, Vigo E-36200, Spain*

² *LESIA, Observatoire de Paris-Meudon, UMR 8109, Meudon F-92190, France*

³ *Instituto de Astrofísica de Andalucía-CSIC, Granada E-18008, Spain*

⁴ *Department of Physics and Astronomy, University of Delaware, Newark, DE-19716, U.S.A.*

⁵ *Institut für Astrophysik, Universität Göttingen, Göttingen D-37077, Germany*

⁶ *Departamento de Ciencias de la Navegación y de la Tierra, Universidade de Coruña, A Coruña E-15011, Spain*

Received 2005 July 27

Abstract. A stability analysis of a structural model of an sdO star is presented. A non-adiabatic code of oscillations is used to search for modes in the frequency range 0.4 to 15 mHz. All of the computed modes were found to be stable. We draw attention, however, to three different stability regions.

Key words: stars: hot subdwarfs, oscillations

1. INTRODUCTION

O-type hot subdwarfs (sdOs) are pre-WD stars with masses around $0.5 M_{\odot}$ and stellar parameters between 40 000 and 100 000 K in T_{eff} and 4.0–6.5 in $\log g$. The few interpretations found in the literature about sdO's physical nature depict them as objects with a C/O core and a helium burning shell (Groth et al. 1985), from where they get their luminosity, and which are mostly devoid of hydrogen in their atmospheres.

As can be inferred from their scattered positions on the HR diagram (HRD), appearing both in the post-AGB (Asymptotic Giant Branch) and post-EHB (Extreme Horizontal Branch) domains, there may be different evolutionary paths which can bring a star to the sdO's loci.

We have started a photometric campaign searching for possible pulsations in these objects which, if successful, could open a new field to gain important information for sdOs. So far, we have observed about 40 sdOs, with three possible pulsators found. Some structural models were constructed for two of these objects and their evolutionary paths calculated on the HRD.

We also present the first preliminary results of pulsational stability of one of these structural models.

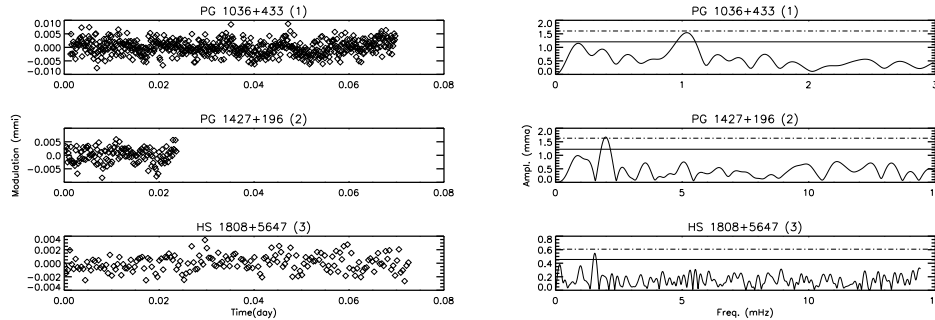


Fig. 1. Light curves and power spectra of promising pulsating sdOs. The horizontal lines are 3 and 4 times the mean Fourier noise.

2. STRUCTURAL MODELS AND EVOLUTIONARY PATHS

The structural models were constructed to account for the physical parameters of sdOs numbers 1 and 2 which were found particularly promising for pulsations in our photometric campaigns (Rodríguez-López et al. 2005) and whose light curves and Fourier transforms are shown in Figure 1. For object number 3 (from a recent campaign) the construction of the models is under way.

Models 1 and 2 were calculated to match the physical parameters of object 1, and models 3 to 6 were constructed to account for object 2. These models were calculated with the stellar evolution code of Jimenez et al. (2004) evolving $Z = 0.02 M_{\odot}$ stars from the main sequence with mass loss on the red giant branch at rates 70–85% higher than the canonical Reimers formula rates. Some relevant properties of the models are given in Table 1.

The complete evolutionary tracks in the HRD of models 3 to 6, and the evolution to the WD phase of models 1 and 2 are shown in Figure 2.

3. STABILITY ANALYSIS AND DISCUSSION

Using the non-adiabatic pulsation code of Moya et al. (2004) we have calculated modes for $\ell = 0, 1, 2, 3, 4$ with frequencies between 0.4 and 15 mHz, for model 1 of Table 1. The structural models were calculated with a refinement of the fractional mass depth parameter $\log q (= \log(1 - M_r / M_{\odot}))$ from 0 to ~ -13 . In Figure 3 the growth rate parameter (η) is plotted versus frequency. A positive value of η would mean we have an unstable mode, while a negative value indicates stability. The plot shows that all of the computed modes were found to be stable.

Table 1. Main physical parameters of the structural models.

| Model number | T_{eff} (K) | $\log g$ | M (M_{\odot}) | η_R | $X(\text{H})$ | $X(\text{He})$ | $X(\text{C})$ | Z |
|--------------|----------------------|----------|---------------------|----------|---------------|----------------|---------------|------|
| 1 | 79 000 | 5.70 | 0.478 | 0.675 | 0.21 | 0.72 | 3.4E-02 | 0.07 |
| 2 | 79 000 | 5.95 | 0.491 | 0.650 | 0.68 | 0.30 | 3.0E-03 | 0.02 |
| 3 | 55 000 | 5.89 | 0.471 | 0.685 | 0.43 | 0.55 | 9.6E-04 | 0.02 |
| 4 | 55 000 | 5.95 | 0.471 | 0.690 | 0.33 | 0.65 | 6.3E-04 | 0.02 |
| 5 | 55 200 | 5.98 | 0.471 | 0.695 | 0.27 | 0.71 | 9.0E-04 | 0.02 |
| 6 | 55 000 | 6.02 | 0.470 | 0.700 | 0.18 | 0.78 | 1.5E-02 | 0.04 |

However, we can notice 3 different regions in the scanned frequency range. Two regions where η achieves less negative values and hence the modes have a tendency to instability: one with low frequencies (from about 0.5 to 2 mHz) corresponding to high radial order g -modes, and other with high frequencies (from about 9 to 12 mHz) corresponding to low radial order p -modes. The modes in the region in between (from 2 to 9 mHz) were found highly stable.

We have plotted the derivative of the work integral ($dW/d\log q$), which gives the net amount of energy gained or lost by the displaced material during one pulsation cycle, and the logarithm of the opacity vs. $\log q$ for a representative mode of each one of these regions for $\ell = 2$. A negative (positive) value of $dW/d\log q$ indicates that this region contributes locally to driving (damping) of the mode.

In the first region (Figure 4 left) the energy concentrates at $\log q \sim -6$ in the proximity of the small bump in the opacity profile. At this depth in the star

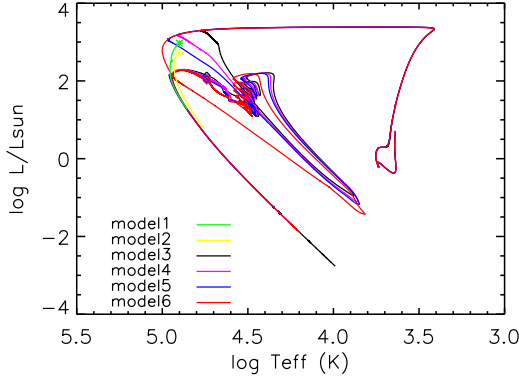


Fig. 2. Evolutionary tracks followed by the models in the HRD. Model 1 is marked with an asterisk and the rest of the models with a diamond.

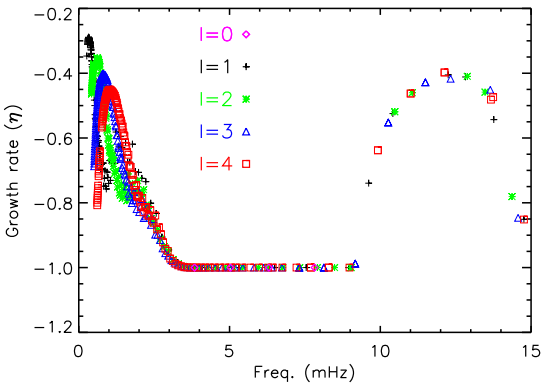


Fig. 3. Growth rate parameter (η) vs. frequency for $\ell = 0,1,2,3,4$ of model 1.

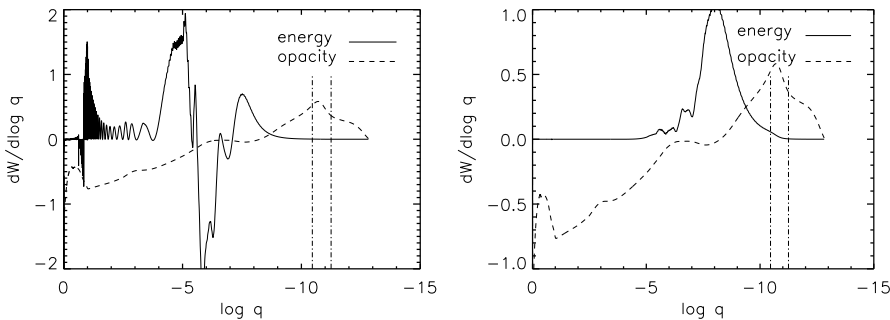


Fig. 4. Left panel. Energy and opacity for the g99 mode at $\nu \sim 0.6$ mHz. Right panel. The g10 mode at $\nu \sim 4.5$ mHz. The dashed-dotted line depicts the convection zone.

the density and temperature are high, making it an important zone in the overall driving of pulsations. Therefore the mode gains energy and becomes a bit more unstable. This opacity bump is due to the C/O partial ionization zone, whose κ -mechanism is the responsible for driving the pulsations found in the PG 1159 spectral class (Starrfield et al. 1983). Our structural model has a low carbon mass fraction, but He enhancement often occurs together with a C enhancement, so we can speculate that by enhancing the metallicity and hence the magnitude of the opacity bump, we might get unstable modes. It might well be that we need accurate envelope compositions to construct individual structural models for each sdO, as it is also the case for the PG 1159 stars (Quirion et al. 2004).

At intermediate frequencies the energy concentrates at $\log q \sim -8$ (Figure 4 right). However, this region is not associated with an opacity bump and the modes are highly stable.

At higher frequencies (Figure 5) the energy shifts even more towards the surface, at $\log q \sim -10$, approaching the highest opacity bump located at $\log q \sim -11$, and the modes have again a tendency to instability. However, we would not expect unstable modes. Even though the opacity bump is strong, the density there is not large enough to drive pulsations. Besides, the low ratio of the thermal to dynamical time scales in this zone would make the energy redistribution too efficient for the mode to become unstable. Work is in progress to test for all these possibilities.

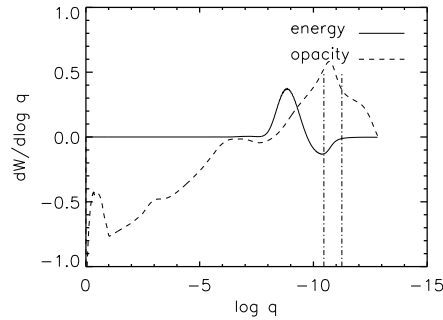


Fig. 5. Energy and opacity for the p3 mode at $\nu \sim 10$ mHz.

ACKNOWLEDGMENTS. We thank the Centro de Supercomputación de Galicia (CESGA) for the use made of their computational facilities. This work was supported by the Spanish MCyT AYA 2003-09499 and ESP2004-03855-C03-01.

REFERENCES

- Groth H. G., Kudritzki R. P., Heber U. 1985, *A&A*, 152, 107
 Heber U. 1986, *A&A*, 155, 33
 Jimenez R., MacDonald J., Dunlop J. S., Padoan P., Peacock J. A. 2004, *MNRAS*, 349, 240
 Moya A., Garrido R., Dupret M. A. 2004, *A&A*, 414, 1081
 Quirion P.-O, Fontaine G., Brassard P. 2004 *ApJ*, 610, 436
 Rodríguez-López C., Ulla A., Garrido R. et al. 2005, in *14th European Workshop on White Dwarfs*, eds. D. Koester & S. Moehler, ASP Conf. Ser., 334, 627.
 Starrfield S., Cox A. N., Hodson S. W., Pesnell W. D. 1983, *ApJ*, 268, L27

A NEW LARGE-AMPLITUDE SLOWLY PULSATING SDB STAR

D. Kilkenny¹, D. O’Donoghue¹, M. D. Reed², N. Hambly³ and H. McGillivray³

¹ *South African Astronomical Observatory, PO Box 9, Observatory 7935, South Africa*

² *Department of Physics, Astronomy and Materials Science, Southwest Missouri State University, 901 S. National Ave., Springfield, MO 65804, U.S.A.*

³ *Wide Field Astronomy Unit, Institute for Astronomy, University of Edinburgh, Blackford Hill, Edinburgh EH9 3HJ, Scotland*

Received 2005 August 1

Abstract. We report the discovery of a new large-amplitude slowly pulsating sdB star, EC 21324–1346. Although we have only a small amount of data, it is clear that the star exhibits more than one mode of variation; the present data can be adequately represented with three or four frequencies in the range 170–330 μHz (about 0.8 to 1.6 hours). The amplitude of the dominant frequency is about 0.004 mag – large for a slowly pulsating sdB star.

Key words: stars: oscillations – stars: horizontal-branch – stars: individual (EC 21324–1346)

1. INTRODUCTION

The slowly pulsating sdB stars were discovered as part of a campaign by E. Green and her collaborators (Green et al. 2003) to find and monitor sdB stars in binary systems. As with the rapidly pulsating sdB stars, the slow pulsators have amplitudes < 0.01 mag – often much less – but longer periods, typically 1–2 hours. The slow pulsators also appear to be multi-periodic and, like the rapid pulsators, the nomenclature for the slow pulsators is undecided – they have been referred to as “Betsy” stars, after the discoverer, but “PG 1716 stars” (after the prototype, PG 1716+426) is more appropriate.

In the Edinburgh-Cape (EC) survey (Stobie et al. 1997; Kilkenny et al. 1997) many new sdB stars have been found. Following the discovery of the fast pulsators (Kilkenny et al. 1997) these are being checked for variability, but generally only for short intervals of ~ 2 hours, so that low-amplitude slow pulsators might have been missed. The star reported here, EC 21324–1346, was of such a large amplitude, that even we could not miss the variability, even in a relatively short run.

EC 21324–1346 is located at $\alpha = 21^{\text{h}} 35^{\text{m}} 13^{\text{s}}$, $\delta = -13^{\circ} 33' 23''$ (2000.0). A preliminary spectral type from the EC survey is “sdB”, but no survey *UBV* photometry has yet been obtained. The photographic magnitude from the plate measurement indicates $B \sim 13$ mag.

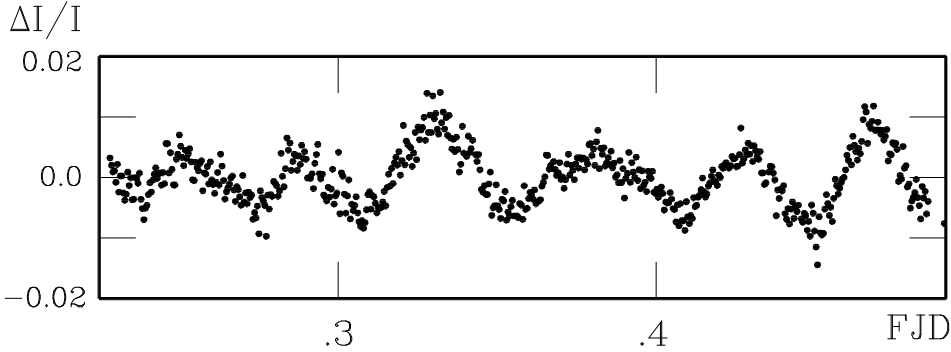


Fig. 1. Relative intensity light curve for EC 21324–1346 on JD 2453259 (40 s integrations; no filter). The abscissa is Fractional (heliocentric) Julian Date.

2. OBSERVATIONS

Observations were made with the University of Cape Town’s frame-transfer CCD on the 1.9 m and 1.0 m telescopes at the Sutherland site of the SAAO. Details are listed in Table 1 and the longest run is shown in Figure 1.

Table 1. UCT CCD observation log for EC 21324–1346

| Date (2003) | JD | Tel (m) | Filter | Run (hr) | Integr. (s) |
|-------------|---------|---------|--------|----------|-------------|
| Jul 15/16 | 2453202 | 1.9 | BG39 | 2.0 | 10 |
| Sep 07/08 | 3258 | 1.0 | – | 4.1 | 30 |
| Sep 09/10 | 3259 | 1.0 | – | 6.3 | 40 |

Table 2. Four frequencies extracted from Fig. 2 data (best fit to two nights).

| Frequency (Hz) | Ampl.(mag) | Period (s) | Period (hr) |
|----------------|------------|------------|-------------|
| 0.000253 | 0.0037 | 3950 | 1.10 |
| 0.000332 | 0.0022 | 3010 | 0.84 |
| 0.000175 | 0.0022 | 5710 | 1.59 |
| 0.000226 | 0.0016 | 4420 | 1.23 |

3. ANALYSIS

The usual Fourier analysis has been carried out. The night JD 2453259 is the longest run, and we found at least four frequencies clearly above the noise level (see Figure 2). Of course, with such a short data set – covering very few cycles – it is optimistic to think we can extract four frequencies. But inspection of Figure 1 indicates that the variations are clearly not mono-periodic and even that probably more than two frequencies are present.

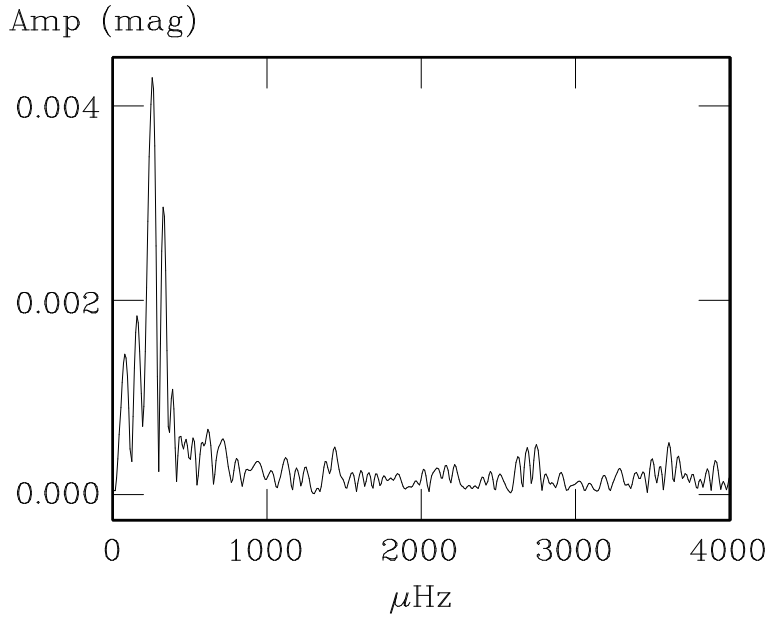


Fig. 2. Periodogram from Fig. 1 data for EC 21324–1346.

We have repeated the analysis for the two consecutive nights – JD 2453258 and JD 2453259 – together. We extract the same four frequencies and Figure 3 shows the best four frequency fit to the data for the two nights.

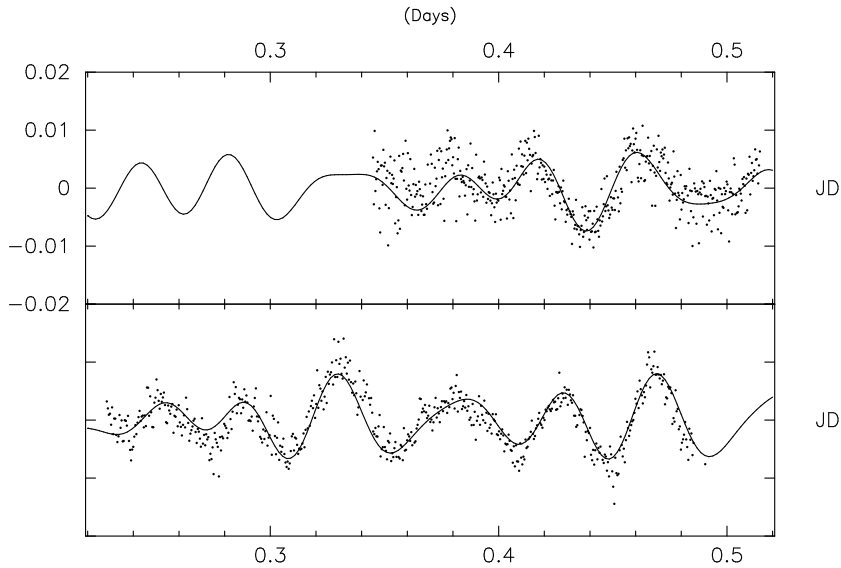


Fig. 3. Four-frequency fit to EC 21324–1346 data for JD 2453258 and 3259.

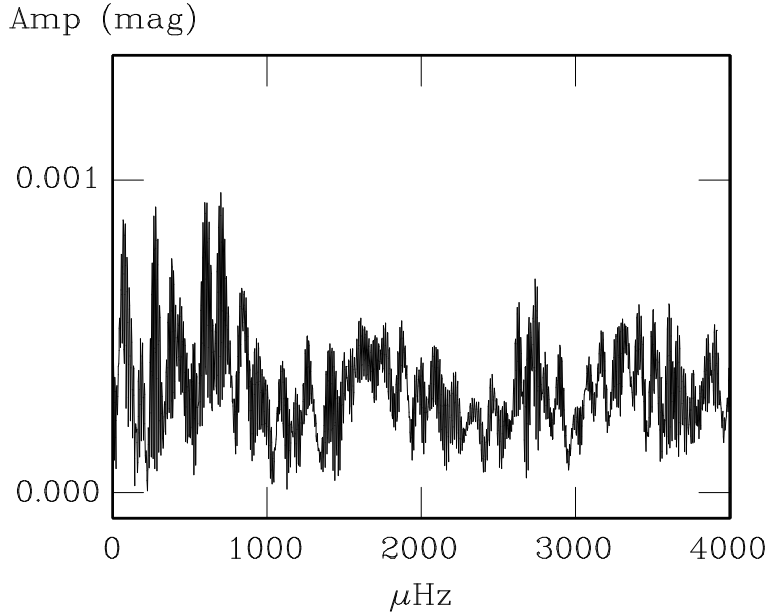


Fig. 4. Periodogram for the EC 21324–1346 data for JD 2453258 and 3259 after the removal of the four strongest frequencies.

4. CONCLUSIONS

EC 21324–1346 is an sdB star which exhibits multi-periodic variation with periods in the range 0.8 to 1.6 hours (see Table 2). It is clearly a slowly-pulsating star of the type discovered by Green et al. (2003) and has rather a large amplitude for this class of star.

REFERENCES

- Green E. M., Fontaine G., Reed M. D., Callerame K., Seitzzahl I. R., White B. A., Hyde E. A., Østensen R., Cordes O., Brassard P. et al. 2003, *ApJ*, 583, L31
 Kilkenney D., O'Donoghue, D., Koen C., Stobie R. S., Chen A. 1997, *MNRAS*, 287, 867
 Kilkenney D., Koen C., O'Donoghue D., Stobie R. S. 1997, *MNRAS*, 285, 640
 Stobie R. S. et al. 1997, *MNRAS*, 287, 848

THE MSST CAMPAIGN: 4 M SPECTROSCOPY OF PG 1605+072

C. S. Jeffery¹, U. Heber², S. Dreizler^{3,4}, S. J. O’Toole^{2,5}, S. L. Schuh^{3,4},
V. M. Woolf^{1,6}, S. Falter^{2,7}, A. Nitta⁸, S. Kleinman⁸, J. Krzesinski⁸ and
M. Billères⁹

¹ *Armagh Observatory, College Hill, Armagh BT61 9DG, U.K.*

² *Remeis-Sternwarte, Astronomisches Institut der Universität
Erlangen-Nürnberg, Sternwartstrasse 7, D-96049 Bamberg, Germany*

³ *Institut für Astrophysik, Universität Göttingen, Friedrich-Hund-Platz 1,
D-37077 Göttingen, Germany*

⁴ *Institut für Astronomie und Astrophysik, Universität Tübingen, Sand 1,
D-72076 Tübingen, Germany*

⁵ *School of Physics, University of Sydney, NSW 2006, Australia*

⁶ *Department of Physics, University of Nebraska at Omaha, 6001 Dodge St.,
Omaha NE 68182, U.S.A.*

⁷ *Max-Planck-Institut für Astronomie, Königstuhl 17, D-69117 Heidelberg,
Germany*

⁸ *Apache Point Observatory, PO Box 59, Sunspot, NM 88349, U.S.A.*

⁹ *European Southern Observatory, Santiago Headquarters, Avenida Alonso de
Cordova 3107, Vitacura, Casilla 19001, Santiago 19, Chile*

Received: 2005 September 30

Abstract. The MultiSite Spectroscopic Telescope (MSST) campaign aimed to provide a detailed view of the short-period pulsating subdwarf B star PG 1605+072. We present results from the part of the campaign undertaken on 4 m telescopes in 2002 May and June.

Key words: stars: hot subdwarfs – stars: oscillations – stars: individual (PG 1605+072)

1. INTRODUCTION

The MultiSite Spectroscopic Telescope (MSST) campaign observed the non-radially pulsating subdwarf B star PG 1605+072 in 2002 May and June (Heber et al. 2003). Spectroscopic observations were obtained on a range of 2 m and 4 m class telescopes, supported by photometry from a large number of observatories, including the Whole Earth Telescope. Other papers describing the spectroscopic results from 2 m telescopes (O’Toole et al. 2005) and the photometry (Schuh et al. 2003, Dreizler et al. 2006) are and will be published elsewhere.

Previous spectroscopic observations of PG 1605+072 with 4 m telescopes had

proved the feasibility and precision of a study of velocity variations (Woolf et al. 2002), compromised only by the quantity of data obtained and issues about timing. The main focus of this part of the MSST was to maximize the length and coverage of the observations in order to obtain higher resolution in both velocity and frequency, and hence to obtain material useful for identifying oscillation modes. As a consequence of the traditional traumas of observational astronomy (time allocation, instrument failure and bad weather), out of eighteen nights originally requested, 7.5 nights were awarded and 24.3 hours of time-resolved spectroscopy was obtained, of which 19.5 hours was usable. This paper introduces the observations, and presents the frequencies derived from the radial velocity measurements.

2. OBSERVATIONS

Time-resolved spectroscopy of spectral resolution $\sim 1 \text{ \AA}$ was carried out during six nights at the Calar Alto 3.5 m telescope (Spain), the European Southern Observatory 3.5 m New Technology Telescope (Chile) and the Apache Point Observatory 3.5 m (New Mexico, U.S.A.).

At Apache Point (APO), we used the red arm of the Dual

Imaging Spectrograph where it was anticipated that velocity changes would be observable in H α . At Calar Alto 3.5 m (CA) telescope, both arms of the TWIN spectrograph were used to obtain spectra simultaneously in the wavelength ranges 5785–6880 \AA and 3850–4950 \AA . At the NTT, the ESO Multi-Mode Instrument (EMMI) was used to obtain spectra in the wavelength range 6400–6700 \AA . However, atmospheric conditions were so poor that none of the EMMI data have proved to be usable.

In all cases, spectra were obtained by trailing the star along the slit (Falter et al. 2003) to give two-dimensional images representing wavelength dispersion in one axis and time in the other. The time resolution is given effectively by the trail-rate along the slit divided by the projected size of the stellar disk on the detector; a higher trail rate provides better time resolution, but lower S/N per resolution element. A summary of the observations is given in Table 1. The integrated sky background is estimated using regions at each end of the slit. Arc-lamp and standard-star calibration images were obtained in order to provide wavelength calibrations and geometric correction.

The data reduction methods have been described by Falter et al. (2003). With the image trailed along the slit at a uniform rate, each two-dimensional image has to be reduced to a series of discrete spectra, with each one accurately time-stamped. The choice of extraction interval is made at this stage to optimize both the signal to noise ratio in individual spectra and the sampling rate. The reduced data products consist of a two-dimensional FITS file containing a series of wavelength calibrated time-tagged spectra for each long-slit trailed spectrum.

Spectra were read directly from the reduced FITS files and resampled onto a logarithmic wavelength scale. Velocities were determined by cross-correlating each spectrum with a template created by summing all spectra from a given series.

Table 1. MSST 4 m observing log.

| Date 2002 | Obs. | Start JD–2445000 | Finish | t_{exp} s | N_{obs} |
|--------------|------|---------------------|---------|-----------------------|------------------|
| May 14 | APO | 409.324 | 409.446 | 3.6 | 1773 |
| May 15 | APO | 410.183 | 410.331 | 4.8 | 1727 |
| May 18 | APO | 413.296 | 413.329 | 4.8 | 471 |
| May 22 | CA | 416.908 | 417.146 | 16.5 | 1065 |
| May 23 | CA | 417.885 | 418.158 | 16.5 | 1213 |
| May 29 | NTT | 424.161 | 424.359 | – | – |
| Total | | | | | 10892 |

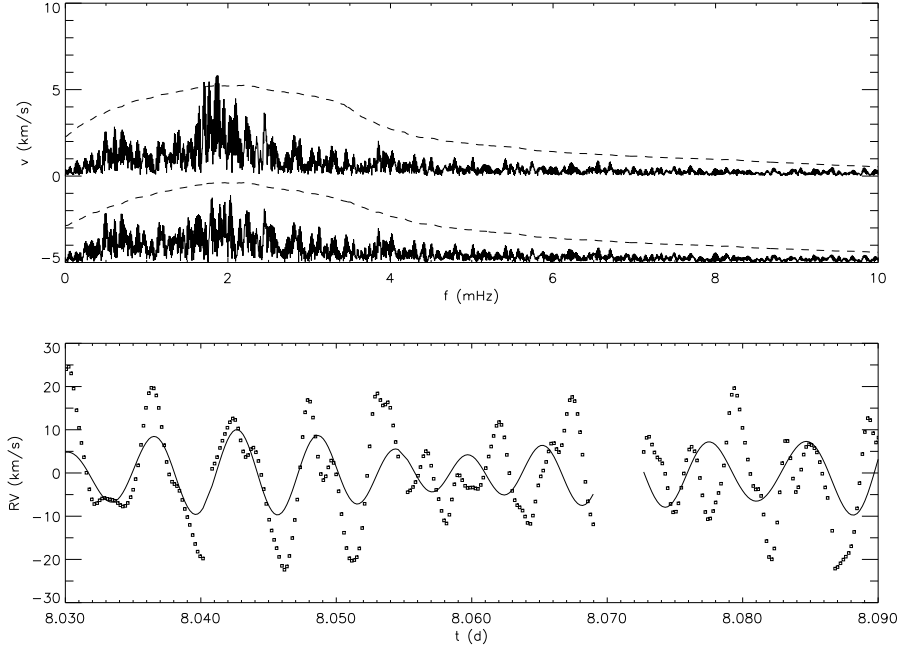


Fig. 1. Best solution for the CA blue spectroscopy. Top: the velocity amplitude spectrum (v) before (above) and after (below) subtraction of the four highest peaks. The dashed line shows the 4σ level in each case. Bottom: part of the radial velocity curve with the best four-frequency solution (solid) from Table 2. Times are in JD-2452410.

Problems with the wavelength calibrations, evident from substantial offsets for individual frames, were corrected by demanding the mean velocity for each frame to be 0 km s^{-1} .

3. FREQUENCY ANALYSIS

Velocity amplitude spectra for each dataset (CA blue, CA red, APO red and APO+CA red) were calculated using a simple Fourier transform. The limited overall coverage restricts the frequency information that can be extracted. All datasets show an excess of power in the range 1.5–2.5 mHz.

Despite apparent similarities in the velocity curves, the amplitude spectra obtained from each arm of the TWIN spectrograph differ considerably from one another. A careful comparison was carried out to look for systematic correlations.

We have formally analyzed only the two CA datasets, which have a formal temporal resolution ($2/T$) of 18 mHz. A detection threshold was defined by a local

Table 2. MSST 4 m frequencies and amplitudes.

| F_b mHz | V_b km/s | P s | F_r mHz | V_r km/s | F_{2m} mHz | V_{2m} km/s |
|--------------|---------------|----------|--------------|---------------|-----------------|------------------|
| 1.705 | 6.0 | 586 | | | | |
| 1.756 | 5.4 | 569 | 1.767 | 8.5 | | |
| 1.867 | 7.2 | 536 | 1.867 | 6.5 | 1.891 | 2.3 |
| 2.095 | 5.4 | 477 | | | 2.076 | 15.4 |

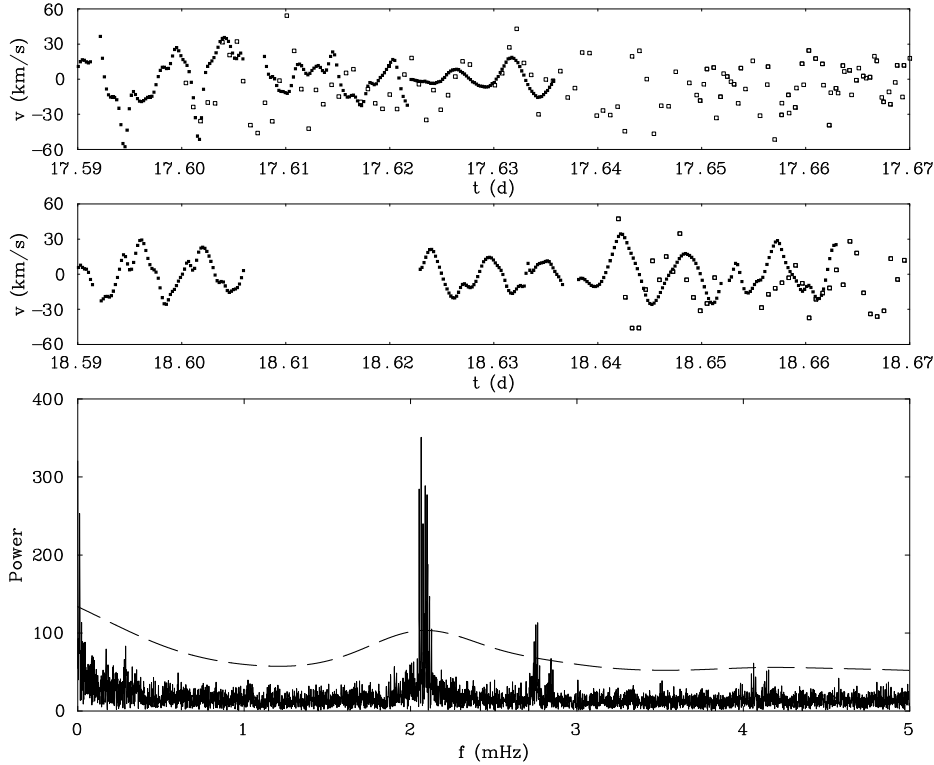


Fig. 2. Top: comparison of 4 m spectroscopy (CA blue: solid symbols) with concurrent radial velocities from the MSST 2 m campaign (open symbols). Times are in JD–2452410. Bottom: power spectrum of 2 m radial velocities for three nights (JD 2452416.61–2452418.98). The dashed line represents the 4σ level.

σ . Any peak above 4σ was deemed real, a sinusoid was fitted and its frequency and amplitude recorded. The data was prewhitened by the fit and the procedure repeated until no peaks exceeded the 4σ level. The solutions are given in Table 2 for the blue (F_b) and red (F_r) arms, and also compared to the MSST 2 m (F_{2m}) results.

These solutions are unsatisfactory. As we know from the 2 m data, there are unresolved frequencies present which suggest that substantial errors should be attached to the amplitudes given in Table 1. It is notable that the signal at 2.076 mHz detected in the 2 m campaign (O’Toole et al. 2005) has a much lower amplitude in the CA data. It is apparent that neither signal at 1.71 and 1.76 mHz was detected in the MSST 2 m campaign (O’Toole et al., 2005). While, given the frequency resolution of our data, the signal at 1.76 mHz may coincide with one at 1.744 mHz in the light curve of Kilkenny et al. (1999). There are sufficient discrepancies between the 2 m and 4 m results to raise a number of questions.

Following the conference at which these first results were presented, we re-analyzed a short section of the 2 m data spanning just three nights (JD 2452416.61–2452418.98) centered on the two nights of the CA observations (O’Toole et al. 2005). Figure 2 shows both 2 m and 4 m data in the regions of overlap where

it will be seen that the level of correlation is not high. It is also clear that the principal signal at 2.076 mHz is present in the 2 m data over these three nights, while it is not seen in the 4 m data. At the very least it would appear that we have oversampled the trailed CA spectra. Reconciling and understanding the remaining discrepancies will require further work.

While O'Toole et al. (2005) note that the 2.076 mHz peak had a much reduced amplitude in early velocity studies (O'Toole et al. 2003; Woolf et al. 2002; O'Toole et al. 2002) compared with contemporary photometric studies (Kilkenny et al. 1999; Koen et al. 1998), it had a larger velocity amplitude in the study by Falter et al. (2003). Although the mode amplitude may be variable over long time scales, we have so far failed to confirm any such variability on a short time scale.

In conclusion, MSST 4 m data should provide a high-time and spectral resolution snapshot of the radial-velocity behavior of PG 1605+072 over short intervals during the more extended 2 m campaign. Further analysis of the combined data from 2 m, 4 m and photometry campaigns remains to be completed.

REFERENCES

- Dreizler S., Schuh S., Heber U. et al. 2006, in preparation
- Falter S., Heber U., Dreizler S. et al. 2003, *A&A*, 401, 289
- Heber U., Dreizler S., Schuh S. L. et al. 2003, in *13th European Workshop on White Dwarfs*, eds. D. de Martino, R. Silvotti, J.-E. Solheim & R. Kalytis, Kluwer, Dordrecht, p. 105
- Heber U., Reid I. N., Werner K. 1999, *A&A*, 348, L25
- Heber U., Napiwotski R., Reid I. N. 1997, *A&A*, 323, 819
- Jeffery C. S., Woolf V. M., Pollacco D. L. 2001, *A&A*, 376, 497
- Kawaler S. D. 1999, in *11th European Workshop on White Dwarfs*, eds. J.-E. Solheim & E. G. Meištas, ASP Conf. Ser., 169, 158
- Kilkenny D., Koen C., O'Donoghue D. et al. 1999, *MNRAS*, 303, 525
- Koen C., O'Donoghue D., Kilkenny D. et al. 1998, *MNRAS*, 296, 317
- Montañès Rodríguez P., Jeffery C. S. 2001, *A&A*, 375, 411
- O'Toole S. J., Bedding T. R., Kjeldsen H., Dall T., Stello D. 2002, *MNRAS*, 334, 471
- O'Toole S. J., Jorgensen M. A. S. G., Kjeldsen H. et al. 2003, *MNRAS*, 340, 856
- O'Toole S. J., Heber U., Jeffery C. S. et al. 2005, *A&A*, 440, 667
- Schuh S. L., Heber U., Dreizler S. et al. 2003, *Baltic Astronomy*, 12, 55
- Woolf V. M., Jeffery C. S., Pollacco D. L. 2002a, *MNRAS*, 329, 497

**SPECTROSCOPIC DETECTION OF G-MODES IN
A LONG-PERIOD PULSATING SDB STAR PG 1627+017**

B.-Q. For¹, E. M. Green¹, D. O'Donoghue², L. L. Kiss³, S. K. Randall⁴,
G. Fontaine⁴, A. P. Jacob³, S. J. O'Toole⁵, E. A. Hyde¹ and T. R. Bedding³

¹ *Steward Observatory, University of Arizona, Tucson, AZ 85721, U.S.A.*

² *South African Astronomical Observatory, P.O. Box 9, Observatory, 7935, South Africa*

³ *School of Physics, University of Sydney, NSW 2006, Australia*

⁴ *Département de Physique, Université de Montréal, C.P. 6128, Succ. Centre-Ville, Montréal, Québec H3C 3J7, Canada*

⁵ *Remeis-Sternwarte, Astronomisches Institut der Universität Erlangen-Nürnberg, Sternwartstr. 7, Bamberg D-96049, Germany*

Received 2005 August 1

Abstract. We have detected low-level velocity variations due to g-mode pulsations in the long-period sdB variable PG 1627+017. The amplitudes are barely detectable at 1.0–1.5 km s⁻¹, despite the fact that this star is one of the brightest ($V = 12.9$) and largest amplitude (0.03 mag) pulsators in its class. The final radial velocity data set includes 84 hours of time-series spectroscopy over a time baseline of 53 days, with typical errors of 5–6 km s⁻¹ per spectrum. Our velocities were combined with previously existing data to derive improved orbital parameters. Unexpectedly, we find that the orbit of PG 1627+017 appears slightly elliptical, supporting Edelman et al.'s recent claim for similar ellipticities in the orbits of several other sdB stars. Our radial velocity power spectrum, after subtracting the orbital motion, shows three possible pulsational peaks at 7201.0 s (138.87 μ Hz), 7014.6 s (142.56 μ Hz) and 7037.3 s (142.10 μ Hz), with amplitudes only 3 to 4 σ above the mean noise level. While only one of the features is statistically likely to be real, all three are tantalizingly close to, or a one day alias of, the three strongest periodicities found in the concurrent photometric campaign. We further attempted to detect pulsational variations in the Balmer line amplitudes. The only detectable periodicity, at 7209 s, is consistent with theoretical expectations as a function of wavelength, and it also allows us to rule out a degree index of $l=3$ or $l=5$ for this mode. Given the extreme weakness of the detected g-mode pulsations, we conclude that more detailed spectroscopic mode identification in long-period sdB pulsators will require larger telescopes, higher efficiency spectral monitoring over longer time baselines, improved longitude coverage, and increased radial velocity precision.

Key words: stars: EHB and post-EHB – stars: oscillations – stars: subdwarfs

MAGNETIC FIELDS IN SDB AND SDO STARS

S. J. O’Toole¹, S. Jordan², U. Heber¹ and S. Friedrich³

¹ *Remeis-Sternwarte Bamberg, Astronomisches Institut der Universität Erlangen-Nürnberg, Sternwartstrasse 7, D-96049 Bamberg, Germany*

² *Astronomisches Rechen-Institut, ZAH, Mönchhofstrasse 12-14, D-69120 Heidelberg, Germany*

³ *Max-Planck-Institut für Extraterrestrische Physik, Giessenbachstrasse, D-85748 Garching, Germany*

Received 2005 August 1

Abstract. We have started a survey of magnetic fields in hot subdwarfs, and here present our current results. The survey was inspired by the discovery of two super-metal-rich sdB stars, which lead to the idea that a correlation may exist between metal abundances and magnetic field strength, similar to that seen in the chemically peculiar A stars. After our initial observations, we find no clear correlation. We will discuss the possible meaning of these results and the implication of our detections for magnetic flux conservation in late stages of stellar evolution.

Key words: stars: magnetic fields – hot subdwarfs

This contribution contains only an expanded discussion of the implications of the detection of 1 kG magnetic fields in hot subdwarf stars. For full details of the observations and analysis of this work, see O’Toole et al. (2005).

In this initial study we have found no clear evidence that the extreme abundances seen in UVO 0512–08 and PG 0909+276 are related to a strong magnetic field. Our other observations of white dwarfs (Aznar-Cuadrado et al. 2004) and central stars of planetary nebulae (Jordan et al. 2005) using the same instrumental setup and reduction procedure have measured similar fields with strengths ranging from -3 kG to +4 kG.

The detection of kilogauss strength magnetic fields raises questions for several areas of hot subdwarf research. Detailed analysis of these is beyond the scope of this work, however we present a qualitative discussion here.

First of all, how are the fields generated? The Sun’s magnetic field is believed to be dynamo-induced; that is, the solar core is rotating at a different speed with respect to the outer layers. Fields in magnetic white dwarfs (and magnetic Ap stars) are thought to be fossil fields. A link has been suggested between these two types of stars, and this would necessarily mean that their magnetic fields are tied to the stellar core, since even a weak stellar wind would destroy fields only existing in the outer layers. In the case of the hot subdwarfs, no firm evidence exists for differential internal rotation, although it has been proposed by Kawaler & Hostler (2005); this implies that dynamo-induced fields are unlikely. The case of fossil

fields is less clear. If the fields are leftover from, for example, the star formation cloud, then we might expect the fields to evolve with the star. It is unclear how binary evolution (CPD–64 481 probably has passed through a common envelope phase) might affect the magnetic field of the star’s progenitor.

Second, what implications, if any, do these results have for any assumptions of conservation of magnetic flux in stars? This is difficult to answer as there is yet no consistent theory that includes magnetic fields, convection, rotation, diffusion and winds in stellar evolution. From an empirical standpoint, however, if magnetic flux is completely conserved in sdB stars, then, based on our measurements, we would expect a population of low-mass white dwarfs with magnetic field strengths of up to ~ 500 kG. The observational statistics is too low at the moment to conclude which way is right.

Another question we might ask is: how would a magnetic field affect gravitational settling and radiative levitation calculations in hot subdwarfs? Naively we might expect such a field to disrupt diffusion, however, abundance anomalies with magnetic fields are also seen in chemically peculiar A stars and are in fact believed to play a role in the element enhancement. We therefore suggest that magnetic fields of around 1 kG should be included in sdB diffusion calculations, at least in a simple way.

Finally, it is well known that a small subset of sdBs pulsate. A magnetic field of ~ 1 kG should have some effect on the pulsations, most obviously as a splitting of a single pulsation mode into a doublet. There are more interesting consequences if the pulsation modes are high-order, however. In the roAp stars, kilogauss-strength fields lead to a region in the stellar atmosphere where magnetic pressure dominates over radiation pressure. This will of course have an additional effect on the nature of the oscillations.

Because the questions outlined above, we feel urged to extend spectropolarimetric measurements to additional sdB and sdO stars. First of all, we lack a sample of “normal” sdBs, i.e. objects which neither pulsate, nor are members of close binary systems, nor have already evolved away from the EHB. Since the pulsating sdB stars are much fainter than the stars studied here, it will be much harder to get similarly accurate measurements of field strength for them. Nevertheless, we have been awarded additional observing time with FORS1 at the VLT to measure one pulsator and several “normal” sdB stars with the same setup.

REFERENCES

- Aznar Cuadrado R., Jordan S., Napiwotzki R. et al. 2004, *A&A*, 423, 1081
Jordan S., Werner K., O’Toole S. J. 2005, *A&A*, 432, 273
Kawaler S. D., Hostler S. 2005, *ApJ*, 621, 432
O’Toole S. J., Jordan S., Friedrich S., Heber U. 2005, *A&A*, 437, 227

PHOTOMETRY OF LSIV–14 116 †

A. Ahmad and C. S. Jeffery

Armagh Observatory, College Hill, Armagh BT61 9DG, Northern Ireland

Received 2005 July 28

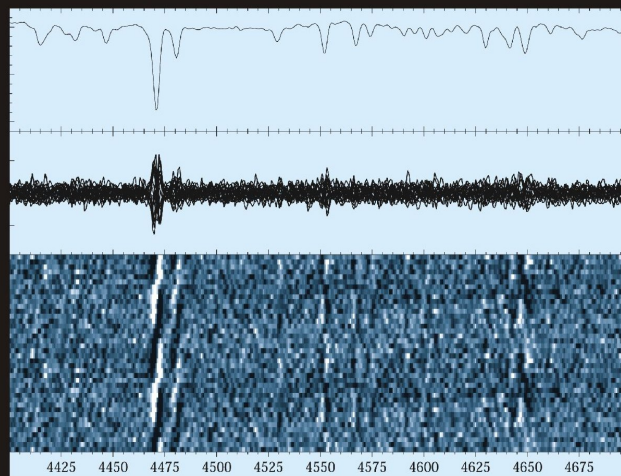
Abstract. Helium-rich subdwarf B (He-sdB) stars form a very small inhomogeneous group of subluminous stars showing varying degrees of helium enrichment. They have been found in the field of our Galaxy as well as in globular clusters. Here we report the first discovery of pulsation in a He-sdB star LSIV–14 116. Two pulsation periods can be clearly identified (1950 and 2900 s). They are more likely to be due to high-order non-radial *g*-mode oscillations than to radial or non-radial *p*-modes.

Key words: stars: chemically peculiar – stars: hot subdwarfs – stars: oscillations – stars: individual (LSIV–14 116)

†This work has been published in: Ahmad A. and Jeffery C. S. 2005, A&A, 437, L51

Proceedings from the Second Meeting on
La Palma '05 **sdO** **Hot Subdwarf Stars**
sdB **and Related Objects**
Roy H. Østensen (Ed.)

These proceedings contain contributions from the second meeting on Hot Subdwarf Stars and Related Objects. The book covers a wide spectrum of topics related to these interesting stars. Included are in depth presentations on the most recent results on the UV upturn phenomenon, reports from the most recent surveys of hot subdwarf stars in the field, in the galactic bulge and in various clusters, studies of the atmospheric properties of different types of subdwarf stars, new results from studies of subdwarf B binaries, and many new asteroseismological studies of new and old pulsating sdB stars.



Time resolved spectroscopy of the sdBV Balloon 090100001.
J. H. Telting et al. (illustration from the book, p. 235-242)